USE OF FALLING WEIGHT DEFLECTOMETER TESTING IN THE PAVEMENT ME AC/AC OVERLAY DESIGN PROCEDURE

by

Nathan Dressler Bech

B.S., University of Pittsburgh, 2015

Submitted to the Graduate Faculty of

Swanson School of Engineering in partial fulfillment

of the requirements for the degree of

Master of Science

University of Pittsburgh

2018

UNIVERSITY OF PITTSBURGH

SWANSON SCHOOL OF ENGINEERING

This thesis was presented

by

Nathan Dressler Bech

It was defended on

May 18th, 2018

and approved by

Luis E. Vallejo, Ph.D., Professor
Department of Civil and Environmental Engineering
University of Pittsburgh

Lev Khazanovich, Ph.D., Professor
Department of Civil and Environmental Engineering
University of Pittsburgh

Julie Marie Vandenbossche, Ph.D., Associate Professor
Department of Civil and Environmental Engineering
University of Pittsburgh
Thesis Advisor

USE OF FALLING WEIGHT DEFLECTOMETER TESTING IN THE PAVEMENT ME AC/AC OVERLAY DESIGN PROCEDURE

Nathan Dressler Bech, M.S.

University of Pittsburgh, 2018

Falling weight deflectometer (FWD) testing consists of applying an impact load to the pavement and recording the deflection of the pavement surface at specified distances from the point of impact. It is used to determine the structural capacity of an existing pavement and to backcalculate the stiffness of each layer in the pavement structure. This research focuses on the use of FWD data when designing asphalt concrete over asphalt concrete (AC/AC) overlays using the Pavement ME design procedure. There are four main components to this study. First, the performance prediction of the Pavement ME AC/AC overlay design procedure is examined in detail and is evaluated using field data from the Long-Term Pavement Performance Program (LTPP). Second, three methods for determining the stiffness of the existing asphalt concrete are compared using field and laboratory data, and the effect that the differences between methods have on design is quantified. Third, additional LTPP data is used to examine the relationship between FWD data and observed pavement distress in order to identify FWD parameters that are correlated with damage in the existing asphalt. Finally, LTPP data is used to develop adjustment factors for the Pavement ME AC/AC overlay design procedure that account for the difference between methods used to determine the stiffness of the existing asphalt.

TABLE OF CONTENTS

LIST OF TABLES

LIST OF FIGURES

ACKNOWLEDGEMENTS

This thesis is the result of work by many people besides myself. First, I would like to thank the members of my committee, Dr. Lev Khazanovich, Dr. Luis Vallejo, and Dr. Julie Vandenbossche, for reviewing and providing feedback on my work. In particular, I would like to thank my committee chair and advisor, Dr. Julie Vandenbossche, for providing guidance, for reviewing all of my writing, and for motivating me to finish this thesis. Second, I would like to thank Dr. John Oyler, Scooter, and Dr. Vikas Khanna, each of whom has helped me significantly over the last six years at Pitt. Third, I would like to thank my co-workers, John DeSantis, Katie Chmay, Nikki Souder, and Kevin Alland for providing assistance, ideas, and camaraderie along the way. Finally, I would like to thank my family, my mom, dad, and sister, for their invaluable support as I finished this work.

ΓΝΟΘΙ ΣΕΑΥΤΟΝ

NOMENCLATURE

Abbreviation	Meaning
AASHTO	Association of State Highway and Transportation Officials
AC	Asphalt concrete
AC/AC	Asphalt concrete over asphalt concrete
ANOVA	Analysis of variance
$d_{0,OWP}$	Deflection at the center of the load plate for FWD testing conducted in the outer wheelpath
$d_{0,ML}$	Deflection at the center of the load plate for FWD testing conducted at mid-lane
DCP	Dynamic cone penetrometer
E*	Dynamic modulus of asphalt concrete
E_{NDT}	Backcalculated stiffness of asphalt concrete
$E_{NDT,OWP}$	Backcalculated stiffness of asphalt concrete for FWD testing conducted in the outer wheelpath
$E_{NDT,ML}$	Backcalculated stiffness of asphalt concrete for FWD testing conducted at mid-lane
$E_{Witczak}$	Asphalt concrete stiffness estimated using the Witczak equation
$E_{Witczak(Aging)}$	Asphalt concrete stiffness estimated using the Witczak equation with binder aging models
$E_{Witczak(No\ aging)}$	Asphalt concrete stiffness estimated using the Witczak equation without binder aging models
FHWA	Federal Highway Administration
FWD	Falling weight deflectometer
LTE	Load transfer efficiency
LTPP	Long-Term Pavement Performance Program
MnDOT	Minnesota Department of Transportation
MDT	Mid-depth asphalt concrete temperature
ML	Mid-lane
MnROAD	Minnesota Road Research Facility
NCHRP	National Cooperative Highway Research Program
NDT	Non-destructive testing
OWP	Outer wheelpath
PennDOT	Pennsylvania Department of Transportation

SMP	Seasonal monitoring program
SR	State route
V_a	Volumetric air content of asphalt concrete
V_{be}	Volumetric effective binder content of asphalt concrete

1.0 INTRODUCTION

The structural condition of the asphalt concrete (AC) in the existing pavement is a critical input for the design of asphalt concrete over asphalt concrete (AC/AC) overlays. Falling weight deflectometer (FWD) testing is a non-destructive method for determining the structural condition of an existing AC pavement. AASHTOWare Pavement ME Design (Pavement ME) is one of the primary pavement design procedures used in the United States. In the Pavement ME AC/AC overlay design procedure, the amount of damage in the asphalt concrete layer of the existing pavement is quantified by comparing the stiffness of the asphalt concrete, backcalculated from the results of FWD testing, to the stiffness of the same layer determined using a predictive equation. This research focuses on how the Pavement ME AC/AC overlay design procedure quantifies damage in the asphalt concrete layer of the existing pavement, whether this methodology is effective, and how it might be improved.

1.1 BACKGROUND

AC/AC overlay design combines several aspects of civil engineering, including mechanics of materials, non-destructive testing, and mechanistic-empirical design. Three topics in particular require a brief introduction: the material properties of asphalt concrete, FWD testing and backcalculation, and the AASHTOWare pavement design software, Pavement ME.

1.1.1 Material properties of asphalt concrete

Asphalt concrete is an engineered mixture with two major components: asphalt cement binder and aggregate. Asphalt binder is a petroleum product produced by fractional distillation of crude oil. Its primary roles in an asphalt concrete mixture are to bind the aggregate particles together and provide stiffness at low temperatures. Asphalt binder is a viscoelastic and temperature-dependent material, so its stiffness depends on both the rate and temperature at which it is loaded. Because it contains asphalt binder, asphalt concrete is also viscoelastic and temperature-dependent. The stiffness of asphalt concrete is described using the dynamic modulus, which is the ratio of stress over strain under cyclic loading at a specified combination of temperature and load frequency. There are several different methods for determining the dynamic modulus of asphalt concrete. These are discussed in detail in Chapter 2. Additionally, asphalt binder becomes stiffer and more brittle over time as it reacts with oxygen in the air. This is called binder aging or binder oxidation. The aggregate in an asphalt concrete mixture should be a durable natural stone. The primary roles of aggregate in an asphalt concrete mixture are to provide stiffness and stability at high temperatures and to provide friction on the road surface. Asphalt concrete mixtures are designed to meet the performance requirements of a paving project, including traffic level and environmental conditions. Parameters commonly used to describe an asphalt concrete mixture include: volumetric air content (V_a) (%), volumetric effective binder content (V_{be}) (%), and aggregate gradation ($P_{3/4}$, $P_{3/8}$, P_4, and P_{200}). The composition of a typical asphalt concrete mixture used in Pennsylvania is shown in Figure 1 (Bhattacharya et al. 2017).

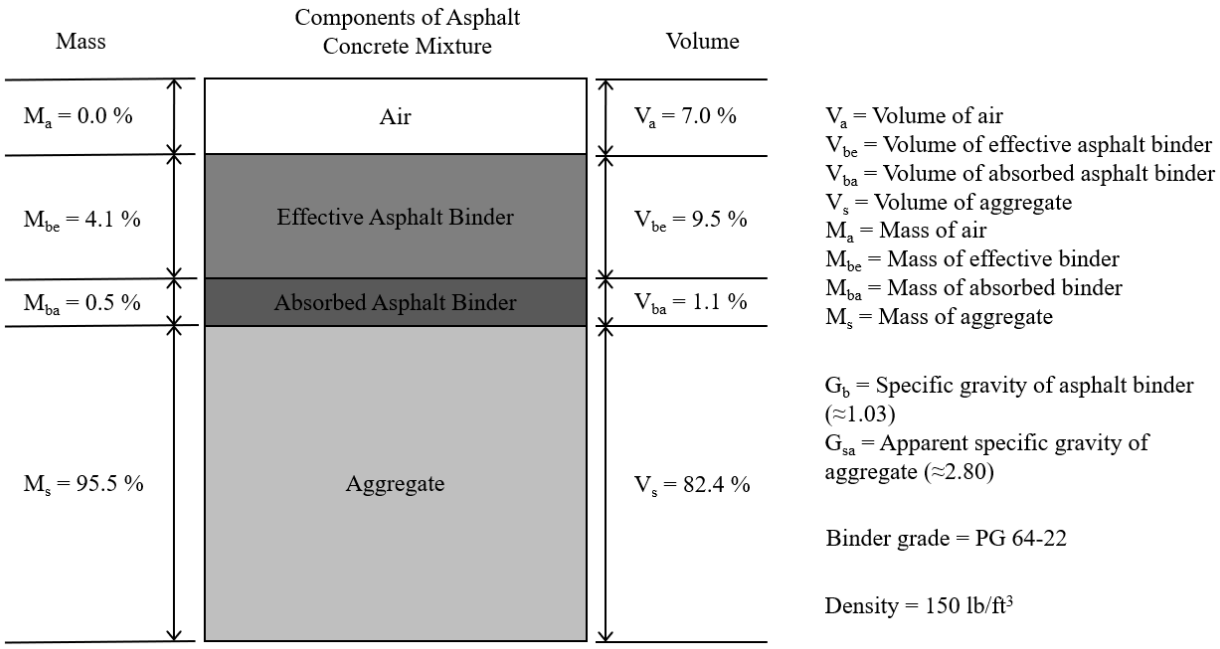

Figure 1. Composition of a typical asphalt concrete base course mixture used in Pennsylvania.

1.1.2 FWD testing and backcalculation

The FWD is a machine that applies an impact load to the surface of a pavement and measures the deflection of the pavement surface at specified distances from the point of impact. For AC pavements, the primary purpose of FWD testing is to determine the stiffness of each layer in the pavement structure. This is accomplished using a process called backcalculation. There are several different types of backcalculation. The type of backcalculation used in this research is iterative backcalculation with static layered elastic analysis. This backcalculation process consists of a series of steps:

1. Perform FWD testing and record maximum surface deflections (the deflection basin).
2. Determine the thickness of each layer in the pavement structure.

3. Estimate the stiffness of each layer in the pavement structure. These estimates are called seed values.
4. Create a virtual model of the pavement structure, including thickness, estimated stiffness, and other (assumed) mechanical properties, for each layer.
5. Use layered elastic analysis to calculate the deflection basin created by a FWD load.
6. Compare the measured and calculated deflection basins. Determine the error from the difference between basins.
7. If the error or the layer stiffness has changed less than a specified amount since the previous iteration, end the process. Otherwise, change the stiffness of layers in the model and repeat steps 5 and 6.

These steps are summarized in Figure 2.

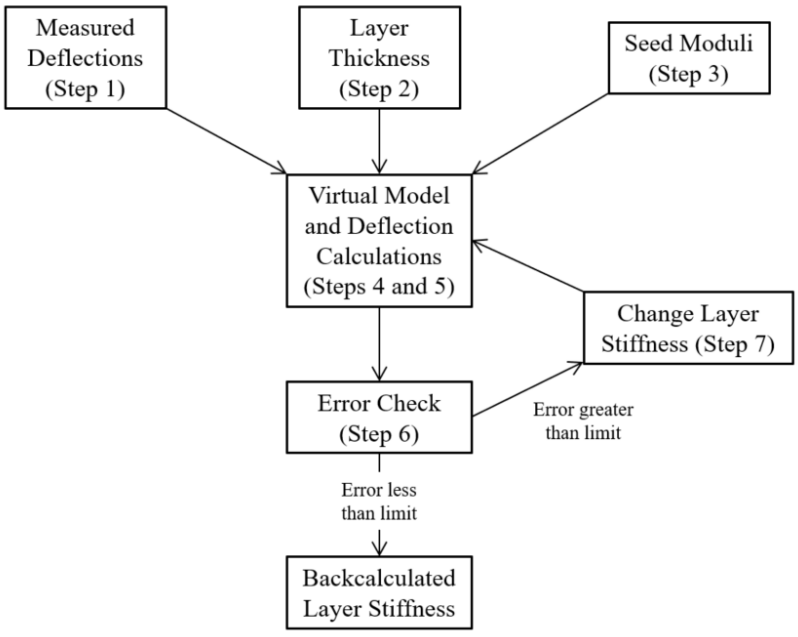

Figure 2. Steps in the iterative backcalculation process using layered elastic analysis.

The estimated stiffness of each layer is equal to the stiffness of that layer at the end of the backcalculation process (when error is less than the error limit in Step 6). The backcalculation for this study was performed in a semi-automated manner using a backcalculation software program, such as EVERCALC 5.0 (WSDOT 2005) or the Pavement ME Backcalculation Tool (ARA Inc. 2017). The backcalculation program contains algorithms that perform Steps 4 through 7 of the backcalculation process automatically. The correct solution to a given backcalculation problem is the set of backcalculated layer stiffness values that minimizes the total error between measured and calculated deflections. Also, the stiffness of each layer must be within reasonable limits for its material. It is important to note that the FWD is a dynamic test, but the layer stiffness determined from backcalculation is a static value because layered elastic analysis models the FWD impact load as static. This discrepancy is discussed in more detail in Chapter 2.

1.1.3 AASHTOWare Pavement ME Design

Pavement ME is a pavement design software program that is based on mechanistic-empirical design principles. Design inputs include the thickness of each pavement layer, the material properties of each layer, the amount of traffic expected over the design period, and the environmental conditions. The program uses a set of mechanistic models to simulate the response of the pavement to traffic and environmental loads. Responses consist of stresses, strains, and deflections at different locations in the pavement structure. Once mechanistic responses have been calculated, empirical transfer functions are used to translate these responses into predicted pavement performance. Transfer functions are statistical relationships between pavement response and pavement performance that were developed using data from pavement test sections. For AC pavements, pavement performance measures include fatigue cracking, longitudinal cracking,

transverse cracking, and rutting. Using Pavement ME, a pavement structure is designed by changing the characteristics of the pavement structure until the predicted pavement performance meets an acceptable threshold. Pavement ME allows the user to change the length of the analysis period and the level of reliability for predicted performance.

Pavement ME uses three levels (Level 1, Level 2, and Level 3) to define each input. Level 1 inputs require the most effort to define but are intended to provide the most accurate information for simulating pavement response. Level 2 and Level 3 inputs require less effort to define and generally provide less accurate information for simulating pavement response. Level 2 and Level 3 inputs are often estimates of Level 1 inputs or correlations with Level 1 inputs. For the Pavement ME AC/AC overlay design procedure, FWD testing of the existing pavement and the mix properties of the asphalt concrete in the existing pavement are the Level 1 inputs used to define the stiffness of the asphalt concrete in the existing pavement. For Level 2 and Level 3, the inputs used to define the stiffness of the asphalt concrete of the existing asphalt concrete are the amount and severity of fatigue cracking in the existing pavement and the subjective condition rating of the existing pavement, respectively.

1.2 MOTIVATION FOR RESEARCH

The main motivation for this research is the implementation of the Pavement ME by the Pennsylvania Department of Transportation (PennDOT). Currently, PennDOT uses the AASHTO Guide for Design of Pavement Structures, 1993 (AASHTO 1993) to design overlays. As part of adopting Pavement ME, PennDOT contracted the University of Pittsburgh to provide guidelines for using FWD testing to establish the inputs for designing an AC/AC overlay using the Pavement

ME. For overlays of existing AC pavements, including the AC/AC overlay design procedure, PennDOT was specifically interested in using FWD testing to define damage in the asphalt concrete layer and to backcalculate the stiffness of the unbound pavement layers.

1.3 RESEARCH OBJECTIVES

There are several objectives for this research. The first objective is to develop a complete understanding of the Pavement ME AC/AC overlay design procedure and to assess the accuracy of distress predictions made by the procedure. This is necessary because the AC/AC overlay design procedure was recently changed by adding a mechanistic reflective cracking model and the new procedure has not been thoroughly evaluated in the literature (ARA Inc. 2015a). The second objective is to examine and compare different methods for determining the stiffness of asphalt concrete in an existing AC pavement. Additionally, the effect of different methods on design will be examined to determine if differences between methods have a significant impact on design. The third objective is to examine the relationship between FWD data and fatigue damage in the asphalt concrete of an existing AC pavements. This investigation is necessary to verify the assumption that FWD testing can be useful in assessing the damage in the AC layer of an existing pavement. The final objective is to use findings from the first three objectives to develop adjustment factors for the backcalculated AC stiffness input used in the Pavement ME AC/AC overlay design procedure. The purpose of the adjustment factors is to improve the accuracy of distress predictions made by this procedure.

1.4 RESEARCH APPROACH

This research makes extensive use of field testing data to address the research objectives. Most of this data was obtained from two pavement performance programs: The Long-Term Pavement Performance Program (LTPP) and the Minnesota Department of Transportation (MnDOT) research facility (MnROAD). Additional data was collected by PennDOT and the University of Pittsburgh from two pavement sections near Pittsburgh, Pennsylvania. The first research objective is addressed by using the Pavement ME AC/AC overlay design procedure to simulate overlaid pavement sections that are included in the LTPP database and comparing predicted and observed pavement distress. The second research objective is addressed by comparing field and laboratory data obtained from instrumented pavement sections at MnROAD and from two sections near Pittsburgh, PA. The third research objective is addressed by performing statistical analysis on field and laboratory data from non-overlaid pavement sections in the LTPP database. The final objective is addressed by simulating the performance of overlaid pavement sections found in the LTPP database with Pavement ME and determining program inputs that produced the best agreement between predicted and observed distress. A regression analysis is then used to determine adjustment factors for the backcalculated asphalt concrete stiffness input used in the Pavement ME AC/AC overlay design procedure.

1.5 STRUCTURE OF THE THESIS

The structure of the thesis is as follows. Chapter 2 contains a literature review of the previous work that has evaluated the Pavement ME AC/AC overlay design procedure and of work that has compared methods for determining the stiffness of asphalt concrete in an existing AC pavement. Chapter 3 provides a detailed description of the Pavement ME AC/AC overlay design procedure, focusing on the mechanistic models and underlying assumptions. The design procedure is also evaluated using field and laboratory data from the LTPP database. The results of the evaluation are used to define objectives for Chapters 4 through 6. Chapter 4 compares three separate methods for determining the stiffness of asphalt concrete in an existing AC pavement using field and laboratory data from MnROAD and PennDOT. Additionally, the effect that differences between methods have on design is evaluated using the Pavement ME design procedure for new AC pavements. The purpose of this is to determine if the dynamic modulus will provide the same predicted performance, regardless of the methodology used to establish it.

Chapter 5 examines the relationship between FWD data and fatigue damage in the asphalt concrete. This is performed using field and laboratory data from the LTPP database. Several parameters are established using FWD data to assess fatigue damage. Relationships between FWD load level, asphalt concrete temperature, and fatigue damage are examined for each parameter. Chapter 6 establishes a method for improving the accuracy of distress predicted when using the Pavement ME AC/AC overlay design procedure. Field and laboratory data for sections in the LTPP database is used to develop adjustment factors for the Level 1 backcalculated asphalt concrete stiffness input used in Pavement ME. Chapter 7 presents the conclusions of this research, identifies limitations of the findings, and provides suggestions for future work.

2.0 LITERATURE REVIEW

2.1 EVALUATION OF THE PAVEMENT ME AC/AC OVERLAY DESIGN PROCEDURE

The Pavement ME AC/AC overlay design procedure is a collection of mechanistic models and calibrated empirical relationships that predicts the amount of distress that will occur in an asphalt concrete overlay placed on an existing AC pavement. There are three levels of design inputs for the AC/AC overlay procedure. The models used to predict distress are the same for all input levels but the way that inputs are used to define damage in the asphalt concrete of the existing pavement is different for each input level. When using Level 1 inputs damage in the asphalt concrete of the existing pavement is defined by the relationship between the backcalculated stiffness of the asphalt concrete (E_{NDT}) and the stiffness of the same asphalt concrete estimated using the Witczak predictive equation ($E_{Witczak}$) (ARA Inc. 2004). E_{NDT} represents the damaged stiffness of the asphalt concrete and $E_{Witczak}$ represents the undamaged stiffness of the asphalt concrete. When Level 2 inputs are used damage in the asphalt concrete of the existing pavement is defined using the observed amount and severity of fatigue cracking in the existing pavement. When Level 3

inputs are used, damage in the asphalt concrete is defined using a subjective rating of the condition of the existing pavement.

Once the amount of damage in the asphalt concrete of the existing pavement has been defined, it is used to reduce the stiffness of the asphalt concrete for mechanistic pavement response calculations. Calculated responses are translated into predicted distress using empirical transfer functions. Thus, the input level (Level 1, 2, or 3) determines the method used to define damage in the asphalt concrete and therefore the amount of predicted distress. The models and procedures used in the Pavement ME for the design of AC/AC overlays are discussed in more detail in Chapter 3.

2.1.1 Level 1 inputs

Only a few studies have been performed to evaluate the use of Pavement ME for designing AC/AC overlays using Level 1 inputs. Additionally, the procedure was significantly revised in August, 2015, when a mechanistic reflective cracking model was added to Version 2.2 (ARA Inc. 2015a). Some of the studies evaluating the procedure were published before the release of this revision.

A study performed at Virginia Tech evaluated the Pavement ME AC/AC overlay design procedure when using Level 1, Level 2, and Level 3 inputs (Loulizi et al. 2008). This study concluded that the use of Level 1 inputs causes the damaged stiffness of the asphalt concrete in the existing pavement to be lower than both the lab-measured dynamic modulus and the dynamic modulus predicted using the Witczak equation.

In a recent draft report from the ongoing research project "FHWA-PROJ-14-0126: Characterizing Existing Hot-Mix Asphalt Layer Damage for Mechanistic-Empirical Pavement Design," LTPP data was used to evaluate the Level 1 procedure. This study concluded that the

assumption E_{NDT} and $E_{Witczak}$ are equal for an undamaged pavement, is not valid. This is critical because this is the underlying assumption of when designing AC/AC overlays with Level 1 inputs using Pavement ME. It was determined that the difference between E_{NDT} and $E_{Witczak}$ is temperature-dependent and temperature-dependent adjustment factors were developed for the Level 1 E_{NDT} input. These are shown in Table 2. Additionally, it was observed that E_{NDT} is consistently greater for pavements with thin asphalt concrete layers than for pavements with thick asphalt concrete layers. Finally, the study recommended that the FWD loading frequency be defined at 30 Hz when using Level 1 inputs.

The study also made several conclusions about the AC/AC overlay design procedure that are not directly related to the Level 1 inputs. It was determined that the ratio of E_{NDT} over $E_{Witczak}$ is not strongly correlated to the amount of fatigue cracking in the existing pavement, and that this can cause a large difference between fatigue cracking predicted using Level 1 inputs and fatigue cracking predicted using Level 2 inputs. Two explanations were given for this. First, it was observed that E_{NDT} can be reduced by up to 50% before fatigue cracking appears at the surface of the pavement. Second, it was determined that not all fatigue cracking initiates at the bottom of the asphalt concrete layer, resulting in a reduction of the E_{NDT} over $E_{Witczak}$ ratio. Rather, some fatigue cracking is bottom-up and some is top-down and the thickness of the asphalt concrete layer dictates which type of cracking type of cracking is most likely to occur. Despite these observations, the overarching assumption that the amount of fatigue cracking in an AC pavement is directly related to the ratio of E_{NDT} over $E_{Witczak}$ was accepted.

Finally, a recent FHWA report recommends that the correction factors developed by Von Quintus and Killingsworth (Table 2) be used to adjust the Level 1 E_{NDT} (Bruinsma et al. 2017).

The same report notes, however, that use of the adjustment factors should be reevaluated once the previously-discussed FHWA study (FHWA-PROJ-14-0126) is completed.

No studies were found that directly evaluate the accuracy of the current AC/AC overlay design procedure with Level 1 inputs by comparing predicted distress to observed distress. Additionally, no studies have been found that examine whether applying adjustment factors (such as those in Table 2) to the E_{NDT} input improves the accuracy of Pavement ME distress predictions. Additional research is required to determine if Pavement ME provides reasonable results when designing AC/AC overlays using Level 1 inputs.

2.1.2 Level 2 inputs

The AC/AC overlay design procedure has not been thoroughly evaluated using Level 2 inputs. Software demonstrations by the developers of the procedure have shown that it can predict both the time history and maximum amount of fatigue cracking with reasonable accuracy for individual pavement sections (Lytton and Von Quintus 2016). However, similar to using the procedure with Level 1 inputs, additional work is required to determine whether the use of the procedure, while using Level 2 inputs, provides reasonable distress predictions across a range of pavement structures.

2.1.3 Level 3 inputs

Similar to using the AC/AC overlay design procedure with Level 2 inputs, the use of Level 3 inputs has not been thoroughly evaluated either. Additional work is required to determine whether using the procedure with Level 3 inputs provides reasonable distress predictions.

2.2 METHODS FOR DETERMINING THE STIFFNESS OF ASPHALT CONCRETE

The stiffness of asphalt concrete is defined using the dynamic modulus, which is the ratio of stress over strain at a specified temperature and load frequency. There are three methods commonly used for determining the dynamic modulus of asphalt concrete:

1. Measuring it in the laboratory using AASHTO T 342 (AASHTO 2015)
2. Estimating it using a predictive equation
3. Performing FWD testing and backcalculation

In Pavement ME, the stiffness of asphalt concrete is described using a dynamic modulus (E*) master curve. The E* master curve is a collection of fitted equations that describes the dynamic modulus of an asphalt concrete mixture as a function of temperature and load frequency. In Pavement ME, E* is a critical design input used to predict the development of both fatigue cracking and rutting for both new and rehabilitated flexible pavement structures. For new AC pavement designs and in AC/AC overlay design, the dynamic modulus master curve of new asphalt concrete can be defined by performing dynamic modulus testing on laboratory samples or by using a predictive equation with inputs from the mixture design.

For the asphalt concrete of the existing pavement, however, the E* master curve is defined using both a predictive equation and FWD testing. First, the Witczak predictive equation, which will be the focus of this study, is used to define the E* master curve of the existing asphalt in an undamaged state. Next, the backcalculated stiffness of the asphalt concrete in the existing pavement is used to define the amount of fatigue damage in this asphalt concrete. Finally, the fatigue damage is used to create a damaged E* master curve, which represents the in-situ, damaged

stiffness of the asphalt concrete in the existing pavement. A more detailed description of this process is provided in Chapter 3. To evaluate and develop inputs for the Pavement ME AC/AC overlay design procedure, it is necessary to understand each of the three different methods for establishing the stiffness of the asphalt concrete in the existing pavement and to understand how these methods are related. Specifically, it is important to check the assumption that each of the three methods results in the same stiffness for the same asphalt concrete mixture tested at the same temperature and load rate. If this assumption is not correct, a relationship between the dynamic moduli established using these different methods can be identified so that each can be corrected to a single master curve that provides the best predicted performances.

Abbreviations are used throughout this study to refer to the three methods for defining asphalt concrete stiffness. The stiffness determined from laboratory dynamic modulus testing is abbreviated as E*. The stiffness estimated using the Witczak dynamic modulus predictive equation is abbreviated as $E_{Witczak}$. Finally, the stiffness determined using FWD testing and backcalculation is abbreviated as E_{NDT}.

2.2.1 Dynamic modulus testing

The stiffness of asphalt concrete is determined in the laboratory using the dynamic modulus test described in AASHTO T 342 (AASHTO 2015). In this test, a haversine axial load is applied to a cylindrical asphalt concrete specimen and the deformation is measured as a function of time. Because asphalt concrete is viscoelastic, the peak strain (ε) lags the peak stress (σ) by a phase angle (φ). The complex modulus of the asphalt concrete is defined by Equation 1.

$$E^*_{complex} = E^* \cos(\varphi) + iE^* \sin(\varphi) \quad (1)$$

Where:

$E^*_{complex}$ = Complex modulus

E* = Dynamic modulus. Equal to the absolute value of the complex modulus ($E^* = |E^*_{complex}|$)

φ = Phase angle

i = Imaginary number

For practical purposes, the stiffness of asphalt concrete is usually defined using the dynamic modulus (E*), which is the absolute value of the complex modulus. By performing multiple dynamic modulus tests at several combinations of load frequency and temperature, one can develop a dynamic modulus master curve that describes the stiffness of an asphalt concrete mixture at any combination of load rate and temperature. The master curve is based on the principle of time-temperature superposition. This principle assumes that, for linear viscoelastic materials, the relationship between load rate and instantaneous stiffness does not change with temperature, but merely shifts left or right. The dynamic modulus master curve for an asphalt concrete mixture consists of a sigmoidal curve, describing the relationship between the dynamic modulus and load rate, and a set of shift factors, describing the relationship between the dynamic modulus and temperature. The sigmoidal curve is defined at a reference temperature, usually 70ºF. The dynamic modulus master curve for a typical asphalt concrete mixture used in Pennsylvania is shown in Figure 3 (Bhattacharya et al. 2017).

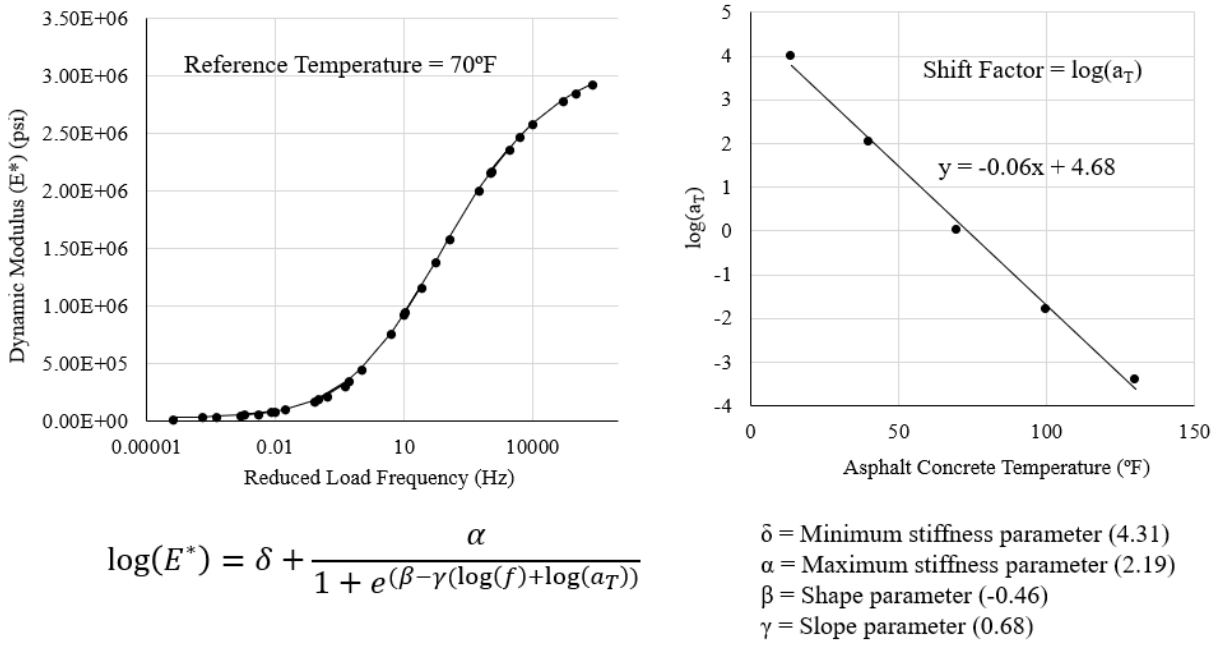

$$\log(E^*) = \delta + \frac{\alpha}{1 + e^{(\beta - \gamma(\log(f) + \log(a_T)))}}$$

Figure 3. Dynamic modulus master curve for a typical asphalt concrete base course mixture used in Pennsylvania.

Performing dynamic modulus testing on asphalt concrete cores pulled from the existing pavement is the most direct method of measuring the stiffness of the asphalt concrete in the existing pavement over a range of temperatures and load frequencies. There are two limitations with using dynamic modulus testing of field cores to determine the stiffness of asphalt concrete in the existing pavement. First, the laboratory dynamic modulus test requires specialized equipment and the test is expensive to perform for most asphalt rehabilitation projects. Second, dynamic modulus test specimens are only 6 in long, so the entire thickness of the asphalt concrete layer in the existing pavement is not considered if it is greater than 6 in. Additionally, it is not possible to test the dynamic modulus of individual asphalt concrete lifts in the existing pavement if they are less than 6 in thick. This usually includes the wearing and binder courses, the two layers most affected by binder aging.

2.2.2 Predictive equations

Predictive equations may be used to estimate the dynamic modulus of an asphalt concrete mix at a specified temperature and load frequency. Such equations require additional information about the asphalt mix, such as binder content, binder grade, air content, and aggregate gradation. These mix parameters can be determined in a laboratory using relatively simple asphalt concrete test procedures. Compared to dynamic modulus testing, predictive equations are a more cost-effective method for determining the dynamic modulus of asphalt concrete. Dynamic modulus predictive equations usually take the form of statistical regressions of laboratory test data. Some commonly used equations of this type are the Witczak, Hirsch, and Al-Khateeb equations (Al-Khateeb et al. 2006; Andrei et al. 1999; Bari 2005; Christensen et al. 2003) Artificial neural networks have also been used to predict the dynamic modulus from asphalt mixture parameters (Ceylan et al. 2007; Kim et al. 2011). The Witczak dynamic modulus predictive equation is used exclusively in this research because it was used to define asphalt stiffness when the national calibration of the Pavement ME AC/AC overlay design procedure was performed (Andrei et al. 1999).

The Witczak equation, which, as previously mentioned, is incorporated into Pavement ME, is based on two volumetric parameters of the asphalt mix (volumetric air voids (V_a), and volumetric effective binder content (V_{be})), the characteristics of the aggregate gradation ($P_{3/8}$, $P_{3/4}$, P_4, and P_{200}), and the grade of the asphalt binder (Andrei et al. 1999). The Witczak equation is shown in Equation 2. Additional details and how the Witczak equation has been incorporated into Pavement ME (including models used to simulate asphalt binder aging) can be found in Chapter 3.

$$\log(E^*) = 3.750063 + 0.029232P_{200} - 0.001767(P_{200})^2 - 0.002841P_4 - 0.058097V_a - 0.802208\left[\frac{V_{be}}{V_{be}+V_a}\right] + \frac{3.871977 - 0.0021P_4 + 0.003958P_{3/8} - 0.000017\left(P_{3/8}\right)^2 + 0.005470P_{3/4}}{1 + e^{(-0.603313 - 0.313351\log(f) - 0.393532\log(\eta))}} \quad (2)$$

Where:

E^* = Dynamic modulus (psi)

η = Asphalt binder viscosity (poise*10^6)

f = Loading frequency (Hz)

V_a = Air void content (%)

V_{be} = Volumetric effective binder content (%)

$P_{3/4}$ = Cumulative percent retained on the 3/4-in sieve

$P_{3/8}$ = Cumulative percent retained on the 3/8-in sieve

P_4 = Cumulative percent retained on the #4 sieve

P_{200} = Percent passing the #200 sieve

Predictive models, however, do not provide an exact measure of the dynamic modulus. First, there is inherent uncertainty in all predictive equations because they are statistical regressions of experimental data. Second, there may be differences between the data used to develop a predictive equation and the way that equation is used in practice. For example, the Witczak equation was developed using mostly lab-mixed, lab-compacted, undamaged asphalt specimens, but is used to predict the dynamic modulus of plant-mixed, field-compacted, damaged asphalt specimens. Additionally, many of the dynamic modulus tests used to fit the Witczak model were performed diametrically, whereas the current dynamic modulus test (AASHTO T342) uses axial loading (AASHTO 2015; Andrei et al. 1999).

It is worth noting that even if the use of the Witczak equation does not provide a "true measure" of the dynamic modulus, it is possible that this method provides the most realistic predicted pavement thicknesses when using Pavement ME for design. This is because the national calibration of the performance prediction curves was performed using dynamic moduli established primarily using the Witczak equation (ARA Inc. 2004).

2.2.3 FWD testing and backcalculation

The stiffness of asphalt concrete in an existing AC pavement can be determined with FWD testing and backcalculation. Importantly, the backcalculated stiffness of the asphalt concrete in the existing pavement corresponds to the temperature of the asphalt at the time the FWD testing is performed and to the load frequency of the FWD. The temperature of the asphalt can be measured directly using thermocouples or can be estimated using a predictive equation or heat transfer model. The load frequency (f) of the FWD is typically defined using the cyclic definition of frequency ($f = 1/t$), where t is the load duration. The typical duration of a Dynatest FWD load pulse is between 15 ms and 35 ms, resulting in a load frequency between 29 Hz and 67 Hz (Ayyala et al. 2016). The Dynatest is the most commonly used type of FWD in the United States, and PennDOT operates three Dynatest FWDs. An FWD test is not directly analogous to a dynamic modulus test, however, and the frequency of the FWD load pulse changes as it travels through the pavement structure due to a variety of dynamic, wave propagation, and viscoelastic effects (Chatti et al. 2017). Work has been performed to model the dynamic behavior of the FWD load in the asphalt pavement structure and to backcalculate the asphalt concrete dynamic modulus master curve from the FWD deflection time history, but this methodology has not been successfully proven using field data (Chatti et al. 2017). Ongoing research regarding the use of FWD testing

in the Pavement ME AC/AC overlay design procedure has suggested that the FWD load frequency may actually be variable and may depend on the structure of the pavement being tested (Ayyala et al. 2016).

In lieu of dynamic modeling and backcalculation, the most common approach for defining the frequency associated with the backcalculated asphalt concrete stiffness is to use a single, representative frequency for all backcalculated moduli. There is some disagreement in defining the representative frequency and how it should be calculated (Ayyala et al. 2016). Table 1 summarizes some of the representative FWD load frequencies reported in the literature. Across these studies, it is assumed that the representative load frequency is specific to the type of FWD used. The representative load frequency is relatively consistent (between 17.9 Hz and 30 Hz) for studies using a Dynatest FWD and either the cyclic definition of frequency ($f = 1/t$) or direct measurement of load frequency. Currently, a FWD load frequency of 30 Hz is recommended for use in Pavement ME (Rao and Von Quintus 2015).

Table 1. Summary of FWD load frequency values used in literature.

Location of Study	Source	Representative FWD Load Frequency (Hz)	Time-Frequency Conversion	Type of FWD
MnROAD	Clyne, et al., 2004	17.9	Load frequency determined from strain gauge time-histories	Dynatest
Virginia Tech Transportation Institute	Loulizi, et al., 2007	5.3	$f = 1/2\pi t$	Dynatest
Kansas State University	Gedafa, et al., 2010	25	$f = 1/t$	Dynatest
CEDEX	Mateos, et al., 2012	15	$f = 1/t$	KUAB
Applied Research Associates, Inc. (ARA)	Ayyala, et al., 2017	30	$f = 1/t$	Dynatest

An alternative method for determining an asphalt concrete dynamic modulus master curve using FWD data was developed as part of this research. The backcalculated stiffness can be used to "calibrate" a master curve that was developed using the Witczak equation, if FWD testing is performed over a wide range of asphalt temperatures for a newly constructed pavement section. This method is described in detail in Chapter 4.

The primary advantage of backcalculation is that it can be performed quickly and cost-effectively, as compared to laboratory dynamic modulus testing or the use of predictive equations when inputs are established by laboratory testing. The primary disadvantage of backcalculation is that a single day of FWD testing cannot define the full relationship between asphalt concrete stiffness, temperature, and load frequency. A relationship between backcalculated stiffness and temperature can be established, but this requires FWD testing at different times of year to capture a full range of asphalt temperatures. Additionally, correct backcalculation of the asphalt concrete stiffness requires accurate layer thickness information and appropriate seed moduli. Collecting this information often requires coring and soils testing that can add to the cost of FWD testing.

2.2.4 Comparison of methods

Several studies have evaluated the relationship between the difference in the stiffness of the asphalt when they were determined using different methods. The relevant findings of these studies are discussed below and are summarized in Table 2. A study performed for the Federal Highway Administration (FHWA), included an analysis of data in the LTPP database. It was concluded that the backcalculated stiffness of asphalt concrete is greater than the resilient modulus of the asphalt concrete determined using indirect tensile testing (Von Quintus and Killingsworth 1998). The resilient modulus of asphalt concrete is the ratio of the cyclic load, applied in indirect tension, over

the recoverable horizontal deformation (ASTM International 2011). Furthermore, the relationship between the backcalculated stiffness and resilient modulus is temperature-dependent. The backcalculated stiffness is equal to the resilient modulus at 41ºF and the backcalculated stiffness is four times greater than the resilient modulus at 104ºF. Temperature-dependent factors were provided for adjusting the backcalculated asphalt stiffness used in the AASHTO 1993 Design Guide (AASHTO 1993; Von Quintus and Killingsworth 1998).

In a study performed at MnROAD, master curves developed using data from dynamic modulus testing performed on field cores and from backcalculation using Evercalc 5.0 were compared for three pavement sections (cells) (Clyne et al. 2004). Testing was performed on Cells 33, 34 and 35 of the Low Volume Road. The majority of pavement research sections at MnROAD are located on the mainline, a portion of Interstate 94 northwest of Minneapolis, Minnesota, and are subjected to mixed traffic at highway speeds. The Low Volume Road is a separate test loop intended to simulate low volume roads in Minnesota. The Low Volume Loop is trafficked by a five-axle semi-trailer and the total number of loads is much less than on the mainline. Each cell had a 4.0-in asphalt concrete layer over a 12-in granular base. A FWD load frequency of 17.9 Hz was calculated using data from strain gauges embedded in the pavement. The backcalculated asphalt stiffness was found to be lower than the dynamic modulus measured in the lab for asphalt concrete temperatures between 30ºF and 100ºF. Results from Cells 34 and 35 showed that variability in the backcalculated moduli within cells was greatest at temperatures less than 50ºF (Clyne et al. 2004).

In research performed at Virginia Tech, master curves were established with data from dynamic modulus testing performed on cores. These master curves were compared to master curves developed using the Witczak equation and moduli backcalculated using ELMOD (Loulizi

et al. 2008). Cores were taken from nine different pavements in Virginia. A FWD load frequency of 5.3 Hz was assumed based on an FWD load pulse duration of 0.03 seconds for a Dynatest FWD. Notably, this is over three times less than the FWD load frequency used at MnROAD for the same type of FWD (Table 1) (Clyne et al. 2004). Dynamic moduli predicted using the Witczak equation were roughly equivalent to lab-measured dynamic moduli for the entire range of temperatures and frequencies considered. Additionally, the backcalculated moduli, averaged over each pavement section, were lower than the dynamic moduli predicted using the Witczak equation (Loulizi et al. 2008).

A study from Kansas State compared the stiffness of asphalt concrete in existing pavements determined using dynamic modulus testing of cores, the Witczak equation, and backcalculation (Gedafa et al. 2010). The analysis was based on data gathered from nine AC pavement sections in Kansas, five of which were newly constructed when FWD testing was performed. A FWD load frequency of 25 Hz, the highest load frequency used in laboratory dynamic modulus testing, was assumed for making comparisons between backcalculated stiffness, laboratory-measured dynamic modulus, and predicted dynamic modulus. Several different backcalculation programs were evaluated, including EVERCALC, MODCOMP, and MODULUS. The backcalculated asphalt concrete stiffness was comparable for all three programs. Additionally, several different predictive equations were evaluated, including the Hirsch equation (Christensen et al. 2003), the revised Witczak equation (Bari 2005), and the original Witczak equation (used in Pavement ME) (Andrei et al. 1999). Of the three predictive equations evaluated, the revised Witczak equation produced the highest estimated asphalt stiffness at low temperatures. Additionally, stiffness estimated using the original Witczak model was lower than the dynamic modulus measured in the laboratory at low temperatures and higher than those measured at high temperatures. Finally, the backcalculated

stiffness and laboratory-measured dynamic modulus were found to be statistically different for all nine sections (Gedafa et al. 2010). The data presented in the Kansas State study was used to compute average relationships between methods. These are shown in Table 2. Only data from the five new sections was used to exclude the effect of damage in the asphalt concrete of the existing pavement. Additionally, only data that used the EVERCALC backcalculation program and the original Witczak predictive model was used because these methods for determining asphalt stiffness are used in the LTPP database and Pavement ME, respectively.

In a study performed at the CEDEX test track in Madrid, dynamic moduli measured on field cores and the moduli backcalculated using EVERCALC 5.0 were compared for four new pavement sections (Mateos et al. 2012). The four sections had asphalt layers between 4.75 in and 6.0 in thick and granular bases between 20 in and 40 in thick. A load frequency of 15 Hz was assumed based on the load duration of the KUAB FWD used in this study. The average backcalculated moduli were roughly equivalent to that determined through laboratory testing on field cores (Mateos et al. 2012).

Table 2. Comparisons of methods for determining the stiffness of asphalt concrete in existing pavements in previous studies.

Location of Study	Author(s)	Relationship between methods	Temp-erature Range (°F)	Frequency Range (Hz)	Stiffness Range (ksi)	FWD Load Frequency (Hz)	Back-calculation Program(s) Used	Range of Asphalt Concrete Thickness (in)	Range of Granular Base Thickness (in)	Notes
Brent Rauhut Engineering, Inc.	Von Quintus and Killingsworth, 1998	$E_{NDT} = 1.00 \times E_{RT,,Lab}$ [1,2]	41	N/A [6]	N/A	NR [7]	MODULUS	NR (Wide range of LTPP sections)		[8]
		$E_{NDT} = 2.8 \times E_{RT,,Lab}$	77							
		$E_{NDT} = 4.0 \times E_{RT,,Lab}$	104							
MnROAD	Clyne, et al., 2004	$E_{NDT} < E^*$ [3]	30 < MDT < 100 [5]	N/A	N/A	17.9	EVERCALC	4	12	None
Virginia Tech Transport-ation Institute	Loulizi, et al., 2007	$E_{Witczak} \approx E^*$ [4]	10 to 130	0.1 to 25	N/A	N/A	N/A	NR	NR	[9]
		$E_{NDT} < E_{Witczak}$	NR	N/A	N/A	5.3	ELMOD			None
Kansas State University	Gedafa, et al., 2010	$E_{NDT} = 1.14 \times E_{Witczak}$	39	N/A	N/A	25 (used to compare methods) 33 to 40 (stated theoretical value)	EVERCALC (MODULUS and MODCOMP also used but not summarized here)	9 to 13	0 to 11	[10]
		$E_{Witczak} = 1.36 \times E^*$		0.1 to 25						
		$E_{NDT} = 1.52 \times E^*$		N/A						
		$E_{NDT} = 0.69 \times E_{Witczak}$	70	N/A						
		$E_{Witczak} = 0.94 \times E^*$		0.1 to 25						
		$E_{NDT} = 0.63 \times E^*$		N/A						
		$E_{NDT} = 0.84 \times E_{Witczak}$	95	N/A						
		$E_{Witczak} = 0.95 \times E^*$		0.1 to 25						
		$E_{NDT} = 0.77 \times E^*$		N/A						
CEDEX	Mateos, et al., 2012	$E_{NDT} \approx E^*$	40 < MDT < 95	N/A	N/A	15	EVERCALC	5 to 6	18 to 32	None
Applied Research Associates, Inc. (ARA)	Ayyala, et al., 2017	$E_{NDT} = 1.0 \times E^*$	MDT < 40	N/A	E* > 1000	30	EVERCALC, MODCOMP	NR (Wide range of LTPP sections)		[11]
		$E_{NDT} = 1.3 \times E^*$	60 < MDT <70	N/A	600 < E* < 800					
		$E_{NDT} = 1.6 \times E^*$	MDT > 90	N/A	E* < 500					

[1] E_{NDT} = Backcalculated stiffness, [2] $E_{RT,Lab}$ = Resilient modulus from laboratory test., [3] E* = Dynamic modulus measured in the laboratory. [4] $E_{Witczak}$ = Dynamic modulus estimated using the Witczak equation. [5] MDT = Mid-depth asphalt temperature. [6] N/A = Not applicable. [7] NR = Not reported. [8] Resilient modulus testing was performed in indirect tension. [9] The difference between $E_{Witczak}$ and E* is smallest at high temperatures and increases as temperature decreases. [10] The BELLS3 model was used to estimate asphalt temperature (Lukanen et al. 2000). Backcalculated asphalt concrete stiffness was adjusted for temperature using a previously-developed empirical relationship (Chen et al. 2000). Binder aging models were used in the calculation of $E_{Witczak}$ (Mirza 1993). [11] E* was determined using dynamic modulus data from the LTPP computed parameters tables. Dynamic modulus data in these tables was derived from the results of several different laboratory test procedures, such as resilient modulus testing, using numerical methods (Kim et al. 2011).

Finally, a draft report from the ongoing research project "FHWA-PROJ-14-0126: Characterizing Existing Hot-Mix Asphalt Layer Damage for Mechanistic-Empirical Pavement Design" used LTPP data to compare backcalculated asphalt concrete stiffness to lab-measured dynamic moduli (Ayyala et al. 2016). A FWD load frequency of 30 Hz was assumed based on the load duration of a Dynatest FWD. It was determined that the backcalculated stiffness is roughly equivalent to the dynamic modulus at low temperatures, but that the backcalculated stiffness is greater than the dynamic modulus at high temperatures. Some of the difference between backcalculated stiffness and dynamic modulus were believed to be caused by aging. Adjustment factors for the Pavement ME backcalculated stiffness input (E_{NDT}), were developed (Ayyala et al. 2016). These can be seen in Table 2.

Several notable trends were seen throughout the literature. First, the majority of studies concluded that the stiffness determined using backcalculation is different from the stiffness determined using either laboratory dynamic modulus testing or predictive equations. There is,

however, no general agreement between authors on the exact relationship between methods. Ayyala, et al. and Von Quintus and Killingsworth both conclude that E_{NDT} is greater than stiffness determined by laboratory testing (E* or $E_{RT,Lab}$), while Clyne et al. and Gedafa, et al. make the opposite conclusion (Ayyala et al. 2016; Clyne et al. 2004; Gedafa et al. 2010; Von Quintus and Killingsworth 1998). Second, half of the studies examined conclude that the relationship between methods changes with the temperature of the asphalt concrete. Ayyala et al. and Von Quintus and Killingsworth determined that E_{NDT} increases relative to stiffness measured in the laboratory as temperature increases (Ayyala et al. 2016; Von Quintus and Killingsworth 1998). Results from Gedafa et al. contradicts this showing that E_{NDT} decreases relative to both $E_{Witczak}$ and E* as temperature increases. Finally, it appears that E* and E_{itczak} are very similar. Both Loulizi et al. and Gedafa, et al. concluded that $E_{Witczak}$ and E* are roughly equivalent at high temperatures, but that $E_{Witczak}$ is greater than E* at low temperatures (Gedafa et al. 2010; Loulizi et al. 2008).

3.0 EVALUATION OF THE PAVEMENT ME AC/AC OVERLAY DESIGN PROCEDURE

In order to develop appropriate inputs for the Pavement ME AC/AC overlay design procedure it was first necessary to fully understand and evaluate this procedure. This chapter includes a detailed description of the AC/AC overlay design procedure, an evaluation of the procedure using observed pavement performance data, and a sensitivity analysis. Adjustment factors for the backcalculated asphalt concrete stiffness input used in the overlay design procedure are also evaluated. The purpose of these adjustment factors, which were found in the existing literature, is to improve the accuracy of distress predictions made by the design procedure. Discussion of the design procedure is mostly limited to the components of the procedure that involve FWD testing.

The Pavement ME AC/AC overlay design procedure is a collection of mechanistic models and calibrated empirical relationships that predict the amount of distress that will occur in an asphalt concrete overlay placed on an existing asphalt concrete pavement. There are three levels of design inputs for the AC/AC overlay procedure. The models used to predict distress are the same for all input levels. However, the way that inputs are used to define the amount of fatigue damage in the asphalt concrete of the existing pavement is different for each input level. In Pavement ME, the amount fatigue damage in asphalt concrete is represented by a non-dimensional damage parameter. As the value of the damage parameter increases, the stiffness of the asphalt concrete decreases. A damage equation, Equation 8, is used to calculate the stiffness of the asphalt

concrete (the damaged stiffness) as a function of the damage parameter. The Level 1 inputs used to define the damage parameter are the backcalculated stiffness of the asphalt concrete (E_{NDT}), which represents the damaged stiffness of the material, and the stiffness of the asphalt concrete estimated using the Witczak equation ($E_{Witczak}$), which represents the undamaged stiffness of the material. The Level 2 inputs used to define the damage parameter are the quantity and severity of fatigue cracking observed in the existing AC pavement. The Level 3 inputs used to define the damage parameter are two separate pavement condition ratings of the existing AC pavement: the structural condition and the environmental condition. The structural condition is correlated to the amount of fatigue cracking in the existing pavement and the environmental condition is correlated to the amount of transverse cracking in the existing pavement. Both condition ratings have several levels: Excellent, good, fair, etc.

The AC/AC overlay design procedure predicts several different distresses: bottom-up fatigue cracking, top-down fatigue cracking, total rutting, asphalt-only rutting, transverse cracking, and IRI. Only bottom-up fatigue cracking and rutting were considered for the purposes of evaluating and analyzing the AC/AC design procedure, because these are the only distresses significantly affected by the amount of fatigue damage in the asphalt concrete of the existing pavement. Top-down cracking was not considered because the top-down cracking models currently used in Pavement ME will soon be replaced (ARA Inc. 2015b). A research project to revise these models is currently in progress (National Cooperative Highway Research Program (NCHRP) Project 1-52: A Mechanistic-Empirical Model for Top-Down Cracking of Hot-Mix Asphalt Layers).

The steps used to predict fatigue cracking in the AC/AC overlay design procedure are shown in Figure 4. First, the damaged stiffness of the asphalt concrete in the existing AC pavement is defined using FWD testing (Level 1), a distress survey (Level 2), or a pavement rating (Level 3). The stiffness of the asphalt concrete in the overlay is defined using either dynamic modulus testing (Level 1) or the Witczak equation (Level 2/3). Second, fatigue cracking in the overlay is predicted separately using two, parallel models. A fracture mechanics-based model is used to predict the percentage of the fatigue cracking in the asphalt concrete of the existing pavement that will reflect through the overlay. Additionally, an asphalt fatigue damage model is used to predict the amount of new fatigue cracking that develops in the overlaid pavement structure as a whole. Finally, the total amount of fatigue cracking in the overlaid pavement section is determined by summing up the fatigue cracking predicted by each model. Pavement ME reports the total amount of fatigue cracking in the overlaid pavement section as "AC total fatigue cracking: bottom up + reflective."

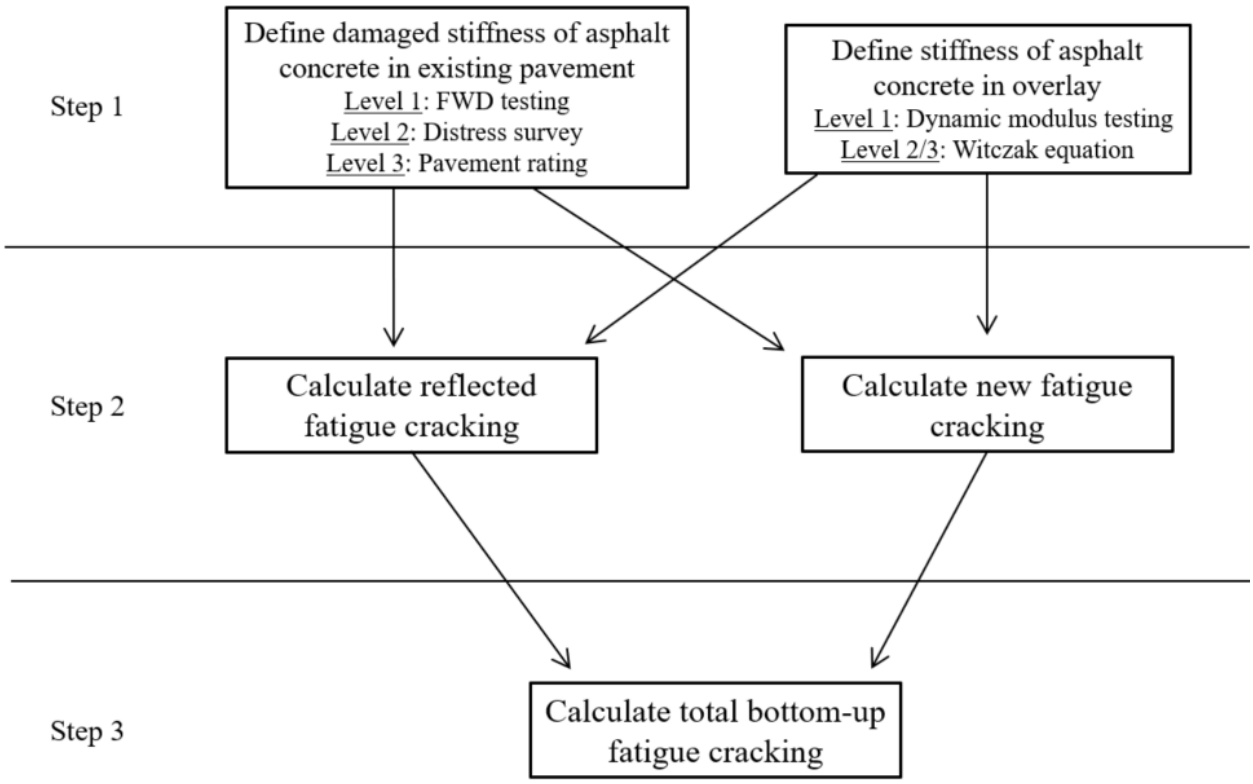

Figure 4. Fatigue cracking prediction in the AC/AC overlay design procedure.

The steps used to predict total rutting in the AC/AC overlay design procedure are shown in Figure 5. First, the damaged stiffness of the asphalt concrete in the existing pavement is defined using FWD testing (Level 1), a distress survey (Level 2), or a pavement rating (input Level 3). The amount of rutting in all the existing pavement layers, the stiffness of the existing unbound layers, and the stiffness of the asphalt concrete overlay are also defined. Rutting in the each of the existing layers is a direct program input. The amount of rutting in each existing pavement layers can be measured directly by trenching or can be estimated. There are several possible methods for determining the stiffness of the existing unbound layers. These include laboratory resilient modulus testing (Level 1), FWD testing and backcalculation (Level 2), dynamic cone penetrometer (DCP) testing (Level 2), California bearing ratio (CBR) testing (Level 2), and correlations based on soil classification (Level 3). The stiffness of the asphalt concrete in the overlay is defined using either dynamic modulus testing (Level 1) or the Witczak equation (Level 2/3). Second, the rutting in all asphalt layers (overlay and existing) is calculated using the asphalt rutting model. This model calculates the amount of plastic strain in the asphalt concrete as a function of resilient strain and total number of traffic loads. Simultaneously, the rutting in all unbound layers is calculated using the unbound layer rutting model. This model uses the same concept of plastic and resilient strain as the asphalt rutting model. Finally, the total rutting is calculated by adding the asphalt rutting and the unbound layer rutting.

A brief preliminary evaluation of the Pavement ME AC/AC overlay design procedure showed that the inputs used to define damage in the asphalt concrete of the existing pavement effect the magnitude of the predicted fatigue cracking and predicted rutting. A more comprehensive evaluation of the AC/AC overlay design procedure was conducted to further investigate this effect.

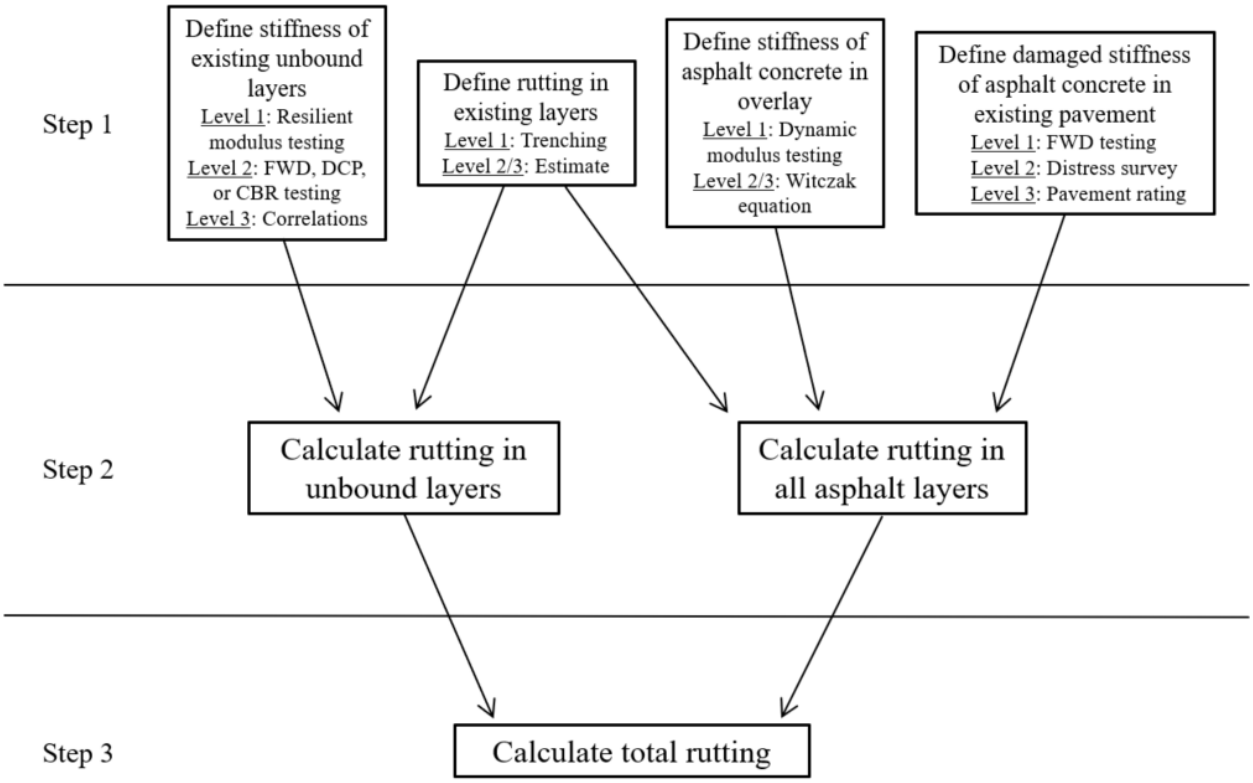

Figure 5. Rutting prediction in the AC/AC overlay design procedure.

Separate evaluations were conducted when using Level 1, Level 2, and Level 3 inputs. When Level 1 inputs are used, the Pavement ME AC/AC overlay design procedure is referred to as the AC/AC design procedure with Level 1 inputs. The same nomenclature is used for Level 2 and Level 3 inputs. The AC/AC procedure with Level 2 or Level 3 inputs does not require the use of FWD data, but it was still evaluated to determine if it can be used as an acceptable alternative to Level 1 inputs.

3.1 LEVEL 1 AC/AC OVERLAY DESIGN

3.1.1 Description

When the AC/AC overlay design procedure is used with Level 1 inputs, the amount of fatigue damage in the asphalt concrete of the existing pavement is quantified by comparing the backcalculated stiffness of this asphalt concrete to the stiffness of the asphalt concrete predicted using the Witczak equation. The backcalculated stiffness (E_{NDT}) represents the in-situ, damaged condition of the asphalt concrete. The predicted stiffness ($E_{Witczak}$) represents the theoretical, undamaged stiffness of the same material. E_{NDT} is determined by performing FWD testing in the outer wheelpath and by backcalculating the stiffness. In addition to E_{NDT}, the mid-depth temperature of the existing asphalt and the load frequency of the FWD are also required. Current recommendations by the developers of Pavement ME state that 30 Hz should be used as the load frequency of the FWD (Ayyala et al. 2016; Bruinsma et al. 2017; Rao and Von Quintus 2015). The input fields for E_{NDT}, asphalt temperature, and FWD load frequency are shown in Figure 6.

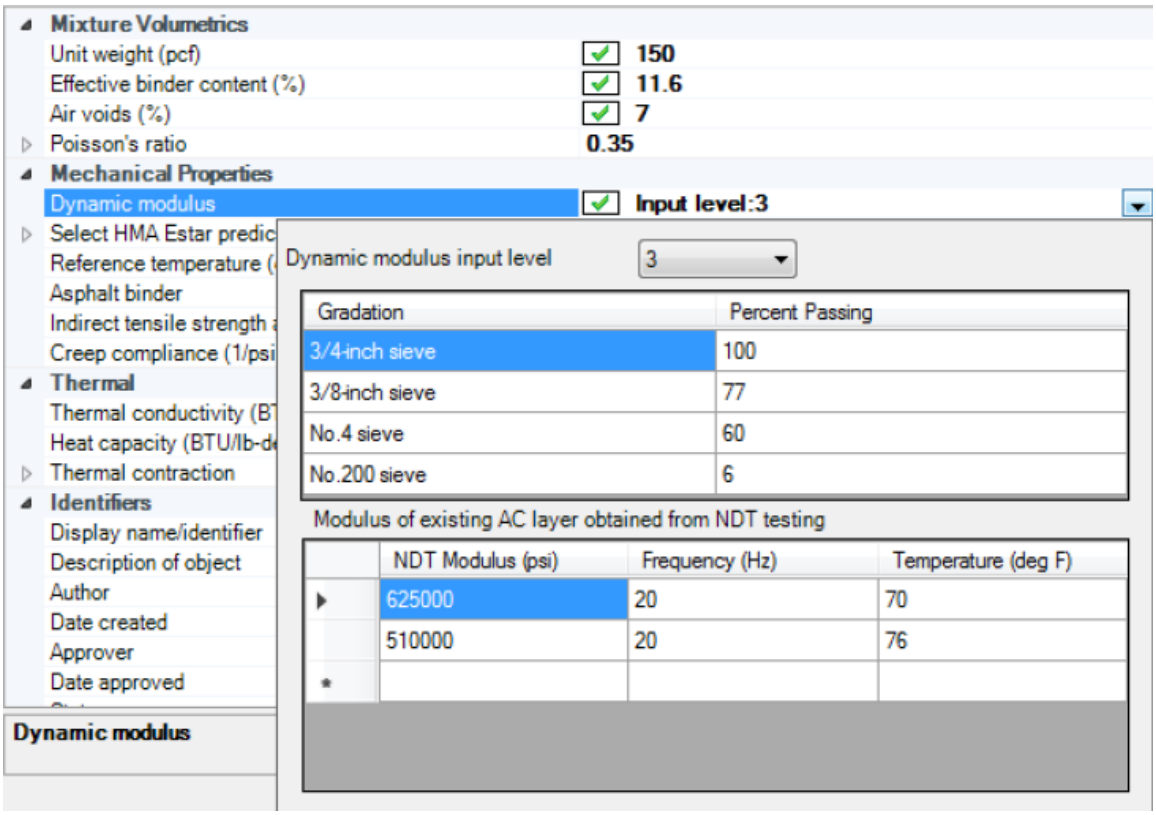

Figure 6. FWD testing input fields.

$E_{Witczak}$ is determined using the Witczak equation, shown in Equation 3 (Andrei et al. 1999). The mix volumetric parameters (air voids (V_a) and effective binder content (V_{be})) and the aggregate gradation ($P_{3/4}$, $P_{3/8}$, P_4, and P_{200}) in Equation 3 are determined by coring the existing asphalt and performing laboratory testing on the core. The load frequency is equal to the load frequency of the FWD. The binder viscosity is calculated in several steps. First, the binder grade of the existing asphalt is determined from lab testing or historical records. Second, the viscosity of the binder is calculated at the mid-depth temperature of the asphalt concrete at the time the FWD test is performed using the A-VTS relationship (Equation 4). The A and VTS parameters used in Equation 4 are selected based on the binder grade of the asphalt concrete in the existing pavement (ASTM International 1998). Typical values for A and VTS binder grades commonly found in

asphalt concrete of existing pavements are shown in Table 3 (ASTM International 1998). Third, the binder viscosity is adjusted for aging, using the binder aging models shown in Equations 5 through 7 (Mirza 1993). The input fields used to calculate $E_{Witczak}$ are shown in Figure 7.

$$\begin{aligned}&\log(E^*)\\&= 3.750063 + 0.029232P_{200} - 0.001767(P_{200})^2 - 0.002841P_4 - 0.058097V_a\\&- 0.802208\left[\frac{V_{be}}{V_{be}+V_a}\right]\\&+ \frac{3.871977 - 0.0021P_4 + 0.003958P_{3/8} - 0.000017\left(P_{3/8}\right)^2 + 0.005470P_{3/4}}{1+e^{(-0.603313-0.313351\log(f)-0.393532\log(\eta))}}\end{aligned} \quad (3)$$

Where:

E^* = Dynamic modulus (psi)

η = Asphalt binder viscosity (poise*10^6)

f = Loading frequency (Hz)

V_a = Air void content (%)

V_{be} = Volumetric effective binder content (%)

$P_{3/4}$ = Cumulative percent retained on the 3/4-in sieve (%)

$P_{3/8}$ = Cumulative percent retained on the 3/8-in sieve (%)

P_4 = Cumulative percent retained on the #4 sieve (%)

P_{200} = Percent passing the #200 sieve (%)

$$\log(log(\eta)) = A + VTS \times \log(T_R) \quad (4)$$

Where:

η = Binder viscosity (poise*10^{-2})

T_R = Binder temperature (Rankine)

A = Intercept of viscosity-temperature susceptibility regression

VTS = Slope of viscosity-temperature susceptibility regression

Table 3. Typical A and VTS values for binder grades commonly found in asphalt concrete in existing pavements.

Binder Grade	A[1]	VTS
PG 76-22	9.715	-3.208
PG 64-22	10.980	-3.680
PG 58-28	11.010	-3.701
AC-20	10.7709	-3.6017
AC-10	11.0134	-3.6954
Pen 85-100	11.8232	-3.621
Pen 120-150	11.8107	-4.0068

[1] The A and VTS values shown were defined using Rolling thin-film oven (RTFO)-aged binder. This represent the viscosity of asphalt binder at mixing/lay-down (ASTM International 1998).

$$\log\left(\log\left(\eta_{aged}\right)\right) = \frac{\log(\log(\eta_{t=0})) + A \times t}{1 + B \times t}$$

$$A = -0.004166 + 1.41213 \times C + C \times \log(MAAT) + D \times \log(\log(\eta_{t=0}))$$

$$B = 0.197725 + 0.068384 \times \log(C) \qquad (5)$$

$$C = 10^{(274.4946 + 193.831 \times \log(T_R) + 33.9366 \times log(T_R)^2}$$

$$D = -14.5521 + 10.47662 \times \log(T_R) - 1.88161 \times \log(T_R)^2$$

Where:

η_{aged} = Aged binder viscosity (Poise*10^{-2})

$\eta_{t=0}$ = Binder viscosity at mix/lay-down (Poise*10^{-2})

MAAT = Mean annual air temperature (ºF)

T = Time (months)

$$\log\left(\log\left(\eta'_{aged}\right)\right) = F_v \times \log(\log\left(\eta_{aged}\right))$$

$$F_v = \frac{1 + 1.0367 \times V_a \times t \times 10^{-4}}{1 + 6.1798 \times t \times 10^{-4}} \tag{6}$$

$$V_a = \frac{V_{a,orig} + 0.011 \times t - 2}{1 + 4.24 \times MAAT \times t \times 10^{-4} + 1.169 \times 10^{-3} \times (\frac{t}{\eta_{orig,77}})} + 2$$

Where:

η'_{aged} = Aged, adjusted binder viscosity (Poise*10^6)

η_{aged} = Aged binder viscosity (from Equation C-6-3) (Poise*10^6)

$\eta_{orig,77}$ = Original binder viscosity at 77°F (Poise*10^6)

$V_{a,orig}$ = Initial air voids (%)

V_a = Adjusted air voids (%)

$$\eta_{t,z} = \frac{\eta'_{aged}(4 + E) - E(\eta_{t=0})(1 - 4z)}{4(1 + Ez)} \tag{7}$$

$$E = 23.83e^{(-0.0308 \times MAAT)}$$

Where:

$\eta_{t,z}$ = Aged binder viscosity at time t and depth z (from Equation C-6-4) (Poise*10^6)

η'_{aged} = Aged, adjusted binder viscosity (from Equation C-6-4) (Poise*10^6)

$\eta_{t=0}$ = Binder viscosity at mix/lay-down (Poise*10^6)

z = Depth (in)

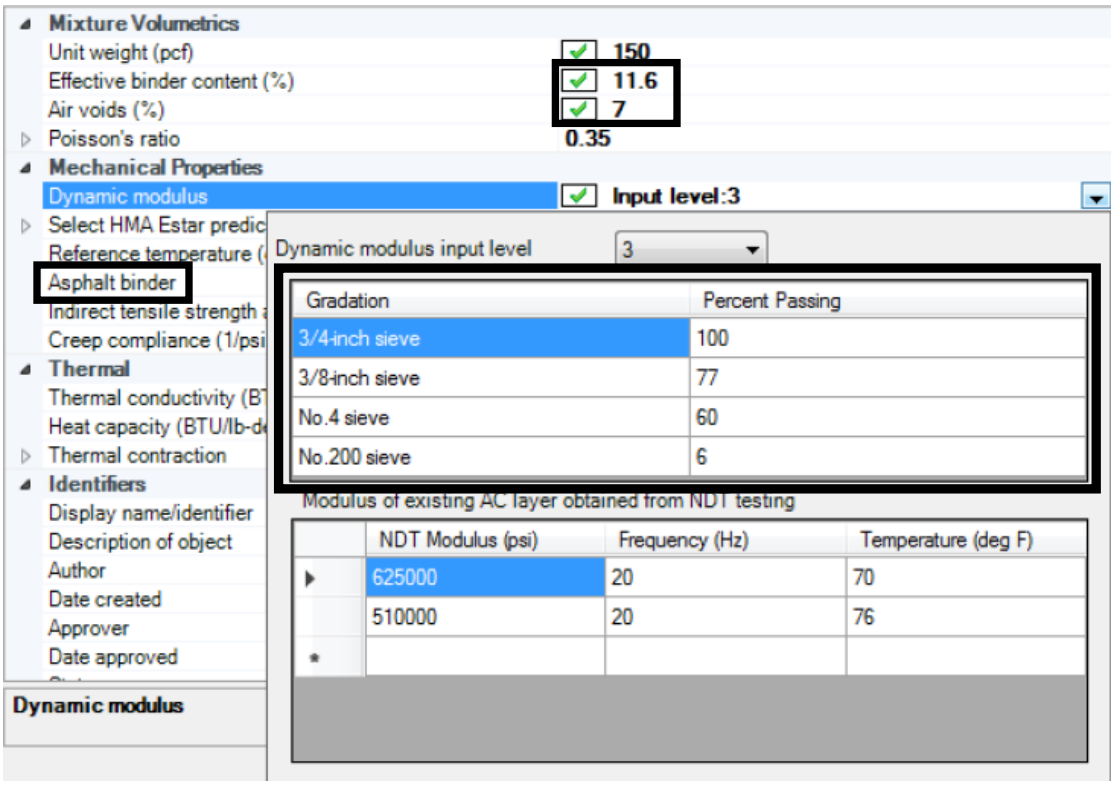

Figure 7. Witczak Equation input fields.

After E_{NDT} and $E_{Witczak}$ are determined, a damage parameter, which represents the damage in the existing asphalt, is calculated using Equation 8 (ARA Inc. 2004).

$$\log(d_{AC}) = 0.2 \times \left[\ln\left(\frac{E_{Witczak} - E_{NDT}}{E_{NDT} - 10^{\delta}}\right) + 0.3\right] \quad (8)$$

Where:

d_{AC} = Damage parameter

$E_{Witczak}$ = Existing asphalt stiffness predicted using the Witczak Equation (psi)

E_{NDT} = Backcalculated stiffness of the existing asphalt (psi)

δ = Base 10 logarithm of the minimum stiffness of the existing asphalt (estimated using the Witczak Equation, in psi)

Note: d_{AC} is defined as zero when E_{NDT} is greater than or equal to $E_{Witczak}$.

Once damage in the asphalt concrete of the existing pavement is quantified, a combination of mechanistic models and an empirical transfer function are used to predict the amount of distress that will occur in the overlaid pavement structure. The reflection of fatigue cracking in the existing pavement through the overlay and the formation of new fatigue cracking in the overlaid pavement structure are predicted separately. Reflection of cracking through the overlay is modeled in two steps. First, the damage parameter determined in Equation 8 is used in the bottom-up fatigue cracking transfer function, shown in Equation 9, to estimate the amount of the fatigue cracking in the existing pavement (ARA Inc. 2004). Note that the amount of fatigue cracking estimated in this way does not necessarily match the amount of fatigue cracking observed in the existing pavement. Rather, it represents the amount of fatigue damage in the asphalt concrete of the existing pavement, which, theoretically, includes cracking that has not yet reached the surface of the existing pavement. Second, a fracture mechanics-based reflective cracking model is used to calculate the percentage of fatigue cracking (estimated using the transfer function shown in Equation 9) that will propagate through the overlay and the time it takes for this to occur. The general form of the reflective cracking model is shown in Equation 10 (Lytton et al. 2010).

$$FC_{Bottom} = \left[\frac{1}{60}\right]\left[\frac{C_4}{1 + e^{(C_1 C_1^* + C_2 C_2^* \times \log(\log(d_{AC}) \times 100))}}\right]$$

$$C_1^* = -2 \times C_2^* \tag{9}$$

$$C_2^* = -2.40874 - 39.748(1 + h_{AC})^{-2.856}$$

Where:

FC_{Bottom} = Area of alligator cracking that initiates from the bottom of the asphalt layers (% total lane area)

d_{AC} = Damage parameter (from Equation C-6-6)

$C_1 = C_2 = 1$

$C_4 = 6000$

h_{AC} = Thickness of asphalt layers (in)

$$\frac{dc}{dN} = A \times (\Delta K)^n \tag{10}$$

Where:

C = Crack length

N = Number of loading cycles

A, n = Fracture properties of asphalt mixture

ΔK = Stress intensity factor amplitude (depends on the stress level, the geometry of the pavement structure, the fracture mode, and the crack length)

The reflective cracking model was developed under NCHRP 1-41, and was designed to predict propagation of a transverse crack through an asphalt overlay (Lytton et al. 2010). The traffic induced fatigue portion of the reflective cracking model is based on the stress caused by a wheel load traversing a single transverse crack in the perpendicular direction (Figure 8). The geometry of actual fatigue cracking is very different from that shown in Figure 8. It consists of multiple branching cracks that orient in different directions with respect to the wheel load.

Therefore, there are significant limitations in the use of the NCHRP 1-41 model to predict the reflection of fatigue cracking. Nevertheless, the NCHRP 1-41 reflective cracking model is currently the best available. It was calibrated to predict fatigue cracking and was implemented in Pavement ME Design Build 2.2, released in August, 2015 (ARA Inc. 2015a; Lytton and Von Quintus 2016).

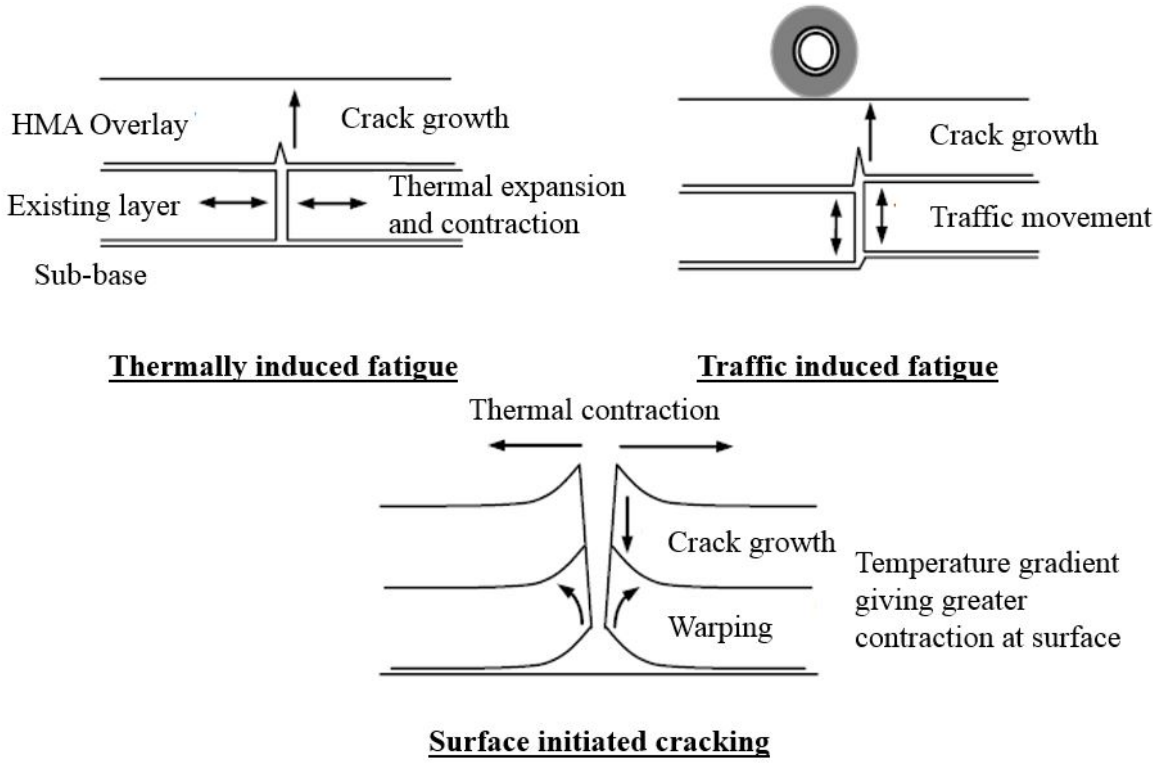

Figure 8. Geometries used to derive stress intensity factors in the NCHRP 1-41 reflective cracking model (Lytton et al. 2010).

The formation of new fatigue cracking in the asphalt concrete of the existing pavement and in the overlay is predicted using the Asphalt Institute fatigue damage model (ARA Inc. 2004). First, the damage parameter calculated in Equation 8 is used in the damaged asphalt stiffness

equation (Equation 11) to determine the damaged dynamic modulus (E*) master curve for the existing asphalt concrete. The effect of fatigue damage on the E* master curve is shown in Figure 9. Note that the damaged master curve is equal to the undamaged master curve when E_{NDT} is equal to $E_{Witczak}$ (ARA Inc. 2004). Next, the damaged master curve is used to determine the stiffness of the asphalt concrete in the existing pavement, which is a critical input for the fatigue damage model, specifically the portion of the model shown in Equation 12b. The fatigue damage model uses the stiffness of the asphalt concrete in the existing pavement, the stiffness of the asphalt concrete in the overlay, and several other inputs to estimate the amount of fatigue damage that accumulates in the overlaid pavement structure. This portion of the model is shown in Equation 12a. Finally, the damage index determined using the fatigue damage model is used in the bottom-up fatigue cracking transfer function, shown in Equation 9, to determine the amount of new fatigue cracking in both the asphalt concrete in the overlay and the asphalt concrete in the existing pavement. It is important to note that the damaged master curve, shown in Figure 9, is also used to estimate the stiffness of the asphalt concrete in the existing pavement for the reflective cracking model discussed previously.

$$E_{Witczak,damaged} = 10^{\delta} + \frac{E_{Witczak} - 10^{\delta}}{1 + e^{-0.3+5\times\log(d_{AC})}} \quad (11)$$

Where:

$E_{Witczak,damaged}$ = Damaged stiffness of existing asphalt (psi)

$E_{Witczak}$ = Predicted, undamaged stiffness of existing asphalt for a specific reduced time (combination of temperature and load frequency) (psi)

d_{AC} = Damage parameter (from Equation 8)

δ = Base 10 logarithm of the minimum stiffness of the existing asphalt (estimated using the Witczak Equation, in psi).

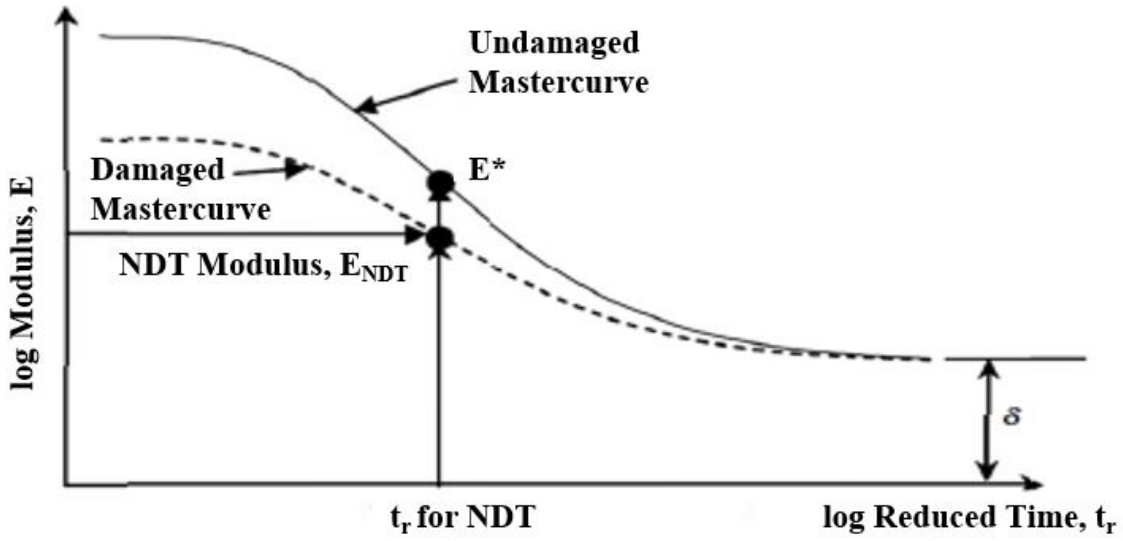

Figure 9. Method for determining the damaged master curve of the existing asphalt concrete (ARA Inc. 2004).

$$DI = \sum (\Delta DI)_{j,m,l,p,T} = \sum \left(\frac{n}{N_{f-HMA}} \right)_{j,m,l,p,T} \quad (12a)$$

Where:

n = Actual number of axle load applications in analysis time increment

j = Axle load interval

m = Axle load type (single, tandem, tridem, quad, or special axle configuration)

l = Truck type using the truck classification groups included in MEPDG

p = Month

T = Median temperature for the five temperature intervals used to subdivide each month (°F)

$N_{f\text{-}HMA}$ = Allowable number of axle load repetitions analysis time increment. A function of the AC dynamic modulus, the tensile strain at critical locations, the asphalt thickness, the asphalt content, and the air voids

$$N_{f-HMA} = k_{f1}(10^{M})(C_H)\beta_{f1}(\varepsilon_t)^{k_{f2}\beta_{f2}}(E_{HMA})^{k_{f3}\beta_{f3}} \quad (12b)$$

Where:

ε_t = Tensile strain at critical location. Calculated by the layered elastic analysis structural response model (JULEA) (in/in)

E_{HMA} = Dynamic modulus of the asphalt concrete (psi)

k_{f1}, k_{f2}, k_{f3} = Global field calibration parameters (from the NCHRP 1-40D re-calibration; k_{f1} = 0.007566, k_{f2} = -3.9492, and k_{f3} = -1.281)

β_{f1}, β_{f2}, β_{f3} = Field calibration constants. For the global calibration effort, these constants are set to 1.0

M = Mixture regression coefficient. Defined by the volumetric properties

$$M = 4.84\left(\frac{V_{be}}{V_a + V_{be}} - 0.69\right) \quad (12c)$$

Where:

V_{be} = Effective asphalt content by volume (%)

V_a = Percent air voids (%)

C_H = Thickness correction term

$$C_H = \frac{1}{0.000398 + \frac{0.003602}{1 + e^{(11.02 - 3.49H_{HMA})}}} \quad (12d)$$

Where:

H_{HMA} = Asphalt concrete thickness (in)

The fatigue damage model, shown in Equation 12, predicts new fatigue cracking initiating at the bottom of the overlay and new fatigue cracking initiating at the bottom of the asphalt concrete in the existing pavement separately. In the penultimate step of predicting fatigue

cracking, new cracking initiating in the existing pavement is input into the reflective cracking model to determine the amount that reaches the surface of the overlaid pavement structure.

When Level 1 inputs are used the total amount of fatigue cracking predicted by the AC/AC overlay design procedure is the sum of fatigue cracking in the existing pavement that is reflected through the overlay, new fatigue cracking that initiates at the bottom of the asphalt concrete in the existing pavement and is reflected through the overlay, and new fatigue cracking that initiates at the bottom of the asphalt in the overlay. This value is reported as "AC total fatigue cracking: bottom up + reflective." The calculation of "AC total fatigue cracking" is shown in Equation 13. A schematic representation of the total fatigue cracking calculation is shown in Figure 10. All the models and functions used to predict total fatigue cracking are summarized in Figure 11.

$$Total\ Cracking = RCR \times FC_{existing} + FC_{new,overlay} + RCR \times FC_{new,existing} \quad (13)$$

Where:

Total Cracking = "AC total fatigue cracking: bottom-up + reflective" (% total lane area)

RCR = Proportion of cracks reflected from underlying layer (0-1). Calculated by reflective cracking model

$FC_{existing}$ = Fatigue cracking in existing asphalt (% total lane area). Calculated from transfer function

$FC_{new,overlay}$ = New fatigue cracking in overlay (% total lane area).

$FC_{new,existing}$ = New fatigue cracking in existing asphalt (% total lane area)

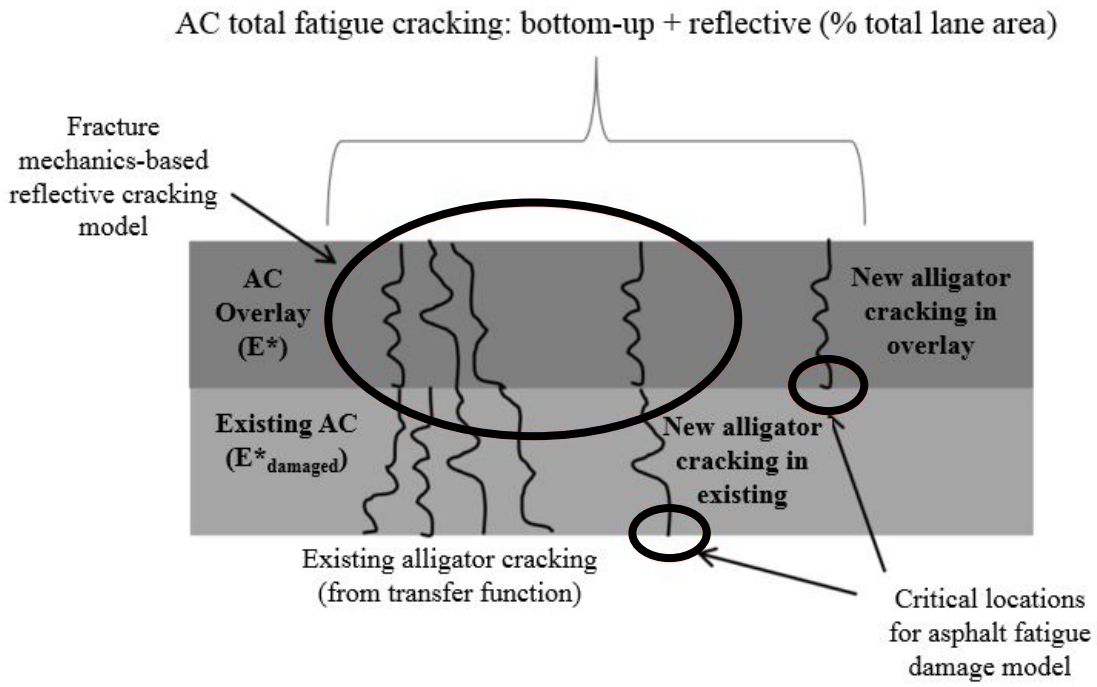

Figure 10. Calculation of total fatigue cracking.

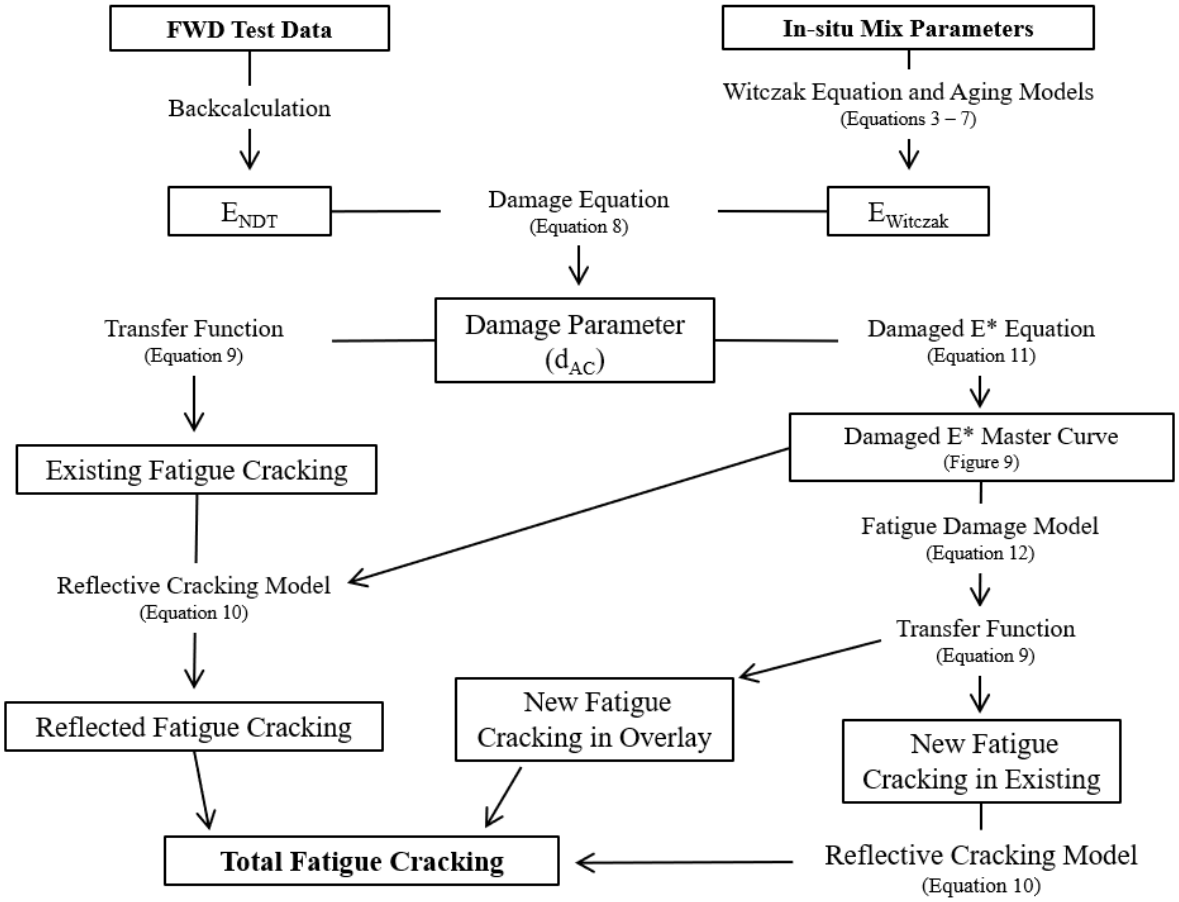

Figure 11. Prediction of total fatigue cracking in the Pavement ME AC/AC overlay design procedure with Level 1 inputs.

Total rutting predicted by the AC/AC overlay design procedure is the sum of the rutting predicted in the asphalt concrete and rutting predicted in the unbound layers, which are determined separately. Only the asphalt rutting is significantly affected by damage in the asphalt concrete of the existing pavement. The damage parameter, calculated using Equation 8, is used in the damaged asphalt stiffness equation, shown in Equation 11, to determine the damaged E* master curve for the existing asphalt concrete. The damaged E* master curve for the asphalt concrete in the existing pavement, the E* master curve for the overlay, and the rutting in the existing asphalt are then used

in the asphalt rutting model, shown in Equation 14, to predict the combined rutting in all of the asphalt concrete layers of the overlaid pavement structure (ARA Inc. 2004). The models and functions used to predict asphalt rutting are summarized in Figure 12.

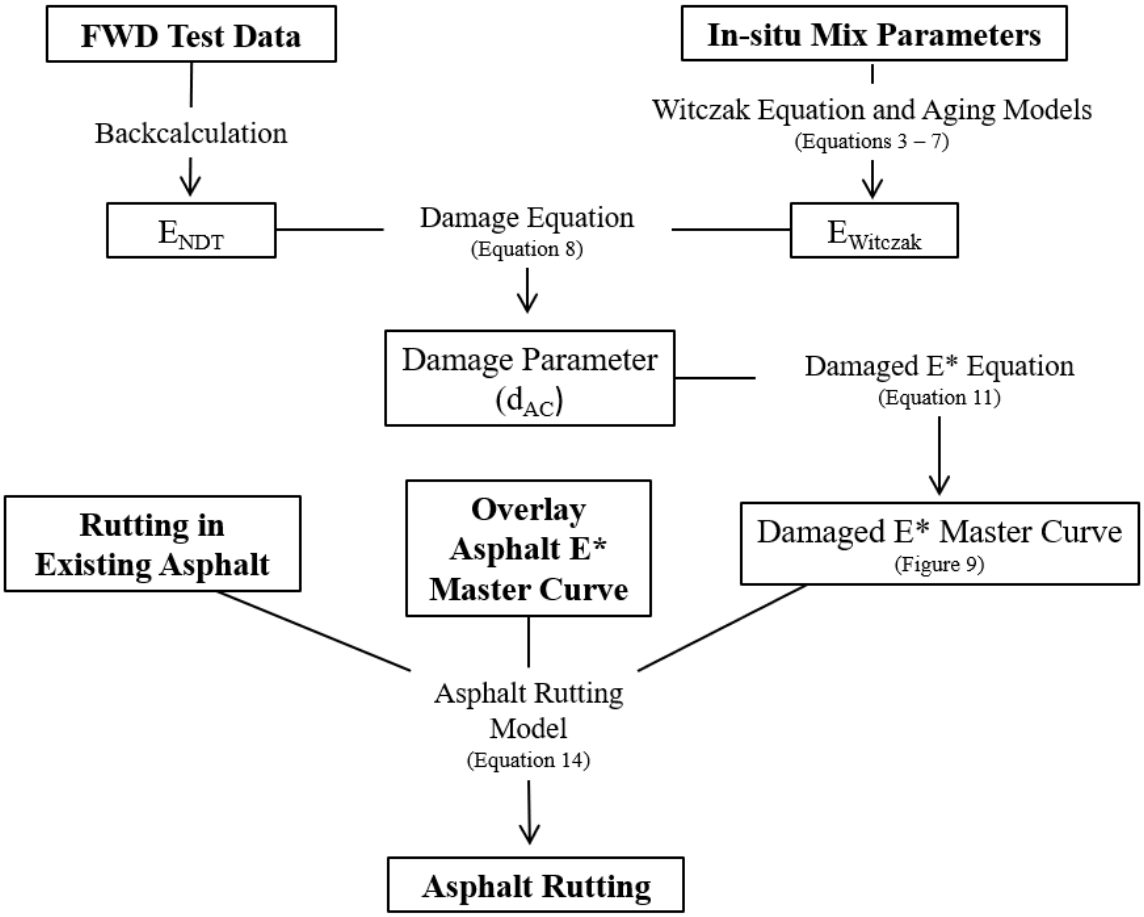

Figure 12. Prediction of total rutting in the Pavement ME AC/AC overlay design procedure with Level 1 inputs.

$$\frac{\varepsilon_p}{\varepsilon_r} = k_1 \times 10^{-3.4488} \times T^{1.5606} \times N^{0.479244}$$

$$k_1 = (C_1 + C_2 \times depth) \times 0.328196^{depth} \quad (14)$$

$$C_1 = -0.1039 \times h_{AC}^2 + 2.4868 \times h_{AC} - 17.342$$

$$C_2 = 0.0172 \times h_{AC}^2 - 1.7331 \times h_{AC} + 27.428$$

Where:

ε_p = Accumulated plastic strain at N repetitions of load (in/in)

ε_r = Resilient strain of the asphalt material as a function of mix properties, temperatures, and time rate of loading (in/in)

N = Number of load repetitions

T = Temperature (^{o}F)

h_{ac} = Total thickness of all asphalt layers (in)

depth = depth to computational point (in)

The current version of the AC/AC overlay design procedure with Level 1 inputs represents a recent major change to the procedure. This change was fully implemented in Pavement ME Version 2.2 in August, 2015 (ARA Inc. 2015a). The original Pavement ME AC/AC overlay design procedure used an empirical model to estimate that amount of fatigue cracking that reflects from the existing pavement through the overlay rather than the current reflective cracking model. The original empirical model was developed using "engineering judgement and a limited amount of published data from Georgia" (ARA Inc. 2004). Additionally, it is unclear if the equation used to calculate the damage parameter (Equation 8), and method used to determine the damaged master curve (Equation 11 and Figure 9), have never been validated using field data (Von Quintus 2017). A Federal Highway Administration (FHWA)-funded study is currently being conducted by Applied Research Associates (ARA) to evaluate and calibrate the methods used in Pavement ME

to determine the amount of fatigue damage in the asphalt concrete of the existing pavement (FHWA Project FHWA-PROJ-14-0126: Characterizing Existing Hot-Mix Asphalt Layer Damage for Mechanistic-Empirical Pavement Design).

3.1.2 Evaluation

LTPP data was used to evaluate whether distress predictions made using the AC/AC overlay design procedure with Level 1 inputs are reasonable and accurate. The Pavement ME AC/AC overlay design procedure was used to predict the performance of 35 LTPP test sections with AC/AC overlays. The predicted distress was compared to observed distress over time for each section. If the predicted and observed performance histories have the same overall shape, then the distress prediction was considered reasonable. A prediction was considered accurate if, in addition to being the same shape, the predicted and observed distress histories have the same critical values (the points at which the rate of distress development changes) and the same maximum values. All comparisons between predicted and observed distress were made at a reliability level of 50%.

The LTPP sections used in the evaluation were chosen to represent a range of damage, from 0% to more than 50% fatigue cracking by total lane area, in the asphalt concrete layer of both the existing pavement structure and the overlaid pavement structure. Sections with no significant distress in both the existing pavement or the overlaid pavement section were excluded. Additionally, all sections analyzed are in wet-freeze climates and/or have asphalt binders similar to those typically used in Pennsylvania. The LTPP sections used to evaluate the Level 1 procedure are summarized in Table 4.

Table 4. LTPP sections used to evaluate the AC/AC overlay design procedure with Level 1 inputs.

State	LTPP ID	AC Thickness (Pre-milling) (in)	AC Thickness (Post-milling) (in)	Overlay Thickness (in)	Binder Grade	E_{NDT} (ksi)	MDT (°F) [1]
CT	9-1803	7	7	1.75	PG 64-28 / AC-20	1096	70
DE	10-0102	4.25	4.25	1.25	AC-20 / AC-20	433	73
IL	17-A310	11.25	11.25	0.5	AC-20 / AC-20	821	61
IA	19-1044	16.25	16.25	3.75	PG 58-28 / Pen 85-100	424	42
KS	20-0159	11.25	6	5.25	PG 64-22 / AC-10	211	90
KS	20-1005	13	12	0.75	PG 64 -22 / AC-5	545	51
KS	20-1009	11	4.5	7.5	AC-20 / AC-20	1138	59
ME	23-1009	5.75	5.75	2.75	AC-20 / Pen 85-100	911	71
MD	24-1634	3.5	3.5	3.25	PG 70-22 / Pen 85-100	987	64
NJ	34-0503	9.25	9.25	4.75	Pen 85-100 / Pen 85-100	1309	51
NJ	34-0504	8.75	8.75	4.75	Pen 85-100 / Pen 85-100	1116	63
NJ	34-0505	9	9	1.75	Pen 85-100 / Pen 85-100	1575	50
NJ	34-0506	9.5	7.5	4	Pen 85-100 / Pen 85-100	599	68
NJ	34-0507	8.25	6.25	7.5	Pen 85-100 / Pen 85-100	819	55
NJ	34-0508	8.75	6.75	7.5	Pen 85-100 / Pen 85-100	1298	58
NJ	34-0509	9.25	7.25	4.25	Pen 85-100 / Pen 85-100	960	65
NJ	34-0903	9	7.5	5.5	PG 64-22 / Pen 85-100	1068	53
NJ	34-0960	9.75	7.25	4.75	PG 64-22 / Pen 85-100	1242	54
NJ	34-0961	9.25	5.5	6.5	PG 64-22 / Pen 85-100	1148	44
NJ	34-0962	9	7.5	4.25	PG 64-22 / Pen 85-100	682	57
NJ	34-1003	7.5	5.5	2.25	AC-20 / AC-20	274	91
NJ	34-1011	9	6.5	4	AC-20 / Pen 85-100	331	89
NJ	34-1030	6	3	4.5	AC-20 / AC-20	313	93
NJ	34-1033	7.5	6.75	2	AC-20 / AC-20	1493	75

Table 4 (continued).

State	LTPP ID	AC Thickness (Pre-milling) (in)	AC Thickness (Post-milling) (in)	Overlay Thickness (in)	Binder Grade	E_{NDT} (ksi)	MDT (°F) [1]
PA	42-1597	6.5	5	6.25	PG 64-22 / AC 20	571	56
MB	83-0502	4.5	4.5	2.75	Pen 150-200 / Pen 150-200	450	98
MB	83-0503	4.75	4.75	5.25	Pen 150-200 / Pen 150-200	430	81
MB	83-0506	5.5	4	3	Pen 150-200 / Pen 150-200	431	73
MB	83-0507	4	3	6.75	Pen 150-200 / Pen 150-200	591	81
MB	83-0508	3.5	2.5	6.5	Pen 150-200 / Pen 150-200	750	106
MB	83-0509	5	4	3.5	Pen 150-200 / Pen 150-200	367	74
MB	83-6451	4	4	2.5	Pen 150-200 / Pen 150-200	593	97
ON	87-1622	5.5	3	4.5	PG 58-28 / Pen 85-100	1112	49
QB	89-1125	5.25	5.25	2	PG 58-28 / Pen 85-100	875	53
QB	89-1127	5	5	2.5	Pen 85-100 / Pen 150-200	709	65

[1] MDT = Mid-depth asphalt temperature at the time of the FWD test.

Information extracted from the LTPP database to be used in Pavement ME is summarized in Table 5. Default values were used for defining all other inputs. The most important Level 1 inputs for evaluating the AC/AC design procedure are the backcalculated stiffness of the existing asphalt concrete (E_{NDT}) and the mid-depth asphalt temperature (MDT) of the existing asphalt. E_{NDT} was established by calculating the mean of all backcalculated asphalt stiffness values for 9-kip drops in the last outer wheelpath FWD test pass performed before the section was overlaid. MDT was established by calculating the mean of all MDT measurements corresponding to the 9-kip drops used to calculate E_{NDT}. The AC/AC design procedure allows multiple E_{NDT} inputs to be entered for a single design, as shown in Figure 6, but only one value was used per section for the

initial evaluation. The effect of using multiple Level 1 E_{NDT} inputs is evaluated below. A FWD load frequency of 30 Hz was assumed for all sections. Global calibration factors were used for all analyses.

Table 5. Level 1 inputs determined from LTPP data.

		Material Properties					
General Info	Pavement Structure	Overlay Asphalt Layers	Existing Asphalt Layers	Unbound Layers	Climate	Traffic	Other Inputs
Overlay placement date	Overlay thickness	Witczak equation inputs from cores	Backcalculated stiffness of existing asphalt (E_{NDT})	Backcalculated stiffness of subbase and subgrade	Closest weather station(s)	AADTT	MDT of existing asphalt
Existing asphalt placement date	Existing asphalt thickness	Binder grade	Witczak equation inputs from cores	Engineering properties of subbase and subgrade		Truck class distribution	Rutting in existing asphalt
	Milled thickness		Binder grade			Overall AADTT growth rate	
	Unbound layer thickness						

The results of the evaluation showed that fatigue cracking performance histories predicted by the AC/AC overlay design procedure with Level 1 inputs have the same shape as observed performance histories, but the predicted performance histories are rarely accurate. Both the predicted cracking performance history and the observed cracking performance history are sigmoidal ("S"-shaped). This indicates that the design procedure is able to reasonably approximate the development of fatigue cracking in an actual pavement section. With regard to accuracy, the predicted performance history often begins to increase and reaches a maximum value much earlier than the observed performance history. An example of this is shown in Figure 13. For 89% of sections in the analysis, distress initiates earlier in the pavement life for predicted fatigue cracking

than for observed fatigue cracking. This is summarized in Figure 14. Additionally, for 49% of sections in the analysis, the predicted fatigue cracking performance history asymptotically approaches a fixed maximum value while the observed performance history curve does not. This might be attributed to the fact that LTPP test sections are rehabilitated or taken out of service when fatigue cracking reaches a threshold level. An example of this is shown in Figure 15.

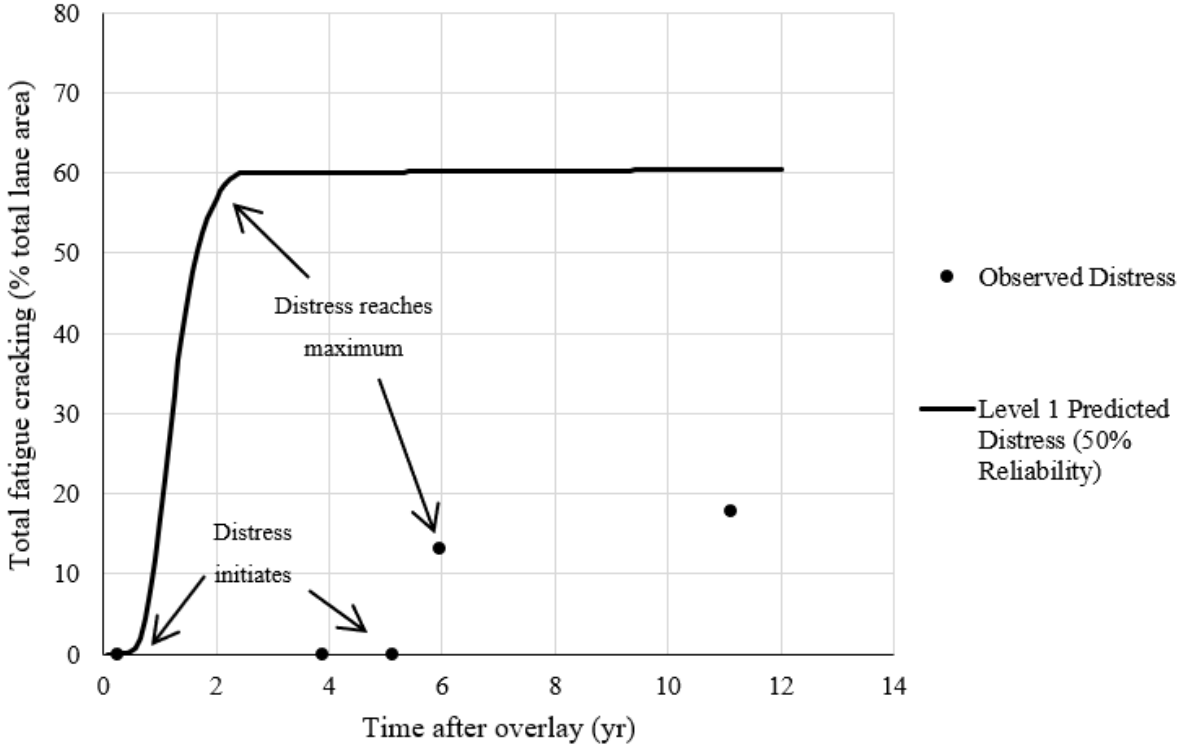

Figure 13. Comparison of predicted and observed fatigue cracking (LTPP Section 34-0962, New Jersey).

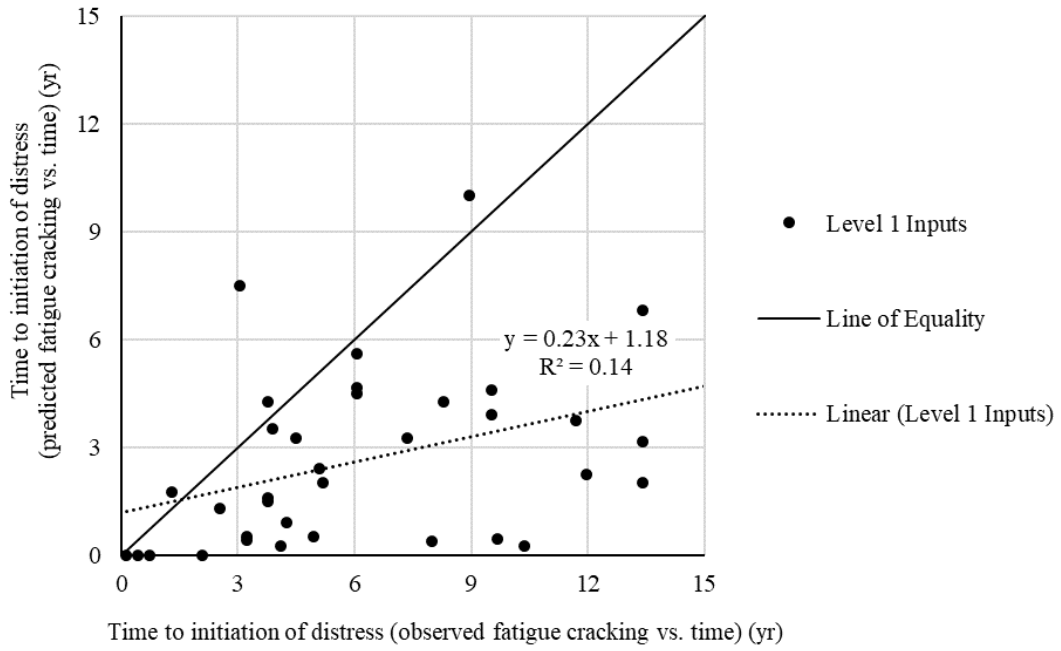

Figure 14. Time to initiation of distress for predicted and observed fatigue cracking.

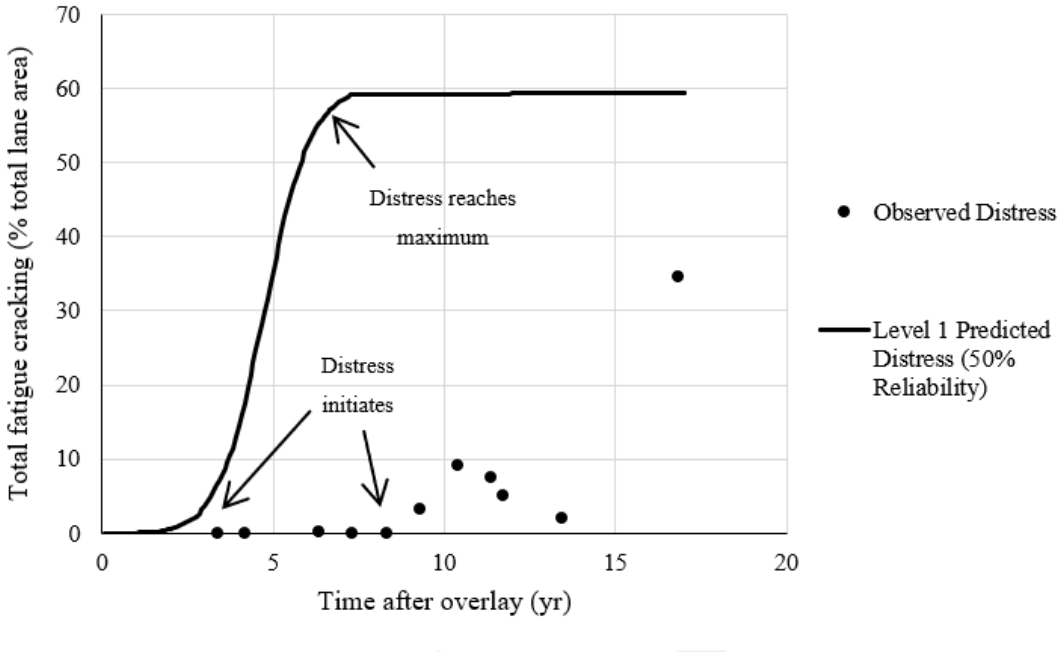

Figure 15. Comparison of predicted and observed fatigue cracking (LTPP Section 34-0503, New Jersey).

Finally, maximum predicted fatigue cracking is more than 10% greater than the maximum observed cracking for 68% of the sections evaluated. The maximum predicted cracking is more than 10% less than observed for 23% of sections evaluated. The predicted and observed fatigue cracking are within 10% of each other for 9% of sections evaluated. This is shown in Figures 16 and 17. Based on a paired t-test, maximum predicted fatigue cracking is greater than maximum observed fatigue cracking at a 95% confidence level (p-value = 0.00).

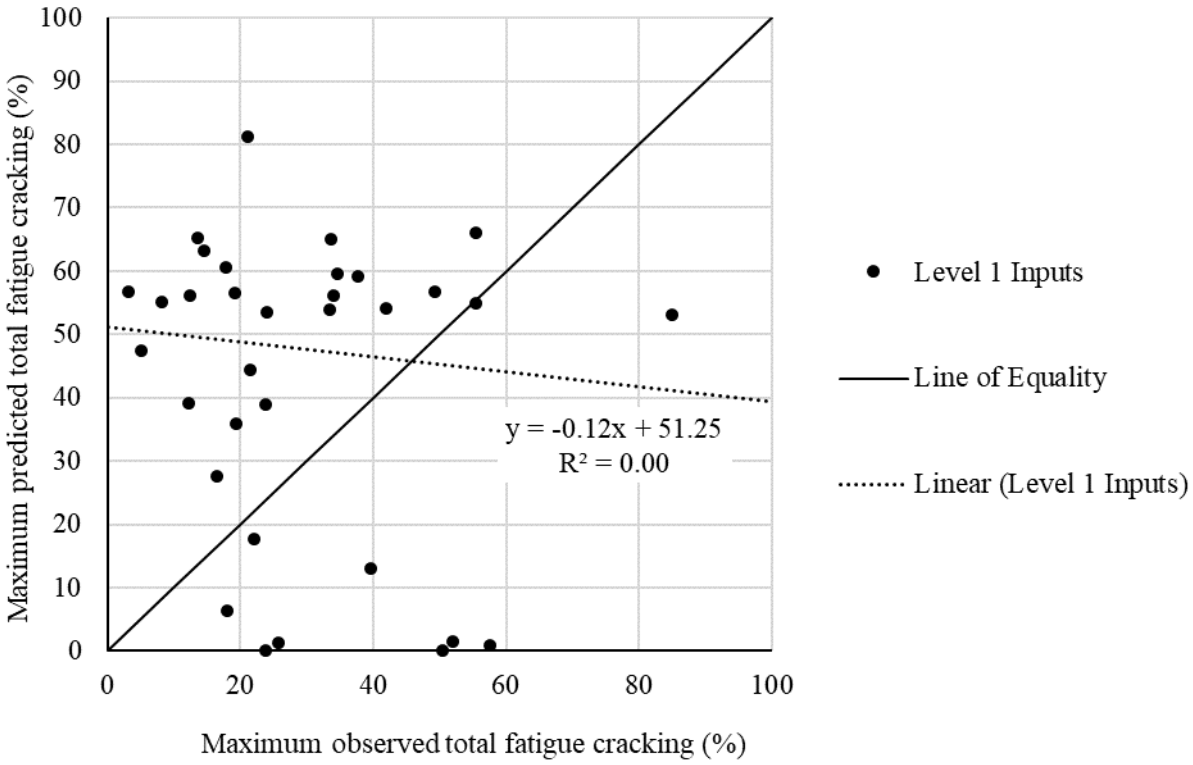

Figure 16. Predicted fatigue cracking vs. observed fatigue cracking (all sections and Level 1 inputs).

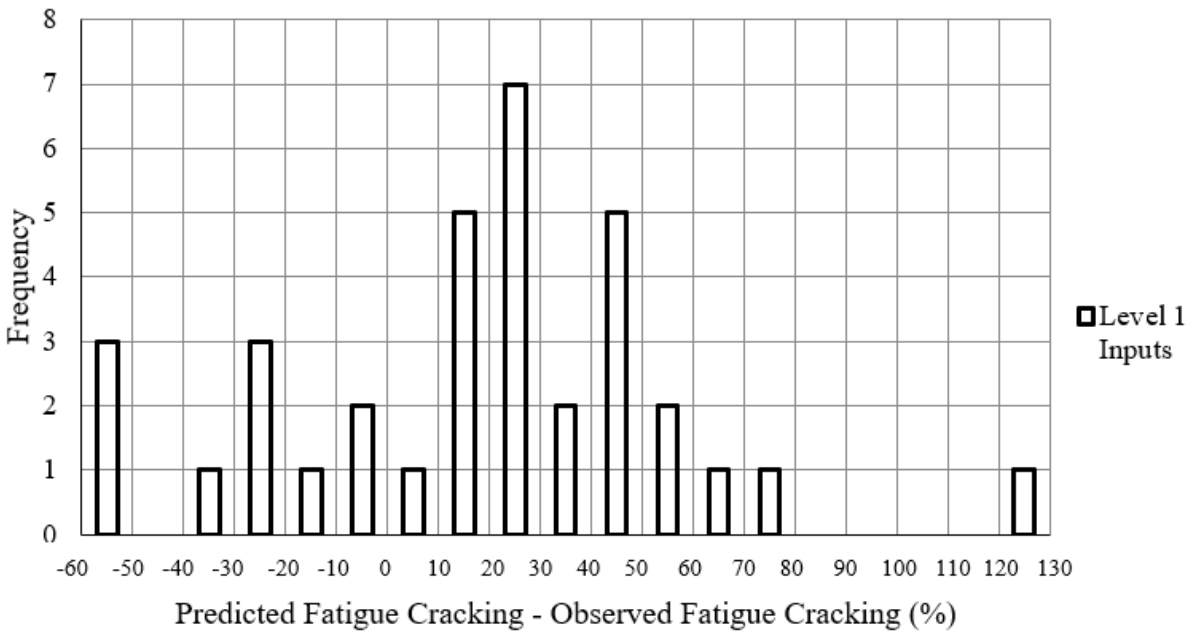

Figure 17. Difference between predicted and observed fatigue cracking (all sections and Level 1 inputs)

In addition to showing the difference between predicted and observed fatigue cracking, the evaluation showed that total rutting performance histories predicted by the AC/AC overlay design procedure with Level 1 inputs have the same shape as observed performance histories and are sometimes accurate. Total rutting is the amount of rutting measured at the pavement surface and is equal to the sum of rutting in all asphalt concrete and unbound layers. Rutting occurs in three phases: primary, secondary, and tertiary. Primary rutting is a rapid increase in permanent deformation that occurs near the beginning of the pavement life. Secondary rutting is a constant, gradual increase in permanent deformation that occurs over the majority of the pavement life. Tertiary rutting is another period of rapid permanent deformation that occurs at the end of the pavement life. Pavement ME only models primary and secondary rutting (ARA Inc. 2004). Both the predicted and observed total rutting performance histories show clear primary and secondary phases of rutting. An example of this is shown in Figure 18. This suggests that Pavement ME is

able to reasonably approximate how rutting develops in an actual pavement section. With regard to accuracy, the transition between primary and secondary rutting occurs at approximately the same time for predicted and observed rutting. This is shown in Figure 19. The difference between time to transition for predicted rutting and time to transition for observed rutting is not significantly different from 0 at a 95% confidence level (p-value = 0.43). Maximum predicted rutting is usually greater than the maximum observed rutting. This is shown in Figures 20 and 21. Based on a paired t-test, maximum predicted total rutting is greater than maximum observed total rutting at a 95% confidence level (p-value = 0.00).

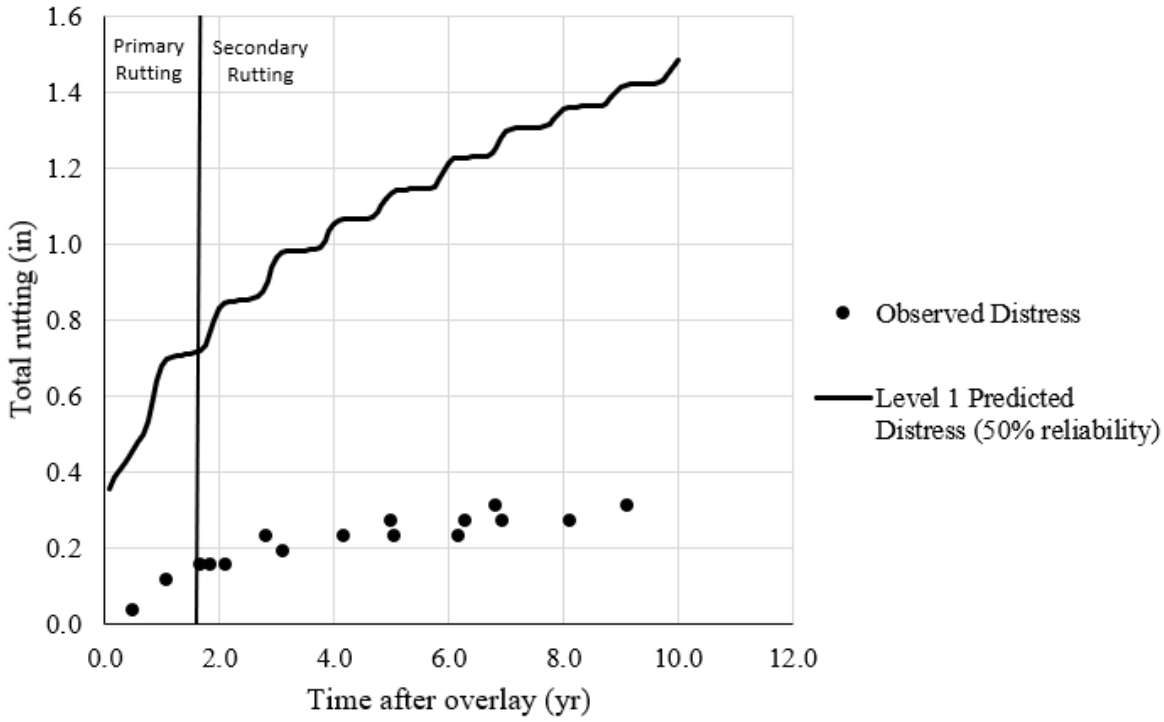

Figure 18. Comparison of predicted and observed total rutting (LTPP Section 10-0102, Delaware).

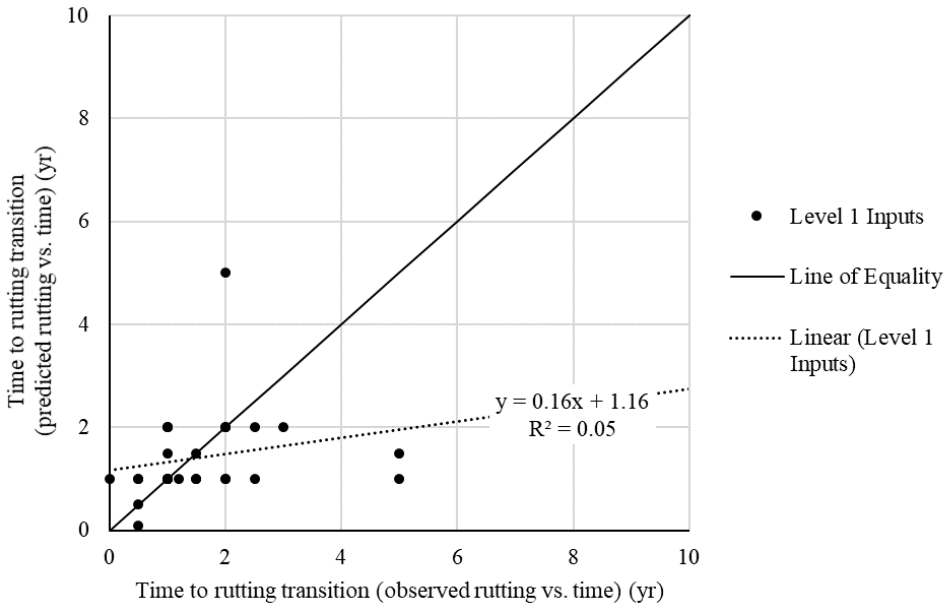

Figure 19. Predicted vs. observed transition between primary and secondary rutting (all sections and Level 1 inputs).

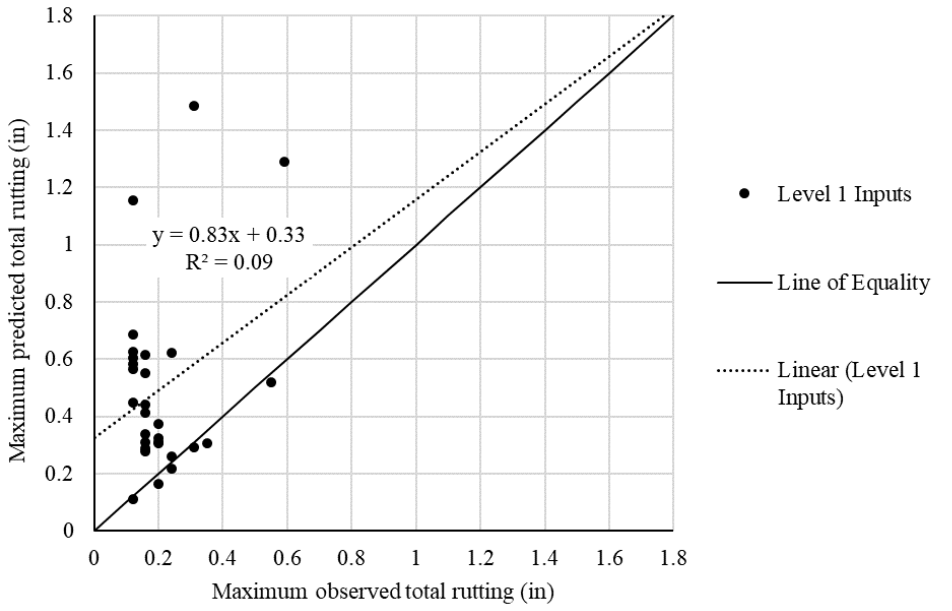

Figure 20. Predicted total rutting vs. observed total rutting (all sections and Level 1 inputs).

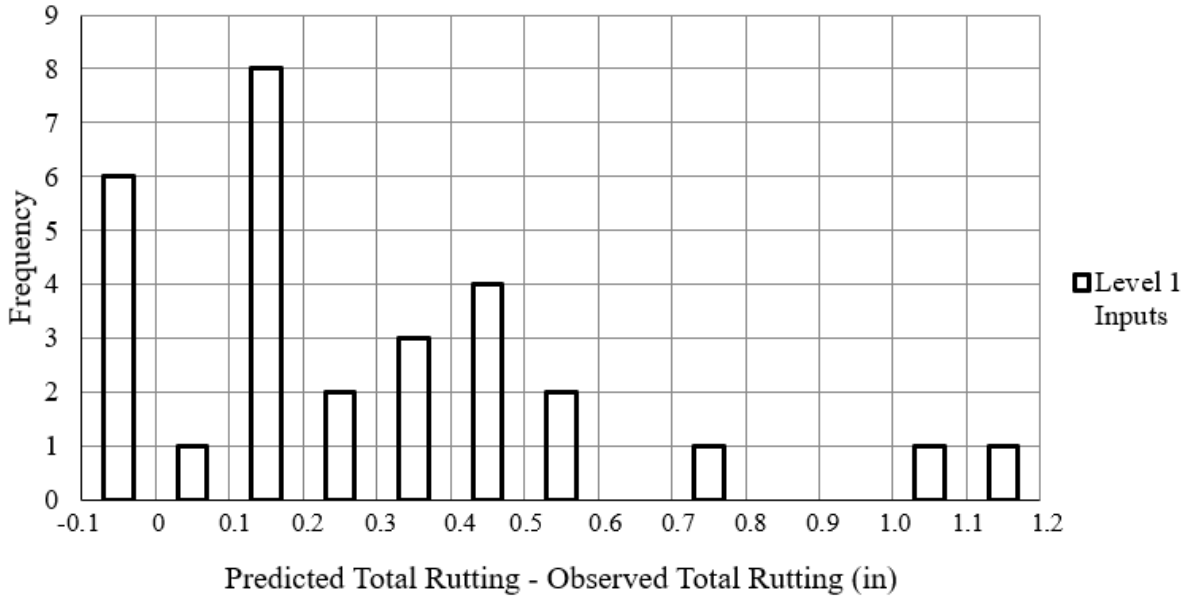

Figure 21. Difference between predicted and observed total rutting (all sections and Level 1 inputs)

The primary conclusion from evaluating the predicted performance using Level 1 inputs is that the predicted fatigue cracking and the predicted total rutting are both greater than the observed distress. The assumption that E_{NDT} is equal to $E_{Witczak}$ when there is no damage in the existing asphalt (see Equation 8) might be contributing to this difference between predicted and observed distress. An investigation of LTPP data showed this assumption is not valid, and that $E_{Witczak}$ is almost always greater than E_{NDT}. The two main reasons for this are:

1. The binder aging models used to calculate the $E_{Witczak}$ over-estimate the effect of binder aging on asphalt stiffness, especially at low temperatures.
2. For most pavements, the assumed 30 Hz load frequency used to calculate $E_{Witczak}$ is higher than the actually load frequency of the FWD.

The effect of the binder aging models on $E_{Witczak}$ is investigated further in Chapters 4 and 5. Additional discussion on the determination of FWD load frequency can be found in Chapter 4.

Because $E_{Witczak}$ tends to be greater than E_{NDT}, the damage parameter calculated in Equation 8 is almost never zero and the predicted distress is almost always greater than the actual distress observed. This problem can be further seen by using the AC/AC overlay design procedure with Level 1 inputs to design an overlay for a new, undamaged pavement. In this extreme case, one would expect minimal fatigue cracking in the first few years after the overlay, but, in fact, the predicted fatigue cracking increases rapidly at the beginning of the design life.

This problem is illustrated by simulating a mill and overlay of a newly constructed pavement in Pennsylvania on State Route 2001 (SR 2001). This pavement consists of 15 in of asphalt concrete over a 6-in granular base and backfill. It was constructed in 2015, and FWD testing was performed in 2016. The stiffness of the existing asphalt was backcalculated as 797 ksi at 74ºF. Traffic is very low, approximately 100 ADTT. The performance of a 1.5-in mill and overlay on this new section was estimated using the AC/AC design procedure with Level 1 inputs. Figure 22 shows the predicted fatigue cracking. It is entirely unrealistic that this pavement should have 20% fatigue cracking after 5 years, with a traffic level of only 100 ADTT.

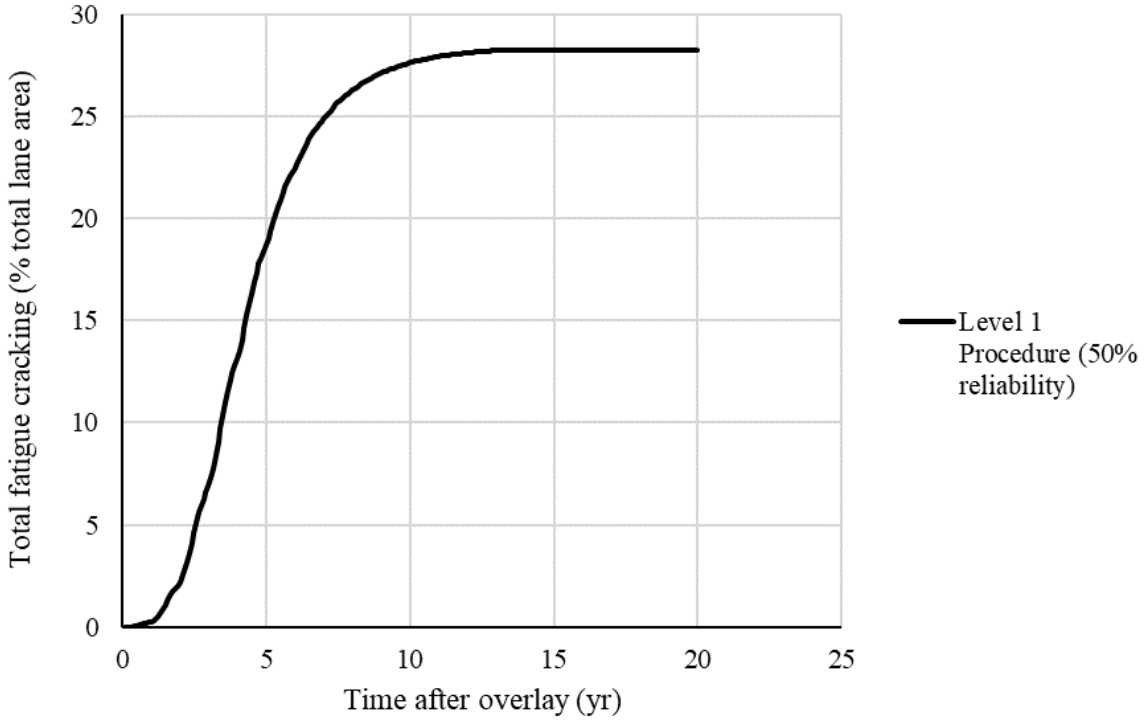

Figure 22. Level 1 performance prediction analysis of overlay placed on an undamaged pavement (PA State Route 2001).

3.1.3 Sensitivity

An analysis was conducted to determine the sensitivity of distress predicted using the AC/AC overlay design procedure to several Level 1 inputs. The inputs examined were the backcalculated stiffness of the asphalt concrete layer in the existing pavement (E_{NDT}) and the mixture parameters for the asphalt concrete in the existing pavement (volumetric air voids (V_a), volumetric effective binder content (V_{be}), and gradation ($P_{3/4}$, $P_{3/8}$, P_4, and P_{200})). All of these inputs affect the value of the damage parameter, calculated using Equation 8, which defines the stiffness of the asphalt

concrete in the existing pavement. Each input was varied one at a time. Interactions between inputs were not examined in this analysis.

Fatigue cracking predicted by the AC/AC overlay design procedure is very sensitive to the Level 1 E_{NDT} input. This was examined using LTPP Section 23-1009, which consists of a 2.7-in asphalt concrete overlay, 5.7 in of existing asphalt concrete, and a 5-in granular base on an A-4 subgrade. The measured E_{NDT} for this section is 911 ksi at a MDT of 71ºF. This input resulted in 39% predicted total fatigue cracking 11 years after being overlaid. Increasing E_{NDT} to 1200 ksi decreases the predicted total fatigue cracking from 39% to 18%. Increasing E_{NDT} further from 1200 ksi to 1250 ksi decreases the predicted total fatigue cracking from 18% to 7%. Finally, decreasing E_{NDT} from 1250 ksi to 1258 ksi, the value of $E_{Witczak}$ at 71ºF, decreases predicted total fatigue cracking from 7% to 0%. These changes are shown in Figure 23. Predicted total rutting is much less sensitive to E_{NDT} than predicted fatigue cracking, as shown in Figure 24. Increasing E_{NDT} from the measured value of 911 ksi to 1200 ksi decreases predicted total rutting by only 0.02 in after 11 years. Increasing E_{NDT} further to 1258 ksi does not decrease predicted total rutting. The sensitivity of both fatigue cracking rutting to E_{NDT} is problematic because the backcalculation process provides an estimate and not an exact measurement of the stiffness of the asphalt concrete in the existing pavement. Significant variability between the actual stiffness of the asphalt concrete and the E_{NDT} can occur even when an average of the E_{NDT} throughout the section is used. The results of backcalculation can be affected by differences between the assumed and actual layer thickness, the initial seed values used, and how layers are combined or sub divided into similar layers. These three factors all contribute to the variability in defining E_{NDT}.

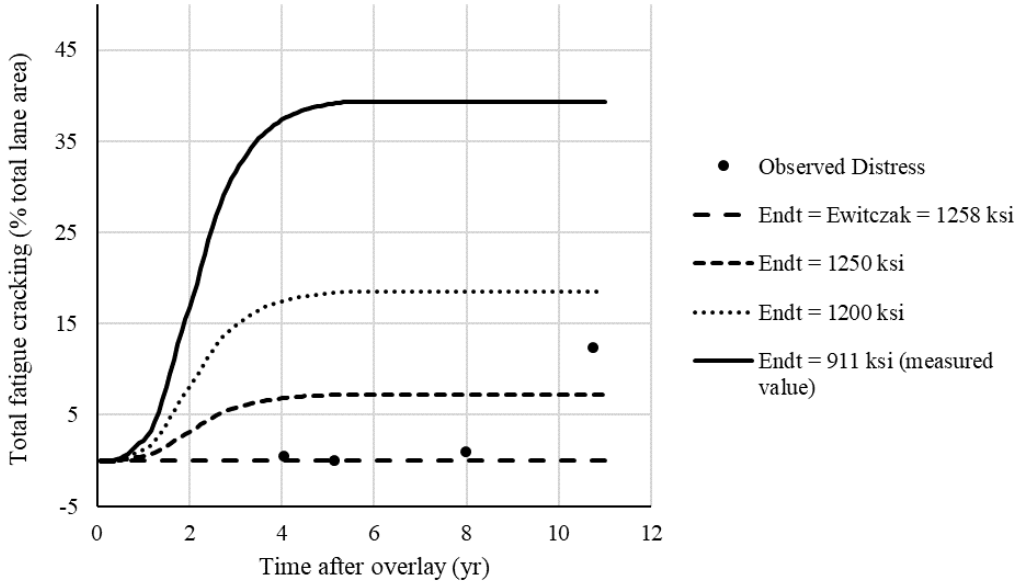

Figure 23. Sensitivity of predicted total fatigue cracking to the E_{NDT} (LTPP Section 23-1009, Maine).

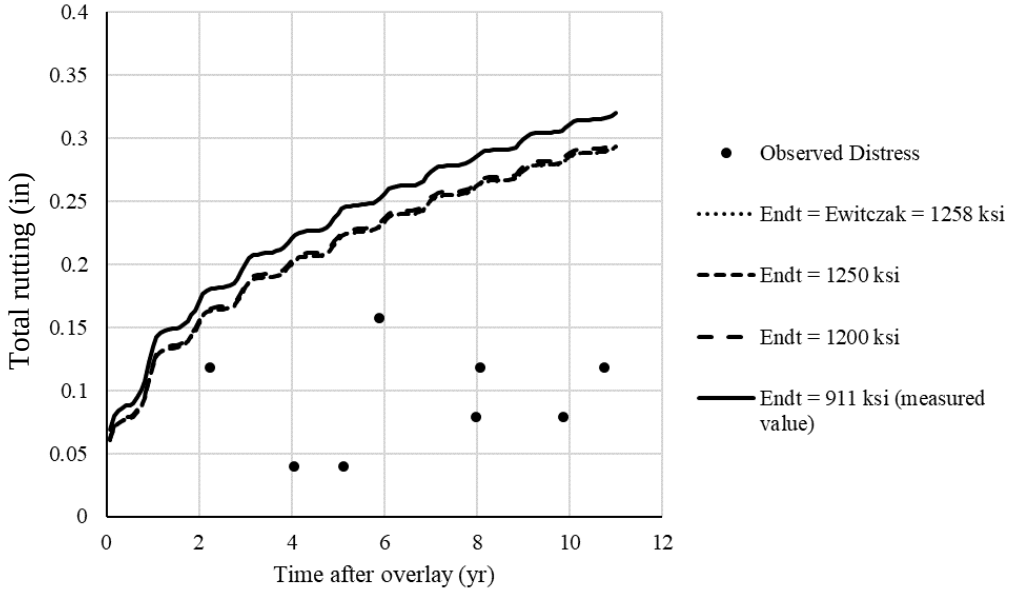

Figure 24. Sensitivity of predicted total rutting to the E_{NDT} (LTPP Section 23-1009, Maine).

Sensitivity to the individual inputs that define $E_{Witczak}$ were also examined. The inputs for V_a, V_{be}, $P_{3/4}$, $P_{3/8}$, P_4, and P_{200} were varied one at a time for both the asphalt concrete in the existing pavement. Section ME 1009 was used for this analysis. Figures 25, 26, and 27 show that predicted fatigue cracking is sensitive to V_a, V_{be}, and the gradation of the asphalt concrete in the existing pavement, respectively. Figures 28, 29, and 30 show that predicted rutting is not very sensitive to V_a, V_{be}, or the gradation of the existing asphalt mixture, respectively. It is important to note that changing the mixture characteristics for the asphalt concrete in the existing pavement can increase or decrease the maximum predicted distress, but it does not change the time at which cracking initiates or reaches a maximum value. A similar sensitivity analysis was conducted using the mixture characteristics of the overlay asphalt concrete. Results of this analysis showed that fatigue cracking and rutting predicted by the AC/AC overlay design procedure with Level 1 inputs are both insensitive to V_a, V_{be}, and gradation of the asphalt concrete mixture used for the overlay.

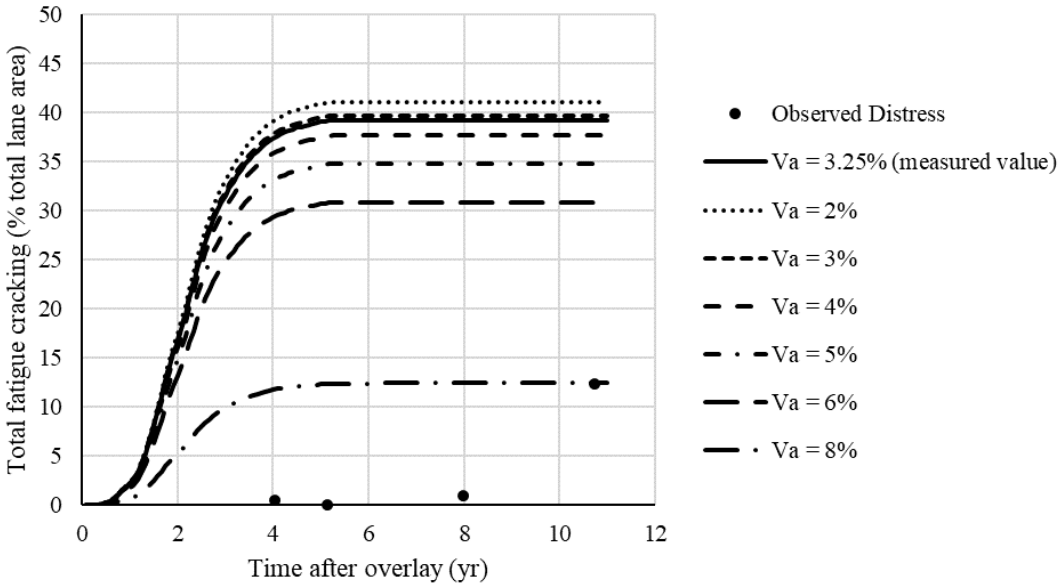

Figure 25. Sensitivity of predicted total fatigue cracking to volumetric air voids content (V_a) of the asphalt concrete in the existing pavement (LTPP Section 23-1009, Maine, E_{NDT} = 911 ksi, MDT = 71°F).

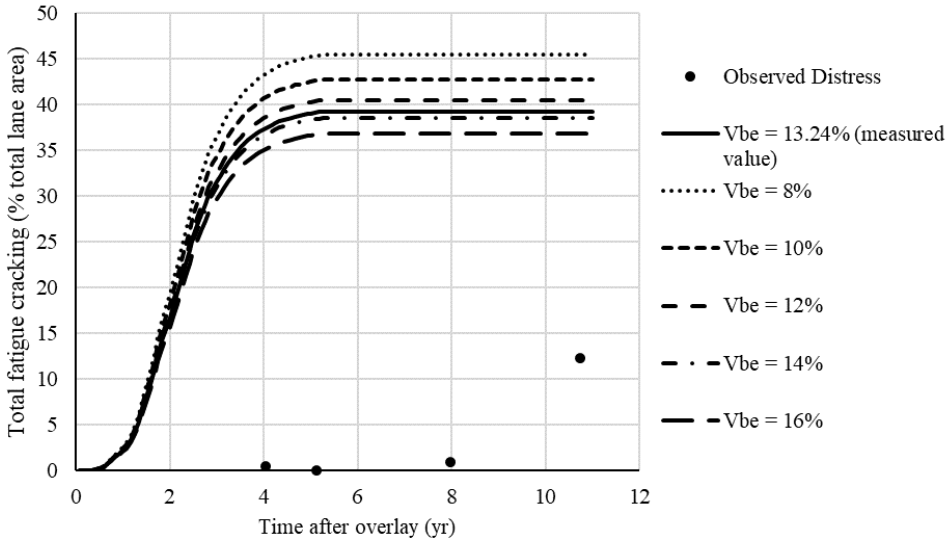

Figure 26. Sensitivity of predicted total fatigue cracking to volumetric effective binder content (V_{be}) of the asphalt concrete in the existing pavement (LTPP Section 23-1009, Maine, E_{NDT} = 911 ksi, MDT = 71°F).

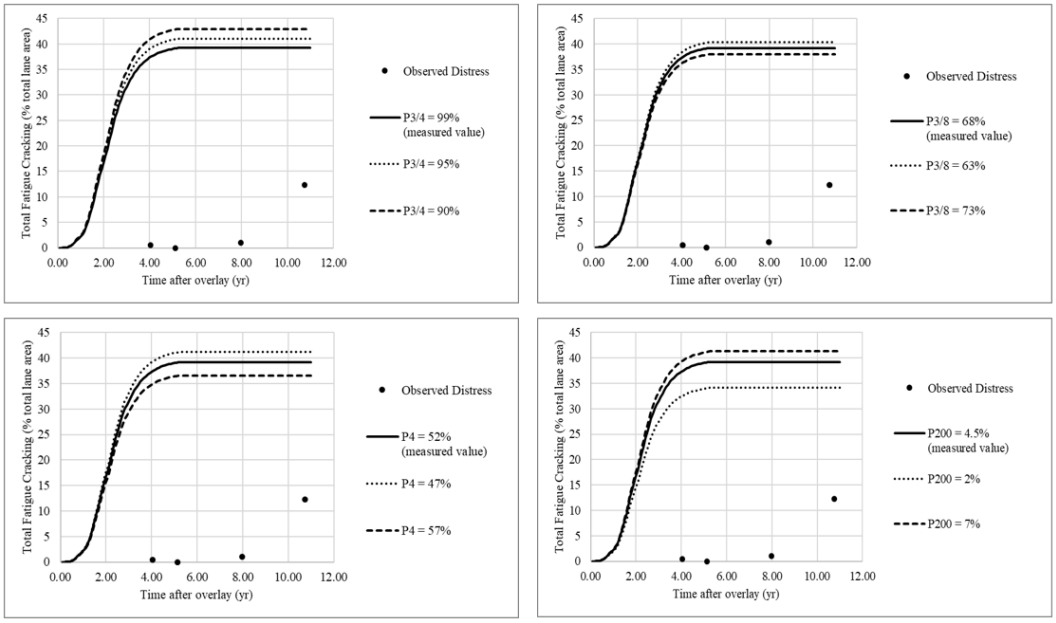

Figure 27. Sensitivity of predicted total fatigue cracking to the aggregate gradation inputs of the asphalt concrete in the existing pavement (LTPP Section 23-1009, Maine, E_{NDT} = 911 ksi, MDT = 71ºF).

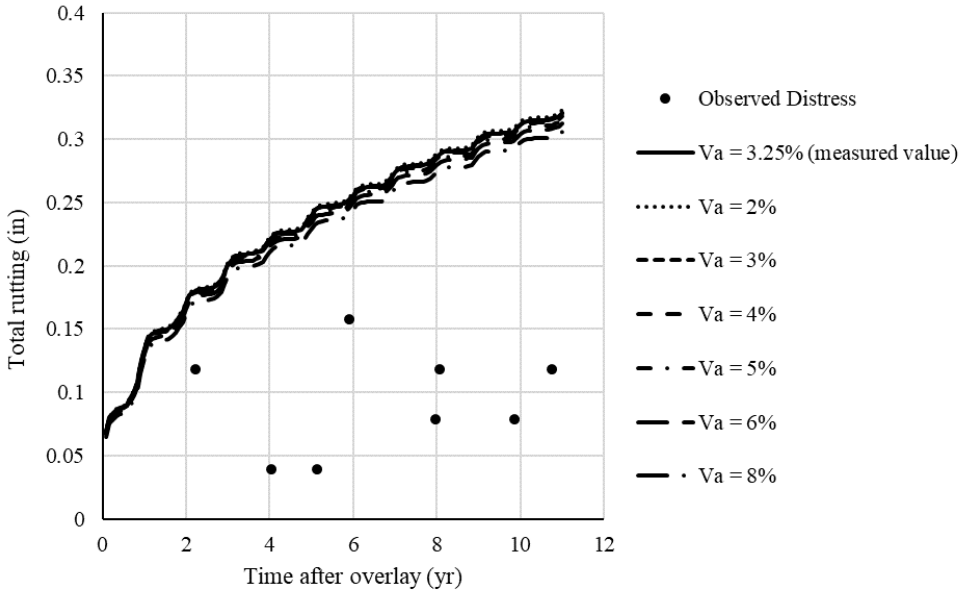

Figure 28. Sensitivity of predicted total rutting to volumetric air voids (Va) of the asphalt concrete in the existing pavement (LTPP Section 23-1009, Maine, E_{NDT} = 911 ksi, MDT = 71ºF).

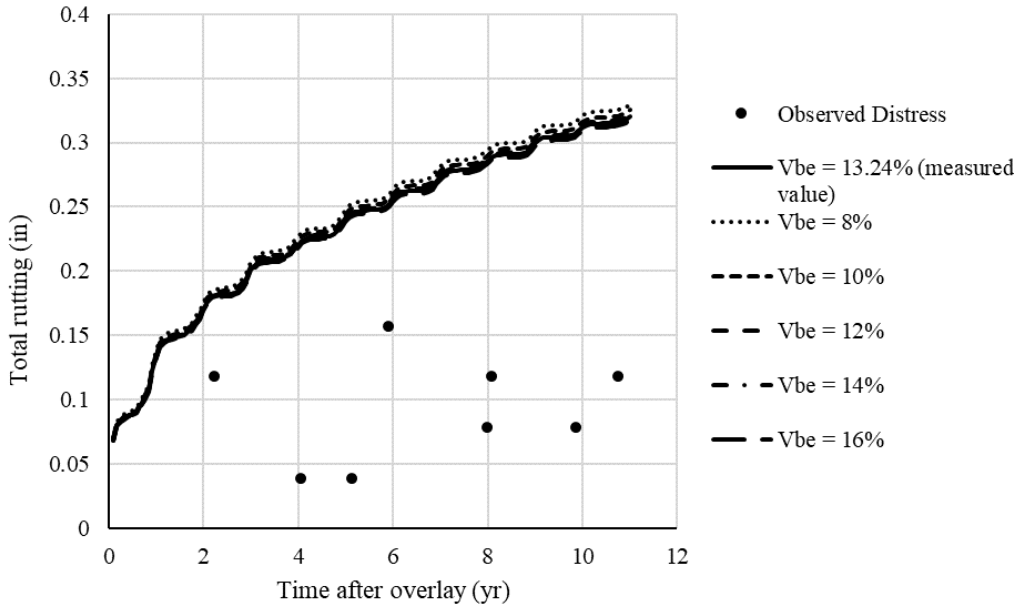

Figure 29. Sensitivity of predicted total rutting to volumetric effective binder content (Vbe) of the asphalt concrete in the existing pavement (LTPP Section 23-1009, Maine, E_{NDT} = 911 ksi, MDT = 71°F).

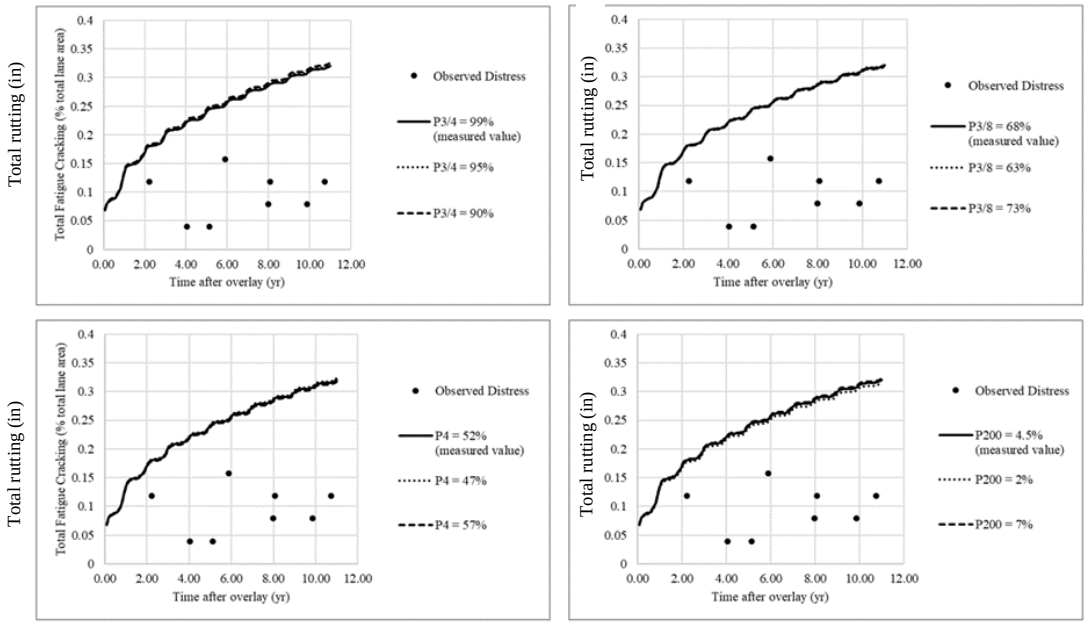

Figure 30. Sensitivity of predicted total rutting to the aggregate gradation inputs of the asphalt concrete in the existing pavement (LTPP Section 23-1009, Maine, E_{NDT} = 911 ksi, MDT = 71°F).

3.1.4 Improving predicted distress by adjusting inputs

Once it was determined that the Pavement ME AC/AC overlay design procedure over predicts observed distress in most cases when Level 1 inputs are used, additional analyses were performed to determine if the accuracy of distress predictions can be improved by altering the Pavement ME program inputs. Three methods of modifying the program inputs were examined:

1. Using multiple values of E_{NDT} determined at different temperatures.
2. Adjusting E_{NDT} to account for the fact that E_{NDT} is measured differently than $E_{Witczak}$ and therefore is not necessarily equal.
3. Adjusting the backcalculated resilient modulus of the unbound layers to account for differences between the backcalculated resilient modulus and the resilient modulus measured in a laboratory.

3.1.4.1 Multiple E_{NDT} inputs

The AC/AC overlay design procedure allows multiple Level 1 E_{NDT} inputs to be entered for a single pavement design. This is shown in Figure 6. The PennDOT Pavement ME Preliminary User Input Guide recommends that multiple FWD test passes should be performed over the course of a day to obtain multiple E_{NDT} inputs for the design procedure (Bhattacharya et al. 2017). This recommendation is based on the assumption that obtaining multiple stiffness measurements at different asphalt temperatures will result in a more accurate estimate of the asphalt condition, because asphalt stiffness is temperature-sensitive.

LTPP Section 87-1622 in Ontario was used to determine if the use of E_{NDT} backcalculated at multiple temperatures over the course of a single day improves the accuracy of the predicted

distress. This section was selected because multiple FWD test passes were performed in a single day on five separate occasions in the year before the section was overlaid. The effect of using multiple E_{NDT} inputs was evaluated for three of these five days. First, an AC/AC overlay design analysis was performed for each test pass individually. The E_{NDT} input for each test pass is the average of the backcalculated stiffness at each of the 11 test points in the outer wheelpath. Only data from 9-kip drops was used. The MDT for each test pass is established by calculating the mean of all MDT measurements corresponding to the 9-kip drops used to calculate E_{NDT}. Second, a design analysis is performed using all of the E_{NDT} and MDT inputs simultaneously. This is the method recommended in the Preliminary User Input Guide (Bhattacharya et al. 2017). The E_{NDT} and MDT inputs for each test pass are entered into a separate row in the fields shown under the heading "Modulus of existing AC layer obtained from NDT testing" in Figure 6. An FWD load frequency of 30 Hz was assumed for all test passes. The E_{NDT} and MDT for each test pass conducted in May, July, and October are summarized in Table 6. Plots of fatigue cracking vs. time and rutting vs. time for each month are shown in Figures 31 through 36.

Table 6. Average E_{NDT} for FWD passes at LTPP Section 87-1622, Ontario.

Test Date	Pass	E_{NDT} (ksi)	MDT (°F)
5/22/1997	1	1077	54
	2	961	59
	3	828	63
7/24/1997	1	711	73
	2	667	78
	3	491	89
	4	421	96
10/30/1997	1	1498	38
	2	1298	45
	3	1112	49

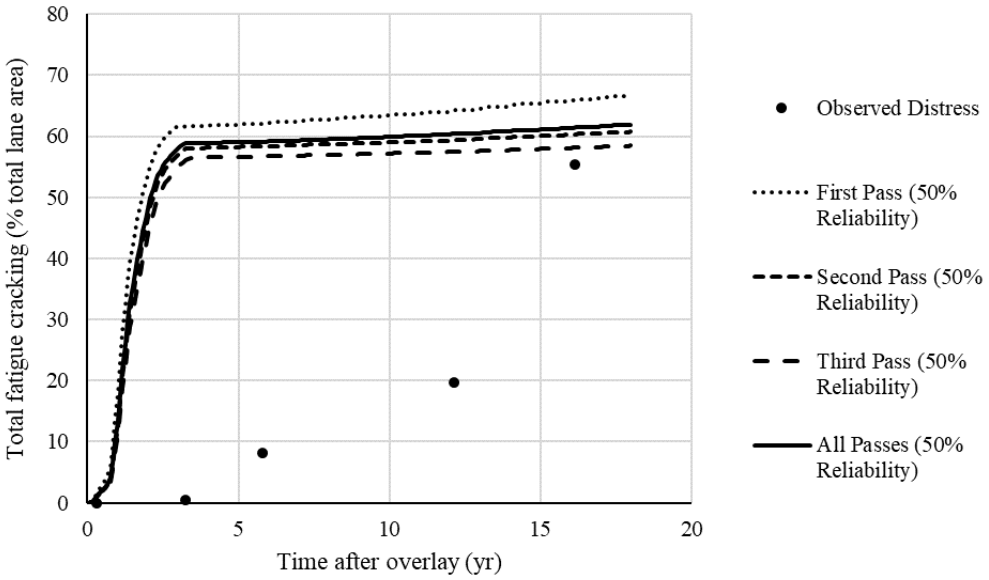

Figure 31. Comparison of predicted and observed fatigue cracking when using multiple E_{NDT} inputs (LTPP Section 87-1622, Ontario, 5/22/1997).

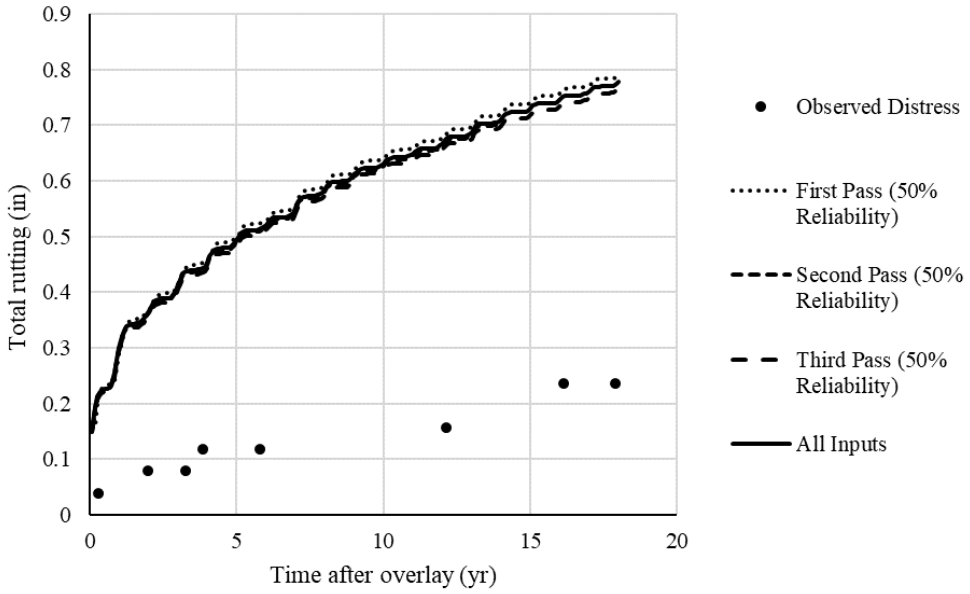

Figure 32. Comparison of predicted and observed total rutting when using multiple E_{NDT} inputs (LTPP Section 87-1622, Ontario, 5/22/1997).

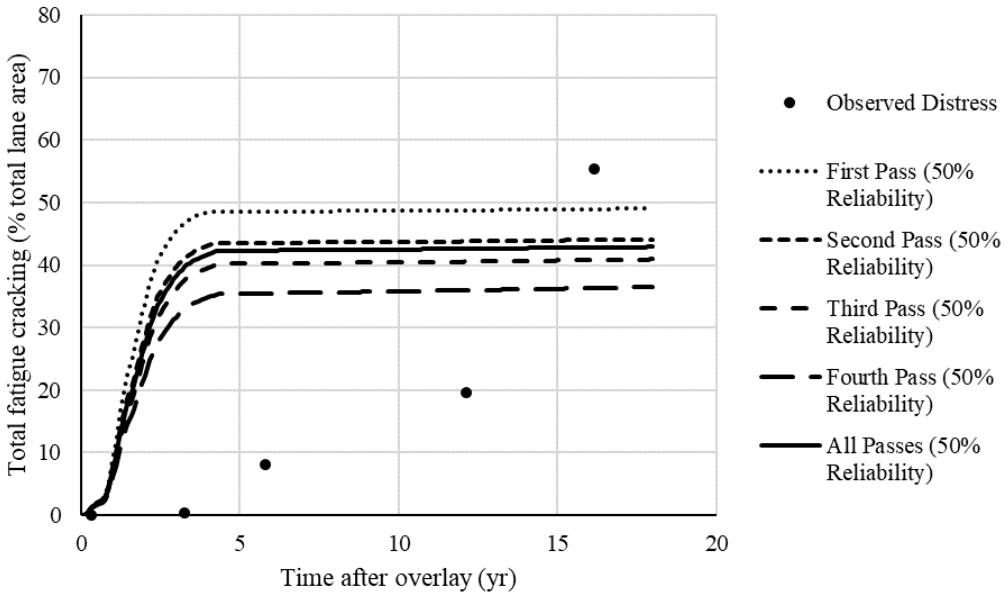

Figure 33. Comparison of predicted and observed fatigue cracking when using multiple E_{NDT} inputs (LTPP Section 87-1622, Ontario, 7/24/1997).

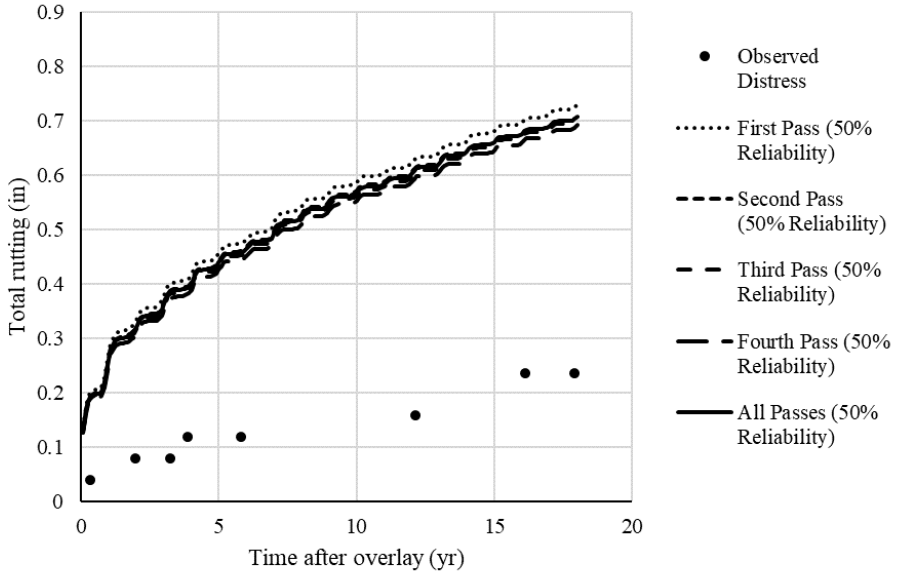

Figure 34. Comparison of predicted and observed total rutting when using multiple E_{NDT} inputs (LTPP Section 87-1622, Ontario, 7/24/1997).

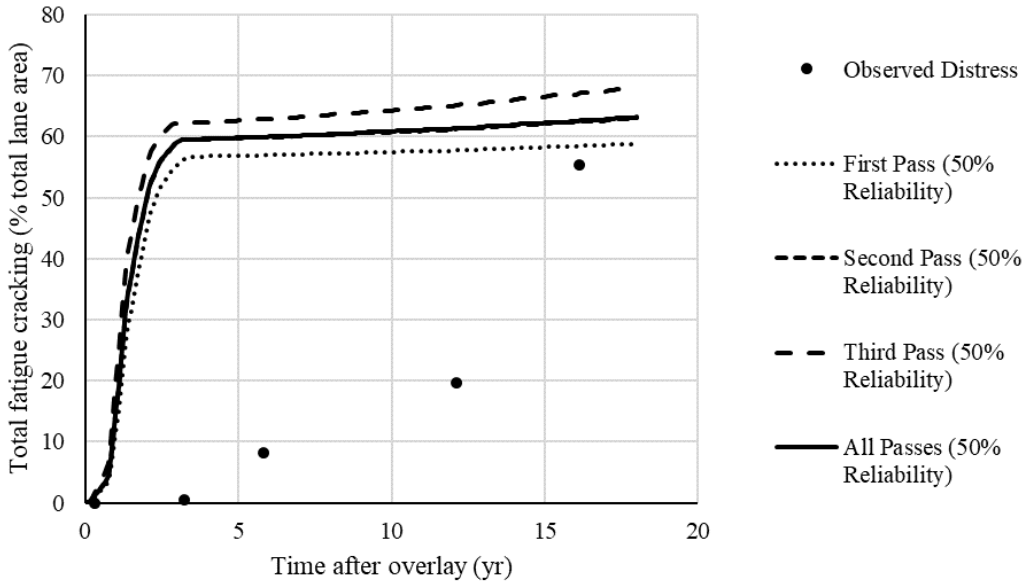

Figure 35. Comparison of predicted and observed fatigue cracking when using multiple E_{NDT} inputs (LTPP Section 87-1622, Ontario, 10/30/1997).

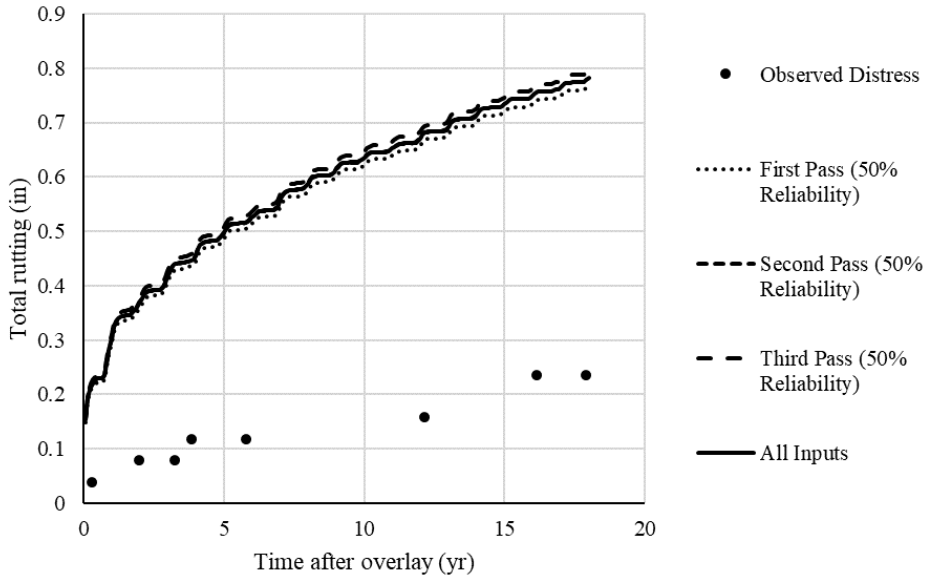

Figure 36. Comparison of predicted and observed total rutting when using multiple E_{NDT} inputs (LTPP Section 87-1622, Ontario, 10/30/1997).

Figures 31 through 36 show that performing multiple test passes at different pavement temperatures and using multiple inputs does not improve the accuracy of the AC/AC overlay design procedure with Level 1 inputs. For both fatigue cracking and rutting, the distress predicted when multiple E_{NDT} inputs determined at multiple temperatures are used simultaneously is similar to the average of the distress predicted by each input individually.

3.1.4.2 E_{NDT} adjustment factors

Several sources have suggested that there is an inherent difference between E_{NDT} and $E_{Witczak,}$ and adjustment factors have been developed for the Level 1 E_{NDT} input that are intended to account for this difference (Ayyala et al. 2017; Gedafa et al. 2010; Von Quintus and Killingsworth 1998). Three sets of E_{NDT} adjustment factors were evaluated using LTPP data from a total of eighteen FWD test passes, which were performed on ten test sections and over a wide range of asphalt temperatures. The adjustment factors evaluated are summarized in Table 7, below, and are also summarized in Table 2 in Chapter 2. First, the average backcalculated asphalt concrete stiffness in the outer wheelpath (E_{NDT}) and the corresponding average MDT over the test pass were determined for each test pass. The E_{NDT} and MDT for each test pass were established using the same method described above for the evaluation of multiple E_{NDT} inputs. Second, the measured MDT was used to determined adjustment factors for each test pass. Finally, E_{NDT} was multiplied by each of the three adjustment factors (Von Quintus and Killingsworth, Gedafa, and Ayyala) to obtain three adjusted E_{NDT} inputs ($E_{NDT,adjusted}$) for each test pass. Table 8 summarizes the adjustment factors proposed in previous research and the adjusted E_{NDT} inputs used for each section. The distress predicted using the adjusted inputs and the distress predicted using the unadjusted inputs were both compared to the observed distress.

Table 7. Adjustment factors for the Level 1 E_{NDT} input

Von Quintus and Killingsworth, 1998		Gedafa, et al., 2010		Ayyala, et al., 2017 [2]		
Asphalt Temperature (°F)	$E_{NDT}/M_{r,IDT}$ [1]	Asphalt Temperature (°F)	$E_{NDT}/E_{Witczak}$	Asphalt Temperature (°F)	E_{Lab} (ksi)	E_{NDT}/E_{Lab}
41	1.0	39	1.14	< 40	> 1000	1.0
77	2.8	70	0.69	60 - 70	600 - 800	1.3
104	4.0	95	0.84	> 90	< 500	1.6

[1] $M_{r,IDT}$ is the total resilient modulus measured in indirect tension. [2] For Ayyala, et al. factors, it is assumed that E_{Lab} is equal to $E_{Witczak}$.

Table 8. Inputs used in E_{NDT} adjustment factor analysis.

				Von Quintus and Killingsworth		Gedafa		Ayyala	
State	LTPP ID	E_{NDT}	MDT	Adjustment Factor	Adjusted E_{NDT}	Adjustment Factor	Adjusted E_{NDT}	Adjustment Factor	Adjusted E_{NDT}
IA	19-1044	424	42.2	1.06	400	1.09	388	1.03	410
KS	20-0159	211	89.6	3.36	63	0.81	261	1.59	132
ME	23-1009	911	70.9	2.50	365	0.70	1310	1.31	694
MD	24-1634	987	63.9	2.15	460	0.78	1268	1.30	759
NJ	34-0961	1148	44.4	1.17	981	1.06	1081	1.07	1077
NJ	34-0962	683	57.0	1.80	379	0.88	777	1.26	544
NJ	34-1011	331	88.8	3.32	100	0.80	412	1.58	209
PA	42-1597	571	56.2	1.76	324	0.89	641	1.24	459
ON	87-1622	1073	42.4	1.07	1002	1.09	984	1.04	1035
ON	87-1622	961	59.1	1.91	504	0.85	1133	1.29	747
ON	87-1622	544	83.3	3.08	177	0.77	707	1.50	363
ON	87-1622	667	78.4	2.86	233	0.74	901	1.43	468
ON	87-1622	421	96.2	3.65	115	0.85	497	1.69	249
ON	87-1622	1020	61.9	2.04	499	0.81	1263	1.29	793
ON	87-1622	1146	54.5	1.67	685	0.92	1251	1.22	941
ON	87-1622	1298	45.0	1.20	1080	1.05	1233	1.08	1207
ON	87-1622	1112	49.3	1.42	785	0.99	1123	1.14	975
QB	89-1125	875	53.2	1.61	543	0.93	937	1.20	730

Adjustment factors provided by the Von Quintus and Killingsworth and the Ayyala studies are greater than 1.00 (they assume that E_{NDT} is greater than $E_{Witczak}$) and increase the difference between predicted and observed fatigue cracking (decrease accuracy). However, factors that assume E_{NDT} is less than $E_{Witczak}$ (the Gedafa factors) decrease the difference between predicted and observed fatigue cracking (increase accuracy) for the sections analyzed. An example of an adjustment factor improving accuracy is shown in Figure 37, but none of the adjustment factors provide a consistent improvement in the ability of the design procedure to predict fatigue cracking. If the unadjusted E_{NDT} input resulted in a poor prediction of the observed distress, then all of the adjusted E_{NDT} would also tend to provide poor predictions. An example of this is shown in Figure 38. On the other hand, if the unadjusted E_{NDT} resulted in an accurate prediction of observed distress, using adjustment factors did not appreciably improve the prediction. This can be seen in Figure 39. The same trends are true for rutting, but the changes in predicted distress caused by adjusting the E_{NDT} input are much smaller than for fatigue cracking.

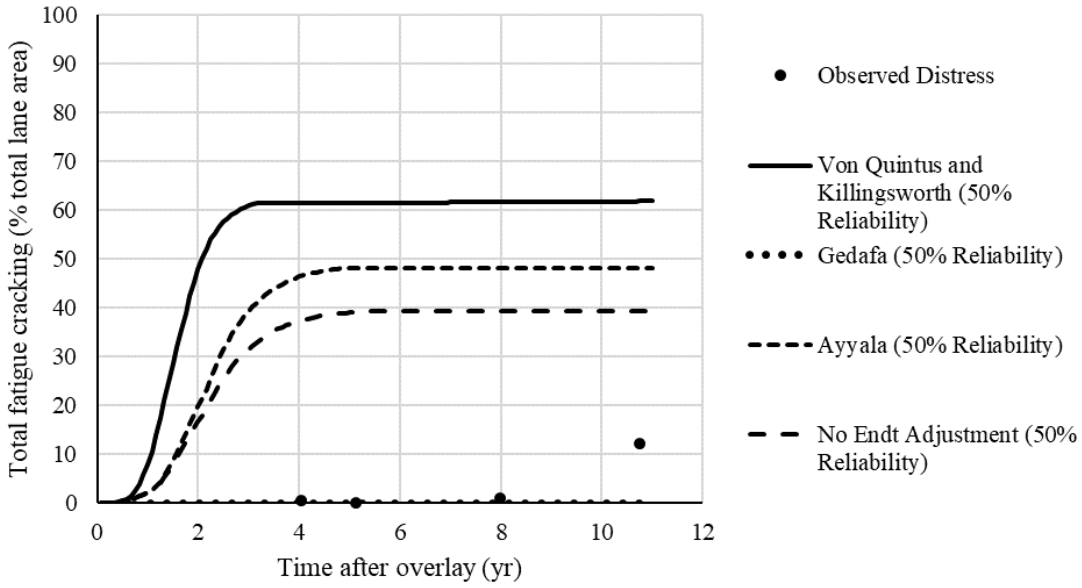

Figure 37. Effect of E_{NDT} adjustment factors on predicted total fatigue cracking (LTPP Section 23-1009, Maine).

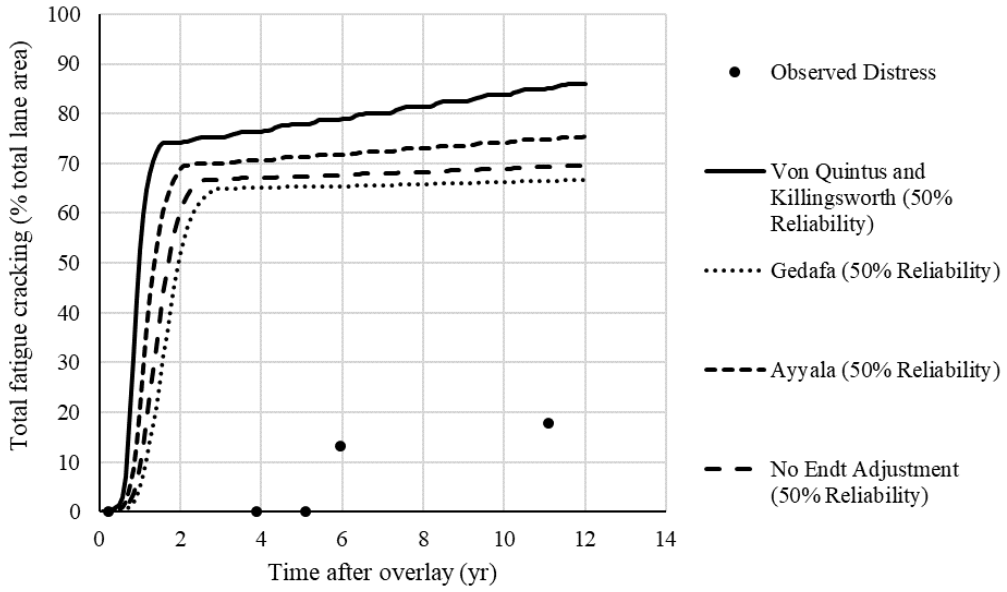

Figure 38. Effect of E_{NDT} adjustment factors on predicted total fatigue cracking

(LTPP Section 34-0962, New Jersey).

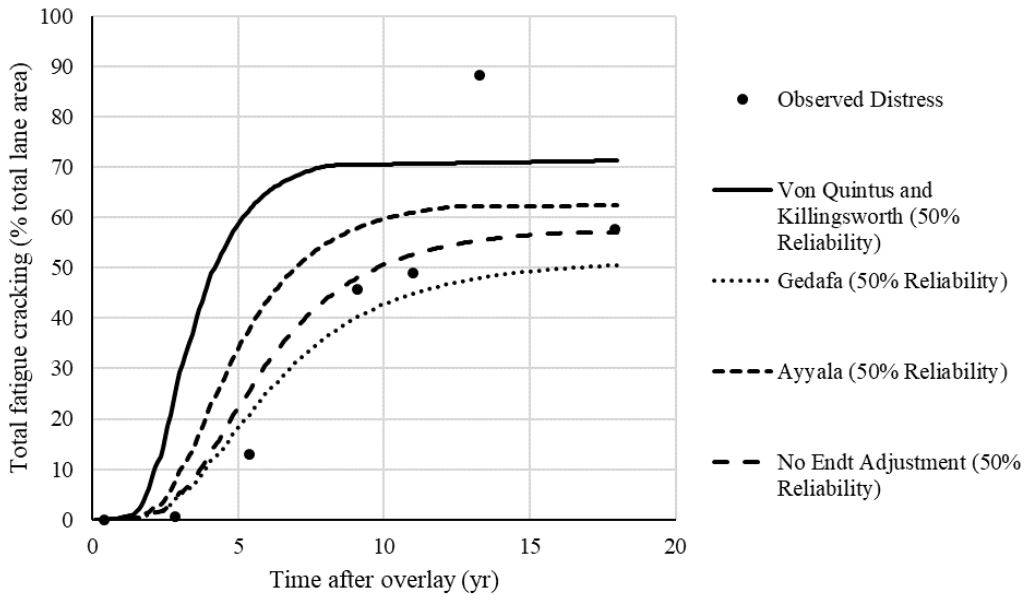

Figure 39. Effect of E_{NDT} adjustment factors on predicted total fatigue cracking (LTPP Section 24-1634, Maryland).

Two additional observations were made during the evaluation of the E_{NDT} adjustment factors. First, when no E_{NDT} adjustment factors are used, the maximum predicted fatigue cracking decreases as the MDT at which FWD was performed increases. This is shown in Figure 40 using FWD data from four test passes performed on Section 87-1622 one year before the section was overlaid. Again, E_{NDT} and MDT for each test pass were calculated using the same method described above. Assuming the amount of damage in the existing asphalt remained constant between April and July, the fact that maximum predicted fatigue cracking decreases as MDT increases suggests that there is a temperature-dependent relationship between $E_{Witczak}$ and E_{NDT}.

Second, when adjustment factors are used to modify E_{NDT}, the relationship between the maximum predicted fatigue cracking and MDT changes. This is shown in Figures 41 through 43. Cracking predicted using the Von Quintus and Killingsworth and the Ayyala adjustment factors is consistent across MDT but the observed distress substantially over predicted in all cases. On the

other hand, fatigue cracking predicted using the Gedafa adjustment factors is closer to the observed fatigue cracking, but the relationship between predicted and observed fatigue cracking is inconsistent across MDT. Ideally, E_{NDT} adjustment factors should lead to distress predictions that are reasonably accurate across the range of MDT. None of the adjustment factors evaluated fulfill this criterion. E_{NDT} adjustment factors were found to have similar, but less pronounced, effects on predicted rutting.

Overall, it appears that applying an adjustment factor to the E_{NDT} input can improve agreement between predicted and observed distress. However, in most cases, it cannot fundamentally change the shape of the predicted distress time history to match the observed distress time history. Finally, it is important to note that these conclusions are based on a very limited analysis. Further discussion of E_{NDT} adjustment factors can be found in Chapter 6.

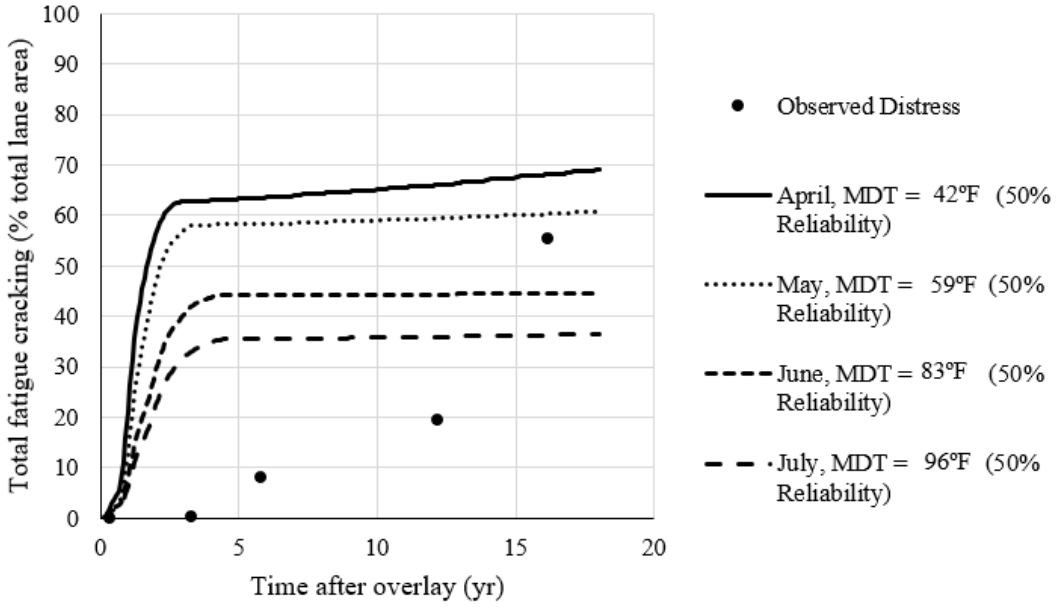

Figure 40. Effect of MDT at the time of FWD testing on predicted total fatigue cracking without E_{NDT} adjustment factors (LTPP Section 87-1622, Ontario).

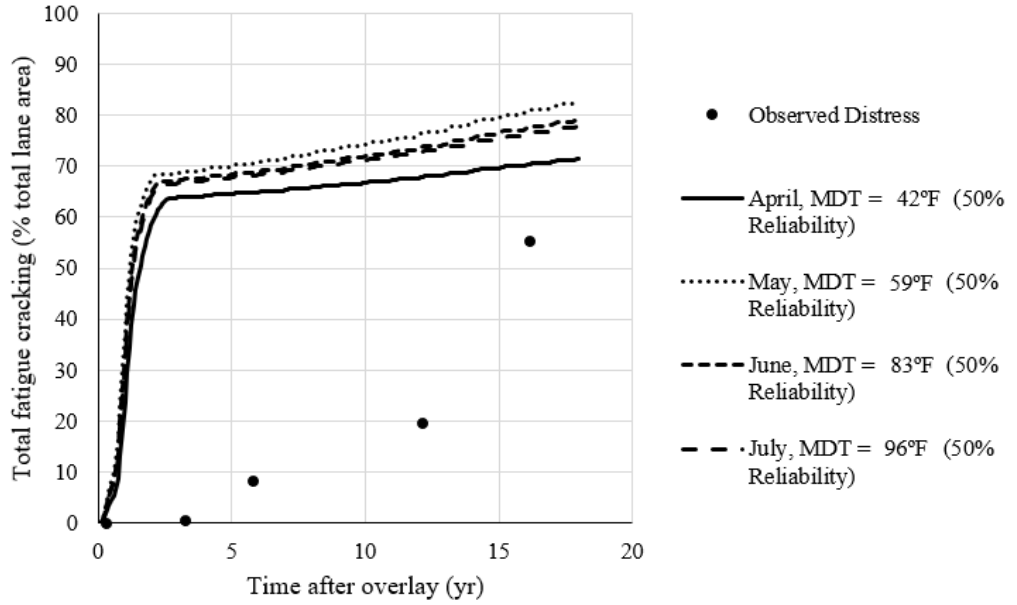

Figure 41. Effect of MDT at the time of FWD testing on predicted total fatigue cracking using Von Quintus and Killingsworth adjustment factors (LTPP Section 87-1622, Ontario).

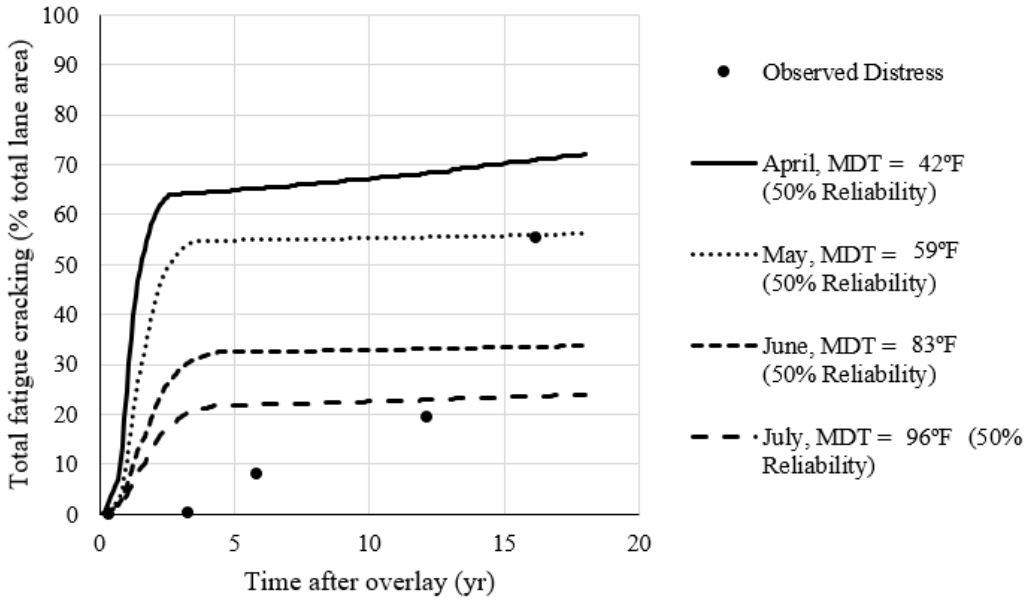

Figure 42. Effect of MDT at the time of FWD testing on predicted total fatigue cracking using Gedafa adjustment factors (LTPP Section 87-1622, Ontario).

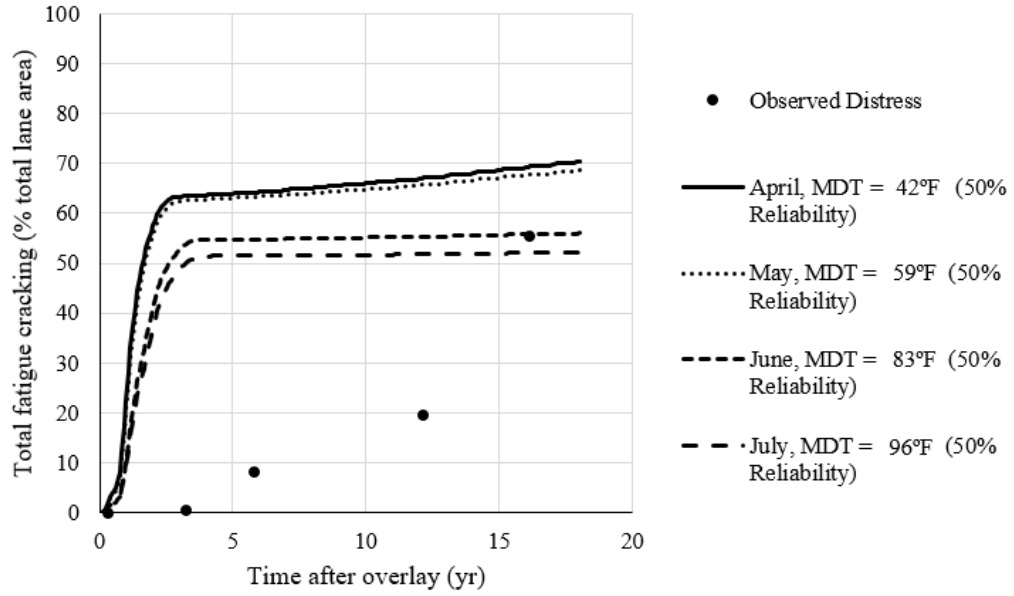

Figure 43. Effect of MDT at the time of FWD testing on predicted total fatigue cracking using Ayyala adjustment factors (LTPP Section 87-1622, Ontario).

3.1.4.3 Adjusted unbound layer stiffness

The PennDOT Pavement ME Preliminary User Input Guide recommends that the backcalculated stiffness of unbound layers be adjusted based on the type of pavement section analyzed. The purpose of the adjustment factors is to convert the backcalculated stiffness of an unbound layer to an equivalent laboratory resilient modulus. The recommended adjustment factors are provided in Table 9 (Bhattacharya et al. 2017; Killingsworth and Von Quintus 1997). The appropriate factor must be entered manually into Pavement ME for each unbound layer. First, the backcalculated stiffness, in-situ water content, and in-situ dry density of the unbound material are entered for each unbound layer. The backcalculated stiffness of the layer is the average over the entire pavement section, excluding outliers. Second, the appropriate adjustment factor is entered for each unbound layer. The special input field for the unbound layer stiffness adjustment factor is shown in Figure 44.

Table 9. Suggested adjustment factors to convert backcalculated unbound layer stiffness to laboratory equivalent resilient modulus.

Layer Type and Material	Layer Description	Adjustment Factor ($M_r/E_{Backcalulated}$)
Aggregate base	Granular base above a stabilized material (sandwich section)	1.43
	Granular base under an AC surface or AC base	0.62
Subgrade	Soil under a stabilized subgrade	0.75
	Soil under a full-depth AC pavement	0.52
	Soil under a flexible pavement with granular base/subbase	0.35

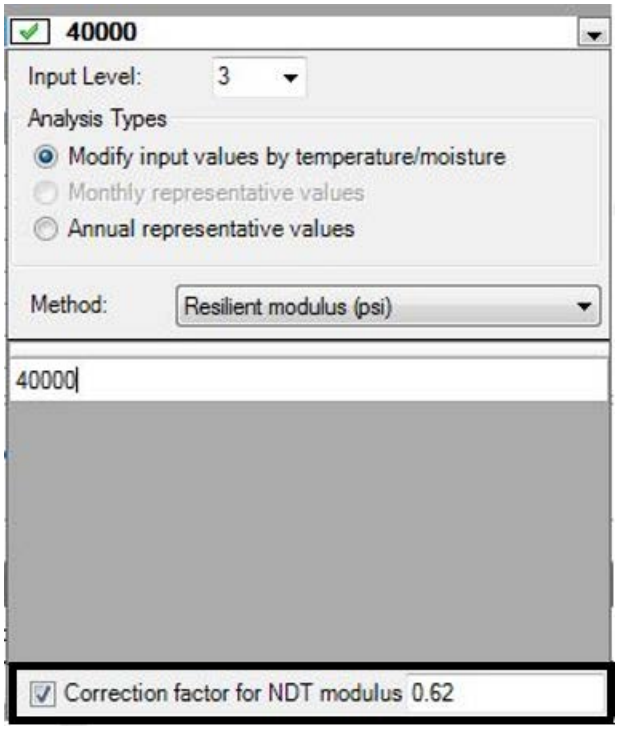

Figure 44. Input field for the unbound layer backcalculated stiffness adjustment factor.

The effect of the unbound layer backcalculated stiffness adjustment factors on predicted distress was evaluated using the same LTPP sections listed in Table C-6-2. The effect of adjusting the unbound layer stiffness on fatigue cracking and total rutting is shown in Figures 45 and 46, respectively.

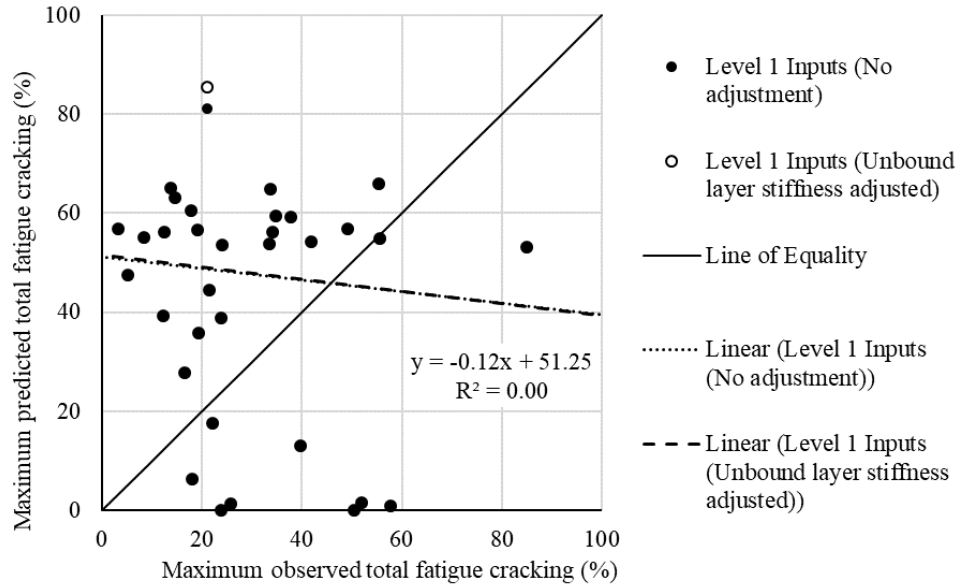

Figure 45. Predicted fatigue cracking with and without adjusted unbound layer stiffnesses vs. observed fatigue cracking.

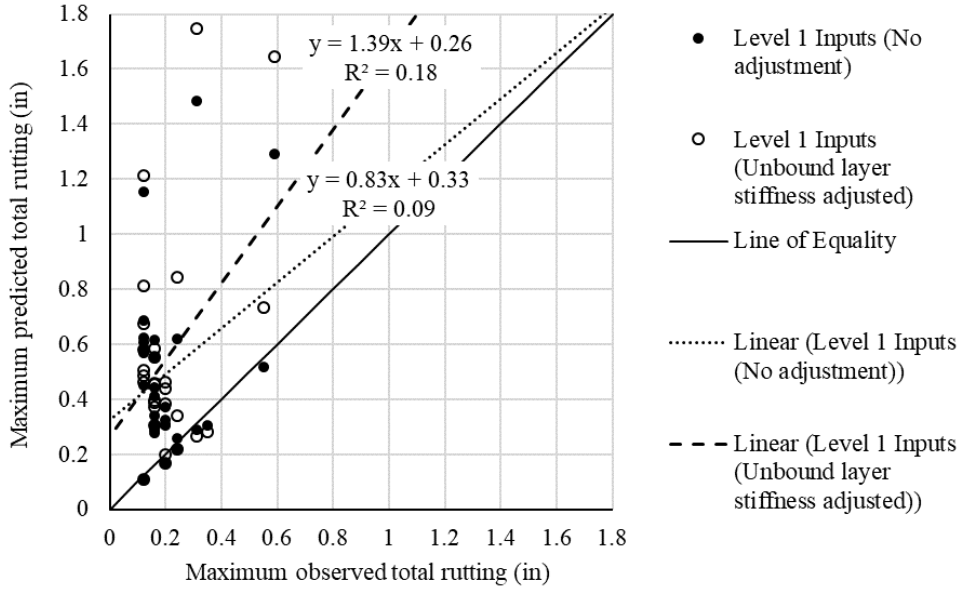

Figure 46. Predicted total rutting with and without adjusted unbound layer stiffnesses vs. observed total rutting.

As shown in Figure 45, adjusting the backcalculated unbound layer stiffness has almost no effect on the accuracy of the predicted fatigue cracking. A paired t-test at a 95% confidence level showed that the difference between the predicted fatigue cracking and the observed fatigue cracking (the quantity (predicted cracking – observed cracking)) is the same with and without unbound layer stiffness adjustment (p-value = 0.32). This is expected, as predicted fatigue cracking is determined primarily by the backcalculated stiffness of the existing asphalt and the reflective cracking model. In contrast, adjusting the backcalculated stiffness of the unbound layers increases the predicted total rutting for most sections. A paired t-test at a 95% confidence level showed that the difference between the predicted total rutting and the observed total rutting (the quantity (predicted rutting – observed rutting)) is significantly greater when the unbound stiffness is adjusted than when it is not adjusted (p-value = 0.01). The increase in the difference between predicted rutting and observed rutting is greatest when the unadjusted backcalculated granular base layer stiffness is less than 15 ksi and/or the unadjusted backcalculated subgrade layer stiffness is less than 25 ksi. The unbound layer stiffness adjustment factors should be used with care in these cases.

3.2 LEVEL 2 AC/AC OVERLAY DESIGN

The AC/AC overlay design procedure was also evaluated with Level 2 inputs to determine its accuracy as compared to when Level 1 inputs are used.

3.2.1 Description

In the AC/AC overlay design procedure with Level 2 inputs, the amount of damage in the asphalt concrete of the existing pavement is defined by the amount and severity of fatigue cracking observed at the surface of the existing pavement, obtained from a distress survey. The amount of fatigue cracking is expressed as a percentage of total lane area, and the severity of fatigue cracking is rated as low, medium, or high, according to the LTPP Distress Identification Guide (Lytton and Von Quintus 2016; Miller and Bellinger 2014). The input fields for defining the amount and severity of fatigue cracking in the existing pavement are shown in Figure 47. Like the AC/AC overlay design procedure when using Level 1 inputs, the use of Level 2 inputs predicts reflected fatigue cracking and new fatigue cracking separately.

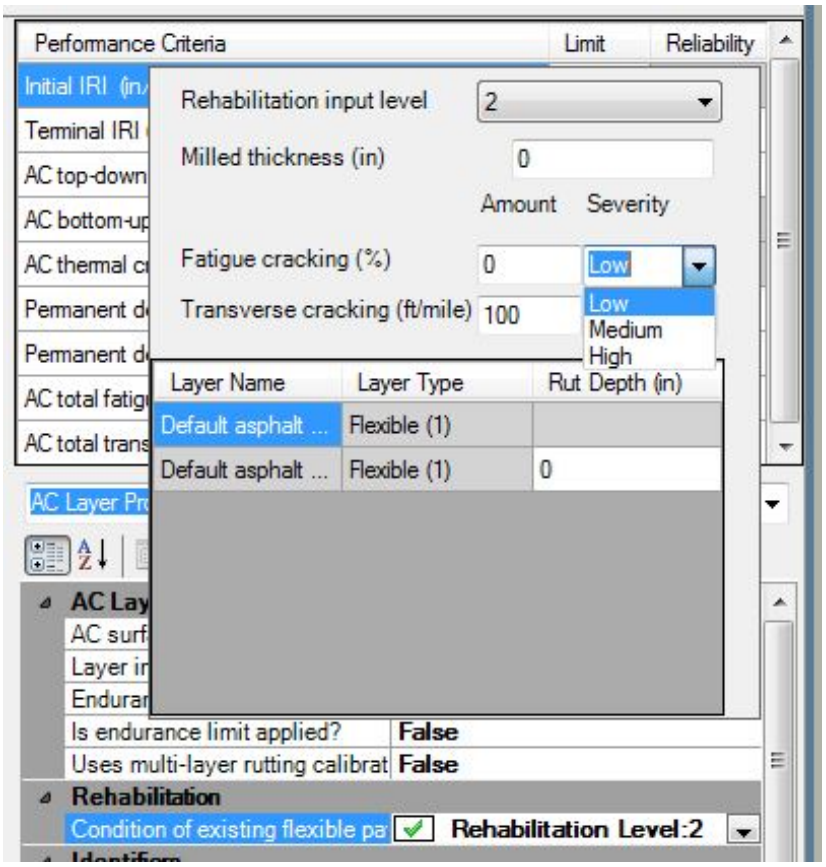

Figure 47. Pavement ME inputs for defining the amount and severity of fatigue cracking in the existing pavement.

Reflected fatigue cracking is predicted using the reflective cracking model described previously and shown in Equation 10 and Figure 8. The amount of fatigue cracking in the existing pavement is used as a direct input for the reflective cracking model. The severity of fatigue cracking in the existing pavement is correlated to a load transfer efficiency (LTE) term in the reflective cracking model. This term defines the amount of load that is transferred over the crack in the existing pavement in the "Traffic induced fatigue" crack growth geometry shown in Figure 8. Low severity fatigue cracking in the existing pavement is correlated to a LTE of 85%, medium severity to a 50% LTE, and high severity to a 30% LTE (Lytton and Von Quintus 2016).

To predict new fatigue cracking, the amount of existing fatigue cracking is first converted to a damage parameter, which is used to develop a master curve that describes the damaged stiffness of the asphalt concrete in the existing pavement. Next, the damaged master curve is used to determine the stiffness of the asphalt concrete in the existing pavement, which is a critical input for the fatigue damage model. The fatigue damage model uses the stiffness of the asphalt concrete in the existing pavement, the stiffness of the asphalt concrete in the overlay, and several other inputs to estimate the amount of fatigue damage that accumulates in the overlaid pavement structure. Finally, the accumulated damage calculated using the fatigue damage model is used in the bottom-up fatigue cracking transfer function to determine the amount of new fatigue cracking in both the overlay and the existing pavement. The predicted total fatigue cracking reported in the Pavement ME AC/AC overlay design procedure with Level 2 inputs is the sum of the existing fatigue cracking in the existing pavement that has reflected through the overlay, the new fatigue cracking initiating at the bottom of the overlay, and the new fatigue cracking initiating at the bottom of the existing pavement and reflecting through the overlay. The mechanistic models and empirical relationships used to predict fatigue cracking in the AC/AC overlay design procedure using Level 2 inputs are summarized in Figure 48.

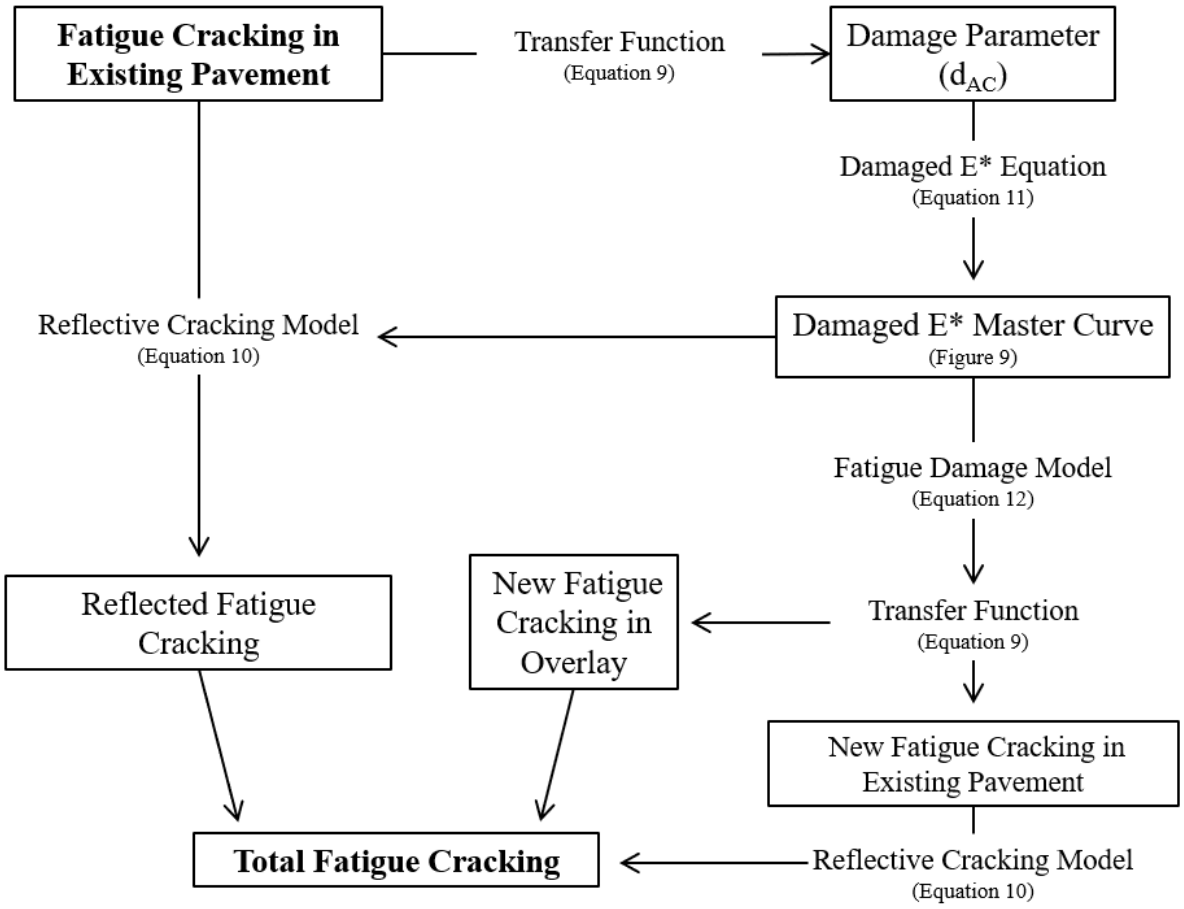

Figure 48. Prediction of total fatigue cracking in the Pavement ME AC/AC overlay design procedure with Level 2 inputs.

The approach for predicting rutting in the asphalt is similar when using either Level 1 or Level 2 inputs. However, when the AC/AC overlay design procedure is used with Level 2 inputs, the damage parameter for the asphalt concrete of the existing pavement is obtained based on the amount of fatigue cracking in the existing pavement, rather than from the backcalculated stiffness of the asphalt concrete in the existing pavement. Once obtained, the damaged stiffness of the asphalt concrete in the existing pavement is used to predict rutting in the asphalt concrete of the

overlaid pavement structure. Figure 49 summarizes the mechanistic models and empirical relationships used to predict asphalt rutting in the AC/AC overlay design procedure using Level 2 inputs.

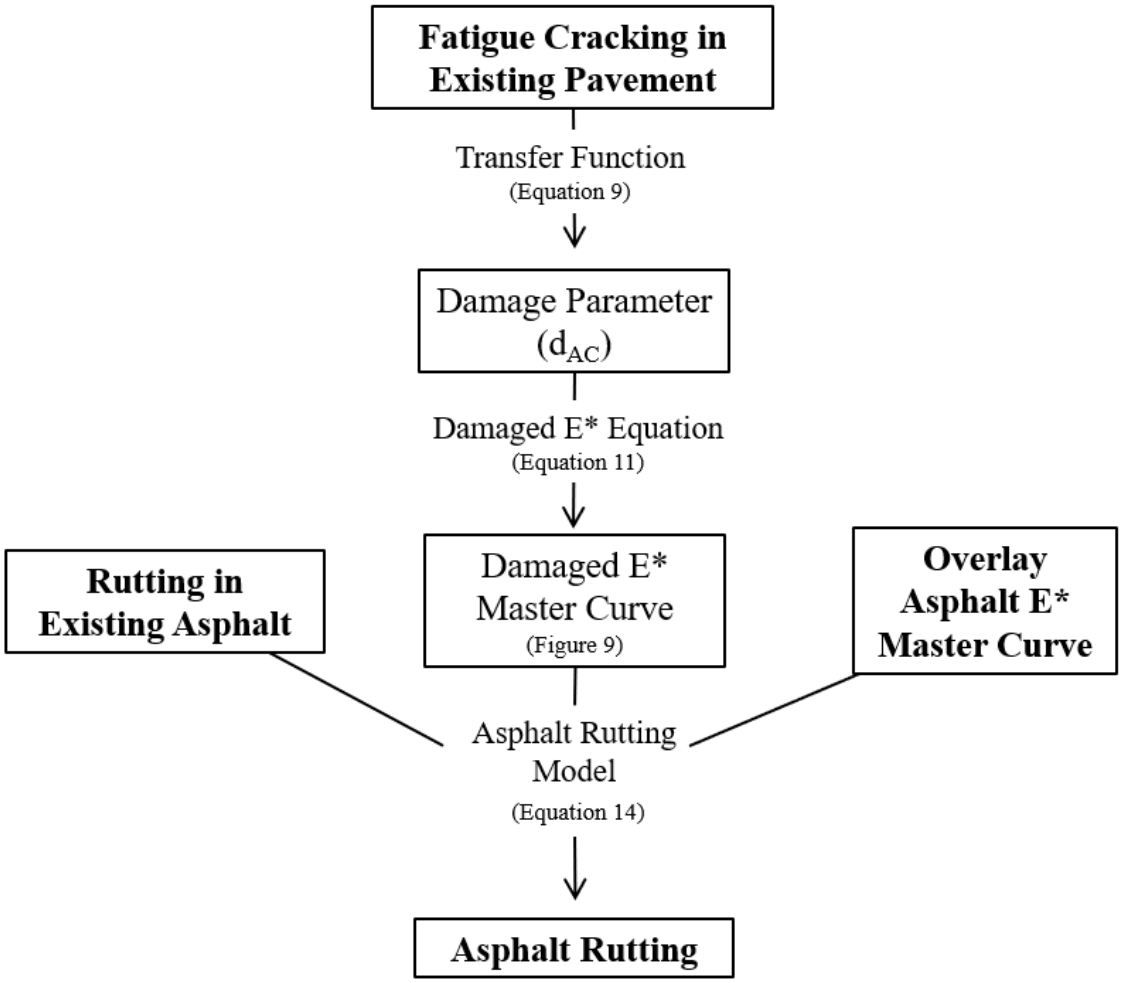

Figure 49. Prediction of total rutting in the Pavement ME AC/AC overlay design procedure with Level 2 inputs.

3.2.2 Evaluation

The use of Level 2 inputs in the AC/AC overlay design procedure was evaluated in the same manner as for the Level 1 inputs. A total of 40 LTPP sections were considered, all of which are located in wet-freeze climates and/or use binders similar to those used in Pennsylvania. These sections are summarized in Table 10. Inputs derived from LTPP data were the same as those listed in Tables 4 and 5, except that the amount and severity of fatigue cracking in the existing pavement was used instead of E_{NDT} and MDT. The amount of fatigue cracking in the existing pavement was taken directly from LTPP distress tables and was confirmed with distress surveys. For some sections, it was noted that the observed fatigue cracking did not fall entirely within the wheelpath and/or other distresses were misclassified and included in the amount of total fatigue cracking. No attempt was made to "clean" the existing fatigue cracking measurements, as the goal of the evaluation was to determine how the design procedure performs across a range of inputs. The cracking severity used in the design process was defined by the level of severity of cracking that makes up the largest proportion of the observed fatigue cracking. For example, if an existing AC pavement had 10% fatigue cracking by total lane area, 3/10 of which was rated low severity, 3/10 medium severity, and 4/10 high severity, the Level 2 input for fatigue cracking in the existing pavement would be defined as 10% high severity. Current user guidelines for Pavement ME do not provide clear instructions for how to define the severity of the fatigue cracking in the existing pavement (Bhattacharya et al. 2017). The method described above was developed as a best guess of the method intended by the developers. The global calibration factors were used again for all analyses.

Table 10. LTPP sections used to evaluate the AC/AC overlay design procedure with Level 2 inputs.

State	LTPP ID	AC Thickness (Pre-milling) (in)	AC Thickness (Post-milling) (in)	Overlay Thickness (in)	Binder Grade	Fatigue Cracking in Existing Pavement (%)	Severity of Fatigue Cracking
CT	9-1803	7	7	1.75	PG 64-28 / AC-20	5.0	Low
DE	10-0102	4.25	4.25	1.25	AC-20 / AC-20	1.5	Low
IL	17-A310	11.25	11.25	0.5	AC-20 / AC-20	0.0	Low
IN	18-2008	13.5	13.5	1.5	AC-20 / AC-20	7.0	Medium
IA	19-1044	16.25	16.25	3.75	PG 58-28 / Pen 85-100	6.4	Medium
KS	20-0159	11.25	6	5.25	PG 64-22 / AC-10	20.4	Low
KS	20-1005	13	12	0.75	PG 64 -22 / AC-5	29.0	Medium
KS	20-1009	11	4.5	7.5	AC-20 / AC-20	0.9	Medium
ME	23-1009	5.75	5.75	2.75	AC-20 / Pen 85-100	28.1	Low
MD	24-1634	3.5	3.5	3.25	PG 70-22 / Pen 85-100	38.7	Low
NJ	34-0502	8.75	8.75	1.75	Pen 85-100 / Pen 85-100	1.7	Low
NJ	34-0503	9.25	9.25	4.75	Pen 85-100 / Pen 85-100	0.0	Low
NJ	34-0504	8.75	8.75	4.75	Pen 85-100 / Pen 85-100	5.1	Low
NJ	34-0505	9	9	1.75	Pen 85-100 / Pen 85-100	11.8	Low
NJ	34-0506	9.5	7.5	4	Pen 85-100 / Pen 85-100	0.0	Low
NJ	34-0507	8.25	6.25	7.5	Pen 85-100 / Pen 85-100	0.3	Medium
NJ	34-0508	8.75	6.75	7.5	Pen 85-100 / Pen 85-100	0.0	Medium
NJ	34-0509	9.25	7.25	4.25	Pen 85-100 / Pen 85-100	0.0	Medium
NJ	34-0903	9	7.5	5.5	PG 64-22 / Pen 85-100	41.7	Medium
NJ	34-0960	9.75	7.25	4.75	PG 64-22 / Pen 85-100	56.2	Low
NJ	34-0961	9.25	5.5	6.5	PG 64-22 / Pen 85-100	33.2	Low
NJ	34-0962	9	7.5	4.25	PG 64-22 / Pen 85-100	20	Low
NJ	34-1003	7.5	5.5	2.25	AC-20 / AC-20	18.7	Low
NJ	34-1011	9	6.5	4	AC-20 / Pen 85-100	7.5	Low

Table 10 (continued).

State	LTPP ID	AC Thickness (Pre-milling) (in)	AC Thickness (Post-milling) (in)	Overlay Thickness (in)	Binder Grade	Fatigue Cracking in Existing Pavement (%)	Severity of Fatigue Cracking
NJ	34-1030	6	3	4.5	AC-20 / AC-20	16.2	Low
NJ	34-1033	7.5	6.75	2	AC-20 / AC-20	0	Low
PA	42-1597	6.5	5	6.25	PG 64-22 / AC-20	0.7	High
VA	51-2021	7.5	7.5	1.75	AC-20 / AC-20	0	Low
MB	83-0502	4.5	4.5	2.75	Pen 150-200 / Pen 150-200	0	Low
MB	83-0503	4.75	4.75	5.25	Pen 150-200 / Pen 150-200	7	Low
MB	83-0504	4.5	4.5	5.5	Pen 150-200 / Pen 150-200	1.2	Medium
MB	83-0505	5.25	5.25	3	Pen 150-200 / Pen 150-200	0	Low
MB	83-0506	5.5	4	3	Pen 150-200 / Pen 150-200	0	Low
MB	83-0507	4	3	6.75	Pen 150-200 / Pen 150-200	1.6	Medium
MB	83-0508	3.5	2.5	6.5	Pen 150-200 / Pen 150-200	0	Low
MB	83-0509	5	4	3.5	Pen 150-200 / Pen 150-200	1.9	Low
MB	83-6451	4	4	2.5	Pen 150-200 / Pen 150-200	0	Low
ON	87-1622	5.5	3	4.5	PG 58-28 / Pen 85-100	5.4	Medium
QB	89-1125	5.25	5.25	2	PG 58-28 / Pen 85-100	40.1	Low
QB	89-1127	5	5	2.5	Pen 85-100 / Pen 150-200	0.6	Low

The results of the evaluation showed that fatigue cracking performance histories predicted by the AC/AC overlay design procedure using Level 2 inputs have the same shape as the observed performance histories but are rarely accurate. Similar to using the procedure with Level 1 inputs, both the predicted fatigue cracking performance history and the observed fatigue cracking performance history trends are both sigmoidal. This indicates that the AC/AC overlay design procedure used along with Level 2 inputs is able to reasonably approximate the development of fatigue cracking in an actual pavement section. Pertaining to accuracy, there is no consistent

relationship between the predicted and observed fatigue cracking performance histories, except that the maximum predicted fatigue cracking is usually less than the maximum observed fatigue cracking. In general, the predicted and observed fatigue cracking performance curves do not increase at the same rate and do not reach a maximum value at the same time. A typical example of this can be seen in Figure 50.

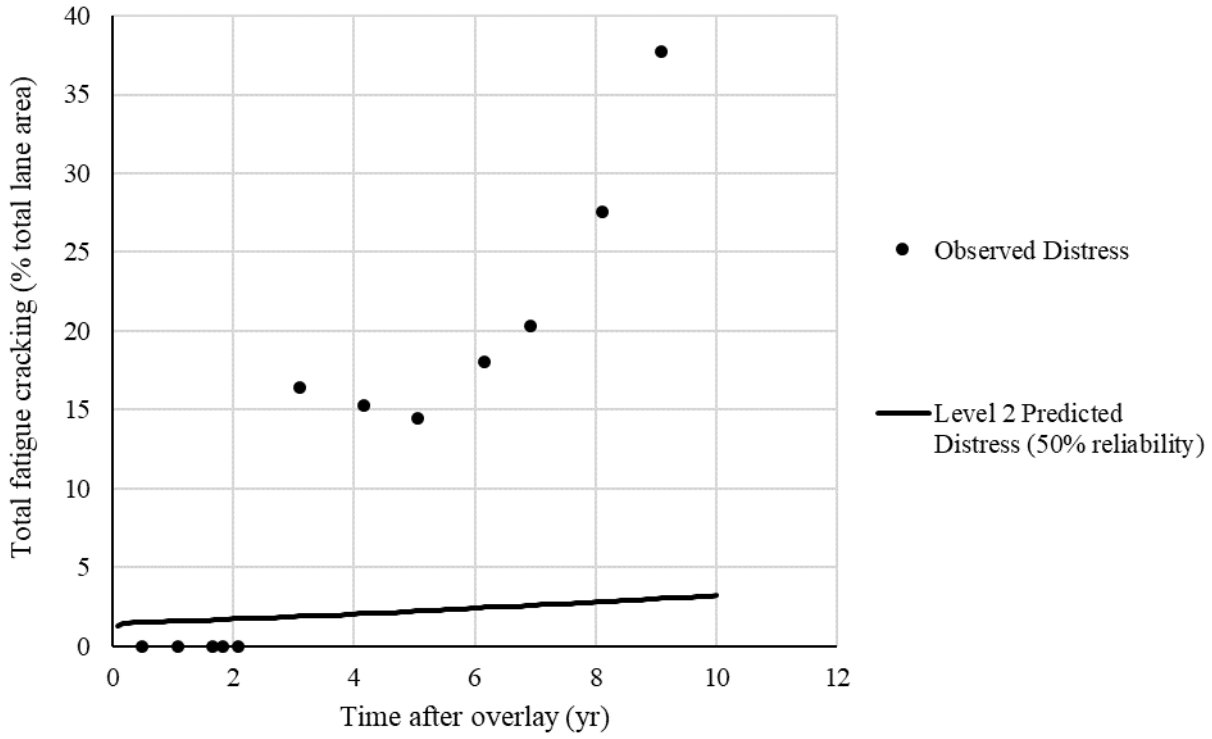

Figure 50. Predicted and observed total fatigue cracking (LTPP Section 10-0102, Delaware).

The inconsistent relationship between predicted and observed fatigue cracking performance histories may be attributed to the manner in which the reflective cracking model addresses cracking severity. The reflective cracking model was developed to address transverse

cracking, and the stress intensity factor used for a given crack depends on the LTE of that crack. The "traffic induced fatigue" crack growth geometry, shown in Figure 8, was used during the calibration of the reflective cracking model for fatigue cracking. The LTE of the cracking in the existing pavement was fixed for different levels of fatigue cracking severity: 85 % LTE for low severity, 50 % LTE for medium severity, and 30% LTE for high severity (Lytton and Von Quintus 2016). As a result, the rate at which predicted cracking develops is very sensitive to the cracking severity input. An example of this is shown in Figure 51. Fatigue cracking severity, while defined in the LTPP Distress Identification Guide, is a highly subjective measurement and could vary significantly along a project (Miller and Bellinger 2014). It is likely that fatigue cracking predictions made by the AC/AC overlay design procedure using Level 2 inputs would be more accurate if the severity of the fatigue cracking in the existing pavement (and the corresponding load transfer efficiency used in the reflective cracking model) were defined as a continuous variable, rather than at fixed levels.

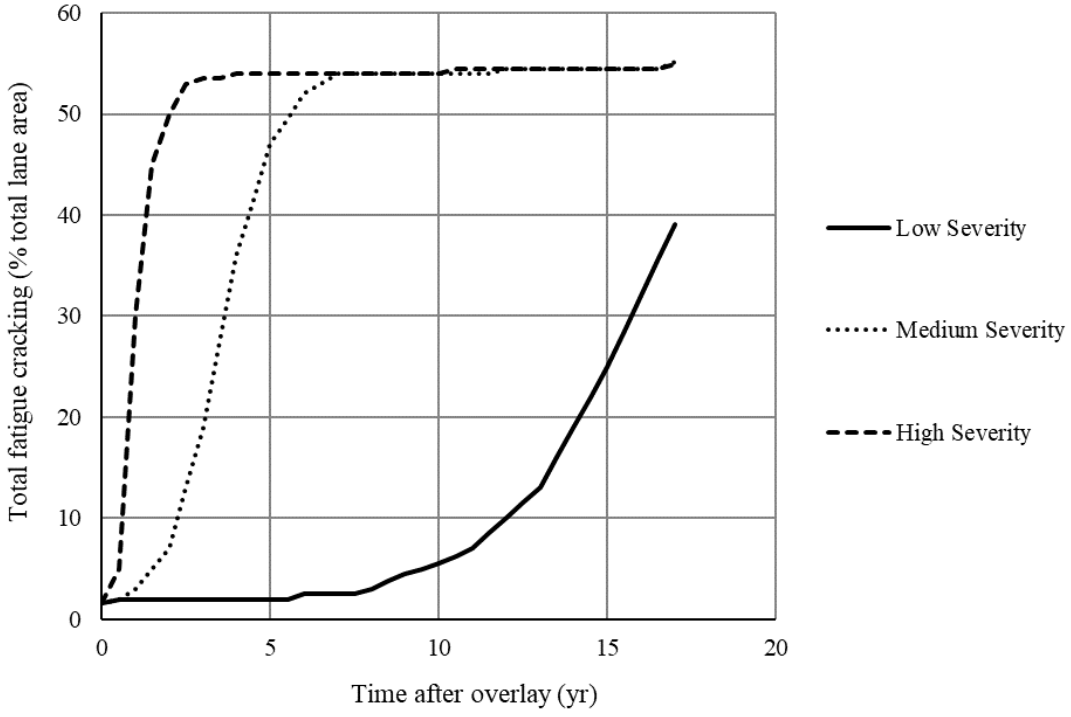

Figure 51. Effect of the severity of fatigue cracking in the existing pavement on the rate of predicted fatigue cracking development.

With regard to the maximum amount of fatigue cracking, the predicted fatigue cracking is less than the observed cracking in most cases, and the predicted cracking is often nearly zero. The relationship between predicted and observed maximum fatigue cracking when using Level 2 inputs is shown in Figures 52 and 53. Using a paired t-test, it was determined that maximum fatigue cracking predicted using Level 2 inputs is less than the maximum observed fatigue cracking at a 95% confidence level (p-value = 0.00). There are two reasons for this. First, the rate at which the predicted distress develops depends heavily on the severity of the cracking in the existing pavement. If the cracking is low severity, the predicted distress will remain close to zero for the entire life of the pavement.

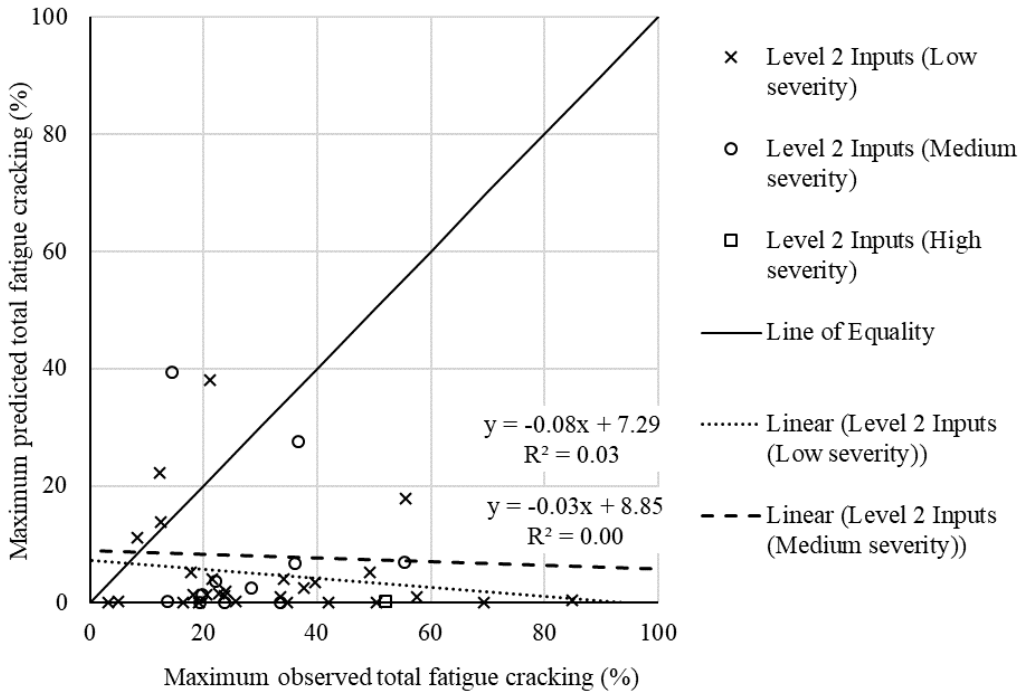

Figure 52. Predicted fatigue cracking vs. observed fatigue cracking (all sections and using Level 2 inputs).

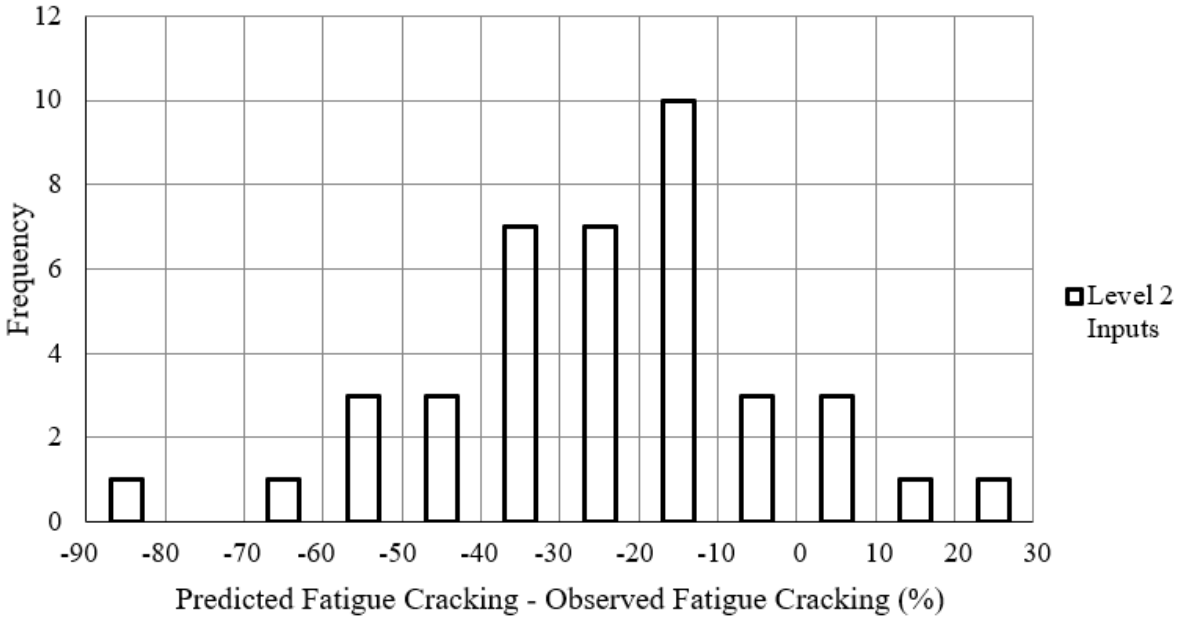

Figure 53. Difference between predicted and observed fatigue cracking (all sections and using Level 2 inputs).

Second, the predicted fatigue cracking is almost always less than the observed fatigue cracking because the predicted fatigue cracking is always less than or equal to the amount of fatigue cracking in the existing pavement, as shown in Figure 54. Altering the amount of fatigue cracking in the existing pavement shows that, given a long enough design period, the predicted fatigue cracking in the overlay asymptotically approaches the amount of fatigue cracking in the existing pavement prior to the placement of the overlay. This is shown in Figure 55. This directly contradicts the fact that the maximum observed fatigue cracking in the overlay is often greater than the fatigue cracking in the existing pavement immediately prior to the placement of the overlay. A comparison of maximum observed fatigue cracking in the overlay and fatigue cracking in the existing pavement prior to the overlay is shown in Figure 56. A paired t-test shows that maximum observed fatigue cracking in the overlay is greater than observed fatigue cracking in the existing pavement at a 95% confidence level (p-value = 0.00). Based on the observation that maximum predicted fatigue cracking in the overlay is always less than or equal to the amount of fatigue cracking in the existing pavement, it appears the fatigue cracking predicted by the reflective cracking model controls the maximum amount of fatigue cracking predicted by the AC/AC overlay design procedure when Level 2 inputs are used.

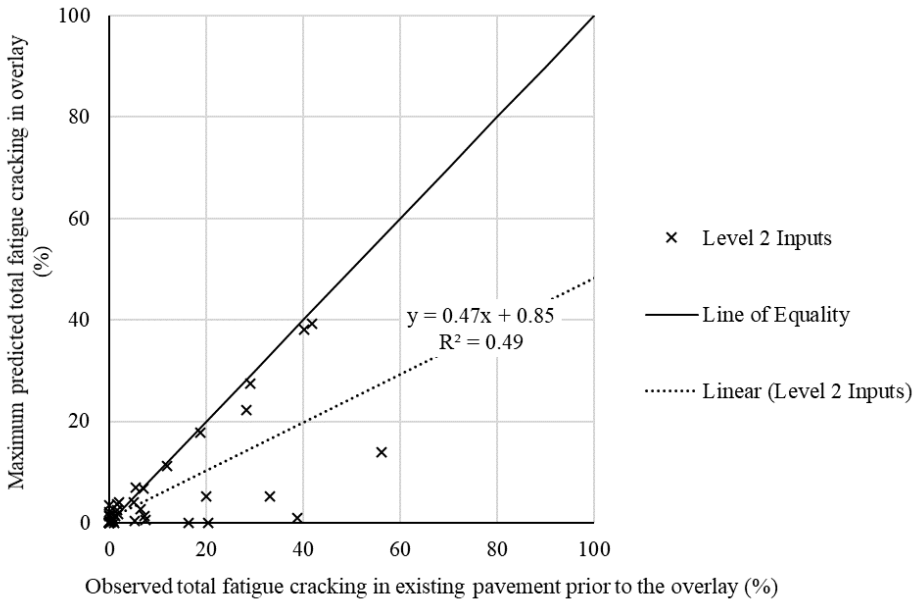

Figure 54. Predicted fatigue cracking in overlay vs. existing fatigue cracking in the existing pavement prior to overlay (all sections and using Level 2 inputs).

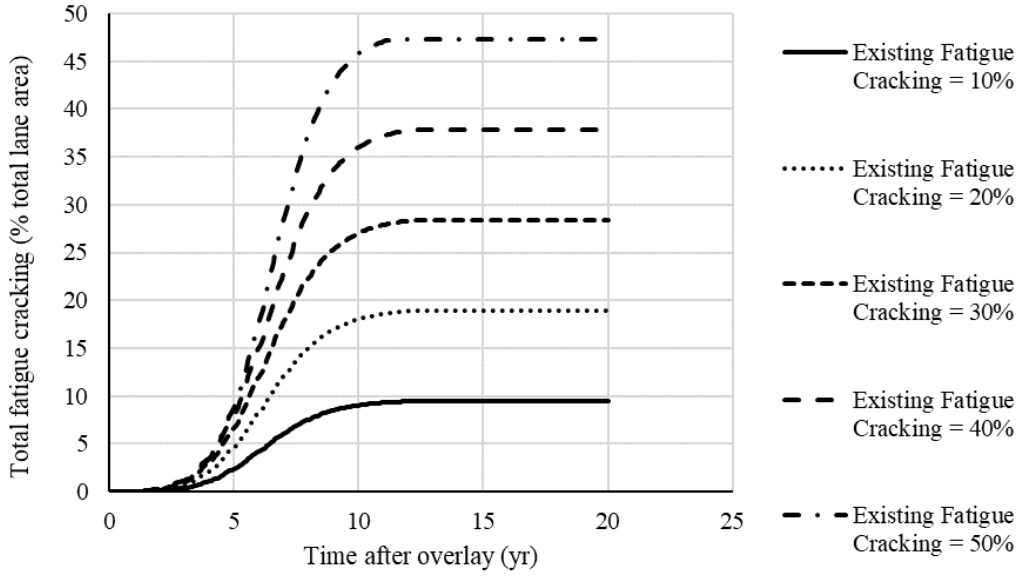

Figure 55. Predicted fatigue cracking performance history for different amounts of fatigue cracking in the existing pavement (LTPP Section 34-1003, New Jersey).

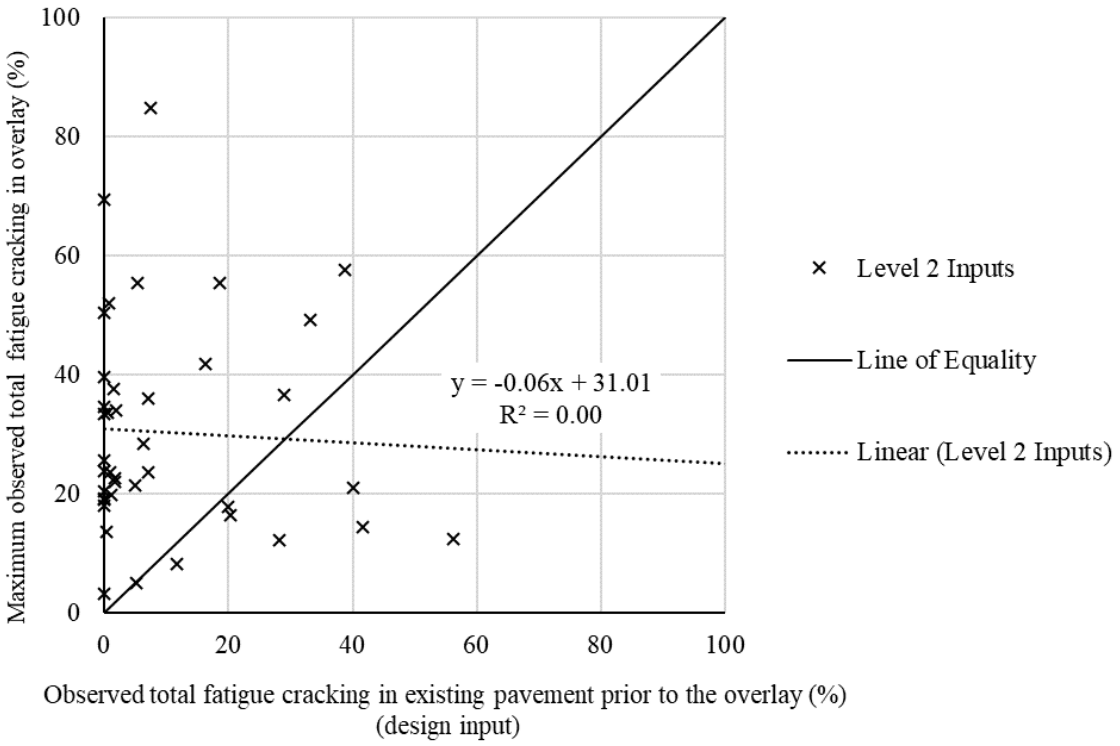

Figure 56. Observed fatigue cracking in overlay vs. fatigue cracking in the existing pavement prior to overlay (all sections and using Level 2 inputs).

Results of the evaluation showed that total rutting performance histories predicted using the AC/AC overlay design procedure and Level 2 inputs have the same shape as observed performance histories and are sometimes accurate. Both the predicted and observed total rutting performance histories show clear primary and secondary phases of rutting. With regard to accuracy, the transition between primary and secondary rutting occurs at approximately the same time for the predicted and observed total rutting, as shown in Figure 57. The difference between time to transition for predicted rutting and time to transition for observed rutting is not significantly different from 0 at a 95% confidence level (p-value = 0.41). The maximum predicted rutting is usually within 0.2 in of the maximum observed rutting, as shown in Figures 58 and 59. Based on

a paired t-test, the difference between maximum predicted total rutting and maximum observed total rutting is not statistically different from 0 at a 95% confidence level (p-value = 0.26). Note that the rutting for all LTPP sections included in this analysis was less than 0.6 in.

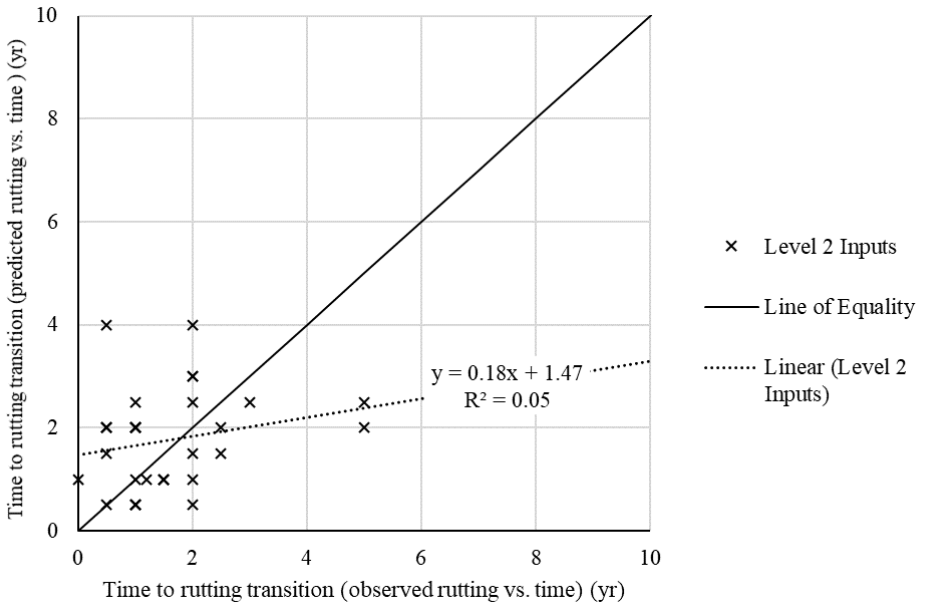

Figure 57. Predicted vs. observed time of transition between primary and secondary rutting (all sections and using Level 2 inputs).

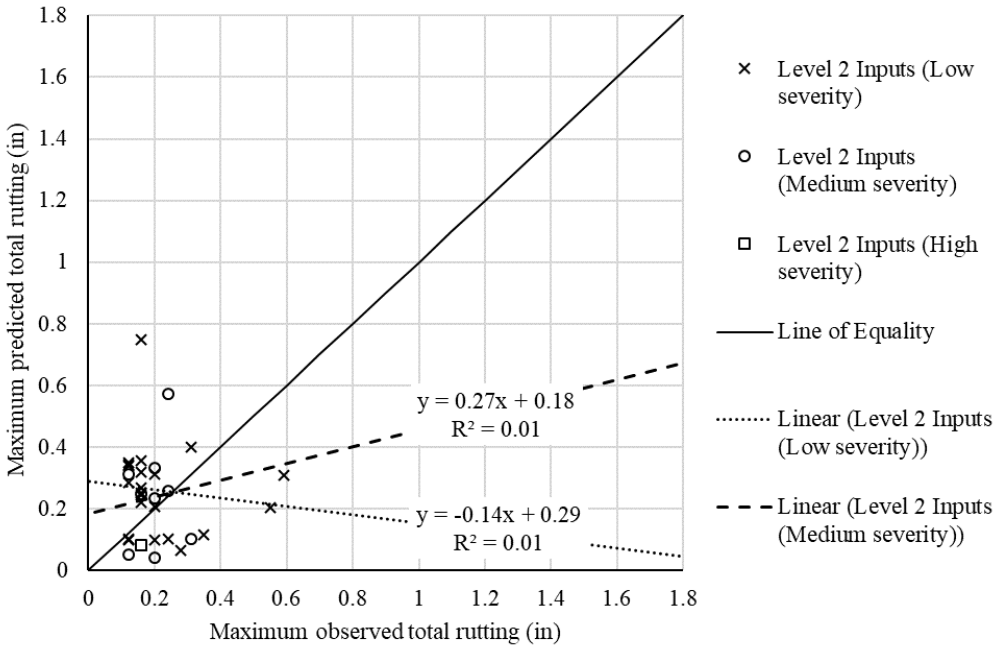

Figure 58. Predicted total rutting vs. observed total rutting (all sections and using Level 2 inputs).

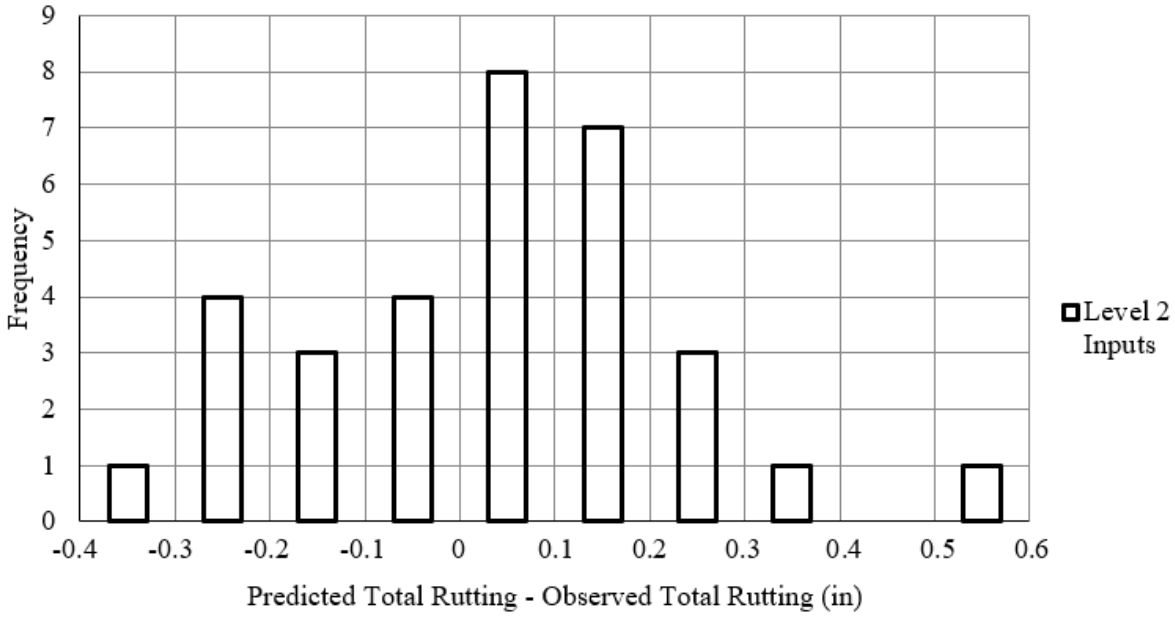

Figure 59. Difference between predicted and observed total rutting (all sections and using Level 2 inputs).

3.2.3 Sensitivity

An analysis was conducted to determine the sensitivity of distress predicted using the AC/AC overlay design procedure to several Level 2 inputs. The inputs examined were the amount (%) and severity (low, medium, or high) of fatigue cracking in the existing pavement prior to the overlay and the mixture parameters for the asphalt concrete in the existing pavement (volumetric air voids (V_a), volumetric effective binder content (V_{be}), and gradation ($P_{3/4}$, $P_{3/8}$, P_4, and P_{200})). All of these inputs affect the magnitude of the damage parameter that defines the stiffness of the asphalt concrete in the existing pavement. Each input was varied one at a time. Interactions between inputs were not examined in this analysis, except for the interaction between the amount and the severity of fatigue cracking in the existing pavement.

It was determined that the maximum amount of predicted fatigue cracking is equal to the amount of fatigue cracking in the existing pavement prior to the overlay, and the rate at which fatigue cracking develops is dictated by the severity of the fatigue cracking in the existing pavement. This is shown in Figure 60. As shown in Figure 61, predicted total rutting increases as the amount of fatigue cracking in the existing pavement prior to the overlay increases, but this effect is not significant unless the amount of fatigue cracking in the existing pavement is greater than 30%.

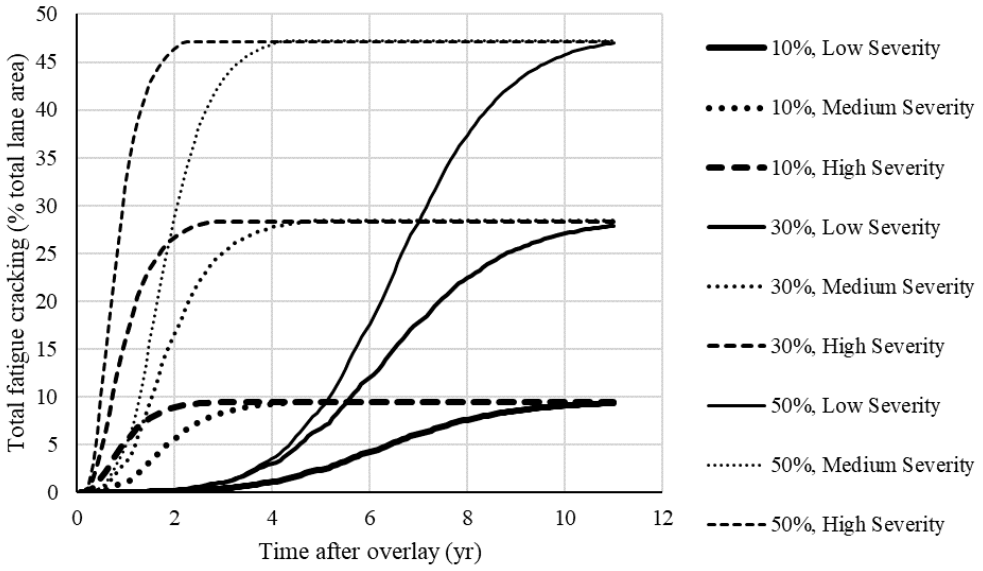

Figure 60. Sensitivity of predicted total fatigue cracking in the overlaid pavement to the amount and severity of fatigue cracking in the existing pavement (LTPP Section 23-1009, Maine).

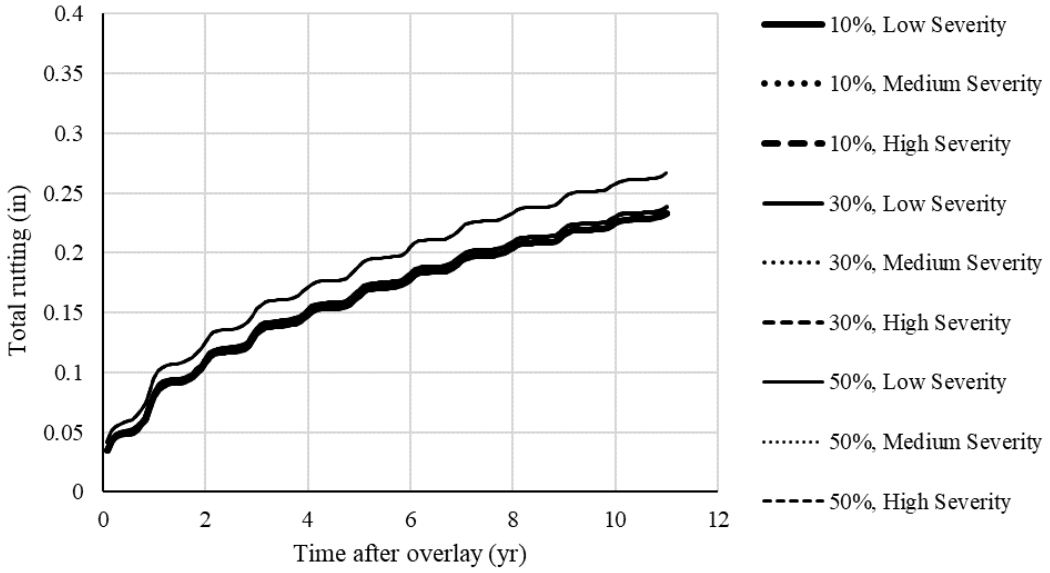

Figure 61. Sensitivity of predicted total rutting in the overlaid pavement to the amount and severity of fatigue cracking in the existing pavement (LTPP Section 23-1009, Maine).

The sensitivity of the predicted distress to the parameters used for defining stiffness with the Witczak equation (V_a, V_{be}, $P_{3/4}$, $P_{3/8}$, P_4, and P_{200}) was also assessed. Each asphalt concrete mixture parameter was varied one at a time for both the asphalt concrete in the existing pavement and the asphalt concrete in the overlay. The relationships between these parameters and the predicted distress are similar to those found for the AC/AC overlay design procedure using Level 1 inputs (Figures 25 through 30). One major difference, however, is that the mixture parameters used to define the asphalt concrete mixture in the overlay affect the amount of distress predicted by the AC/AC overlay design procedure when using Level 2 inputs. This is not the case when the AC/AC overlay design procedure is used with Level 1 inputs.

3.3 LEVEL 3 AC/AC OVERLAY DESIGN

3.3.1 Description

Similar to the AC/AC overlay design procedure using Level 2 inputs, when Level 3 inputs are used the Pavement ME AC/AC overlay design procedure quantifies damage in the existing asphalt using observed distress rather than field or laboratory testing. The condition of the existing pavement is defined using subjective pavement ratings, one rating for the structural condition and one rating for the environmental condition. The structural condition rating is correlated to the amount of fatigue cracking in the existing pavement and the environmental condition rating is correlated to the amount of transverse cracking in the existing pavement. The correlations recommended in the PennDOT Pavement ME Preliminary User Input Guide are summarized in Tables 11 and 12

(Bhattacharya et al. 2017). It is not clear how structural condition rating inputs are used to establish the amount of damage in the existing asphalt in the AC/AC overlay design procedure.

Table 11. Pavement ME Level 3 structural condition ratings.

Structural Rating	Existing alligator cracking (All levels of severity) (% total lane area)
Excellent	Less than 5
Good	5 – 15
Fair	15 – 35
Poor	35 – 50
Very Poor	Greater than 50

Table 12. Pavement ME Level 3 environmental condition ratings.

Structural Rating	Existing transverse cracking (All levels of severity) (ft/mi)
Excellent	Less than 50
Good	50 – 150
Fair	150 – 400
Poor	400 – 800
Very Poor	Greater than 800

3.3.2 Evaluation

The use of Level 3 inputs in the AC/AC overlay design procedure was evaluated using the same LTPP sections included in the analysis of the Level 2 inputs. These sections are listed in Table 10. The structural and environmental condition ratings were determined using observed distress in the existing pavement and the correlations shown in Tables 11 and 12. The Level 3 inputs used to evaluate the design procedure are summarized in Table 13. The evaluation showed that the use

of Level 3 inputs in AC/AC procedure results in an under prediction of total fatigue cracking for the majority of the sections, but to a lesser extent than when Level 2 inputs are used. This can be seen in Figures 62 and 63. Based on a paired t-test, the maximum fatigue cracking predicted when using Level 3 inputs is less than maximum observed fatigue cracking at a 95% confidence level (p-value = 0.00). The use of Level 3 inputs provides reasonable predictions for total rutting for most sections. This is shown in Figures 64 and 65. Maximum predicted total rutting is less than the maximum observed total rutting at a 95% confidence level (p-value = 0.00). Note that the rutting for all LTPP sections included in this analysis was less than 0.6 in.

Table 13. LTPP sections used to evaluate the AC/AC overlay design procedure with Level 3 inputs.

State	LTPP ID	AC Thickness (Pre-milling) (in)	AC Thickness (Post-milling) (in)	Overlay Thickness (in)	Structural Condition Rating	Environmental Condition Rating
CT	9-1803	7	7	1.75	Excellent	Very Poor
DE	10-0102	4.25	4.25	1.25	Excellent	Excellent
IL	17-A310	11.25	11.25	0.5	Excellent	Excellent
IN	18-2008	13.5	13.5	1.5	Good	Very Poor
IA	19-1044	16.25	16.25	3.75	Good	Very Poor
KS	20-0159	11.25	6	5.25	Fair	Very Poor
KS	20-1005	13	12	0.75	Fair	Excellent
KS	20-1009	11	4.5	7.5	Excellent	Very Poor
ME	23-1009	5.75	5.75	2.75	Fair	Fair
MD	24-1634	3.5	3.5	3.25	Poor	Good
NJ	34-0502	8.75	8.75	1.75	Excellent	Fair
NJ	34-0503	9.25	9.25	4.75	Excellent	Poor
NJ	34-0504	8.75	8.75	4.75	Good	Very Poor
NJ	34-0505	9	9	1.75	Good	Very Poor
NJ	34-0506	9.5	7.5	4	Good	Fair
NJ	34-0507	8.25	6.25	7.5	Excellent	Poor
NJ	34-0508	8.75	6.75	7.5	Excellent	Poor
NJ	34-0509	9.25	7.25	4.25	Excellent	Good
NJ	34-0903	9	7.5	5.5	Poor	Excellent
NJ	34-0960	9.75	7.25	4.75	Very Poor	Poor
NJ	34-0961	9.25	5.5	6.5	Fair	Poor
NJ	34-0962	9	7.5	4.25	Fair	Excellent
NJ	34-1003	7.5	5.5	2.25	Fair	Excellent

Table 13 (continued).						
State	LTPP ID	AC Thickness (Pre-milling) (in)	AC Thickness (Post-milling) (in)	Overlay Thickness (in)	Structural Condition Rating	Environmental Condition Rating
NJ	34-1011	9	6.5	4	Good	Very Poor
NJ	34-1030	6	3	4.5	Fair	Excellent
NJ	34-1033	7.5	6.75	2	Excellent	Very Poor
PA	42-1597	6.5	5	6.25	Excellent	Very Poor
VA	51-2021	7.5	7.5	1.75	Excellent	Excellent
MB	83-0502	4.5	4.5	2.75	Excellent	Good
MB	83-0503	4.75	4.75	5.25	Good	Fair
MB	83-0504	4.5	4.5	5.5	Excellent	Fair
MB	83-0505	5.25	5.25	3	Excellent	Excellent
MB	83-0506	5.5	4	3	Excellent	Excellent
MB	83-0507	4	3	6.75	Excellent	Good
MB	83-0508	3.5	2.5	6.5	Excellent	Good
MB	83-0509	5	4	3.5	Excellent	Good
MB	83-6451	4	4	2.5	Excellent	Excellent
ON	87-1622	5.5	3	4.5	Good	Very Poor
QB	89-1125	5.25	5.25	2	Poor	Fair
QB	89-1127	5	5	2.5	Excellent	Very Poor

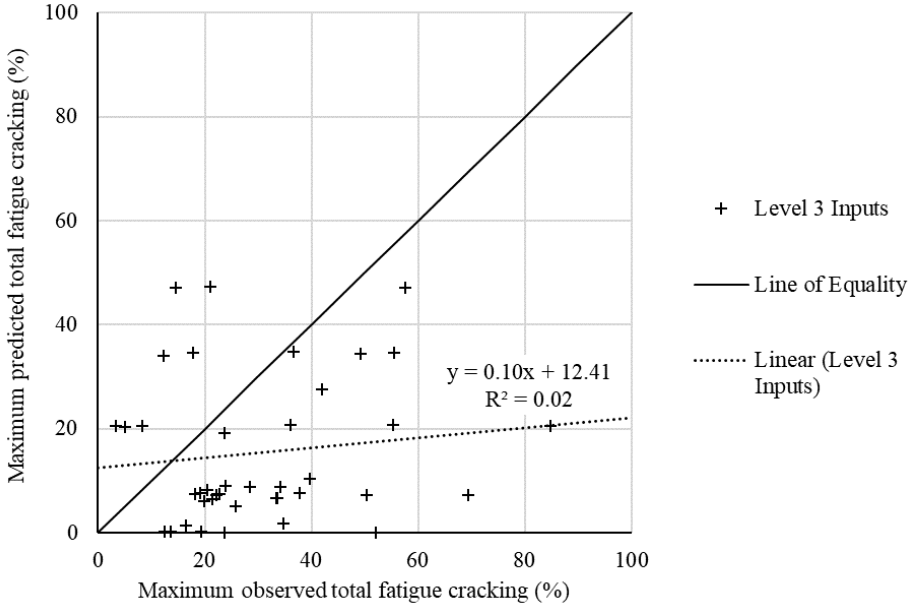

Figure 62. Predicted fatigue cracking vs. observed fatigue cracking (all sections and Level 3 inputs)

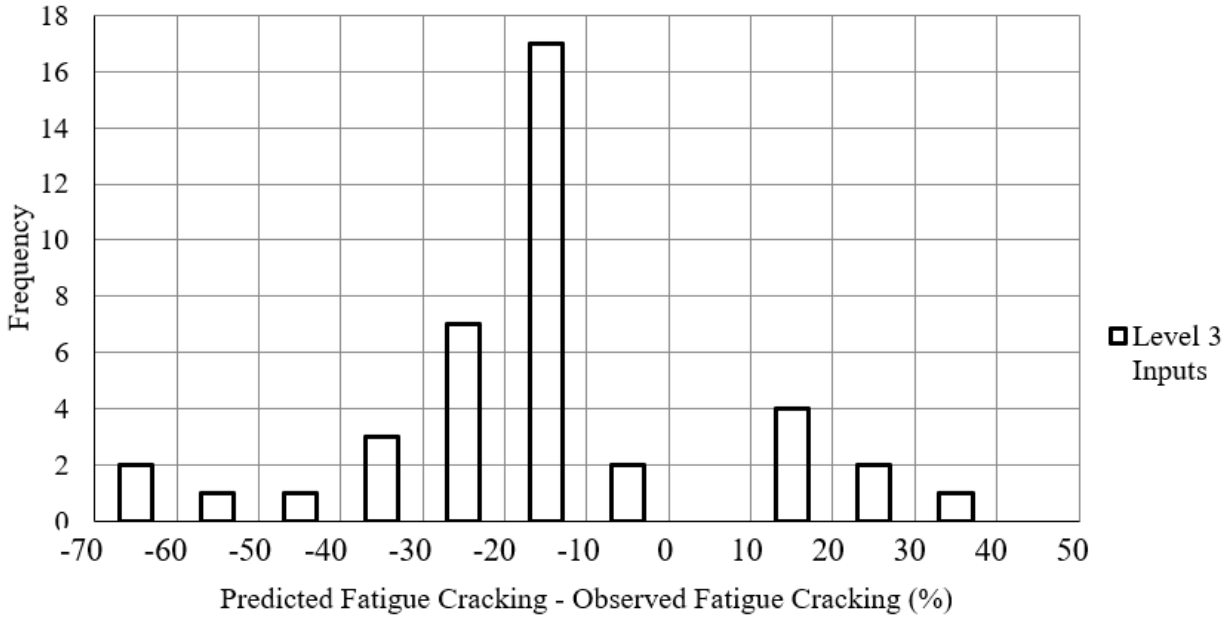

Figure 63. Difference between predicted and observed fatigue cracking (all sections and Level 3 inputs).

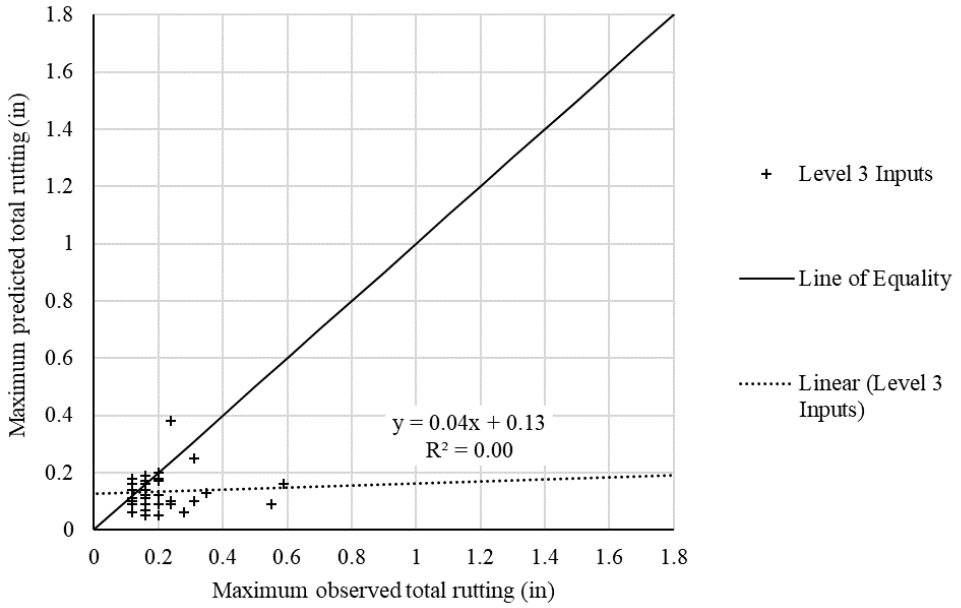

Figure 64. Predicted total rutting vs. observed total rutting (all sections and Level 3 inputs)

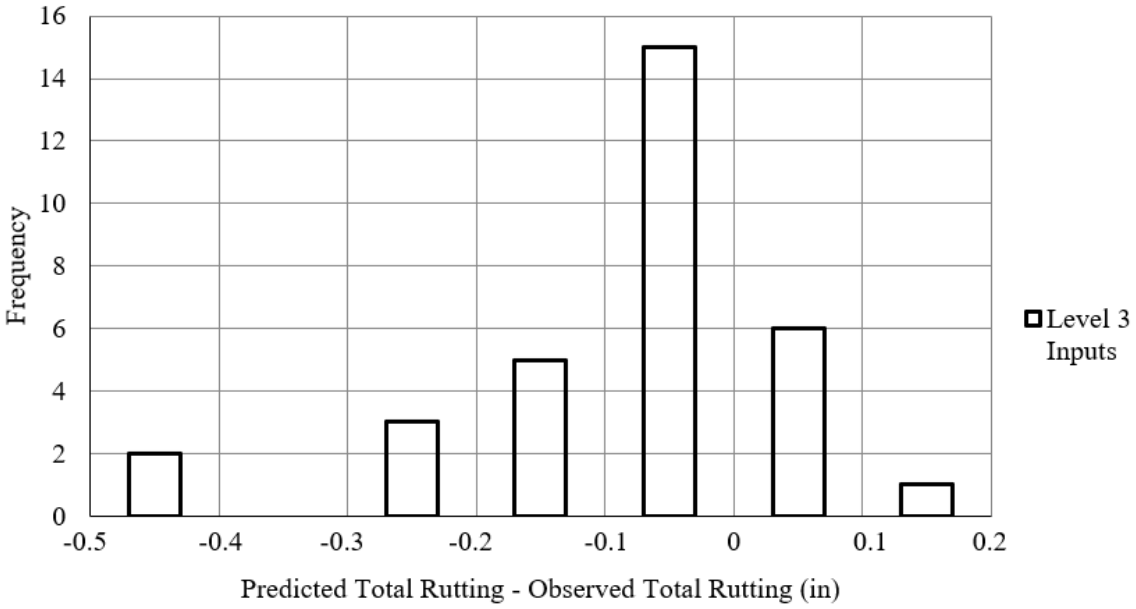

Figure 65. Difference between predicted and observed total rutting (all sections and Level 3 inputs).

3.4 CONCLUSIONS

The Pavement ME AC/AC overlay design procedure was evaluated using Level 1, Level 2, and Level 3 inputs. The results of this evaluation showed that the predicted distress is greater than the observed distress for both fatigue cracking and total rutting when Level 1 inputs are used. It is suspected that this is due to an inherent difference between E_{NDT} and $E_{Witczak}$, which are used to estimate the amount of fatigue damage in the asphalt concrete layer of the existing pavement. Additionally, when Level 1 inputs are used, the predicted distress is very sensitive to E_{NDT} and is moderately sensitive to the mixture parameters of the asphalt concrete in the existing pavement. The use of Level 2 inputs, results in a predicted fatigue cracking that is less than the observed fatigue cracking and a predicted total rutting that is approximately equal to the observed total

rutting. When using Level 2 inputs, the maximum predicted fatigue cracking in the overlay is equal to the amount of fatigue cracking in the existing pavement. The rate at which predicted cracking develops in the overlay is dictated by the severity of the fatigue cracking in the existing pavement. When Level 3 inputs are used, the predicted distress is less than the observed distress for both fatigue cracking and total rutting. These conclusions are consistent with the draft report by Ayyala, et al., which found that there is an inherent difference between E_{NDT} and $E_{Witczak}$ and that there is a large difference between fatigue cracking predicted using Level 1 inputs and fatigue cracking predicted using Level 2 inputs (Ayyala et al. 2016).

Three methods for improving the accuracy of predicted distress when using Level 1 inputs were evaluated. First, it was determined that using multiple values of E_{NDT} established at different temperatures does not change the accuracy of the predicted distress. Second, it was shown that adjustments factors for E_{NDT} can increase the accuracy of the predicted distress but cannot fundamentally change the shape of the predicted performance history. Finally, it was determined that applying adjustment factors to backcalculated unbound layer stiffness does not have a significant effect on the predicted fatigue cracking but can increase the predicted rutting.

This evaluation of the Pavement ME AC/AC overlay design procedure challenged two of the primary assumptions on which this procedure is based. These are:

1. E_{NDT} and $E_{Witczak}$ are equal at an equal temperature and load frequency.
2. FWD data can be used to quantify fatigue damage in the asphalt concrete layer of an existing pavement.

Three specific questions were defined to determine the validity of these two assumptions and to direct further research. The questions are:

1. What relationships exist between the stiffness of asphalt concrete in an existing pavement determined using these three different methods? How do differences between methods affect the pavement design obtained using Pavement ME?
2. What relationships exist between FWD parameters (parameters derived from FWD data) and fatigue damage in the asphalt concrete layer of an existing pavement? Are these relationships statistically significant?
3. Can the answers to the first two questions be used to improve the accuracy of distress predictions made using the Pavement ME AC/AC overlay design procedure?

Question 1 is addressed in Chapter 4 by directly comparing the three primary methods for determining asphalt concrete stiffness. These comparisons are performed using data from MnROAD and PennDOT pavement sections. Question 1 is also addressed in Chapter 5 using data from the LTPP database. Question 2 is addressed in Chapter 5 by performing statistical analysis on data from the LTPP database. Question 3 is addressed in Chapter 6 using the Pavement ME AC/AC overlay design procedure, additional LTPP data, and regression analyses.

4.0 METHODS FOR DETERMINING THE STIFFNESS OF ASPHALT CONCRETE IN AN EXISTING PAVEMENT

There are three main methods used for determining the dynamic modulus of asphalt concrete in an existing pavement:

1. Measure the dynamic modulus of cores taken from the existing pavement in the laboratory in accordance with AASHTO T 342 (AASHTO 2015).
2. Determine the volumetric and gradation mixture parameters in the laboratory for cores taken from the existing pavement and use this to estimate the dynamic modulus using a predictive equation.
3. Perform FWD testing and backcalculate the dynamic modulus.

The second and third methods are of particular interest because they are used within the Pavement ME AC/AC overlay design procedure to estimate fatigue damage in the asphalt concrete of the existing pavement. The design procedure assumes that these two methods are equivalent, but some existing literature and the current evaluation of the design procedure suggest that this assumption is not accurate. There is no consensus in the existing literature in defining the relationship between these methods. Thus, the relationship between methods was examined by direct comparison using field and laboratory data from two different sources. The impact of different methods on the design was also examined using Pavement ME.

4.1 COMPARISON OF DYNAMIC MODULI OBTAINED USING FIELD AND LABORATORY DATA

A comparison of the dynamic moduli obtained using the three different methods was performed using data from three AC pavement sections at MnROAD and two AC pavement sections near Pittsburgh, PA. As previously described, MnROAD is a test road maintained by the Minnesota Department of Transportation and is located on Interstate 94 in Albertville, Minnesota. The test road is divided into discrete experimental sections (cells). The two AC pavements in Pennsylvania are relatively low volume state roads maintained by the PennDOT, District 11.

Data from MnROAD Cells 15, 16, and 21 were used to establish the asphalt concrete stiffness vs. temperature relationships using each of the three methods previously described (MnDOT 2016). All cells were constructed in 1993 and removed in 2008 (Johnson et al. 2009). The pavement structure for these cells is detailed in Table 14.

Table 14. Pavement structure of MnROAD cells.

	Cell 15	Cell 16	Cell 21
Total Asphalt Concrete Thickness (in)	11.0	8.0	8.0
Base Thickness (in)	N/A	28	23
Base Material	N/A	Class 3. Sp. Granular Base[1]	Class 5 Sp. Granular Base[1]
Subgrade AASHTO Classification	A-6	A-6	A-6
Depth to Rigid Layer (ft)	13	13	11

[1] See MnDOT construction specifications for additional information on these materials (MnDOT 2018).

The dynamic modulus of the asphalt concrete in the existing pavement was measured for four cores extracted from Cell 21. A master curve was established based on an average of the four cores tested. Additional cores were taken from each section and mixture parameters for each asphalt mixture were measured in the laboratory. The binder grade for each asphalt mixture was established from construction records. Additionally, representative complex modulus and phase angle data for each binder grade were determined by testing extracted binder. This information is summarized in Table 15. All asphalt mixtures were dense-graded. FWD testing was performed several times over the life of each cell and the asphalt temperature was measured using thermocouples. Backcalculation of the FWD data was performed using Evercalc 5.0. A stiff layer was assumed, representing the high-water table at MnROAD, and the depth to the stiff layer was obtained using the "line of influence" method (Rhode and Scullion 1990). The seed values used for backcalculation were based on typical seasonal values for the MnROAD construction materials (Ovik et al. 2000). The stiffness of the asphalt concrete in the existing pavement was backcalculated at two stations within each cell.

Table 15. Asphalt mix parameters of MnROAD cells.

Cell	15			16			21		
Asphalt Course	Wearing	Binder	Base	Wearing	Binder	Base	Wearing	Binder	Base
Thickness (in)	1.25	4.5	5.5	1.5	3.25	3.0	1.5	3.25	3.0
Binder Grade	AC-20 (PG 64-22)			AC-20 (PG 64-22)			Pen 120/150 (PG 58-28)		
Air Voids (V_a) (%)	8.3	9.9	7.9	5.4	8.1	9.6	4.2	5.6	6.8
Effective Binder Content (V_{be}) (%)	10.5	10.4	10.9	10.3	9.9	10.0	11.8	11.7	11.4
P_{38} (%)[1]	100			100			99.9		
P_{34} (%)[1]	85.6			84.3			84.3		
P_4 (%)[1]	69.5			68.2			68.6		
P_{200} (%)[1]	4.40			4.53			4.76		

[1] Gradation information represents the entire asphalt core. Gradation information for individual asphalt concrete courses was not available.

In order to exclude the effects of damage and post-construction compaction due to traffic on the stiffness of the asphalt concrete, only FWD test data collected at mid-lane was used. The assumption that there was minimal damage in the asphalt at the mid-lane locations was confirmed through distress surveys. Very little fatigue cracking was observed in any of the cells, but significant longitudinal cracking in the wheelpath and transverse cracking was observed in all cells (MnDOT 2016). Furthermore, the effect of asphalt binder aging on asphalt concrete stiffness was accounted for by using only FWD data collected between 1996 and 2005. All cells were constructed in 1993, and it was assumed that any significant increase in asphalt concrete stiffness due to binder aging would have occurred by 1996 when FWD testing began. The asphalt concrete stiffness determined using the Witczak equation was calculated with binder aging (using the binder

aging models described in Chapter 3) and without binder aging (Mirza 1993). The load frequency of the Dynatest FWD used at MnROAD was assumed to be 30 Hz, since this is the recommended value provided by the developers of Pavement ME (Rao and Von Quintus 2015).

The three methods for determining the stiffness of asphalt concrete in the existing pavement were compared using stiffness vs. temperature plots. These are shown in Figures 66, 67, and 68 for Cells 15, 16, and 21, respectively. The stiffness of the asphalt concrete layer was backcalculated at two different locations in each cell. It was also estimated using the Witczak equation and the volumetrics and aggregate gradations obtained from testing field cores. The binder grade, shown in Table 15, was assumed based on the binder grade provided in the original mixture design information. Cores were extracted at mid-lane so that dynamic modulus testing could be performed in the laboratory only for Cell 21. A FWD load frequency of 30 Hz was used to generate the stiffness vs. temperature curves shown in Figures 66 through 68 for the Witczak equation and dynamic modulus testing methods.

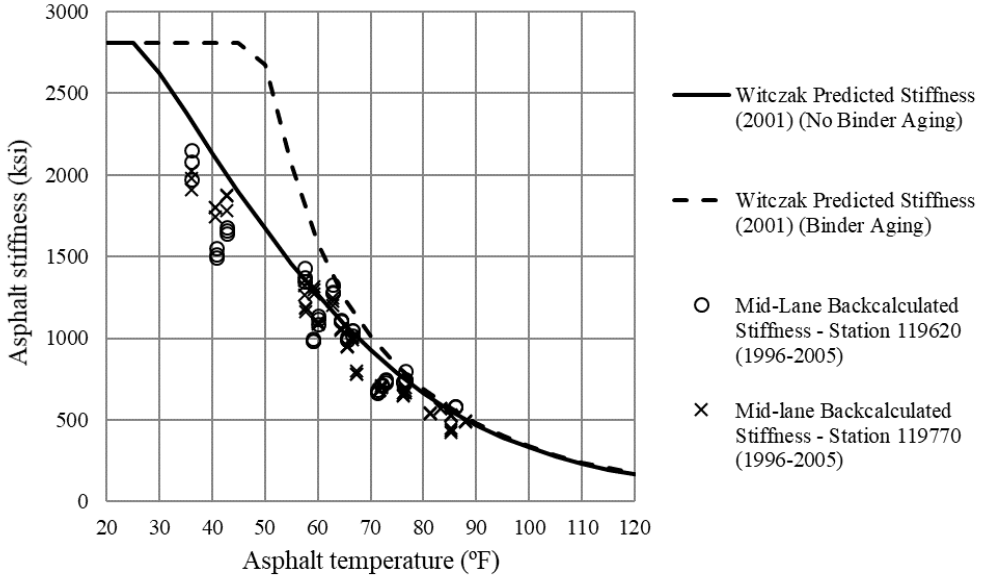

Figure 66. Stiffness of the asphalt concrete in the existing pavement (MnROAD Cell 15).

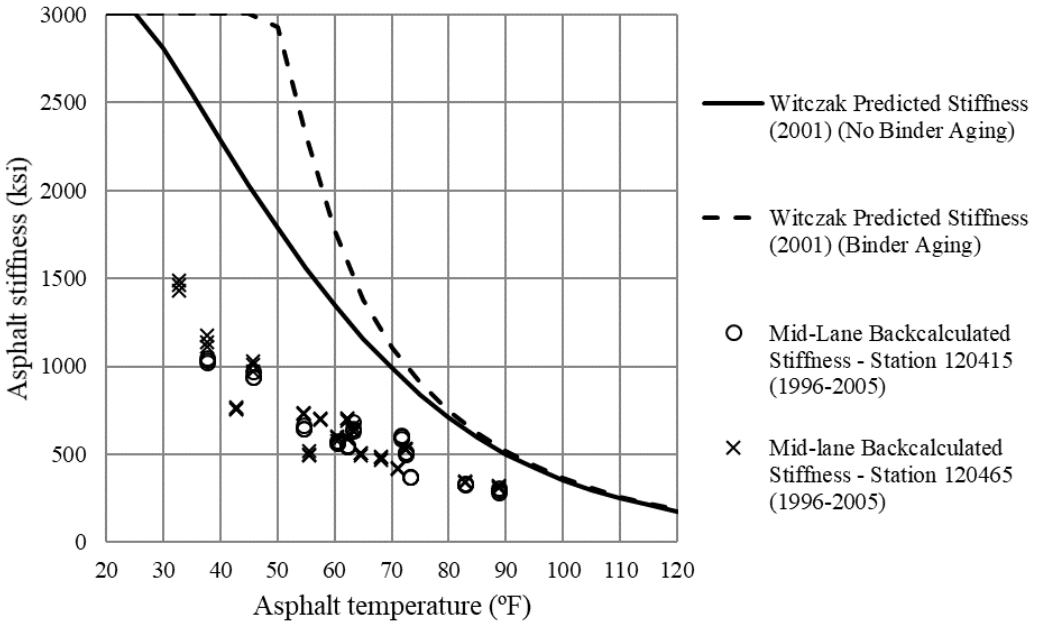

Figure 67. Stiffness of the asphalt concrete in the existing pavement (MnROAD Cell 16).

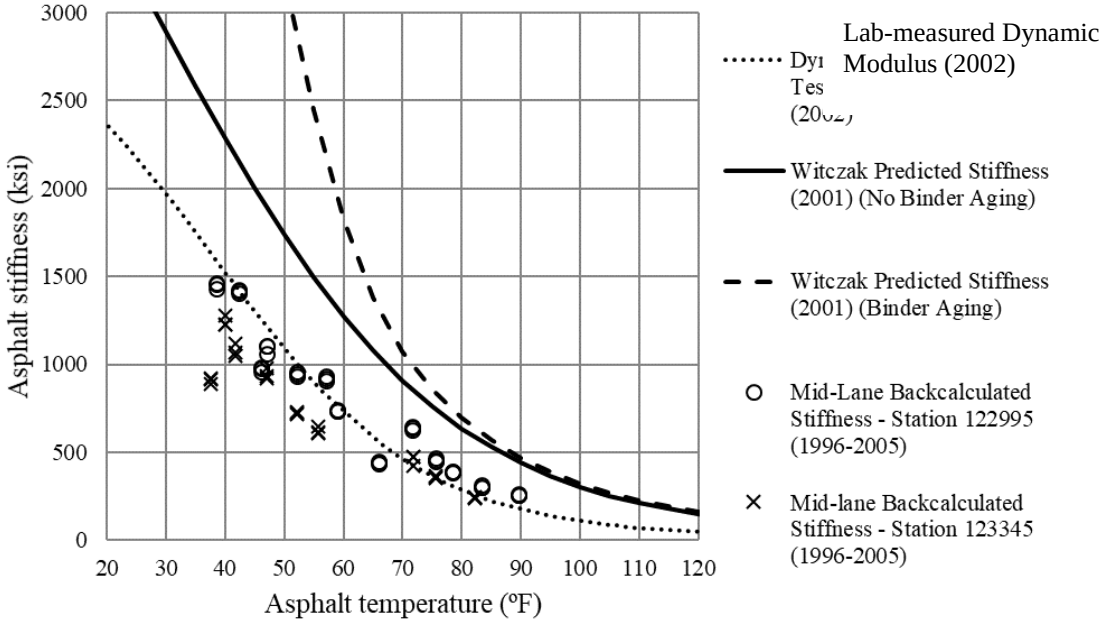

Figure 68. Stiffness of the asphalt concrete in the existing pavement (MnROAD Cell 21).

For Cell 15, the backcalculated stiffness of the asphalt concrete is similar to the stiffness predicted using the Witczak equation if binder aging is neglected. For Cells 16 and 21, however, the backcalculated stiffness is lower than the Witczak stiffness at all asphalt temperatures. This trend is consistent with a study performed by Clyne et al. for cells on the Low Volume Road at MnROAD (Clyne et al. 2004). Additionally, the difference between the curves with and without binder aging increases as the asphalt temperature decreases. The asphalt stiffness predicted with binder aging considered reaches a maximum value at approximately 50ºF. For Cell 21, the backcalculated stiffness is similar to the stiffness obtained based on the dynamic modulus testing performed on cores from this cell. This trend agrees with observations made at the CEDEX test track (Mateos et al. 2012), but not with observations by Clyne et al. Finally, the stiffness estimated using the Witczak equation, both corrected and not corrected for aging, is greater than the stiffness obtained from laboratory testing for Cell 21. This is consistent with observations made for the sections in Virginia (Loulizi et al. 2008).

Data collected at two PennDOT AC pavement sections, State Route 18 (SR 18), in Beaver Falls, Pennsylvania and State Route 2001 (SR 2001), near Monongahela, Pennsylvania, was also used to establish stiffness vs. temperature relationships using each of the three methods. The section on SR 18 section was constructed in 2007 while the section on SR 2001 was constructed in 2015. For both sections, FWD testing was performed in June, 2016 and coring of the asphalt concrete layer was performed in July, 2016. The pavement structures for both Pennsylvania sections are summarized in Table 16. The layer thickness information was obtained from the PennDOT Pavement History web application and confirmed by coring and DCP testing (PennDOT 2015). The subgrade soil classification was estimated using the Arizona State Soil Unit Map web application (Zapata and Cary 2012).

Table 16. Pavement structure of SR 18 and SR 2001 sections in Pennsylvania.

	SR 18	SR 2001
Total Asphalt Concrete Thickness (in)	14.5	14.5
Base Thickness (in)	8	6
Base Material	PennDOT 2A Granular Base	PennDOT 2A Granular Base
Subgrade AASHTO Classification	A-4	A-6
Depth to Stiff Layer (ft)	Infinite	Infinite

For both Pennsylvania sections, the asphalt concrete surface consisted of sub-layers, or courses: wearing course, binder course, and base course. The dynamic modulus of the asphalt concrete base course was measured for six cores, three taken from the outer wheelpath and three taken from mid-lane. Using only the mid-lane cores, representative master curves were developed for the asphalt concrete base course for each section. Additional laboratory testing was performed to determine the volumetric properties of the asphalt concrete base course. The aggregate gradation and binder grade of the asphalt concrete base course were assumed based on information obtained from PennDOT (Bhattacharya et al. 2017). The dynamic modulus, mixture volumetric properties, aggregate gradation, and binder grade of the wearing and binder asphalt concrete courses were also based on information obtained from PennDOT (Bhattacharya et al. 2017). All asphalt mixtures for the Pennsylvania sections were dense-graded. The asphalt concrete mix information for the Pennsylvania sections is summarized in Table 17.

Table 17. Asphalt mix parameters of SR 18 and SR 2001 sections in Pennsylvania.

Section	SR 18			SR 2001		
Asphalt Course	Wearing	Binder	Base	Wearing	Binder	Base
Thickness (in)	1.5[1]	2.5[1]	10.25[1]	1.5[1]	2.5[1]	10.5[1]
Binder Grade	PG 64-22			PG 64-22		
Air Voids (V_a) (%)	7.0	7.0	8.6[1]	7.0	7.0	6.0[1]
Effective Binder Content (V_{be}) (%)	12.0	9.9	4.8[1]	12.0	9.9	8.1[1]
P_{38} (%)	100	97.5	87.8	100	97.5	87.8
P_{34} (%)	96.8	69.3	53.7	96.8	69.3	53.7
P_4 (%)	62.8	44.7	38.2	62.8	44.7	38.2
P_{200} (%)	4.78	4.62	3.98	4.78	4.62	3.98

[1] Thickness of all asphalt concrete courses and V_a and V_{be} of the base course were measured in the laboratory. All other values were assumed based on information provided by PennDOT.

For each Pennsylvania section, FWD testing was performed continuously for approximately 12 hours at 11 stations distributed longitudinally along the pavement section. Testing was performed in passes, alternating between a pass where tests were performed in the outer wheelpath and then at mid-lane. The asphalt temperature during FWD testing was measured using temperature holes drilled in the asphalt concrete. Backcalculation of the FWD data was performed using Evercalc 5.0. For SR 18, the granular base and subgrade were combined for the backcalculation analysis and an infinite subgrade was assumed. For SR 2001, the granular base and subgrade were treated as separate layers in the backcalculation analysis and an infinite subgrade was assumed. The seed values used for backcalculation were based on asphalt concrete dynamic modulus information provided by PennDOT (Bhattacharya et al. 2017) and on the results of DCP testing performed at both sections.

As with the MnROAD cells, only FWD test data collected at mid-lane was used to reduce the effects of damage and post-construction compaction due to traffic on the stiffness of the asphalt

concrete. The assumption that there was minimal damage in the asphalt at the mid-lane was confirmed through distress surveys. Very little cracking was observed in either of the Pennsylvania sections. The stiffness was estimated using Witczak equation and was adjusted to account for aging of the binder (using the binder aging models detailed in Chapter 3). The stiffness was also estimated without consideration of binder aging (Mirza 1993). A Dynatest FWD was used for all FWD testing on the Pennsylvania sections, therefore a load frequency of 30 Hz was assumed for the FWD.

The three methods for determining the stiffness of the asphalt concrete in the existing pavement were compared using stiffness vs. temperature plots. These are shown in Figures 69 and 70 for sections SR 18 and SR 2001, respectively. As previously described, the stiffness of the asphalt concrete was backcalculated at 11 different locations in each section. It was also predicted using the Witczak equation based on the volumetrics obtained from testing field cores and assumed binder grades and aggregate gradations (Table 17). Finally, the weighted average dynamic modulus of the asphalt concrete layer was calculated using dynamic modulus data from laboratory testing of the asphalt concrete base course and dynamic modulus data provided by PennDOT for the asphalt concrete wearing and binder courses (Bhattacharya et al. 2017). Weights were assigned based on the thickness of each asphalt concrete layer. The weighted average dynamic modulus represents the measured dynamic modulus of all asphalt concrete layers combined. An FWD load frequency of 30 Hz was used to generate the stiffness vs. temperature curves shown in Figures 69 and 70 for the Witczak equation and dynamic modulus testing methods.

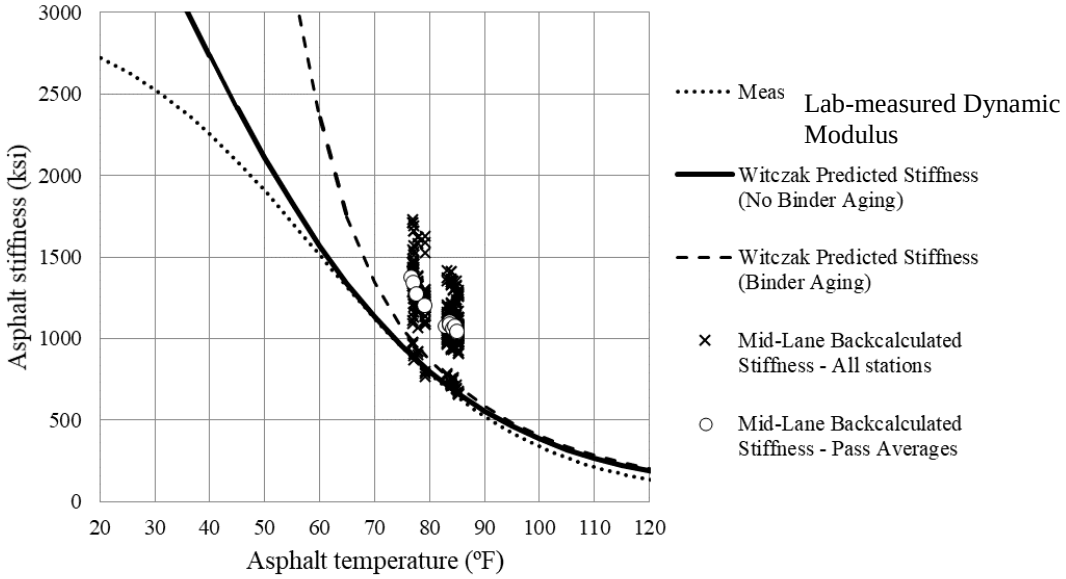

Figure 69. Stiffness of the asphalt concrete in the exiting pavement (SR 18, Pennsylvania).

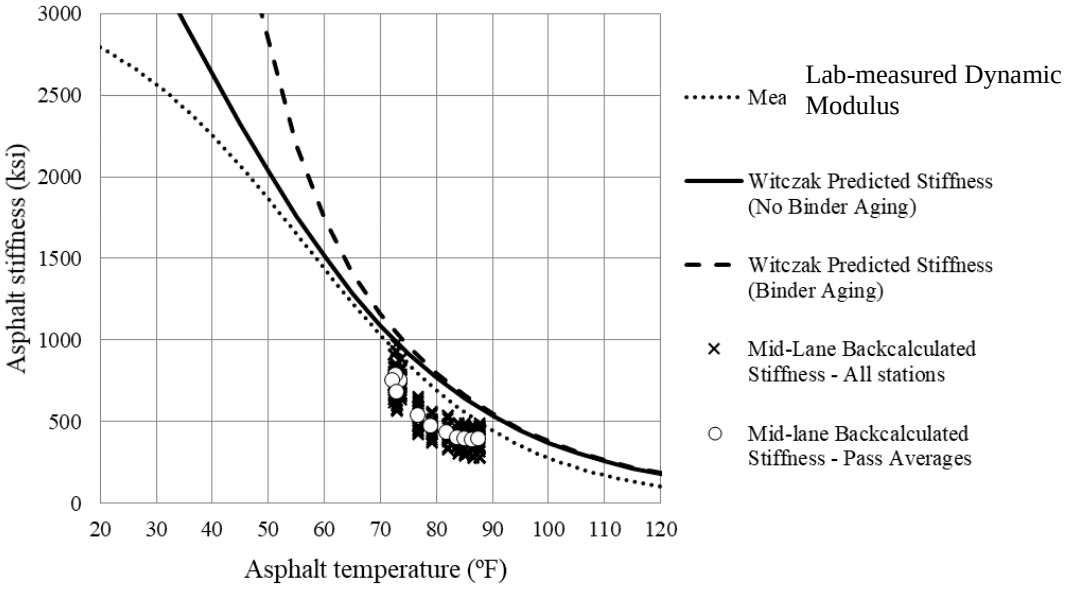

Figure 70. Stiffness of the asphalt concrete in the existing pavement (SR 2001, Pennsylvania).

The measured dynamic modulus is nearly identical for both Pennsylvania sections. This is expected because both pavement structures use the same mixture designs, including the same asphalt binder for all mixtures for each asphalt layer, and have similar layer thicknesses. One would expect the measured stiffness from SR 18 to be greater than that from SR 2001 due to binder oxidation because SR 18 is older (SR 18 was 9 years old at the time of testing and SR 2001 was 1 year old). This is not seen, however, because binder oxidation only affects the top few inches of the asphalt concrete, and only the base course was tested for both Pennsylvania sections. The stiffness estimated with the Witczak equation without binder aging considered is also nearly identical for both Pennsylvania sections. Again, this is because both pavement structures use the same mixture designs and have similar pavement structures. The stiffness estimated using the Witczak with binder aging considered is slightly greater at low asphalt temperatures for SR 18 than for SR 2001 because SR 18 is 8 years older than SR 2001. Additionally, the stiffness estimated using the Witczak equation with binder aging considered is greater than stiffness predicted without binder aging being considered for both SR 18 and SR 2001. As was seen with the MnROAD cells, the difference between the curves when binder aging is considered and is not considered increases as the asphalt temperature decreases. The stiffness predicted using the Witczak equation reaches a maximum value at approximately 50ºF when binder aging is not considered.

The backcalculated stiffness of the asphalt concrete layer is up to 700 ksi greater for SR 18 than for SR 2001 at the same asphalt temperature. This is unexpected because the two Pennsylvania sections are so similar. The large difference in backcalculated stiffness could be due to more binder oxidation in SR 18 than in SR 2001. However, such a large increase in stiffness would require most of the thickness of the asphalt to be oxidized, and this is not supported by the

measured dynamic modulus. Additionally, there is much more variability in the backcalculated stiffness at SR 18 than at SR 2001. This may be due to damage in the asphalt concrete at mid-lane at SR 18. The section of SR 18 tested is on an inclined curve, and large wheel wander could result in more damage at mid-lane than would occur on a straight and level section.

For SR 18, the backcalculated stiffness is greater than the stiffness predicted using the Witczak equation. For SR 2001, the backcalculated stiffness is less than the stiffness predicted using the Witczak equation. This is true for both when accounting for and when not accounting for binder aging when using the Witczak equation. There are three possible explanations for this difference between the Pennsylvania sections. First, there may be some difference in the stiffness estimated using the Witczak equation between sections. The air void content is higher and the effective binder content is lower for SR 18 than for SR 2001, as shown in Table 17, but this does not seem to have a significant effect on the predicted stiffness between the sections. Second, binder aging may cause the backcalculated stiffness to be greater for SR 18 than for SR 2001. Third, the properties of the pavement structure (other than asphalt concrete layer thickness, the asphalt concrete mix properties, and the asphalt binder oxidation) may affect the load frequency of the FWD. This would affect the relationship between the backcalculated asphalt stiffness and the stiffness estimated using the Witczak, which was determined based on an assumed FWD load frequency of 30 Hz. The relationship between pavement structure and FWD load frequency has not yet been fully investigated.

Finally, for both SR 18 and SR 2001, the stiffness estimated using the Witczak equation without consideration of binder aging and the measured dynamic modulus are very similar at asphalt temperatures above approximately 50ºF. The stiffness estimated using the Witczak

equation and adjusted for binder aging are similar to the measured dynamic modulus at asphalt temperatures above approximately 70ºF.

There are two notable results gleaned from comparing the three methods. First, based on the Pennsylvania sections, there is more variability in the backcalculated stiffness along a pavement section when the section has more damage. This makes it more difficult to develop an appropriate design input using the backcalculated stiffness of damaged asphalt concrete. Second, based on data from four of the five sections examined, the backcalculated stiffness is less than or equal to the stiffness estimated using the Witczak equation across a range of temperatures. This suggests that there is some inherent difference between these two values, which are assumed to be equal when used in Pavement ME to quantify fatigue damage in the asphalt concrete.

4.2 COMPARISON OF METHODS USING PAVEMENT ME

Comparing the three methods for determining the stiffness of asphalt concrete in an existing pavement revealed that each method produces different results. The Pavement ME new flexible pavement design module was used to quantify how the differences between methods affect predicted performance. The new flexible pavement design module was used because it allows the asphalt stiffness to be defined directly using each of three methods. Inputs in the AC/AC overlay procedure do not allow the stiffness of the asphalt concrete in the existing pavement to be defined in this way. Only the three MnROAD cells were used in this analysis. Each cell was modeled using the pavement structures summarized in Table 14. The stiffness of the asphalt concrete was entered into Pavement ME differently for each method of determining the asphalt concrete stiffness.

Dynamic moduli measured in the lab were entered directly into Pavement ME using the Level 1 dynamic modulus input fields. Complex modulus and phase angle data obtained from laboratory testing of extracted asphalt binder was entered into the Level 1 input fields for these properties. Pavement ME uses a statistical regression to construct the dynamic modulus master curve for the asphalt concrete from the asphalt dynamic modulus, binder complex modulus, and binder phase angle. For the Witczak equation, the volumetric properties and aggregate gradation of the asphalt concrete were entered into the Level 3 input fields and the binder grade was selected using the drop-down menus. The asphalt concrete mixture volumetric data and aggregate gradation data were entered separately for each asphalt lift.

For backcalculation, "calibration" was required to convert the backcalculated moduli to Level 1 inputs for Pavement ME. First, a master curve representative of the in-situ asphalt was created using the Witczak equation with the volumetrics, aggregate gradation, and binder grade for each asphalt lift. Binder aging models were not used. Next, the backcalculated stiffness and the asphalt stiffness predicted by the representative master curve were plotted on the same set of stiffness vs. temperature axes. Finally, the frequency at which the Witczak stiffness was calculated was changed until the Witczak stiffness was approximately equal to the backcalculated stiffness across a range of temperatures. This "matching frequency" was found to be 1.08 Hz for Cell 21, Station 122995, as shown in Figure 71.

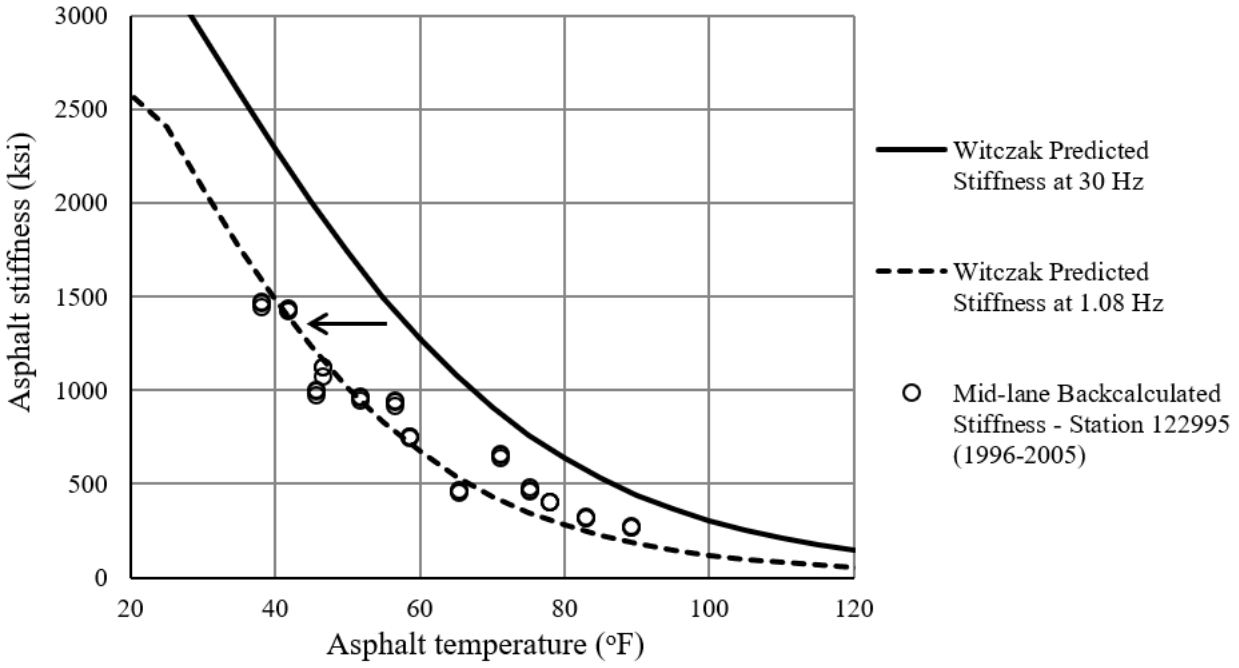

Figure 71. Adjusting load frequency to match Witczak predicted moduli with backcalculated moduli (MnROAD Cell 21, Station 122995).

The representative master curve was then used to create a matrix of asphalt dynamic moduli at several combinations of temperature and load frequency that could be used as Level 1 Pavement ME inputs. The frequencies for this matrix were shifted an amount equal to the logarithmic difference between the frequency initially used to predict stiffness using the Witczak equation (30 Hz in Figure 71) and the "matching frequency." This master curve calibration procedure was performed for each station where moduli were backcalculated, and a separate Pavement ME analysis was run for each station. The matching frequency for Cell 15 is significantly higher than for Cells 16 and 21, which have roughly equal matching frequencies, as show in Table 18. This trend roughly correlates with the asphalt concrete layer thickness.

Table 18. Matching frequencies for MnROAD cells.

Cell	Station	Matching Frequency (Hz)	Average Asphalt Concrete Thickness (in)
15	119620	14.6	11.25
15	119770	15.4	11.25
16	120415	0.305	8.0
16	120465	0.257	8.0
21	122995	1.08	7.75
21	123345	0.365	7.75

The Pavement ME inputs for Cell 21 for the dynamic modulus testing on field cores, Witczak equation, and backcalculation methods are summarized in Tables 19 through 22. Pavement ME inputs for Cells 15 and 16 were established in the same manner as for Cell 21.

Table 19. Dynamic modulus testing method Level 1 stiffness inputs (MnROAD Cell 21).

	Dynamic Modulus (ksi)			
	Frequency (Hz)			
Temperature (ºF)	1	5	10	25
14	1513	1941	2382	2524
39	460	788	1407	1540
68	99	257	331	424
104	17	36	57	131
130	4	17	29	71

Table 20. Witczak Equation method Level 3 stiffness inputs (MnROAD Cell 21).

	Asphalt Course		
Property	Wearing	Binder	Base
Thickness (in)	1.5	3.25	3.0
Binder Grade	Pen 120-150	Pen 120-150	Pen 120-150
Air Voids (V_a) (%)	4.2	5.6	6.8
Effective Binder Content (V_{be}) (%)	11.8	11.7	11.4
P_{38} (%)[1]	99.9		
P_{34} (%)[1]	84.3		
P_4 (%)[1]	68.6		
P_{200} (%)[1]	4.76		

[1] Gradation information represents entire asphalt core. Gradation information for individual lifts was not available.

Table 21. Backcalculation method Level 1 stiffness inputs (MnROAD Cell 21, Station 122995.

Matching frequency = 1.08 Hz).

	Dynamic Modulus (ksi)			
	Frequency (Hz)			
Temperature (ºF)	1.39	2.78	27.75	138.76
14	1820	1990	2561	2953
39	864	989	1469	1848
68	190	232	426	624
104	46	58	116	186
130	16	20	39	62

Table 22. Lab testing method and backcalculation method Level 1 binder inputs (MnROAD Cell 21).

Temperature (ºF)	Binder Complex Modulus (psi)	Phase Angle (degrees)
95	18.3	63.9
113	3.59	70.2
140	0.331	80.1

A design period of 15 years was used for all Pavement ME analyses because all cells were constructed in 1993 and removed in 2008. Traffic data from MnROAD were used to establish traffic inputs that represented the actual traffic for Cells 15, 16, and 21 between 1993 and 2008. The initial average annual daily truck traffic (AADTT) was set at 1391 in the design lane. Vehicle class distributions, growth rates by vehicle class, and monthly adjustment factors were also established using MnROAD traffic data. The same traffic inputs were used for all Pavement ME analyses. The climate inputs were based on weather data from the Crystal Airport northwest of Minneapolis, Minnesota. The default threshold values for predicted distress were used along with a 50% reliability.

Table 23 shows the predicted distress and the observed surface distress for Cells 15, 16, and 21. All predicted distress is reported at a 50% level of reliability for comparison to observed distress. If the predicted distress exceeds the threshold criterion, the approximate pavement age at which this occurred is listed in parentheses. All observed distress measurements are based on distress surveys performed in April, 2008, which is at the end of the pavement life (MnDOT 2016). Very little fatigue cracking was recorded on the distress surveys. Cell 15 had 0.5% fatigue cracking by total lane area, and Cells 16 and 21 both had 0% fatigue cracking. Additionally, the distress surveys do not distinguish between bottom-up and top-down cracking. Thus, Table 23 shows total longitudinal cracking measured in the wheelpath (ft/mi) for each cell, rather than distinguishing between bottom-up and top-down cracking.

Table 23. Predicted and measured distress for MnROAD Cells 15, 16, and 21.

.		Distress				
	Method for Determining Existing Asphalt Stiffness	Total Rutting (in)	AC Rutting (in)	AC Thermal Cracking (ft/mi)	AC Bottom-up cracking (%)	AC Top-down Cracking (ft/mi)
	Threshold	0.75	0.25	1000	25	2000
Cell 15	Witczak Equation	0.74	0.22	1296 (9 yr)	1.72	0
	Backcalculation Station 119620	0.72	0.20	872	2.20	0
	Backcalculation Station 119770	0.73	0.20	872	2.23	0
	Observed Distress	0.29	Not measured	4615	5481 (ft/mi)[1]	
Cell 16	Witczak Equation	0.83 (10 yr)	0.28 (12 yr)	1613 (7 yr)	6.91	25
	Backcalculation Station 120415	1.26 (3.5 yr)	0.60 (3 yr)	1497 (7.5 yr)	12.40	3400 (10.25 yr)
	Backcalculation Station 120465	1.29 (3.25 yr)	0.62 (3 yr)	1497 (7.5 yr)	13.00	3700 (8.5 yr)
	Observed Distress	0.39	Not measured	5945	2988 (ft/mi) [1]	
Cell 21	Witczak Equation	0.88 (7 yr)	0.30 (10.5 yr)	355	2.27	0
	Backcalculation Station 122995	1.14 (4 yr)	0.50 (3.5 yr)	1189 (13 yr)	2.97	250
	Backcalculation Station 123345	1.33 (3 yr)	0.65 (2.25 yr)	1189 (13 yr)	3.97	400
	Dynamic Modulus Test	1.07 (5 yr)	0.45 (4.5 yr)	1189 (13 yr)	2.7	200
	Observed Distress	0.53	Not measured	2017	2999 (ft/mi) [1]	

[1] Distress surveys do not distinguish between top-down and bottom-up cracking. The observed distress corresponding to both bottom-up and top-down cracking is total longitudinal cracking in the wheelpath (ft/mi).

The predicted and measured distresses shown in Table 23 are significantly different. Measured thermal cracking is two to three times greater than the predicted thermal cracking for Cells 15 and 16. This might be attributed to the low temperature binder performance inputs being selected based on typical values for that binder grade, and not measured values. Predicted total rutting is at least two times greater than measured total rutting across all methods of estimating asphalt stiffness and for all cells. Finally, there is no consistent relationship between predicted bottom-up and top-down cracking and observed longitudinal cracking in the wheelpath.

The method used to estimate the stiffness of the asphalt concrete in the existing pavement has a different effect on each predicted distress. First, there is no clear relationship between the method of estimating asphalt stiffness and predicted thermal cracking. Cell 15 fails by thermal cracking in nine years when the Witczak equation is used but does not fail due to thermal cracking when backcalculation is used, even though there is little difference in moduli between the Witczak and backcalculation methods, as shown in Figure 66. In contrast, predicted thermal cracking in Cell 16 is almost identical for the Witczak and backcalculation methods, even though these two methods give very different estimates of asphalt stiffness (Figure 67). The lack of correlation between the method for estimating asphalt stiffness and thermal cracking occurs because the amount of thermal cracking predicted by Pavement ME is determined primarily by low-temperature properties of the binder and not by the stiffness of the asphalt concrete. Differences between thermal cracking predicted by the Witczak method and thermal cracking predicted by the other two methods are caused by differences in how Pavement ME calculates binder viscosity at different input levels. For the Witczak method, using Level 3 inputs, the binder viscosity at a specified temperature is calculated using typical values of the A and VTS parameters, which describe the relationship between binder viscosity and temperature. The details of this calculation

and typical values of the A and VTS parameters can be found in Chapter 3. For the laboratory-measured dynamic modulus and backcalculation methods, both of which use Level 1 inputs, the relationship between binder viscosity and temperature is defined using laboratory-measured complex modulus data, as shown in Table 22.

The method used to predict asphalt concrete stiffness has a large effect on predicted asphalt rutting. A substantial variation in asphalt stiffness obtained between methods is correlated to a large difference in predicted rutting. In Cells 16 and 21, asphalt stiffness estimated using backcalculation is lower than stiffness estimated using the Witczak equation, as shown in Figures 67 and 68. Consequently, the AC rutting predicted using the backcalculated stiffness is between 66% and 121% greater than that predicted using Witczak stiffness. For Cell 16 specifically, AC rutting predicted using the backcalculated stiffness is 0.60 in, two times greater than the 0.28 in of AC rutting predicted using asphalt stiffness determined with the Witczak equation. For Cell 15, backcalculation and the Witczak equation give similar values for asphalt stiffness, as shown in Figure 66, and asphalt rutting, as can be seen in Table 23. As shown in Figure 68, for Cell 21, the asphalt stiffness estimated using the dynamic modulus testing is between the stiffness estimated using the other two methods. The asphalt rutting predicted using the laboratory-measured dynamic modulus is also between that predicted using the other two methods, as can be seen in Table 23. It was not possible to compare predicted asphalt rutting to actual asphalt rutting because only total rutting data was available. Predicted total rutting was at least two times greater than the observed total rutting for all cells.

The method used to determine the stiffness of the asphalt concrete in the existing pavement also has a large effect on the predicted bottom-up and top-down cracking. The magnitude of this effect correlates to the difference in stiffness between the three methods. For example, in Cell 16,

the stiffness estimated using backcalculation is much lower than the stiffness estimated using the Witczak equation. This can be seen in Figure 67. Approximately 7% fatigue cracking is predicted when the Witczak equation is used to estimate the asphalt stiffness, but approximately 13% is predicted when backcalculation is used. The predicted top-down cracking in Cell 16 is much greater when backcalculation is used (average of 3550 ft/mi) than when the Witczak equation is used (25 ft/mi). For Cell 15, the asphalt stiffness and the top-down cracking estimated using backcalculation and the Witczak equation are similar, as evident in Figure 66 and Table 23, respectively. Finally, it should be noted that, for Cell 21, using the asphalt stiffness measured in the lab provided a similar predicted performance as when using the backcalculated stiffness (for all distresses). Over all three cells, using the Witczak equation to determine the stiffness of the asphalt concrete in the existing pavement resulted in the most accurate fatigue cracking predictions. No single method for determining asphalt stiffness provided the most accurate estimation of top-down cracking over all cells.

4.3 CONCLUSIONS

The three main methods for determining the stiffness of asphalt concrete in an existing pavement, dynamic modulus testing of field cores, predictive models, and backcalculation, were compared using data collected at MnROAD and in Pennsylvania. By comparing moduli at a fixed frequency, it was found that there are differences in the asphalt stiffness determined using each of the three methods. Most notably, the backcalculated asphalt stiffness is less than or equal to the asphalt stiffness determined using the Witczak equation (at a load frequency of 30 Hz) for four of the five sections examined. The effect that the difference between methods has on design was quantified

using the new flexible pavement design module in Pavement ME. It was found that predicted rutting, bottom-up cracking, and top-down cracking are most affected by the method used to determine the stiffness of the asphalt concrete in the existing pavement. No single method for determining asphalt stiffness provided the most accurate distress predictions across all distresses.

The results of the analysis performed in this chapter provides a preliminary answer to the first question posed at the end of Chapter 3. It appears that there is a difference between the backcalculated stiffness (E_{NDT}) and stiffness estimated using the Witczak equation and binder aging models ($E_{Witczak}$). The Pavement ME AC/AC overlay design procedure assumes that these two methods are equivalent for the purpose of estimating fatigue damage in the asphalt concrete of the existing pavement. Additionally, it appears that difference between methods significantly affects the design of new AC pavements in Pavement ME. The results of this chapter, however, are based on a sample size of only five pavement sections. The relationship between E_{NDT} and $E_{Witczak}$ is examined further in Chapter 5 using data from many LTPP sections.

5.0 INVESTIGATION OF FWD PARAMETERS USING LTPP DATA

An evaluation of the Pavement ME AC/AC overlay design procedure was performed in Chapter 3. The results of this evaluation challenged two of the primary assumptions on which the procedure is built. The first assumption, that E_{NDT} and $E_{Witczak}$ are equal when compared at a constant temperature and load frequency, was partially addressed in Chapter 4. Direct comparisons were made between three different methods for determining the stiffness of asphalt concrete in an existing pavement. These comparisons suggested that E_{NDT} is actually less than $E_{Witczak}$ when compared at the same temperature and load. Only five pavement sections were examined in Chapter 4, however, so additional analysis is required to elucidate the relationship between E_{NDT} and $E_{Witczak}$. The second assumption, that FWD data can be used to quantify fatigue damage in the asphalt concrete layer of an existing pavement, has not yet been addressed in this research.

An investigation using data from the LTPP database was conducted to determine the validity of the two major assumptions described above. This investigation is based on parameters derived from FWD test data, including the ratio of E_{NDT} over $E_{Witczak}$, which is used in Pavement ME. Each FWD parameter is analyzed in three steps:

1. The theoretical value of the parameter is hypothesized for a pavement with no fatigue damage in the asphalt concrete. For the ratio of E_{NDT} over $E_{Witczak}$, the hypothesized value

with no fatigue damage is 1.00. This is equivalent to assuming that E_{NDT} is equal to $E_{Witczak}$ when there is not fatigue damage in the asphalt concrete of the existing pavement. The hypothesized value of the parameter is then evaluated using LTPP data from pavement sections with no visible distress.

2. The relationship between the FWD parameter, FWD load level, and MDT at the time of FWD testing is examined using LTPP data from pavement sections with no visible distress. This is performed to determine if load level and/or MDT must be considered when examining the relationship between the FWD parameter and fatigue damage.
3. The relationship between the FWD parameter and fatigue damage is examined using LTPP data from distressed pavement sections. The amount of observed fatigue cracking in the pavement is used as an indicator of the amount of fatigue damage in the asphalt concrete. This analysis is intended to confirm or refute the assumption that FWD data can effectively be used to quantify fatigue damage in the asphalt concrete layer of an existing pavement.

5.1 LONG-TERM PAVEMENT PERFORMANCE PROGRAM

The LTPP program is an ongoing project to collect and process high-quality information and performance data for pavement structures in the United States and Canada. The LTPP InfoPave database contains data for more than 2,500 pavement sections, collected between 1988 and the present. A typical LTPP pavement section is 500 ft long. Distress surveys, FWD testing, and material testing are performed on each LTPP section at intervals of one month to five years. Additional surveys and testing are performed on a section whenever there is a major structural change, such as an overlay.

5.1.1 Data source

There are 1,574 sections in the LTPP database for which the original pavement structure has an asphalt concrete surface. However, only 397 of these sections were included in the analysis of FWD parameters. All asphalt concrete sections in wet-freeze climates were included because these experience climatic conditions similar to those in Pennsylvania and often use similar asphalt binder grades. Additionally, all seasonal monitoring program (SMP) sections with binder grades similar to those used in Pennsylvania were included. SMP sections have a large amount of FWD data collected at frequent intervals over a wide range of temperatures, so they are useful for examining changes in FWD parameters with respect to both time and temperature.

Several types of data were extracted from the LTPP database for each section. The five main types of data used in the analysis of the FWD parameters are:

1. Observed Surface Distress: The amount of observed fatigue cracking (alligator cracking) and wheelpath longitudinal cracking over the life of the pavement was obtained for all sections. In the LTPP database, both of these distresses are recorded for the entire pavement section. However, FWD testing on LTPP sections is only conducted in the outer wheelpath and at mid-lane, so the total observed distress cannot be compared to FWD parameters on a one-to-one basis since only a portion of the distressed surface area is being tested. It was initially assumed that, on average, fatigue cracking in the outer wheelpath is equal to one half of the total fatigue cracking in the section because fatigue cracking should occur predominately in the two wheelpaths. Similarly, it was assumed that longitudinal cracking is also evenly distributed between the wheelpaths.

In order to test these assumptions, observed pavement distress was reviewed manually for a subset of the LTPP sections used in the analysis. This subset includes 56 sections, mostly SMP sections, which represent 67% of the FWD data included in the overall analysis. These sections are listed in Table 24. Scanned paper distress surveys and pictures of the 56 LTPP sections were used to sum the total distress only in the outer wheelpath. Distress in the outer wheelpath was compared to the total distress obtained from the LTPP database. Figures 72 and 73 show weighted linear regressions of the outer wheelpath distress vs. the total distress for fatigue cracking and wheelpath longitudinal cracking, respectively. Weights were assigned so that each LTPP section had the same overall weight. As shown in Figure 72, fatigue cracking in the outer wheelpath is approximately 43% of total fatigue cracking, compared to the assumed 50%. This is most likely because the total fatigue cracking recorded in the LTPP database often includes cracking between or outside the wheelpaths. Longitudinal cracking in the outer wheelpath is approximately 25% of the total longitudinal wheelpath cracking, compared to the assumed 50%. It is possible that the relationship between total and outer wheelpath longitudinal cracking, shown in Figure 73, is unduly influenced by data from a few sections that are not representative of the true trend.

Table 24. LTPP sections for which the distress surveys were analyzed.

State	LTPP ID	State	LTPP ID	State	LTPP ID	State	LTPP ID
AL	1-0101	MN	27-1018	NM	35-1112	VT	50-1683
AL	1-0102	MN	27-1028	NY	36-0801	VA	51-0113
CO	8-1053	MN	27-6251	NY	36-0802	VA	51-0114
CT	9-1803	MS	28-1016	NC	37-1028	WY	56-1007
DE	10-0102	MS	28-1802	OH	39-0901	MB	83-0502
GA	13-1005	MT	30-0114	OK	40-4165	MB	83-0503
GA	13-1031	ME	31-0114	PA	42-1597	MB	83-0506
ID	16-1010	NH	33-1001	SD	46-9187	MB	83-0507
KS	20-0159	NJ	34-0501	TX	48-1060	MB	83-0508
KS	20-1005	NJ	34-0961	TX	48-1068	MB	83-0509
ME	23-1009	NJ	34-0962	TX	48-1077	MB	83-1801
ME	23-1026	NJ	34-1003	TX	48-1122	ON	87-1622
MD	24-1634	NJ	34-1011	UT	49-1001	QB	89-1125
MA	25-1002	NJ	34-1030	VT	50-1002	SK	90-6045

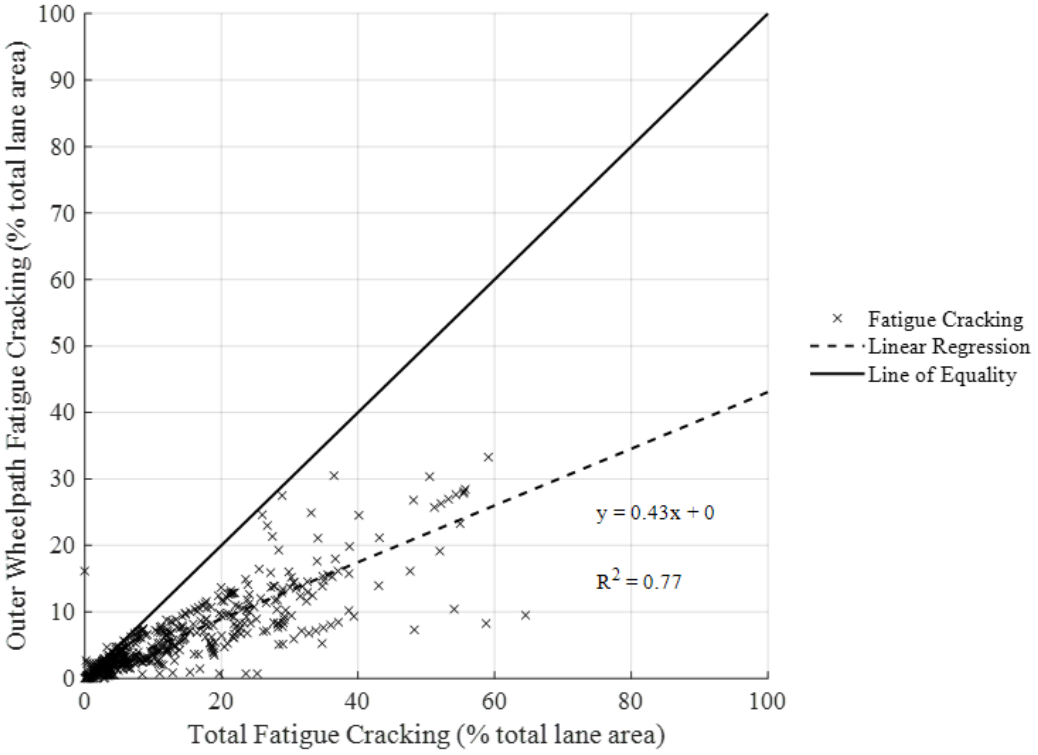

Figure 72. Outer wheelpath vs. total fatigue cracking for a subset of LTPP sections.

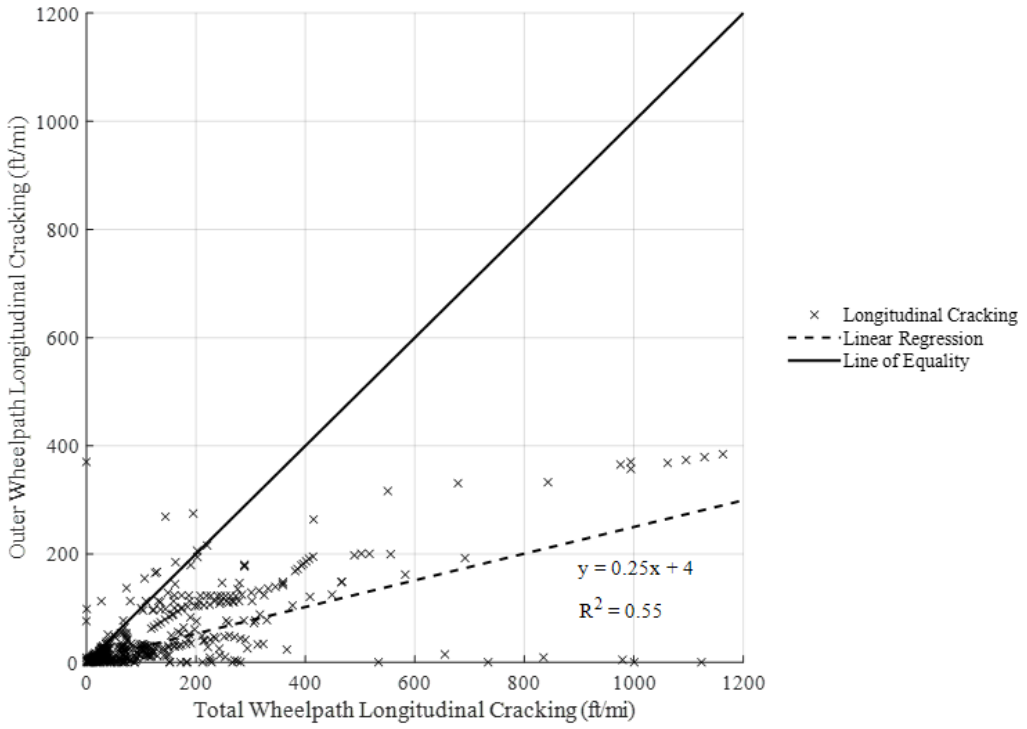

Figure 73. Outer wheelpath vs. total wheelpath longitudinal cracking for a subset of LTPP sections.

2. FWD Deflections: The deflection basin, consisting of the maximum deflection for each FWD sensor, was obtained for each FWD drop performed over the life of the sections. According to the LTPP standard procedure, FWD testing of AC pavements is performed in passes, alternating between the outer wheelpath and mid-lane. The outer wheelpath test pass is performed first and the mid-lane test pass is performed second. Test locations are spaced either 25 ft or 50 ft apart along the 500-ft test section. Figure 74 shows the LTPP standard test plan for AC pavements (Schmalzer 2006). Sixteen FWD drops are performed at each test location, four at each of the standard FWD load levels: 6 kip, 9 kip, 12 kip, and 16 kip. Maximum deflections for each drop are normalized to the target load.

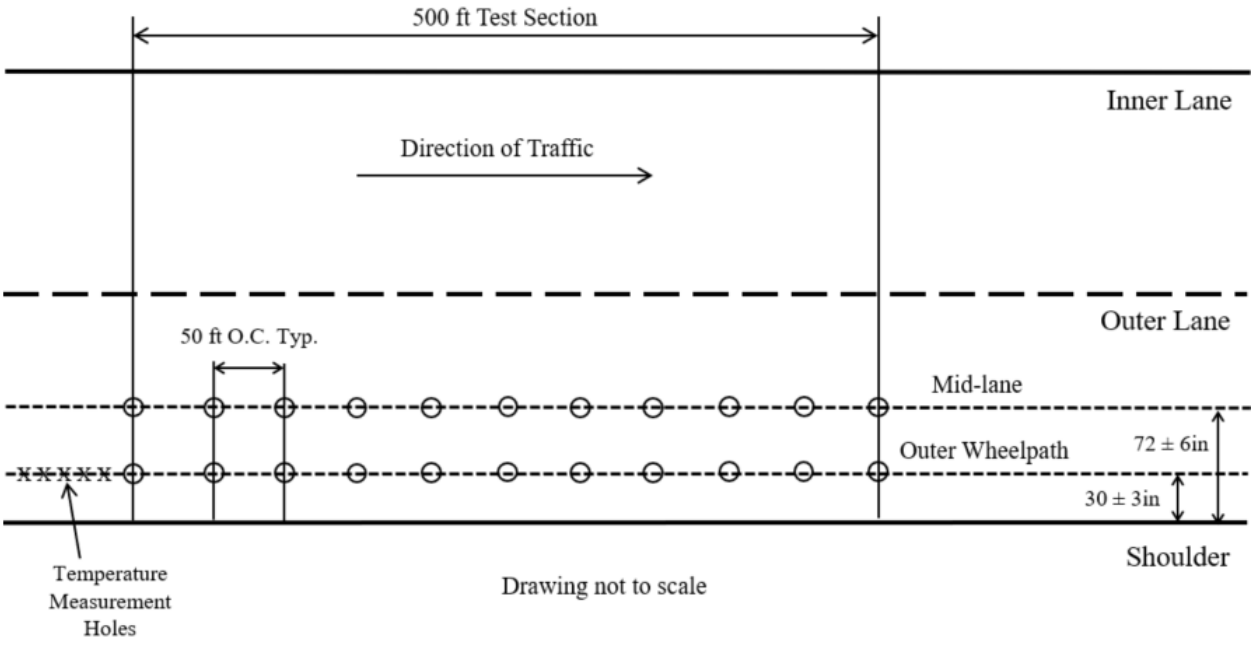

Figure 74. LTPP FWD test plan for flexible pavement sections.

3. Layer Moduli: The backcalculated stiffness (modulus) of all pavement layers was obtained for each FWD drop performed over the life of each section. Layer moduli in the LTPP database were backcalculated in a semi-automated procedure using the backcalculation programs EVERCALC and MODCOMP (Von Quintus et al. 2015). For this analysis, erroneous backcalculated moduli were identified and removed using error codes provided in the LTPP database and by manually reviewing the backcalculated moduli. Two criteria were used to identify erroneous backcalculated moduli for removal. The criteria are:

    a. One or more of the backcalculated moduli associated with the FWD drop is a round number (e.g. 400 ksi for the backcalculated stiffness of the asphalt concrete or 100 ksi for the granular base), indicating that the backcalculation program converged to a user-defined stiffness limit. Convergence to a user-defined stiffness limit

indicates that the backcalculated stiffness of the asphalt concrete layer is likely incorrect.

b. The backcalculated asphalt modulus is more than three standard deviations greater than the mean backcalculated asphalt stiffness (calculated from all LTPP sections) at the same mid-depth asphalt temperature.

If the backcalculated modulus for an FWD drop met either of the criteria, the backcalculated asphalt concrete stiffness from that drop was removed from the analysis.

4. Asphalt Temperature: Asphalt temperature data was obtained for all days on which FWD testing was performed. During LTPP FWD testing, the asphalt temperature is measured using temperature holes drilled to different depths in the asphalt layer. Temperature holes are drilled at one or both ends of the 500-ft test section, as shown in Figure 74. Asphalt temperature is recorded every 30 min. Linear interpolation was used to estimate the mid-depth asphalt temperature (MDT) at the time each FWD drop was made.

5. Asphalt Mixture Information: Asphalt mix information was obtained for a subset of the sections used in the analysis. This subset includes 116 sections, which represent 71% of the FWD data included in the overall analysis. The asphalt mixture information collected includes all of the mixture parameters necessary to estimate the stiffness of the asphalt concrete using the Witczak equation: percent air voids (V_a), effective binder content by volume (V_{be}), and aggregate gradation ($P_{3/4}$, $P_{3/8}$, P_4, and P_{200}). See Chapter 3 for a detailed description of the Witczak equation. These parameters were obtained through laboratory testing of field samples and thus represent the in-situ properties of the asphalt concrete in the existing pavement. The LTPP database contains a considerable amount of information

from lab testing of asphalt concrete extracted from existing pavements, but this data was often incomplete and required some processing to obtain the inputs in the Witczak equation. This processing included calculating the Witczak equation inputs from other asphalt concrete mix parameters (using Equations 15 through 18), excluding outlying or erroneous data, and making assumptions about the values of mixture parameters based on partial information. Quality levels were established for each type of LTPP data used to establish the inputs for the Witczak equation. The quality levels are summarized in Table 25.

Table 25. Quality of data used to develop inputs for the Witczak Equation.

	Level of Data Quality		
Type of Data	A	B	C
Bulk specific gravity of asphalt mix (G_{mb})	Lab testing of cores	Assumed same as Level A data from similar/adjacent layer	Mix design
Maximum specific gravity of the asphalt mix (G_{mm})	Lab testing of cores	Mix design	Assumed same as similar/adjacent layer
Bulk specific gravity of the aggregate (G_{sb})	Lab testing of extracted aggregate	Mix design	Assumed same as similar/adjacent layer
Percent binder by weight (P_b) (%)	Lab testing of cores	Mix design	Assumed same as similar/adjacent layer
Asphalt Concrete Aggregate Gradation ($P_{3/4}$, $P_{3/8}$, P_4, P_{200})	Lab testing of extracted aggregate	Mix design	Assumed same as similar/adjacent layer
Binder Grade	Mixture design or historical records	Assumed same as similar/adjacent layer	Assumed based on a similar pavement in the same state

Level A data is the highest quality and is based on laboratory testing of cores taken in the outer wheelpath. If multiple sets of cores were taken at different times in the pavement life, the mix information from these cores was averaged. Averaging was performed to account for the reduction in the air void content of asphalt concrete in an existing pavement that occurs over time due to compaction by traffic. If the bulk specific gravity of the aggregate (G_{sb}) was not reported directly, it was calculated using the bulk specific gravities of the coarse ($G_{sb,ca}$) and fine ($G_{sb,fa}$) extracted aggregate and the aggregate gradation. The calculated G_{sb} is the average of $G_{sb,ca}$ and $G_{sb,fa}$, weighted by the percentages of coarse (retained on a #4 sieve) and fine (passing a #4 sieve) aggregate in the asphalt concrete mixture. The G_{sb} determined in this way was considered Level A data. Mixture design data was assigned a higher quality level than assumed data from all types of data except the bulk specific gravity of the asphalt mix (G_{mb}). For several sections, significant differences were observed between a G_{mb} that was measured for a core pulled from the existing pavements and a G_{mb} that was measured on a mixture design specimen. G_{mb} significantly influences V_a and V_{be}, both of which are critical inputs in the Witczak equation. Therefore, the Level A G_{mb} from the asphalt concrete in an existing pavement that is similar to the pavement in question was preferred over a G_{mb} established based on mixture design information. A section was not used in the analysis unless at least Level C data could be obtained for all data for each asphalt concrete layer in the pavement structure.

With the data obtained from the LTPP database, the volumetric inputs for the Witczak equation (V_a and V_{be}) were calculated using Equations 15 through 18. All of the asphalt mixture information used in this chapter can be found in Appendix A.

$$V_a = \left(1 - \frac{G_{mb}}{G_{mm}}\right) \times 100 \quad (15)$$

Where:

V_a = Air voids (%)

G_{mb} = Bulk specific gravity of the AC mixture

G_{mm} = Maximum theoretical specific gravity of the AC mixture

$$P_s = 100 - P_b \quad (16)$$

Where:

P_s = Percentage of aggregate in mix by weight (%)

P_b = Percentage of binder in mix by weight (%)

$$VMA = 100 - \left(\frac{G_{mb}(P_s)}{G_{sb}}\right) \quad (17)$$

Where:

VMA = Voids in mineral aggregate (%)

$$V_{be} = VMA - V_a \quad (18)$$

Where:

V_{be} = Effective asphalt content by volume (%)

All the LTPP data used in the analysis was organized with respect to the date and time that FWD testing was performed. Linear interpolation with respect to time and distance along the pavement section was used to estimate MDT for each FWD drop. Next, the mean, standard deviation, median, maximum, and minimum values of the maximum deflections, the backcalculated moduli, and MDT were calculated for each FWD pass. This was performed

separately for mid-lane and outer wheelpath passes. Finally, linear interpolation was used to estimate the amount of distress in the pavement section on the date each FWD pass was conducted.

Only FWD data collected on the original pavement structure prior to the placement of the overlay was used in the analysis of the FWD parameters. All data from FWD testing conducted on overlaid or otherwise structurally modified pavement structures was excluded because it is not possible to quantify the amount of distress in pavement layers concealed by the overlay.

5.2 FWD PARAMETERS CONSIDERED

A FWD parameter was defined as any quantitative value that is derived from the results of FWD testing and provides information about the tested pavement structure. The focus of this analysis is on FWD parameters that can provide information about the amount of damage in the asphalt concrete layer of an existing AC pavement. Many parameters were examined, but the following four were determined to be the most informative: $d_{0,OWP}/d_{0,ML}$, $E_{NDT,OWP}/E_{NDT,ML}$, $E_{NDT,OWP}/E_{Witczak(Aging)}$, and $E_{NDT,OWP}/E_{Witczak(No\ aging)}$.

5.2.1 $d_{0,OWP}/d_{0,ML}$

The parameter $d_{0,OWP}/d_{0,ML}$ is the ratio of the center-plate deflection (d_0) when FWD testing is performed in the outer wheelpath over the center-plate deflection for a mid-lane test. Center-plate deflection is the maximum deflection recorded at the center of the FWD load plate, directly under the load. For AC pavements, d_0 is generally considered to be representative of the stiffness of the asphalt concrete surface layer. If fatigue damage in asphalt concrete causes a reduction in the

stiffness of the material, d_0 should increase. Additionally, it was assumed that most fatigue damage in the asphalt concrete occurs in the wheelpaths. Thus, the ratio of d_0 measured in the outer wheelpath ($d_{0,OWP}$) over d_0 measured at mid-lane ($d_{0,ML}$) should be an indicator of fatigue damage in the asphalt concrete in the outer wheelpath. FWD testing of LTPP sections is conducted in passes, as shown in Figure 74, so data from consecutive passes is paired together and the ratio $d_{0,OWP}/d_{0,ML}$ was calculated for each pair of test passes. The $d_{0,OWP}/d_{0,ML}$ parameter for each pair of test passes was calculated in several steps. A separate value of $d_{0,OWP}/d_{0,ML}$ was calculated for each FWD load level.

First, the average center-plate deflection was calculated for the outer wheelpath test pass ($d_{0,OWP}$) and for the mid-lane test pass ($d_{0,ML}$). The average MDT was also calculated for the outer wheelpath test pass (MDT_{OWP}) and for the mid-lane test pass (MDT_{ML}). Second, $d_{0,ML}$ was adjusted to account for the small difference in MDT that occurs between consecutive FWD test passes. This adjustment was performed using a regression between $d_{0,ML}$ and MDT that was fitted using data from all LTPP sections included in the analysis that had no visible distress. A separate regression between $d_{0,ML}$ and MDT was used for each FWD load level. The regression used to adjust $d_{0,ML}$ at the 9-kip load level is shown in Figure 75. The adjustment of $d_{0,ML}$ was performed in three steps:

1. MDT_{OWP} and MDT_{OWP} were used with the regression to estimate $d_{0,ML}$ for the outer wheelpath pass temperature ($d_{0,ML(1)}$) and the mid-lane pass temperature ($d_{0,ML(2)}$).
2. The change in $d_{0,ML}$ between the outer wheelpath and mid-lane passes ($\Delta d_{0,ML}$) was computed by subtracting $d_{0,ML(2)}$ from $d_{0,ML(1)}$ ($\Delta d_{0,ML} = d_{0,ML(1)} - d_{0,ML(2)}$).

3. The temperature-adjusted value of $d_{0,ML}$ ($d_{0,ML(adj)}$) was computed by adding $\Delta d_{0,ML}$ to the original value of $d_{0,ML}$ ($d_{0,ML(adj)} = d_{0,ML} + \Delta d_{0,ML}$).

It is important to note that the difference in temperature between consecutive test passes is relatively small for most pairs of test passes. Among all LTPP sections used in this analysis, the mean difference in temperature between mid-lane and outer wheelpath test passes ($MDT_{ML} - MDT_{OWP}$) is -1.7ºF, with a standard deviation of 2.2ºF. Note that the outer wheelpath test pass is performed first. A histogram of the difference between the average MDT for consecutive outer wheelpath and mid-lane test passes is shown in Figure 76. The final step to calculate $d_{0,OWP}/d_{0,ML}$ was to divide $d_{0,OWP}$ by the temperature-adjusted value of $d_{0,ML}$ ($d_{0,OWP}/d_{0,ML} = d_{0,OWP}/ d_{0,ML(adj)}$).

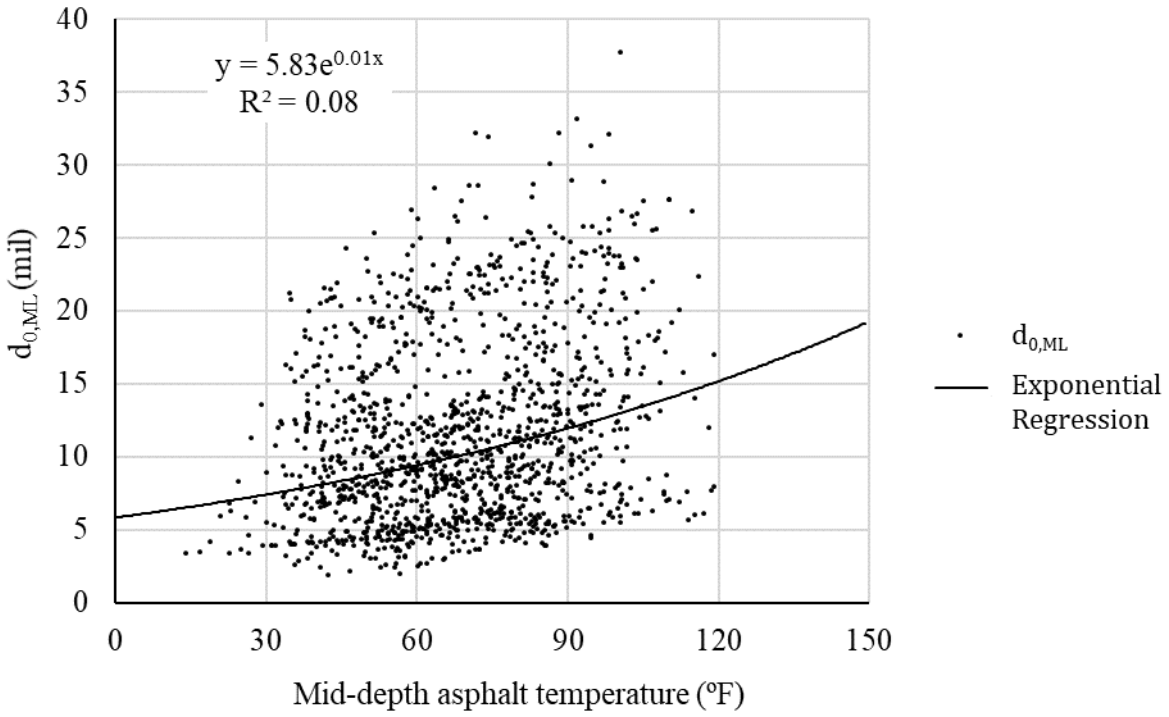

Figure 75. Relationship between $d_{0,ML}$ and MDT used to account for difference in MDT between consecutive test passes (9-kip load level).

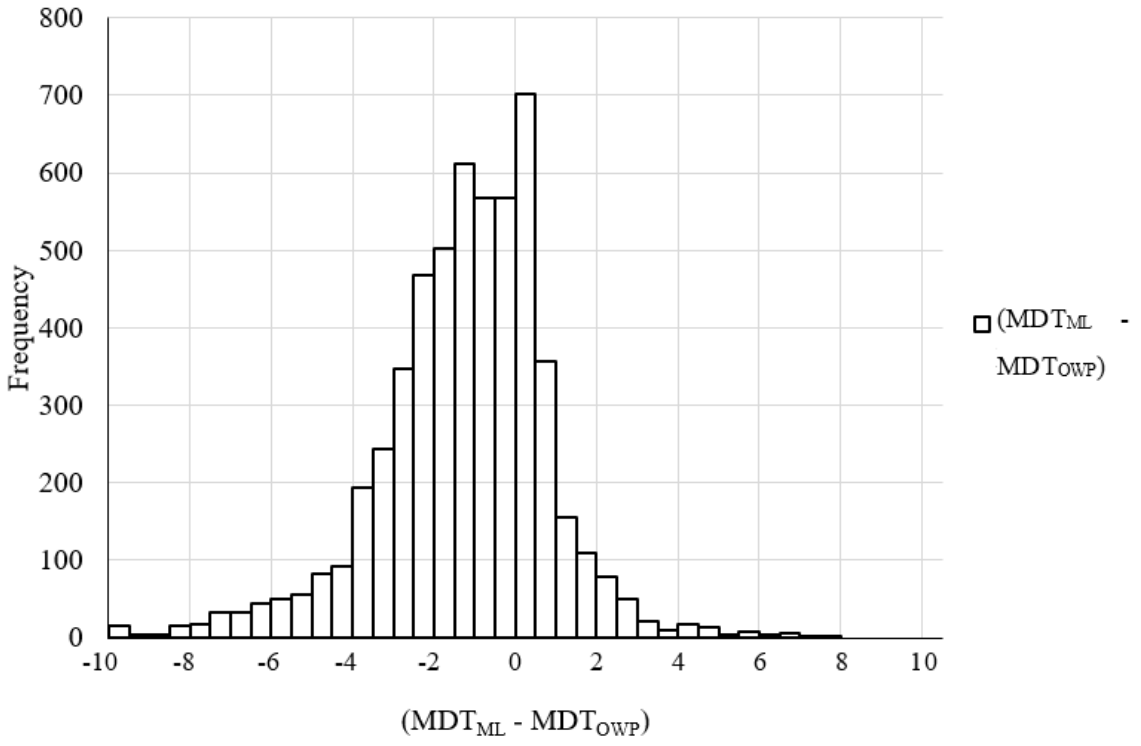

Figure 76. Distribution of the difference in average MDT between consecutive outer wheelpath and mid-lane test passes for LTPP sections.

The assumption that $d_{0,OWP}/d_{0,ML}$ is 1.00 for an undamaged pavement section was tested using FWD data collected from LTPP sections with no visible distress (0% observed fatigue cracking and 0 ft/mi longitudinal cracking). The mean of $d_{0,OWP}/d_{0,ML}$ for a pavement section with no visible distress, calculated from 5490 data points and 248 different LTPP sections, is 1.06 and the standard deviation of $d_{0,OWP}/d_{0,ML}$ is 0.10. The parameter is normally distributed with a slight positive skew, as shown in Figure 77. A one-sided t-test indicated that the mean of $d_{0,OWP}/d_{0,ML}$ is greater than 1.00 at a 95% confidence level (p-value = 0.00). Additional compaction of the asphalt concrete under traffic and/or proximity to the pavement edge or the longitudinal shoulder joint may cause the mean value of $d_{0,OWP}/d_{0,ML}$ to be greater than 1.00. Variability in the parameter is likely due to variability in asphalt thickness transversely across the section.

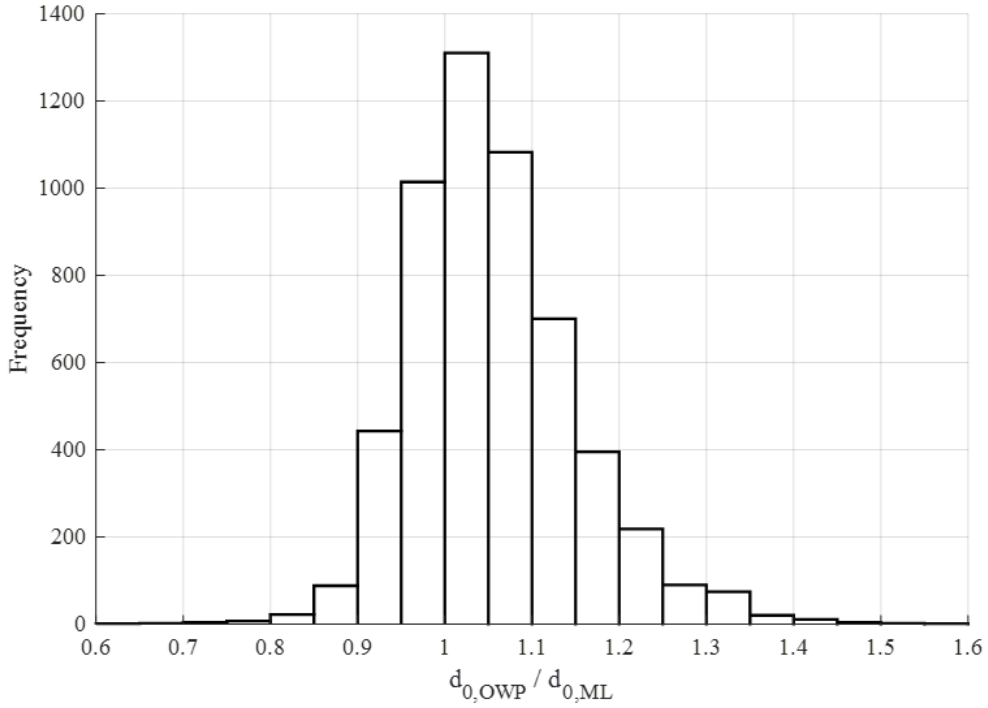

Figure 77. Distribution of the $d_{0,OWP}/d_{0,ML}$ parameter for pavements with no visible distress.

5.2.2 $E_{NDT,OWP}/E_{NDT,ML}$

$E_{NDT,OWP}/E_{NDT,ML}$ is the ratio of the backcalculated asphalt concrete stiffness based on FWD testing in the outer wheelpath ($E_{NDT,OWP}$) over the backcalculated asphalt concrete stiffness based on FWD testing at mid-lane ($E_{NDT,ML}$). It was assumed that damage in asphalt concrete causes a reduction in the stiffness of the material, so the backcalculated stiffness of the asphalt concrete layer can be used as an indicator of fatigue damage in that layer. Additionally, it was assumed that most fatigue damage occurs in the wheelpath. Thus, the ratio of $E_{NDT,OWP}$ over $E_{NDT,ML}$ should be an indicator of fatigue damage in the asphalt concrete in the outer wheelpath of the existing pavement. Data from consecutive FWD passes was paired together and the ratio $E_{NDT,OWP}/E_{NDT,ML}$ was calculated

for each pair of test passes. $E_{NDT,ML}$ was adjusted to account for the slight difference in mid-depth asphalt temperature between two consecutive FWD passes. This was performed using the same procedure described for $d_{0,OWP}/d_{0,ML}$. The regression between $E_{NDT,ML}$ and MDT for the 9-kip load level is shown in Figure 78.

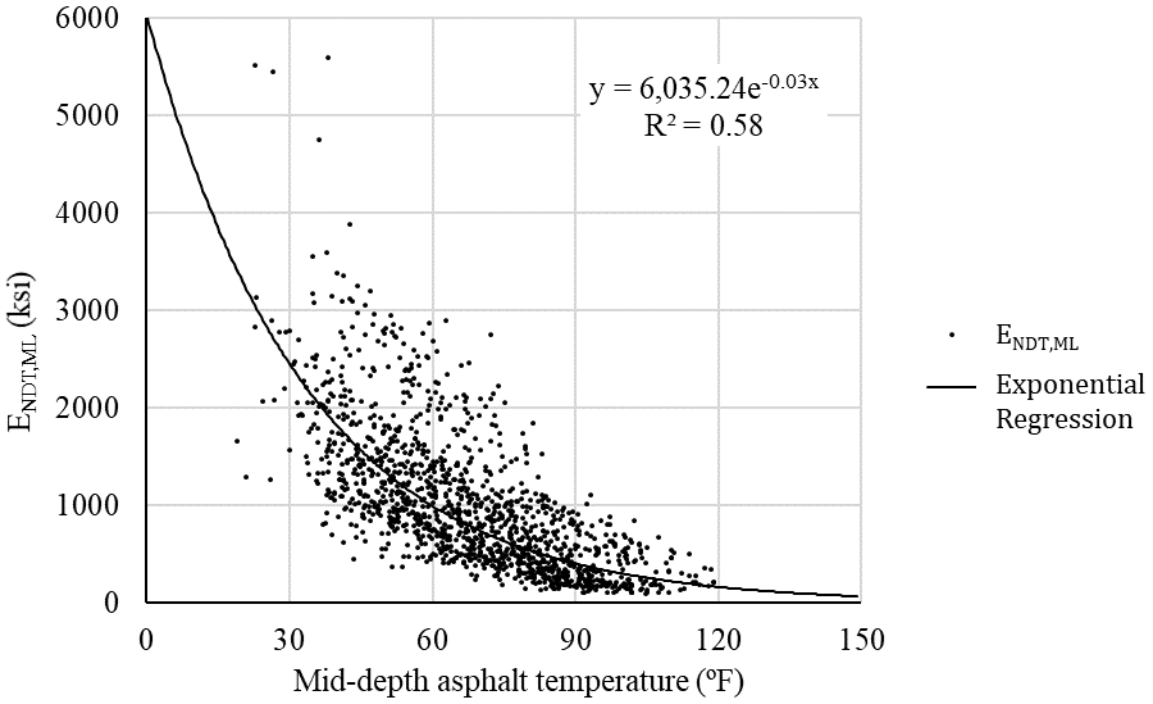

Figure 78. Relationship between $E_{NDT,ML}$ and MDT used to account for difference in MDT between consecutive FWD test passes (9-kip load level).

The mean of $E_{NDT,OWP}/E_{NDT,ML}$ for a section with no visible distress, calculated from 5490 data points and 248 different LTPP sections, is 1.04 and the standard deviation is 0.23. The parameter is normally distributed with a slight positive skew, as shown in Figure 79. Statistically, the mean of $E_{NDT,OWP}/E_{NDT,ML}$ is greater than 1.00 at a 95% confidence level (p-value = 0.00). Compaction of the asphalt concrete by traffic in the outer wheelpath may cause the mean value of

$E_{NDT,OWP}/E_{NDT,ML}$ to be slightly greater than 1.00. Variability in $E_{NDT,OWP}/E_{NDT,ML}$ is likely influenced by unknown variability in pavement layer thickness, which is magnified by the backcalculation process.

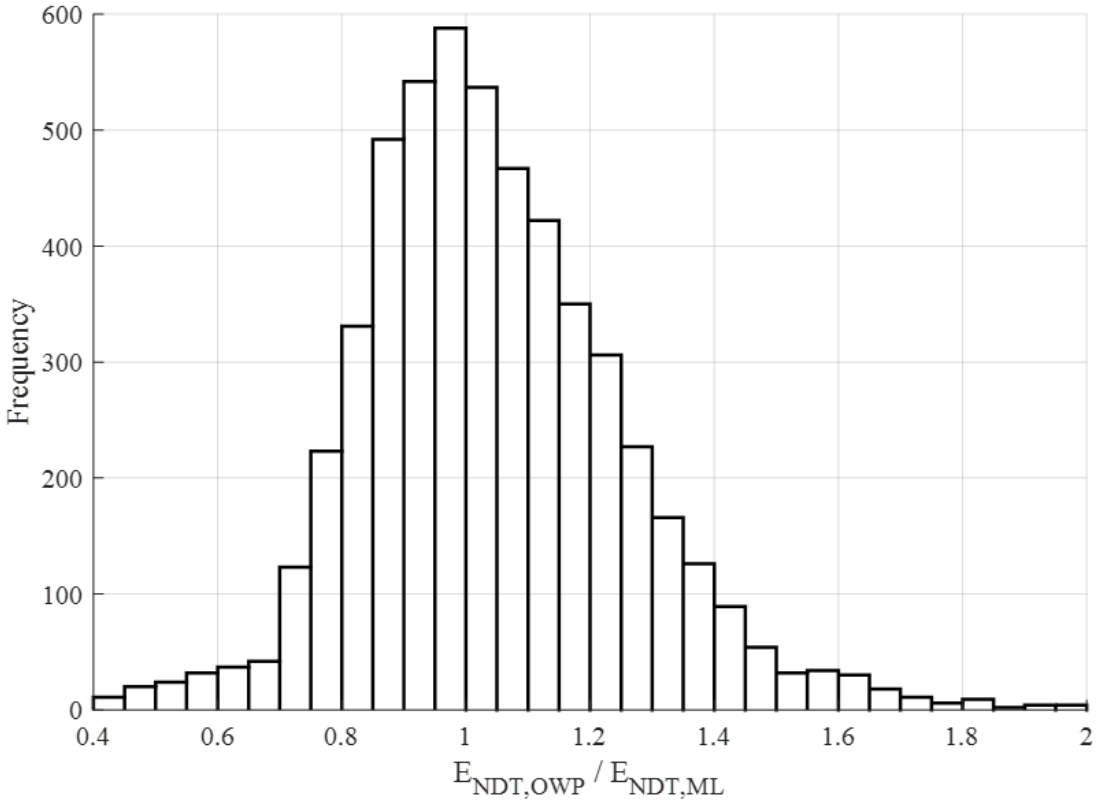

Figure 79. Distribution of $E_{NDT,OWP}/E_{NDT,ML}$ for pavements with no visible distress.

5.2.3 $E_{NDT,OWP}/E_{Witczak(Aging)}$

$E_{NDT,OWP}/E_{Witczak(Aging)}$ is the ratio of the backcalculated asphalt concrete stiffness based on FWD testing in the outer wheelpath ($E_{NDT,OWP}$) over the asphalt concrete stiffness estimated using the Witczak equation and adjusted for binder aging ($E_{Witczak(Aging)}$). As previously discussed, fatigue

damage in the asphalt concrete of the existing pavement can be detected by comparing the backcalculated asphalt concrete stiffness in a damaged location to that in an undamaged location. Fatigue damage in the asphalt concrete can also be detected by comparing E_{NDT} in a damaged location to the theoretical undamaged stiffness of the asphalt concrete, estimated using the Witczak equation. To correctly make this comparison, one must know the load frequency of the FWD. Load frequency is one of the necessary inputs for the Witczak equation, and the frequency used in the Witczak equation must be equal to the FWD load frequency to make a meaningful comparison between E_{NDT} and $E_{Witczak}$. The FWD load frequency can change between sections, but the relationship between load frequency, pavement structure, and asphalt temperature is not well understood. A constant FWD load frequency of 30 Hz was assumed for this analysis. This is the value currently recommend by the developers of the Pavement ME AC/AC overlay design procedure (Rao and Von Quintus 2015). Additionally, $E_{Witczak}$ may be estimated with or without being adjusted for binder aging ($E_{Witczak(Aging)}$ or $E_{Witczak(No\ aging)}$). The same binder aging models incorporated into Pavement ME were used to determine $E_{Witczak(Aging)}$ in this analysis. See Chapter 3 for a description of these binder aging models and how they are used in conjunction with the Witczak equation. $E_{NDT,OWP}/E_{Witczak(Aging)}$ is the FWD parameter used in the Pavement ME AC/AC overlay design procedure to define the amount of fatigue damage in the asphalt concrete of the existing pavement (ARA Inc. 2004).

The assumed value of $E_{NDT,OWP}/E_{Witczak(Aging)}$ was evaluated using FWD data collected from LTPP sections with no visible distress. The mean value of $E_{NDT,OWP}/E_{Witczak(Aging)}$ for a pavement section with no visible distress, calculated using 3726 data points and 72 different LTPP sections, is 0.64 and the standard deviation is 0.36. Note that only sections with sufficient asphalt concrete mix information to calculate $E_{Witczak}$ were included the analysis of $E_{NDT,OWP}/E_{Witczak(Aging)}$. The

parameter is log-normally distributed with a positive skew, as shown in Figure 80. $E_{NDT,OWP}/E_{Witczak(Aging)}$ was transformed using the base 10 logarithm for the purpose of statistical testing. The transformed distribution, which is approximately normal with a slight negative skew, is shown in Figure 81. The mean value of $\log(E_{NDT,OWP}/E_{Witczak(Aging)})$ for a pavement section with no visible distress is -0.26 and the standard deviation is 0.24. A t-test performed on $\log(E_{NDT,OWP}/E_{Witczak(Aging)})$ indicated that mean of the transformed parameter is less than 0.00 (equivalent to $E_{NDT,OWP}/E_{Witczak(Aging)} = 1.00$) at a 95% confidence level (p-value = 0.00).

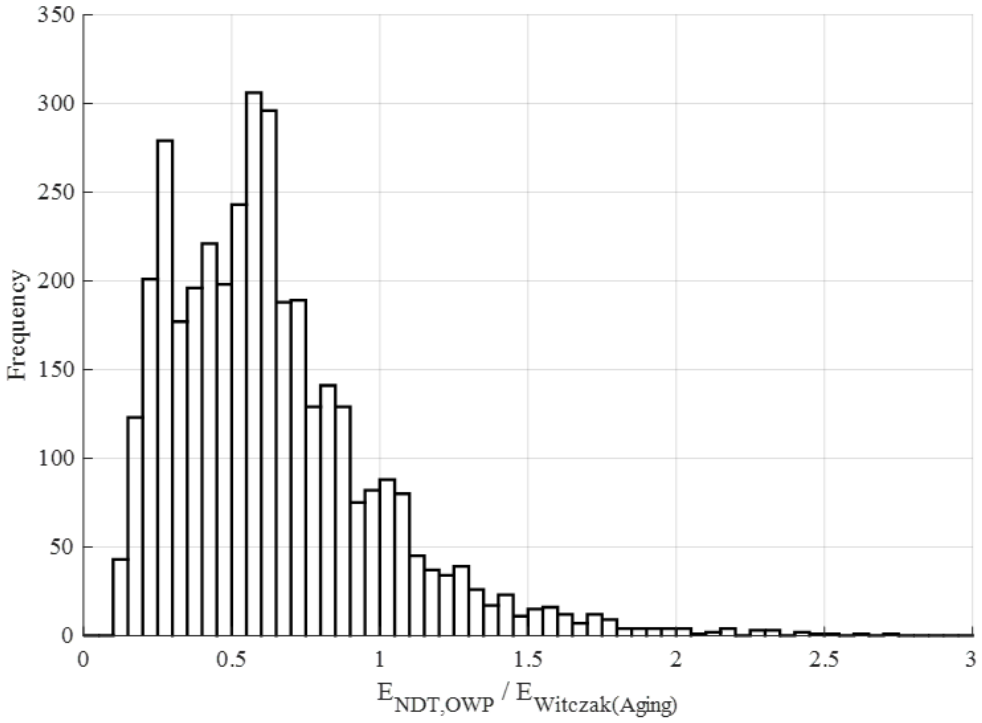

Figure 80. Distribution of $E_{NDT,OWP}/E_{Witczak(Aging)}$ for pavements with no visible distress.

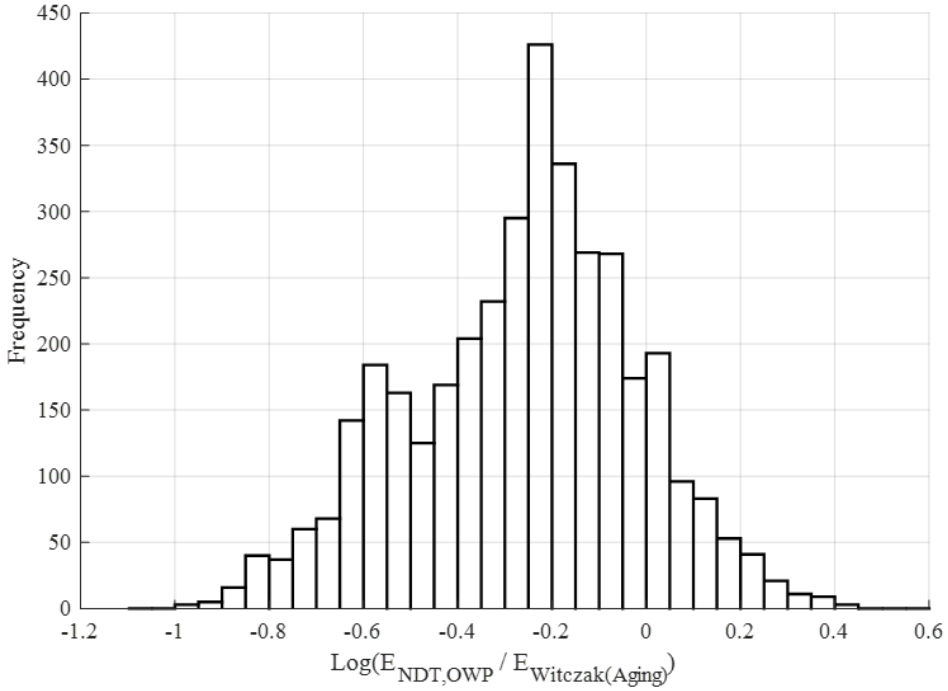

Figure 81. Distribution of log($E_{NDT,OWP}/E_{Witczak(Aging)}$) for pavements with no visible distress.

There are two related reasons that the observed mean value of $E_{NDT,OWP}/E_{Witczak(Aging)}$ is significantly less than the initially assumed value. First, the binder aging models used to estimate $E_{Witczak(Aging)}$ in the denominator of the parameter increase the value of $E_{Witczak(Aging)}$ by an unrealistically large amount. Binder aging is generally considered to affect only the top few inches of in-place asphalt (Mirza 1993), but the binder aging models, as they are used to determine $E_{Witczak(Aging)}$ in Pavement ME, significantly affect the entire thickness of the asphalt concrete in the existing pavement. This increases the average stiffness of the entire asphalt concrete layer to a very high value, particularly at low temperatures, as shown in Figure 82. The binder aging model also places a maximum limit on the asphalt binder viscosity, which causes $E_{Witczak(Aging)}$ to reach a maximum value at approximately 50ºF. This can also be seen in Figure 82. Second, the observed

mean value of $E_{NDT,OWP}/E_{Witczak(Aging)}$ may be less than the assumed value of 1.00 because the assumed FWD load frequency of 30 Hz may be higher than the actual FWD load frequency for many of the pavement sections included in this analysis. If the asphalt concrete stiffness in the numerator ($E_{NDT,OWP}$) actually corresponds to a load frequency lower than the 30Hz used to calculate the asphalt stiffness in the denominator ($E_{Witczak(Aging)}$), then the ratio of the two values will be less than 1.00.

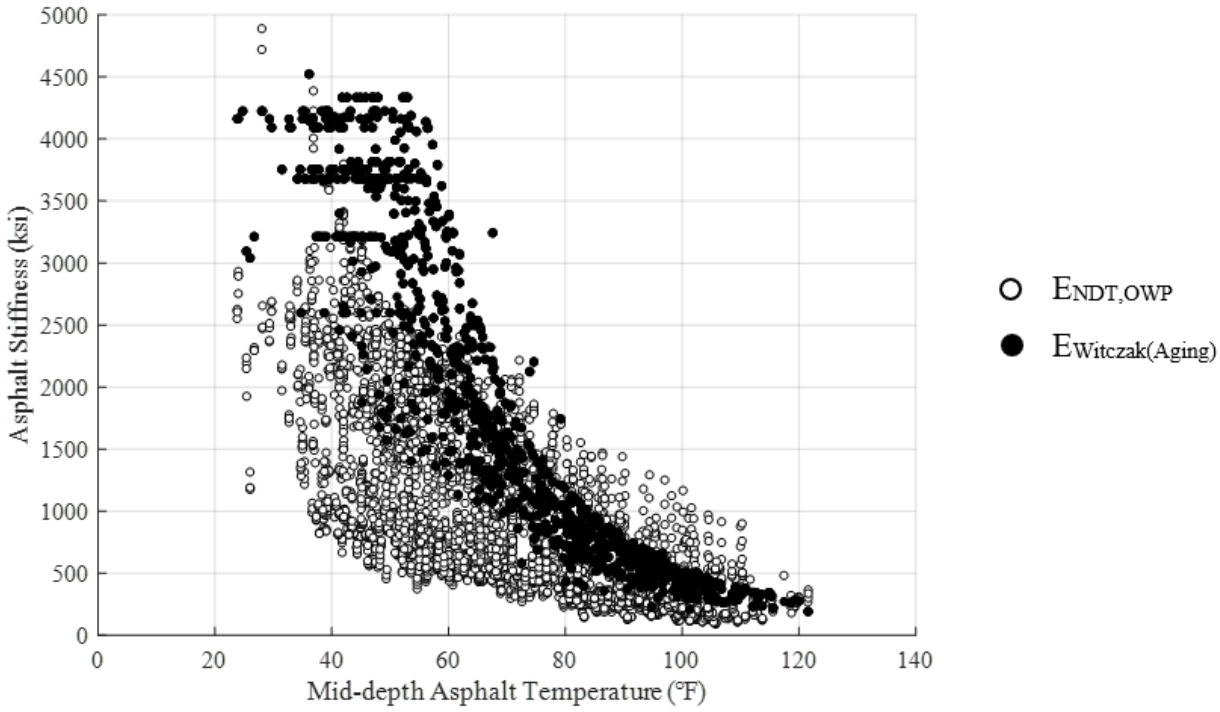

Figure 82. $E_{NDT,OWP}$ and $E_{Witczak(Aging)}$ vs. MDT.

5.2.4 $E_{NDT,OWP}/E_{Witczak(No\ aging)}$

$E_{NDT,OWP}/E_{Witczak(No\ aging)}$ is the ratio of the backcalculated asphalt concrete stiffness in the outer wheelpath ($E_{NDT,OWP}$) over the theoretical undamaged asphalt concrete stiffness, estimated using the Witczak equation **without** adjusting for binder aging ($E_{Witczak(No\ aging)}$). The mean value of $E_{NDT,OWP}/E_{Witczak(No\ aging)}$ for undamaged pavement sections (no visible distress), calculated from 3810 data points and 72 different LTPP sections, is 0.82 and the standard deviation is 0.41 The parameter is log-normally distributed with a positive skew, as shown in Figure 83. $E_{NDT,OWP}/E_{Witczak(No\ aging)}$ was transformed using the base 10 logarithm for the purpose of statistical testing. The transformed distribution, which is approximately normal, is shown in Figure 84. The mean value of $\log(E_{NDT,OWP}/E_{Witczak(No\ aging)})$ for a pavement section with no visible distress is -0.15 and the standard deviation is 0.22. A t-test performed on $\log(E_{NDT,OWP}/E_{Witczak(No\ aging)})$ indicated that mean of the transformed parameter is less than 0.00 (equivalent to $E_{NDT,OWP}/E_{Witczak(No\ aging)} = 1.00$) at a 95% confidence level (p-value = 0.00).

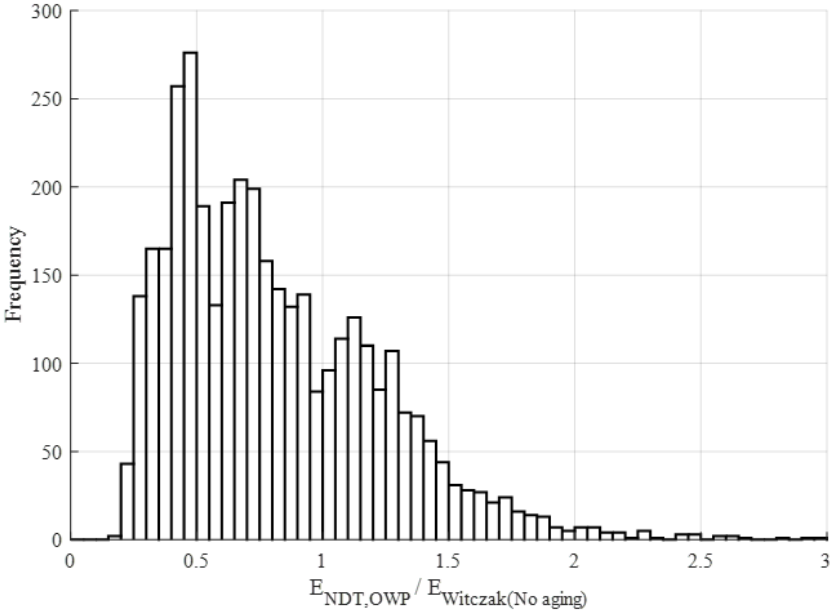

Figure 83. Distribution of $E_{NDT,OWP}/E_{Witczak(No\ aging)}$ for pavements with no visible distress.

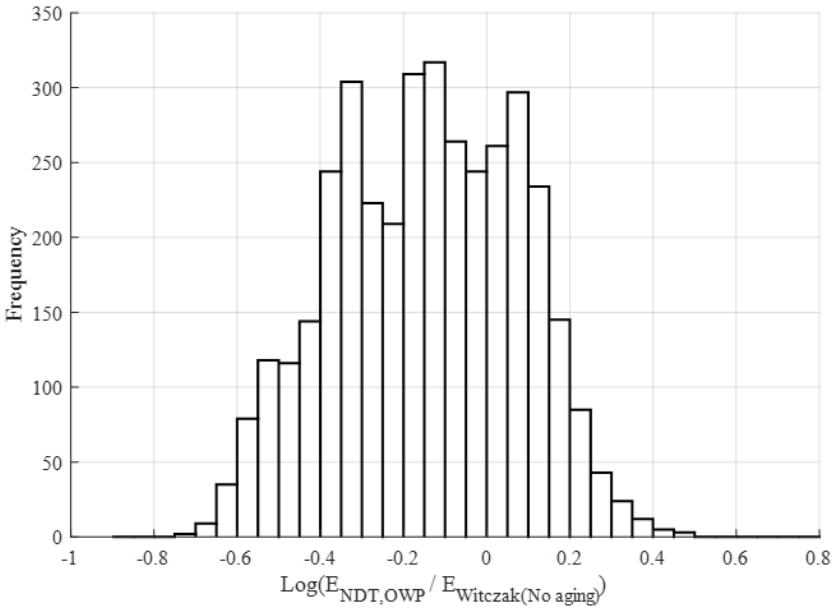

Figure 84. Distribution of $\log(E_{NDT,OWP}/E_{Witczak(No\ aging)})$ for pavements with no visible distress.

The observed mean value of $E_{NDT,OWP}/E_{Witczak(No\ aging)}$ is significantly less than 1, but to a lesser extent than $E_{NDT,OWP}/E_{Witczak(Aging)}$. For $E_{NDT,OWP}/E_{Witczak(Aging)}$, the binder aging adjustment caused $E_{Witczak}$ to be greater than $E_{NDT,OWP}$, especially at low temperatures. This is shown in Figure 82. Without adjusting for binder aging, however, there is still a difference between $E_{Witczak}$ and $E_{NDT,OWP}$, as shown in Figure 85. This difference can most likely be attributed to the fact that the assumed FWD load frequency of 30 Hz is higher than the actual FWD load frequency for many of the pavement sections in the analysis. A comparison of Figure 85 and Figure 82 shows that $E_{Witczak(No\ aging)}$ provides a better estimate of $E_{NDT,OWP}$ than $E_{Witczak(Aging)}$,, especially at low temperatures.

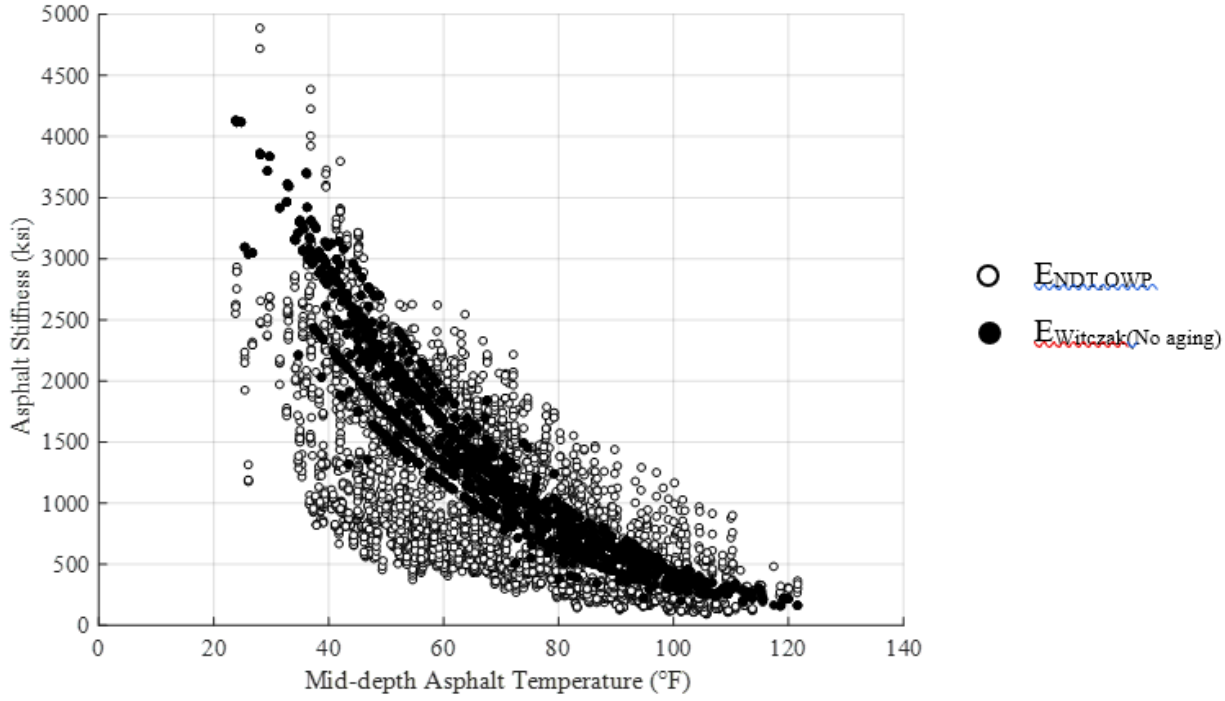

Figure 85. $E_{NDT,OWP}$ and $E_{Witczak(No\ aging)}$ vs. MDT.

5.3 EFFECT OF LOAD AND MDT ON THE FWD PARAMETERS

The preliminary investigation of the FWD parameters suggests that they are all dependent on both the FWD load magnitude and the MDT at the time FWD testing is performed. Thus, the relationship between the FWD parameter and the FWD load magnitude and the relationship between the FWD parameter and MDT were examined. This analysis was performed using a pool of data from many different LTPP sections. The data used in the analysis of each FWD parameter is summarized in Table 26. Additionally, in order to mitigate the effect of fatigue damage on the FWD parameter, only data from FWD testing on pavements with no visible distress (0% fatigue cracking by total lane area and 0 ft/mi longitudinal cracking in the wheelpath) was used in this analysis. Fatigue cracking in the AC pavements initiates at the bottom of the asphalt concrete layer and propagates to the surface of the pavement over time. Thus, it is possible that a pavement with no visible distress may have fatigue damage in the form of fatigue cracking that has not yet reached the surface of the pavement. This was not accounted for in the analysis of FWD parameters with respect to load magnitude and MDT, but it was considered in the subsequent analysis of the relationship between FWD parameters and fatigue damage.

Table 26. Summary of data used in assessing the effect of load magnitude and MDT on FWD parameters.

FWD Parameter	Number of LTPP Sections	Number of FWD Parameter Data Points
$d_{0,OWP}/d_{0,ML}$	248	5490
$E_{NDT,OWP}/E_{NDT,ML}$	248	5490
$E_{NDT,OWP}/E_{Witczak(Aging)}$	72	3726
$E_{NDT,OWP}/E_{Witczak(No\ aging)}$	72	3810

5.3.1 $d_{0,OWP}/d_{0,ML}$

First, $d_{0,OWP}/d_{0,ML}$ was examined with respect to FWD load magnitude. The mean of $d_{0,OWP}/d_{0,ML}$ appears to decrease slightly as the load magnitude changes, as shown in Figure 86. Paired t-tests were conducted between all pairs of load magnitude (6 kips and 9 kips, 6 kips, and 12 kips, 6 kips and 16 kips, etc.) to determine if $d_{0,OWP}/d_{0,ML}$ differs significantly between with magnitude. Paired t-tests were used to account for the effect of correlations between $d_{0,OWP}/d_{0,ML}$ data points collected from the same LTPP section at different points in the pavement life. Data was paired within test passes. Test passes without data for all four load levels were excluded from the paired t-tests. The details and results of the paired t-tests are shown in Table 27. The results confirm the initial impression that the mean of $d_{0,OWP}/d_{0,ML}$ is affected by load magnitude. Furthermore, it is shown that, for all pairs of load magnitude, the mean of $d_{0,OWP}/d_{0,ML}$ is significantly smaller at the higher load magnitude. This suggests that the mean of $d_{0,OWP}/d_{0,ML}$ decreases as the FWD load magnitude increases.

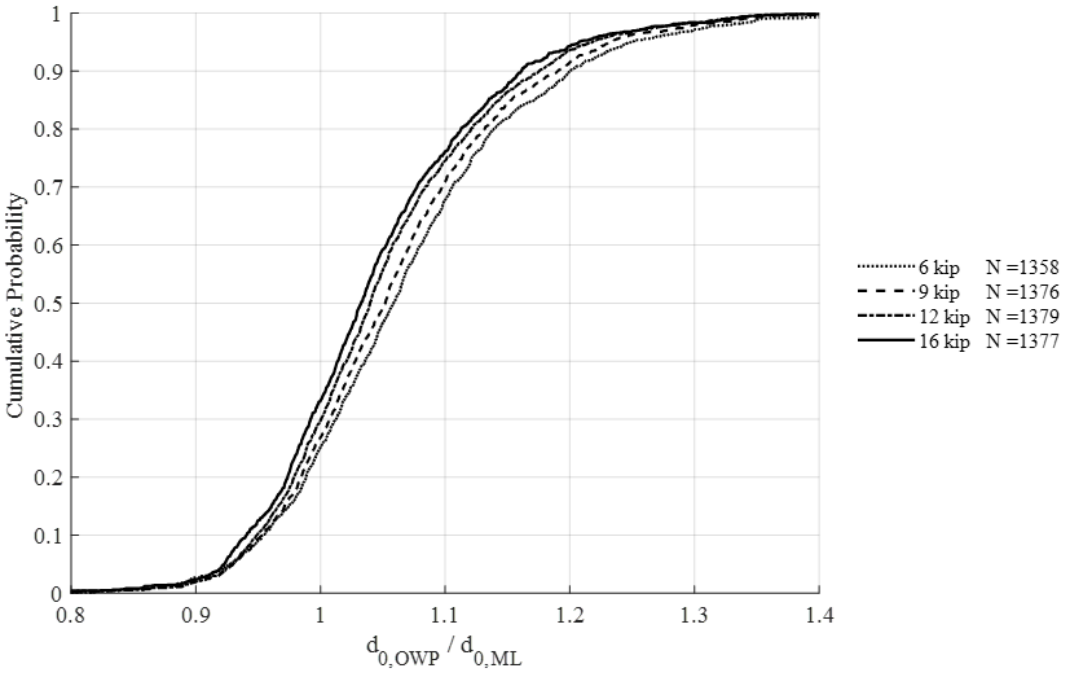

Figure 86. Distribution of $d_{0,OWP}/d_{0,ML}$ with respect to FWD load magnitude.

Table 27. Results of paired t-tests to determine the effect of FWD load magnitude on the mean of $d_{0,OWP}/d_{0,ML}$.

Null Hypothesis	$\mu_i - \mu_j = 0$					
Alternative Hypothesis	$\mu_i - \mu_j > 0$					
Load Level for μ_i	6 kips	6 kips	6 kips	9 kips	9 kips	12 kips
Load Level for μ_j	9 kips	12 kips	16 kips	12 kips	16 kips	16 kips
Reject Null Hypothesis?	Yes	Yes	Yes	Yes	Yes	Yes
Confidence Level	95%	95%	95%	95%	95%	95%
p-value	0.00	0.00	0.00	0.00	0.00	0.00

Statistical testing demonstrated that there is a significant relationship between $d_{0,OWP}/d_{0,ML}$ and FWD load magnitude. Thus, all further analysis of $d_{0,OWP}/d_{0,ML}$ was conducted using only data collected at a single load level. Separate, parallel analyses of the relationship between $d_{0,OWP}/d_{0,ML}$

and MDT were conducted using data from the 9-kip and 16-kip loads. The 9-kip load was selected because it is commonly used for routine FWD testing of AC pavements. The 16-kip load was selected because it is the other FWD load level most different from the 9-kip level, and thus the most likely to have a different effect on FWD parameters. The mean of $d_{0,OWP}/d_{0,ML}$ at the 9-kip load, calculated from 1376 data points and 247 different LTPP sections, is 1.06 and the standard deviation is 0.10. The mean of $d_{0,OWP}/d_{0,ML}$ at the 16-kip load, calculated from 1377 data points and 246 different LTPP sections, is 1.04 and the standard deviation is 0.09. The $d_{0,OWP}/d_{0,ML}$ parameter is normally distributed with a slight positive skew for both the 9-kip and 16-kip load magnitudes.

Second, $d_{0,OWP}/d_{0,ML}$ was examined with respect to MDT. As shown in Figures 87 and 89, there appears to be almost no correlation between $d_{0,OWP}/d_{0,ML}$ and MDT. However, if the data is divided into bins by MDT and cumulative probability distributions are plotted, it appears that the mean of $d_{0,OWP}/d_{0,ML}$ decreases as MDT increases. Cumulative probability distributions of $d_{0,OWP}/d_{0,ML}$ are shown in Figures 88 and 90 for the 9-kip and 16-kip load magnitudes, respectively.

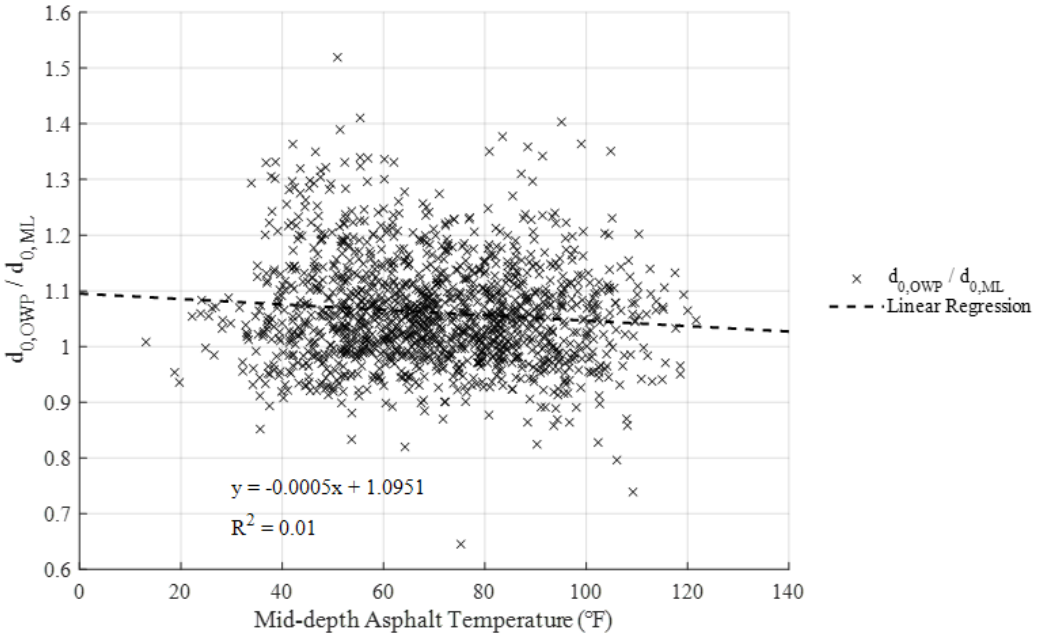

Figure 87. $d_{0,OWP}/d_{0,ML}$ vs. MDT (9-kip load).

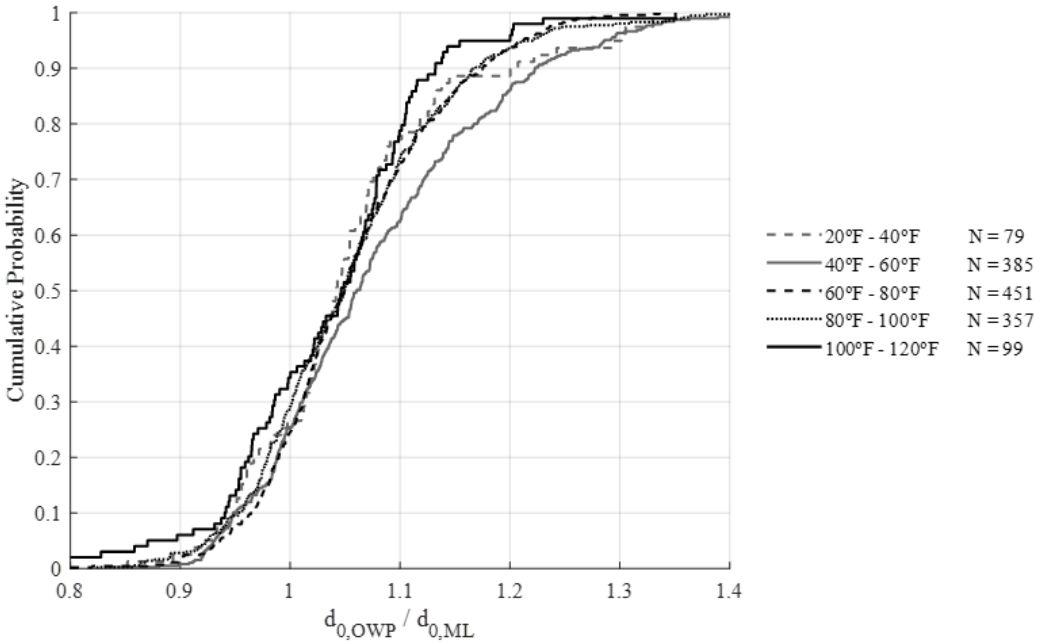

Figure 88. Distribution of $d_{0,OWP}/d_{0,ML}$ with respect to MDT (9-kip load).

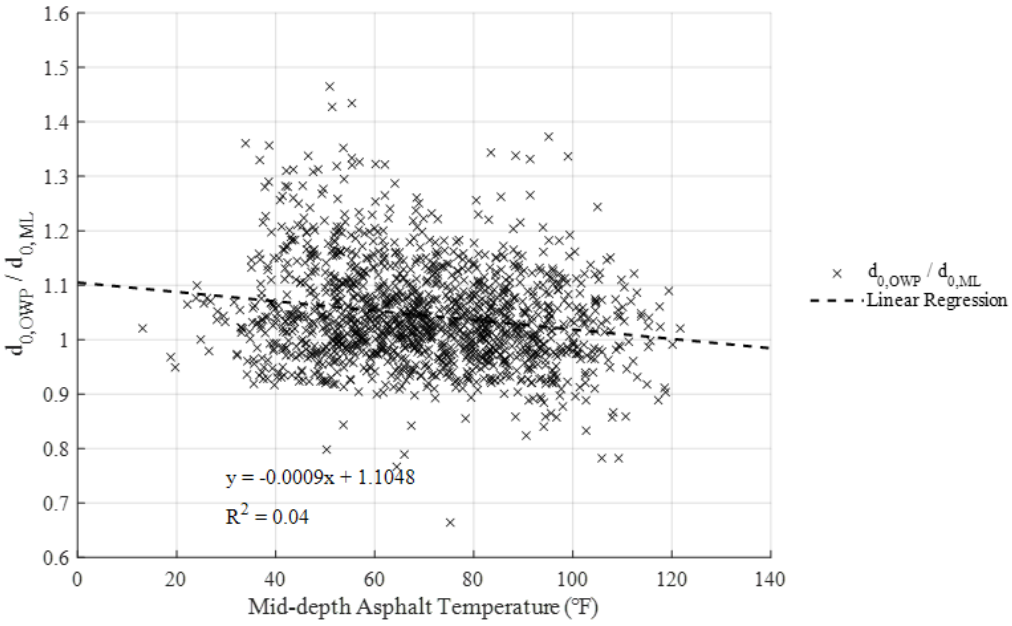

Figure 89. $d_{0,OWP}/d_{0,ML}$ vs. MDT (16-kip load).

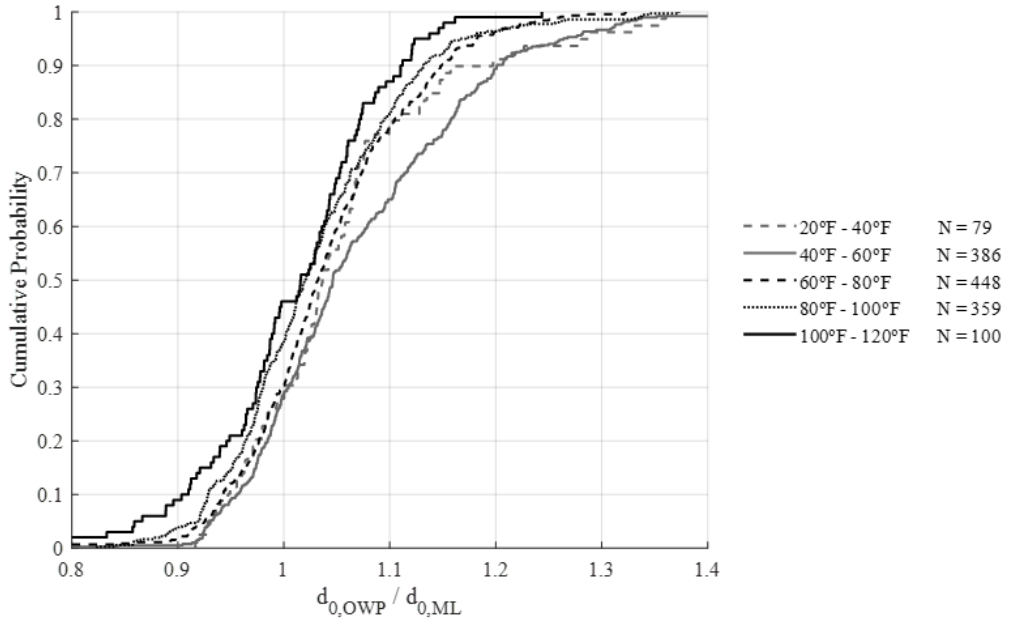

Figure 90. Distribution of $d_{0,OWP}/d_{0,ML}$ with respect to MDT (16-kip load).

In order to determine if $d_{0,OWP}/d_{0,ML}$ changes significantly with respect to MDT, a one-way analysis of variance (ANOVA) was performed. For the ANOVA, a model is used to describe two sources of variability in the sample data: variability due to factors of interest (such as MDT) and variability due to random error. The total variance of the sample data is divided according to the model into components that are attributed to factors (also called effects) and a component that is attributable to random error. Each factor in ANOVA is defined at multiple, discrete levels, also called treatments. This is called a fixed-effects model. Statistical hypothesis testing is performed by comparing the total variance attributable to the levels of each factor to the total variance attributable to random error. The F-statistic is used to determine if a factor has a significant effect on the mean. The F-statistic is the ratio of the mean sum of squares due to treatments (MST) over the mean sum of squares due to error (MSE). A p-value is determined by comparing the calculated F-statistic to the F-distribution. The p-value indicates the significance level of the treatment's effect on the mean. An ANOVA is similar to performing multiple two-sample t-tests to determine the effect of a factor but results in less Type I error. ANOVA can be performed with one factor (one-way ANOVA), two factors (two-way ANOVA), or multiple factors. When two or more factors are used, it is also possible to quantify the effect of interactions between the factors.

For the one-way ANOVA performed here, the factor is MDT and the response is the mean of $d_{0,OWP}/d_{0,ML}$. The ANOVA was conducted with fixed effects. Bins were used to define discrete levels of MDT. MDT was divided into 10ºF-wide bins, starting with 40ºF to 50 ºF and ending with 100ºF to 110 ºF. Each $d_{0,OWP}/d_{0,ML}$ data point was assigned to one of these bins based on its associated MDT. An ANOVA was performed separately for the 9-kip and 16-kip loads.

The results of the one-way ANOVA, detailed in Table 28, indicate that $d_{0,OWP}/d_{0,ML}$ changes significantly between 40ºF and 110ºF for both the 9-kip and 16-kip loads. Furthermore,

examining the mean of $d_{0,OWP}/d_{0,ML}$ for each MDT level shows that $d_{0,OWP}/d_{0,ML}$ decreases as MDT increases. This finding agrees with the previous observation made based on Figures 88 and 90. The mean and standard deviation of $d_{0,OWP}/d_{0,ML}$ for each MDT level are summarized in Table 29. The results of the ANOVA were used to perform a Tukey's test for comparing all pairs of means. Tukey's test is a single-step multiple comparison statistical hypothesis test. Tukey's test compares all possible pairs of means between groups and identifies pairs of means that are significantly different. The null hypothesis is that all pairs of means are equal. Tukey's test is based on an overall confidence level, and the confidence level of each paired comparison is at least equal to the overall confidence level. Tukey's test assumes that all observations are independent, the data within each group is normally distributed, and the variance within each group is equal (Tukey 1949).

Tukey's test was performed at an overall 95% confidence level. Note that the pairwise comparisons use the same null hypothesis and alternative hypothesis as an ANOVA. The pairwise mean comparisons, shown in Table 30, indicate that the mean of $d_{0,OWP}/d_{0,ML}$ is significantly different between high and low values of MDT. For example, the mean of $d_{0,OWP}/d_{0,ML}$ at the 40ºF and 50ºF level is significantly different from the mean at the 90ºF and 100ºF level for both the 9-kip and 16-kip loads. Exploratory analysis using ANOVA and Tukey's test demonstrated that there is a significant difference in $d_{0,OWP}/d_{0,ML}$ between low and high temperatures, but these tests do not account for possible correlations between data points from the same section. Paired t-tests were conducted to exclude the possible effect of correlations.

Table 28. Results of one-way ANOVA for the effect of MDT on the mean of $d_{0,OWP}/d_{0,ML}$ (9-kip and 16-kip loads).

FWD Load	9 kips	16 kips
Null Hypothesis	$\mu_1 = \mu_2 = \ldots = \mu_n$	
Alternative Hypothesis	At least one $\mu_i \neq \mu_j$	
Minimum MDT (ºF)	40	
Maximum MDT (ºF)	110	
Reject Null Hypothesis?	Yes	Yes
Confidence Level	95%	95%
p-value	0.00	0.00

Table 29. Mean and standard deviation of $d_{0,OWP}/d_{0,ML}$ for individual MDT levels (9-kip and 16-kip loads).

FWD Load	9 kips			16 kips		
MDT	Mean	Standard Deviation	Number of Data Points	Mean	Standard Deviation	Number of Data Points
40ºF - 50ºF	1.08	0.115	153	1.07	0.107	152
50ºF - 60ºF	1.08	0.107	232	1.07	0.101	234
60ºF - 70ºF	1.06	0.084	247	1.05	0.085	247
70ºF - 80ºF	1.05	0.085	204	1.03	0.079	201
80ºF - 90ºF	1.06	0.086	212	1.04	0.078	212
90ºF - 100ºF	1.04	0.099	145	1.02	0.093	147
100ºF - 110ºF	1.03	0.096	76	1.01	0.084	76

Table 30. Results of Tukey's test for pairwise comparisons of levels of MDT ($d_{0,OWP}/d_{0,ML}$, 9-kip and 16-kip loads).

FWD Load		9 kips		16 kips	
Lower MDT	Upper MDT	Reject Null Hypothesis?	p-value	Reject Null Hypothesis?	p-value
40ºF - 50ºF	50ºF - 60ºF	No	0.98	No	0.97
40ºF - 50ºF	60ºF - 70ºF	No	0.26	No	0.03
40ºF - 50ºF[1]	**70ºF - 80ºF**	No	0.02	**Yes**	**0.00**
40ºF - 50ºF	**80ºF - 90ºF**	No	0.33	**Yes**	**0.00**
40ºF - 50ºF	**90ºF - 100ºF**	**Yes**	**0.01**	**Yes**	**0.00**
40ºF - 50ºF	**100ºF - 110ºF**	**Yes**	**0.00**	**Yes**	**0.00**
50ºF - 60ºF	60ºF - 70ºF	No	0.69	No	0.18
50ºF - 60ºF	**70ºF - 80ºF**	No	0.11	**Yes**	**0.00**
50ºF - 60ºF	80ºF - 90ºF	No	0.77	No	0.02
50ºF - 60ºF	**90ºF - 100ºF**	No	0.03	**Yes**	**0.00**
50ºF - 60ºF	**100ºF - 110ºF**	**Yes**	**0.01**	**Yes**	**0.00**
60ºF - 70ºF	70ºF - 80ºF	No	0.91	No	0.75
60ºF - 70ºF	80ºF - 90ºF	No	1.00	No	0.96
60ºF - 70ºF	90ºF - 100ºF	No	0.55	No	0.05
60ºF - 70ºF	100ºF - 110ºF	No	0.24	No	0.06
70ºF - 80ºF	80ºF - 90ºF	No	0.90	No	1.00
70ºF - 80ºF	90ºF - 100ºF	No	0.99	No	0.71
70ºF - 80ºF	100ºF - 110ºF	No	0.78	No	0.57
80ºF - 90ºF	90ºF - 100ºF	No	0.54	No	0.39
80ºF - 90ºF	100ºF - 110ºF	No	0.23	No	0.32
90ºF - 100ºF	100ºF - 110ºF	No	0.98	No	1.00

[1] Significant comparisons are in bold.

Paired t-tests were conducted to determine if $d_{0,OWP}/d_{0,ML}$ is significantly lower at a high MDT than at a low MDT. A bin from 40ºF to 60ºF was selected to represent a low MDT and a bin from 90ºF to 110ºF was selected to represent a high MDT. Data was paired by LTPP section. For each section, all $d_{0,OWP}/d_{0,ML}$ data points in the 40ºF - 60ºF bin were averaged to obtain a representative value of $d_{0,OWP}/d_{0,ML}$ at a low MDT. The same was performed for the 90ºF - 110ºF bin. All sections without data in both MDT bins were excluded from the analysis. As a result of this restriction, only 42 sections were included in the paired t-test for the 9-kip load and 45 sections for the 16-kip load. The data used in the paired t-test for the 9-kip load are summarized in Table 31. The details and results of the paired t-tests for both load magnitudes are summarized in Table 32.

Table 31. Data used in a paired t-test to determine the effect of MDT on $d_{0,OWP}/d_{0,ML}$ (9-kip load).

State	LTPP ID	Mean of $d_{0,OWP}/d_{0,ML}$ for 40-60 bin	Mean of $d_{0,OWP}/d_{0,ML}$ for 90-110 bin	Number of data points in 40-60 bin	Number of data points in 90-110 bin
GA	13-1031	1.11	0.96	18	12
IL	17-B320	1.01	1.02	1	1
IA	19-0107	1.11	1.17	1	1
KS	20-0111	0.98	0.86	1	1
KS	20-0162	0.97	0.90	1	1
KS	20-0903	1.10	1.11	1	1
ME	23-1026	1.05	1.01	14	4
MI	26-0116	1.02	1.09	3	1
MI	26-0124	1.05	1.02	3	1
MN	27-0501	1.04	1.03	2	2
MN	27-1018	1.06	1.07	2	1
MN	27-A330	1.11	1.01	1	1
MN	27-C350	1.07	1.06	1	2
MO	29-A320	1.24	0.97	1	1
MO	29-A351	1.24	1.10	1	2
MO	29-B350	1.02	0.96	1	1

Table 31 (continued).

State	LTPP ID	Mean of $d_{0,OWP}/d_{0,ML}$ for 40-60 bin	Mean of $d_{0,OWP}/d_{0,ML}$ for 90-110 bin	Number of data points in 40-60 bin	Number of data points in 90-110 bin
MT	30-8129	1.09	1.09	30	18
NE	31-0114	0.97	1.05	8	13
NE	31-1030	1.15	1.20	14	3
NE	31-A350	1.32	1.15	2	1
NE	31-A351	1.10	1.05	1	1
NE	31-A353	1.15	1.20	2	1
NV	32-0101	1.04	1.14	12	8
NM	35-1112	1.11	1.10	26	23
NY	36-0801	0.95	0.99	23	8
NY	36-0859	0.97	0.95	1	1
OH	39-0105	1.10	1.14	1	1
OH	39-0901	1.05	0.92	3	4
PA	42-1597	1.00	0.89	1	1
SD	46-9187	1.27	1.24	32	6
TX	48-1122	1.22	1.01	1	2
UT	49-1001	1.18	1.12	14	2
VA	51-0113	1.05	1.00	17	3
VA	51-0114	0.98	1.00	30	21
WI	55-0114	1.14	0.96	1	1
WI	55-0115	1.00	1.08	2	1
WI	55-0120	1.08	1.07	1	1
WI	55-0122	1.04	1.05	1	1
WI	55-0806	1.03	1.01	1	1
MB	83-A331	1.02	0.96	1	1
MB	83-A350	0.92	0.97	1	2
MB	83-A351	1.15	0.94	1	1

Table 32. Results of paired t-test to determine the effect of MDT on the mean of $d_{0,OWP}/d_{0,ML}$ (9-kip and 16-kip loads).

FWD Load	9 kips	16 kips
Null Hypothesis	$\mu_1 - \mu_2 = 0$	
Alternative Hypothesis	$\mu_1 - \mu_2 > 0$	
MDT Range for μ_1	40ºF - 60ºF	
MDT Range for μ_2	90ºF - 110ºF	
Reject Null Hypothesis?	Yes	Yes
Confidence Level	95%	95%
p-value	0.00	0.00

The results of the paired t-tests indicate that the mean of $d_{0,OWP}/d_{0,ML}$ is significantly lower at a high MDT than at a low MDT for both loads. Assuming there are no additional, unknown factors that affect $d_{0,OWP}/d_{0,ML}$, this suggests that MDT does have a significant effect on the $d_{0,OWP}/d_{0,ML}$ parameter. Further analysis of $d_{0,OWP}/d_{0,ML}$ must account for this relationship.

The same statistical analyis described above for $d_{0,OWP}/d_{0,ML}$ was also performed for the other three FWD parameters, $E_{NDT,OWP}/E_{NDT,ML}$, $E_{NDT,OWP}/E_{Witczak(Aging)}$, and $E_{NDT,OWP}/E_{Witczak(No\ aging)}$. For each parameter, the main conclusions of the analysis are described and tabulated. Deviations from the analysis of $d_{0,OWP}/d_{0,ML}$ are noted and described

5.3.2 $E_{NDT,OWP}/E_{NDT,ML}$

First, $E_{NDT,OWP}/E_{NDT,ML}$ is examined with respect to FWD load. As shown in Figure 91, it appears that $E_{NDT,OWP}/E_{NDT,ML}$ increases as the load increases. Paired t-tests were conducted between all pairs of load levels to determine if $E_{NDT,OWP}/E_{NDT,ML}$ increases significantly with load magnitude. The paired t-tests were set up for $E_{NDT,OWP}/E_{NDT,ML}$ in the same manner performed for $d_{0,OWP}/d_{0,ML}$.

The details and results of the paired t-tests are shown in Table 33. The results show that, for all pairs of load levels, the mean of $E_{NDT,OWP}/E_{NDT,ML}$ is significantly greater for the higher load level. This confirms the initial assumption that $E_{NDT,OWP}/E_{NDT,ML}$ increases with load magnitude.

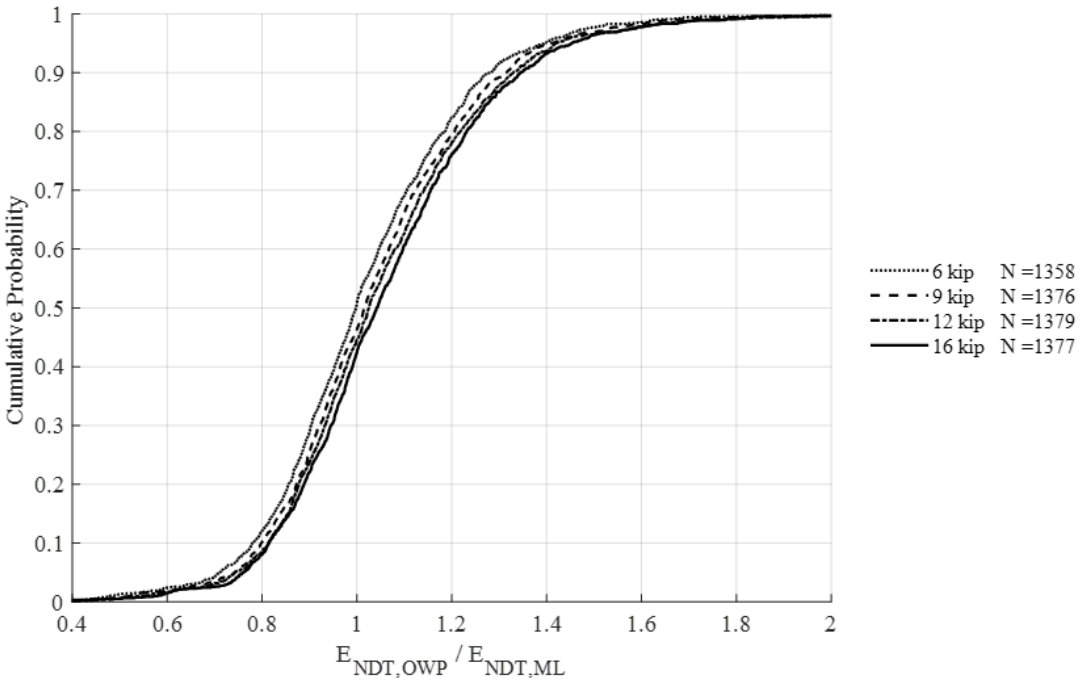

Figure 91. Distribution of $E_{NDT,OWP}/E_{NDT,ML}$ with respect to FWD load magnitude.

Table 33. Results of paired t-tests to determine the effect of FWD load magnitude on the mean of $E_{NDT,OWP}/E_{NDT,ML}$.

Null Hypothesis	$\mu_i - \mu_j = 0$					
Alternative Hypothesis	$\mu_i - \mu_j < 0$					
Load Level for μ_i	6 kips	6 kips	6 kips	9 kips	9 kips	12 kips
Load Level for μ_j	9 kips	12 kips	16 kips	12 kips	16 kips	16 kips
Reject Null Hypothesis?	Yes	Yes	Yes	Yes	Yes	Yes
Confidence Level	95%	95%	95%	95%	95%	95%
p-value	0.00	0.00	0.00	0.00	0.00	0.00

Statistical testing demonstrated that there is a significant relationship between $E_{NDT,OWP}/E_{NDT,ML}$ and FWD load magnitude. All further analysis of $E_{NDT,OWP}/E_{NDT,ML}$ is conducted using only data collected at a single load. Separate, parallel analyses of the relationship between $E_{NDT,OWP}/E_{NDT,ML}$ and MDT were conducted using data from the 9-kip and 16-kip loads. The mean of $E_{NDT,OWP}/E_{NDT,ML}$ at the 9-kip load, calculated based on 1376 data points and 247 different LTPP sections, is 1.04 and the standard deviation is 0.23. The mean of $E_{NDT,OWP}/E_{NDT,ML}$ at the 16-kip load, calculated based on 1377 data points and 246 different LTPP sections, is 1.07 and the standard deviation is 0.24. For both loads, $E_{NDT,OWP}/E_{NDT,ML}$ is normally distributed with a slight positive skew.

As shown in Figures 92 and 94, a very weak positive correlation exists between $E_{NDT,OWP}/E_{NDT,ML}$ and MDT for both the 9-kip and 16-kip loads. The relationship between $E_{NDT,OWP}/E_{NDT,ML}$ and MDT becomes much clearer if the data is divided into bins by MDT and cumulative probability distributions are plotted. Cumulative probability distributions for $E_{NDT,OWP}/E_{NDT,ML}$ are shown in Figures 93 and 95 for the 9-kip and 16-kip loads, respectively.

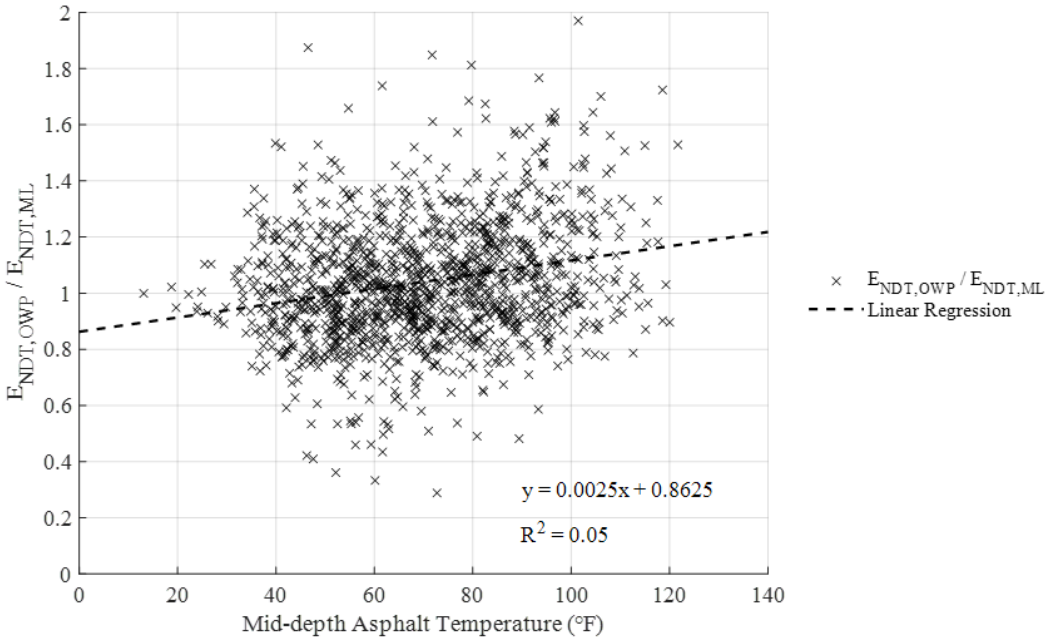

Figure 92. $E_{NDT,OWP}/E_{NDT,ML}$ vs MDT (9-kip load).

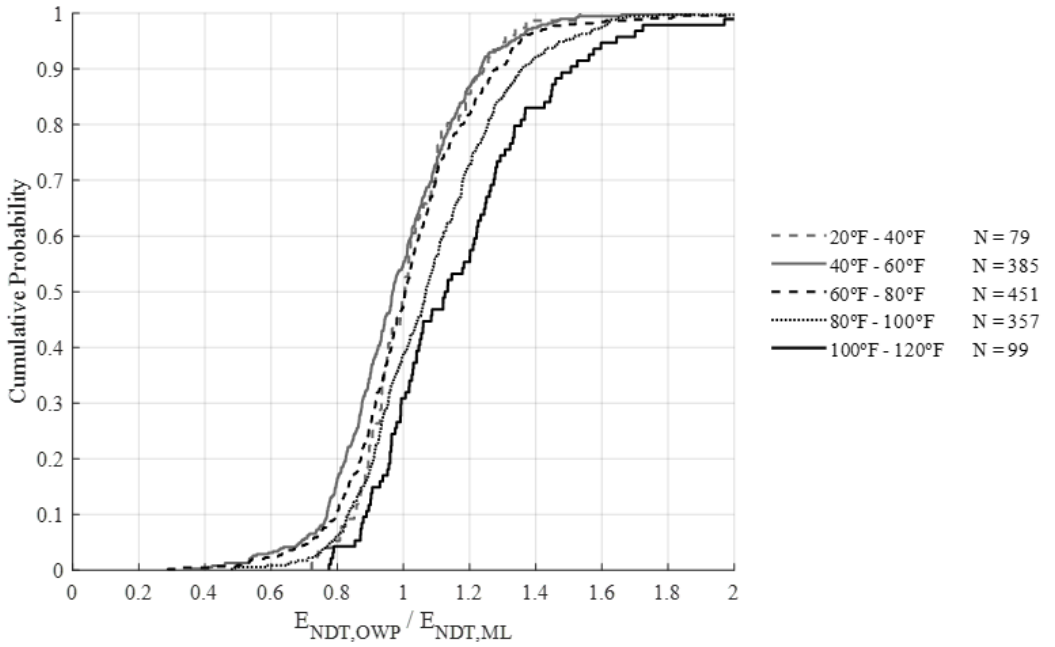

Figure 93. Distribution of $E_{NDT,OWP}/E_{NDT,ML}$ with respect to MDT (9-kip load).

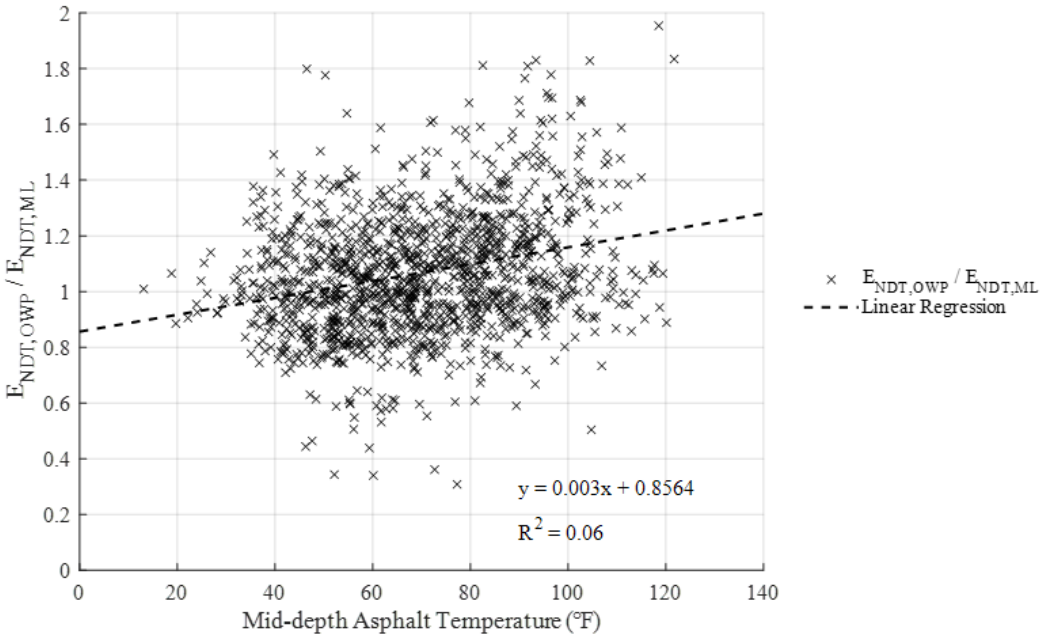

Figure 94. $E_{NDT,OWP}/E_{NDT,ML}$ vs MDT (16-kip load).

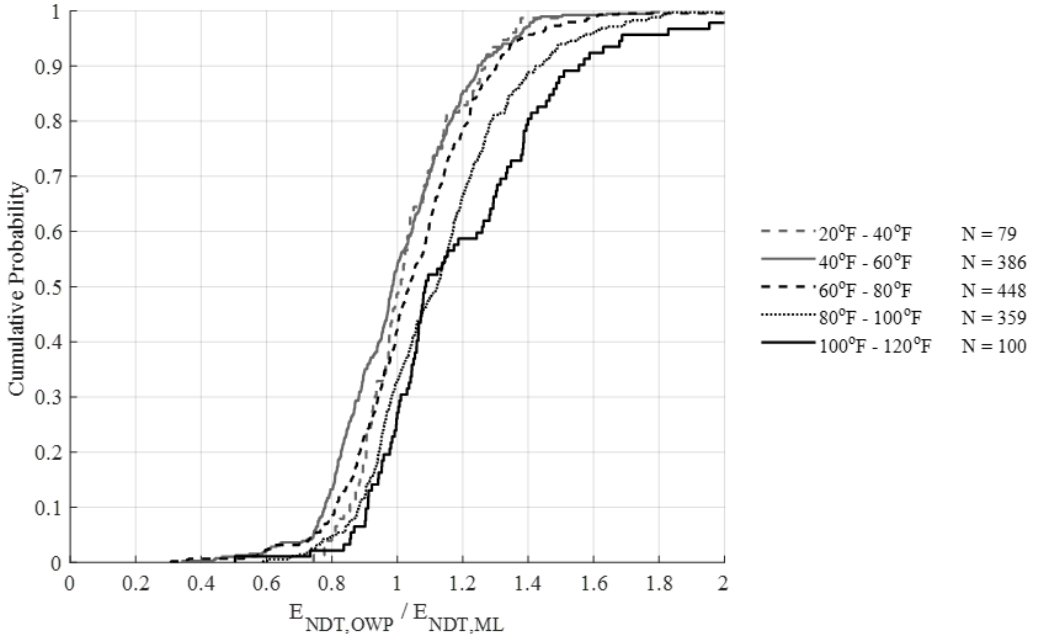

Figure 95. Distribution of $E_{NDT,OWP}/E_{NDT,ML}$ with respect to MDT (16-kip load).

A one-way ANOVA was performed to test the assumption that $E_{NDT,OWP}/E_{NDT,ML}$ increases as MDT increases. The same temperature bins used to perform the ANOVA for $d_{0,OWP}/d_{0,ML}$ were used for $E_{NDT,OWP}/E_{NDT,ML}$. The results of the ANOVA, detailed in Table 34, indicate that the mean of $E_{NDT,OWP}/E_{NDT,ML}$ does change significantly between 40ºF and 110ºF for both the 9-kip and 16-kip loads. Additionally, examining the mean of $E_{NDT,OWP}/E_{NDT,ML}$ for each level of the MDT factor shows that $E_{NDT,OWP}/E_{NDT,ML}$ increases as MDT increases, confirming the initial assumption based on Figures 92 through 95. The mean and standard deviation of $E_{NDT,OWP}/E_{NDT,ML}$ for each MDT level are summarized in Table 35.

Tukey's test was performed at a 95% overall confidence level to compare all pairs of the MDT factor level. The pairwise comparisons, shown in Table 36, indicate that the mean of $E_{NDT,OWP}/E_{NDT,ML}$ is significantly different for several combinations of MDT levels. The majority of significantly different MDT levels are not consecutive. For example, the 40ºF to 50ºF level is not significantly different from the 50ºF to 60ºF level. Furthermore, most significantly different pairs of levels include one level in the low MDT range (40ºF to 60ºF) and one level in the high MDT range (90ºF to 110ºF). Tukey's test indicates there is a significant difference in $E_{NDT,OWP}/E_{NDT,ML}$ between low and high temperatures, but it does not account for possible correlations between data points from the same section. Paired t-tests were performed in order to account for the possible effect of correlations.

Table 34. Results of one-way ANOVA for the effect of MDT on the mean of $E_{NDT,OWP}/E_{NDT,ML}$ (9-kip and 16-kip loads).

FWD Load	9 kips	16 kips
Null Hypothesis	$\mu_1 = \mu_2 = \ldots = \mu_n$	
Alternative Hypothesis	At least one $\mu_i \neq \mu_j$	
Minimum MDT (ºF)	40	
Maximum MDT (ºF)	110	
Reject Null Hypothesis?	Yes	Yes
Simultaneous Confidence Level	95%	95%
p-value	0.00	0.00

Table 35. Mean and standard deviation of $E_{NDT,OWP}/E_{NDT,ML}$ for individual MDT levels (9-kip and 16-kip loads).

FWD Load	9 kips			16 kips		
MDT	Mean	Standard Deviation	Number of Data Points	Mean	Standard Deviation	Number of Data Points
40ºF - 50ºF	0.99	0.215	153	1.01	0.205	153
50ºF - 60ºF	0.98	0.194	232	1.00	0.201	232
60ºF - 70ºF	1.00	0.209	247	1.03	0.209	247
70ºF - 80ºF	1.05	0.300	204	1.08	0.270	204
80ºF - 90ºF	1.06	0.196	212	1.10	0.205	212
90ºF - 100ºF	1.13	0.249	145	1.18	0.257	145
100ºF - 110ºF	1.18	0.264	76	1.21	0.301	76

Table 36. Results of Tukey's test for pairwise comparisons of levels of the MDT ($E_{NDT,OWP}/E_{NDT,ML}$, 9-kip and 16-kip loads).

Lower MDT	Upper MDT	Reject Null Hypothesis?	p-value	Reject Null Hypothesis?	p-value
40ºF - 50ºF	50ºF - 60ºF	No	1.00	No	1.00
40ºF - 50ºF	60ºF - 70ºF	No	1.00	No	0.94
40ºF - 50ºF	70ºF - 80ºF	No	0.17	No	0.05
40ºF - 50ºF[1]	**80ºF - 90ºF**	No	0.08	**Yes**	**0.00**
40ºF - 50ºF	**90ºF - 100ºF**	**Yes**	**0.00**	**Yes**	**0.00**
40ºF - 50ºF	**100ºF - 110ºF**	**Yes**	**0.00**	**Yes**	**0.00**
50ºF - 60ºF	60ºF - 70ºF	No	0.91	No	0.67
50ºF - 60ºF	**70ºF - 80ºF**	No	0.02	**Yes**	**0.00**
50ºF - 60ºF	**80ºF - 90ºF**	**Yes**	**0.00**	**Yes**	**0.00**
50ºF - 60ºF	**90ºF - 100ºF**	**Yes**	**0.00**	**Yes**	**0.00**
50ºF - 60ºF	**100ºF - 110ºF**	**Yes**	**0.00**	**Yes**	**0.00**
60ºF - 70ºF	70ºF - 80ºF	No	0.29	No	0.30
60ºF - 70ºF	80ºF - 90ºF	No	0.14	No	0.02
60ºF - 70ºF	**90ºF - 100ºF**	**Yes**	**0.00**	**Yes**	**0.00**
60ºF - 70ºF	**100ºF - 110ºF**	**Yes**	**0.00**	**Yes**	**0.00**
70ºF - 80ºF	80ºF - 90ºF	No	1.00	No	0.97
70ºF - 80ºF	90ºF - 100ºF	No	0.05	**Yes**	**0.00**
70ºF - 80ºF	**100ºF - 110ºF**	**Yes**	**0.00**	**Yes**	**0.00**
80ºF - 90ºF	90ºF - 100ºF	No	0.10	No	0.03
80ºF - 90ºF	**100ºF - 110ºF**	**Yes**	**0.00**	**Yes**	**0.01**
90ºF - 100ºF	100ºF - 110ºF	No	0.70	No	0.97

[1] Significant comparisons are in bold.

Paired t-tests were conducted to determine if the mean of $E_{NDT,OWP}/E_{NDT,ML}$ is significantly greater at a high MDT than at a low MDT. A bin from 40ºF to 60ºF was selected to represent a low MDT and a bin from 90ºF to 110ºF was selected to represent a high MDT. The paired t-tests for $E_{NDT,OWP}/E_{NDT,ML}$ were performed in the same manner as the paired t-tests for $d_{0,OWP}/d_{0,ML}$. As a result, only 41 sections for the 9-kip load and 45 sections for the 16-kip load were included in the paired t-tests for $E_{NDT,OWP}/E_{NDT,ML}$. These are the same LTPP sections used in the paired t-tests performed for $d_{0,OWP}/d_{0,ML}$, except LTPP Section 27-A330 was excluded from the 9-kip load analysis because it was found to have erroneous backcalculation data. The details and results of

the paired t-tests for $E_{NDT,OWP}/E_{NDT,ML}$ are summarized in Table 37. The results indicate that the mean of $E_{NDT,OWP}/E_{NDT,ML}$ is significantly greater at high temperatures than at low temperatures, confirming the initial observation that $E_{NDT,OWP}/E_{NDT,ML}$ increases as MDT increases. Further analysis of $E_{NDT,OWP}/E_{NDT,ML}$ must account for this relationship.

Table 37. Results of paired t-tests to determine the effect of MDT on the mean of $E_{NDT,OWP}/E_{NDT,ML}$ (9-kip and 16-kip loads).

FWD Load	9 kips	16 kips
Null Hypothesis	$\mu_1 - \mu_2 = 0$	
Alternative Hypothesis	$\mu_1 - \mu_2 > 0$	
MDT Range for μ_1	40ºF - 60ºF	
MDT Range for μ_2	90ºF - 110ºF	
Reject Null Hypothesis?	Yes	Yes
Confidence Level	95%	95%
p-value	0.00	0.01

5.3.3 $E_{NDT,OWP}/E_{Witczak(Aging)}$

The relationship between $E_{NDT,OWP}/E_{Witczak(Aging)}$ and FWD load was analyzed using the log transformation of the FWD parameter, $\log(E_{NDT,OWP}/E_{Witczak(Aging)})$. Based on Figure 96, it appears that the mean of $\log(E_{NDT,OWP}/E_{Witczak(Aging)})$ increases as the FWD load increases. Paired t-tests were conducted for all pairs of load levels to determine if $\log(E_{NDT,OWP}/E_{Witczak(Aging)})$ increases significantly with increasing load. The paired t-tests were performed for $\log(E_{NDT,OWP}/E_{Witczak(Aging)})$ the same manner as for the previous two parameters. The details and results of the paired t-tests are shown in Table 38. The results show that, for all pairs of load levels, the mean of $\log(E_{NDT,OWP}/E_{Witczak(Aging)})$ is significantly greater for the higher load level. This confirms the initial hypothesis that $\log(E_{NDT,OWP}/E_{Witczak(Aging)})$ increases as the load level increases.

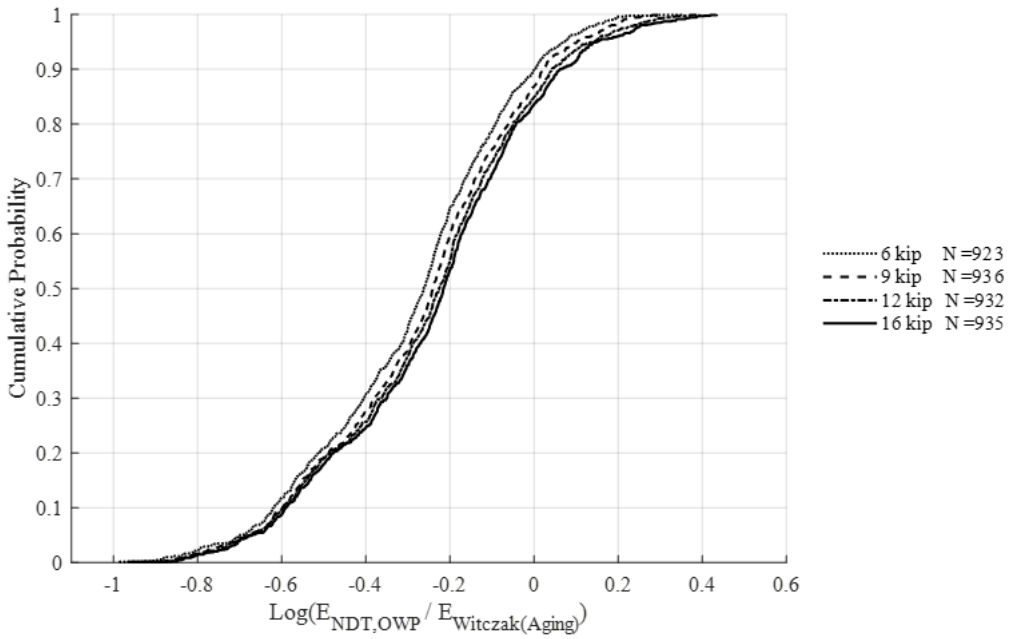

Figure 96. Distribution of $\log(E_{NDT,OWP}/E_{Witczak(Aging)})$ with respect to FWD load.

Table 38. Results of paired t-tests to determine the effect of FWD load level on the mean of $\log(E_{NDT,OWP}/E_{Witczak(Aging)})$.

Null Hypothesis	$\mu_i - \mu_j = 0$					
Alternative Hypothesis	$\mu_i - \mu_j < 0$					
Load Level for μ_i	6 kip	6 kip	6 kip	9 kip	9 kip	12 kip
Load Level for μ_j	9 kip	12 kip	16 kip	12 kip	16 kip	16 kip
Reject Null Hypothesis?	Yes	Yes	Yes	Yes	Yes	Yes
Confidence Level	95%	95%	95%	95%	95%	95%
p-value	0.00	0.00	0.00	0.00	0.00	0.00

Paired t-tests indicated that there is a significant relationship between $\log(E_{NDT,OWP}/E_{Witczak(Aging)})$ and FWD load, so all further analyses of $\log(E_{NDT,OWP}/E_{Witczak(Aging)})$ are conducted using only data collected at a single load level. Separate, parallel analyses of the relationship between $\log(E_{NDT,OWP}/E_{Witczak(Aging)})$ and MDT were conducted using data from the 9-kip and 16-kip load levels. The mean of $\log(E_{NDT,OWP}/E_{Witczak(Aging)})$ at the 9-kip load, calculated from 936 data points and 71 different LTPP sections, is -0.27 and the standard deviation is 0.24. The mean of $\log(E_{NDT,OWP}/E_{Witczak(Aging)})$ at a 16-kip load, calculated from 935 data points and 71 different LTPP sections, is -0.24 and the standard deviation is 0.25. For both load levels, $\log(E_{NDT,OWP}/E_{Witczak(Aging)})$ is approximately normally distributed with a slight negative skew.

As shown in Figures 97 and 99, there appears to be a weak positive correlation between $\log(E_{NDT,OWP}/E_{Witczak(Aging)})$ and MDT for both the 9-kip and 16-kip loads. The positive correlation between $\log(E_{NDT,OWP}/E_{Witczak(Aging)})$ and MDT becomes much clearer if the data is divided into bins by MDT and cumulative probability distributions are plotted. Cumulative probability distributions of $\log(E_{NDT,OWP}/E_{Witczak(Aging)})$ are shown in Figures 98 and 100 for the 9-kip and 16-kip load levels, respectively.

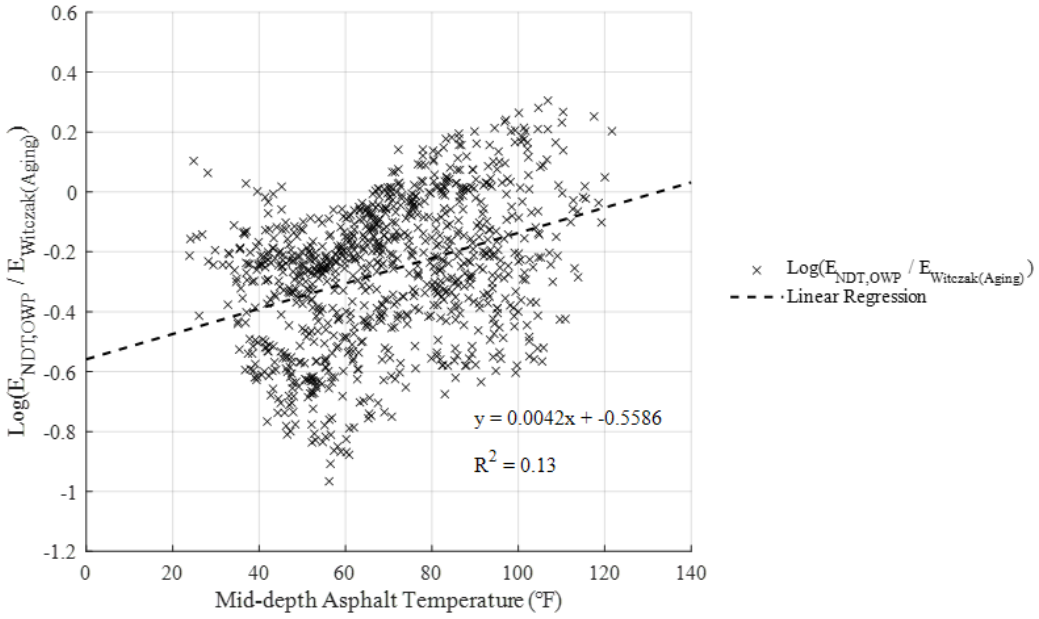

Figure 97. Log($E_{NDT,OWP}/E_{Witczak(Aging)}$) vs MDT (9-kip load).

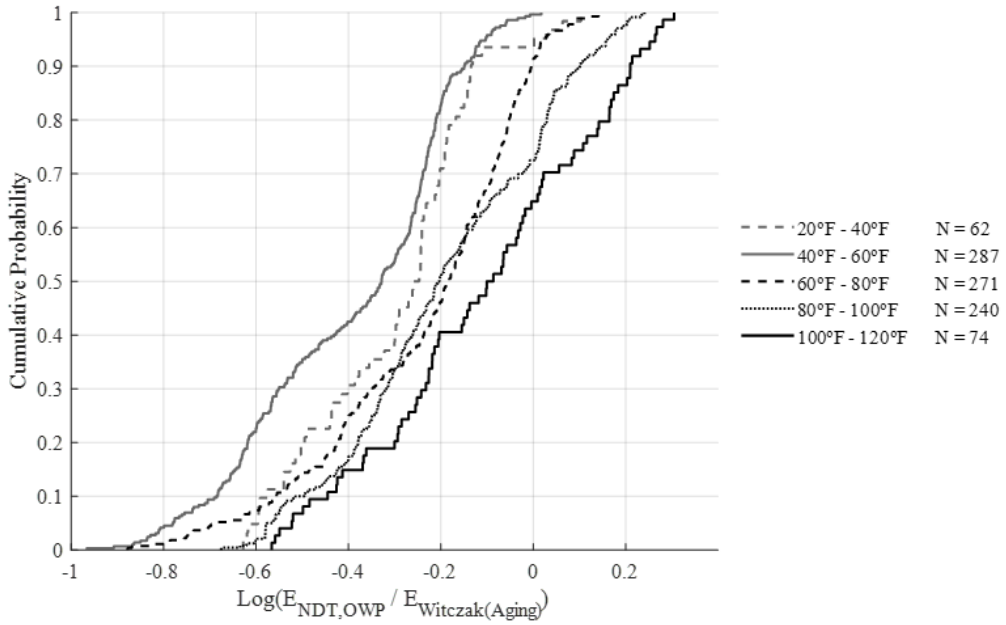

Figure 98. Distribution of log($E_{NDT,OWP}/E_{Witczak(Aging)}$) with respect to MDT (9-kip load).

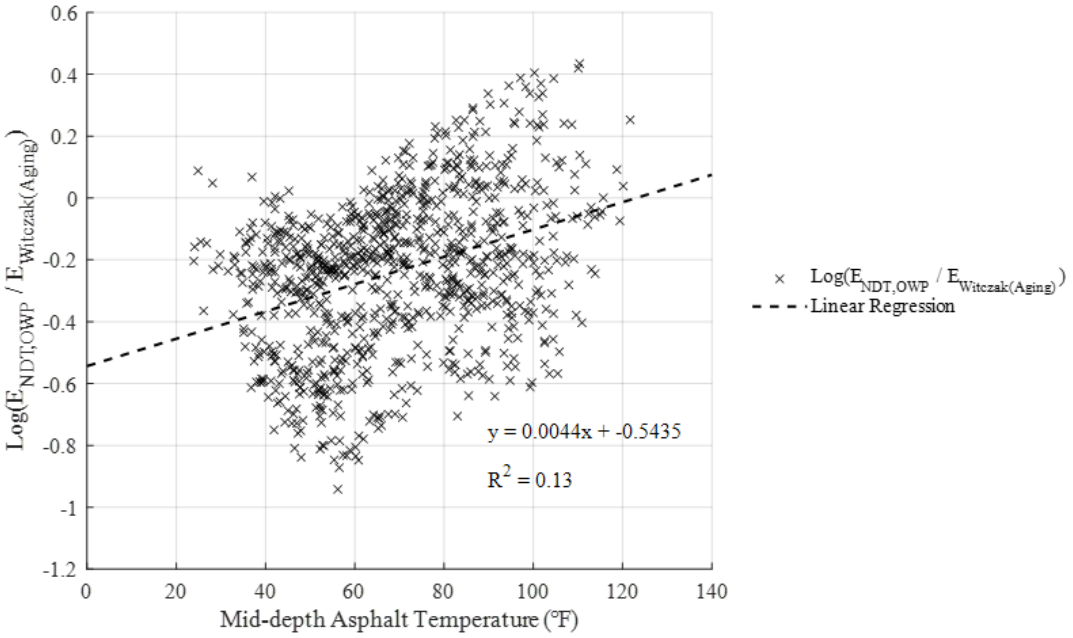

Figure 99. Log($E_{NDT,OWP}/E_{Witczak(Aging)}$) vs MDT (16-kip load).

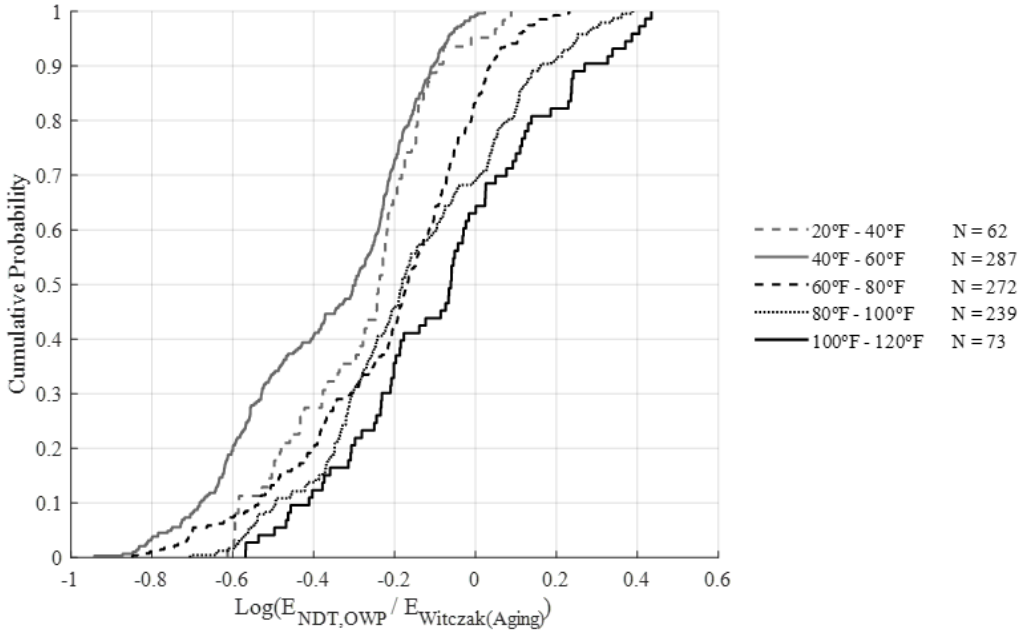

Figure 100. Distribution of log($E_{NDT,OWP}/E_{Witczak(Aging)}$) with respect to MDT (16-kip load).

An ANOVA was performed to test the assumption that $\log(E_{NDT,OWP}/E_{Witczak(Aging)})$ increases as MDT increases. The same temperature bins used to perform the ANOVA for $d_{0,OWP}/d_{0,ML}$ and $E_{NDT,OWP}/E_{NDT,ML}$ were used for $\log(E_{NDT,OWP}/E_{Witczak(Aging)})$. The results of the ANOVA, detailed in Table 39, indicate that the mean of $\log(E_{NDT,OWP}/E_{Witczak(Aging)})$ changes significantly between 40ºF and 110ºF for both the 9-kip and 16-kip load levels. Furthermore, the mean of $\log(E_{NDT,OWP}/E_{Witczak(Aging)})$ increases as MDT increases. The mean and standard deviation of $\log(E_{NDT,OWP}/E_{Witczak(Aging)})$ for each MDT level are summarized in Table 38. Tukey's test was performed at a 95% overall confidence level to compare all pairs of the MDT levels. The pairwise comparisons, shown in Table 39, indicate that the mean of $\log(E_{NDT,OWP}/E_{Witczak(Aging)})$ is significantly different for all pairwise comparisons that include lower MDTs. For example, the mean of $\log(E_{NDT,OWP}/E_{Witczak(Aging)})$ for a MDT at the 40ºF to 50ºF level is significantly different than the mean of $\log(E_{NDT,OWP}/E_{Witczak(Aging)})$ at the 60ºF to 70ºF, 70ºF to 80ºF, 80ºF to 90ºF, or 90ºF to 100ºF level. Additionally, the mean of $\log(E_{NDT,OWP}/E_{Witczak(Aging)})$ is not significantly different for all pairs of levels above 60ºF to 70ºF.

Table 39. Results of one-way ANOVA for the effect of MDT on the mean of $\log(E_{NDT,OWP}/E_{Witczak(Aging)})$ (9-kip and 16-kip loads).

FWD Load	9 kips	16 kips
Null Hypothesis	$\mu_1 = \mu_2 = \ldots = \mu_n$	
Alternative Hypothesis	At least one $\mu_i \neq \mu_j$	
Minimum MDT (ºF)	40	
Maximum MDT (ºF)	110	
Reject Null Hypothesis?	Yes	Yes
Simultaneous Confidence Level	95%	95%
p-value	0.00	0.00

Table 40. Mean and standard deviation of $\log(E_{NDT,OWP}/E_{Witczak(Aging)})$ for individual MDT levels (9-kip and 16-kip loads).

FWD Load	9 kips			16 kips		
MDT	Mean	Standard Deviation	Number of Data Points	Mean	Standard Deviation	Number of Data Points
40ºF - 50ºF	-0.38	0.21	126	-0.36	0.22	126
50ºF - 60ºF	-0.40	0.22	161	-0.38	0.23	161
60ºF - 70ºF	-0.28	0.22	159	-0.25	0.23	159
70ºF - 80ºF	-0.18	0.20	112	-0.16	0.21	113
80ºF - 90ºF	-0.19	0.22	144	-0.16	0.24	144
90ºF - 100ºF	-0.19	0.23	96	-0.15	0.25	95
100ºF - 110ºF	-0.13	0.25	57	-0.09	0.27	57

Table 41. Results of Tukey's test for pairwise comparisons of levels of MDT ($\text{Log}(E_{NDT,OWP}/E_{Witczak(Aging)})$, 9-kip and 16-kip loads).

FWD Load		9 kips		16 kips	
Lower MDT	Upper MDT	Reject Null Hypothesis?	p-value	Reject Null Hypothesis?	p-value
40ºF - 50ºF	50ºF - 60ºF	No	0.98	No	0.99
40ºF - 50ºF[1]	**60ºF - 70ºF**	**Yes**	**0.00**	**Yes**	**0.00**
40ºF - 50ºF	**70ºF - 80ºF**	**Yes**	**0.00**	**Yes**	**0.00**
40ºF - 50ºF	**80ºF - 90ºF**	**Yes**	**0.00**	**Yes**	**0.00**
40ºF - 50ºF	**90ºF - 100ºF**	**Yes**	**0.00**	**Yes**	**0.00**
40ºF - 50ºF	**100ºF - 110ºF**	**Yes**	**0.00**	**Yes**	**0.00**
50ºF - 60ºF	**60ºF - 70ºF**	**Yes**	**0.00**	**Yes**	**0.00**
50ºF - 60ºF	**70ºF - 80ºF**	**Yes**	**0.00**	**Yes**	**0.00**
50ºF - 60ºF	**80ºF - 90ºF**	**Yes**	**0.00**	**Yes**	**0.00**
50ºF - 60ºF	**90ºF - 100ºF**	**Yes**	**0.00**	**Yes**	**0.00**
50ºF - 60ºF	**100ºF - 110ºF**	**Yes**	**0.00**	**Yes**	**0.00**
60ºF - 70ºF	70ºF - 80ºF	No	0.01	No	0.01
60ºF - 70ºF	80ºF - 90ºF	No	0.01	No	0.01
60ºF - 70ºF	90ºF - 100ºF	No	0.04	No	0.02
60ºF - 70ºF	**100ºF - 110ºF**	**Yes**	**0.00**	**Yes**	**0.00**
70ºF - 80ºF	80ºF - 90ºF	No	1.00	No	1.00
70ºF - 80ºF	90ºF - 100ºF	No	1.00	No	1.00
70ºF - 80ºF	100ºF - 110ºF	No	0.70	No	0.66

Table 41 (continued).

FWD Load		9 kips		16 kips	
Lower MDT	Upper MDT	Reject Null Hypothesis?	p-value	Reject Null Hypothesis?	p-value
80ºF - 90ºF	90ºF - 100ºF	No	1.00	No	1.00
80ºF - 90ºF	100ºF - 110ºF	No	0.55	No	0.59
90ºF - 100ºF	100ºF - 110ºF	No	0.56	No	0.74

[1] Significant comparisons are in bold.

Paired t-tests were performed to determine if the mean of $\log(E_{NDT,OWP}/E_{Witczak(Aging)})$ is significantly greater at a high MDT than at a low MDT. A bin from 40ºF to 60ºF was selected to represent a low MDT and a bin from 90ºF to 110ºF was selected to represent a high MDT. The paired t-tests for the mean of $\log(E_{NDT,OWP}/E_{Witczak(Aging)})$ were set up in the same manner as the paired t-tests performed for $d_{0,OWP}/d_{0,ML}$ and $E_{NDT,OWP}/E_{NDT,ML}$. A total of 26 sections were included in the paired t-tests for the 9-kip load and 27 sections for the 16-kip load. The data used in the paired t-test for the 9-kip load is summarized in Table 42. The same sections, plus LTPP Section 55-0116, were included in the paired t-test performed for the 16-kip load. The details and results of the paired t-tests are summarized in Table 43.

Table 42. Data used in a paired t-test to determine the effect of MDT on $\log(E_{NDT,OWP}/E_{Witczak(Aging)})$ (9-kip load).

State	LTPP ID	Mean of $\log(E_{NDT,OWP}/E_{Witczak(Aging)})$ for 40ºF to 60ºF Bin	Mean of $\log(E_{NDT,OWP}/E_{Witczak(Aging)})$ for 90ºF to 110ºF Bin	Number of Data Points in 40ºF to 60ºF Bin	Number of Data Points in 90ºF to 110ºF Bin
GA	13-1031	-0.80	-0.50	17	12
ME	23-1026	-0.60	-0.37	14	4
MI	26-0116	-0.28	-0.15	3	1
MN	27-0501	-0.28	0.03	2	2
MN	27-1018	-0.24	0.02	2	1
MN	27-C350	-0.22	0.15	1	2
MO	29-B350	-0.39	-0.07	1	1

Table 42 (continued).

State	LTPP ID	Mean of $\log(E_{NDT,OWP}/E_{Witczak(Aging)})$ for 40ºF to 60ºF Bin	Mean of $\log(E_{NDT,OWP}/E_{Witczak(Aging)})$ for 90ºF to 110ºF Bin	Number of Data Points in 40ºF to 60ºF Bin	Number of Data Points in 90ºF to 110ºF Bin
MT	30-8129	-0.22	0.18	30	18
NE	31-0114	-0.06	-0.36	8	13
NE	31-1030	-0.58	-0.60	14	3
NE	31-A350	-0.74	-0.58	2	1
NE	31-A351	-0.61	-0.58	1	1
NE	31-A353	-0.67	-0.56	2	1
NV	32-0101	-0.28	-0.22	12	8
NM	35-1112	-0.22	0.01	26	21
NY	36-0801	-0.35	-0.16	23	8
OH	39-0105	-0.17	0.21	1	1
PA	42-1597	-0.36	-0.28	1	1
SD	46-9187	-0.59	-0.34	32	6
TX	48-1122	-0.78	-0.03	1	1
UT	49-1001	-0.21	0.12	14	2
VA	51-0113	-0.22	-0.15	17	3
VA	51-0114	-0.34	-0.20	30	21
WI	55-0114	-0.45	-0.27	1	1
WI	55-0120	-0.34	-0.13	1	1
WI	55-0806	-0.39	-0.46	1	1

Table 43. Results of paired t-tests to determine the effect of MDT on the mean of $\log(E_{NDT,OWP}/E_{Witczak(Aging)})$ (9-kip and 16-kip loads).

FWD Load	9 kips	16 kips
Null Hypothesis	$\mu_1 - \mu_2 = 0$	
Alternative Hypothesis	$\mu_1 - \mu_2 > 0$	
MDT Range for μ_1	40ºF - 60ºF	
MDT Range for μ_2	90ºF - 110ºF	
Reject Null Hypothesis?	Yes	Yes
Confidence Level	95%	95%
p-value	0.00	0.00

The results of the paired t-tests indicate that the mean of $\log(E_{NDT,OWP}/E_{Witczak(Aging)})$ is significantly greater at a high MDT than at a low MDT for both load levels. These results confirm the initial assumption that $\log(E_{NDT,OWP}/E_{Witczak(Aging)})$ increases as MDT increases. Further analysis of $\log(E_{NDT,OWP}/E_{Witczak(Aging)})$ must account for the relationship between $\log(E_{NDT,OWP}/E_{Witczak(Aging)})$ and MDT.

5.3.4 $E_{NDT,OWP}/E_{Witczak(No\ aging)}$

The relationship between $E_{NDT,OWP}/E_{Witczak(No\ aging)}$ and FWD load was analyzed using the log transformation of the FWD parameter, $\log(E_{NDT,OWP}/E_{Witczak(No\ aging)})$. As shown in Figure 101, it appears that $\log(E_{NDT,OWP}/E_{Witczak(No\ aging)})$ increases as the load increases. Paired t-tests were conducted between all pairs of load levels to determine if the mean of $\log(E_{NDT,OWP}/E_{Witczak(No\ aging)})$ increases significantly with load. The paired t-tests were set up for $\log(E_{NDT,OWP}/E_{Witczak(No\ aging)})$ the same manner adopted for the other three parameters. The details and results of the paired t-tests are shown in Table 44. The results show that, for all pairs of load levels, the mean of $\log(E_{NDT,OWP}/E_{Witczak(No\ aging)})$ is significantly greater for the higher load. This confirms $\log(E_{NDT,OWP}/E_{Witczak(No\ aging)})$ increases as the FWD load increases.

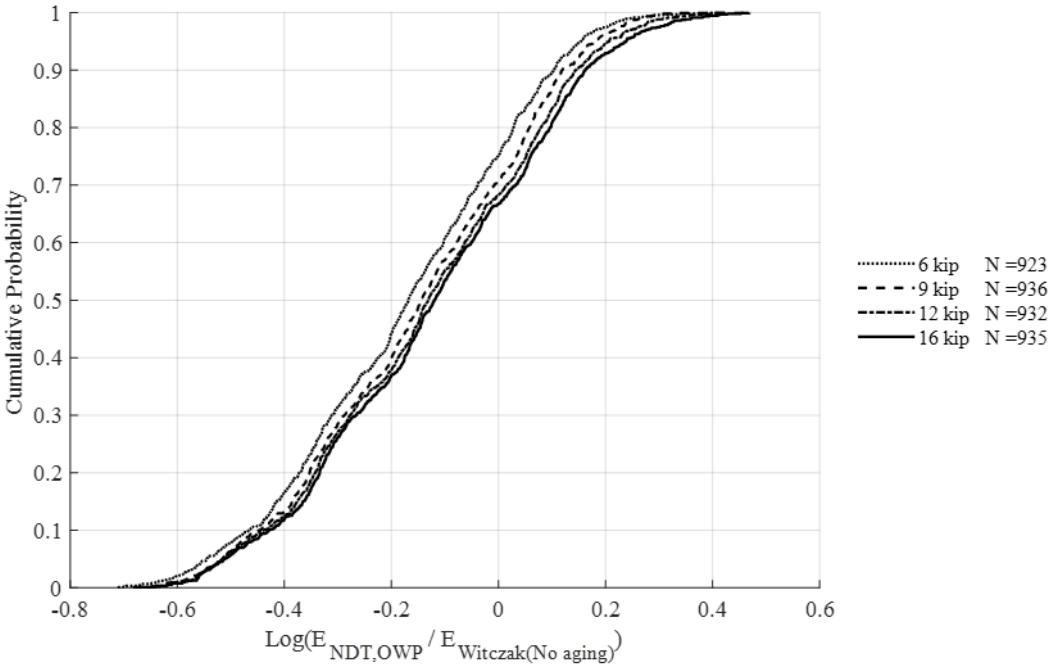

Figure 101. Distribution of $E_{NDT,OWP}/E_{Witczak(No\ aging)}$ with respect to FWD load.

Table 44. Results of paired t-tests to determine the effect of FWD load on the mean of $\log(E_{NDT,OWP}/E_{Witczak(No\ aging)})$.

Null Hypothesis	$\mu_i - \mu_j = 0$					
Alternative Hypothesis	$\mu_i - \mu_j < 0$					
Load Level for μ_i	6 kips	6 kips	6 kips	9 kips	9 kips	12 kips
Load Level for μ_j	9 kips	12 kips	16 kips	12 kips	16 kips	16 kips
Reject Null Hypothesis?	Yes	Yes	Yes	Yes	Yes	Yes
Confidence Level	95%	95%	95%	95%	95%	95%
p-value	0.00	0.00	0.00	0.00	0.00	0.00

Statistical testing demonstrated that the mean of $\log(E_{NDT,OWP}/E_{Witczak(No\ aging)})$ for each FWD load is significantly greater than the mean of $\log(E_{NDT,OWP}/E_{Witczak(No\ aging)})$ for all lower load levels. Thus, further analysis of $\log(E_{NDT,OWP}/E_{Witczak(No\ aging)})$ was conducted using only data

collected at a single load level. Separate, parallel analyses of the relationship between $\log(E_{NDT,OWP}/E_{Witczak(No\ aging)})$ and MDT were conducted using data from the 9-kip and 16-kip loads. The mean of $\log(E_{NDT,OWP}/E_{Witczak(No\ aging)})$ at the 9-kip load, calculated based on 936 data points and 71 different LTPP sections, is -0.15 and the standard deviation is 0.22. The mean of $\log(E_{NDT,OWP}/E_{Witczak(No\ aging)})$ at the 16-kip load level, calculated based on 935 data points and 71 different LTPP sections, is -0.12 and the standard deviation is 0.23. For both load levels, $\log(E_{NDT,OWP}/E_{Witczak(No\ aging)})$ is approximately normally distributed.

As shown in Figures 102 and 104, there is a very weak positive correlation between $\log(E_{NDT,OWP}/E_{Witczak(No\ aging)})$ and MDT for both the 9-kip and 16-kip loads. Cumulative probability distributions of the $\log(E_{NDT,OWP}/E_{Witczak(No\ aging)})$ data, divided into bins by MDT, are shown in Figures 103 and 105 for the 9-kip and 16-kip loads, respectively. Based on these plots, it appears that $\log(E_{NDT,OWP}/E_{Witczak(No\ aging)})$ is greater at high temperatures than at low temperatures. On the other hand, it appears that $\log(E_{NDT,OWP}/E_{Witczak(No\ aging)})$ for MDTs between 80ºF to 100ºF is less than the mean of $\log(E_{NDT,OWP}/E_{Witczak(No\ aging)})$ for MDTs between 60ºF to 80ºF. Thus, it is assumed that $\log(E_{NDT,OWP}/E_{Witczak(No\ aging)})$ is related to MDT, but the nature of this relationship is unclear.

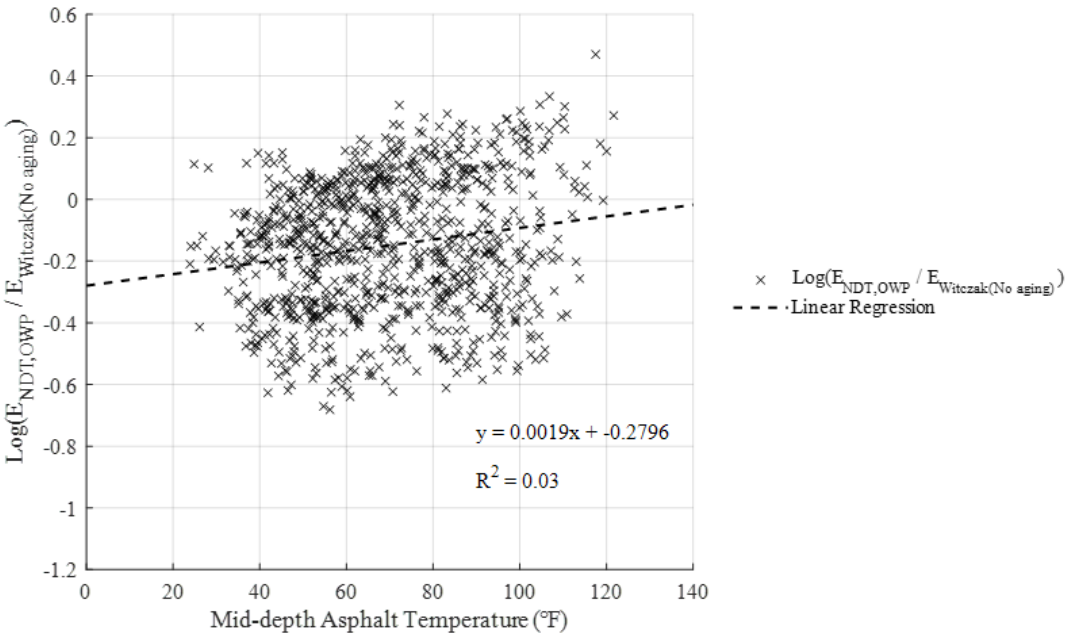

Figure 102. $E_{NDT,OWP}/E_{Witczak(No\ aging)}$ vs MDT (9-kip load).

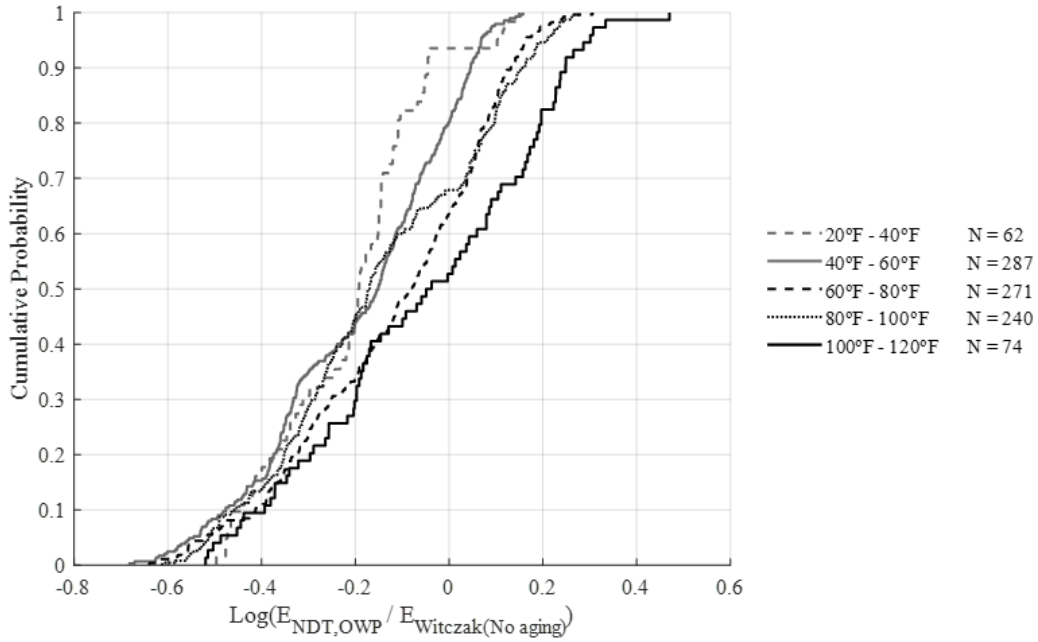

Figure 103. Distribution of $E_{NDT,OWP}/E_{Witczak(No\ aging)}$ with respect to MDT (9-kip load).

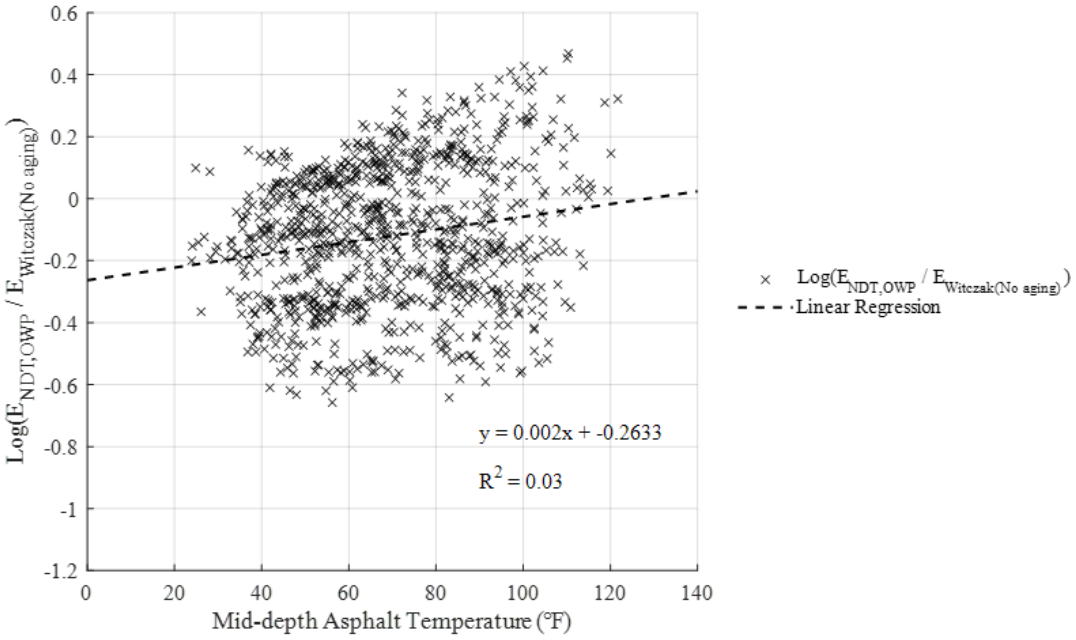

Figure 104. $E_{NDT,OWP}/E_{Witczak(No\ aging)}$ vs MDT (16-kip load).

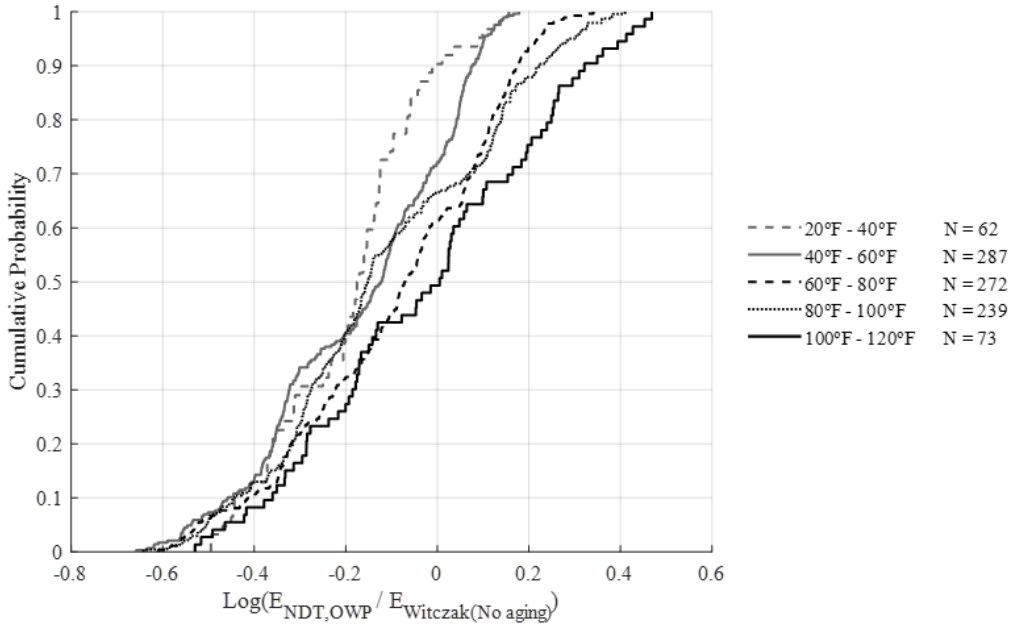

Figure 105. Distribution of $E_{NDT,OWP}/E_{Witczak(No\ aging)}$ with respect MDT (16-kip load).

An ANOVA was performed to test the initial assumption that $\log(E_{NDT,OWP}/E_{Witczak(No\ aging)})$ changes as a function of MDT. The same temperature bins used to perform an ANOVA for all other parameters were used for $\log(E_{NDT,OWP}/E_{Witczak(No\ aging)})$. The results of the ANOVA, detailed in Table 45, indicate that the mean of $\log(E_{NDT,OWP}/E_{Witczak(Aging)})$ changes significantly between 40ºF to 110ºF for both the 9-kip and 16-kip load levels. The mean and standard deviation of $\log(E_{NDT,OWP}/E_{Witczak(No\ aging)})$ for each MDT level are summarized in Table 46. The is no clear trend between the mean of $\log(E_{NDT,OWP}/E_{Witczak(No\ aging)})$ and the MDT. Tukey's test was performed at a 95% overall confidence level to compare all pairs of the MDT bins. The pairwise comparisons show that the mean of $\log(E_{NDT,OWP}/E_{Witczak(No\ aging)})$ is the same for all pairs of MDT levels except the 40ºF to 50ºF level and 70ºF to 80ºF level. This was the case for both the 9-kip and 16-kip loads.

Table 45. Results of one-way ANOVA for the effect of MDT on the mean of $\log(E_{NDT,OWP}/E_{Witczak(No\ aging)})$ (9-kip and 16-kip loads).

FWD Load	9 kips	16 kips
Null Hypothesis	$\mu_1 = \mu_2 = \ldots = \mu_n$	
Alternative Hypothesis	At least one $\mu_i \neq \mu_j$	
Minimum MDT (ºF)	40	
Maximum MDT (ºF)	110	
Reject Null Hypothesis?	Yes	Yes
Simultaneous Confidence Level	95%	95%
p-value	0.00	0.00

Table 46. Mean and standard deviation of $\log(E_{NDT,OWP}/E_{Witczak(No\ aging)})$ for individual MDT levels (9-kip and 16-kip loads).

FWD Load	9 kips			16 kips		
MDT	Mean	Standard Deviation	Number of Data Points	Mean	Standard Deviation	Number of Data Points
40ºF - 50ºF	-0.21	0.20	126	-0.18	0.21	126
50ºF - 60ºF	-0.19	0.20	161	-0.16	0.20	161
60ºF - 70ºF	-0.13	0.21	159	-0.11	0.22	159
70ºF - 80ºF	-0.10	0.22	112	-0.07	0.23	113
80ºF - 90ºF	-0.14	0.22	144	-0.11	0.24	144
90ºF - 100ºF	-0.16	0.23	96	-0.12	0.25	95
100ºF - 110ºF	-0.08	0.26	57	-0.05	0.27	57

Paired t-tests were conducted to determine conclusively if there is a significant relationship between $\text{Log}(E_{NDT,OWP}/E_{Witczak(No\ aging)})$ and MDT. The paired t-tests for the mean of $\log(E_{NDT,OWP}/E_{Witczak(No\ aging)})$ is performed in the same manner as the paired t-tests performed for all other parameters. The same LTPP sections used in the paired t-tests for $\log(E_{NDT,OWP}/E_{Witczak(Aging)})$ were used in the paired t-tests for $\log(E_{NDT,OWP}/E_{Witczak(No\ aging)})$. These sections are listed in Table 42. The details and results of the paired t-tests for $\log(E_{NDT,OWP}/E_{Witczak(No\ aging)})$ are summarized in Table 47. Note that the alternative hypothesis used in the paired t-tests for $\log(E_{NDT,OWP}/E_{Witczak(No\ aging)})$ is different than that used in the paired t-tests for $\log(E_{NDT,OWP}/E_{Witczak(Aging)})$.

Table 47. Results of paired t-tests to determine the effect of MDT on the mean of $\log(E_{NDT,OWP}/E_{Witczak(No\ aging)})$ (9-kip and 16-kip loads).

FWD Load	9 kips	16 kips
Null Hypothesis	$\mu_1 - \mu_2 = 0$	
Alternative Hypothesis	$\mu_1 - \mu_2 \neq 0$	
MDT Range for μ_1	40ºF - 60ºF	
MDT Range for μ_2	90ºF - 110ºF	
Reject Null Hypothesis?	No	No
Confidence Level	95%	95%
p-value	0.54	0.26

The results of the paired t-tests indicate that the mean of $\log(E_{NDT,OWP}/E_{Witczak(No\ aging)})$ does not change significantly with respect to MDT. This result refutes the initial assumption that there is a relationship between $\log(E_{NDT,OWP}/E_{Witczak(No\ aging)})$ and MDT. The results of the paired t-test also contradict the results of the ANOVA, that the mean of $\log(E_{NDT,OWP}/E_{Witczak(No\ aging)})$ changes with respect to MDT. It is possible that a non-linear relationship exists between $\log(E_{NDT,OWP}/E_{Witczak(No\ aging)})$ and MDT, but this possibility was not examined in more detail. Further analysis of $\log(E_{NDT,OWP}/E_{Witczak(No\ aging)})$ should conservatively assume that there is some relationship between $\log(E_{NDT,OWP}/E_{Witczak(Aging)})$ and MDT and that the effect of MDT must be considered.

The analysis of four FWD parameters, $d_{0,OWP}/d_{0,ML}$, $E_{NDT,OWP}/E_{NDT,ML}$, $E_{NDT,OWP}/E_{Witczak(Aging)}$, and $E_{NDT,OWP}/E_{Witczak(No\ aging)}$, with respect to FWD load level and MDT resulted in several notable conclusions:

- All four FWD parameters are significantly affected by the FWD load level. This can be mitigated by using only data from one load level when analyzing FWD parameters.

- Three of the four FWD parameters are significantly affected by MDT. For $d_{0,OWP}/d_{0,ML}$, the parameter decreases as MDT increases. For $E_{NDT,OWP}/E_{NDT,ML}$ and $E_{NDT,OWP}/E_{Witczak(Aging)}$, the parameter increases as MDT increases. For $E_{NDT,OWP}/E_{Witczak(Aging)}$, the nature of the relationship between the parameter and MDT is unclear. For all parameters, the relationship between the FWD parameter and MDT must be accounted for when performing further analyses.
- The interaction between FWD load and MDT does not appear to affect the mean of the FWD parameters examined. This interaction was not examined explicitly, but the relationship between parameters and MDT does not appear to change between the 9-kip and 16-kip loads.

Based on these conclusions, it was determined that further analyses of the relationship between FWD parameters and fatigue damage should be conducted using FWD data collected only at one load level and must account for the effect of MDT.

5.4 FWD PARAMETERS AND FATIGUE DAMAGE IN THE ASPHALT CONCRETE

Once the FWD parameters were evaluated for pavements with no visible distress, the same FWD parameters were used to examine the relationship between FWD data and fatigue damage in AC pavements. Observed distress, specifically outer wheelpath (OWP) fatigue cracking, was used as an indicator of fatigue damage in the asphalt concrete layer of the existing pavement. It was assumed that all fatigue cracking initiates at the bottom of the asphalt concrete layer and propagates

to the surface of the pavement over time. Based on this assumption, it is possible that a pavement may have fatigue damage at the bottom of the pavement that has not yet propagated to the surface of the pavement.

The relationship between FWD parameters and OWP fatigue cracking was analyzed with the objective of answering the following questions:

1. Can FWD parameters be used to estimate the development of fatigue damage in the asphalt concrete layer of an existing pavement? Specifically:
    a. Is there a significant correlation between the FWD parameters and time when there is **no** visible fatigue cracking in a pavement section? Can the FWD parameters be used to detect fatigue damage caused by fatigue cracking at the bottom of the pavement that has not reached the surface of the pavement?
    b. Is there a significant correlation between any of the FWD parameters and OWP fatigue cracking when there is visible distress? Can any of the FWD parameters provide information regarding the extent and severity of fatigue damage in the asphalt concrete once fatigue cracking has reached the surface of the pavement?
    c. Is there a significant correlation between any of the FWD parameters and OWP fatigue cracking over the whole life of a pavement section? Can any of the FWD parameters provide information about the extent and severity of fatigue damage in the asphalt concrete over the entire life of a pavement section?
2. Is the $E_{NDT,OWP}/E_{Witczak(Aging)}$ parameter, which is currently used in the Pavement ME AC/AC overlay design procedure, meaningfully related to fatigue damage and OWP fatigue cracking? Can $E_{NDT,OWP}/E_{Witczak(Aging)}$ or any of the other FWD parameters be used

to adjust the E_{NDT} input used in Pavement ME to more successfully quantify the amount of fatigue damage in the asphalt concrete of the existing pavement?

The relationship between FWD parameters and fatigue damage was analyzed both for individual LTPP sections and using combined data from multiple LTPP sections. Both of these analyses were conducted using a two-way ANOVA with MDT as the first factor and either section age or amount of visible fatigue cracking as the second factor. Both factors were grouped into bins for the purpose of performing the ANOVA. Additionally, only data from the 9-kip load was used in this analysis because previous analyses showed the FWD load has a significant effect on all FWD parameters.

For this analysis, it was initially assumed that there is a significant relationship between fatigue damage and FWD parameters. Statistical testing was performed to either confirm or refute this assumption. Additionally, for each FWD parameter, the effect of fatigue damage on the FWD parameter was hypothesized. These hypothesized relationships are described below and summarized in Table 48.

- $d_{0,OWP}/d_{0,ML}$ – The d_0 deflection when FWD testing is performed in an area of fatigue cracking (fatigue damage) will be greater than d_0 when FWD testing is performed in an adjacent area with no fatigue cracking. Therefore $d_{0,OWP}/d_{0,ML}$ should increase as fatigue damage in the outer wheelpath increases relative to fatigue damage at mid-lane.
- $E_{NDT,OWP}/E_{NDT,ML}$ – E_{NDT} when FWD testing is performed in an area with fatigue damage will be less than E_{NDT} when FWD testing is performed in an adjacent area with no fatigue

damage. Therefore $E_{NDT,OWP}/E_{NDT,ML}$ should decrease as fatigue damage in the outer wheelpath increases relative to fatigue damage at mid-lane.

- $E_{NDT,OWP}/E_{Witczak(Aging)} - E_{NDT}$ when FWD testing is performed in on a pavement with fatigue damage should be less than the estimated stiffness of the asphalt concrete without fatigue damage ($E_{Witczak(Aging)}$). Therefore $E_{NDT,OWP}/E_{Witczak(Aging)}$ should decrease as fatigue damage in the outer wheelpath increases.
- $E_{NDT,OWP}/E_{Witczak(No\ aging)} - E_{NDT}$ when FWD testing is performed in on a pavement with fatigue damage should be less than the estimated stiffness of the asphalt concrete without fatigue damage ($E_{Witczak(No\ aging)}$). Therefore $E_{NDT,OWP}/E_{Witczak(No\ aging)}$ should decrease as fatigue damage in the outer wheelpath increases.

Table 48. Hypothesized effect of fatigue damage on FWD parameters.

FWD Parameter	Effect of Fatigue Damage on Parameter
$d_{0,OWP}/d_{0,ML}$	Increase
$E_{NDT,OWP}/E_{NDT,ML}$	Decrease
$E_{NDT,OWP}/E_{Witczak(Aging)}$	Decrease
$E_{NDT,OWP}/E_{Witczak(No\ aging)}$	Decrease

5.4.1 FWD parameters and fatigue damage for individual sections

A two-way ANOVA was used to analyze nine individual LTPP sections. The pavement structures and approximate traffic levels of the nine LTPP sections are listed in Table 49. These particular sections were selected based on two criteria. First, each section has fatigue cracking that develops over the life of the section. Specifically, there is a period of time with no visible fatigue cracking

followed by a period of time during which fatigue cracking steadily increases. Second, each section has a large amount of FWD test data distributed over the entire life of the pavement section, including the periods of no visible fatigue cracking and increasing fatigue cracking. All nine LTPP sections are SMP sections.

Table 49. LTPP sections considered for the within section analysis.

State	LTPP ID	Asphalt Concrete Thickness (in)	Granular Base Thickness (in)	AADTT[1] over Analysis Period
AL	1-0101	7.5	8	1000
ID	16-1010	11	5	250
MT	30-0114	7.5	12	300
NE	31-0114	6.5	12	450
NY	36-0801	5	8	Less than 100
OK	40-4165	8	24	300
VA	51-0113	4	8	800
VA	51-0114	7.5	12	800
MB	83-1801	4.5	19	500

[1] AADTT = Average annual daily truck traffic

The same two-way ANOVA analysis was performed for each FWD parameter for each of the nine sections. This analysis is described in detail only for $d_{0,OWP}/d_{0,ML}$ for LTPP Section 83-1801 in Manitoba. Details of the analysis for all other FWD parameters and sections can be found in Appendix B.

The two-way ANOVA is a statistical method for quantifying the effect of two independent variables (factors) on a third, dependent variable (response). For this analysis, the response is the FWD parameter and the factors are the MDT at time of FWD testing and the section age or OWP fatigue cracking at the time of FWD testing. Each FWD parameter data point represents an average value for a single FWD pass and has a corresponding MDT, section age, and OWP fatigue

cracking. The two-way ANOVA was conducted with fixed effects, meaning that each factor is defined at several discrete levels. Thus, bins were used to define discrete levels of the MDT, section age, and OWP fatigue cracking factors. MDT was the first factor for all two-way ANOVA analyses. MDT was divided into bins with a width of 20ºF, starting at 40ºF and continuing to 120ºF. Data collected when the MDT was less than 40ºF were excluded from the analysis because the stiffness of asphalt concrete, and thus the value of the FWD parameters, is relatively constant below 40ºF. Additionally, erroneous FWD parameters are much more likely to be found when the MDT is below 40ºF due to frozen unbound layers in the pavement structure. For all individual section analyses, the same bins ranges were used to define levels of the MDT factor.

The second factor for the two-way ANOVA was either section age or OWP fatigue cracking. For section age, the time history of the pavement section was divided into bins based on visual examination of performance history plots. The performance history plot used to define the bin categories for section age for the analysis of LTPP Section 83-1801 in Manitoba is shown in Figure 106. Note that section age bins are not necessarily all the same width. Rather, the width of each bin is selected to include a sufficiently large amount of FWD data. The performance history plots used to define section age bins for all individual sections and all FWD parameters are shown in Appendix C. OWP fatigue cracking was divided into bins starting with no visible fatigue cracking (0% by total lane area) and increasing in intervals of 5% OWP fatigue cracking. The fatigue cracking bin categories used for the analysis of LTPP Section 83-1801 are shown in Figure 107. The same outer wheelpath fatigue cracking bin categories were used to define levels of the OWP fatigue cracking factor for all individual section analyses. The bin categories used for each of the factors in the two-way ANOVA for the within section analysis are summarized in Table 50.

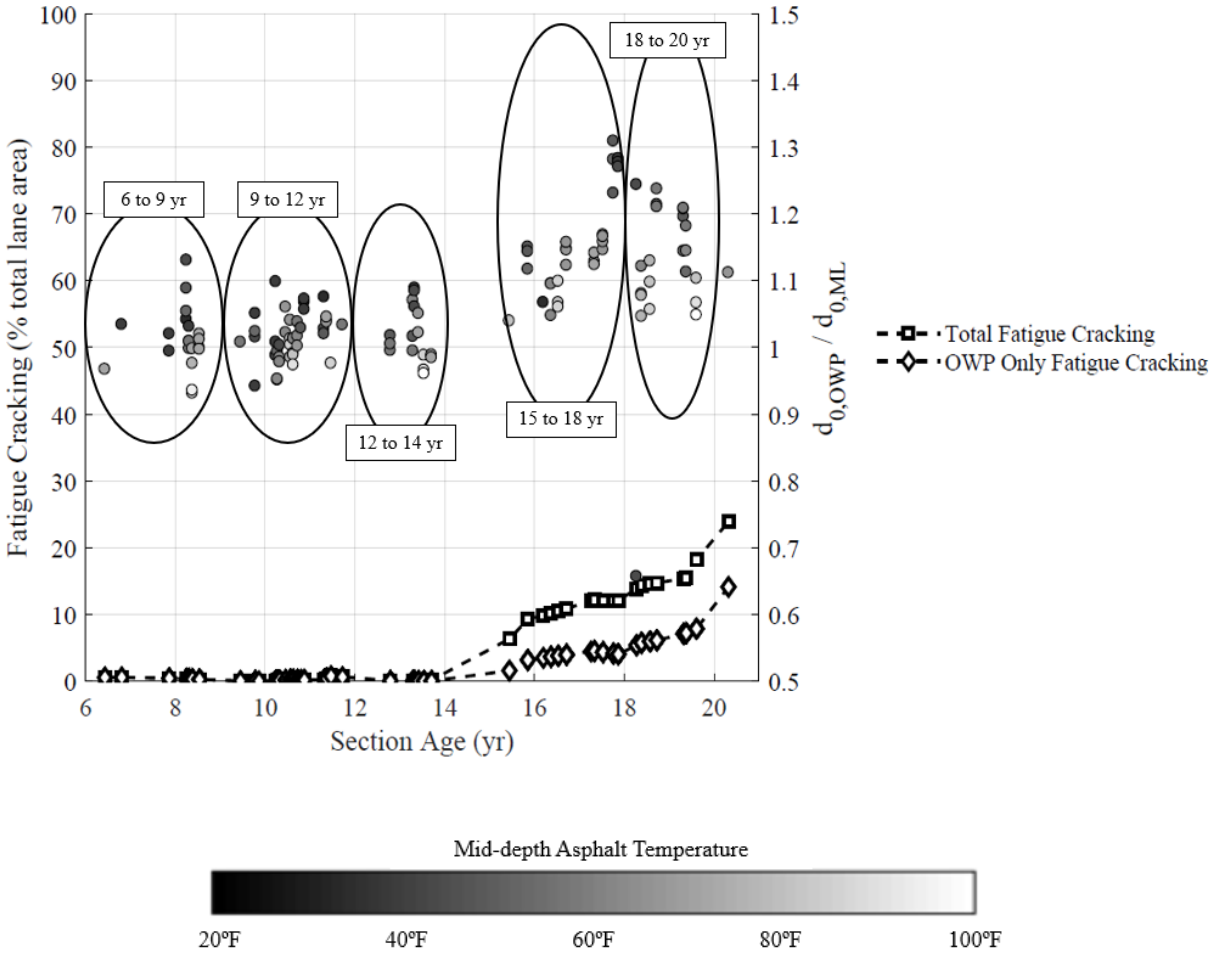

Figure 106. Performance history plot used to establish section age bin categories for two-way ANOVA ($d_{0,OWP}/d_{0,ML}$, LTPP Section 83-1801, Manitoba).

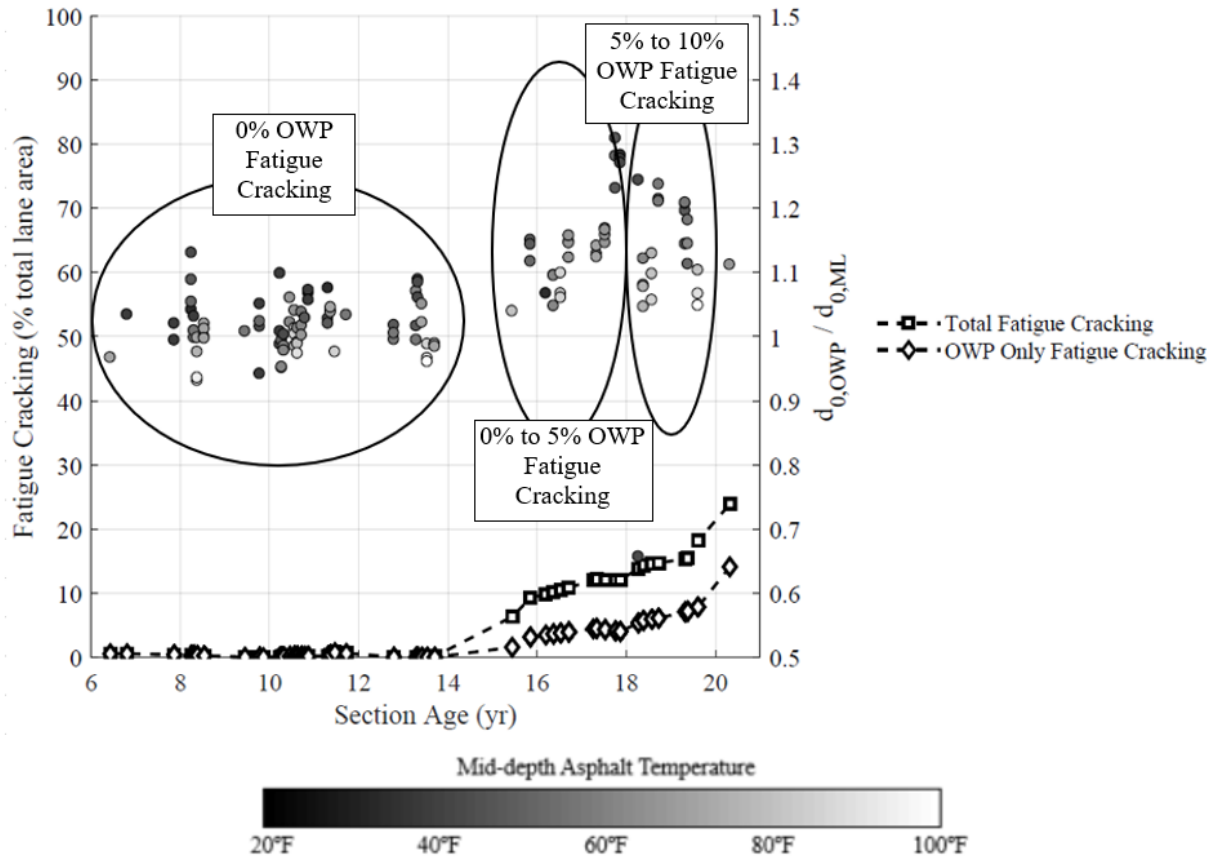

Figure 107. Fatigue cracking bin categories used for two-way ANOVA analysis ($d_{0,OWP}/d_{0,ML}$, LTPP Section 83-1801, Manitoba).

Table 50. Bin categories used to define factors for two-way ANOVA analysis of individual LTPP sections.

	Factor 1	Factor 2	
Factor Level	MDT	Section Age	Outer Wheelpath Fatigue Cracking
1	40ºF to 60 ºF	Determined using time-history plot	0%
2	60ºF to 80ºF		0% to 5%
3	80ºF to 100ºF		5% to 10%
4	100ºF to 120ºF		Greater than 10%

In order to obtain meaningful results from the two-way ANOVA, the response data must be evenly distributed across all the levels for each factor. The response data for each level of the section age or fatigue cracking factor must include data from all levels of the MDT factor and vice versa. In order to satisfy this requirement, if there were not enough FWD parameter data points at a specific level of a factor, all the data points at that level of that factor were removed from the analysis. For example, in the analysis of LTPP Section 83-1801 in Manitoba, only 2 of the 128 FWD parameter data points had a MDT between 100ºF to 120ºF and these data points were not evenly distributed over the various categories of section age or fatigue cracking. As a result, these two data points were not included in the two-way ANOVA analysis. All of the data used to analyze the relationship between $d_{0,OWP}/d_{0,ML}$ and fatigue damage for LTPP Section 83-1801, including the FWD parameter, MDT, section age, OWP fatigue cracking, and all factor levels, is shown in Table 51. Note that the data in Table 51 is the same data represented in Figures 106 and 107.

Table 51. Data used in two-way ANOVA analysis of relationship between $d_{0,OWP}/d_{0,ML}$ and fatigue damage (LTPP Section 83-1801, Manitoba).

$d_{0,OWP}/d_{0,ML}$	MDT (ºF)	Section Age (yr)	OWP Fatigue Cracking (% total lane area)	MDT Level	Section Age Level	OWP Fatigue Cracking Level
1.12	42	8.2	0.0	1	1	1
1.06	49	8.2	0.0	1	1	1
1.06	54	8.2	0.0	1	1	1
1.02	46	8.3	0.0	1	1	1
0.99	57	8.3	0.0	1	1	1
0.98	58	8.3	0.0	1	1	1
0.99	72	8.4	0.0	2	1	1
0.98	80	8.4	0.0	2	1	1
0.94	90	8.4	0.0	3	1	1
0.93	96	8.4	0.0	3	1	1
1.02	69	8.5	0.0	2	1	1
0.99	71	8.5	0.0	2	1	1
1.00	73	8.5	0.0	2	1	1
0.98	74	8.5	0.0	2	1	1
1.02	58	9.5	0.0	1	2	1

Table 51 (continued).

$d_{0,OWP}/d_{0,ML}$	MDT (°F)	Section Age (yr)	OWP Fatigue Cracking (% total lane area)	MDT Level	Section Age Level	OWP Fatigue Cracking Level
1.02	43	9.8	0.0	1	2	1
1.02	51	9.8	0.0	1	2	1
1.01	43	10.2	0.0	1	2	1
0.96	47	10.3	0.0	1	2	1
0.98	53	10.3	0.0	1	2	1
0.95	62	10.3	0.0	2	2	1
1.00	43	10.3	0.0	1	2	1
0.97	54	10.3	0.0	1	2	1
0.97	61	10.3	0.0	2	2	1
0.96	63	10.3	0.0	2	2	1
1.01	65	10.5	0.0	2	2	1
1.07	66	10.5	0.0	2	2	1
1.02	66	10.6	0.0	2	2	1
1.01	78	10.6	0.0	2	2	1
1.01	83	10.6	0.0	3	2	1
1.00	86	10.6	0.0	3	2	1
1.00	63	10.6	0.0	2	2	1
1.03	72	10.6	0.0	2	2	1
0.98	81	10.6	0.0	3	2	1
0.97	92	10.6	0.0	3	2	1
1.03	56	10.7	0.0	1	2	1
1.00	60	10.7	0.0	2	2	1
1.00	66	10.7	0.0	2	2	1
1.01	47	10.8	0.0	1	2	1
1.02	42	11.3	0.0	1	2	1
1.00	46	11.3	0.0	1	2	1
1.03	50	11.4	0.0	1	2	1
1.04	65	11.4	0.0	2	2	1
1.02	73	11.4	0.0	2	2	1
1.01	85	11.5	0.0	3	2	1
1.01	59	11.7	0.0	1	2	1
1.02	49	12.8	0.0	1	3	1
0.99	57	12.8	0.0	1	3	1
0.98	59	12.8	0.0	1	3	1
0.97	47	13.3	0.0	1	3	1
1.01	55	13.3	0.0	1	3	1
1.04	61	13.3	0.0	2	3	1
1.06	41	13.3	0.0	1	3	1
1.08	43	13.3	0.0	1	3	1
1.03	70	13.4	0.0	2	3	1
1.02	74	13.4	0.0	2	3	1
0.99	85	13.5	0.0	3	3	1
0.97	94	13.5	0.0	3	3	1
0.98	62	13.7	0.0	2	3	1
0.98	68	13.7	0.0	2	3	1
0.98	71	13.7	0.0	2	3	1
1.06	81	15.4	1.6	3	4	2
1.11	48	15.9	3.2	1	4	2
1.14	48	15.9	3.2	1	4	2
1.07	53	15.9	3.2	1	4	2
1.06	63	16.4	3.6	2	4	2

Table 51 (continued).						
$d_{0,OWP}/d_{0,ML}$	MDT (°F)	Section Age (yr)	OWP Fatigue Cracking (% total lane area)	MDT Level	Section Age Level	OWP Fatigue Cracking Level
1.09	65	16.4	3.6	2	4	2
1.09	65	16.4	3.6	2	4	2
1.09	83	16.5	3.8	3	4	2
1.09	86	16.5	3.8	3	4	2
1.06	86	16.5	3.8	3	4	2
1.16	65	16.7	3.9	2	4	2
1.12	65	16.7	3.9	2	4	2
1.14	65	16.7	3.9	2	4	2
1.11	65	16.7	3.9	2	4	2
1.15	68	17.3	4.5	2	4	2
1.15	73	17.3	4.5	2	4	2
1.12	75	17.3	4.5	2	4	2
1.14	68	17.5	4.3	2	4	2
1.14	68	17.5	4.3	2	4	2
1.13	69	17.5	4.3	2	4	2
1.15	69	17.5	4.3	2	4	2
1.33	47	17.8	4.1	1	4	2
1.26	49	17.8	4.1	1	4	2
1.30	52	17.8	4.1	1	4	2
1.27	43	17.9	4.0	1	4	2
1.24	42	18.3	5.4	1	5	3
0.97	44	18.3	5.4	1	5	3
1.13	64	18.4	5.7	2	5	3
1.09	71	18.4	5.7	2	5	3
1.07	76	18.4	5.7	2	5	3
1.05	80	18.4	5.7	2	5	3
1.13	78	18.6	5.9	2	5	3
1.10	83	18.6	5.9	3	5	3
1.07	89	18.6	5.9	3	5	3
1.18	53	18.7	6.1	1	5	3
1.23	57	18.7	6.1	1	5	3
1.23	60	18.7	6.1	1	5	3
1.22	46	19.3	7.1	1	5	3
1.21	51	19.3	7.1	1	5	3
1.13	54	19.3	7.1	1	5	3
1.15	55	19.3	7.1	1	5	3
1.21	52	19.4	7.2	1	5	3
1.22	58	19.4	7.2	1	5	3
1.19	64	19.4	7.2	2	5	3
1.11	84	19.6	7.8	3	5	3
1.08	92	19.6	7.8	3	5	3

A two-way ANOVA was performed three times for each FWD parameter and each individual LTPP section. Three analyses were performed to answer the three parts of the first question proposed at the beginning of this section:

a. Is there a significant correlation between $d_{0,OWP}/d_{0,ML}$ and time when there is **no** visible distress in the existing pavement?
b. Is there a significant correlation between $d_{0,OWP}/d_{0,ML}$ and OWP fatigue cracking when there is visible distress?
c. Is there a significant correlation between $d_{0,OWP}/d_{0,ML}$ and OWP fatigue cracking over the entire life of the pavement section?

For each two-way ANOVA, a subset of the data provided in Table 51 was used. The subset of factor levels required for each analysis is summarized in Table 52. All two-way ANOVAs are performed at a 95% confidence level. For every two-way ANOVA, the null hypothesis is that the mean of the FWD parameter is equal for all levels of both factors ($\mu_{11} = \mu_{12} = \ldots = \mu_{nn}$). The alternative hypothesis is that the means are not equal for one or more combination of factor levels (at least one $\mu_{ij} \neq \mu_{ji}$).

Table 52. Factor levels used in two-way ANOVA for the effect of MDT and section age on $d_{0,OWP}/d_{0,ML}$ when there is no visible distress (LTPP Section 83-1801, Manitoba).

	Factor 1	Factor 2	
Question Number	MDT Levels	Section Age Levels[1]	OWP Fatigue Cracking Levels
1	40ºF to 60 ºF, 60ºF to 80 ºF, 80ºF to 100 ºF	6 yr to 9 yr, 9 yr to 12 yr, 12 yr to 14 yr	0%
2	40ºF to 60 ºF, 60ºF to 80 ºF, 80ºF to 100 ºF	15 yr to 18 yr, 18 yr to 20 yr	0% to 5%, 5% to 10%
3	40ºF to 60 ºF, 60ºF to 80 ºF, 80ºF to 100 ºF	All	0%, 0% to 5%, 5% to 10%

[1] See Figure 106 for determination of levels of section age factor.

First, a two-way ANOVA was performed using only FWD data points with **no** visible distress (0% fatigue cracking). The results of this analysis, shown in Table 53, indicate that MDT and the interaction between MDT and section age (MDT * Section Age) have a significant effect on $d_{0,OWP}/d_{0,ML}$, but section age does not have a significant effect. Main effects and interaction plots are shown in Figures 108 and 109, respectively. Figure 108 shows that the mean of $d_{0,OWP}/d_{0,ML}$ decreases as MDT increases. This is the same trend that was observed previously for LTPP sections with no visible distress. Figure 108 also shows that the mean of $d_{0,OWP}/d_{0,ML}$ increases as section age increases, but this trend is not significant. Finally, Figure 109 shows that the effect of MDT on $d_{0,OWP}/d_{0,ML}$ is greater for the 6 yr to 9 yr level of section age than for the 9 yr to 12 yr and 12 yr to 14 yr levels.

Table 53. Results of two-way ANOVA analysis for the effect of MDT and section age on the mean of $d_{0,OWP}/d_{0,ML}$ when there is no visible distress (LTPP Section 83-1801, Manitoba).

Source of Variation	Degrees of Freedom	Adjusted Sum of Squares	Mean Square	F-value	p-value
MDT	2	0.016	0.008	8.31	0.00
Section Age	2	0.001	0.001	0.65	0.53
MDT * Section Age	4	0.011	0.003	2.94	0.03
Error	53	0.050	0.001		
Total	61	0.072			

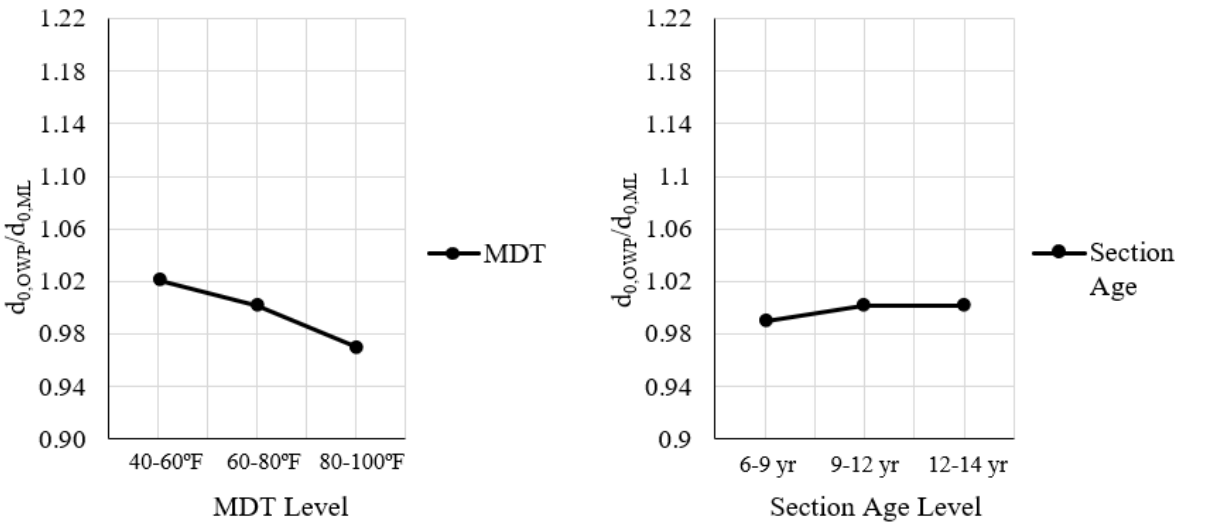

Figure 108. Main effects of the MDT and section age factors when there is no visible distress ($d_{0,OWP}/d_{0,ML}$, LTPP Section 83-1801, Manitoba).

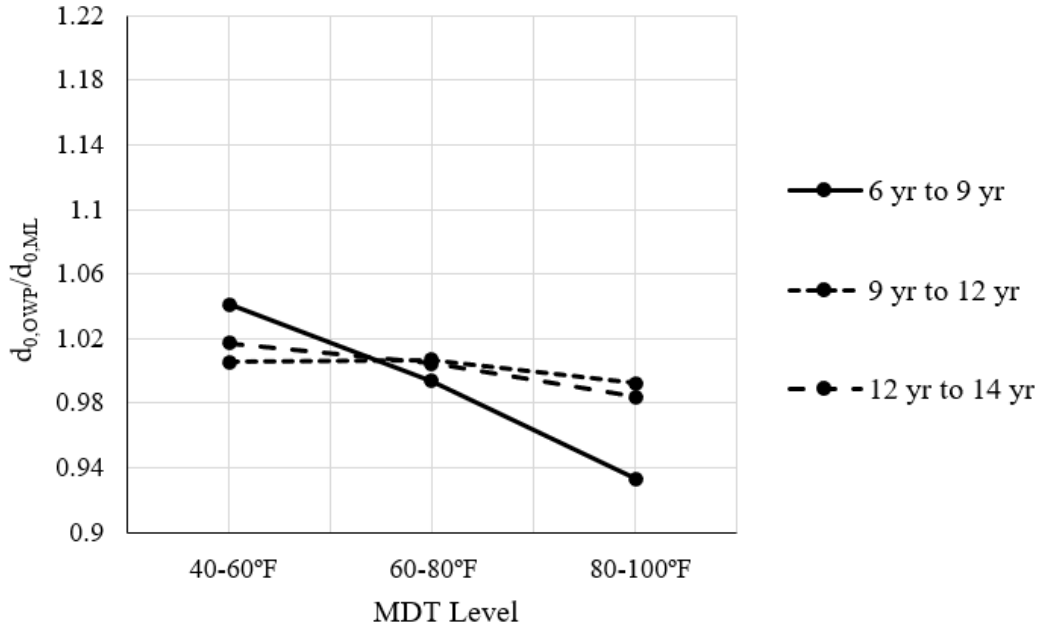

Figure 109. Interaction of the MDT and section age factors when there is no visible distress ($d_{0,OWP}/d_{0,ML}$, LTPP Section 83-1801, Manitoba).

Additionally, Tukey's test was also conducted at a 95% overall confidence level for each factor in order to identify which pairs of factor levels are significantly different. The null hypothesis for this test is that the mean of the FWD parameter is equal for all pairs of factor levels being examined ($\mu_i = \mu_j$, where $i \neq j$). This null hypothesis was rejected for MDT and not rejected for section age. The pairwise comparisons from Tukey's test, shown in Table 54, indicate that the mean of $d_{0,OWP}/d_{0,ML}$ for the 80ºF to 100ºF level of the MDT is significantly different from the mean at any lower levels, but that the mean of $d_{0,OWP}/d_{0,ML}$ is not significantly different between the 40ºF to 60ºF and 60ºF to 80ºF levels. The results in Table 54 also indicate that the mean of $d_{0,OWP}/d_{0,ML}$ does not change significantly with respect to the section age factor.

Table 54. Results of Tukey's test for MDT and section age factors when there is no visible distress (LTPP Section 83-1801, Manitoba).

MDT				Section Age			
Lower Factor Level	Upper Factor Level	Reject Null Hypothesis ?	p-value	Lower Factor Level	Upper Factor Level	Reject Null Hypothesis?	p-value
40ºF to 60ºF	60ºF to 80ºF	No	0.08	6 yr to 9 yr	9 yr to 12 yr	No	0.53
40ºF to 60ºF[1]	**80ºF to 100ºF**	**Yes**	**0.00**	6 yr to 9 yr	12 yr to 14 yr	No	0.63
60ºF to 80ºF	**80ºF to 100ºF**	**Yes**	**0.05**	9 yr to 12 yr	12 yr to 14 yr	No	1.00

[1] Significant comparisons are in bold.

Second, a two-way ANOVA was performed using only FWD data points with visible distress. Note that OWP fatigue cracking was used as the second factor instead of section age for this analysis. The results, shown in Table 55, indicate that MDT has a significant effect on $d_{0,OWP}/d_{0,ML}$, but OWP fatigue cracking and the interaction between MDT and OWP fatigue cracking do not have significant effects. A main effects plot, shown in Figure 110, indicates that

the mean of $d_{0,OWP}/d_{0,ML}$ decreases as MDT increases, which is the same trend observed previously when there is no visible distress. Figure 110 also shows that the mean of $d_{0,OWP}/d_{0,ML}$ remains almost constant as OWP fatigue cracking increases, but this trend is not significant.

Table 55. Results of two-way ANOVA analysis for the effect of MDT and OWP fatigue cracking on the mean of $d_{0,OWP}/d_{0,ML}$ when there is visible distress (LTPP Section 83-1801, Manitoba).

Source of Variation	Degrees of Freedom	Adjusted Sum of Squares	Mean Square	F-value	p-value
MDT	2	0.092	0.046	12.25	0.00
OWP Fatigue Cracking	1	0.001	0.001	0.22	0.64
MDT * OWP Fatigue Cracking	2	0.003	0.001	0.39	0.68
Error	40	0.150	0.004		
Total	45	0.242			

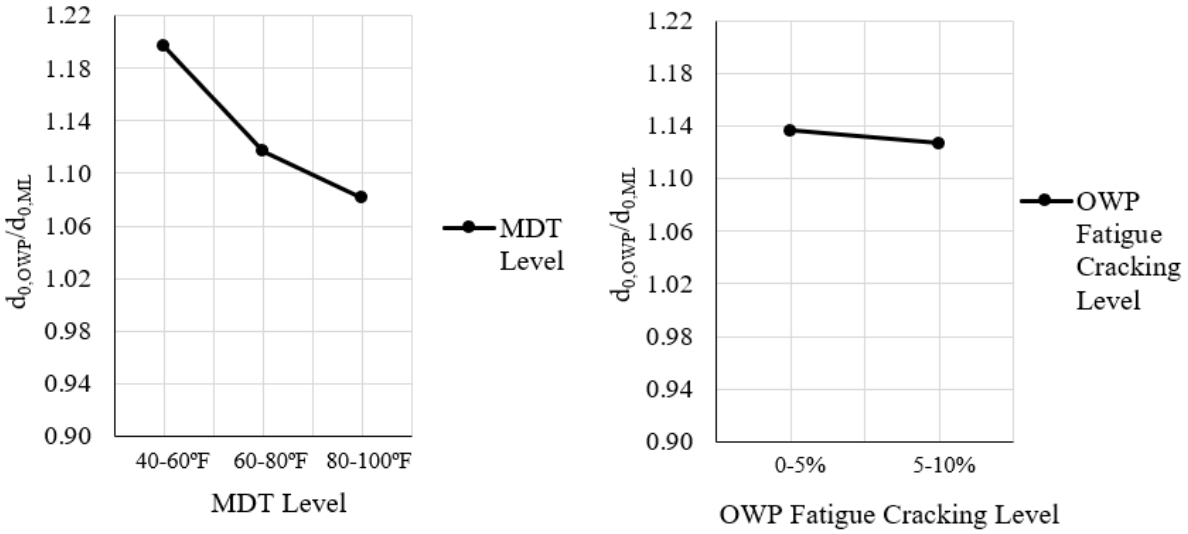

Figure 110. Main effects of the MDT and OWP fatigue cracking factors when there is visible distress ($d_{0,OWP}/d_{0,ML}$, LTPP Section 83-1801, Manitoba).

Again, Tukey's test was conducted at a 95% overall confidence level for each factor to identify which pairs of factor levels are significantly different. The null hypothesis was rejected for MDT but not rejected for section age. The pairwise comparisons, shown in Table 56, indicate that the mean of $d_{0,OWP}/d_{0,ML}$ for the 80ºF to 100ºF level is not significantly different from the mean for the 60ºF to 80ºF level, but that the mean of $d_{0,OWP}/d_{0,ML}$ is significantly different between all other pairs of MDT levels. The results also indicate that the mean of $d_{0,OWP}/d_{0,ML}$ does not change significantly with respect to OWP fatigue cracking.

Table 56. Results of Tukey's test for MDT and OWP fatigue cracking factors when there is visible distress (LTPP Section 83-1801, Manitoba).

MDT				OWP Fatigue Cracking			
Lower Factor Level	Upper Factor Level	Reject Null Hypothesis?	p-value	Lower Factor Level	Upper Factor Level	Reject Null Hypothesis ?	p-value
40ºF to 60ºF[1]	**60ºF to 80ºF**	**Yes**	**0.00**	0% to 5%	5% to 10%	No	0.64
40ºF to 60ºF	**80ºF to 100ºF**	**Yes**	**0.00**				
60ºF to 80ºF	80ºF to 100ºF	No	0.37				

[1] Significant comparisons are in bold.

Finally, a two-way ANOVA was performed using all the FWD data in Table 51. The results of this analysis, shown in Table 57, indicate that MDT, OWP fatigue cracking, and the interaction between MDT and OWP fatigue cracking all have a significant effect on $d_{0,OWP}/d_{0,ML}$. Main effects and interaction plots are shown in Figures 111 and 112, respectively. Figure 111 shows that the mean of $d_{0,OWP}/d_{0,ML}$ decreases as MDT increases, which is the same relationship observed for the previous two analyses. Figure 111 also shows that the mean of $d_{0,OWP}/d_{0,ML}$ increases as OWP fatigue cracking increases. This result confirms the initial hypothesis that

$d_{0,OWP}/d_{0,ML}$ increases as fatigue cracking increases. Figure 112 shows that the difference between $d_{0,OWP}/d_{0,ML}$ at the 0% fatigue cracking level and $d_{0,OWP}/d_{0,ML}$ at the 5% to 10% fatigue cracking level is greater at an MDT between 40ºF to 60ºF than at a MDT between 80ºF to 100ºF. This suggests that $d_{0,OWP}/d_{0,ML}$ may provide more information about fatigue damage in the asphalt concrete when FWD testing is conducted at a low temperature than when it is conducted at a high temperature.

Table 57. Results of two-way ANOVA analysis for the effects of MDT and section age on the mean of $d_{0,OWP}/d_{0,ML}$ over the entire pavement life (LTPP Section 83-1801, Manitoba).

Source of Variation	Degrees of Freedom	Adjusted Sum of Squares	Mean Square	F-value	p-value
MDT	2	0.101	0.050	23.63	0.00
OWP Fatigue Cracking	2	0.371	0.186	87.16	0.00
MDT * OWP Fatigue Cracking	4	0.031	0.008	3.65	0.01
Error	99	0.211	0.002		
Total	107	0.809			

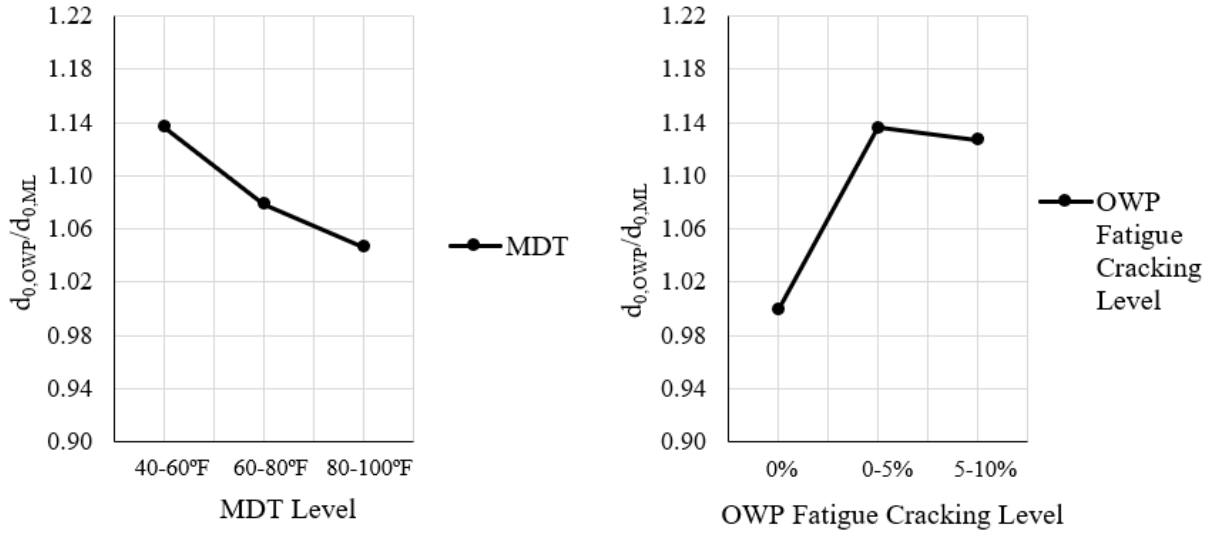

Figure 111. Main effects of MDT and OWP fatigue cracking factors over the entire pavement life ($d_{0,OWP}/d_{0,ML}$, LTPP Section 83-1801, Manitoba).

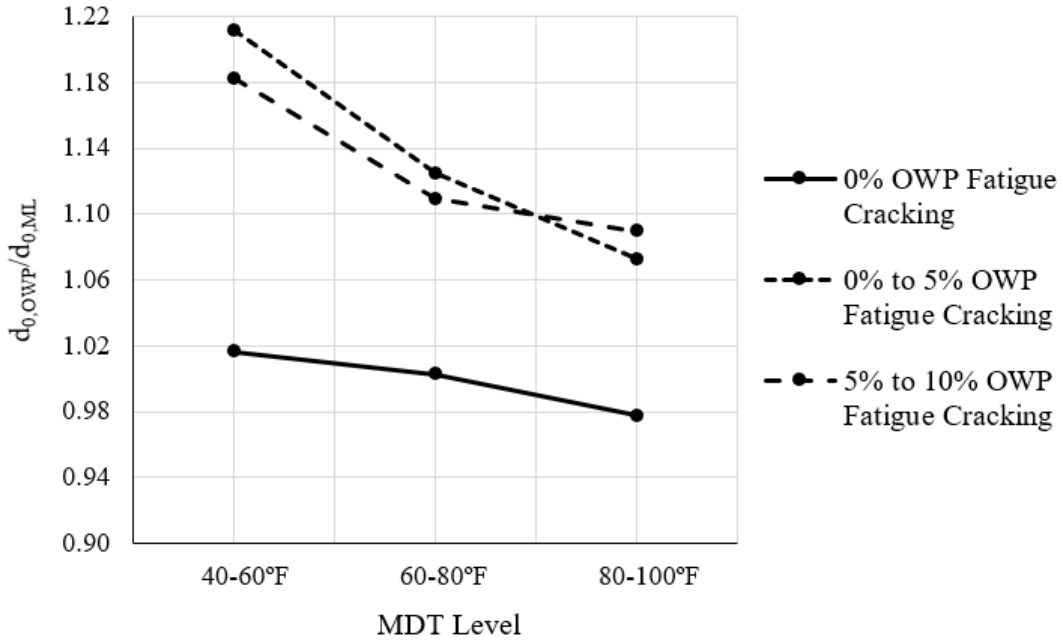

Figure 112. Interaction of MDT and OWP fatigue cracking factors over the entire pavement life ($d_{0,OWP}/d_{0,ML}$, LTPP Section 83-1801, Manitoba).

Tukey's test was conducted at a 95% overall confidence level for each factor to identify, which pairs of factor levels are significantly different. The null hypothesis was rejected for both MDT and OWP fatigue cracking. The pairwise comparisons from the Tukey's test are shown in Table 58. Similar to the previous Tukey's test, the mean of $d_{0,OWP}/d_{0,ML}$ at the 80ºF to 100ºF MDT level is not significantly different from the mean at the 60ºF to 80ºF MDT level, but that the mean of $d_{0,OWP}/d_{0,ML}$ is significantly different between all other pairs of MDT levels. The results also show that the 0% to 5% and 5% to 10% OWP fatigue cracking levels are significantly different from the 0% fatigue cracking level. Furthermore, the 0% to 5% and 5% to 10% OWP fatigue cracking levels are not significantly different from one another.

Table 58. Results of Tukey's test for MDT and OWP fatigue cracking factors over the entire pavement life (LTPP Section 83-1801, Manitoba).

MDT				OWP Fatigue Cracking			
Lower Factor Level	Upper Factor Level	Reject Null Hypothesis?	p-value	Lower Factor Level	Upper Factor Level	Reject Null Hypothesis?	p-value
40ºF to 60ºF[1]	**60ºF to 80ºF**	**Yes**	**0.00**	**0%**	**0% to 5%**	**Yes**	**0.00**
40ºF to 60ºF	**80ºF to 100ºF**	**Yes**	**0.00**	**0%**	**5% to 10%**	**Yes**	**0.00**
60ºF to 80ºF	80ºF to 100ºF	No	0.07	0% to 5%	5% to 10%	No	0.81

[1] Significant comparisons are in bold.

The following conclusions can be made based on the three two-way ANOVA analyses for LTPP Section 83-1801 in Manitoba:

1. The $d_{0,OWP}/d_{0,ML}$ parameter decreases as MDT increases. This agrees with the previous analysis of the relationship between $d_{0,OWP}/d_{0,ML}$ and MDT for LTPP sections with no visible distress. For this section, the relationship between $d_{0,OWP}/d_{0,ML}$ and MDT is significant over the entire life of the pavement section, including periods with visible distress and periods without visible distress.
2. There is not a significant relationship between $d_{0,OWP}/d_{0,ML}$ and section age when there is no visible distress. This answers Question 1a, and suggests, for this section, that it is not possible to detect fatigue cracking that has not yet reached the surface of the pavement.
3. There is not a significant relationship between $d_{0,OWP}/d_{0,ML}$ and OWP fatigue cracking when there is visible distress. This answers Question 1b, and indicates, for this section, that FWD parameters cannot provide information about the severity of fatigue damage in the pavement once there is visible distress.
4. The $d_{0,OWP}/d_{0,ML}$ parameter increases as OWP fatigue cracking increases over the entire life of the pavement section. This result supports the initial hypothesis that $d_{0,OWP}/d_{0,ML}$ increases as fatigue damage increases. The result also answers Question 1c, and suggests that, for this section, $d_{0,OWP}/d_{0,ML}$ provides useful information about the amount of fatigue damage in the asphalt concrete over the entire life of the pavement.

The three two-way ANOVA analyses of $d_{0,OWP}/d_{0,ML}$ performed for LTPP Section 83-1801 were also performed for each other FWD parameter and for the other eight individual LTPP sections. The ANOVA analyses of the $E_{NDT,OWP}/E_{Witczak(Aging)}$, and $E_{NDT,OWP}/E_{Witczak(No\ aging)}$ parameters were

performed using the log transformations of these parameters, $\log(E_{NDT,OWP}/E_{Witczak(Aging)})$, and $\log(E_{NDT,OWP}/E_{Witczak(No\ aging)})$, respectively. The results of each individual section analysis are summarized in Table 59. Each percentage in this table is the percentage of the individual sections for which the relationship between the FWD parameter and the factor is significant and is also the same as the hypothesized relationship shown in Table 48. Note that the percentage only includes sections for which there was sufficient FWD data to perform the two-way ANOVA. Detailed results of the analysis conducted for each FWD parameter and each individual section can be found in Appendix C.

Table 59. Summary of two-way ANOVA analysis of FWD parameters for individual LTPP sections.

		LTPP Sections with Significant Relationship between FWD Parameter and Dependent Variable			
	Dependent Variable	$d_{0,OWP}/d_{0,ML}$	$E_{NDT,OWP}/E_{NDT,ML}$	$\log(E_{NDT,OWP}/E_{Witczak(Aging)})$	$\log(E_{NDT,OWP}/E_{Witczak(No\ aging)})$
No Fatigue Cracking	MDT	50% (3/6)[1]	33% (2/6)	83% (5/6)	33% (2/6)
	Section Age	67% (4/6)	67% (4/6)	50% (3/6)	17% (1/6)
	Interaction	50% (3/6)	33% (2/6)	67% (4/6)	33% (2/6)
After Development of Fatigue Cracking	MDT	40% (2/5)	60% (3/5)	60% (3/5)	60% (3/5)
	OWP Fatigue Cracking	20% (1/5)	40% (2/5)	20% (1/5)	20% (1/5)
	Interaction	25% (1/4)	25% (1/4)	60% (3/5)	40% (2/5)
Entire Pavement Life	MDT	33% (3/9)	56% (5/9)	78% (7/9)	56% (5/9)
	OWP Fatigue Cracking	78% (7/9)	56% (5/9)	44% (4/9)	22% (2/9)
	Interaction	50% (3/6)	33% (2/6)	50% (3/6)	33% (3/9)

[1] Fractions in parentheses are the number of sections with a significant relationship over the number of total sections with sufficient FWD data to perform a two-way ANOVA.

5.4.1.1 Conclusions from individual sections analysis

Multiple two-way ANOVAs were performed for four FWD parameters and nine individual LTPP sections. The objective of the analysis was to answer several specific questions regarding the relationship between FWD parameters and fatigue damage. These questions and corresponding answers, based on the analysis performed, are listed below.

1. Question: Can FWD parameters be used to estimate the development of fatigue damage in the asphalt concrete layer of the existing pavement? Specifically:
    a. Question: Is there a significant correlation between the FWD parameters and time when there is **no** visible fatigue cracking in a pavement section? Can FWD parameters be used to detect fatigue damage prior to the development of fatigue cracking at the pavement surface?

       Answer: Analysis of individual LTPP sections has shown that FWD parameters can be used to detect fatigue damage in the asphalt concrete caused by fatigue cracking that has not yet reached the surface of the pavement. However, this is not true for all pavement sections, as shown in Table 59. Furthermore, the percentage of sections for which the FWD parameter can be used to detect fatigue cracking that has not reached the surface of the pavement depends on the FWD parameter used. As shown in Table 59, fatigue damage was detected in 67% of sections using the $d_{0,OWP}/d_{0,ML}$ and $E_{NDT,OWP}/E_{NDT,ML}$ parameters, but in only 17% of sections using $E_{NDT,OWP}/E_{Witczak(No\ aging)}$. It was not possible to determine a clear relationship between the thickness of the asphalt concrete layer and the ability of the FWD parameter to detect fatigue cracking that is not visible at the pavement surface. It

is important to note that only a small number of individual sections were analyzed and conclusions made from this analysis should be interpreted accordingly.

While it has been shown that FWD parameters may be used to detect fatigue cracking before it reaches the surface of the pavement, this information obtained from FWD testing may not be practically useful. First, it is necessary to collect FWD data at regular intervals over a long period of time to determine if a significant change in the FWD parameter has occurred. Figure 106 is a representative example of the amount of FWD data required. In this figure, each $d_{0,OWP}/d_{0,ML}$ data point represents two FWD test passes. Collecting this much FWD data is generally not practical for transportation agencies. Second, as shown in Table 59, even with a large amount of FWD data, the likelihood that a given FWD parameter will be able to detect "invisible" fatigue cracking is at most 67%.

b. Question: Is there a significant correlation between any of the FWD parameters and OWP fatigue cracking when there is visible distress?

   Answer: The relationship between the FWD parameter and OWP fatigue cracking when there is visible distress is significant for, at most, 40% of the individual sections across all FWD parameters. This suggests that FWD parameters may not be useful for quantifying the extent and severity of fatigue damage once fatigue cracking has reached the pavement surface.

c. Question: Is there a significant correlation between any of the FWD parameters and OWP fatigue cracking over the whole life of a pavement section?

   Answer: As shown in Table 59, the percentage of individual sections with a significant relationship between the FWD parameter and OWP fatigue cracking

over the entire life of the pavement section varies widely between FWD parameters. The relationship is significant for 78% of sections when $d_{0,OWP}/d_{0,ML}$ is used, but it is significant for only 22% of sections when $\log(E_{NDT,OWP}/E_{Witczak(No\ aging)})$ is used. This suggests that $d_{0,OWP}/d_{0,ML}$ is the best parameter for determining information about fatigue damage in the asphalt concrete. It should be noted, however, that only a small number of individual sections were analyzed.

2. Question: Is the $E_{NDT,OWP}/E_{Witczak(Aging)}$ parameter, which is currently used in the Pavement ME AC/AC overlay design procedure, meaningfully related to fatigue damage and OWP fatigue cracking? Can $E_{NDT,OWP}/E_{Witczak(Aging)}$ or any of the other FWD parameters be used to adjust the E_{NDT} input used in Pavement ME to more successfully quantify the amount of fatigue damage in the asphalt concrete of the existing pavement?

   Answer: As shown in Table 59, $E_{NDT,OWP}/E_{Witczak(Aging)}$ is significantly related to OWP fatigue cracking over the entire life of the pavement section for 44% of sections. Additionally, $E_{NDT,OWP}/E_{Witczak(Aging)}$ is significantly related to OWP fatigue cracking for 50% of sections when there is no visible distress in the pavement. These results suggest it is not entire unreasonable to use $E_{NDT,OWP}/E_{Witczak(Aging)}$ to characterize fatigue damage in the asphalt concrete. More investigation, however, is required due to the small number of sections analyzed.

5.4.2 FWD parameters and fatigue damage using data from multiple sections

Two-way ANOVAs were also performed to analyze the relationship between FWD parameters and fatigue damage using a compilation of data from many different LTPP sections. This analysis was conducted to answer the questions proposed at the beginning of this section:

1. Can FWD parameters be used to estimate the development of fatigue damage in the asphalt concrete layer of an existing pavement? Specifically:
    b. Is there a significant correlation between any of the FWD parameters and OWP fatigue cracking when there is visible distress?
    c. Is there a significant correlation between any of the FWD parameters and OWP fatigue cracking over the whole life of a pavement section?
2. Is the $E_{NDT,OWP}/E_{Witczak(Aging)}$ parameter, which is currently used in the Pavement ME AC/AC overlay design procedure, meaningfully related to fatigue damage and OWP fatigue cracking?

Only 56 sections with OWP fatigue cracking information were included in the analysis. These sections are a mixture of SMP sections, which have a large amount of FWD data, and sections that were overlaid, which exhibited a significant amount of fatigue cracking in the existing pavement. Note that, unlike the analysis of individual LTPP sections, not all sections in this analysis have FWD data distributed over the entire life of the pavement section. The sections used in the analysis and the number of FWD data points for each section are listed in Table 60.

Table 60. LTPP sections included in the analysis of the relationship between FWD parameters and fatigue damage.

Section Information		Number of FWD Data Points	
State	LTPP ID	$d_{0,OWP}/d_{0,ML}$ and $E_{NDT,OWP}/E_{NDT,ML}$	$Log(E_{NDT,OWP}/E_{Witczak(Aging)})$ and $Log(E_{NDT,OWP}/E_{Witczak(No\ aging)})$
AL	1-0101	91	91
AL	1-0102	78	78
CO	8-1053	101	99
CT	9-1803	83	83
DE	10-0102	6	5
GA	13-1005	74	74
GA	13-1031	106	103
ID	16-1010	75	72
KS	20-0159	2	2
KS	20-1005	23	23
ME	23-1009	1	1
ME	23-1026	59	58
MD	24-1634	53	53
MA	25-1002	99	98
MN	27-1018	41	40
MN	27-1028	69	0
MN	27-6251	76	0
MS	28-1016	47	47
MS	28-1802	78	53
MT	30-0114	90	87
NE	31-0114	94	90
NH	33-1001	90	89
NJ	34-0501	14	0
NJ	34-0961	1	1
NJ	34-0962	1	1
NJ	34-1003	2	2
NJ	34-1011	1	1
NJ	34-1030	6	6
NM	35-1112	103	100
NY	36-0801	143	143
NY	36-0802	9	9
NC	37-1028	59	59
OH	39-0901	124	0
OK	40-4165	68	53
PA	42-1597	8	8
SD	46-9187	72	72
TX	48-1060	92	90

Table 60 (continued).

Section Information		Number of FWD Data Points	
State	LTPP ID	$d_{0,OWP}/d_{0,ML}$ and $E_{NDT,OWP}/E_{NDT,ML}$	$Log(E_{NDT,OWP}/E_{Witczak(Aging)})$ and $Log(E_{NDT,OWP}/E_{Witczak(No\ aging)})$
TX	48-1068	92	91
TX	48-1077	80	76
TX	48-1122	123	118
UT	49-1001	77	77
VT	50-1002	139	138
VT	50-1683	2	0
VA	51-0113	90	88
VA	51-0114	120	118
WY	56-1007	86	85
MB	83-0502	1	1
MB	83-0503	1	1
MB	83-0506	1	1
MB	83-0507	1	1
MB	83-0508	1	0
MB	83-0509	1	1
MB	83-1801	129	127
ON	87-1622	58	58
QB	89-1125	1	1
SK	90-6405	77	0

The two-way ANOVA was conducted in the same manner as was done for individual LTPP sections. Each LTPP section has many FWD parameter data points, each of which represent the average value of the FWD parameter for a single FWD pass. Every data point has an associated MDT and OWP fatigue cracking. First, the FWD parameter data points and associated MDT and OWP fatigue cracking from all LTPP sections were combined into a single data set. Next, the MDT and the OWP fatigue cracking for each FWD parameter data point were each assigned to a level. The same bin categories used to define levels of MDT and OWP fatigue cracking for individual sections were used to assign factor levels for this data analysis. These categories are shown in Table 50. The two-way ANOVA was performed separately for each FWD parameter,

and the main effects and second-order interactions of the factors were determined. A Tukey test was also performed to determine which levels of each factor are significantly different from one another. The results of each analysis are described separately.

5.4.2.1 $d_{0,OWP}/d_{0,ML}$

As shown in Figure 113, there is a very weak correlation between $d_{0,OWP}/d_{0,ML}$ and OWP fatigue cracking for the pooled data. The two-way ANOVA was conducted to determine if there is a significant relationship between $d_{0,OWP}/d_{0,ML}$ and OWP fatigue cracking. The results of this analysis, shown in Table 61, indicate that MDT, OWP fatigue cracking, and the interaction between MDT and OWP fatigue cracking are all significant at a 95% confidence level.

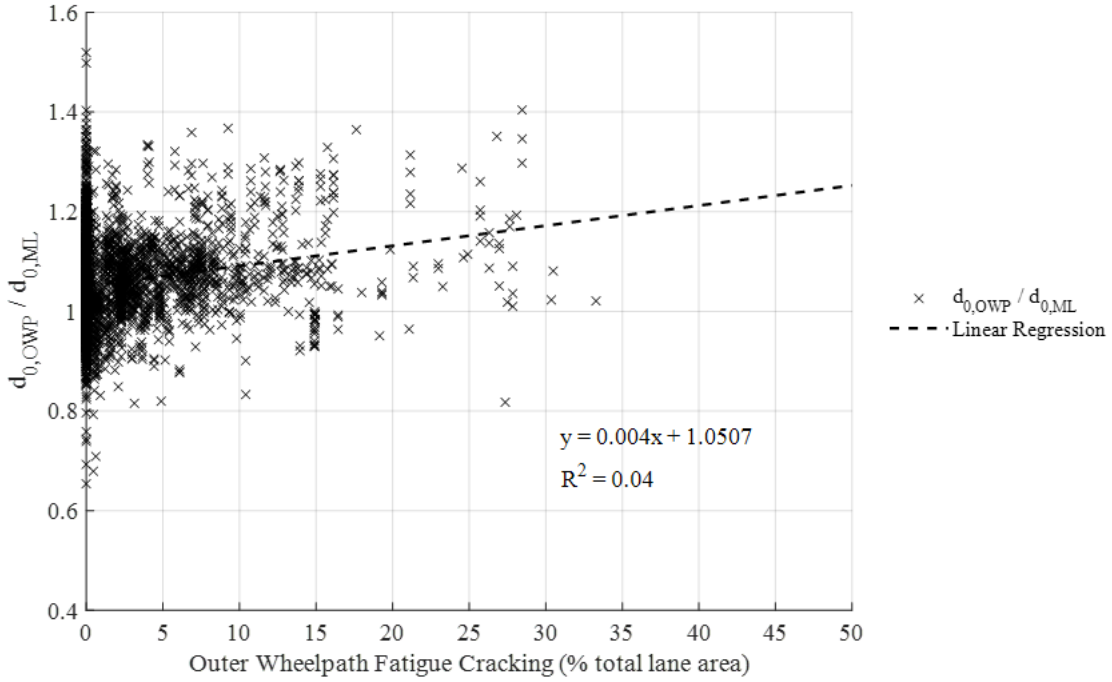

Figure 113. $d_{0,OWP}/d_{0,ML}$ vs. OWP fatigue cracking (56 LTPP sections, 9-kip load).

Table 61. Results of the two-way ANOVA of the effects of MDT and OWP fatigue cracking on $d_{0,OWP}/d_{0,ML}$ over the entire pavement life based on 56 LTPP sections.

Source of Variation	Degrees of Freedom	Adjusted Sum of Squares	Mean Square	F-value	p-value
MDT	3	0.315	0.105	13.24	0.00
OWP Fatigue Cracking	3	0.439	0.146	18.46	0.00
MDT * OWP Fatigue Cracking	9	0.388	0.043	5.43	0.00
Error	2907	23.039	0.008		
Total	2922	24.554			

Main effects plots are shown in Figure 114. The main effects plot for MDT shows that $d_{0,OWP}/d_{0,ML}$ decreases as MDT increases. This trend was previously observed in the analysis of sections without visible distress (Table 29) and in some of the individual LTPP sections (Table 59). Tukey's test was performed at a 95% overall confidence level for MDT. The results, shown in Table 62, indicate that $d_{0,OWP}/d_{0,ML}$ at the 40ºF to 60ºF level is significantly different from $d_{0,OWP}/d_{0,ML}$ at all other MDT levels, but that $d_{0,OWP}/d_{0,ML}$ is not significantly different for all MDT levels above 60ºF. This trend is similar to what was observed for sections with no visible distress (Table 30). Figure 114 also shows that $d_{0,OWP}/d_{0,ML}$ increases as OWP fatigue cracking increases. This supports the initial hypothesis that $d_{0,OWP}/d_{0,ML}$ increases as OWP fatigue cracking increases. The results of Tukey's test, shown in Table 62, indicate that $d_{0,OWP}/d_{0,ML}$ is significantly different for all combinations of factor levels except 0% and 0% to 5% and 5% to 10% and greater than 10% OWP fatigue cracking. Additionally, it is notable that the total change in the mean of $d_{0,OWP}/d_{0,ML}$ between the lowest and highest levels of MDT is roughly equivalent to the total change between the lowest and highest levels of OWP fatigue cracking.

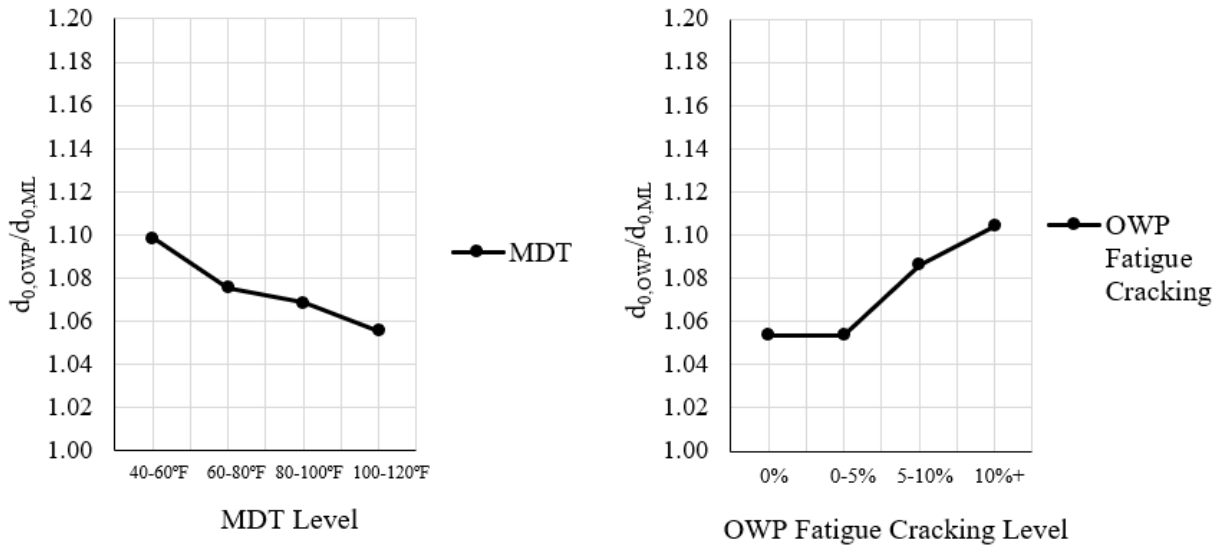

Figure 114. Main effects of the MDT and OWP fatigue cracking factors based on 56 LTPP sections ($d_{0,OWP}/d_{0,ML}$).

Table 62. Results of Tukey's test for MDT and OWP fatigue cracking factors over the entire pavement life based on 56 LTPP sections ($d_{0,OWP}/d_{0,ML}$).

MDT				OWP Fatigue Cracking			
Lower Factor Level	Upper Factor Level	Reject Null Hypothesis ?	p-value	Lower Factor Level	Upper Factor Level	Reject Null Hypothesis ?	p-value
40°F to 60°F[1]	**60°F to 80°F**	**Yes**	**0.00**	0%	0% to 5%	No	1.00
40°F to 60°F	**80°F to 100°F**	**Yes**	**0.00**	**0%**	**5% to 10%**	**Yes**	**0.00**
40°F to 60°F	**100°F to 120°F**	**Yes**	**0.00**	**0%**	**Greater than 10%**	**Yes**	**0.00**
60°F to 80°F	80°F to 100°F	No	0.62	**0% to 5%**	**5% to 10%**	**Yes**	**0.00**
60°F to 80°F	100°F to 120°F	No	0.15	**0% to 5%**	**Greater than 10%**	**Yes**	**0.00**
80°F to 100°F	100°F to 120°F	No	0.55	5% to 10%	Greater than 10%	No	0.32

[1] Significant comparisons are in bold.

Finally, Figure 115 shows the interaction between MDT and OWP fatigue cracking. The difference between $d_{0,OWP}/d_{0,ML}$ at the 0% OWP fatigue cracking level and $d_{0,OWP}/d_{0,ML}$ at the greater than 10% fatigue cracking level is larger at a MDT between 40ºF to 60ºF than at a MDT between 100ºF to 120ºF. This suggests that $d_{0,OWP}/d_{0,ML}$ may provide more information about fatigue damage in the asphalt concrete when FWD testing is conducted at a low MDT than at a high MDT.

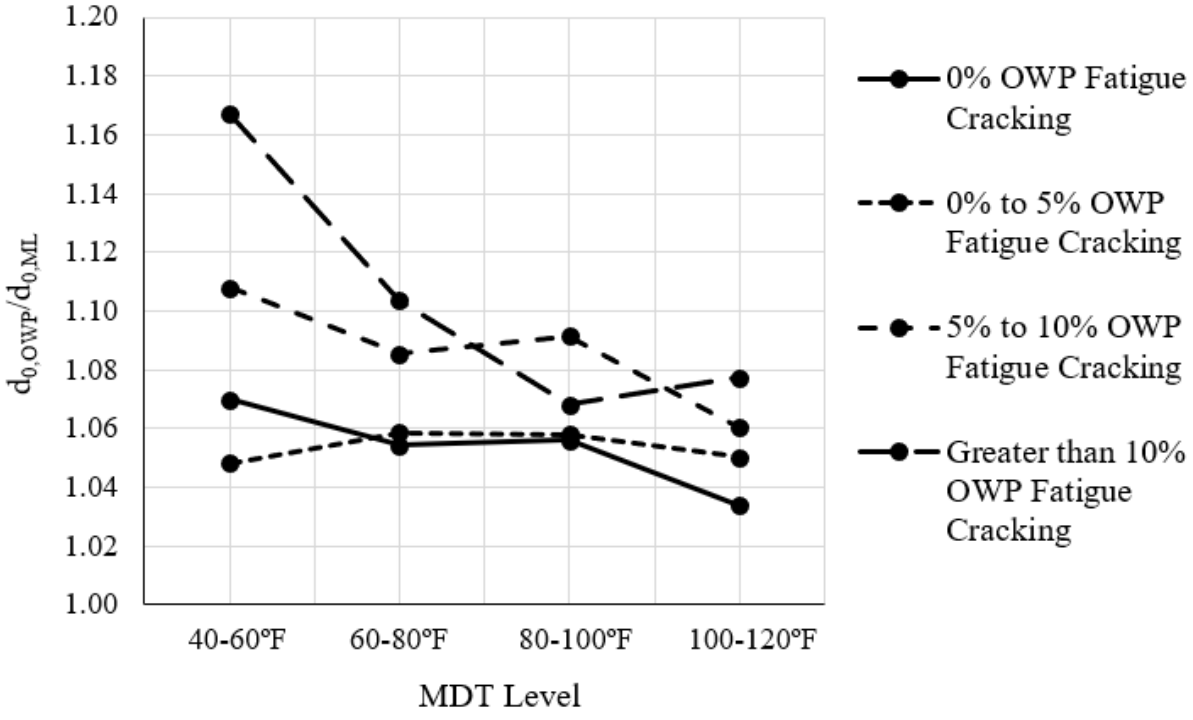

Figure 115. Interaction of the MDT and OWP fatigue cracking factors based on 56 LTPP sections ($d_{0,OWP}/d_{0,ML}$).

5.4.2.2 $E_{NDT,OWP}/E_{NDT,ML}$

As shown in Figure 116, there is almost no correlation between $E_{NDT,OWP}/E_{NDT,ML}$ and OWP fatigue cracking when data for all 56 LTPP sections is considered. A two-way ANOVA was conducted at a 95% confidence level to determine if a significant relationship exists between $E_{NDT,OWP}/E_{NDT,ML}$ and OWP fatigue cracking. The results of this analysis, shown in Table 63, indicate that MDT and the interaction between MDT and OWP fatigue cracking are significant, but that and OWP fatigue cracking alone is not significant.

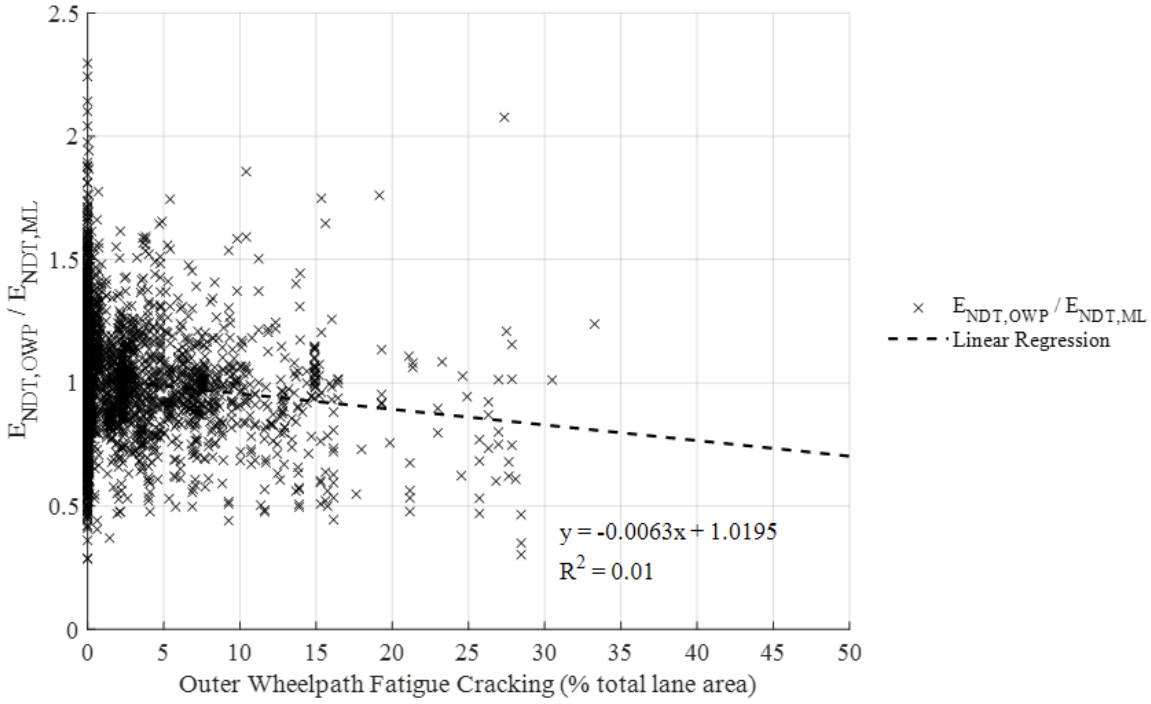

Figure 116. $E_{NDT,OWP}/E_{NDT,ML}$ vs. OWP fatigue cracking (56 LTPP sections, 9-kip load).

Table 63. Results of two-way ANOVA analysis for the effects of MDT and OWP fatigue cracking on $E_{NDT,OWP}/E_{NDT,ML}$ over the entire pavement life based on 56 LTPP sections.

Source of Variation	Degrees of Freedom	Adjusted Sum of Squares	Mean Square	F-value	p-value
MDT	3	4.144	1.381	26.62	0.00
OWP Fatigue Cracking	3	0.388	0.129	2.49	0.06
MDT * OWP Fatigue Cracking	9	1.169	0.130	2.50	0.01
Error	2855	148.121	0.052		
Total	2870	155.395			

Main effects plots are shown in Figure 117. The main effects plot for MDT shows that $E_{NDT,OWP}/E_{NDT,ML}$ increases as MDT increases. This trend was previously observed in the analysis of sections without visible distress (Table 35) and in the analysis of some individual LTPP sections (Table 59). Tukey's test was performed at a 95% overall confidence level for the MDT factor. The results, shown in Table 64, indicate that $E_{NDT,OWP}/E_{NDT,ML}$ is significantly different for all combinations of MDT bins. Figure 117 also shows that $E_{NDT,OWP}/E_{NDT,ML}$ decreases as OWP fatigue cracking increases, but this trend is not significant at the 95% confidence level. The results of Tukey's test for OWP fatigue cracking, shown in Table 64, confirm that $E_{NDT,OWP}/E_{NDT,ML}$ is not significantly different for any combinations of OWP fatigue cracking levels. Additionally, as shown in Figure 117, the total change in the mean of $E_{NDT,OWP}/E_{NDT,ML}$ between the lowest and highest levels of MDT is more than two times the change between the lowest and highest levels of OWP fatigue cracking. This suggests that it is relatively difficult to distinguish the effect of OWP fatigue cracking on $E_{NDT,OWP}/E_{NDT,ML}$ from the effect of MDT.

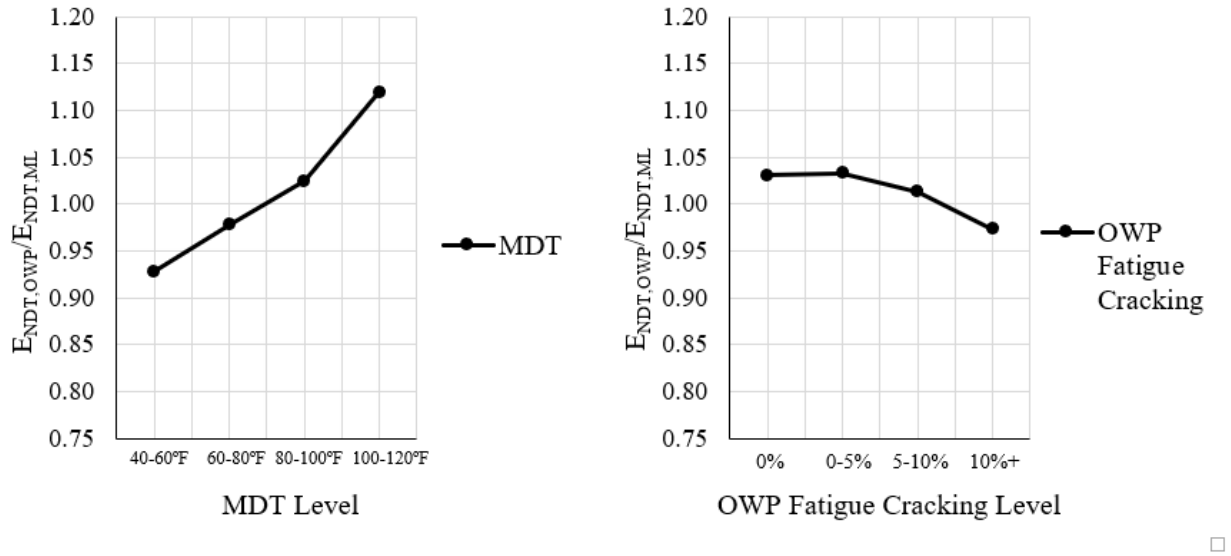

Figure 117. Main effects of the MDT and OWP fatigue cracking factors based on 56 LTPP sections ($E_{NDT,OWP}/E_{NDT,ML}$).

Table 64. Results of Tukey's test for MDT and OWP fatigue cracking factors over the entire pavement life based on 56 LTPP sections ($E_{NDT,OWP}/E_{NDT,ML}$).

MDT				OWP Fatigue Cracking			
Lower Factor Level	Upper Factor Level	Reject Null Hypothesis ?	p-value	Lower Factor Level	Upper Factor Level	Reject Null Hypothesis ?	p-value
40°F to 60°F[1]	**60°F to 80°F**	**Yes**	**0.00**	0%	0% to 5%	No	1.00
40°F to 60°F	**80°F to 100°F**	**Yes**	**0.00**	0%	5% to 10%	No	0.76
40°F to 60°F	**100°F to 120°F**	**Yes**	**0.00**	0%	Greater than 10%	No	0.06
60°F to 80°F	**80°F to 100°F**	**Yes**	**0.01**	0% to 5%	5% to 10%	No	0.70
60°F to 80°F	**100°F to 120°F**	**Yes**	**0.00**	0% to 5%	Greater than 10%	No	0.05
80°F to 100°F	**100°F to 120°F**	**Yes**	**0.00**	5% to 10%	Greater than 10%	No	0.46

[1] Significant comparisons are in bold.

Finally, Figure 118 shows the effect of the interaction between MDT and OWP fatigue cracking. The difference between $E_{NDT,OWP}/E_{NDT,ML}$ at either the 0% or 0% to 5% OWP fatigue cracking level and $E_{NDT,OWP}/E_{NDT,ML}$ at the greater than 10% fatigue cracking level is larger at a low MDT (40ºF to 60ºF) than at a high MDT (100ºF to 120ºF). This suggests that $E_{NDT,OWP}/E_{NDT,ML}$ may provide more information about fatigue damage in the asphalt concrete when FWD testing is conducted at a low MDT than when it is conducted at a high MDT.

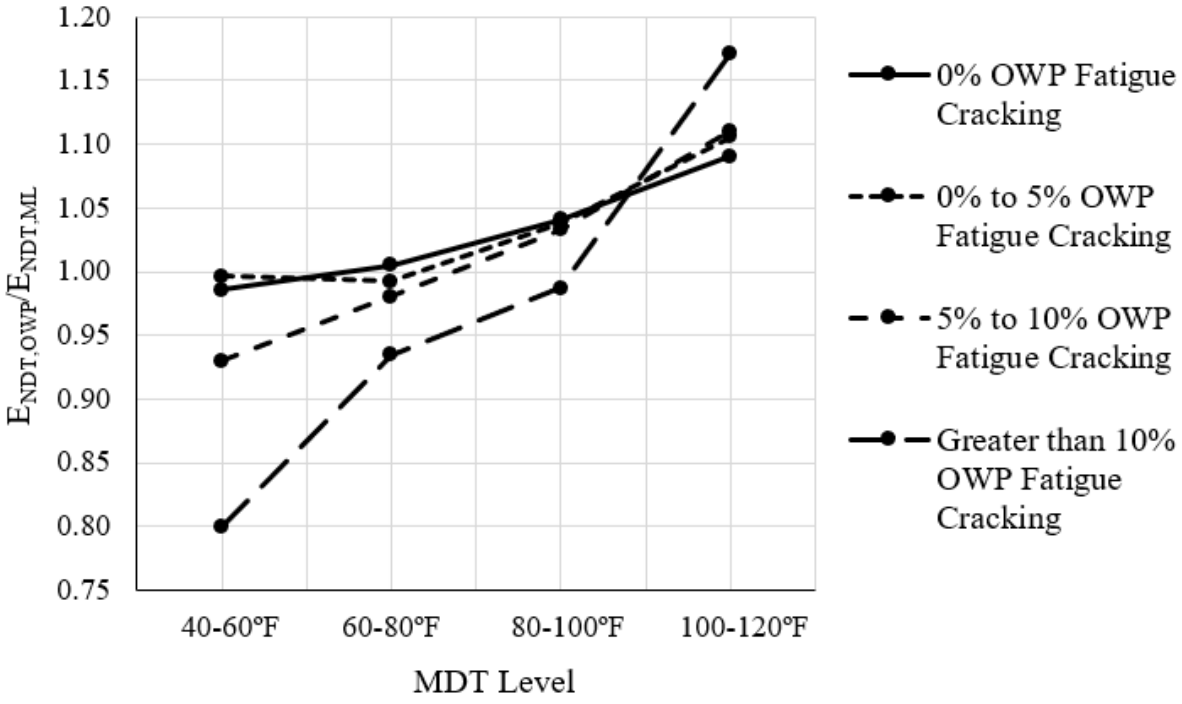

Figure 118. Interaction of the MDT and OWP fatigue cracking factors based on 56 LTPP sections ($E_{NDT,OWP}/E_{NDT,ML}$).

5.4.2.3 $E_{NDT,OWP}/E_{Witczak(Aging)}$

Similar to the previous two parameters, there is a very weak correlation between $\log(E_{NDT,OWP}/E_{Witczak(Aging)})$ and OWP fatigue cracking for the pooled data. This is shown in Figure 119. A two-way ANOVA was conducted to determine if there is a significant relationship between $\log(E_{NDT,OWP}/E_{Witczak(Aging)})$ and OWP fatigue cracking. The results of the ANOVA, shown in Table 65, indicate that MDT, OWP fatigue cracking, and the interaction between MDT and OWP fatigue cracking are all significant at a 95% confidence level.

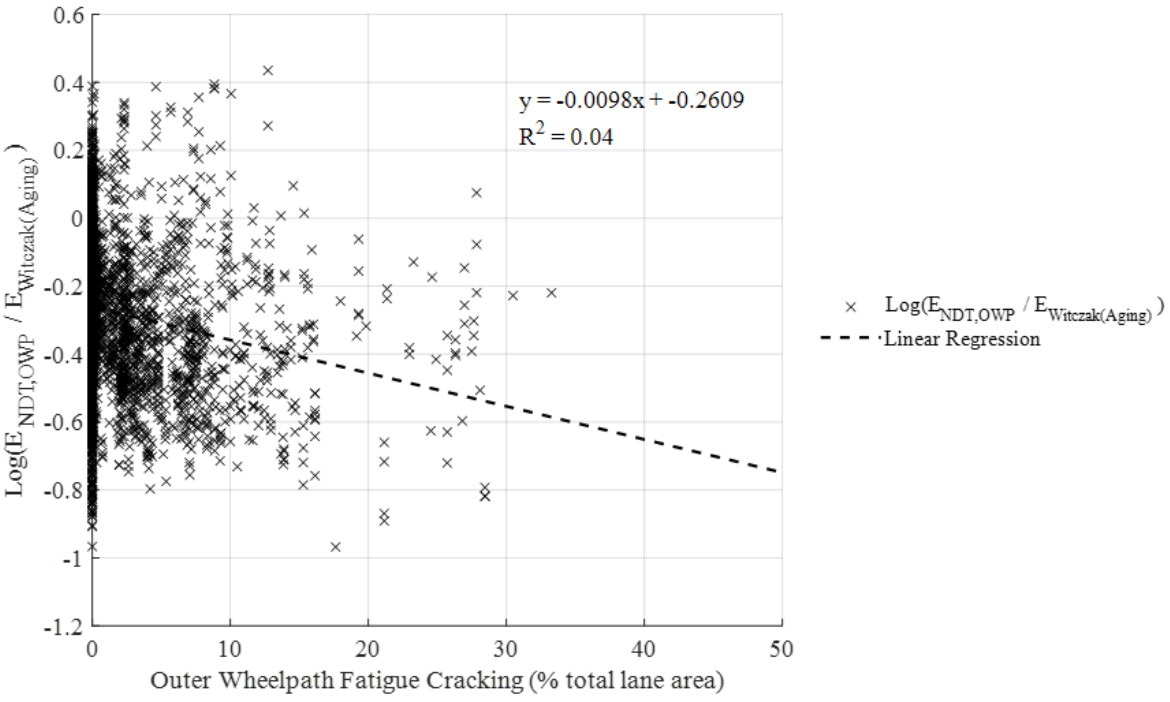

Figure 119. $\log(E_{NDT,OWP}/E_{Witczak(Aging)})$ vs. OWP fatigue cracking (56 LTPP sections, 9-kip load).

Table 65. Results of two-way ANOVA analysis for the effects of MDT and OWP fatigue cracking on $\log(E_{NDT,OWP}/E_{NDT(Aging)})$ over the entire pavement life based on 56 LTPP sections.

Source of Variation	Degrees of Freedom	Adjusted Sum of Squares	Mean Square	F-value	p-value
MDT	3	25.755	8.585	237.83	0.00
OWP Fatigue Cracking	3	1.023	0.341	9.44	0.00
MDT * OWP Fatigue Cracking	9	1.181	0.131	3.63	0.00
Error	2561	92.447	0.036		
Total	2576	138.774			

Main effects plots are shown in Figure 120. The main effects plot for MDT shows that $\log(E_{NDT,OWP}/E_{NDT(Aging)})$ increases as MDT increases. This is the same trend observed in the analysis of sections without visible distress (Table 40) and in the analysis for most of the individual LTPP sections (Table 59). The results of Tukey's test performed at a 95% overall confidence level, shown in Table 66, indicate that $\log(E_{NDT,OWP}/E_{NDT(Aging)})$ is significantly different for all combinations of MDT categories. This conclusion is somewhat different from the analysis of $\log(E_{NDT,OWP}/E_{NDT(Aging)})$ and MDT with no visible distress, which found that $\log(E_{NDT,OWP}/E_{NDT(Aging)})$ does not change significantly at a MDT greater than 70ºF (Table 41) Figure 120 also shows that $\log(E_{NDT,OWP}/E_{NDT(Aging)})$ decreases as OWP fatigue cracking increases.

This result supports the initial hypothesis that $E_{NDT,OWP}/E_{NDT(Aging)}$ decreases as fatigue damage increases. The results of Tukey's test, shown in Table 66, indicate that $\log(E_{NDT,OWP}/E_{NDT(Aging)})$ is significantly different for all combinations of OWP fatigue cracking levels, except between 0% to 5% and 5% to 10% and between 5% to 10% and greater than 10%. Additionally, as shown in Figure 120, the change in $\log(E_{NDT,OWP}/E_{NDT(Aging)})$ between the extreme levels of MDT is more than double the change between the extreme levels of OWP fatigue cracking. This suggests that it may be difficult to distinguish between the effect of OWP fatigue cracking from the effect of MDT.

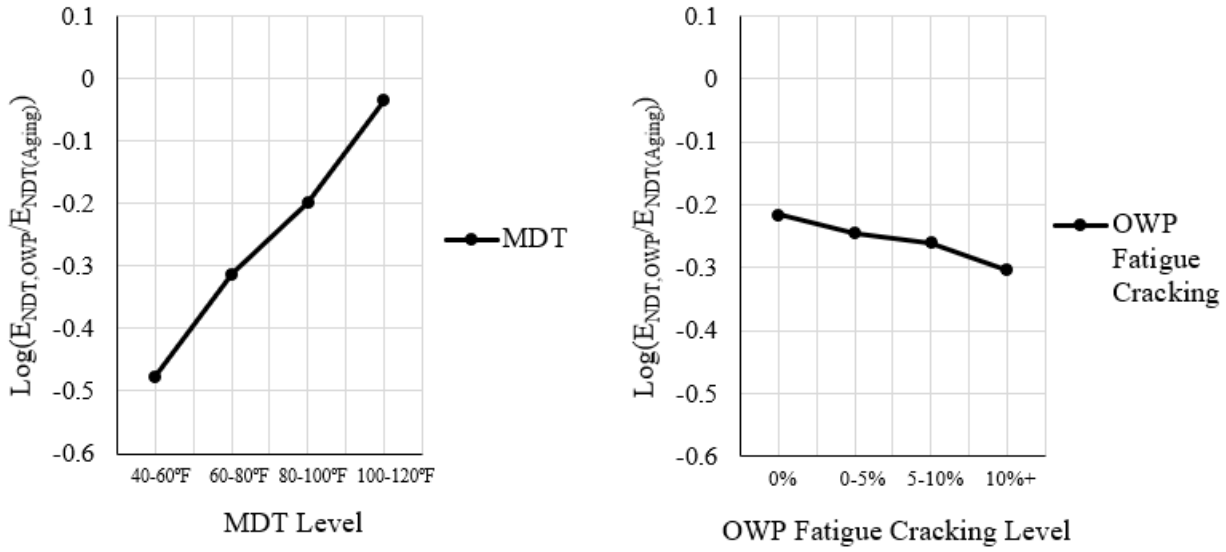

Figure 120. Main effects of the MDT and OWP fatigue cracking factors based on 56 LTPP sections ($\text{Log}(E_{NDT,OWP}/E_{NDT(Aging)})$).

Table 66. Results of Tukey's test for MDT and OWP fatigue cracking factors over the entire pavement life based on 56 LTPP sections ($Log(E_{NDT,OWP}/E_{NDT(Aging)})$).

MDT				OWP Fatigue Cracking			
Lower Factor Level	Upper Factor Level	Reject Null Hypothesis?	p-value	Lower Factor Level	Upper Factor Level	Reject Null Hypothesis?	p-value
40ºF to 60ºF[1]	**60ºF to 80ºF**	**Yes**	**0.00**	**0%**	**0% to 5%**	**Yes**	**0.01**
40ºF to 60ºF	**80ºF to 100ºF**	**Yes**	**0.00**	**0%**	**5% to 10%**	**Yes**	**0.01**
40ºF to 60ºF	**100ºF to 120ºF**	**Yes**	**0.00**	**0%**	**Greater than 10%**	**Yes**	**0.00**
60ºF to 80ºF	**80ºF to 100ºF**	**Yes**	**0.00**	0% to 5%	5% to 10%	No	0.76
60ºF to 80ºF	**100ºF to 120ºF**	**Yes**	**0.00**	**0% to 5%**	**Greater than 10%**	**Yes**	**0.02**
80ºF to 100ºF	**100ºF to 120ºF**	**Yes**	**0.00**	5% to 10%	Greater than 10%	No	1.00

[1] Significant comparisons are in bold

Figure 121 shows the effect of the interaction between MDT and OWP fatigue cracking on $log(E_{NDT,OWP}/E_{NDT(Aging)})$. Similar to the previous two FWD parameters, the difference between $log(E_{NDT,OWP}/E_{NDT(Aging)})$ at 0% fatigue cracking and $log(E_{NDT,OWP}/E_{NDT(Aging)})$ at greater than 10% fatigue cracking is larger at lower levels of MDT (40ºF to 60ºF and 60ºF to 80ºF) than at higher levels of MDT (80ºF to 100ºF and 100ºF to 120ºF). This suggests that $log(E_{NDT,OWP}/E_{NDT(No\ aging)})$ may provide more information about fatigue damage in the asphalt concrete when FWD testing is conducted at lower levels of MDT than at higher levels of MDT.

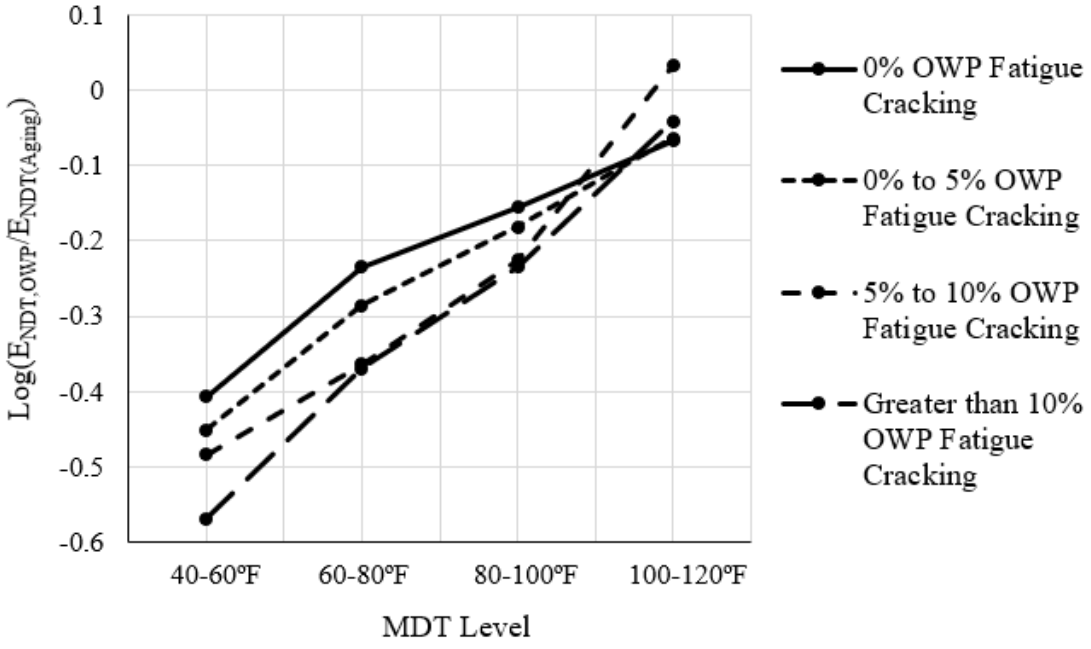

Figure 121. Interaction of the MDT and OWP fatigue cracking factors based on 56 LTPP sections ($Log(E_{NDT,OWP}/E_{NDT(Aging)})$).

5.4.2.4 $E_{NDT,OWP}/E_{Witczak(No\ aging)}$

As with all other parameters, there is a very weak correlation between $log(E_{NDT,OWP}/E_{Witczak(No\ aging)})$ and OWP fatigue cracking when combining the 56 LTPP sections. This is shown in Figure 122. The two-way ANOVA was conducted to determine if there is a significant relationship between $log(E_{NDT,OWP}/E_{Witczak(No\ aging)})$ and OWP fatigue cracking. The results of this analysis, shown in Table 67, indicate that MDT, OWP fatigue cracking, and the interaction between MDT and OWP fatigue cracking are all significant at a 95% confidence level.

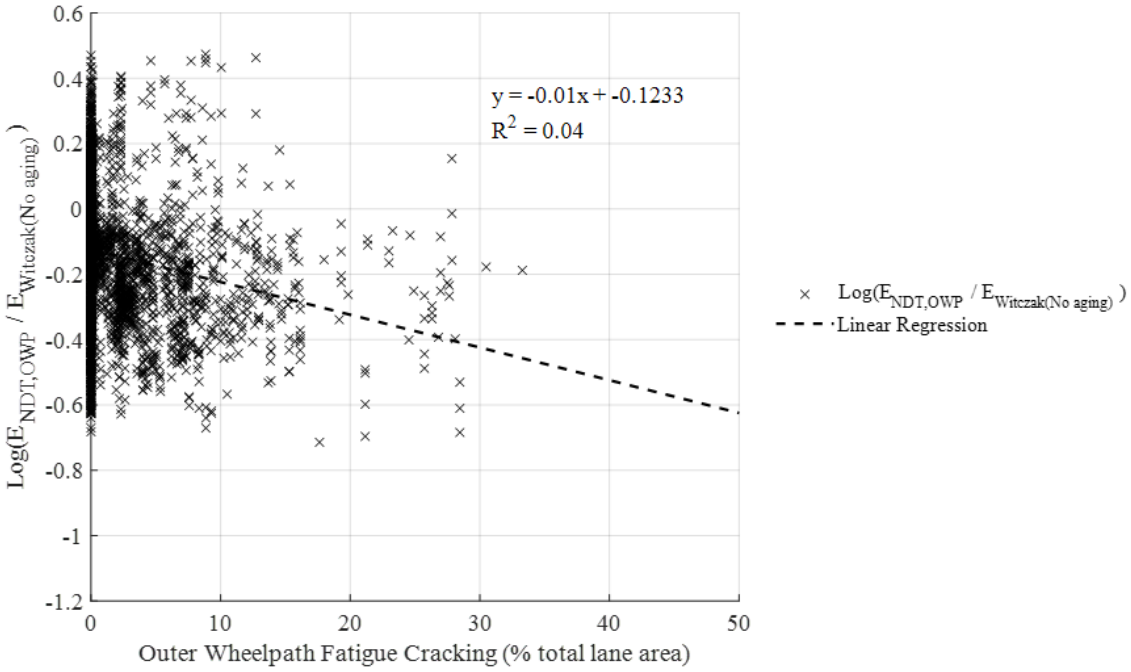

Figure 122. Log($E_{NDT,OWP}/E_{Witczak(No\ aging)}$) vs. OWP fatigue cracking (56 LTPP sections, 9-kip load)

Table 67. Results of two-way ANOVA analysis for the effects of MDT and OWP fatigue cracking on log($E_{NDT,OWP}/E_{Witczak(No\ aging)}$) over the entire pavement life based on 56 LTPP sections.

Source of Variation	Degrees of Freedom	Adjusted Sum of Squares	Mean Square	F-value	p-value
MDT	3	8.341	2.780	72.18	0.00
OWP Fatigue Cracking	3	1.970	0.657	17.05	0.00
MDT * OWP Fatigue Cracking	9	1.321	0.147	3.81	0.00
Error	2561	98.644	0.039		
Total	2576	117.669			

Main effects plots are shown in Figure 123. The main effects plot for MDT shows that $\log(E_{NDT,OWP}/E_{NDT(No\ aging)})$ increases as MDT increases. This contradicts the analysis of sections without visible distress, which concluded that the relationship between $\log(E_{NDT,OWP}/E_{NDT(No\ aging)})$ and MDT is significant but unclear. The relationship between $\log(E_{NDT,OWP}/E_{NDT(No\ aging)})$ and MDT shown in Figure 123 does, however, agree with the analysis of some of the individual LTPP sections (Table 59). The results of Tukey's test performed at a 95% simultaneous confidence level, shown in Table 68, indicate that $\log(E_{NDT,OWP}/E_{NDT(No\ aging)})$ is significantly different for all combinations of MDT levels, except the 60ºF to 80ºF level and the 80ºF to 100ºF level. This conclusion is different from the analysis of $\log(E_{NDT,OWP}/E_{NDT(No\ aging)})$ and MDT with no visible distress, which found that $\log(E_{NDT,OWP}/E_{NDT(No\ aging)})$ is significantly different only between the 40ºF to 50ºF and 70ºF to 80ºF levels.

Figure 123 also shows that $\log(E_{NDT,OWP}/E_{NDT(No\ aging)})$ decreases as OWP fatigue cracking increases. This result supports the initial hypothesis that $E_{NDT,OWP}/E_{NDT(No\ aging)}$ decreases as fatigue damage increases. The results of Tukey's test, shown in Table 68, indicate that $\log(E_{NDT,OWP}/E_{NDT(No\ aging)})$ is significantly different for all combinations of OWP fatigue cracking levels, except 0% to 5% and 5% to 10% and 5% to 10% and greater than 10%. Similar to $\log(E_{NDT,OWP}/E_{NDT(Aging)})$, the total change in $\log(E_{NDT,OWP}/E_{NDT(No\ aging)})$ between the extreme levels of MDT is approximately two times the total change between the extreme levels of OWP fatigue cracking. This suggests that it may be relatively difficult to distinguish the effect of OWP fatigue cracking from the effect of MDT.

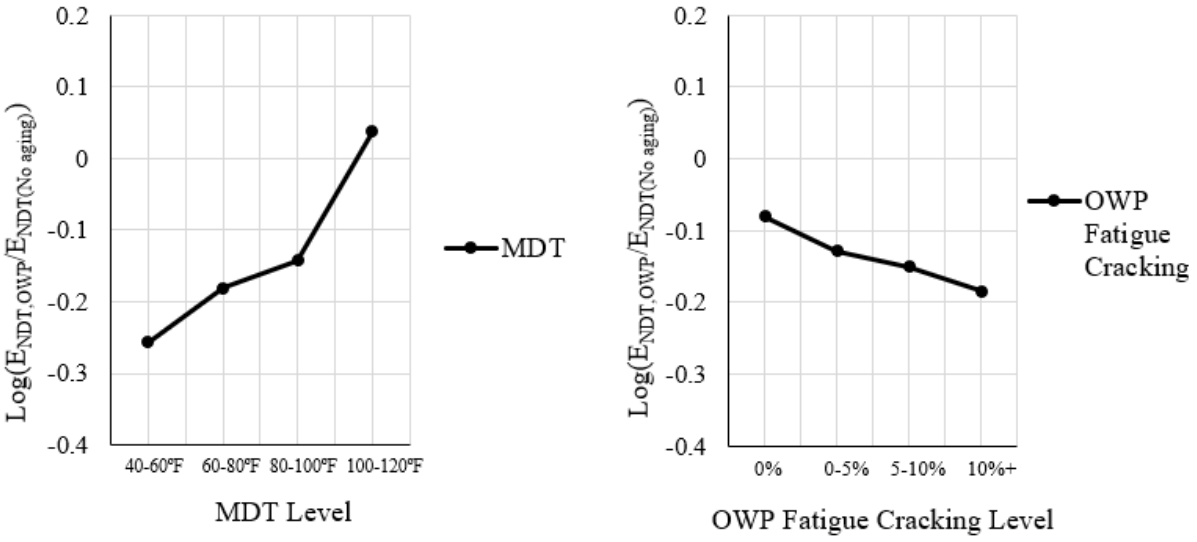

Figure 123. Main effects of the MDT and OWP fatigue cracking factors based on 56 LTPP sections ($Log(E_{NDT,OWP}/E_{NDT(No\ aging)})$).

Table 68. Results of Tukey's test for MDT and OWP fatigue cracking factors over the entire pavement life based on 56 LTPP sections ($Log(E_{NDT,OWP}/E_{NDT(No\ aging)})$).

MDT				OWP Fatigue Cracking			
Lower Factor Level	Upper Factor Level	Reject Null Hypothesis?	p-value	Lower Factor Level	Upper Factor Level	Reject Null Hypothesis?	p-value
40°F to 60°F[1]	**60°F to 80°F**	**Yes**	**0.00**	**0%**	**0% to 5%**	**Yes**	**0.00**
40°F to 60°F	**80°F to 100°F**	**Yes**	**0.00**	**0%**	**5% to 10%**	**Yes**	**0.00**
40°F to 60°F	**100°F to 120°F**	**Yes**	**0.00**	**0%**	**Greater than 10%**	**Yes**	**0.00**
60°F to 80°F	**80°F to 100°F**	**Yes**	**0.03**	0% to 5%	5% to 10%	No	0.48
60°F to 80°F	**100°F to 120°F**	**Yes**	**0.00**	**0% to 5%**	**Greater than 10%**	**Yes**	**0.03**
80°F to 100°F	**100°F to 120°F**	**Yes**	**0.00**	5% to 10%	Greater than 10%	No	0.46

[1] Significant comparisons are in bold.

Figure 124 shows the effect of the interaction between the MDT and OWP fatigue cracking on log($E_{NDT,OWP}/E_{NDT(No\ aging)}$). The same as log($E_{NDT,OWP}/E_{NDT(Aging)}$), the difference between log($E_{NDT,OWP}/E_{NDT(No\ aging)}$) at 0% fatigue cracking and log($E_{NDT,OWP}/E_{NDT(No\ aging)}$) at greater than 10% fatigue cracking is larger at lower levels of MDT (40ºF to 60ºF and 60ºF to 80ºF) than at higher levels of MDT (80ºF to 100ºF and 100ºF to 120ºF). This suggests that log($E_{NDT,OWP}/E_{NDT(No\ aging)}$) may provide more information about fatigue damage in the asphalt concrete when FWD testing is conducted at lower temperatures than at higher temperatures.

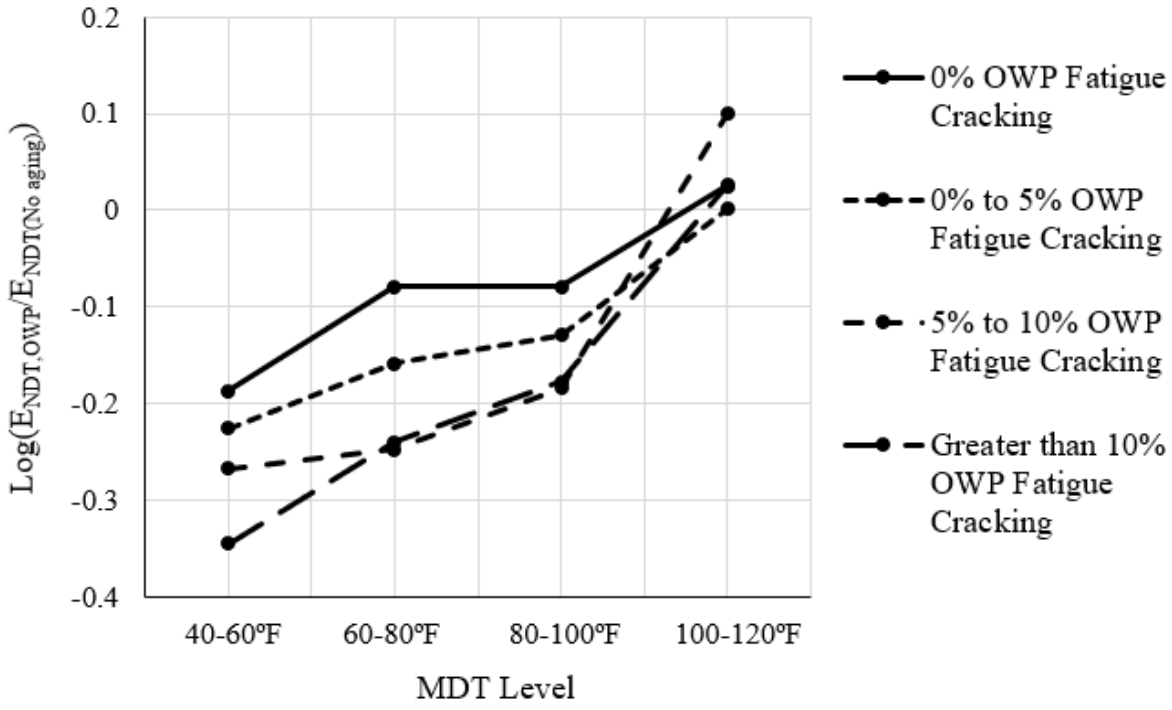

Figure 124. Interaction of the MDT and OWP fatigue cracking factors based on 56 LTPP sections (Log($E_{NDT,OWP}/E_{NDT(No\ aging)}$)).

5.4.2.5 Conclusions from multiple sections analysis

The relationship between FWD parameters and fatigue damage in the asphalt concrete of an existing pavement was examined using data from 56 LTPP sections. Two-way ANOVAs were performed with MDT and OWP fatigue cracking as factors and the FWD parameter as the response. The objective of the analysis was to answer several specific questions regarding the relationship between FWD parameters and fatigue damage. These questions and corresponding answers, based on the analysis performed, are listed below.

1. Question: Can FWD parameters be used to estimate the development of fatigue damage in the asphalt concrete layer of the existing pavement? Specifically:
    b. Question: Is there a significant correlation between any of the FWD parameters and OWP fatigue cracking when there is visible distress?

       Answer: Analysis of the composite data from many LTPP sections has shown that there is a significant relationship between most FWD parameters and OWP fatigue cracking once fatigue cracking has reached the surface of the pavement. Based on the analysis of data from 56 LTPP sections, only $E_{NDT,OWP}/E_{NDT,ML}$ is not significantly related to OWP fatigue cracking.

       Furthermore, Tukey's test has shown that FWD parameters are not significantly different for all levels of OWP fatigue cracking greater than 0%. As shown in Table 69, for all FWD parameters, the mean of the parameter is not significantly different between the 5% to 10% level and the greater than 10% level. Additionally, the mean of the FWD parameter is not significantly different between the 0% to 5% and the 5% to 10% levels for $\log(E_{NDT,OWP}/E_{Witczak(Aging)})$ or

$\log(E_{NDT,OWP}/E_{Witczak(No\ aging)})$. These findings suggest that FWD parameters may provide no more information than observed fatigue cracking once fatigue cracking reaches a specified threshold. It appears that this threshold is approximately 10% OWP fatigue cracking for $d_{0,OWP}/d_{0,ML}$ and approximately 5% OWP fatigue cracking for $E_{NDT,OWP}/E_{Witczak(Aging)}$ and $E_{NDT,OWP}/E_{Witczak(No\ aging)}$.

Table 69. Results of Tukey's test for the OWP fatigue cracking factor when there is visible distress using data from 56 LTPP sections

		Significant Difference between Levels?			
Lower Factor Level	Upper Factor Level	$d_{0,OWP}/d_{0,ML}$	$E_{NDT,OWP}/E_{NDT,ML}$	$\log(E_{NDT,OWP}/E_{Witczak(Aging)})$	$\log(E_{NDT,OWP}/E_{Witczak(No\ aging)})$
0% to 5%	5% to 10%	**Yes**	No	No	No
0% to 5%	Greater than 10%	**Yes**	No	**Yes**	**Yes**
5% to 10%	Greater than 10%	No	No	No	No

c. Question: Is there a significant correlation between any of the FWD parameters and OWP fatigue cracking over the whole life of a pavement section?

Answer: Analysis of combined data from 56 LTPP sections has shown that there is a significant relationship between most FWD parameters and OWP fatigue cracking over the entire life of the pavement section. All FWD parameters except $E_{NDT,OWP}/E_{NDT,ML}$ are significantly related to OWP fatigue cracking over all levels of OWP fatigue cracking. However, Tukey's test has shown that FWD parameters are not significantly different for all combinations of levels of OWP fatigue cracking. As previously discussed, there appears to be a threshold of fatigue

cracking above which FWD parameters no longer provide useful information about fatigue damage. On the other hand, all FWD parameters (except $E_{NDT,OWP}/E_{NDT,ML}$) are significantly different at the 0% OWP fatigue cracking level than at any higher level of OWP fatigue cracking. This is shown in Table 70. This suggests that FWD parameters can provide useful information about fatigue damage when there is little or no fatigue cracking. There is one exception to this trend. The mean of $d_{0,OWP}/d_{0,ML}$ does not change significantly between the 0% OWP fatigue cracking level and the 0% to 5% fatigue cracking level.

Table 70. Results of Tukey's test for the OWP fatigue cracking factor over the entire pavement life using data from 56 LTPP sections.

		Significant Difference between Levels?			
Lower Factor Level	Upper Factor Level	$d_{0,OWP}/d_{0,ML}$	$E_{NDT,OWP}/E_{NDT,ML}$	$\log(E_{NDT,OWP}/E_{Witczak(Aging)})$	$\log(E_{NDT,OWP}/E_{Witczak(No\ aging)})$
0%	0% to 5%	No	No	**Yes**[1]	**Yes**
0%	5% to 10%	**Yes**	No	**Yes**	**Yes**
0%	Greater than 10%	**Yes**	No	**Yes**	**Yes**
0% to 5%	5% to 10%	**Yes**	No	No	No
0% to 5%	Greater than 10%	**Yes**	No	**Yes**	**Yes**
5% to 10%	Greater than 10%	No	No	No	No

[1] Significant comparisons are in bold.

2. Question: Is the $E_{NDT,OWP}/E_{Witczak(Aging)}$ parameter, which is currently used in the Pavement ME AC/AC overlay design procedure, meaningfully related to fatigue damage and OWP fatigue cracking? Can $E_{NDT,OWP}/E_{Witczak(Aging)}$ or any of the other FWD parameters be used

to adjust the E_{NDT} input used in Pavement ME to more successfully quantify the amount of fatigue damage in the asphalt concrete of the existing pavement?

Answer: Analysis of combined data from 56 LTPP sections has shown that $E_{NDT,OWP}/E_{Witczak(Aging)}$ is significantly related to OWP fatigue cracking, and thus fatigue damage. This suggests that the use of $E_{NDT,OWP}/E_{Witczak(Aging)}$ to characterize fatigue damage in Pavement ME is not unreasonable.

It remains unclear, however, how $E_{NDT,OWP}/E_{Witczak(Aging)}$ or any other FWD parameter can be used to adjust the E_{NDT} input and more successfully quantify fatigue damage. Analysis of FWD parameters has demonstrated that all FWD parameters are significantly related to FWD load level and MDT at the time of FWD testing. These relationships must be accounted for if FWD parameters are to be used to quantify fatigue damage. The effect of load level on the FWD parameter can be mitigated by only performing FWD testing at a single load level. The effect of MDT on the FWD parameter is more difficult to isolate. A two-way ANOVA using combined data has shown that, for all FWD parameters, the effect of the MDT on the FWD parameter is at least as large as the effect of fatigue damage. The effects of MDT and fatigue damage can be isolated for a single pavement section using a two-way ANOVA, but this requires an impractically large amount of FWD data. Alternatively, it may be possible to remove the effect of MDT and isolate the effect of fatigue damage by adjusting the value of the FWD parameter based on the MDT at the time of FWD testing.

In addition to answering the questions above, the results of two-way ANOVA were used to evaluate the hypothesized relationships between FWD parameters and fatigue damage. The results supported three of the four hypothesized relationships, but were unable to verify the relationship between $E_{NDT,OWP}/E_{NDT,ML}$ and fatigue damage. This is shown in Table 71.

Table 71. Hypothesized and observed effect of fatigue damage on FWD parameters.

FWD Parameter	Hypothesized Effect of Fatigue Damage on Parameter	Observed Effect of Fatigue Damage on Parameter
$d_{0,OWP}/d_{0,ML}$	Increase	Increase
$E_{NDT,OWP}/E_{NDT,ML}$	Decrease	Unclear
$E_{NDT,OWP}/E_{Witczak(Aging)}$	Decrease	Decrease
$E_{NDT,OWP}/E_{Witczak(No\ aging)}$	Decrease	Decrease

5.5 CONCLUSIONS

LTPP data was analyzed to examine two of the underlying assumptions used in the Pavement ME AC/AC overlay design procedure. These are:

1. E_{NDT} and $E_{Witczak}$ are equal at an equal temperature and load frequency.
2. FWD data can be used to quantify fatigue damage in the asphalt concrete of an existing pavement.

Four FWD parameters were examined: $d_{0,OWP}/d_{0,ML}$, $E_{NDT,OWP}/E_{NDT,ML}$, $E_{NDT,OWP}/E_{Witczak(Aging)}$, and $E_{NDT,OWP}/E_{Witczak(No\ aging)}$. It was determined that all four parameters

are significantly affected by the FWD load magnitude. Additionally, three of the four FWD parameters are significantly affected by MDT at the time of FWD testing. For $d_{0,OWP}/d_{0,ML}$, the parameter decreases as MDT increases. For $E_{NDT,OWP}/E_{NDT,ML}$ and $E_{NDT,OWP}/E_{Witczak(Aging)}$, the parameter increases as MDT increases. The nature of the relationship between $E_{NDT,OWP}/E_{Witczak(No\ aging)}$ and MDT is unclear. It was concluded that, for all FWD parameters, the relationship between the FWD parameter and MDT must be accounted for when investigating fatigue damage.

Findings from the first portion of this chapter refute the assumption that E_{NDT} and $E_{Witczak}$ are equal at an equal temperature and load frequency. Specifically, it was determined that E_{NDT} is less than $E_{Witczak}$ at an equal temperature and assumed load frequency of 30 Hz. Furthermore, it was determined that the relationship between E_{NDT} and $E_{Witczak}$ depends on the temperature of the asphalt concrete at the time of FWD testing. $E_{Witczak}$ is much greater than E_{NDT} at low asphalt temperatures, but the $E_{Witczak}$ and E_{NDT} are almost identical at high temperatures. This is shown in Figure 82.

The relationship between FWD parameters and fatigue damage was investigated using a two-way ANOVA, which simultaneously accounts for the effects of MDT and fatigue damage. The relationship was examined within individual LTPP sections and using combined data from 56 LTPP sections. Several conclusions were made based on the results of this analysis:

- FWD parameters can be used to detect fatigue damage caused by fatigue cracking that has not yet reached the surface of the pavement. This method of detecting fatigue damage is impractical, however, because a very large amount of FWD data is required.
- FWD parameters can provide information about the amount of fatigue damage in the asphalt concrete after fatigue cracking has reached the surface of the pavement. However,

there appears to be a threshold above which FWD parameters are no longer significantly correlated with fatigue cracking and provide no useful information about fatigue damage in the asphalt concrete.

- Most FWD parameters can provide information about fatigue damage in the asphalt concrete over the entire life of the pavement, except when fatigue cracking is greater than the threshold,
- There is a significant correlation between $E_{NDT,OWP}/E_{Witczak(Aging)}$, which is used to quantify fatigue damage in the Pavement ME AC/AC overlay design procedure, and fatigue damage in the asphalt concrete.

Overall, the results of the analysis support the assumption used in Pavement ME, that FWD data can be used to quantify fatigue damage in the asphalt concrete of an existing pavement. The findings detailed in this chapter were used to inform the development of adjustment factors for the E_{NDT} input used in the Pavement ME AC/AC overlay design procedure. This is explained in Chapter 6.

6.0 DEVELOPMENT OF ADJUSTMENT FACTORS FOR USE IN THE PAVEMENT ME AC/AC OVERLAY DESIGN PROCEDURE

The primary directive of this research is to develop appropriate inputs for the Pavement ME design procedures. An evaluation of the AC/AC overlay design procedure revealed that it does not accurately predict either fatigue cracking or total rutting in most cases. When Level 1 inputs are used the AC/AC design procedure tends to over predict both fatigue cracking and total rutting. This is the result of how the amount of fatigue damage in the asphalt concrete of the existing pavement is estimated using the relationship between backcalculated stiffness (E_{NDT}) and predicted stiffness ($E_{Witczak}$). When Level 2 inputs are used, the AC/AC overlay design procedure tends to under predict fatigue cracking. The predicted fatigue cracking in the overlay is never greater than the amount of fatigue cracking observed in the existing pavement just prior to the placement of the overlay. Based on these observations, it appears that the Pavement ME AC/AC overlay design procedure could be modified to improve the predicted distress. The simplest approach is to modify the design inputs.

It was determined that the best way to improve distress predictions without altering the Pavement ME software is to develop adjustment factors for the Level 1 backcalculated asphalt concrete stiffness (E_{NDT}) input. There are three reasons this approach was selected. First, E_{NDT} adjustment factors have been suggested by other researchers (Ayyala et al. 2016; Gedafa et al. 2010; Von Quintus and Killingsworth 1998). These factors were evaluated in Chapter 3. This

evaluation demonstrated that most of the previously suggested adjustment factors do not increase the accuracy of distress predictions. However, the evaluation also demonstrated that manipulating the E_{NDT} input can be used to change the amount of fatigue cracking and rutting predicted by the Pavement ME AC/AC overlay design procedure.

Second, the analysis conducted in Chapters 4 and 5 has shown that there is a significant, inherent difference between E_{NDT} and $E_{Witczak}$. Note that Pavement ME uses $E_{Witczak}$, and a binder aging model to establish the asphalt concrete stiffness. The difference between E_{NDT} and $E_{Witczak(Aging)}$ causes the AC/AC design procedure, which uses the relationship between E_{NDT} and $E_{Witczak(Aging)}$ to estimate fatigue damage in the asphalt concrete of the existing pavement, to greatly over-estimate fatigue cracking in the overlay. E_{NDT} adjustment factors can directly account for the difference between E_{NDT} and $E_{Witczak(Aging)}$, mitigating the problem of over-estimated distress in the overlay.

Finally, the E_{NDT} input, rather than any other single Pavement ME input or combination of inputs, was selected to address problems with predicted distress because it has been shown (in Chapter 5) that the relationship between E_{NDT} and $E_{Witczak(Aging)}$ can provide information regarding fatigue damage in the asphalt concrete. This is the underlying assumption of the Pavement ME AC/AC overlay design procedure when Level 1 inputs are used. If this assumption was not supported, it would have been necessary to develop an entirely different method for determining fatigue damage in the asphalt concrete of the existing pavement.

6.1 ADJUSTMENT FACTORS FOR THE BACKCALCULATED ASPHALT STIFFNESS

Two major questions have to be answered before adjustment factors for the E_{NDT} input can be developed:

1. What parameters should be included in the development of the E_{NDT} adjustment factors?
2. What method should be used to develop the E_{NDT} adjustment factors?

The parameters to be considered in the development of E_{NDT} adjustment factors were identified based on the analysis conducted in previous appendices. Chapters 4 and 5 demonstrated that there is an inherent difference between E_{NDT} and $E_{Witczak(Aging)}$, so both of these parameters were considered. Furthermore, it was shown that relationship between E_{NDT} and $E_{Witczak(Aging)}$ is a function of the MDT at the time of FWD testing, so MDT must be considered in the development of E_{NDT} adjustment factors. Finally, it was demonstrated that the relationship between $E_{NDT,OWP}/E_{Witczak(Aging)}$ is a function of the amount of fatigue cracking in the pavement. The same analysis also showed that $E_{NDT,OWP}/E_{Witczak(Aging)}$ is influenced by the interaction between fatigue cracking and MDT. Thus, fatigue cracking in the existing pavement and the interaction of fatigue cracking and MDT likely both influence the adjustment factors. The parameters and interactions that must be considered when developing E_{NDT} adjustment factors are:

- $E_{NDT,OWP}$ – The backcalculated stiffness of the asphalt concrete in the existing pavement, averaged over one FWD pass. The Pavement ME AC/AC overlay design procedure is sensitive to this Level 1 input.

- $E_{Witczak(Aging)}$ – The stiffness of the asphalt concrete in the existing pavement, estimated using the Witczak equation and the binder aging model. This is calculated internally within Pavement ME for the AC/AC overlay design procedure.
- MDT – The mid-depth temperature of the asphalt concrete in the existing pavement, averaged over one FWD pass. The Pavement ME AC/AC overlay design procedure is sensitive to this Level 1 input.
- Fatigue cracking in the existing pavement. This is not a Level 1 input in the Pavement ME AC/AC overlay design procedure.
- The effect of the interaction between fatigue cracking in the existing pavement and MDT at the time of FWD testing.

The method selected to develop an E_{NDT} adjustment factor has three steps:

1. Use the Pavement ME AC/AC overlay design procedure to model LTPP sections with overlays. Use LTPP data, including asphalt mix parameters, backcalculated layer stiffness, and traffic, to determine program inputs and predict the performance of the overlaid pavement section.
2. For each section, determine the "best fit" E_{NDT} input ($E_{NDT(Best\ fit)}$) for which fatigue cracking predicted by the AC/AC overlay design procedure matches the actual fatigue cracking observed in the overlaid pavement section.
3. Develop E_{NDT} adjustment factors based on the relationship between $E_{NDT(Best\ fit)}$, the measured backcalculated asphalt concrete stiffness ($E_{NDT(Measured)}$), MDT, and observed fatigue cracking in the existing pavement before overlay.

This "best fit" method for developing E_{NDT} adjustment factors was selected because knowing $E_{NDT(Best\ fit)}$ means that it is possible to examine and adjust each step in the damage prediction process used in the AC/AC design procedure. Specifically, if $E_{NDT(Best\ fit)}$ is known, it is possible to quantify the value of the damage parameter (determined using Equation 8) for each section. The main disadvantage of the "best fit" method is that there is minimal data available to establish $E_{NDT(Best\ fit)}$ since there are not many overlaid pavement sections in the LTPP database with FWD testing performed just before the overlay along with a significant amount of fatigue cracking in the overlaid pavement structure.

6.1.1 Sections used to develop the E_{NDT} adjustment factor

The same LTPP sections used to evaluate the Pavement ME AC/AC overlay design procedure in Chapter 3 were used to develop the E_{NDT} adjustment factors. Details of the LTPP sections used to develop the E_{NDT} adjustment factors are shown in Table 72. All of the sections in Table 72 are in wet-freeze climatic zones and have binder grades similar to those currently and/or historically used in Pennsylvania. All $E_{NDT(Measured)}$ values used in this analysis are based on deflections measured for a 9-kip load.

Table 72. LTPP sections used to develop the E_{NDT} adjustment factor.

State	LTPP ID	AC Thickness (Pre-milling) (in)	AC Thickness (Post-milling) (in)	Overlay Thickness (in)	Binder Grade	E_{NDT} (measured) (ksi)	MDT (ºF)	Fatigue Cracking in Existing Pavement (% total lane area)	Severity of Fatigue Cracking in Existing Pavement
CT	9-1803	7	7	1.75	PG 64-28 / AC-20	1096	70	5.0	Low
DE	10-0102	4.25	4.25	1.25	AC-20 / AC-20	433	73	1.5	Low
IL	17-A310	11.25	11.25	0.5	AC-20 / AC-20	821	61	0.0	N/A
IA	19-1044	16.25	16.25	3.75	PG 58-28 / Pen 85-100	424	42	6.4	Medium
KS	20-0159	11.25	6	5.25	PG 64-22 / AC-10	211	90	20.4	Low
KS	20-1005	13	12	0.75	PG 64 -22 / AC-5	545	51	29.0	Medium
KS	20-1009	11	4.5	7.5	AC-20 / AC-20	1138	59	0.9	Medium
ME	23-1009	5.75	5.75	2.75	AC-20 / Pen 85-100	911	71	28.1	Low
MD	24-1634	3.5	3.5	3.25	PG 70-22 / Pen 85-100	523	64	38.7	Low
NJ	34-0503	9.25	9.25	4.75	Pen 85-100 / Pen 85-100	1309	51	0.0	N/A
NJ	34-0504	8.75	8.75	4.75	Pen 85-100 / Pen 85-100	1116	63	5.1	Low
NJ	34-0505	9	9	1.75	Pen 85-100 /Pen 85-100	1575	50	11.8	Low
NJ	34-0506	9.5	7.5	4	Pen 85-100 / Pen 85-100	599	68	0.0	N/A
NJ	34-0507	8.25	6.25	7.5	Pen 85-100 / Pen 85-100	819	55	0.3	Medium
NJ	34-0508	8.75	6.75	7.5	Pen 85-100 / Pen 85-100	1298	58	0.0	N/A
NJ	34-0509	9.25	7.25	4.25	Pen 85-100 / Pen 85-100	960	65	0.0	N/A
NJ	34-0903	9	7.5	5.5	PG 64-22 / Pen 85-100	1068	53	41.7	Medium
NJ	34-0960	9.75	7.25	4.75	PG 64-22 / Pen 85-100	1242	54	56.2	Low
NJ	34-0961	9.25	5.5	6.5	PG 64-22 / Pen 85-100	1148	44	33.2	Low
NJ	34-0962	9	7.5	4.25	PG 64-22 / Pen 85-100	682	57	20.0	Low
NJ	34-1003	7.5	5.5	2.25	AC-20 / AC-20	274	91	18.7	Unknown
NJ	34-1011	9	6.5	4	AC-20 / Pen 85-100	331	89	7.5	Low
NJ	34-1030	6	3	4.5	AC-20 / AC-20	313	93	16.2	Unknown
NJ	34-1033	7.5	6.75	2	AC-20 / AC-20	1493	75	0.0	N/A
PA	42-1597	6.5	5	6.25	PG 64-22 / AC 20	571	56	0.7	High
MB	83-0502	4.5	4.5	2.75	Pen 150-200 / Pen 150-200	450	98	0.0	N/A
MB	83-0503	4.75	4.75	5.25	Pen 150-200 / Pen 150-200	430	81	7.1	Low

Table 72 (continued).

State	LTPP ID	AC Thickness (Pre-milling) (in)	AC Thickness (Post-milling) (in)	Overlay Thickness (in)	Binder Grade	E_{NDT} (measured) (ksi)	MDT (ºF)	Fatigue Cracking in Existing Pavement (% total lane area)	Severity of Fatigue Cracking in Existing Pavement
MB	83-0506	5.5	4	3	Pen 150-200 / Pen 150-200	431	73	0.0	N/A
MB	83-0507	4	3	6.75	Pen 150-200 / Pen 150-200	591	81	1.6	Medium
MB	83-0508	3.5	2.5	6.5	Pen 150-200 / Pen 150-200	750	106	0.0	N/A
MB	83-0509	5	4	3.5	Pen 150-200 / Pen 150-200	367	74	1.9	Low
MB	83-6451	4	4	2.5	Pen 150-200 / Pen 150-200	593	97	0.0	N/A
ON	87-1622	5.5	3	4.5	PG 58-28 / Pen 85-100	1112	49	5.4	Medium
QB	89-1125	5.25	5.25	2	PG 58-28 / Pen 85-100	875	53	40.1	Low
QB	89-1127	5	5	2.5	Pen 85-100 / Pen 150-200	709	65	0.6	Low

6.1.2 Determination of "best fit" E_{NDT} inputs

For each section in Table 72, $E_{NDT(Best\ fit)}$ was established by adjusting the E_{NDT} input such that the predicted fatigue cracking in the overlay is equal to the observed fatigue cracking in the overlay. Several steps are required to determine the appropriate value of $E_{NDT(Best\ fit)}$ for each section. First, the AC/AC overlay design is performed using all of the measured inputs, including $E_{NDT(Measured)}$, MDT, a FWD load frequency of 30 Hz, measured thicknesses of all pavement layers, backcalculated stiffness of all unbound layers, the measured mixture parameters for all asphalt concrete layers, and the measured traffic. This is exactly the same analysis performed to evaluate the AC/AC overlay design procedure using Level 1 inputs in Chapter 3. The predicted fatigue cracking over time determined from this first Pavement ME run was compared to the observed fatigue cracking over time. An example of this is shown in Figure 125 for LTPP Section 23-1009 in Maine.

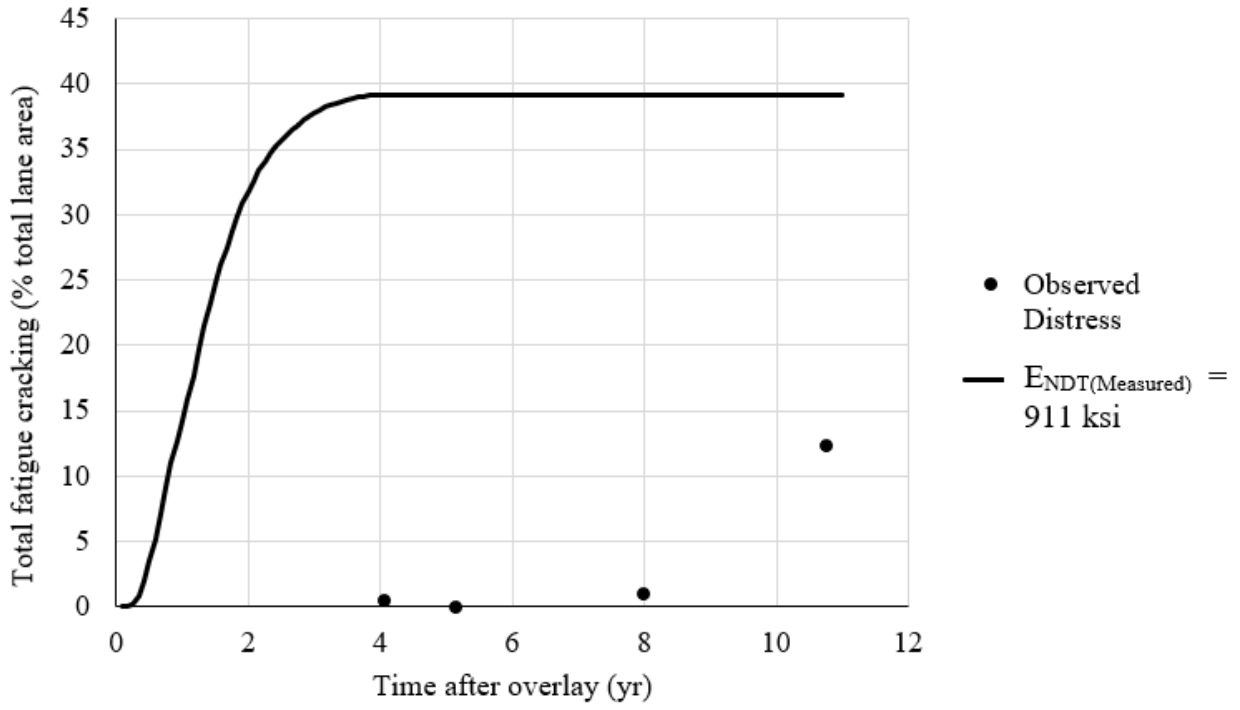

Figure 125. Predicted and observed fatigue cracking using measured E_{NDT} input (LTPP Section 23-1009, Maine).

For most sections, the performance history has a sigmoidal shape, as shown in Figure 125, where predicted fatigue cracking asymptotically approaches a maximum value as time increases. For some sections, however, predicted fatigue cracking does not reach an asymptotic maximum value by the end of the analysis period. An example of this is shown in Figure 126 for LTPP Section 34-0508 in New Jersey. Here, it appears that the predicted performance history is also sigmoidal, but that the asymptotic upper portion of the curve is cut off. The sigmoidal shape of the predicted fatigue cracking performance history and the discrepancy between Figures 125 and 126 are both consequences of the models used to predict fatigue cracking in the AC/AC overlay design procedure.

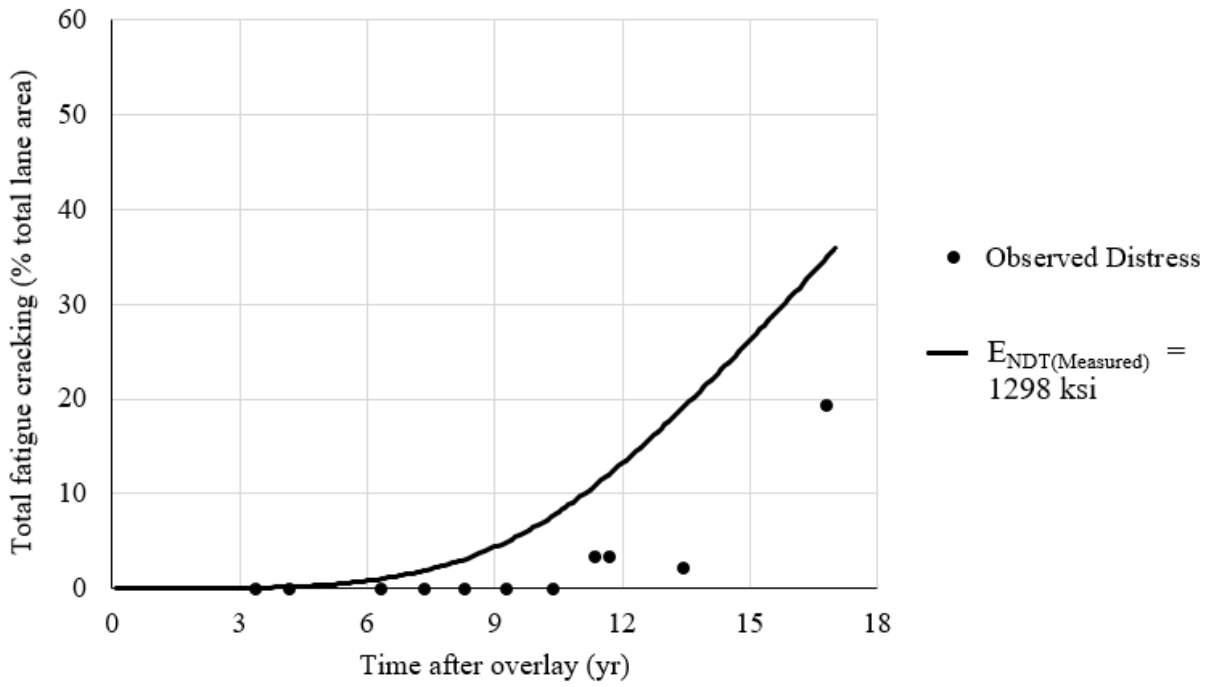

Figure 126. Predicted and observed fatigue cracking using measured E_{NDT} input (LTPP Section 34-0508, New Jersey).

Prediction of fatigue cracking in the overlaid pavement structure is fully explained in Chapter 3. The three steps that determine the performance histories shown in Figures 125 and 126 are:

1. The fatigue damage equation, shown in Equation 19, is used to calculate a damage parameter (d_{AC}) that represents the amount of fatigue damage in the asphalt concrete layer of the existing pavement.

$$\log(d_{AC}) = 0.2 \times \left[\ln\left(\frac{E_{Witczak} - E_{NDT}}{E_{NDT} - 10^{\delta}}\right) + 0.3\right] \quad (19)$$

Where:

d_{AC} = Damage parameter

$E_{Witczak}$ = Existing asphalt stiffness predicted using the Witczak equation (psi)

E_{NDT} = Backcalculated stiffness of the existing asphalt (psi)

δ = Base 10 logarithm of the minimum stiffness of the existing asphalt (estimated using the Witczak equation, in psi)

Note: d_{AC} is defined as zero when E_{NDT} is greater than or equal to $E_{Witczak}$

2. The bottom-up fatigue cracking transfer function, shown in Equation 20, is used to convert d_{AC} into an equivalent amount of fatigue cracking in the existing pavement. Note that this equivalent fatigue cracking is not related to the actual amount of fatigue cracking observed in the existing pavement, but rather represents the amount of fatigue damage in the asphalt concrete.

$$FC_{Bottom} = \left[\frac{1}{60}\right]\left[\frac{C_4}{1 + e^{(C_1 C_1^* + C_2 C_2^* \times \log(d_{AC} \times 100))}}\right]$$
$$C_1^* = -2 \times C_2^* \quad (20)$$
$$C_2^* = -2.40874 - 39.748(1 + h_{AC})^{-2.856}$$

Where:

FC_{Bottom} = Area of fatigue cracking that initiates from the bottom of the asphalt concrete layers (% total lane area)

d_{AC} = Damage parameter (from Equation 19)

$C_1 = C_2 = 1$

$C_4 = 6000$

h_{AC} = Thickness of asphalt concrete layers (in)

3. The equivalent fatigue cracking in the existing pavement is used as an input for the reflective cracking model. The reflective cracking model uses information such as traffic and the relative stiffness of each layer in the pavement structure to determine the rate at which the equivalent fatigue cracking propagates to the surface of the overlaid pavement structure. With enough simulated traffic loads, the full amount of equivalent fatigue cracking will eventually be propagated to the surface of the overlaid pavement structure, regardless of the thickness of the overlay or the relative stiffness of the pavement layers.

With respect to the predicted performance history, as shown in Figures 125 and 126, the damage equation (Equation 19) and bottom-up fatigue cracking transfer function (Equation 20) dictate the maximum value for which the predicted fatigue cracking becomes asymptotic. The reflective cracking model creates the sigmoidal shape of the predicted performance history and determines how long it takes the predicted fatigue cracking to reach its maximum value.

As discussed in Chapter 3, the implementation of the reflective cracking model in the Pavement ME AC/AC overlay design procedure is not well documented. Based on the limited number of sections included in this analysis, it was not possible to determine exactly how the reflective cracking model affects the rate at which predicted fatigue cracking develops for a given section. Thus, the reflective cracking model was bypassed for the purpose of determining $E_{NDT(Best\ fit)}$. Note that this means the adjustment factors developed using $E_{NDT(Best\ fit)}$ do not account for the rate at which predicted fatigue cracking develops and there is no guarantee that using these adjustment factors will provide an improved estimate of how fatigue cracking develops over time in an overlaid pavement. Rather, the adjustment factors are designed to provide a more accurate estimate of fatigue damage in the asphalt concrete of the existing pavement and of the amount of fatigue cracking that will ultimately occur in the overlay. Considering that the reflective cracking

model was bypassed, $E_{NDT(Best\ fit)}$ was determined differently for LTPP sections in which fatigue cracking had fully propagated through the overlay than for sections in which it had not fully propagated.

For sections in which the equivalent fatigue cracking fully propagated through the overlay, as shown in Figure 125, $E_{NDT(Best\ fit)}$ was determined by adjusting the E_{NDT} input until the maximum value for which the fatigue cracking becomes asymptotic matched the observed maximum value of fatigue cracking at the end of the analysis period. This is shown in Figure 127. $E_{NDT(Best\ fit)}$ determined in this manner thus represents the actual amount of fatigue damage in the asphalt concrete of the existing pavement and the amount of fatigue cracking that will eventually propagate to the surface of the overlay. Using $E_{NDT(Best\ fit)}$ and $E_{Witczak}$ as inputs for the fatigue damage equation, shown in Equation 19, one can estimate the actual value of d_{AC} for the existing pavement before overlay. Additionally, using this d_{AC} value as the input for the bottom-up fatigue cracking transfer function, shown in Equation 20, will yield the maximum value at which the fatigue cracking becomes asymptotic. This is the same maximum value that was used to match predicted and observed fatigue cracking, as shown in Figure 127.

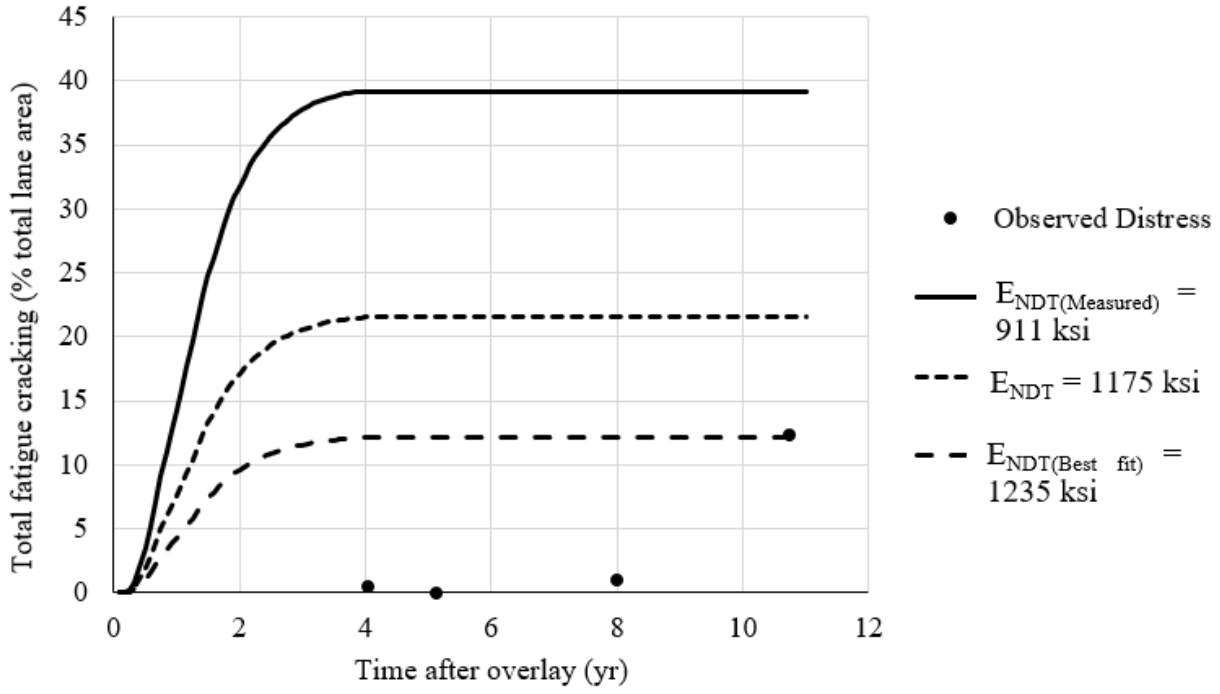

Figure 127. Determination of $E_{NDT(Best\ fit)}$ by modifying the E_{NDT} input to match the maximum predicted fatigue cracking to the maximum observed fatigue cracking (LTPP Section 23-1009, Maine).

For sections in which the equivalent fatigue cracking did not fully propagate through the overlay, as shown in Figure 126, the amount of traffic used in the AC/AC overlay design analysis was increased until the maximum value for which the predicted fatigue cracking is asymptotic became apparent. This is shown in Figure 128. Traffic was increased to reveal the maximum fatigue cracking, but not so much that the fatigue damage model would create additional predicted fatigue cracking. As discussed in Chapter 3, the fatigue damage model does not have a large effect on total fatigue cracking predicted by the AC/AC overlay design procedure unless the traffic is extremely high or the stiffness of the asphalt concrete is extremely low. Once traffic was increased, $E_{NDT(Best\ fit)}$ was determined by changing the E_{NDT} input until the maximum value for which the fatigue cracking becomes asymptotic matched the observed maximum value of fatigue cracking at

the end of the analysis period. This is shown in Figure 129. $E_{NDT(Best\ fit)}$ determined in this manner also represents the actual amount of fatigue damage in the asphalt concrete of the existing pavement and the amount of fatigue cracking that will eventually propagate to the surface of the overlay.

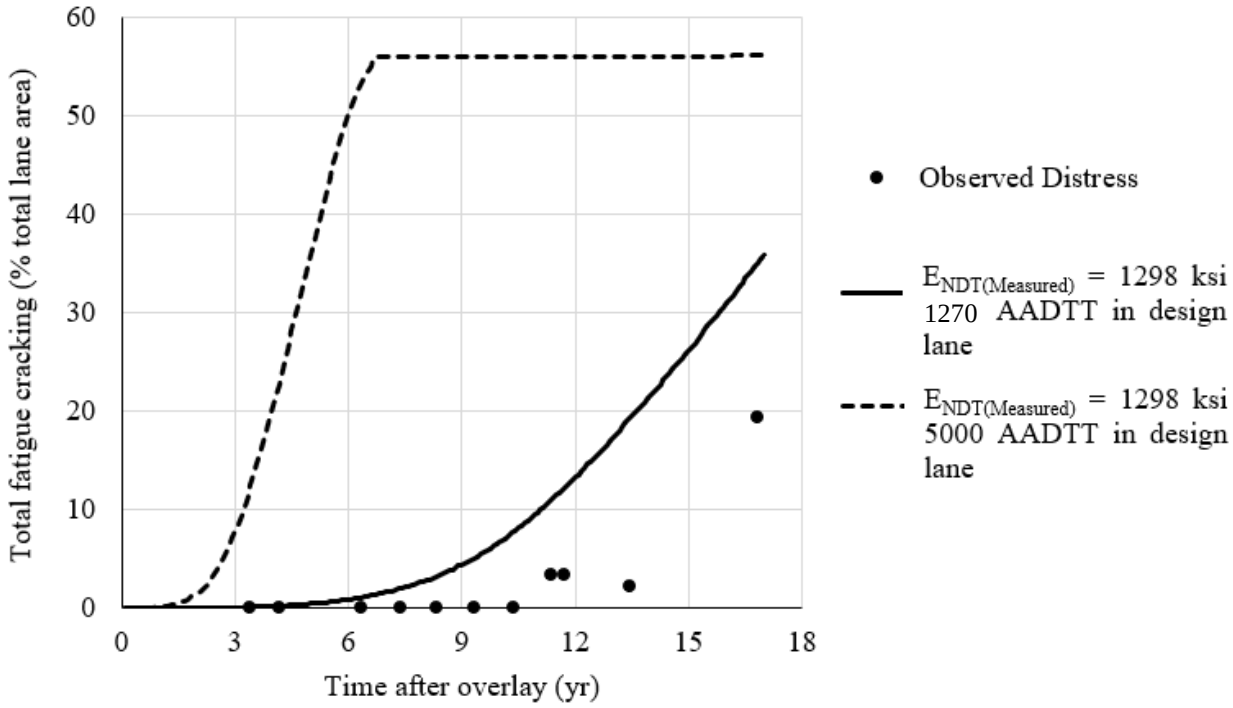

Figure 128. Determining maximum value for which the predicted fatigue cracking becomes asymptotic by increasing traffic input (LTPP Section 34-0508, New Jersey).

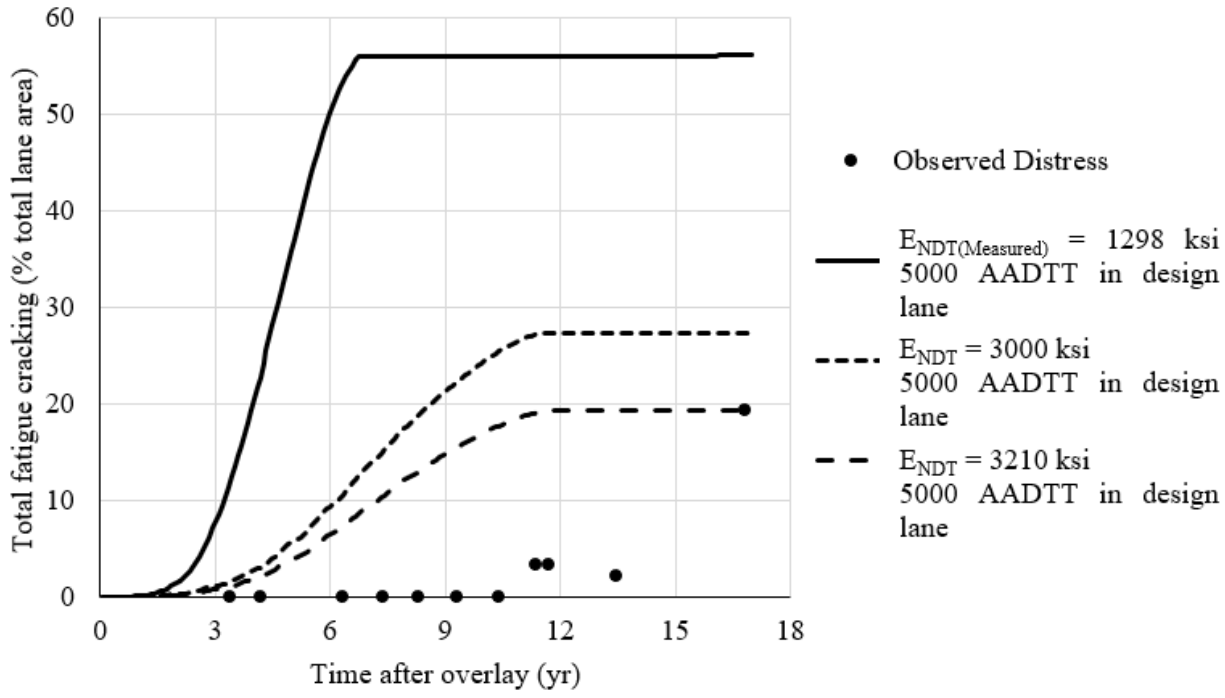

Figure 129. Determination of $E_{NDT(Best\ fit)}$ by modifying E_{NDT} input to match maximum predicted fatigue cracking to maximum observed fatigue cracking (LTPP Section 34-0508, New Jersey).

$E_{NDT(Best\ fit)}$ was determined for all 35 LTPP sections listed in Table 72. The performance history plots used to determine $E_{NDT(Best\ fit)}$ for all sections are shown in Appendix D. $E_{NDT(Best\ fit)}$, $E_{Witczak}$, predicted fatigue cracking in the overlay, observed fatigue cracking in the overlay, as well as other relevant details for each LTPP section are shown in Table 73.

Table 73. $E_{NDT(Best\ fit)}$, $E_{NDT(Measured)}$, $E_{Witczak(Aging)}$, and other data used to develop the E_{NDT} adjustment factor.

State	LTPP ID	E_{NDT} (Best fit) (ksi)	E_{NDT} (Measured) (ksi)	$E_{Witczak}$ (Aging) (ksi)	Predicted Fatigue Cracking in Overlay (Best fit) (% total lane area)	Observed Fatigue Cracking in Overlay (% total lane area)	MDT (°F)	Fatigue Cracking in Existing Pavement (% total lane area)	Fatigue Cracking Severity
CT	9-1803	1660	1096	1790	22.2	21.5	70	5.0	Low
DE	10-0102	995	433	1140	37.5	37.7	73	1.5	Low
IL	17-A310	2100	821	2235	19.5	19.2	61	0.0	N/A
IA	19-1044[1]	3650	424	4120	28.4	28.4	42	6.4	Medium
KS	20-0159	795	211	830	17.6	16.5	90	20.4	Low
KS	20-1005	2040	545	2650	36.5	36.6	51	29.0	Medium
KS	20-1009	2520	1138	2710	23.6	23.7	59	0.9	Medium
ME	23-1009	1250	911	1275	12.6	12.3	71	28.1	Low
MD	24-1634	800	523	2515	57.4	57.6	64	38.7	Low
NJ	34-0503	3295	1309	4085	34.5	34.7	51	0.0	N/A
NJ	34-0504	1940	1116	1955	4.2	5.1	63	5.1	Low
NJ	34-0505	3855	1575	3880	8.3	8.3	50	11.8	Low
NJ	34-0506	1595	599	1600	5.9	3.3	68	0.0	N/A
NJ	34-0507	3760	819	3855	13.8	13.7	55	0.3	Medium
NJ	34-0508	3210	1298	3380	19.4	19.4	58	0.0	N/A
NJ	34-0509	1810	960	2185	33.7	33.4	65	0.0	N/A
NJ	34-0903	4095	1068	4195	14.8	14.5	53	41.7	Medium
NJ	34-0960	3940	1562	4000	12.4	12.5	54	56.2	Low
NJ	34-0961	2200	1540	4145	49.3	49.2	44	33.2	Low
NJ	34-0962	3335	1069	3465	17.9	17.9	57	20.0	Low
NJ	34-1003	265	274	655	55.4	55.5	91	18.7	Unknown
NJ	34-1011[1]	100	331	730	85.3	84.9	89	7.5	Low
NJ	34-1030	525	313	780	41.9	41.9	93	16.2	Unknown
NJ	34-1033[1]	605	1473	1185	50.5	50.4	75	0.0	N/A
PA	42-1597	1450	571	2955	52.0	52.0	56	0.7	High
MB	83-0502	235	450	310	39.9	39.7	98	0.0	N/A
MB	83-0503	555	430	610	24.0	23.7	81	7.1	Low
MB	83-0506	870	431	925	24.4	24.0	73	0.0	N/A
MB	83-0507	690	591	700	22.0	22.1	81	1.6	Medium
MB	83-0508[1]	240	750	260	25.0	25.7	106	0.0	N/A
MB	83-0509	735	367	885	34.2	34.1	74	1.9	Low
MB	83-6451	320	593	350	22.0	18.1	97	0.0	N/A
ON	87-1622	1670	1112	3920	55.4	55.4	49	5.4	Medium
QB	89-1125	3505	875	3710	21.1	21.1	53	40.1	Low
QB	89-1127	2510	709	2945	33.6	33.6	65	0.6	Low

[1] These sections are outliers and were not used to develop the E_{NDT} adjustment factors.

The data shown in Table 73 lead to several conclusions about the relationship between $E_{NDT(Measured)}$, $E_{NDT(Best\ fit)}$, and $E_{Witczak(Aging)}$. First, the magnitude of $E_{NDT(Best\ fit)}$ is more similiar to $E_{Witczak(Aging)}$ than $E_{NDT(Measured)}$ is to $E_{Witczak(Aging)}$. This is shown in Figure 130.

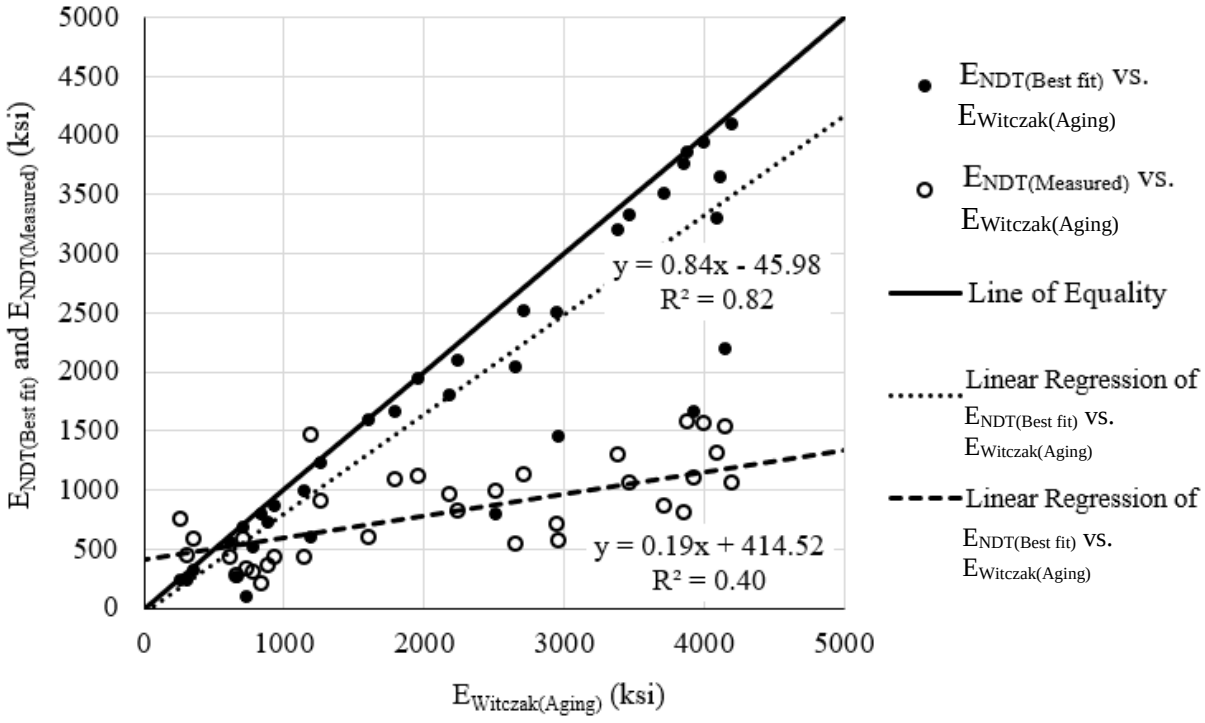

Figure 130. $E_{NDT(Best\ fit)}$ and $E_{NDT(Measured)}$ vs. $E_{Witczak(Aging)}$. E_{NDT} adjustment factor sections (9-kip load).

Also shown in Figure 130, the difference between $E_{NDT(Best\ fit)}$ and $E_{NDT(Measured)}$ increases as $E_{Witczak(Aging)}$ increases. This is caused primarily by the fact that relationship between $E_{NDT(Measured)}$ and $E_{Witczak(Aging)}$ depends on the MDT of the asphalt concrete at the time FWD testing is performed. This relationship was examined in detail in Chapter 5. As shown in Figure 131, the ratio $E_{NDT(Measured)}/E_{Witczak(Aging)}$ increases as MDT increases. Note that the log transformation of $E_{NDT(Measured)}/E_{Witczak(Aging)}$ is used because it was determined in Chapter 5 that the parameter $E_{NDT}/E_{Witczak(Aging)}$ is log-normally distributed. $E_{NDT(Measured)}/E_{Witczak(Aging)}$ is approximately 1.00

($Log(E_{NDT(Measured)}/E_{Witczak(Aging)}) = 0.00$) at 100ºF, which corresponds to a $E_{Witczak(Aging)}$ that is less than 1000 ksi, as shown in Figure 130. In contrast, $E_{NDT(Measured)}/E_{Witczak(Aging)}$ is approximately 0.30 ($Log(E_{NDT(Measured)}/ E_{Witczak(Aging)}) \approx -0.50$) at 50ºF, which corresponds to $E_{Witczak(Aging)}$ of approximately 4000 ksi, as shown in Figure 130. The relationship between $log(E_{NDT(Measured)}/E_{Witczak(Aging)})$ and MDT shown in Figure 131 similar to that seen in Figure 99 in Chapter 5.

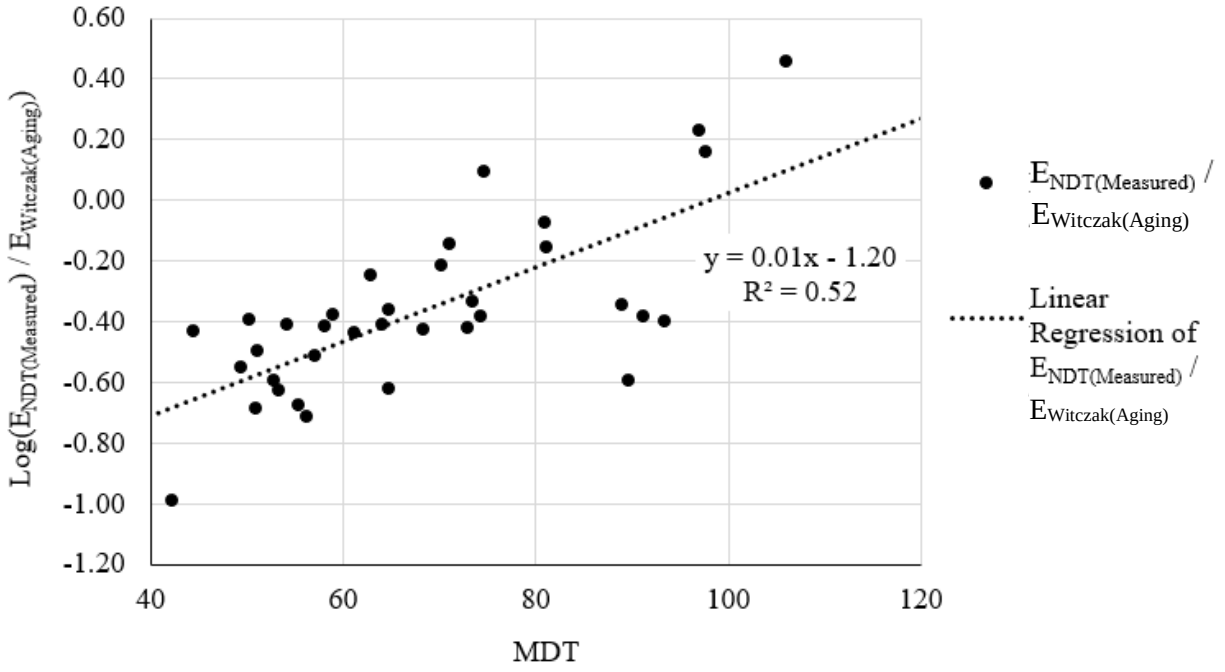

Figure 131. $Log(E_{NDT(Measured)}/E_{Witczak(Aging)})$ vs. MDT. E_{NDT} adjustment factor sections (9-kip load).

Unlike the relationship between $E_{NDT(Measured)}/E_{Witczak(Aging)}$ and MDT, there is no apparent relationship between $E_{NDT(Best\ fit)}/E_{Witczak(Aging)}$ and MDT. This is shown in Figure 132. The process in establishing $E_{NDT(Best\ fit)}$ removes the temperature-dependent relationship between $E_{NDT(Measured)}$ and $E_{Witczak(Aging)}$.

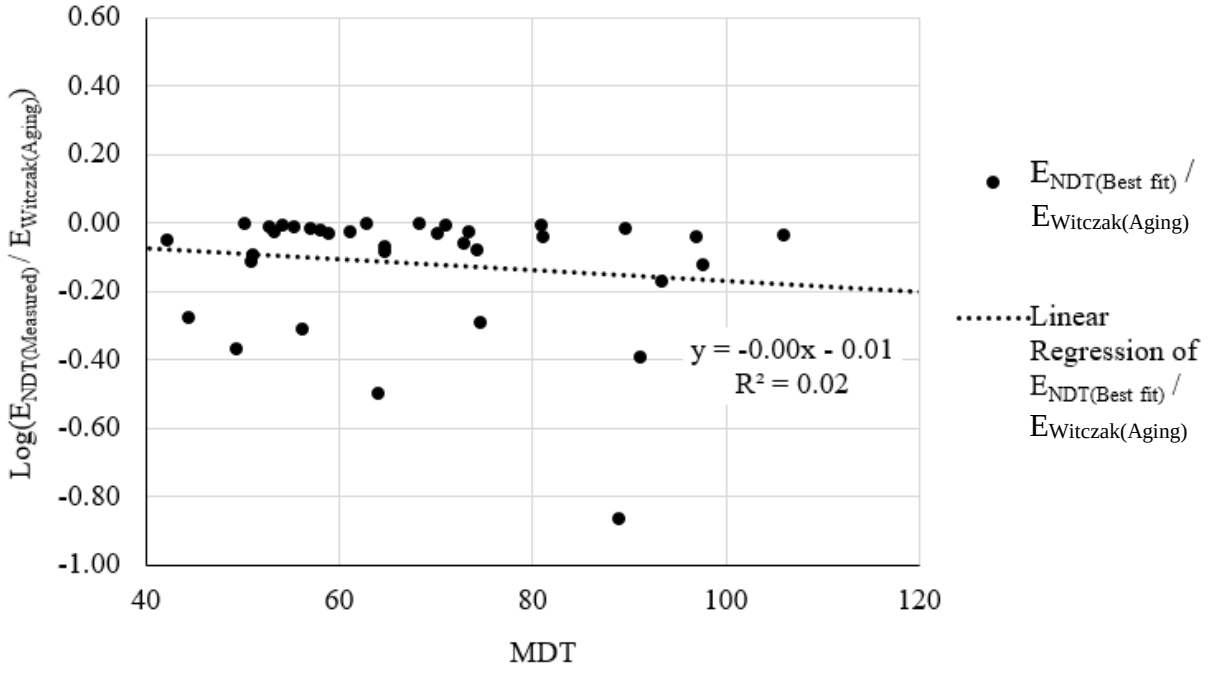

Figure 132. Log($E_{NDT(Best\ fit)}/E_{Witczak(Aging)}$) vs. MDT. E_{NDT} adjustment factor sections (9-kip load).

Unlike the relationship between $E_{NDT(Measured)}/E_{Witczak(Aging)}$ and MDT, there does not appear to be a strong relationship between $E_{NDT(Measured)}/E_{Witczak(Aging)}$ and fatigue cracking in the existing pavement. This is shown in Figure 133. Nevertheless, the relationship between log($E_{NDT(Measured)}/E_{Witczak(Aging)}$) and fatigue cracking shown in Figure 133 is similar to that shown in Figure 119 in Chapter 5. An analysis of the data in Figure 119 demonstrates that log($E_{NDT(Measured)}/E_{Witczak(Aging)}$) decreases as fatigue cracking in the existing pavement increases. Note that Figure 133 shows total fatigue cracking, while Figure 119 shows fatigue cracking in the outer wheelpath only. Finally, there is no apparent relationship between log($E_{NDT(Best\ fit)}/E_{Witczak(Aging)}$) and fatigue cracking in the existing pavement. This is shown in Figure 134.

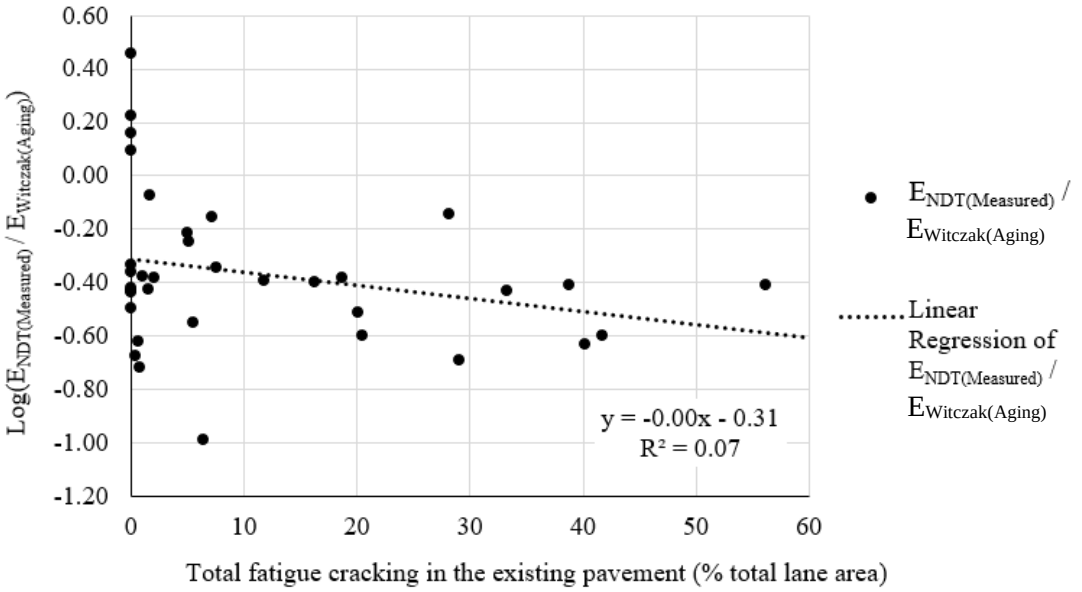

Figure 133. Log($E_{NDT(Measured)}/E_{Witczak(Aging)}$) vs. total fatigue cracking. E_{NDT} adjustment factor sections (9-kip load).

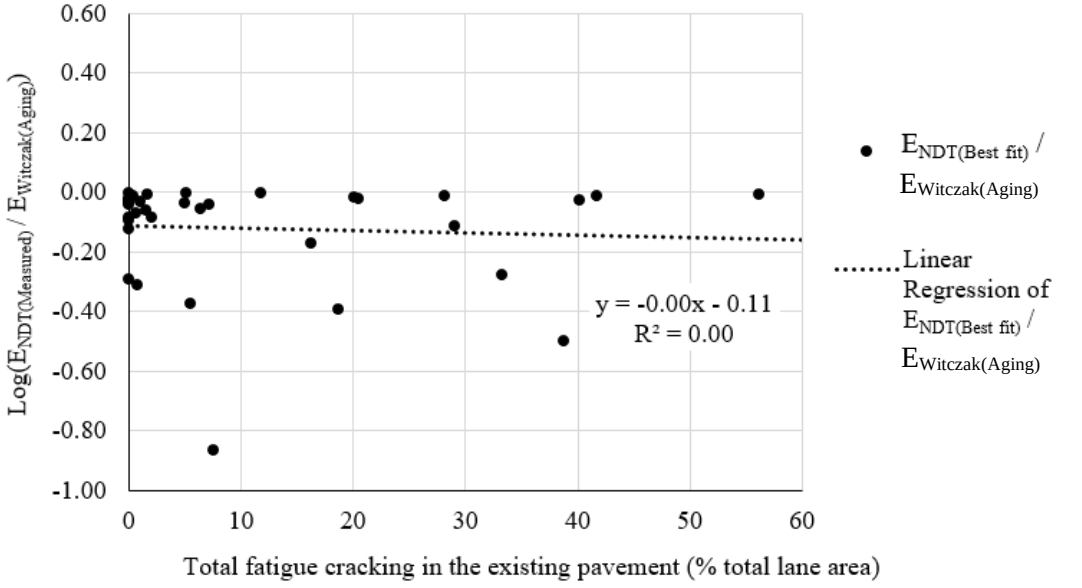

Figure 134. Log($E_{NDT(Best\ fit)}/E_{Witczak(Aging)}$) vs. total fatigue cracking. E_{NDT} adjustment factor sections (9-kip load).

As a result of the relationship between $E_{NDT(Measured)}/E_{Witczak(Aging)}$ and MDT and the similarity of $E_{NDT(Best\ fit)}$ to $E_{Witczak(Aging)}$, $E_{NDT(Best\ fit)}$ is greater than $E_{NDT(Measured)}$ for almost all sections. This is shown in Figure 135.

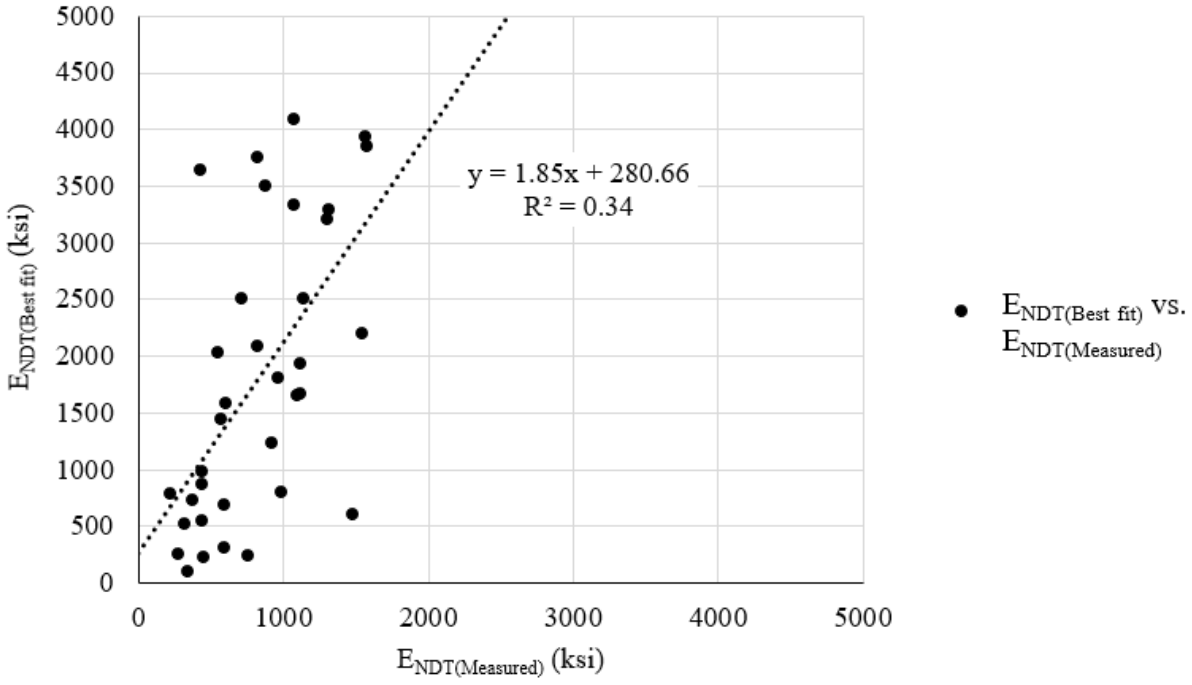

Figure 135. $E_{NDT(Best\ fit)}$ vs. $E_{NDT(Measured)}$. E_{NDT} adjustment factor sections (9-kip load).

Furthermore, as shown in Figure 136, the ratio of $E_{NDT(Best\ fit)}/E_{NDT(Measured)}$ decreases as MDT increases. This is not surprising, considering that a similar relationship exists between $E_{Witczak(Aging)}/E_{NDT(Measured)}$ and MDT, and $E_{NDT(Best\ fit)}$ is very similar to $E_{Witczak(Aging)}$. Finally, as shown in Figure 137, there is no clear relationship between $E_{NDT(Best\ fit)}/E_{NDT(Measured)}$ and fatigue cracking in the existing pavement.

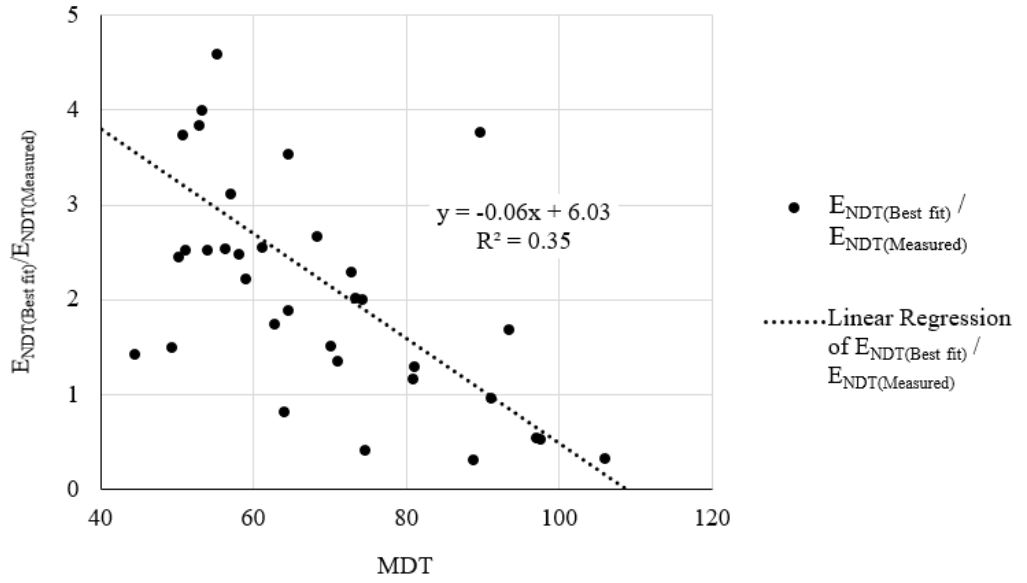

Figure 136. $E_{NDT(Best\ fit)}/E_{NDT(Measured)}$ vs. MDT. E_{NDT} adjustment factor sections (9-kip load).

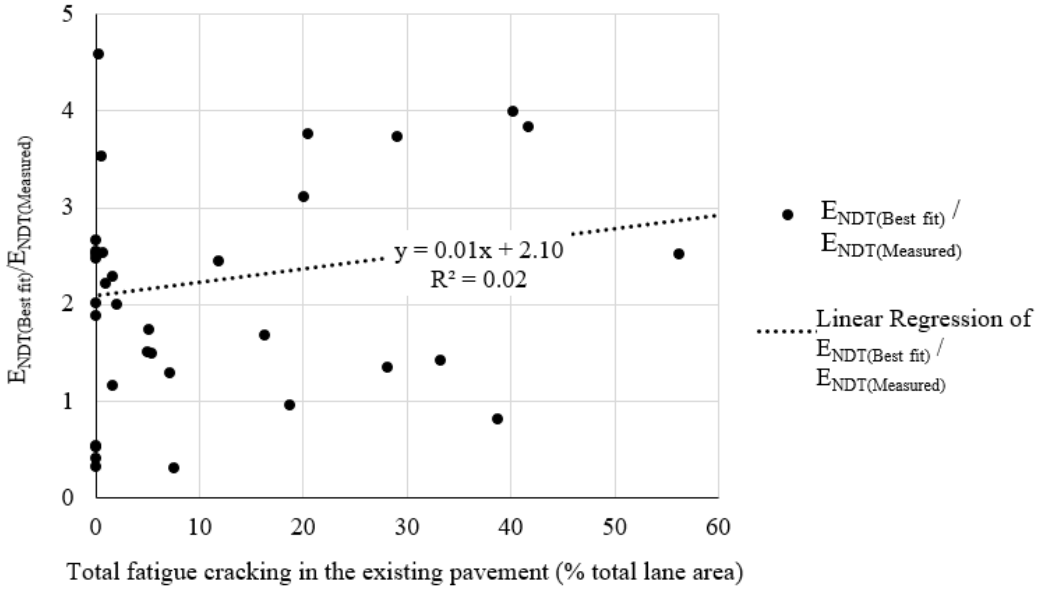

Figure 137. $E_{NDT(Best\ fit)}/E_{NDT(Measured)}$ vs. total fatigue cracking in the existing pavement. E_{NDT} adjustment factor sections (9-kip load).

6.1.3 Development of E_{NDT} adjustment factors

As previously discussed, it was determined that E_{NDT}, $E_{Witczak}$, MDT, fatigue cracking in the existing pavement, and the interaction of fatigue cracking and MDT should all be accounted for in the development of the E_{NDT} adjustment factor. Both $E_{NDT(Best\ fit)}$ and $E_{NDT(Measured)}$ were also included in the development of the adjustment factor. A multivariate regression analysis was selected for developing an adjustment factor that can account for all of the significant variables and interactions identified in the previous analyses.

The ratio $E_{NDT(Best\ fit)}/E_{NDT(Measured)}$ was selected as the response variable for the regression analysis and MDT and fatigue cracking in the existing pavement were selected as predictors. $E_{NDT(Best\ fit)}/E_{NDT(Measured)}$ was chosen as the response variable to eliminate $E_{Witczak}$ as an explicit term in the regression. It also allows the adjustment factor can be determined without performing the steps necessary for establishing $E_{Witczak}$. $E_{Witczak}$ is implicitly included in the ratio of $E_{NDT(Best\ fit)}$ over $E_{NDT(Measured)}$, which is a simplification of $(E_{NDT(Best\ fit)}/E_{Witczak(Aging)})/(E_{NDT(Measured)}/E_{Witczak(Aging)})$. MDT and fatigue cracking were chosen as predictors because these parameters and their interaction were shown to have a significant impact on the relationship between $E_{NDT(Measured)}$ and $E_{Witczak(Aging)}$.

Before the regression analysis was performed, several outlying data points were removed from the data set shown in Table 73. Each row in Table 73 is one data point used for perfroming the regression analysis. Two criteria were established to identify outliers:

1. $E_{NDT(Measured)}$ should be reasonable for the measured value of MDT.
2. Observed and predicted fatigue cracking in the overlaid pavement section should not excessively large (greater than 60%).

Data points that did not meet both of these criteria were removed from the data set. The purpose of the first criterion is to remove data points with excessively high or low backcalculated asphalt concrete stiffness caused by backcalculation errors. The first criterion was evaluated by plotting $E_{NDT(Measured)}$ vs. MDT and visually identifying outlying data points. The plot used to identify outliers is shown in Figure 138. Data from LTPP Sections 19-1044 in Iowa, 34-1033 in New Jersey, and 83-0508 in Manitoba were removed based on the first criterion. The purpose of the second criterion is to remove data points with unrealistically high values of predicted fatigue cracking in the overlaid pavement structure. Unrealistically high predicted fatigue cracking inflates $E_{NDT(Best\ fit)}/E_{NDT(Measured)}$ resulting in a single data point having a substantial effect the results of the regression analysis. Data from LTPP Section 34-1011 in New Jersey was removed based on the second criterion. The observed fatigue cracking in the overlay was 85.3% for this section, which resulted in a $E_{NDT(Best\ fit)}/E_{NDT(Measured)}$ ratio of 8.61.

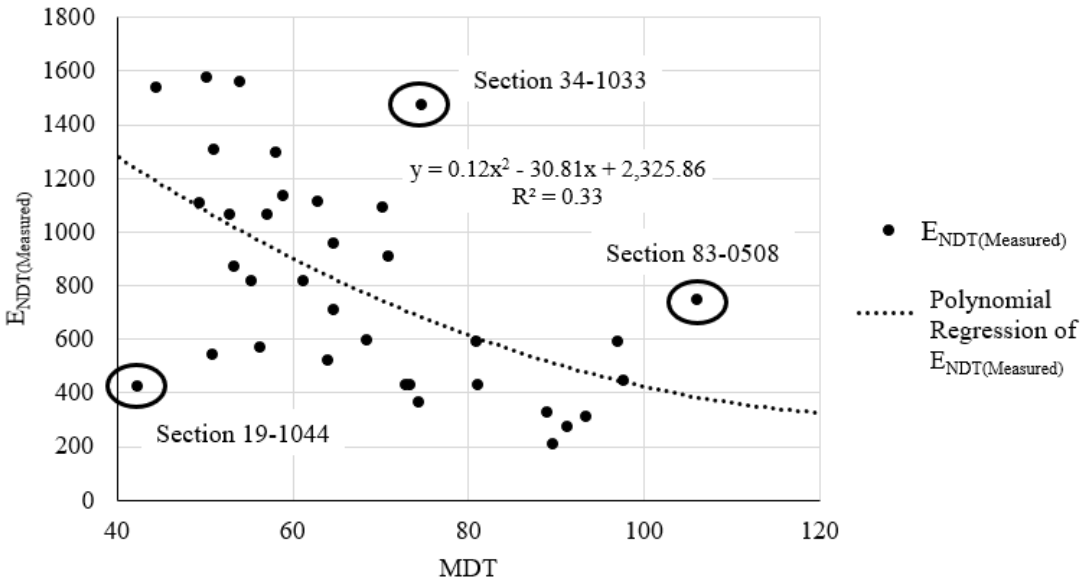

Figure 138. $E_{NDT(Measured)}$ vs. MDT plot used to identify outlying data points.

Using the revised data set with outliers removed, a multivariate linear regression analysis was performed with $E_{NDT(Best\ fit)}/E_{NDT(Measured)}$ as the response and MDT (ºF) and fatigue cracking in the existing pavement (% total lane area) as the predictors. The severity of the fatigue cracking in the existing pavement was not included because this is a subjective measurement and was unknown for some sections. The second-order interaction between MDT and fatigue cracking was also included in the model. All of the data used to create the regression is shown in Table 73. The multivariate linear regression derived from this first analysis is shown in Equation 21. The coefficient of determination (R^2) of this regression is 31%. As shown in Table 74, the constant and the MDT coefficient of the regression are significant at a 95% confidence level, but the fatigue cracking and interaction coefficients are not significant.

$$\frac{E_{NDT(Best\ fit)}}{E_{NDT(Measured)}} = 5.1900 - 0.0455 \times MDT - 0.0587 \times CRACK + 0.0011 \times (MDT \times CRACK) \quad (21)$$

Where:

$E_{NDT(Best\ fit)}$ = Best fit backcalculated asphalt concrete stiffness (ksi)

$E_{NDT(Measured)}$ = Measured backcalculated asphalt concrete stiffness. Average of all values over one FWD test pass for a 9-kip load (ksi)

MDT = Average mid-depth asphalt concrete temperature during one FWD test pass (ºF)

CRACK = Total fatigue cracking in the existing pavement when FWD testing is performed (% total lane area)

Table 74. Significance of coefficients for the first multivariate linear regression.

Term	Coefficient	Standard Error of the Coefficient	t-statistic	p-value
Constant	5.1900	1.070	4.85	0.00
MDT (ºF)	-0.0455	0.016	-2.92	0.01
CRACK (%)	-0.0587	0.058	-1.01	0.32
MDT*CRACK	0.0011	0.001	1.13	0.27

Additionally, residual plots for the regression model show two minor violations of the assumptions of a linear regression analysis. First, as shown in Figure 139, the residuals of the regression are not exactly normally distributed. The distribution of the residuals is slightly tailed. Second, it appears that the variance of the residuals is not constant. As shown in Figure 140, the plot of residuals vs. fitted values is somewhat funnel-shaped. A transformation of the response variable ($E_{NDT(Best\ fit)}/E_{NDT(Measured)}$) was performed to correct the non-normal residuals and non-constant variance. Using the Box-Cox method, the optimal value of λ was found to be 0.09 (Box and Cox 1964). This value was rounded to $\lambda = 0.00$, and the base 10 logarithm was instead used to transform $E_{NDT(Best\ fit)}/E_{NDT(Measured)}$. This transformation was chosen for simplicity.

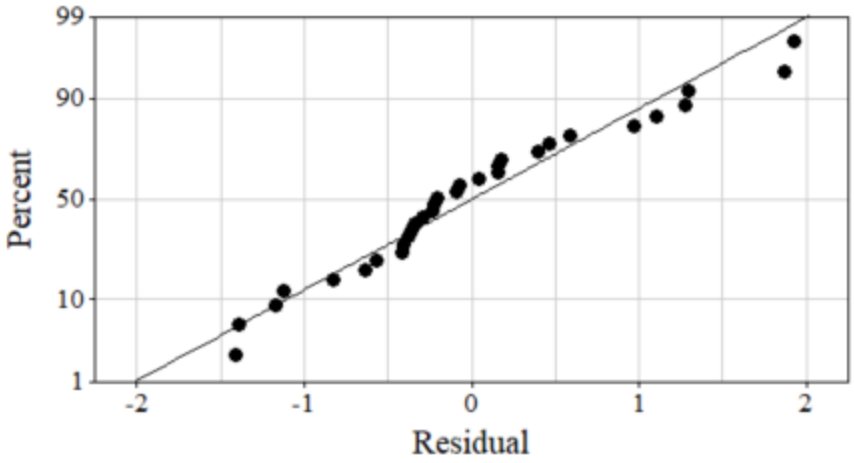

Figure 139. Normal probability plot of residuals for the first regression.

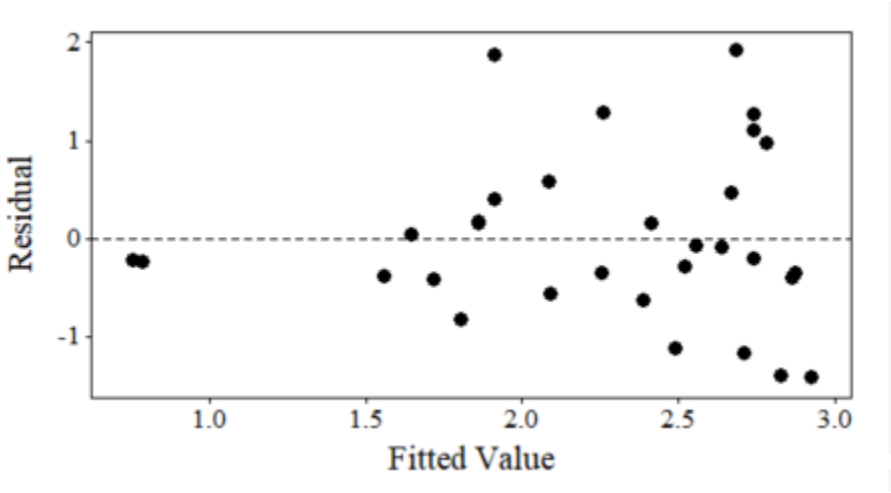

Figure 140. Residuals vs. fitted values plot for the first regression.

A second multivariate linear regression analysis was performed with $\log(E_{NDT(Best\ fit)}/E_{NDT(Measured)})$ as the response and MDT (ºF) and fatigue cracking in the existing pavement (% total lane area) as the predictors. The second-order interaction between MDT and fatigue cracking was also included. This regression is shown in Equation 22. It has an R^2 of 48%. As shown in

Table 75, the constant, the MDT coefficient, the fatigue cracking coefficient, and the interaction are all significant at a 95% confidence level. As shown in Figure 141, the transformation of $E_{NDT(Best\ fit)}/E_{NDT(Measured)}$ has improved the normality of the residuals. Additionally, as shown in Figure 142, the transformation has somewhat stabilized the variance of the residuals.

$$Log\left(\frac{E_{NDT(Best\ fit)}}{E_{NDT(Measured)}}\right) = 1.1920 - 0.0136 \times MDT - 0.0230 \times CRACK + 0.0004 \times (MDT \times CRACK) \quad (22)$$

Where:

Log = Base 10 logarithm

$E_{NDT(Best\ fit)}$ = Best fit backcalculated asphalt concrete stiffness (ksi)

$E_{NDT(Measured)}$ = Measured backcalculated asphalt concrete stiffness. Average of all values over one FWD test pass for a 9-kip load (ksi)

MDT = Average mid-depth asphalt concrete temperature during one FWD test pass (ºF)

CRACK = Total fatigue cracking in the existing pavement when FWD testing is performed (% total lane area)

Table 75. Significance of coefficients for the second multivariate linear regression.

Term	Coefficient	Standard Error of the Coefficient	t-statistic	p-value
Constant	1.1920	0.206	5.78	0.00
MDT (ºF)	-0.0136	0.003	-4.54	0.00
CRACK (%)	-0.0230	0.011	-2.05	0.05
MDT*CRACK	0.0004	0.000	2.14	0.04

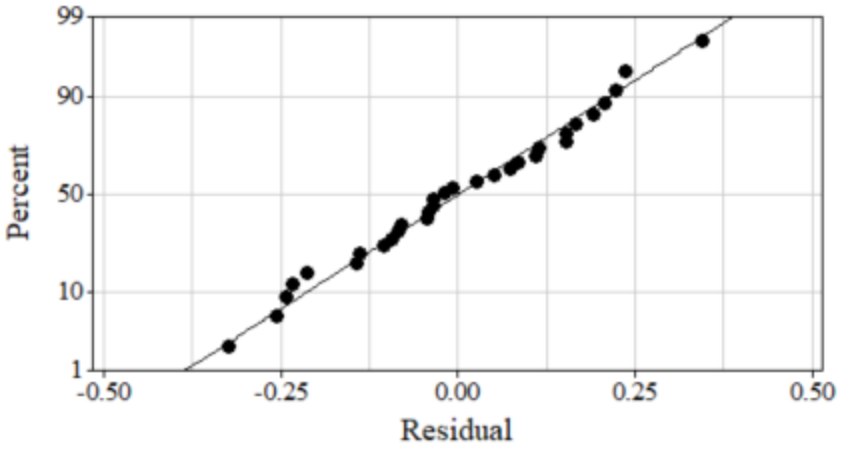

Figure 141. Normal probability plot of residuals for the second regression.

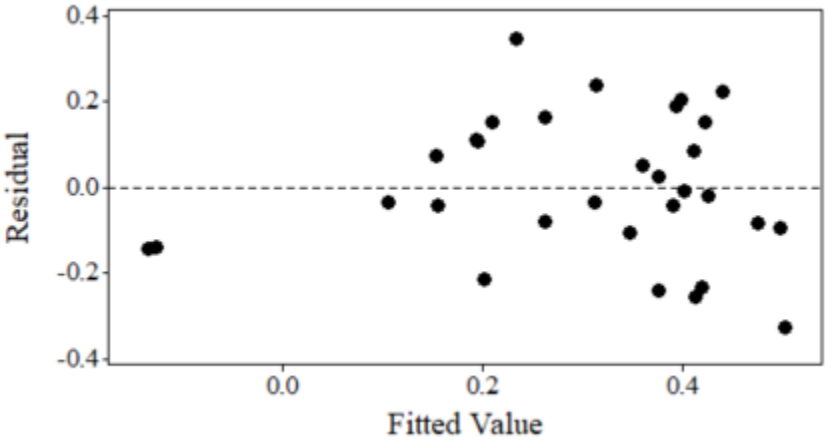

Figure 142. Residuals vs. fitted values plot for the second regression.

The second regression seemed reasonable, but a contour plot revealed that it extrapolates over approximately one quarter of its range. As shown in Figure 143, the data points used to develop the second regression do not cover the upper right quadrant of the contour plot. In this region, the regression analysis has extrapolated the relationship between $\log(E_{NDT(Best\ fit)}/E_{NDT(Measured)})$, MDT, and fatigue cracking. In general, extrapolation outside the inference space

should be avoided. The extrapolation shown in Figure 143 is particularly problematic because $\log(E_{NDT(Best\ fit)}/E_{NDT(Measured)})$ increases significantly in the region of extrapolation. In order to reduce the size of the extrapolation region, the data point for LTPP Section 34-0960 in New Jersey was removed from the data set. This is shown in Figure 143. A final multivariate linear regression was created with the revised data set using the same response, predictors, and interaction.

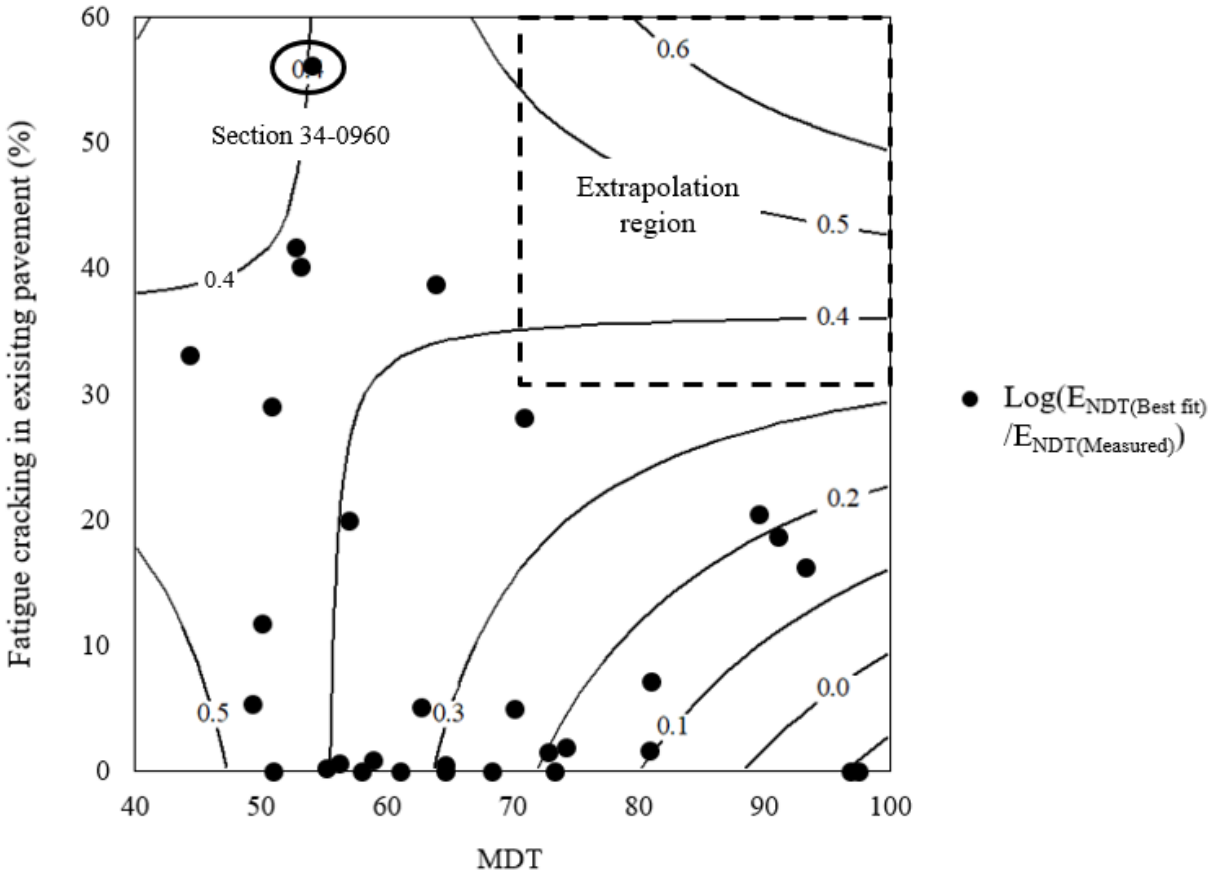

Figure 143. Contour plot of the second regression with overlaid data points.

The final multivariate linear regression is shown in Equation 23. The R^2 of this regression is 47%. As shown in Table 76, the constant, the MDT coefficient, and the interaction between MDT and fatigue cracking are all significant at a 95% confidence level. The fatigue cracking coefficient is significant at a 90% confidence level. Similar to the second regression, the residuals are normally distributed and have a relatively stable variance.

$$Log\left(\frac{E_{NDT(Best\ fit)}}{E_{NDT(Measured)}}\right) = 1.1980 - 0.0137 \times MDT - 0.0236 \times CRACK + 0.0004 \times (MDT \times CRACK) \quad (23)$$

Where:

Log = Base 10 logarithm

$E_{NDT(Best\ fit)}$ = Best fit backcalculated asphalt concrete stiffness (ksi)

$E_{NDT(Measured)}$ = Measured backcalculated asphalt concrete stiffness. Average of all values over one FWD test pass for a 9-kip load (ksi)

MDT = Average mid-depth asphalt concrete temperature during FWD test pass (ºF)

CRACK = Total fatigue cracking in the existing pavement when FWD testing is performed (% total lane area)

Table 76. Significance of coefficients for the final multivariate linear regression.

Term	Coefficient	Standard Error of the Coefficient	t-statistic	p-value
Constant	1.1980	0.213	5.63	0.00
MDT (ºF)	-0.0137	0.003	-4.44	0.00
CRACK (%)	-0.0236	0.012	-1.97	0.06
MDT*CRACK	0.0004	0.000	2.09	0.05

A contour plot of the final regression and the data points used to develop it is shown in Figure 144. There is an extrapolation region in the final regression, but it is smaller than that in the second regression. As shown in Figure 144, the extrapolation region for the final regression covers MDT greater than 75ºF and fatigue cracking greater than 25%. The regression shown in Equation 23 should not be used to estimate $\log(E_{NDT(Best\ fit)}/E_{NDT(Measured)})$ in this region.

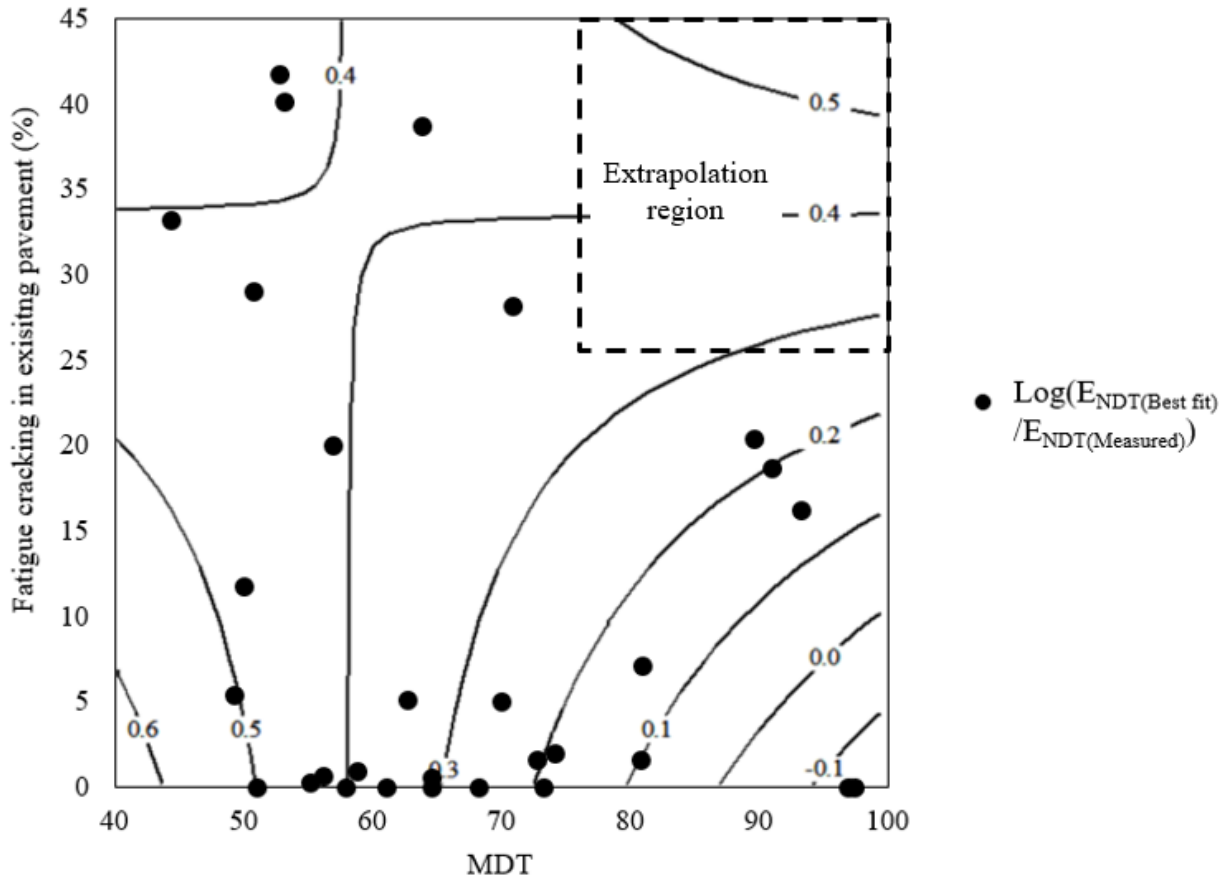

Figure 144. Contour plot of the final regression with overlaid data points.

6.1.4 Using the E_{NDT} adjustment factors

The regression equation shown in Equation 23 can be used to determine an adjusted Level 1 E_{NDT} input ($E_{NDT(Best\ fit)}$) for the Pavement ME AC/AC overlay design procedure. The following steps should be used to determine $E_{NDT(Best\ fit)}$ for a given design:

1. Perform FWD testing in the outer wheelpath of the existing AC pavement. Backcalculate the stiffness off the asphalt concrete layer at each test location. Use only data for a 9-kip load level. Calculate $E_{NDT(Measured)}$, which is the mean backcalculated stiffness of the asphalt concrete layer along the test section.
2. Determine the mean MDT (ºF) over the time period in which the FWD testing was performed.
3. Perform a distress survey of the test section and determine the amount of fatigue cracking in the existing pavement section as a percentage of total lane area.
4. Calculate $Log(E_{NDT(Best\ fit)}/E_{NDT(Measured)})$ using Equation 23 along with the average MDT from Step 3 and the fatigue cracking in the existing pavement from Step 4 as inputs.
5. Calculate $E_{NDT(Best\ fit)}/E_{NDT(Measured)}$ from $log(E_{NDT(Best\ fit)}/E_{NDT(Measured)})$.
6. Multiply $E_{NDT(Measured)}$ by $E_{NDT(Best\ fit)}/E_{NDT(Measured)}$ to determine $E_{NDT(Best\ fit)}$.
7. Use $E_{NDT(Best\ fit)}$ instead of $E_{NDT(Measured)}$ as the Level 1 input for the Pavement ME AC/AC overlay design procedure.

With one exception, this procedure should be used only when MDT is between 40ºF to 100ºF and when fatigue cracking in the existing pavement is between 0% and 45%. The procedure should not be used to estimate $E_{NDT(Best\ fit)}$ if MDT is greater than 75ºF **and** fatigue cracking is greater than

25%. Finally, the regression shown in Equation 23 was developed using $E_{NDT(Best\ fit)}$ data points that represent the damage in the existing asphalt concrete and the amount of fatigue cracking that will ultimately develop in the overlay. This procedure is intended to improve the accuracy of the maximum fatigue cracking predicted by the AC/AC overlay design procedure, but not the rate at which this distress develops over the life of the overlay.

6.2 CONCLUSIONS

Based on an evaluation of the Pavement ME AC/AC overlay design procedure conducted in Chapter 3, it was determined that adjustment factors for the Level 1 E_{NDT} input should be developed to improve the accuracy of predicted distress. The results of the analysis conducted in Chapters 4 and 5 were used to identify parameters that should be included in the development of an E_{NDT} adjustment factor. Several LTPP sections with overlays were modelled in the AC/AC overlay design procedure and the "best fit" E_{NDT} input was identified for each section. A multivariate linear regression analysis was performed for estimating $\log(E_{NDT(Best\ fit)}/E_{NDT(Measured)})$ as a function of MDT and fatigue cracking in the existing pavement. This relationship can be used to determine the adjusted E_{NDT} inputs for the Pavement ME AC/AC overlay design procedure over a wide range of MDT and fatigue cracking in the existing pavement.

7.0 CONCLUSIONS

The primary goal of this research was to determine how the Pavement ME AC/AC overlay design procedure quantifies fatigue damage in the asphalt concrete layer of an existing pavement, whether this methodology accurately predicts distress in the overlaid pavement structure, and how this methodology might be improved. The research was conducted in five main phases:

1. A literature review was performed to obtain information about the performance of the Pavement ME AC/AC overlay design procedure and the assumptions required to use the procedure. Additional information was obtained regarding the various methods available for determining the stiffness of asphalt concrete and how these relate to one another.
2. The Pavement ME AC/AC overlay design procedure was described and then evaluated using data from LTPP sections. In the design procedure, the amount of fatigue damage in the asphalt concrete of the existing pavement is determined by the relationship between the backcalculated stiffness of the asphalt concrete in the existing pavement (E_{NDT}) and the stiffness estimated using the Witczak equation ($E_{Witczak}$). Evaluation of the design procedure showed that it over predicts both fatigue cracking and rutting in the overlaid pavement structure when Level 1 inputs (derived from FWD testing) are used. It was suspected that the over prediction is due to an inherent difference between E_{NDT} and $E_{Witczak}$.

3. In order to investigate the relationship between E_{NDT} and $E_{Witczak}$, three different methods for determining the stiffness of asphalt concrete in an existing pavement were examined: laboratory dynamic modulus testing, predictive equations (the Witczak equation), and backcalculation from FWD data. Field and laboratory data was used to demonstrate that each of these methods can produce a different estimate of stiffness for the same asphalt concrete. Furthermore, it was shown that the method used to estimate the stiffness of the asphalt concrete can have a significant effect on pavement design using Pavement ME. The results of this investigation supported the hypothesis that there is an inherent difference between E_{NDT} and $E_{Witczak}$.
4. Additional LTPP data was analyzed to confirm that there is a relationship between FWD data and fatigue damage in the asphalt concrete of the existing pavement. Observed fatigue cracking was used to represent fatigue damage in the asphalt concrete. Several FWD parameters were defined and relationships between these parameters, temperature, and observed distress were investigate. It was determined that there is a significant relationship between FWD data and fatigue damage in the asphalt concrete layer of an existing pavement. This analysis also confirmed that there is an inherent difference between E_{NDT} and $E_{Witczak}$.
5. In order to improve the accuracy of the Pavement ME AC/AC overlay design procedure, an adjustment factor was developed for the Level 1 backcalculated asphalt stiffness (E_{NDT}) input. These adjustment factors account for the temperature of the asphalt concrete at the time FWD testing is performed and the amount of fatigue cracking in the existing pavement, both of which were shown to affect the relationship between E_{NDT} and $E_{Witczak}$.

There are several limitations to the findings of this research. Related to these limitations, there are also several possible directions for future work. Limitations and directions for future work are described below.

- The backcalculated stiffness adjustment factor proposed here is only a gross adjustment to the Pavement ME design procedure. Without access to the Pavement ME code, it was not possible to change any of the underlying models in the procedure, particularly Equation 8, which defines the amount of fatigue damage in the asphalt concrete of the existing pavement. Future work could focus on revising how to define fatigue damage in the asphalt concrete of the existing pavement. Many types of information regarding the existing pavement, including multiple FWD parameters, observed distress, and the details of the pavement structure, could all be used to estimate fatigue damage.
- This research has only considered mean values, calculated over entire pavement sections, when examining the relationship between FWD parameters and observed distress. Future work could focus on increasing the amount of information provided by FWD parameters by examining relationships between different statistics of the parameters, such as median, maximum, minimum, and coefficient of variation, and how these are related to observed distress.
- Finally, this research takes a largely data-driven, empirical approach to evaluating the amount of fatigue damage in asphalt concrete and ignores the mechanistic approach. Specifically, no attempt was made to model the dynamic behavior of the existing pavement structure or to backcalculate the dynamic modulus master curve of the asphalt concrete form FWD deflection time histories. It seems likely that the most effective method for

determining the amount of fatigue damage in the asphalt concrete is neither purely empirical nor purely mechanistic, and future work on this problem should include both approaches.

APPENDIX A

ASPHALT CONCRETE MIX INFORMATION FROM THE LTPP DATABASE

This appendix contains the asphalt concrete mix information used as inputs for the Witczak equation in Chapters 3, 5, and 6. The mix information represents average values for each section, obtained by processing raw data obtained from the LTPP database. The steps used to process the raw data are explained in Chapter 5.

Table 77. Key to binder grade codes used in mix information table.

Binder Grade Code	Binder Grade	A	VTS
2	AC 5	11.2614	-3.7914
3	AC 10	11.0134	-3.6954
4	AC 20	10.7709	-3.6017
5	AC 30	10.6316	-3.5480
6	AC 40	10.5338	-3.5104
13	Pen 120-150	11.0897	-3.7252
14	Pen 85-100	10.8232	-3.6210
15	Pen 60-70	10.6508	3.5537
16	PG 64-22	10.980	-3.680
18	PG 58-28	11.010	-3.701
19	PG 64-28	10.312	-3.440
20	PG 76-28	9.200	-3.024
21	PG 70-28	9.715	-3.217
22	PG 64-10	11.432	-3.842
99	PG 70-22	10.299	-3.426

Table 78. Asphalt concrete mix information obtained from the LTPP database.

State	LTPP ID	Layer Construct-ion Date	Section Structure Number	Section Layer Number	Average Layer Thickness (in)	Section Age at Layer Construct-ion (yr)	MAAT (°F)	Binder Grade Code	Air Voids (V_a) (%)	Effective Binder Content (V_{be}) (%)	$P_{3/4}$ (%)	$P_{3/8}$ (%)	P_4 (%)	P_{200} (%)
AL	1-0101	3/1/1993	1	2	1.2	0	63.5	4	6.95	10.71	98.3	78.2	61.3	5.90
AL	1-0101	3/1/1993	1	1	6.2	0	63.5	4	7.38	8.53	91.2	69.8	51.2	6.38
AL	1-0102	3/1/1993	1	2	1.4	0	63.5	4	5.28	11.79	98.3	78.2	61.3	5.90
AL	1-0102	3/1/1993	1	1	2.8	0	63.5	4	1.87	9.33	91.2	69.8	51.2	6.38
CO	8-1053	2/1/1984	1	1	4.6	0	51.2	3	1.97	13.04	100.0	82.3	55.8	6.83
CO	8-1053	6/1/2000	2	3	2.2	16	51.2	20	3.89	12.95	100.0	82.0	52.5	8.95
CO	8-1053	6/1/2000	2	2	1.9	16	51.2	3	1.08	13.39	100.0	86.5	59.5	8.60
CO	8-1053	6/1/2000	2	1	2.7	16	51.2	3	1.97	13.04	100.0	82.3	55.8	6.83
CT	9-1803	7/1/1985	1	2	3.0	0	50.4	4	6.25	9.90	100.0	77.0	52.0	4.80
CT	9-1803	7/1/1985	1	1	4.1	0	50.4	4	1.22	7.10	78.5	54.5	43.5	5.35
CT	9-1803	6/1/2000	2	3	1.8	14	50.4	19	3.96	13.97	100.0	85.7	59.7	4.00
CT	9-1803	6/1/2000	2	2	3.0	14	50.4	4	6.25	9.90	100.0	77.0	52.0	4.80
CT	9-1803	6/1/2000	2	1	4.1	14	50.4	4	1.22	7.10	78.5	54.5	43.5	5.35
DE	10-0102	5/1/1996	1	2	1.3	0	55.1	4	8.43	9.80	100.0	95.8	63.0	7.20
DE	10-0102	5/1/1996	1	1	3.0	0	55.1	4	6.28	7.32	92.2	69.8	48.8	6.80
DE	10-0102	9/1/1996	2	3	1.2	0	55.1	4	15.00	12.00	100.0	97.5	40.0	3.50
DE	10-0102	9/1/1996	2	2	1.3	0	55.1	4	8.43	9.80	100.0	95.8	63.0	7.20
DE	10-0102	9/1/1996	2	1	3.0	0	55.1	4	6.28	7.32	92.2	69.8	48.8	6.80
GA	13-1005	6/1/1986	1	3	1.4	0	64.5	5	4.87	7.78	99.0	74.0	50.5	7.35
GA	13-1005	6/1/1986	1	2	2.2	0	64.5	5	6.99	6.04	99.0	74.0	50.5	7.35
GA	13-1005	6/1/1986	1	1	4.0	0	64.5	5	3.27	5.92	95.5	57.5	44.0	6.55

Table 78 (continued).

State	LTPP ID	Layer Construct-ion Date	Section Structure Number	Section Layer Number	Average Layer Thickness (in)	Section Age at Layer Construct-ion (yr)	MAAT (°F)	Binder Grade Code	Air Voids (V_a) (%)	Effective Binder Content (V_{be}) (%)	$P_{3/4}$ (%)	$P_{3/8}$ (%)	P_4 (%)	P_{200} (%)
GA	13-1031	6/1/1981	1	2	3.0	0	59.2	4	4.60	11.68	96.5	77.5	59.5	7.10
GA	13-1031	6/1/1981	1	1	8.2	0	59.2	4	4.16	8.05	87.5	69.0	47.5	7.00
ID	16-1010	10/1/1969	1	2	5.0	0	44.1	14	4.11	12.87	100.0	95.5	63.5	7.55
ID	16-1010	10/1/1969	1	1	5.7	0	44.1	15	3.64	12.35	100.0	75.0	52.0	6.60
IL	17-A310	10/1/1986	1	4	0.8	0	56.4	4	6.40	9.60	100.0	99.0	58.0	5.00
IL	17-A310	10/1/1986	1	3	2.3	0	56.4	4	3.70	11.20	92.0	56.0	38.0	4.00
IL	17-A310	10/1/1986	1	2	3.5	0	56.4	4	3.70	11.20	92.0	56.0	38.0	4.00
IL	17-A310	10/1/1986	1	1	4.7	0	56.4	4	3.70	11.20	92.0	56.0	38.0	4.00
IL	17-A310	7/1/1991	2	5	0.5	4	56.4	4	3.70	12.40	100.0	99.0	58.0	5.00
IL	17-A310	7/1/1991	2	4	0.8	4	56.4	4	6.40	9.60	100.0	99.0	58.0	5.00
IL	17-A310	7/1/1991	2	3	2.3	4	56.4	4	3.70	11.20	92.0	56.0	38.0	4.00
IL	17-A310	7/1/1991	2	2	3.5	4	56.4	4	3.70	11.20	92.0	56.0	38.0	4.00
IL	17-A310	7/1/1991	2	1	4.7	4	56.4	4	3.70	11.20	92.0	56.0	38.0	4.00
IN	18-2008	1/1/1980	1	3	1.0	0	50.7	4	7.14	8.90	100.0	100.0	99.0	4.00
IN	18-2008	1/1/1980	1	2	2.1	0	50.7	4	5.42	7.03	100.0	53.0	35.0	1.00
IN	18-2008	1/1/1980	1	1	10.3	0	50.7	4	4.98	7.27	81.0	45.0	31.0	1.00
IN	18-2008	6/1/1994	2	4	1.5	14	50.7	4	7.70	10.10	100.0	94.5	67.5	4.40
IN	18-2008	6/1/1994	2	3	1.0	14	50.7	4	7.14	8.90	100.0	100.0	99.0	4.00
IN	18-2008	6/1/1994	2	2	2.1	14	50.7	4	5.42	7.03	100.0	53.0	35.0	1.00
IN	18-2008	6/1/1994	2	1	10.3	14	50.7	4	4.98	7.27	81.0	45.0	31.0	1.00
IA	19-0101	11/1/1992	1	2	1.8	0	52.6	3	9.01	6.17	100.0	76.0	53.3	5.43
IA	19-0101	11/1/1992	1	1	5.9	0	52.6	3	7.74	6.72	94.3	64.2	45.8	4.93
IA	19-0103	11/1/1992	1	3	2.1	0	52.6	3	6.19	6.37	100.0	76.0	53.3	5.43
IA	19-0103	11/1/1992	1	2	1.7	0	52.6	3	4.91	6.62	94.3	64.2	45.8	4.93
IA	19-0103	11/1/1992	1	1	8.4	0	52.6	3	4.25	7.73	95.0	68.0	49.3	5.87
IA	19-0104	11/1/1992	1	3	1.8	0	52.6	3	6.20	6.37	100.0	76.0	53.3	5.43

Table 78 (continued).

State	LTPP ID	Layer Construct-ion Date	Section Structure Number	Section Layer Number	Average Layer Thickness (in)	Section Age at Layer Construct-ion (yr)	MAAT (°F)	Binder Grade Code	Air Voids (V_a) (%)	Effective Binder Content (V_{be}) (%)	$P_{3/4}$ (%)	$P_{3/8}$ (%)	P_4 (%)	P_{200} (%)
IA	19-0104	11/1/1992	1	2	5.2	0	52.6	3	5.46	6.89	94.3	64.2	45.8	4.93
IA	19-0104	11/1/1992	1	1	12.4	0	52.6	3	5.06	8.27	95.0	68.0	49.3	5.87
IA	19-0105	11/1/1992	1	3	1.8	0	52.6	3	10.83	6.05	100.0	76.0	53.3	5.43
IA	19-0105	11/1/1992	1	2	1.8	0	52.6	3	6.45	6.81	94.3	64.2	45.8	4.93
IA	19-0105	11/1/1992	1	1	4.7	0	52.6	3	5.75	7.91	95.0	68.0	49.3	5.87
IA	19-0106	11/1/1992	1	3	1.9	0	52.6	3	7.44	6.28	100.0	76.0	53.3	5.43
IA	19-0106	11/1/1992	1	2	5.1	0	52.6	3	5.48	7.11	94.3	64.2	45.8	4.93
IA	19-0106	11/1/1992	1	1	9.2	0	52.6	3	6.20	7.87	95.0	68.0	49.3	5.87
IA	19-0108	11/1/1992	1	3	1.9	0	52.6	3	6.62	6.43	100.0	76.0	53.3	5.43
IA	19-0108	11/1/1992	1	2	4.1	0	52.6	3	5.73	6.98	94.3	64.2	45.8	4.93
IA	19-0108	11/1/1992	1	1	4.5	0	52.6	3	9.02	5.92	83.0	19.7	5.3	2.17
IA	19-0109	11/1/1992	1	3	2.5	0	52.6	3	5.80	6.59	100.0	76.0	53.3	5.43
IA	19-0109	11/1/1992	1	2	4.9	0	52.6	3	5.99	6.85	94.3	64.2	45.8	4.93
IA	19-0109	11/1/1992	1	1	4.8	0	52.6	3	11.85	3.64	83.0	19.7	5.3	2.17
IA	19-0110	11/1/1992	1	4	2.5	0	52.6	3	6.11	6.37	100.0	76.0	53.3	5.43
IA	19-0110	11/1/1992	1	3	5.4	0	52.6	3	4.30	7.16	94.3	64.2	45.8	4.93
IA	19-0110	11/1/1992	1	2	3.2	0	52.6	3	4.10	8.05	95.0	68.0	49.3	5.87
IA	19-0110	11/1/1992	1	1	4.4	0	52.6	3	11.96	4.10	83.0	19.7	5.3	2.17
IA	19-0111	11/1/1992	1	4	2.5	0	52.6	3	5.32	6.42	100.0	76.0	53.3	5.43
IA	19-0111	11/1/1992	1	3	1.9	0	52.6	3	6.48	6.81	94.3	64.2	45.8	4.93
IA	19-0111	11/1/1992	1	2	7.4	0	52.6	3	4.75	7.99	95.0	68.0	49.3	5.87
IA	19-0111	11/1/1992	1	1	4.4	0	52.6	3	10.96	5.93	83.0	19.7	5.3	2.17
IA	19-0112	11/1/1992	1	4	2.4	0	52.6	3	11.47	6.01	100.0	76.0	53.3	5.43
IA	19-0112	11/1/1992	1	3	2.1	0	52.6	3	10.72	6.45	94.3	64.2	45.8	4.93
IA	19-0112	11/1/1992	1	2	12.4	0	52.6	3	3.58	8.09	95.0	68.0	49.3	5.87
IA	19-0112	11/1/1992	1	1	4.1	0	52.6	3	13.95	2.75	83.0	19.7	5.3	2.17

Table 78 (continued).

State	LTPP ID	Layer Construct-ion Date	Section Structure Number	Section Layer Number	Average Layer Thickness (in)	Section Age at Layer Construct-ion (yr)	MAAT (°F)	Binder Grade Code	Air Voids (V_a) (%)	Effective Binder Content (V_{be}) (%)	$P_{3/4}$ (%)	$P_{3/8}$ (%)	P_4 (%)	P_{200} (%)
IA	19-0159	11/1/1992	1	3	1.5	0	52.6	3	8.05	6.81	100.0	76.0	53.3	5.43
IA	19-0159	11/1/1992	1	2	2.5	0	52.6	3	6.31	6.65	94.3	64.2	45.8	4.93
IA	19-0159	11/1/1992	1	1	9.0	0	52.6	3	4.88	5.65	95.0	68.0	49.3	5.87
IA	19-1044	7/1/1971	1	2	3.2	0	49.0	14	8.34	9.35	100.0	72.0	54.0	7.10
IA	19-1044	7/1/1971	1	1	13.0	0	49.0	14	4.90	8.20	100.0	78.0	64.0	9.00
IA	19-1044	9/1/2002	2	5	1.7	31	49.0	18	5.26	9.10	100.0	87.5	68.5	6.70
IA	19-1044	9/1/2002	2	4	2.0	31	49.0	18	5.63	10.10	100.0	79.0	61.0	4.45
IA	19-1044	9/1/2002	2	3	1.0	31	49.0	14	5.79	11.42	100.0	99.0	80.0	10.00
IA	19-1044	9/1/2002	2	2	2.2	31	49.0	14	8.34	9.35	100.0	72.0	54.0	7.10
IA	19-1044	9/1/2002	2	1	13.0	31	49.0	14	4.90	8.20	100.0	78.0	64.0	9.00
KS	20-0159	11/1/1993	1	2	2.0	0	55.2	3	13.03	5.60	100.0	83.5	65.5	7.95
KS	20-0159	11/1/1993	1	1	9.3	0	55.2	3	9.26	5.88	90.7	63.7	54.0	8.00
KS	20-0159	10/1/2001	2	5	1.2	8	55.2	16	5.35	9.60	100.0	97.5	69.5	7.35
KS	20-0159	10/1/2001	2	4	1.3	8	55.2	16	6.26	8.40	100.0	90.0	56.0	8.10
KS	20-0159	10/1/2001	2	3	2.8	8	55.2	16	6.99	6.52	97.7	83.3	69.7	13.60
KS	20-0159	10/1/2001	2	1	6.0	8	55.2	3	9.26	5.88	90.7	63.7	54.0	8.00
KS	20-1005	9/1/1971	1	4	2.0	0	55.3	2	4.67	11.08	100.0	83.0	64.5	9.45
KS	20-1005	9/1/1971	1	3	2.2	0	55.3	2	8.60	9.06	100.0	86.0	53.0	8.65
KS	20-1005	9/1/1971	1	2	4.6	0	55.3	2	9.64	10.81	100.0	79.0	55.0	8.00
KS	20-1005	9/1/1971	1	1	4.2	0	55.3	2	9.64	10.53	100.0	79.0	55.0	8.00
KS	20-1005	11/1/2000	2	5	0.8	28	55.3	16	18.20	9.55	100.0	98.0	47.5	6.95
KS	20-1005	11/1/2000	2	4	1.1	28	55.3	2	4.67	11.08	100.0	83.0	64.5	9.45
KS	20-1005	11/1/2000	2	3	2.2	28	55.3	2	8.60	9.06	100.0	86.0	53.0	8.65
KS	20-1005	11/1/2000	2	2	4.6	28	55.3	2	9.64	10.81	100.0	79.0	55.0	8.00
KS	20-1005	11/1/2000	2	1	4.2	28	55.3	2	9.64	10.53	100.0	79.0	55.0	8.00
KS	20-1009	1/1/1985	1	2	2.4	0	55.8	4	4.18	10.36	100.0	83.5	65.5	7.95

Table 78 (continued).

State	LTPP ID	Layer Construct-ion Date	Section Structure Number	Section Layer Number	Average Layer Thickness (in)	Section Age at Layer Construct-ion (yr)	MAAT (°F)	Binder Grade Code	Air Voids (V_a) (%)	Effective Binder Content (V_{be}) (%)	$P_{3/4}$ (%)	$P_{3/8}$ (%)	P_4 (%)	P_{200} (%)
KS	20-1009	1/1/1985	1	1	8.7	0	55.8	4	5.36	10.28	100.0	84.5	66.0	7.50
KS	20-1009	8/1/1995	2	4	1.5	10	55.8	4	7.74	8.49	100.0	69.0	49.0	4.80
KS	20-1009	8/1/1995	2	3	6.1	10	55.8	4	3.71	10.95	100.0	72.0	52.0	4.70
KS	20-1009	8/1/1995	2	1	4.5	10	55.8	4	5.36	10.28	100.0	84.5	66.0	7.50
KS	20-1010	9/1/1980	1	3	2.2	0	55.9	13	2.54	6.15	100.0	79.5	63.0	6.80
KS	20-1010	9/1/1980	1	2	2.4	0	55.9	13	2.69	6.36	100.0	83.5	68.0	7.35
KS	20-1010	9/1/1980	1	1	4.2	0	55.9	13	5.41	5.65	100.0	84.5	66.0	7.50
ME	23-1009	9/1/1970	1	2	1.0	0	45.7	14	4.43	16.09	100.0	99.0	75.5	5.65
ME	23-1009	9/1/1970	1	1	4.7	0	45.7	14	2.99	12.63	99.0	61.5	47.5	4.30
ME	23-1009	8/1/1993	2	4	1.5	23	45.7	4	6.58	11.04	100.0	84.5	53.5	6.65
ME	23-1009	8/1/1993	2	3	1.2	23	45.7	4	6.58	12.31	100.0	98.0	85.0	6.00
ME	23-1009	8/1/1993	2	2	1.0	23	45.7	14	4.43	16.09	100.0	99.0	75.5	5.65
ME	23-1009	8/1/1993	2	1	4.7	23	45.7	14	2.99	12.63	99.0	61.5	47.5	4.30
ME	23-1026	7/1/1973	1	2	1.0	0	43.2	3	10.61	9.96	100.0	95.5	61.0	9.70
ME	23-1026	7/1/1973	1	1	5.9	0	43.2	3	2.37	11.53	78.0	50.5	37.5	5.55
ME	23-1026	9/1/1996	2	4	1.6	8	43.2	4	5.01	13.57	100.0	94.0	71.0	7.00
ME	23-1026	9/1/1996	2	3	0.5	8	43.2	4	5.01	13.13	100.0	86.0	57.0	7.00
ME	23-1026	9/1/1996	2	2	1.0	8	43.2	3	10.61	9.96	100.0	95.5	61.0	9.70
ME	23-1026	9/1/1996	2	1	5.9	8	43.2	3	2.37	11.53	78.0	50.5	37.5	5.55
MD	24-1634	6/1/1976	1	1	3.6	0	55.6	14	2.11	12.10	100.0	97.0	68.5	6.60
MD	24-1634	5/1/1998	2	3	1.5	22	55.6	99	6.66	10.99	100.0	87.5	48.5	4.68
MD	24-1634	5/1/1998	2	2	1.7	22	55.6	99	5.12	8.62	90.5	66.3	42.0	4.58
MD	24-1634	5/1/1998	2	1	3.6	22	55.6	14	2.11	12.10	100.0	97.0	68.5	6.60
MA	25-1002	5/1/1982	1	2	1.4	0	48.3	4	5.25	15.77	100.0	97.0	67.0	3.75
MA	25-1002	5/1/1982	1	1	6.4	0	48.3	4	5.98	12.19	97.5	58.5	39.5	3.25
MI	26-0116	8/1/1995	1	3	1.8	0	48.5	14	2.50	13.27	100.0	88.3	58.0	6.73

Table 78 (continued).

State	LTPP ID	Layer Construct-ion Date	Section Structure Number	Section Layer Number	Average Layer Thickness (in)	Section Age at Layer Construct-ion (yr)	MAAT (°F)	Binder Grade Code	Air Voids (V_a) (%)	Effective Binder Content (V_{be}) (%)	$P_{3/4}$ (%)	$P_{3/8}$ (%)	P_4 (%)	P_{200} (%)
MI	26-0116	8/1/1995	1	2	2.1	0	48.5	14	2.50	9.22	86.3	57.5	34.7	5.07
MI	26-0116	8/1/1995	1	1	12.1	0	48.5	14	7.29	8.00	85.0	53.0	38.3	5.40
MN	27-0501	7/1/1969	1	2	1.4	0	39.1	14	0.47	10.26	100.0	80.0	63.3	5.83
MN	27-0501	7/1/1969	1	1	5.3	0	39.1	14	4.96	9.19	100.0	79.3	63.7	5.60
MN	27-1018	1/1/1979	1	2	1.6	0	43.9	13	2.94	13.16	100.0	84.5	69.5	3.25
MN	27-1018	1/1/1979	1	1	2.8	0	43.9	13	9.46	10.09	100.0	86.5	72.5	2.70
MN	27-1018	6/1/1995	2	3	2.7	16	43.9	13	1.87	11.02	100.0	85.0	70.0	5.00
MN	27-1018	6/1/1995	2	2	0.6	16	43.9	13	2.94	13.16	100.0	84.5	69.5	3.25
MN	27-1018	6/1/1995	2	1	2.8	16	43.9	13	9.46	10.09	100.0	86.5	72.5	2.70
MN	27-B320	9/1/1981	1	1	5.4	0	39.6	14	4.85	8.49	99.5	83.5	67.5	6.00
MN	27-B330	9/1/1981	1	1	7.4	0	39.6	14	4.85	8.49	99.5	83.5	67.5	6.00
MN	27-B340	9/1/1981	1	1	6.3	0	39.6	14	4.85	8.49	99.5	83.5	67.5	6.00
MN	27-C330	1/1/1972	1	3	1.6	0	41.3	14	1.93	11.19	100.0	84.5	68.0	5.15
MN	27-C330	1/1/1972	1	2	2.0	0	41.3	13	5.17	10.39	100.0	78.0	64.0	5.30
MN	27-C330	1/1/1972	1	1	6.0	0	41.3	13	10.72	9.78	100.0	78.0	64.0	5.30
MN	27-C340	1/1/1972	1	3	1.4	0	41.3	14	1.93	11.19	100.0	84.5	68.0	5.15
MN	27-C340	1/1/1972	1	2	2.0	0	41.3	13	5.17	10.39	100.0	78.0	64.0	5.30
MN	27-C340	1/1/1972	1	1	5.7	0	41.3	13	10.72	9.78	100.0	78.0	64.0	5.30
MN	27-C350	1/1/1972	1	3	1.5	0	41.3	14	1.93	11.19	100.0	84.5	68.0	5.15
MN	27-C350	1/1/1972	1	2	2.0	0	41.3	13	5.17	10.39	100.0	78.0	64.0	5.30
MN	27-C350	1/1/1972	1	1	5.6	0	41.3	13	10.72	9.78	100.0	78.0	64.0	5.30
MN	27-D350	1/1/1980	1	3	0.7	0	43.5	14	5.55	9.18	99.5	88.0	73.5	5.65
MN	27-D350	1/1/1980	1	2	1.2	0	43.5	13	10.02	8.14	99.5	88.0	73.5	5.65
MN	27-D350	1/1/1980	1	1	2.3	0	43.5	13	10.02	8.14	99.5	88.0	73.5	5.65
MS	28-1016	11/1/1986	1	3	0.8	0	62.9	5	2.20	15.59	100.0	80.5	55.0	6.35
MS	28-1016	11/1/1986	1	2	1.4	0	62.9	5	6.88	13.55	100.0	80.5	55.0	6.35

Table 78 (continued).

State	LTPP ID	Layer Construct-ion Date	Section Structure Number	Section Layer Number	Average Layer Thickness (in)	Section Age at Layer Construct-ion (yr)	MAAT (°F)	Binder Grade Code	Air Voids (V_a) (%)	Effective Binder Content (V_{be}) (%)	$P_{3/4}$ (%)	$P_{3/8}$ (%)	P_4 (%)	P_{200} (%)
MS	28-1016	11/1/1986	1	1	5.4	0	62.9	5	8.91	9.63	100.0	80.0	62.0	6.40
MS	28-1802	6/1/1982	1	3	1.3	0	65.1	4	5.19	12.60	100.0	80.5	55.0	6.35
MS	28-1802	6/1/1982	1	2	1.8	0	65.1	4	5.19	10.14	100.0	80.5	55.0	6.35
MS	28-1802	6/1/1982	1	1	4.9	0	65.1	6	6.68	9.53	100.0	79.0	56.0	6.50
MO	29-1002	4/1/1986	1	3	1.2	0	55.5	4	4.54	6.66	100.0	77.0	56.5	10.25
MO	29-1002	4/1/1986	1	2	1.6	0	55.5	4	4.54	6.66	100.0	77.0	56.5	10.25
MO	29-1002	4/1/1986	1	1	4.0	0	55.5	4	3.10	8.55	97.0	72.5	53.5	9.05
MO	29-A350	5/1/1974	1	3	1.1	0	56.1	15	2.04	8.37	96.5	59.0	40.5	3.85
MO	29-A350	5/1/1974	1	2	2.2	0	56.1	15	2.04	8.84	96.5	59.0	40.5	3.85
MO	29-A350	5/1/1974	1	1	5.6	0	56.1	15	4.04	11.53	97.5	70.0	51.5	10.15
MO	29-B320	4/1/1986	1	3	1.6	0	55.5	4	4.54	6.66	100.0	77.0	56.5	10.25
MO	29-B320	4/1/1986	1	2	1.6	0	55.5	4	4.54	6.66	100.0	77.0	56.5	10.25
MO	29-B320	4/1/1986	1	1	4.0	0	55.5	4	3.10	8.55	97.0	72.5	53.5	9.05
MO	29-B340	4/1/1986	1	3	1.4	0	55.5	4	4.54	6.66	100.0	77.0	56.5	10.25
MO	29-B340	4/1/1986	1	2	1.1	0	55.5	4	4.54	6.66	100.0	77.0	56.5	10.25
MO	29-B340	4/1/1986	1	1	3.9	0	55.5	4	3.10	8.55	97.0	72.5	53.5	9.05
MO	29-B350	4/1/1986	1	3	1.5	0	55.5	4	4.54	6.66	100.0	77.0	56.5	10.25
MO	29-B350	4/1/1986	1	2	1.3	0	55.5	4	4.54	6.66	100.0	77.0	56.5	10.25
MO	29-B350	4/1/1986	1	1	4.0	0	55.5	4	3.10	8.55	97.0	72.5	53.5	9.05
MT	30-0114	10/1/1998	1	1	7.5	0	45.9	21	4.75	7.40	100.0	73.3	45.0	5.77
MT	30-0114	7/1/2016	2	2	2.9	18	45.9	22	3.80	7.58	100.0	65.0	39.0	5.40
MT	30-0114	7/1/2016	2	1	5.0	18	45.9	21	4.75	7.40	100.0	73.3	45.0	5.77
MT	30-8129	6/1/1988	1	1	3.0	0	44.8	14	2.18	12.17	100.0	80.5	60.0	7.40
MT	30-8129	6/1/2003	2	2	4.0	15	44.8	21	4.14	10.59	100.0	73.0	40.0	3.50
MT	30-8129	6/1/2003	2	1	3.0	15	44.8	14	2.18	12.17	100.0	80.5	60.0	7.40
NE	31-0114	7/1/1995	1	1	6.6	0	52.5	3	5.64	11.68	100.0	87.0	74.0	6.90

Table 78 (continued).

State	LTPP ID	Layer Construct-ion Date	Section Structure Number	Section Layer Number	Average Layer Thickness (in)	Section Age at Layer Construct-ion (yr)	MAAT (°F)	Binder Grade Code	Air Voids (V_a) (%)	Effective Binder Content (V_{be}) (%)	$P_{3/4}$ (%)	$P_{3/8}$ (%)	P_4 (%)	P_{200} (%)
NE	31-0115	7/1/1995	1	2	6.7	0	52.5	3	5.30	11.24	100.0	90.3	76.8	6.73
NE	31-0115	7/1/1995	1	1	8.4	0	52.5	3	4.62	9.82	96.0	70.0	51.5	3.05
NE	31-0121	7/1/1995	1	2	4.8	0	52.5	3	3.28	11.03	100.0	90.3	76.8	6.73
NE	31-0121	7/1/1995	1	1	4.0	0	52.5	3	7.13	8.77	94.5	48.8	24.3	2.95
NE	31-1030	5/1/1982	1	2	2.0	0	51.7	3	1.26	12.55	98.5	93.0	75.0	10.60
NE	31-1030	5/1/1982	1	1	5.2	0	51.7	3	4.07	12.31	99.5	97.0	85.5	9.40
NE	31-A330	5/1/1982	1	2	2.0	0	51.7	3	1.26	12.55	98.5	93.0	75.0	10.60
NE	31-A330	5/1/1982	1	1	5.2	0	51.7	3	4.07	12.31	99.5	97.0	85.5	9.40
NE	31-A340	5/1/1982	1	2	1.9	0	51.7	3	1.26	12.55	98.5	93.0	75.0	10.60
NE	31-A340	5/1/1982	1	1	5.1	0	51.7	3	4.07	12.31	99.5	97.0	85.5	9.40
NE	31-A350	5/1/1982	1	2	2.0	0	51.7	3	1.26	12.55	98.5	93.0	75.0	10.60
NE	31-A350	5/1/1982	1	1	6.5	0	51.7	3	4.07	12.31	99.5	97.0	85.5	9.40
NE	31-A351	5/1/1982	1	2	2.3	0	51.7	3	1.26	12.55	98.5	93.0	75.0	10.60
NE	31-A351	5/1/1982	1	1	7.0	0	51.7	3	4.07	12.31	99.5	97.0	85.5	9.40
NE	31-A353	5/1/1982	1	3	2.3	0	51.7	3	1.26	12.55	98.5	93.0	75.0	10.60
NE	31-A353	5/1/1982	1	2	3.6	0	51.7	3	1.26	12.55	98.5	93.0	75.0	10.60
NE	31-A353	5/1/1982	1	1	4.7	0	51.7	3	4.07	12.31	99.5	97.0	85.5	9.40
NV	32-0101	8/1/1995	1	1	7.2	0	50.8	4	7.69	6.88	92.3	70.0	59.7	4.67
NH	33-1001	1/1/1981	1	2	1.2	0	46.3	3	3.03	12.53	99.0	74.5	51.0	3.60
NH	33-1001	1/1/1981	1	1	7.2	0	46.3	4	8.59	8.14	72.5	48.0	33.0	3.25
NJ	34-0502	11/1/1968	1	2	2.9	0	52.7	14	5.41	13.57	100.0	99.0	69.0	7.00
NJ	34-0502	11/1/1968	1	1	5.8	0	52.7	14	4.23	11.79	78.0	54.0	42.0	5.00
NJ	34-0502	8/1/1992	2	3	1.7	23	52.7	14	4.27	10.40	98.7	82.0	53.3	6.93
NJ	34-0502	8/1/1992	2	2	2.9	23	52.7	14	5.41	13.57	100.0	99.0	69.0	7.00
NJ	34-0502	8/1/1992	2	1	5.8	23	52.7	14	4.23	11.79	78.0	54.0	42.0	5.00
NJ	34-0503	11/1/1968	1	2	3.0	0	52.7	14	5.39	11.61	100.0	99.0	69.0	7.00

Table 78 (continued).

State	LTPP ID	Layer Construct-ion Date	Section Structure Number	Section Layer Number	Average Layer Thickness (in)	Section Age at Layer Construct-ion (yr)	MAAT (°F)	Binder Grade Code	Air Voids (V_a) (%)	Effective Binder Content (V_{be}) (%)	$P_{3/4}$ (%)	$P_{3/8}$ (%)	P_4 (%)	P_{200} (%)
NJ	34-0503	11/1/1968	1	1	6.2	0	52.7	14	4.23	11.55	78.0	54.0	42.0	5.00
NJ	34-0503	7/1/1992	2	4	1.7	23	52.7	14	4.03	10.47	98.7	82.0	53.3	6.93
NJ	34-0503	7/1/1992	2	3	3.0	23	52.7	14	4.30	9.81	93.5	69.2	51.5	6.78
NJ	34-0503	7/1/1992	2	2	3.0	23	52.7	14	5.39	11.61	100.0	99.0	69.0	7.00
NJ	34-0503	7/1/1992	2	1	6.2	23	52.7	14	4.23	11.55	78.0	54.0	42.0	5.00
NJ	34-0504	11/1/1968	1	2	3.0	0	52.7	14	8.07	11.28	100.0	99.0	69.0	7.00
NJ	34-0504	11/1/1968	1	1	5.7	0	52.7	14	8.09	11.08	78.0	54.0	42.0	5.00
NJ	34-0504	8/1/1992	2	4	1.8	23	52.7	14	3.31	12.44	99.3	87.3	60.7	6.50
NJ	34-0504	8/1/1992	2	3	2.9	23	52.7	14	1.39	11.07	95.0	71.7	54.7	5.93
NJ	34-0504	8/1/1992	2	2	3.0	23	52.7	14	8.07	11.28	100.0	99.0	69.0	7.00
NJ	34-0504	8/1/1992	2	1	5.7	23	52.7	14	8.09	11.08	78.0	54.0	42.0	5.00
NJ	34-0505	11/1/1968	1	2	3.0	0	52.7	14	5.24	11.62	100.0	99.0	69.0	7.00
NJ	34-0505	11/1/1968	1	1	6.1	0	52.7	14	5.70	11.37	78.0	54.0	42.0	5.00
NJ	34-0505	8/1/1992	2	3	1.8	23	52.7	14	3.47	11.96	99.3	87.3	60.7	6.50
NJ	34-0505	8/1/1992	2	2	3.0	23	52.7	14	5.24	11.62	100.0	99.0	69.0	7.00
NJ	34-0505	8/1/1992	2	1	6.1	23	52.7	14	5.70	11.37	78.0	54.0	42.0	5.00
NJ	34-0506	11/1/1968	1	2	3.0	0	52.7	14	9.44	11.11	100.0	99.0	69.0	7.00
NJ	34-0506	11/1/1968	1	1	6.5	0	52.7	14	5.66	11.37	78.0	54.0	42.0	5.00
NJ	34-0506	8/1/1992	2	4	1.9	23	52.7	14	3.07	12.01	99.3	87.3	60.7	6.50
NJ	34-0506	8/1/1992	2	3	2.0	23	52.7	14	2.35	10.83	95.0	71.7	54.7	5.93
NJ	34-0506	8/1/1992	2	2	0.9	23	52.7	14	9.44	11.11	100.0	99.0	69.0	7.00
NJ	34-0506	8/1/1992	2	1	6.5	23	52.7	14	5.66	11.37	78.0	54.0	42.0	5.00
NJ	34-0507	11/1/1968	1	2	3.0	0	52.7	14	6.74	10.27	100.0	99.0	69.0	7.00
NJ	34-0507	11/1/1968	1	1	5.3	0	52.7	14	4.91	9.48	78.0	54.0	42.0	5.00
NJ	34-0507	8/1/1992	2	5	1.9	23	52.7	14	3.47	9.45	99.3	87.3	60.7	6.50
NJ	34-0507	8/1/1992	2	4	2.9	23	52.7	14	2.11	12.86	95.0	71.7	54.7	5.93

Table 78 (continued).

State	LTPP ID	Layer Construct-ion Date	Section Structure Number	Section Layer Number	Average Layer Thickness (in)	Section Age at Layer Construct-ion (yr)	MAAT (°F)	Binder Grade Code	Air Voids (V_a) (%)	Effective Binder Content (V_{be}) (%)	$P_{3/4}$ (%)	$P_{3/8}$ (%)	P_4 (%)	P_{200} (%)
NJ	34-0507	8/1/1992	2	3	2.6	23	52.7	14	3.87	10.54	95.0	71.7	54.7	5.93
NJ	34-0507	8/1/1992	2	2	1.0	23	52.7	14	6.74	9.92	100.0	99.0	69.0	7.00
NJ	34-0507	8/1/1992	2	1	5.3	23	52.7	14	4.91	11.07	78.0	54.0	42.0	5.00
NJ	34-0508	11/1/1968	1	2	3.0	0	52.7	14	5.37	11.30	100.0	99.0	69.0	7.00
NJ	34-0508	11/1/1968	1	1	5.8	0	52.7	14	3.77	11.58	78.0	54.0	42.0	5.00
NJ	34-0508	8/1/1992	2	5	1.8	23	52.7	14	3.77	10.52	98.7	82.0	53.3	6.93
NJ	34-0508	8/1/1992	2	4	3.3	23	52.7	14	3.38	9.51	93.5	69.2	51.5	6.78
NJ	34-0508	8/1/1992	2	3	2.5	23	52.7	14	3.22	8.99	93.5	69.2	51.5	6.78
NJ	34-0508	8/1/1992	2	2	0.9	23	52.7	14	5.37	11.30	100.0	99.0	69.0	7.00
NJ	34-0508	8/1/1992	2	1	5.8	23	52.7	14	3.77	11.58	78.0	54.0	42.0	5.00
NJ	34-0509	11/1/1968	1	2	3.2	0	52.7	14	3.70	11.81	100.0	99.0	69.0	7.00
NJ	34-0509	11/1/1968	1	1	6.2	0	52.7	14	4.30	11.54	78.0	54.0	42.0	5.00
NJ	34-0509	7/1/1992	2	4	1.8	23	52.7	14	2.94	10.21	98.7	82.0	53.3	6.93
NJ	34-0509	7/1/1992	2	3	2.5	23	52.7	14	3.82	9.26	93.5	69.2	51.5	6.78
NJ	34-0509	7/1/1992	2	2	1.1	23	52.7	14	3.70	11.81	100.0	99.0	69.0	7.00
NJ	34-0509	7/1/1992	2	1	6.2	23	52.7	14	4.30	11.54	78.0	54.0	42.0	5.00
NJ	34-0559	11/1/1968	1	2	3.0	0	53.2	14	8.24	11.26	89.7	67.3	51.3	7.27
NJ	34-0559	11/1/1968	1	1	5.6	0	53.2	14	10.15	10.83	91.7	58.7	45.3	8.60
NJ	34-0559	7/1/1992	2	4	1.9	23	53.2	14	3.41	12.84	98.2	82.0	54.8	6.67
NJ	34-0559	7/1/1992	2	3	2.5	23	53.2	14	3.03	12.30	95.0	71.7	54.7	5.93
NJ	34-0559	7/1/1992	2	2	1.0	23	53.2	14	8.24	11.26	89.7	67.3	51.3	7.27
NJ	34-0559	7/1/1992	2	1	5.6	23	53.2	14	10.15	10.83	91.7	58.7	45.3	8.60
NJ	34-0560	11/1/1968	1	2	2.9	0	53.2	14	8.24	11.26	89.7	67.3	51.3	7.27
NJ	34-0560	11/1/1968	1	1	5.6	0	53.2	14	10.15	10.83	91.7	58.7	45.3	8.60
NJ	34-0560	7/1/1992	2	4	1.0	23	53.2	14	3.41	13.77	97.5	82.5	45.0	4.20
NJ	34-0560	7/1/1992	2	3	2.3	23	53.2	14	4.25	12.25	93.0	64.0	47.0	8.30

Table 78 (continued).

State	LTPP ID	Layer Construct-ion Date	Section Structure Number	Section Layer Number	Average Layer Thickness (in)	Section Age at Layer Construct-ion (yr)	MAAT (°F)	Binder Grade Code	Air Voids (V_a) (%)	Effective Binder Content (V_{be}) (%)	$P_{3/4}$ (%)	$P_{3/8}$ (%)	P_4 (%)	P_{200} (%)
NJ	34-0560	7/1/1992	2	2	1.0	23	53.2	14	8.24	11.26	89.7	67.3	51.3	7.27
NJ	34-0560	7/1/1992	2	1	5.6	23	53.2	14	10.15	10.83	91.7	58.7	45.3	8.60
NJ	34-0901	3/1/1970	1	2	1.5	0	53.2	14	7.50	8.00	100.0	99.0	82.5	9.45
NJ	34-0901	3/1/1970	1	1	7.4	0	53.2	14	7.50	8.00	93.0	65.5	50.0	9.10
NJ	34-0901	4/1/1998	2	4	2.2	28	53.2	18	3.41	10.16	96.2	83.5	50.8	5.64
NJ	34-0901	4/1/1998	2	3	2.7	28	53.2	16	7.50	11.40	96.2	83.5	50.8	5.64
NJ	34-0901	4/1/1998	2	1	6.5	28	53.2	14	7.50	8.00	93.0	65.5	50.0	9.10
NJ	34-0902	3/1/1970	1	2	3.0	0	53.2	14	7.50	8.00	100.0	99.0	82.5	9.45
NJ	34-0902	3/1/1970	1	1	6.7	0	53.2	14	7.50	8.00	93.0	65.5	50.0	9.10
NJ	34-0902	4/1/1998	2	4	2.6	28	53.2	18	4.62	9.72	94.9	78.3	44.3	4.91
NJ	34-0902	4/1/1998	2	3	2.5	28	53.2	16	4.62	11.40	94.9	78.3	44.3	4.91
NJ	34-0902	4/1/1998	2	2	0.6	28	53.2	14	7.50	8.00	100.0	99.0	82.5	9.45
NJ	34-0902	4/1/1998	2	1	6.7	28	53.2	14	7.50	8.00	93.0	65.5	50.0	9.10
NJ	34-0903	3/1/1970	1	2	1.4	0	52.8	14	3.04	15.49	100.0	99.0	82.5	9.45
NJ	34-0903	3/1/1970	1	1	7.4	0	52.8	14	2.19	11.91	93.0	65.5	50.0	9.10
NJ	34-0903	4/1/1998	2	4	2.1	27	52.8	16	4.48	11.39	94.9	77.9	43.6	4.83
NJ	34-0903	4/1/1998	2	3	3.3	27	52.8	16	4.48	11.16	94.9	77.9	43.6	4.83
NJ	34-0903	4/1/1998	2	1	7.4	27	52.8	14	2.19	11.91	93.0	65.5	50.0	9.10
NJ	34-0960	3/1/1970	1	2	3.6	0	52.8	14	3.21	15.46	100.0	99.0	82.5	9.45
NJ	34-0960	3/1/1970	1	1	6.4	0	52.8	14	2.74	11.85	93.0	65.5	50.0	9.10
NJ	34-0960	4/1/1998	2	4	2.7	27	52.8	16	4.78	11.04	95.4	78.0	45.1	5.29
NJ	34-0960	4/1/1998	2	3	2.1	27	52.8	16	4.78	10.81	95.4	78.0	45.1	5.29
NJ	34-0960	4/1/1998	2	2	0.9	27	52.8	14	3.21	15.46	100.0	99.0	82.5	9.45
NJ	34-0960	4/1/1998	2	1	6.4	27	52.8	14	2.74	11.85	93.0	65.5	50.0	9.10
NJ	34-0961	3/1/1970	1	2	3.0	0	52.8	14	3.21	15.46	100.0	99.0	82.5	9.45
NJ	34-0961	3/1/1970	1	1	6.3	0	52.8	14	2.74	11.85	93.0	65.5	50.0	9.10

Table 78 (continued).

State	LTPP ID	Layer Construct-ion Date	Section Structure Number	Section Layer Number	Average Layer Thickness (in)	Section Age at Layer Construct-ion (yr)	MAAT (°F)	Binder Grade Code	Air Voids (V_a) (%)	Effective Binder Content (V_{be}) (%)	$P_{3/4}$ (%)	$P_{3/8}$ (%)	P_4 (%)	P_{200} (%)
NJ	34-0961	4/1/1998	2	4	2.8	28	52.8	16	5.64	11.23	94.6	79.6	45.5	5.86
NJ	34-0961	4/1/1998	2	3	3.6	28	52.8	16	4.01	9.28	94.6	79.6	45.5	5.86
NJ	34-0961	4/1/1998	2	1	5.6	28	52.8	14	2.74	11.85	93.0	65.5	50.0	9.10
NJ	34-0962	3/1/1970	1	2	2.4	0	52.8	14	3.21	15.46	100.0	99.0	82.5	9.45
NJ	34-0962	3/1/1970	1	1	6.6	0	52.8	14	2.74	11.85	93.0	65.5	50.0	9.10
NJ	34-0962	4/1/1998	2	4	2.7	28	52.8	16	4.34	11.69	95.9	83.6	49.9	5.08
NJ	34-0962	4/1/1998	2	3	1.5	28	52.8	16	4.01	9.28	95.9	83.6	49.9	5.08
NJ	34-0962	4/1/1998	2	2	0.9	28	52.8	14	3.21	15.46	100.0	99.0	82.5	9.45
NJ	34-0962	4/1/1998	2	1	6.6	28	52.8	14	2.74	11.85	93.0	65.5	50.0	9.10
NJ	34-1003	12/1/1973	1	2	1.6	0	52.5	4	4.19	12.19	100.0	94.5	67.0	6.75
NJ	34-1003	12/1/1973	1	1	5.9	0	52.5	4	4.59	9.25	88.5	55.0	45.0	4.00
NJ	34-1003	4/1/1994	2	3	2.2	20	52.5	4	4.86	15.10	99.0	81.0	52.0	6.00
NJ	34-1003	4/1/1994	2	1	5.5	20	52.5	4	4.59	9.25	88.5	55.0	45.0	4.00
NJ	34-1011	3/1/1970	1	2	1.4	0	52.8	14	3.20	15.59	100.0	99.0	82.5	9.45
NJ	34-1011	3/1/1970	1	1	7.6	0	52.8	14	2.74	11.58	93.0	65.5	50.0	9.10
NJ	34-1011	4/1/1998	2	4	1.8	28	52.8	4	6.51	10.10	95.6	81.5	48.3	4.56
NJ	34-1011	4/1/1998	2	3	2.1	28	52.8	4	3.58	10.75	97.0	80.0	55.0	7.40
NJ	34-1011	4/1/1998	2	1	6.6	28	52.8	14	2.74	11.58	93.0	65.5	50.0	9.10
NJ	34-1030	7/1/1969	1	2	1.8	0	49.6	4	4.56	13.27	100.0	99.0	71.5	5.65
NJ	34-1030	7/1/1969	1	1	4.2	0	49.6	4	3.14	7.45	81.5	53.5	41.5	9.00
NJ	34-1030	7/1/1997	2	4	2.7	28	49.6	4	4.45	8.55	97.8	85.9	54.8	5.19
NJ	34-1030	7/1/1997	2	3	1.9	28	49.6	4	4.00	6.83	92.5	69.5	49.0	4.90
NJ	34-1030	7/1/1997	2	1	3.1	28	49.6	4	3.14	7.45	81.5	53.5	41.5	9.00
NJ	34-1033	5/1/1974	1	2	1.2	0	52.5	4	1.72	16.61	100.0	98.0	70.0	7.00
NJ	34-1033	5/1/1974	1	1	6.2	0	52.5	4	5.15	11.80	87.3	66.8	47.0	6.00
NJ	34-1033	9/1/1998	2	3	2.0	24	52.5	4	9.20	15.86	98.0	79.0	49.5	5.45

Table 78 (continued).

State	LTPP ID	Layer Construct-ion Date	Section Structure Number	Section Layer Number	Average Layer Thickness (in)	Section Age at Layer Construct-ion (yr)	MAAT (°F)	Binder Grade Code	Air Voids (V_a) (%)	Effective Binder Content (V_{be}) (%)	$P_{3/4}$ (%)	$P_{3/8}$ (%)	P_4 (%)	P_{200} (%)
NJ	34-1033	9/1/1998	2	2	0.5	24	52.5	4	1.72	16.61	100.0	98.0	70.0	7.00
NJ	34-1033	9/1/1998	2	1	6.2	24	52.5	4	5.15	11.80	87.3	66.8	47.0	6.00
NM	35-1112	6/1/1984	1	1	6.2	0	62.2	14	6.38	9.12	100.0	80.0	63.5	8.05
NY	36-0801	8/1/1994	1	2	1.2	0	48.4	4	8.51	13.27	100.0	100.0	84.0	3.00
NY	36-0801	8/1/1994	1	1	3.8	0	48.4	4	5.95	10.19	82.0	71.0	53.0	5.00
NY	36-0802	8/1/1994	1	3	0.9	0	49.4	4	10.39	12.20	100.0	100.0	83.3	2.67
NY	36-0802	8/1/1994	1	2	2.1	0	49.4	4	6.66	10.32	87.7	65.3	47.3	4.33
NY	36-0802	8/1/1994	1	1	4.6	0	49.4	4	6.51	10.62	88.0	68.2	45.0	5.62
NY	36-1644	8/1/1980	1	3	1.0	0	42.1	4	8.20	11.00	100.0	87.5	54.5	4.15
NY	36-1644	8/1/1980	1	2	1.3	0	42.1	4	6.64	8.40	100.0	100.0	73.5	5.80
NY	36-1644	8/1/1980	1	1	6.3	0	42.1	4	6.64	8.40	92.5	67.5	46.5	4.45
NY	36-B330	8/1/1980	1	3	1.0	0	42.1	4	8.20	11.00	100.0	100.0	73.5	5.80
NY	36-B330	8/1/1980	1	2	1.3	0	42.1	4	6.64	8.40	92.5	67.5	46.5	4.45
NY	36-B330	8/1/1980	1	1	6.3	0	42.1	4	6.64	8.40	92.5	67.5	46.5	4.45
NC	37-1028	5/1/1982	1	2	1.6	0	60.6	4	4.86	14.26	100.0	95.5	78.0	5.60
NC	37-1028	5/1/1982	1	1	8.2	0	60.6	4	7.37	8.68	87.5	46.0	34.0	2.60
OH	39-0105	11/1/1995	1	3	1.9	0	51.7	4	19.30	7.32	100.0	88.8	52.5	5.83
OH	39-0105	11/1/1995	1	2	2.1	0	51.7	4	19.38	5.95	92.3	69.3	50.3	5.90
OH	39-0105	11/1/1995	1	1	3.8	0	51.7	4	5.01	9.51	63.0	50.0	33.7	6.77
OH	39-0109	11/1/1995	1	3	1.8	0	51.7	4	11.73	7.42	100.0	88.8	52.5	5.83
OH	39-0109	11/1/1995	1	2	5.2	0	51.7	4	11.09	6.67	92.3	69.3	50.3	5.90
OH	39-0109	11/1/1995	1	1	3.9	0	51.7	4	5.01	6.74	85.0	13.3	7.0	3.47
OH	39-0160	11/1/1995	1	3	1.8	0	51.7	4	12.00	7.39	100.0	88.8	52.5	5.83
OH	39-0160	11/1/1995	1	2	2.1	0	51.7	4	11.14	6.66	92.3	69.3	50.3	5.90
OH	39-0160	11/1/1995	1	1	11.0	0	51.7	4	5.01	9.51	63.0	50.0	33.7	6.77
OK	40-4165	6/1/1984	1	2	2.7	0	59.1	4	4.81	5.97	100.0	94.1	72.5	7.23

Table 78 (continued).

State	LTPP ID	Layer Construct-ion Date	Section Structure Number	Section Layer Number	Average Layer Thickness (in)	Section Age at Layer Construct-ion (yr)	MAAT (°F)	Binder Grade Code	Air Voids (V_a) (%)	Effective Binder Content (V_{be}) (%)	$P_{3/4}$ (%)	$P_{3/8}$ (%)	P_4 (%)	P_{200} (%)
OK	40-4165	6/1/1984	1	1	5.5	0	59.1	4	6.48	3.62	90.5	63.0	48.0	5.38
PA	42-1597	9/1/1980	1	2	1.5	0	47.2	4	2.11	12.80	100.0	89.0	61.0	5.85
PA	42-1597	9/1/1980	1	1	4.9	0	47.2	4	7.70	8.00	84.0	51.5	35.0	4.60
PA	42-1597	7/1/2000	2	5	1.8	20	47.2	16	6.31	10.38	100.0	89.0	50.5	4.35
PA	42-1597	7/1/2000	2	4	2.4	20	47.2	16	7.01	9.65	97.0	74.0	49.5	4.70
PA	42-1597	7/1/2000	2	3	2.1	20	47.2	16	7.01	9.65	97.0	74.0	49.5	4.70
PA	42-1597	7/1/2000	2	1	4.9	20	47.2	4	7.70	8.00	84.0	51.5	35.0	4.60
PA	42-A330	9/1/1971	1	2	1.7	0	50.2	4	2.38	13.50	100.0	96.5	59.0	6.75
PA	42-A330	9/1/1971	1	1	7.0	0	50.2	4	1.84	8.90	86.5	57.0	45.0	6.85
SD	46-0804	6/1/1993	1	1	7.0	0	44.4	13	4.13	11.00	100.0	78.3	59.0	4.37
SD	46-9187	5/1/1989	1	2	2.2	0	46.4	14	6.85	10.30	99.5	74.0	55.5	6.45
SD	46-9187	5/1/1989	1	1	3.3	0	46.4	13	6.24	10.50	100.0	72.5	52.5	6.95
TX	48-1060	3/1/1986	1	2	1.7	0	71.1	4	6.62	8.64	100.0	95.0	65.0	5.75
TX	48-1060	3/1/1986	1	1	5.8	0	71.1	4	4.00	6.81	78.5	64.0	53.0	6.85
TX	48-1068	3/1/1987	1	2	3.1	0	64.2	4	4.30	11.14	100.0	81.0	53.5	6.05
TX	48-1068	3/1/1987	1	1	7.8	0	64.2	4	4.53	12.93	80.0	57.0	45.0	9.00
TX	48-1068	11/1/2000	2	3	2.5	13	64.2	16	5.75	5.16	100.0	86.0	65.5	4.50
TX	48-1068	11/1/2000	2	2	2.1	13	64.2	4	4.30	11.14	100.0	81.0	53.5	6.05
TX	48-1068	11/1/2000	2	1	7.8	13	64.2	4	4.53	12.93	80.0	57.0	45.0	9.00
TX	48-1077	1/1/1982	1	2	1.2	0	61.9	3	1.84	11.28	100.0	97.0	54.0	4.00
TX	48-1077	1/1/1982	1	1	3.7	0	61.9	4	2.35	9.41	88.0	68.0	57.0	7.00
TX	48-1122	2/1/1974	1	2	1.4	0	69.6	3	6.26	9.98	100.0	97.5	57.0	4.50
TX	48-1122	2/1/1974	1	1	1.6	0	69.6	3	4.32	11.12	97.0	67.5	46.0	5.65
UT	49-1001	11/1/1980	1	1	5.1	0	55.1	3	1.28	13.98	100.0	77.0	58.5	7.35
VT	50-1002	8/1/1984	1	2	3.0	0	45.9	14	3.37	10.78	99.5	79.0	58.5	3.70
VT	50-1002	8/1/1984	1	1	5.5	0	45.9	14	1.76	11.35	74.5	52.5	36.5	2.85

Table 78 (continued).

State	LTPP ID	Layer Construct-ion Date	Section Structure Number	Section Layer Number	Average Layer Thickness (in)	Section Age at Layer Construct-ion (yr)	MAAT (°F)	Binder Grade Code	Air Voids (V_a) (%)	Effective Binder Content (V_{be}) (%)	$P_{3/4}$ (%)	$P_{3/8}$ (%)	P_4 (%)	P_{200} (%)
VA	51-0113	11/1/1995	1	2	1.7	0	57.9	4	8.98	10.24	99.5	85.5	51.5	5.85
VA	51-0113	11/1/1995	1	1	2.3	0	57.9	4	2.65	11.22	95.5	75.2	46.5	4.62
VA	51-0114	11/1/1995	1	2	3.4	0	57.9	4	9.60	10.17	99.5	85.5	51.5	5.85
VA	51-0114	11/1/1995	1	1	3.9	0	57.9	4	6.67	10.76	95.5	75.2	46.5	4.62
VA	51-2021	5/1/1985	1	2	1.3	0	51.5	4	5.89	11.17	100.0	93.5	75.5	7.50
VA	51-2021	5/1/1985	1	1	6.2	0	51.5	4	6.74	10.09	100.0	78.0	55.0	4.00
VA	51-2021	10/1/1995	2	3	1.7	10	51.5	4	9.20	9.87	100.0	84.0	64.0	6.00
VA	51-2021	10/1/1995	2	2	1.3	10	51.5	4	5.89	11.17	100.0	93.5	75.5	7.50
VA	51-2021	10/1/1995	2	1	6.2	10	51.5	4	6.74	10.09	100.0	78.0	55.0	4.00
WI	55-0114	10/31/1997	1	3	1.9	0	43.4	18	10.01	12.18	100.0	90.0	70.3	4.87
WI	55-0114	10/31/1997	1	2	5.8	0	43.4	18	10.01	12.18	100.0	90.0	70.3	4.87
WI	55-0114	10/31/1997	1	1	11.5	0	43.4	18	6.06	11.29	98.0	82.3	62.3	2.17
WI	55-0116	10/31/1997	1	3	2.1	0	43.4	18	3.94	12.63	100.0	90.0	70.3	4.87
WI	55-0116	10/31/1997	1	2	2.0	0	43.4	18	7.82	10.86	98.0	82.3	62.3	2.17
WI	55-0116	10/31/1997	1	1	12.3	0	43.4	18	5.92	8.45	91.7	53.0	37.3	3.03
WI	55-0120	10/31/1997	1	3	1.6	0	43.4	18	9.35	12.27	100.0	90.0	70.3	4.87
WI	55-0120	10/31/1997	1	2	1.9	0	43.4	18	8.14	11.04	98.0	82.3	62.3	2.17
WI	55-0120	10/31/1997	1	1	4.7	0	43.4	18	12.26	4.46	97.3	48.0	25.3	4.13
WI	55-0806	11/30/1997	1	2	2.1	0	43.6	18	6.08	11.28	100.0	92.7	73.7	4.70
WI	55-0806	11/30/1997	1	1	5.1	0	43.6	18	5.10	11.67	99.3	88.3	69.7	3.90
WY	56-1007	7/1/1980	1	1	2.8	0	45.8	3	1.79	13.23	99.5	84.5	60.0	6.70
MB	83-0502	9/1/1971	1	3	0.2	0	37.7	2	8.34	6.08	100.0	81.0	61.0	5.00
MB	83-0502	9/1/1971	1	2	1.9	0	37.7	2	8.34	6.08	100.0	81.0	61.0	5.00
MB	83-0502	9/1/1971	1	1	2.3	0	37.7	2	10.56	5.64	100.0	81.2	61.2	5.74
MB	83-0502	9/1/1989	2	4	2.7	18	37.7	2	4.67	7.30	100.0	81.7	63.0	5.83
MB	83-0502	9/1/1989	2	3	0.2	18	37.7	2	8.34	6.08	100.0	81.0	61.0	5.00

Table 78 (continued).

State	LTPP ID	Layer Construct-ion Date	Section Structure Number	Section Layer Number	Average Layer Thickness (in)	Section Age at Layer Construct-ion (yr)	MAAT (°F)	Binder Grade Code	Air Voids (V_a) (%)	Effective Binder Content (V_{be}) (%)	$P_{3/4}$ (%)	$P_{3/8}$ (%)	P_4 (%)	P_{200} (%)
MB	83-0502	9/1/1989	2	2	1.9	18	37.7	2	8.34	6.08	100.0	81.0	61.0	5.00
MB	83-0502	9/1/1989	2	1	2.3	18	37.7	2	10.56	5.64	100.0	81.2	61.2	5.74
MB	83-0503	9/1/1971	1	3	0.2	0	37.7	2	8.34	6.13	100.0	81.0	61.0	5.00
MB	83-0503	9/1/1971	1	2	2.1	0	37.7	2	8.34	6.13	100.0	81.0	61.0	5.00
MB	83-0503	9/1/1971	1	1	2.4	0	37.7	2	10.56	4.76	100.0	81.2	61.2	5.74
MB	83-0503	9/1/1989	2	4	5.3	18	37.7	2	4.13	10.02	100.0	81.7	63.0	5.83
MB	83-0503	9/1/1989	2	3	0.2	18	37.7	2	8.34	6.13	100.0	81.0	61.0	5.00
MB	83-0503	9/1/1989	2	2	2.1	18	37.7	2	8.34	6.13	100.0	81.0	61.0	5.00
MB	83-0503	9/1/1989	2	1	2.4	18	37.7	2	10.56	4.55	100.0	81.2	61.2	5.74
MB	83-0504	9/1/1971	1	3	0.3	0	37.7	2	6.14	6.28	100.0	81.0	61.0	5.00
MB	83-0504	9/1/1971	1	2	1.9	0	37.7	2	6.14	6.28	100.0	81.0	61.0	5.00
MB	83-0504	9/1/1971	1	1	2.3	0	37.7	2	8.65	5.11	100.0	81.2	61.2	5.74
MB	83-0504	9/1/1989	2	4	5.6	18	37.7	2	3.52	9.32	100.0	81.7	63.0	5.83
MB	83-0504	9/1/1989	2	3	0.3	18	37.7	2	6.14	6.28	100.0	81.0	61.0	5.00
MB	83-0504	9/1/1989	2	2	1.9	18	37.7	2	6.14	6.28	100.0	81.0	61.0	5.00
MB	83-0504	9/1/1989	2	1	2.3	18	37.7	2	8.65	5.11	100.0	81.2	61.2	5.74
MB	83-0505	9/1/1971	1	3	0.2	0	37.7	2	8.96	5.53	100.0	81.0	61.0	5.00
MB	83-0505	9/1/1971	1	2	2.4	0	37.7	2	8.96	5.53	100.0	81.0	61.0	5.00
MB	83-0505	9/1/1971	1	1	2.7	0	37.7	2	8.31	4.94	100.0	81.2	61.2	5.74
MB	83-0505	9/1/1989	2	4	3.1	18	37.7	2	3.57	10.59	100.0	81.7	63.0	5.83
MB	83-0505	9/1/1989	2	3	0.2	18	37.7	2	8.96	5.53	100.0	81.0	61.0	5.00
MB	83-0505	9/1/1989	2	2	2.4	18	37.7	2	8.96	5.53	100.0	81.0	61.0	5.00
MB	83-0505	9/1/1989	2	1	2.7	18	37.7	2	8.31	4.94	100.0	81.2	61.2	5.74
MB	83-0506	9/1/1971	1	2	2.9	0	37.7	2	6.50	6.29	100.0	81.0	61.0	5.00
MB	83-0506	9/1/1971	1	1	2.6	0	37.7	2	8.75	5.10	100.0	81.2	61.2	5.74
MB	83-0506	9/1/1989	2	3	3.1	18	37.7	2	4.64	9.30	100.0	81.7	63.0	5.83

Table 78 (continued).

State	LTPP ID	Layer Construct-ion Date	Section Structure Number	Section Layer Number	Average Layer Thickness (in)	Section Age at Layer Construct-ion (yr)	MAAT (°F)	Binder Grade Code	Air Voids (V_a) (%)	Effective Binder Content (V_{be}) (%)	$P_{3/4}$ (%)	$P_{3/8}$ (%)	P_4 (%)	P_{200} (%)
MB	83-0506	9/1/1989	2	2	1.5	18	37.7	2	6.50	6.29	100.0	81.0	61.0	5.00
MB	83-0506	9/1/1989	2	1	2.6	18	37.7	2	8.75	5.10	100.0	81.2	61.2	5.74
MB	83-0507	9/1/1971	1	2	1.9	0	37.7	2	8.34	5.38	100.0	81.0	61.0	5.00
MB	83-0507	9/1/1971	1	1	2.3	0	37.7	2	10.56	2.55	100.0	81.2	61.2	5.74
MB	83-0507	9/1/1989	2	3	6.8	18	37.7	2	4.13	10.19	100.0	81.7	63.0	5.83
MB	83-0507	9/1/1989	2	2	0.8	18	37.7	2	8.34	5.38	100.0	81.0	61.0	5.00
MB	83-0507	9/1/1989	2	1	2.3	18	37.7	2	10.56	2.55	100.0	81.2	61.2	5.74
MB	83-0508	9/1/1971	1	2	1.9	0	37.7	2	7.28	6.36	100.0	81.0	61.0	5.00
MB	83-0508	9/1/1971	1	1	1.7	0	37.7	2	8.94	4.83	100.0	81.2	61.2	5.74
MB	83-0508	9/1/1989	2	3	6.6	18	37.7	2	3.93	9.56	100.0	80.0	60.3	5.83
MB	83-0508	9/1/1989	2	2	0.9	18	37.7	2	7.28	6.36	100.0	81.0	61.0	5.00
MB	83-0508	9/1/1989	2	1	1.7	18	37.7	2	8.94	4.83	100.0	81.2	61.2	5.74
MB	83-0509	9/1/1971	1	2	2.3	0	37.7	2	8.21	6.18	100.0	81.0	61.0	5.00
MB	83-0509	9/1/1971	1	1	2.8	0	37.7	2	8.33	5.03	100.0	81.2	61.2	5.74
MB	83-0509	9/1/1989	2	3	3.5	18	37.7	2	5.07	8.65	100.0	80.0	60.3	5.83
MB	83-0509	9/1/1989	2	2	1.3	18	37.7	2	8.21	6.18	100.0	81.0	61.0	5.00
MB	83-0509	9/1/1989	2	1	2.8	18	37.7	2	8.33	5.03	100.0	81.2	61.2	5.74
MB	83-1801	1/1/1984	1	2	2.2	0	37.7	2	4.51	10.08	100.0	89.5	63.0	5.70
MB	83-1801	1/1/1984	1	1	2.2	0	37.7	2	7.45	9.77	100.0	86.5	66.5	5.10
MB	83-6451	9/1/1971	1	3	0.2	0	37.7	2	7.85	5.93	100.0	86.0	62.0	5.00
MB	83-6451	9/1/1971	1	2	1.8	0	37.7	2	7.85	5.93	100.0	86.0	62.0	5.00
MB	83-6451	9/1/1971	1	1	2.1	0	37.7	2	8.31	6.10	100.0	83.0	61.0	6.70
MB	83-6451	9/1/1989	2	4	2.6	18	37.7	2	5.33	10.25	100.0	84.0	65.0	6.40
MB	83-6451	9/1/1989	2	3	0.2	18	37.7	2	7.85	5.93	100.0	86.0	62.0	5.00
MB	83-6451	9/1/1989	2	2	1.8	18	37.7	2	7.85	5.93	100.0	86.0	62.0	5.00
MB	83-6451	9/1/1989	2	1	2.1	18	37.7	2	8.31	6.10	100.0	83.0	61.0	6.70

Table 78 (continued).

State	LTPP ID	Layer Construct-ion Date	Section Structure Number	Section Layer Number	Average Layer Thickness (in)	Section Age at Layer Construct-ion (yr)	MAAT (°F)	Binder Grade Code	Air Voids (V_a) (%)	Effective Binder Content (V_{be}) (%)	$P_{3/4}$ (%)	$P_{3/8}$ (%)	P_4 (%)	P_{200} (%)
ON	87-1622	6/1/1976	1	3	1.1	0	47.1	14	5.79	7.98	100.0	86.0	61.5	3.80
ON	87-1622	6/1/1976	1	2	3.1	0	47.1	14	3.53	10.26	100.0	73.0	52.0	3.80
ON	87-1622	6/1/1976	1	1	1.5	0	47.1	14	9.19	3.95	100.0	95.0	84.0	4.95
ON	87-1622	7/1/1998	2	5	2.2	22	47.1	18	2.83	9.10	100.0	78.5	49.6	2.80
ON	87-1622	7/1/1998	2	4	2.4	22	47.1	18	4.41	8.50	97.5	66.5	49.8	1.70
ON	87-1622	7/1/1998	2	2	1.8	22	47.1	14	3.53	10.26	100.0	73.0	52.0	3.80
ON	87-1622	7/1/1998	2	1	1.5	22	47.1	14	9.19	3.95	100.0	95.0	84.0	4.95
QB	89-1125	8/1/1978	1	1	5.2	0	41.4	14	3.89	8.16	94.0	67.0	50.0	4.00
QB	89-1125	6/1/1996	2	2	1.9	18	41.4	18	7.34	8.79	100.0	98.0	49.0	4.85
QB	89-1125	6/1/1996	2	1	5.2	18	41.4	14	3.89	8.16	94.0	67.0	50.0	4.00
QB	89-1127	11/1/1978	1	2	1.7	0	40.7	2	2.37	11.79	100.0	86.5	60.5	3.75
QB	89-1127	11/1/1978	1	1	3.2	0	40.7	2	2.59	8.54	96.0	65.5	45.5	4.50
QB	89-1127	8/1/1994	2	3	2.5	15	40.7	14	6.59	10.01	100.0	74.0	61.5	3.20
QB	89-1127	8/1/1994	2	2	1.7	15	40.7	2	2.37	11.79	100.0	86.5	60.5	3.75
QB	89-1127	8/1/1994	2	1	3.2	15	40.7	2	2.59	8.54	96.0	65.5	45.5	4.50

APPENDIX B

TWO-WAY ANOVA RESULTS FOR ALL INDIVIDUAL SECTIONS AND ALL FWD PARAMETERS

This appendix contains detailed results of the two-way ANOVA conducted for each individual section and for each FWD parameter in Chapter 5.

Table 79. Results of the two-way ANOVA of $d_{0,OWP}/d_{0,ML}$ for individual LTPP sections.

					Question 1a			Question 1b			Question 1c		
State	LTPP ID	AC Thickness (in)	Granular Base Thickness (in)	Traffic (AADTT)	MDT	Section Age	Interaction	MDT	OWP Fatigue Cracking	Interaction	MDT	OWP Fatigue Cracking	Interaction
AL	1-0101	7.5	8	1000	S[1]	S	N[3]	Insufficient data			S	S	N/A[4]
ID	16-1010	11	6	250	S	S	S	Insufficient data			N	N	N
MT	30-0114	7.5	12	300	Insufficient data			S*[2]	S	S	S*	S	N/A
NE	31-0114	6.5	12	450	N	S	N	Insufficient data			S*	S	S
NY	36-0801	5	8	Less than 100	S*	S*	S	S*	S*	N	S*	S*	N
OK	40-4165	8	24	300	Insufficient data			Insufficient data			N	S	N
VA	51-0113	4	8	800	Insufficient data			S	N	N	S	S	S
VA	51-0114	7.5	12	800	N	S	N	N	N	N/A	S*	S	N/A
MB	83-1801	4.5	19	500	S	N	S	S	N	N	S	S	S

[1] S = Relationship between $d_{0,OWP}/d_{0,ML}$ and the factor is significant at a 95% confidence level and equal to the hypothesized relationship in Table 48. [2] S* = Relationship between $d_{0,OWP}/d_{0,ML}$ and the factor is significant at a 95% confidence level but is **not** the same as the hypothesized relationship in Table 48. [3] N = Relationship between $d_{0,OWP}/d_{0,ML}$ and the factor is not significant. [4] N/A = Insufficient FWD data to determine the effect of interactions.

Table 80. Results of the two-way ANOVA of $E_{NDT,OWP}/E_{NDT,ML}$ for individual LTPP sections.

					Question 1a			Question 1b			Question 1c		
State	LTPP ID	AC Thickness (in)	Granular Base Thickness (in)	Traffic (AADTT)	MDT	Section Age	Interaction	MDT	OWP Fatigue Cracking	Interaction	MDT	OWP Fatigue Cracking	Interaction
AL	1-0101	7.5	8	1000	S[1]	S	N[3]	Insufficient data			S	N	N/A[4]
ID	16-1010	11	6	250	N	N	S	Insufficient data			N	N	N
MT	30-0114	7.5	12	300	Insufficient data			S	S	S	S	S	N/A
NE	31-0114	6.5	12	450	N	S	N	Insufficient data			N	S	N
NY	36-0801	5	8	Less than 100	N	N	N	S	N	N	S	N	S
OK	40-4165	8	24	300	Insufficient data			Insufficient data			S*[2]	N	N
VA	51-0113	4	8	800	Insufficient data			S	N	N	S	S	S
VA	51-0114	7.5	12	800	N	S	N	N	S	N/A	N	S	N/A
MB	83-1801	4.5	19	500	S	S	S	Y	N	N	S	S	N

[1] S = Relationship between $E_{NDT,OWP}/E_{NDT,ML}$ and the factor is significant at a 95% confidence level and equal to the hypothesized relationship in Table 48. [2] S* = Relationship between $E_{NDT,OWP}/E_{NDT,ML}$ and the factor is significant at a 95% confidence level but is **not** the same as the hypothesized relationship in Table 48. [3] N = Relationship between $E_{NDT,OWP}/E_{NDT,ML}$ and the factor is not significant. [4] N/A = Insufficient FWD data to determine the effect of interactions.

Table 81. Results of the two-way ANOVA of $\log(E_{NDT,OWP}/E_{Witczak(Aging)})$ for individual LTPP sections.

					Question 1a			Question 1b			Question 1c		
State	LTPP ID	AC Thickness (in)	Granular Base Thickness (in)	Traffic (AADTT)	MDT	Section Age	Interaction	MDT	OWP Fatigue Cracking	Interaction	MDT	OWP Fatigue Cracking	Interaction
AL	1-0101	7.5	8	1000	S[1]	S*[2]	S	Insufficient data			S	N[3]	N/A[4]
ID	16-1010	11	6	250	S	S	S	Insufficient data			N	N	N
MT	30-0114	7.5	12	300	Insufficient data			S*	N	S	S	N	N/A
NE	31-0114	6.5	12	450	S*	S	N	Insufficient data			S*	S	N
NY	36-0801	5	8	Less than 100	S	N	S	S	S	S	S	N	S
OK	40-4165	8	24	300	Insufficient data			Insufficient data			S	N	N
VA	51-0113	4	8	800	Insufficient data			S	N	S	S	S	S
VA	51-0114	7.5	12	800	S	S	S	N	N	N	S	S	N/A
MB	83-1801	4.5	19	500	S	S*	N	S	N	N	S	S	S

[1] S = Relationship between $\log(E_{NDT,OWP}/E_{Witczak(Aging)})$ and the factor is significant at a 95% confidence level and equal to the hypothesized relationship in Table 48. [2] S* = Relationship between $\log(E_{NDT,OWP}/E_{Witczak(Aging)})$ and the factor is significant at a 95% confidence level but is **not** the same as the hypothesized relationship in Table 48. [3] N = Relationship between $\log(E_{NDT,OWP}/E_{Witczak(Aging)})$ and the factor is not significant. [4] N/A = Insufficient FWD data to determine the effect of interactions.

Table 82. Results of the two-way ANOVA of $\log(E_{NDT,OWP}/E_{Witczak(No\ aging)})$ for individual LTPP sections.

					Question 1a			Question 1b			Question 1c		
State	LTPP ID	AC Thickness (in)	Granular Base Thickness (in)	Traffic (AADTT)	MDT	Section Age	Interaction	MDT	OWP Fatigue Cracking	Interaction	MDT	OWP Fatigue Cracking	Interaction
AL	1-0101	7.5	8	1000	N[3]	S*[2]	S[1]	Insufficient data			N	N	N/A[4]
ID	16-1010	11	6	250	S	S	S	Insufficient data			S	S*	N
MT	30-0114	7.5	12	300	Insufficient data			S*	S*	S	S*	N	N/A
NE	31-0114	6.5	12	450	S*	N	N	Insufficient data			S*	S*	N
NY	36-0801	5	8	Less than 100	N	S*	N	S	N	N	S	N	N
OK	40-4165	8	24	300	Insufficient data			Insufficient data			S	N	N
VA	51-0113	4	8	800	Insufficient data			S	N	S	S	S	S
VA	51-0114	7.5	12	800	N	S*	N	N	N	N	N	N	N/A
MB	83-1801	4.5	19	500	S	S*	N	S	N	N	S	S	S

[1] S = Relationship between $\log(E_{NDT,OWP}/E_{Witczak(No\ aging)})$ and the factor is significant at a 95% confidence level and equal to the hypothesized relationship in Table 48. [2] S* = Relationship between $\log(E_{NDT,OWP}/E_{Witczak(No\ aging)})$ and the factor is significant at a 95% confidence level but is **not** the same as the hypothesized relationship in Table 48. [3] N = Relationship between $\log(E_{NDT,OWP}/E_{Witczak(No\ aging)})$ and the factor is not significant. [4] N/A = Insufficient FWD data to determine the effect of interactions

APPENDIX C

PERFORMANCE HISTORY PLOTS USED TO DEFINE SECTION AGE BINS FOR ALL INDIVIDUAL SECTIONS AND ALL FWD PARAMETERS

This appendix contains performance history plots used to define section age bins used for the two-way ANOVA in Chapter 5. Thirty-six plots are shown, one for each individual section and each FWD parameter.

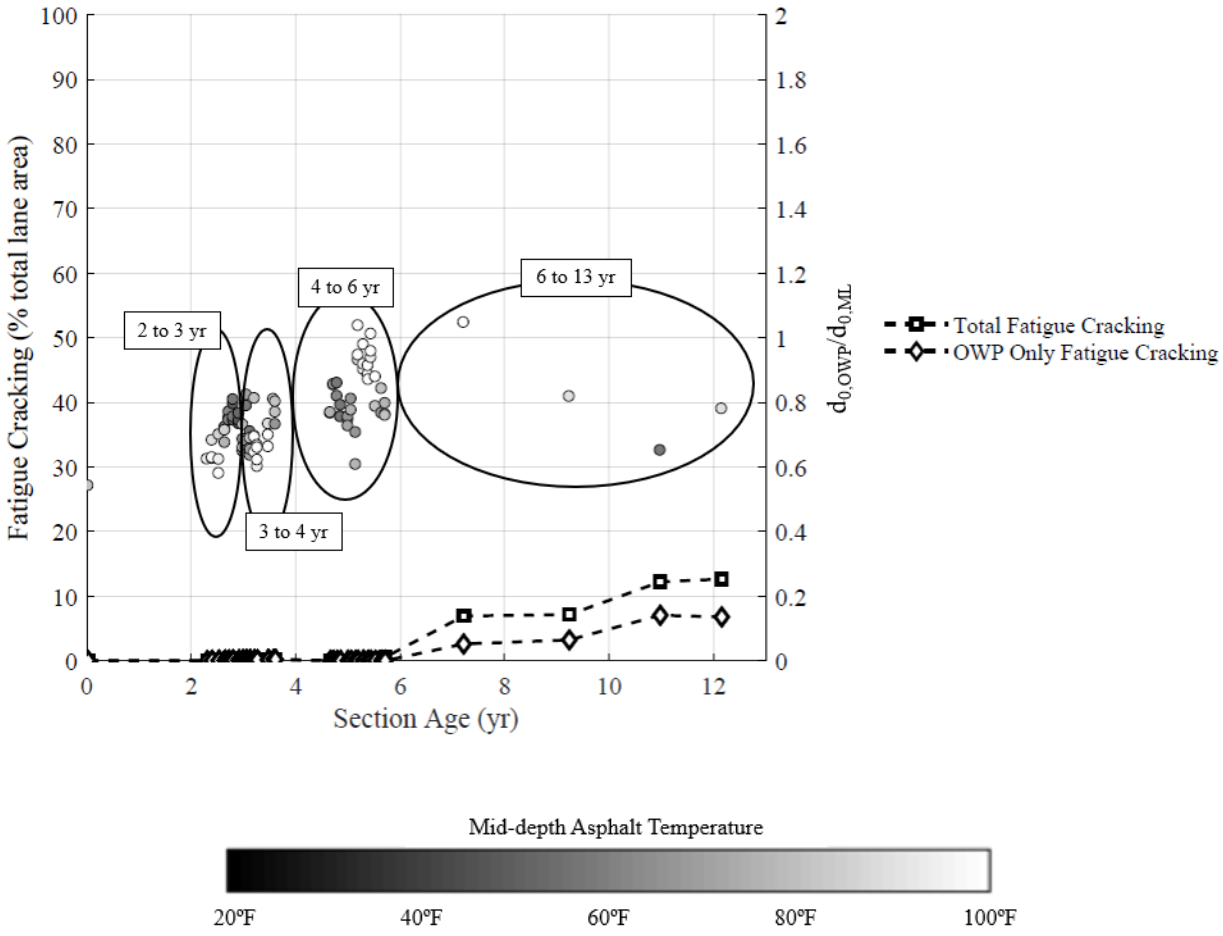

Figure 145. Performance history plot used to establish section age bin categories for two-way ANOVA ($d_{0,OWP}/d_{0,ML}$, LTPP Section 1-0101, Alabama).

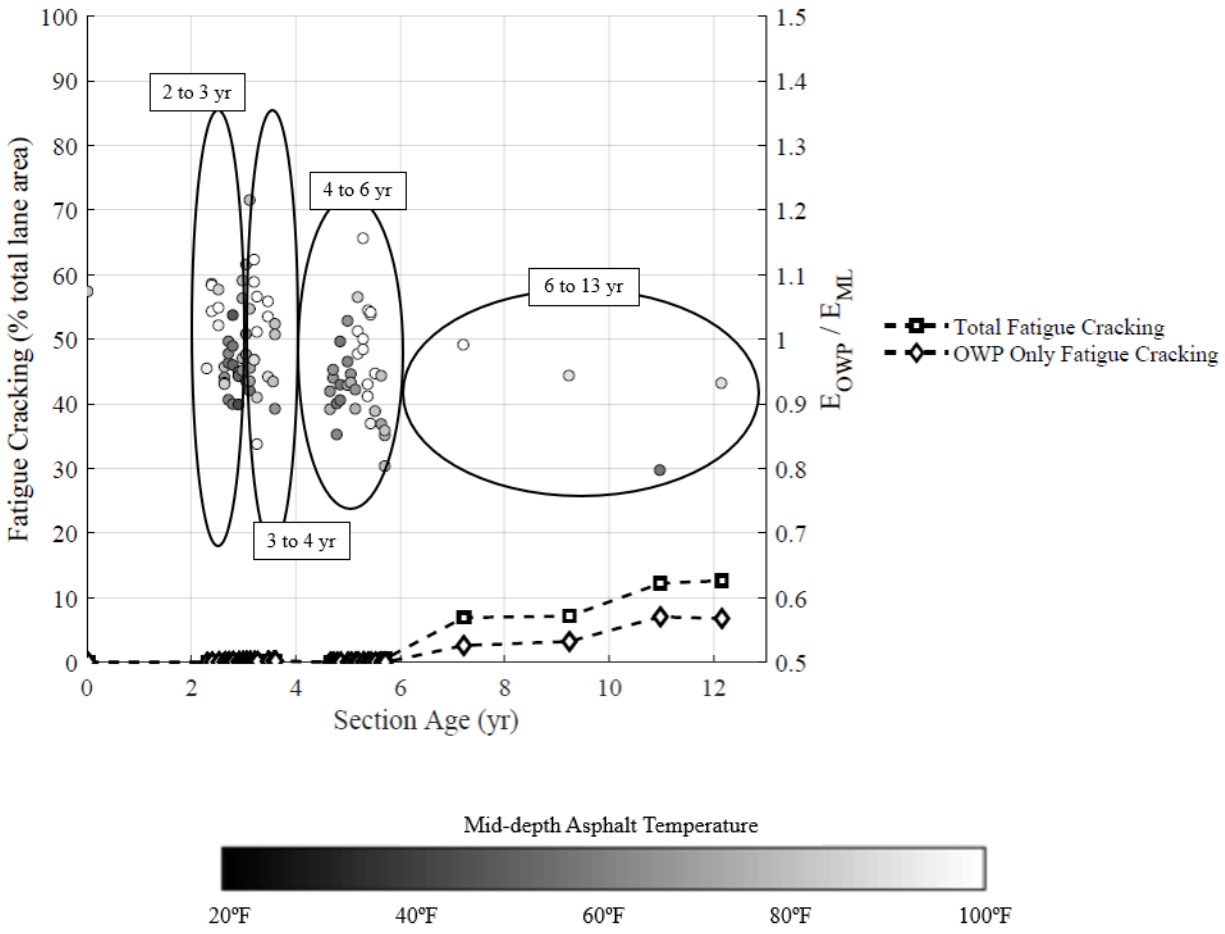

Figure 146. Performance history plot used to establish section age bin categories for two-way ANOVA ($E_{NDT,OWP}/E_{NDT,ML}$, LTPP Section 1-0101, Alabama).

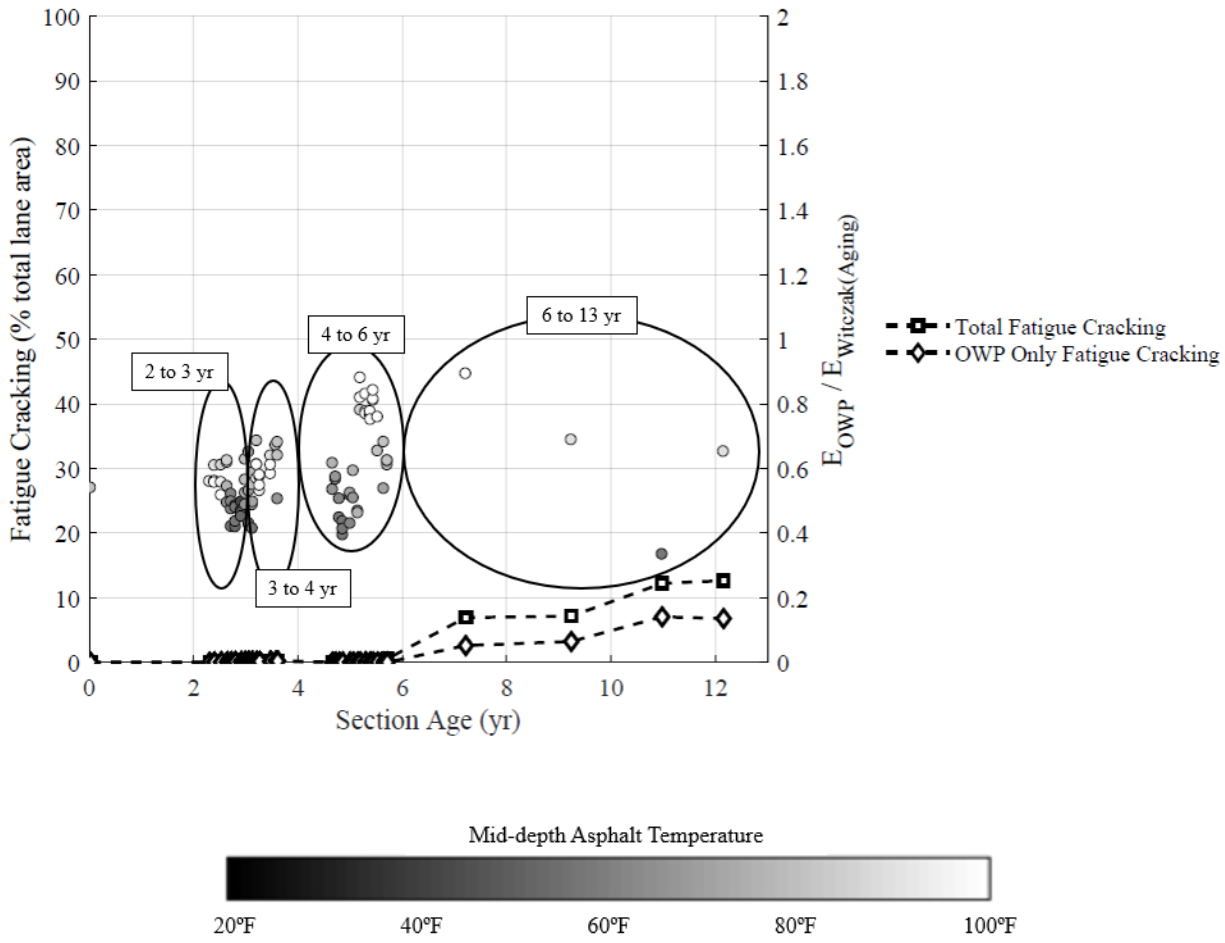

Figure 147. Performance history plot used to establish section age bin categories for two-way ANOVA ($E_{NDT,OWP}/E_{Witczak(Aging)}$, LTPP Section 1-0101, Alabama).

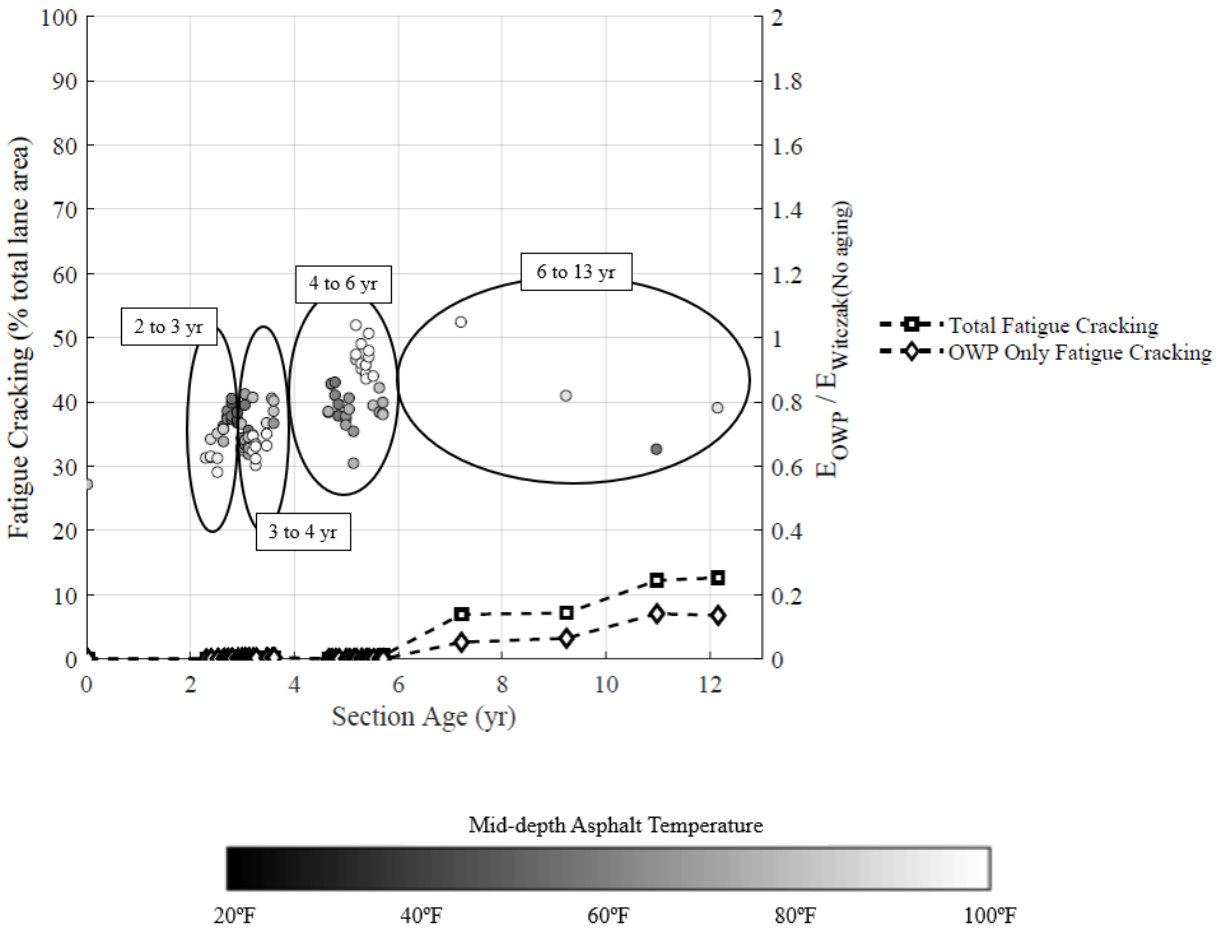

Figure 148. Performance history plot used to establish section age bin categories for two-way ANOVA ($E_{NDT,OWP}/E_{Witczak(No\ aging)}$, LTPP Section 1-0101, Alabama).

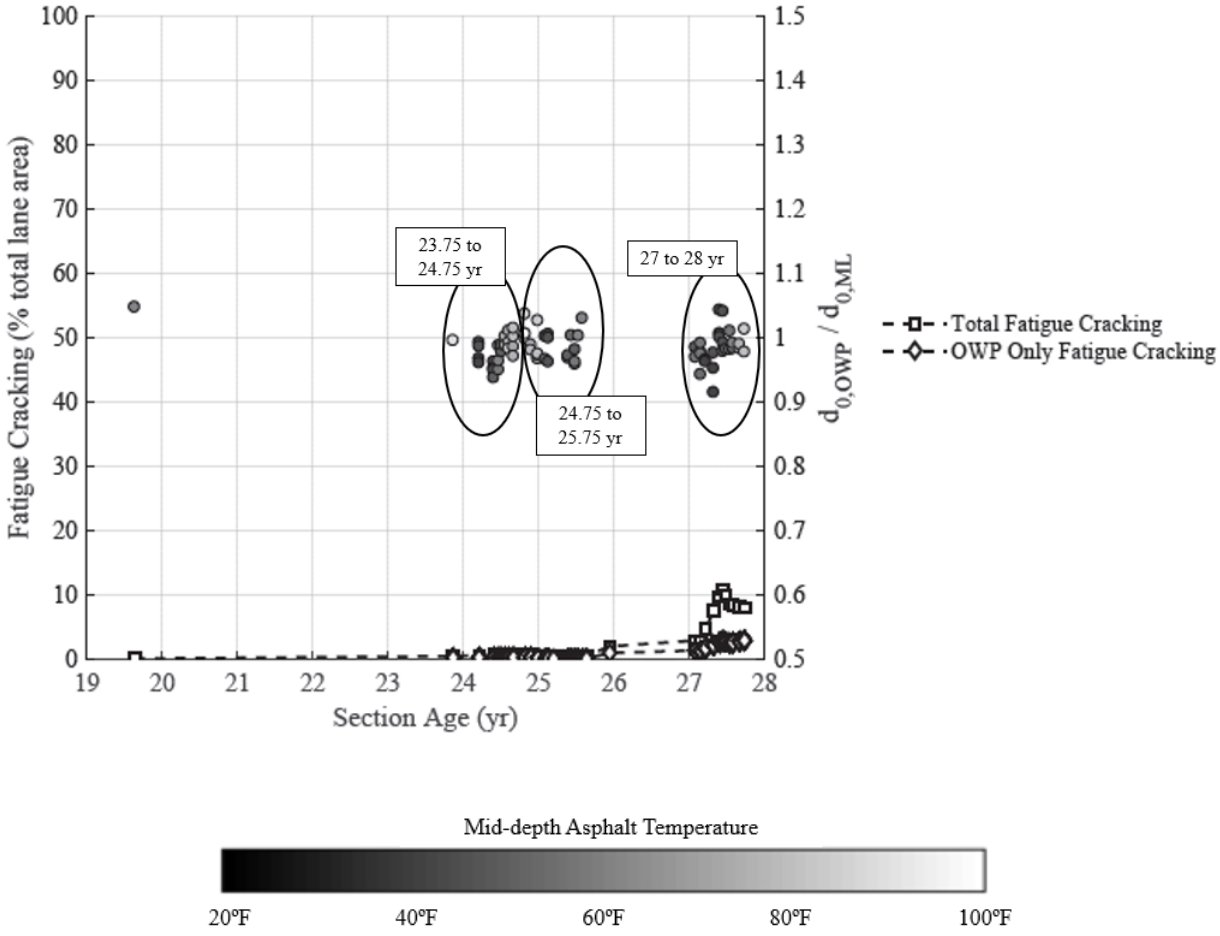

Figure 149. Performance history plot used to establish section age bin categories for two-way ANOVA ($d_{0,OWP}/d_{0,ML}$, LTPP Section 16-1010, Idaho).

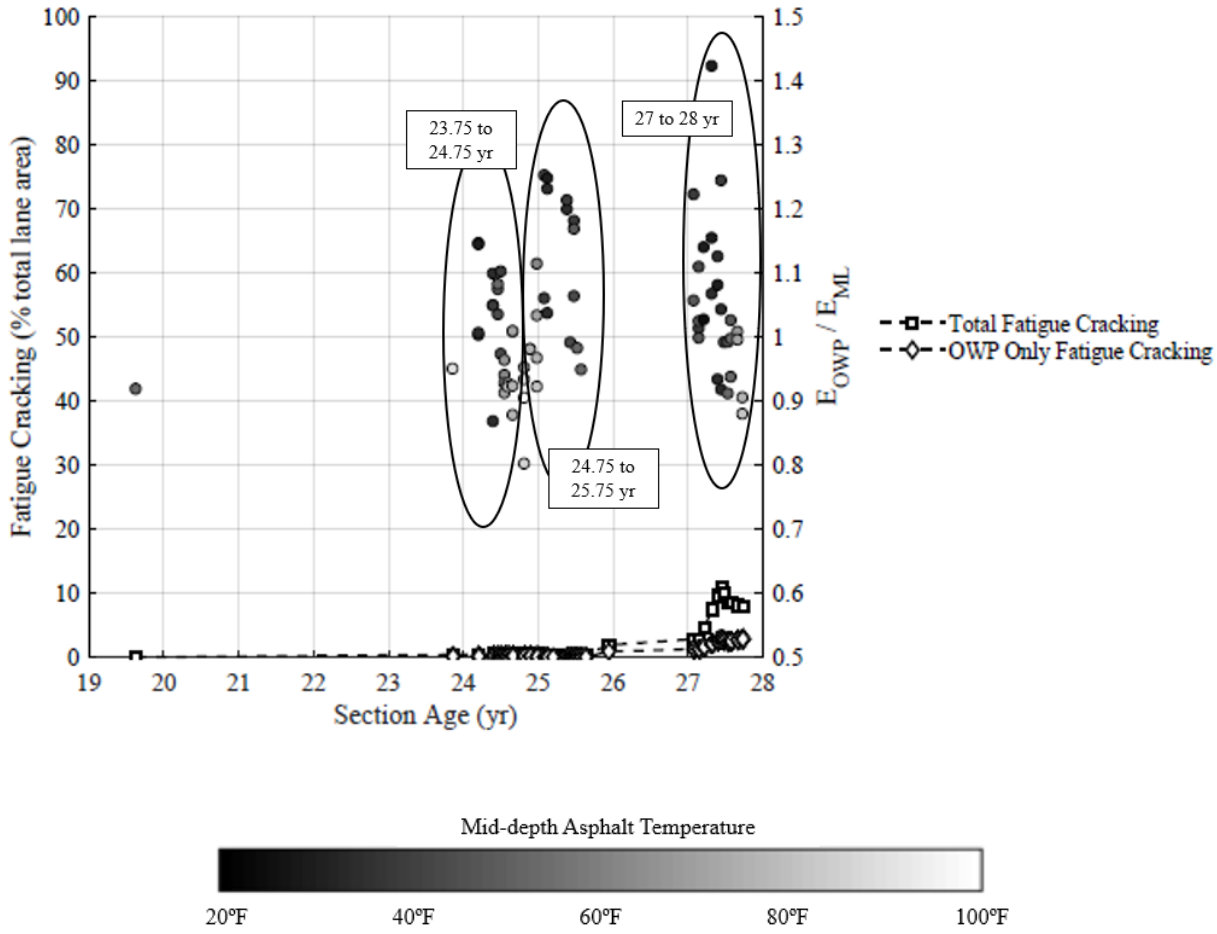

Figure 150. Performance history plot used to establish section age bin categories for two-way ANOVA ($E_{NDT,OWP}/E_{NDT,ML}$, LTPP Section 16-1010, Idaho).

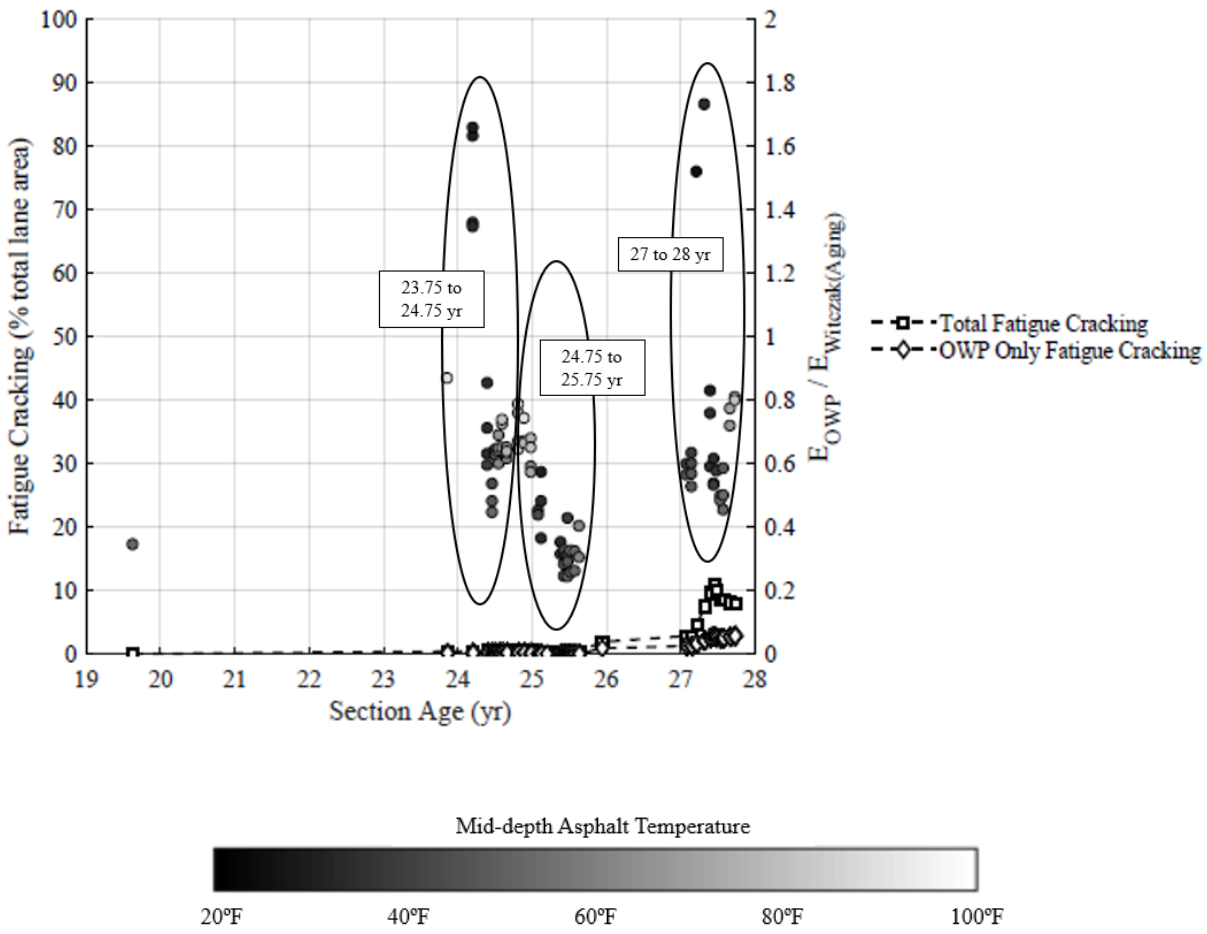

Figure 151. Performance history plot used to establish section age bin categories for two-way ANOVA ($E_{NDT,OWP}/E_{Witczak(Aging)}$, LTPP Section 16-1010, Idaho).

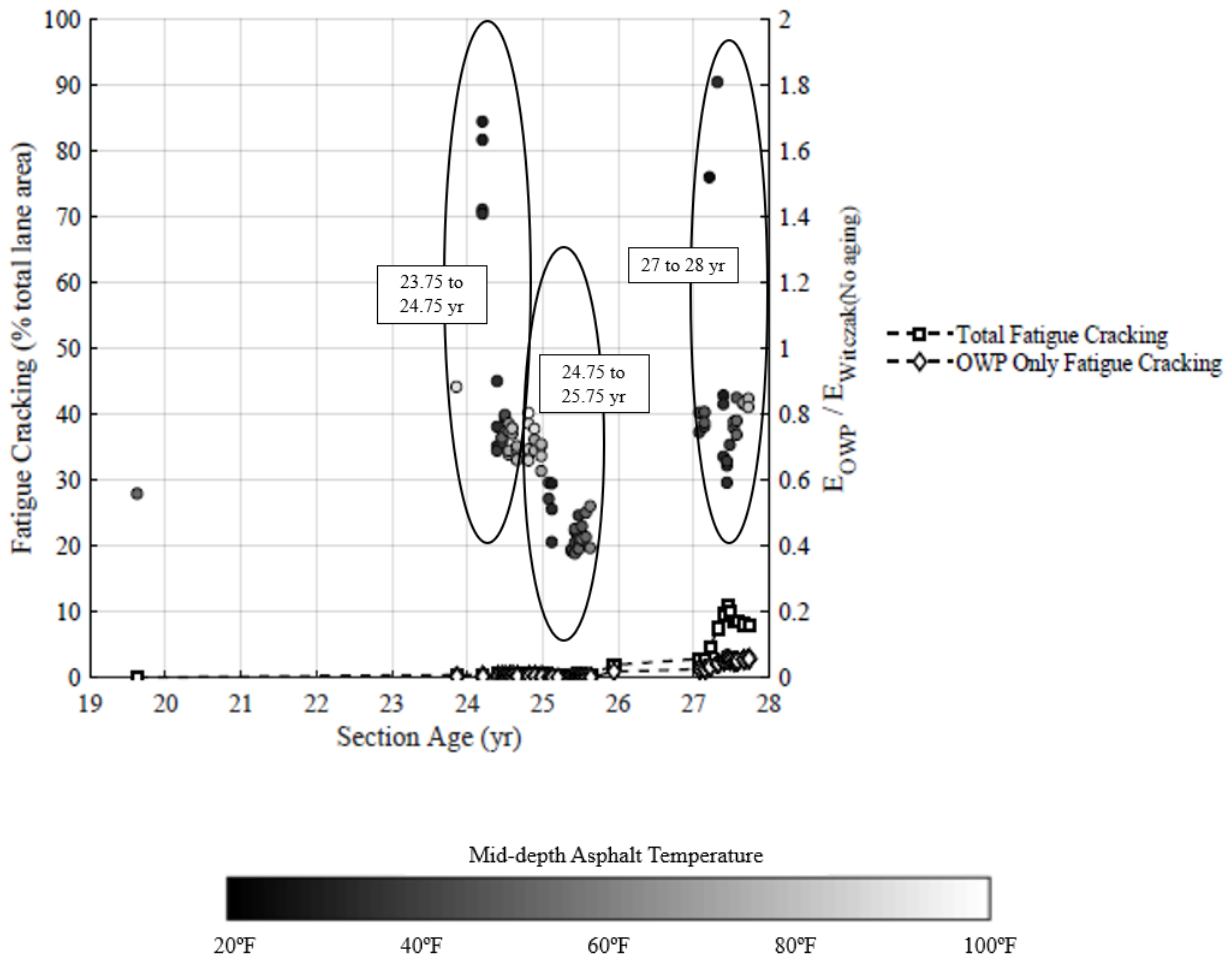

Figure 152. Performance history plot used to establish section age bin categories for two-way ANOVA ($E_{NDT,OWP}/E_{Witczak(No\ aging)}$, LTPP Section 16-1010, Idaho).

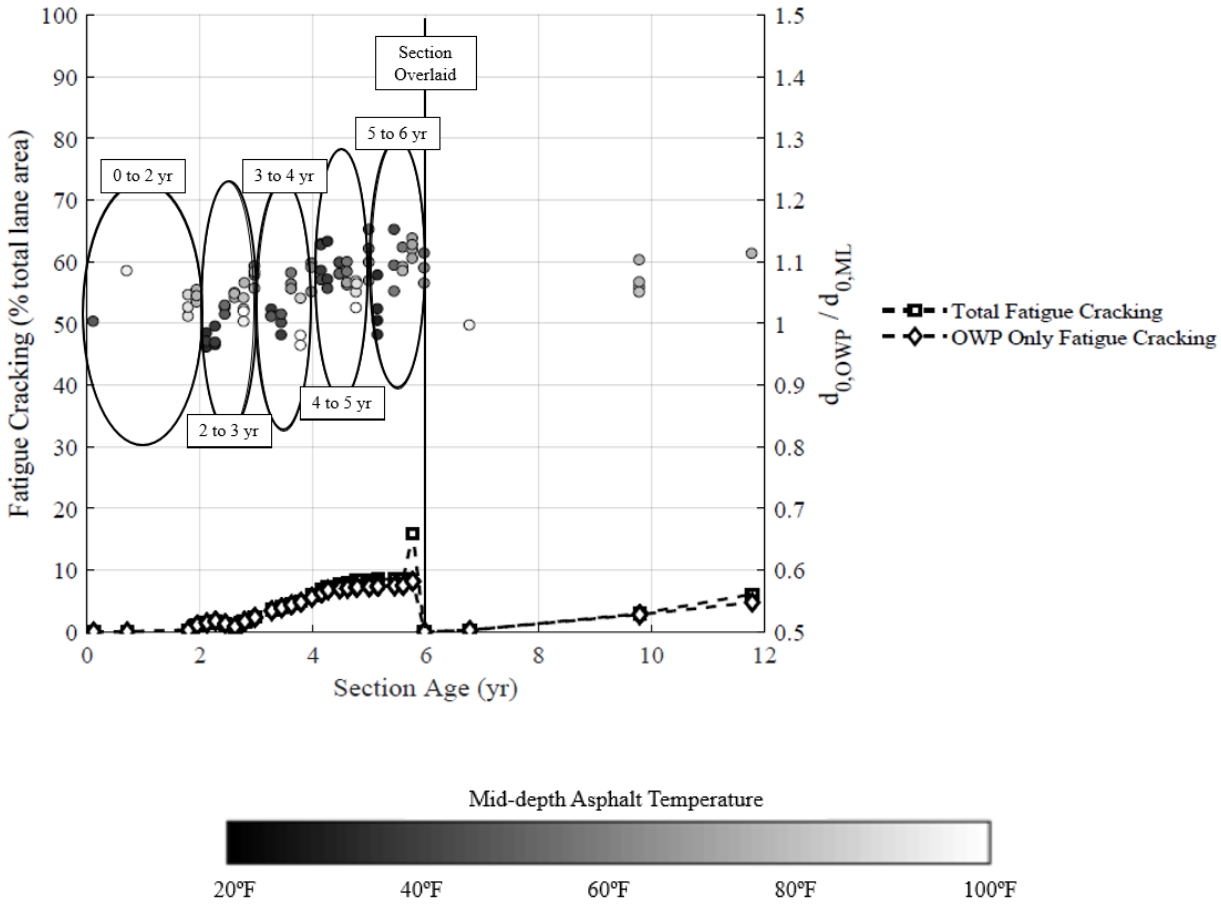

Figure 153. Performance history plot used to establish section age bin categories for two-way ANOVA ($d_{0,OWP}/d_{0,ML}$, LTPP Section 30-0114, Montana).

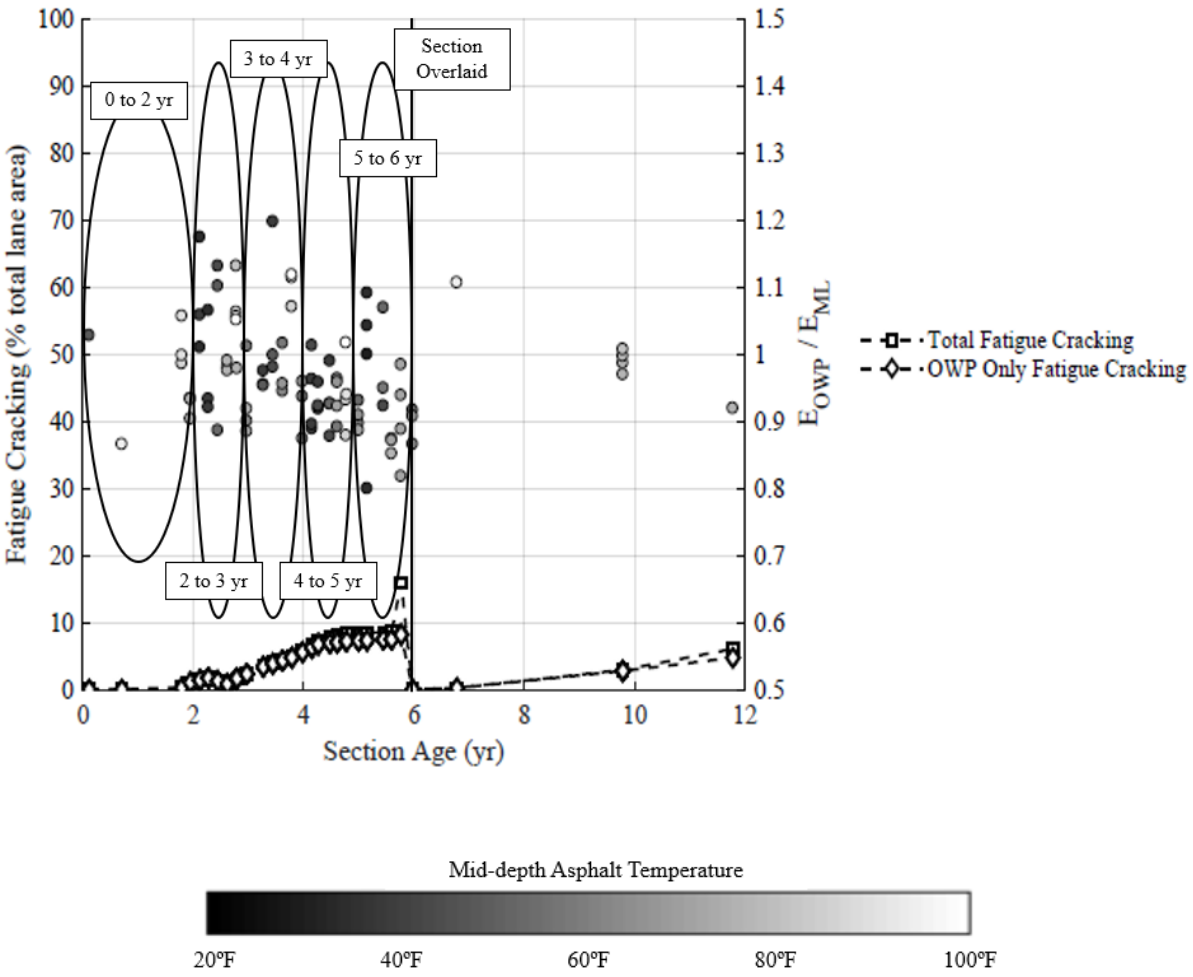

Figure 154. Performance history plot used to establish section age bin categories for two-way ANOVA ($E_{NDT,OWP}/E_{NDT,ML}$, LTPP Section 30-0114, Montana).

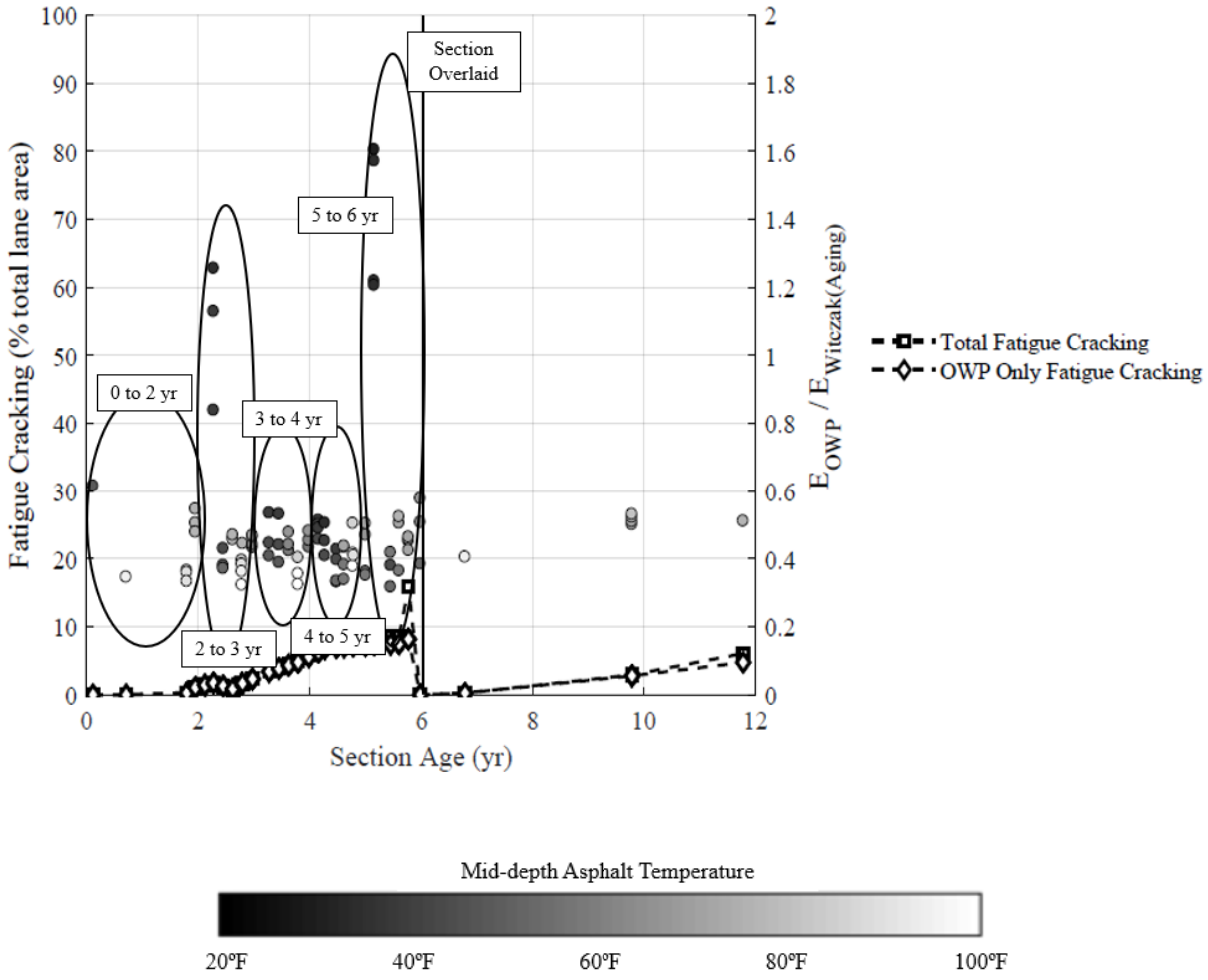

Figure 155. Performance history plot used to establish section age bin categories for two-way ANOVA ($E_{NDT,OWP}/E_{Witczak(Aging)}$, LTPP Section 30-0114, Montana).

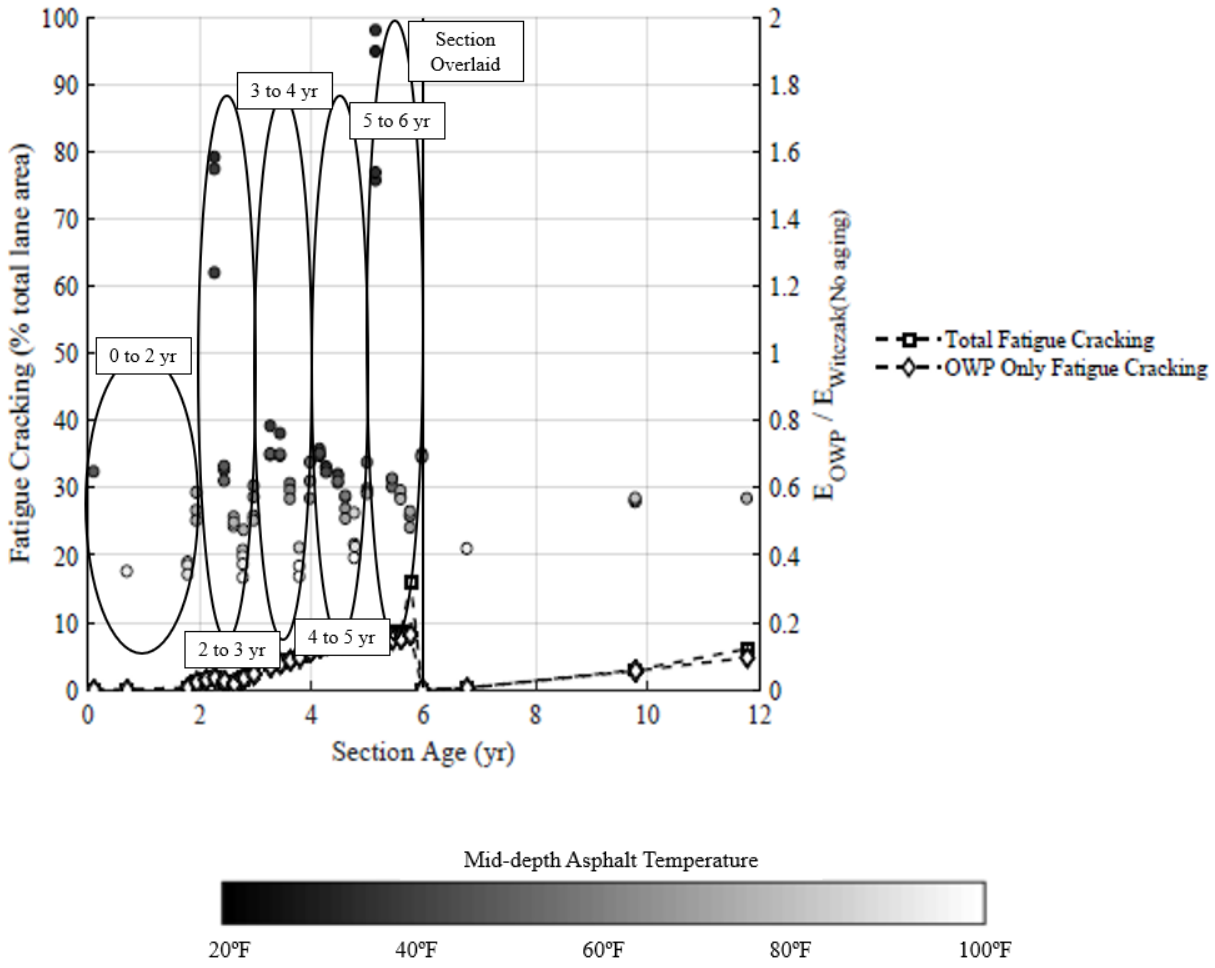

Figure 156. Performance history plot used to establish section age bin categories for two-way ANOVA ($E_{NDT,OWP}/E_{Witczak(No\ aging)}$, LTPP Section 30-0114, Montana).

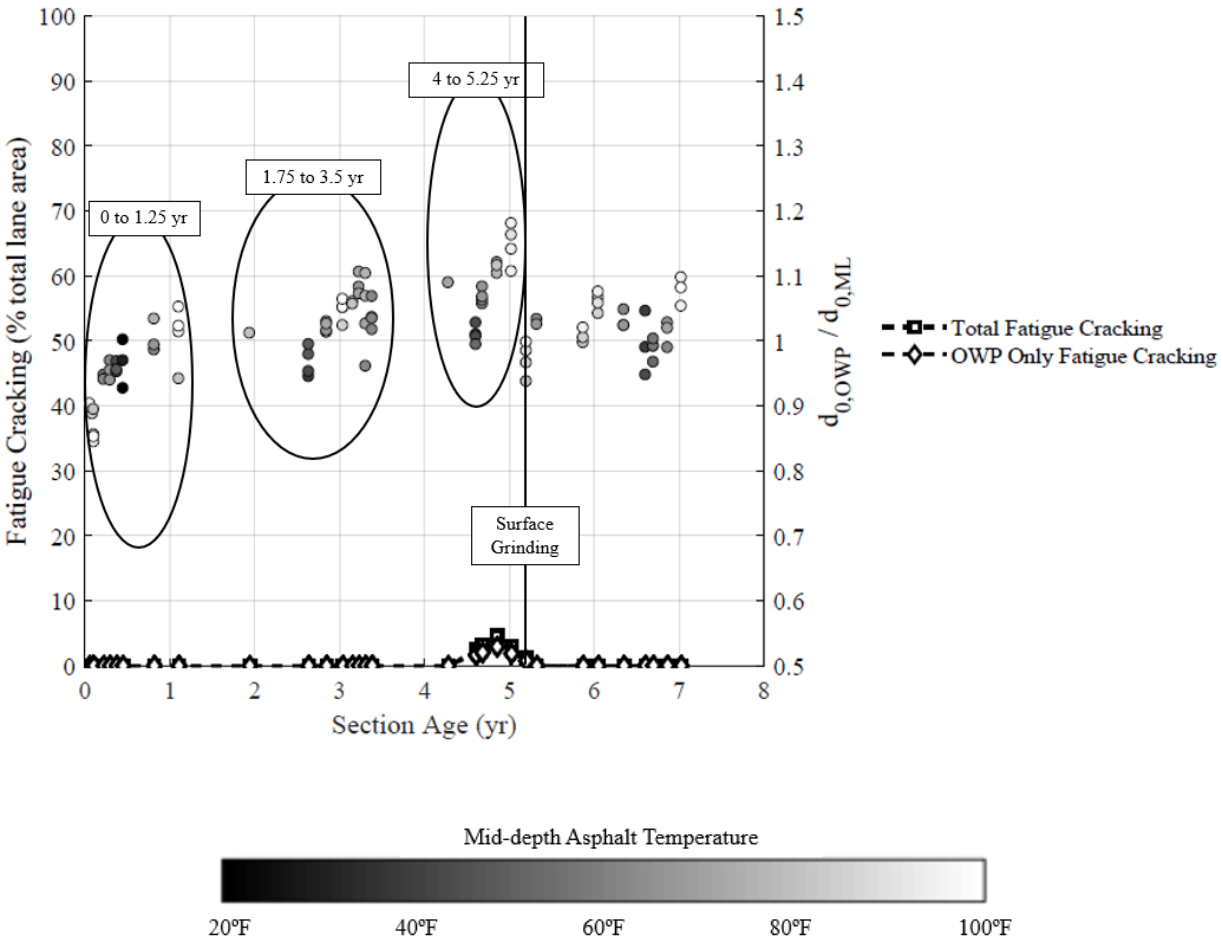

Figure 157. Performance history plot used to establish section age bin categories for two-way ANOVA ($d_{0,OWP}/d_{0,ML}$, LTPP Section 31-0114, Nebraska).

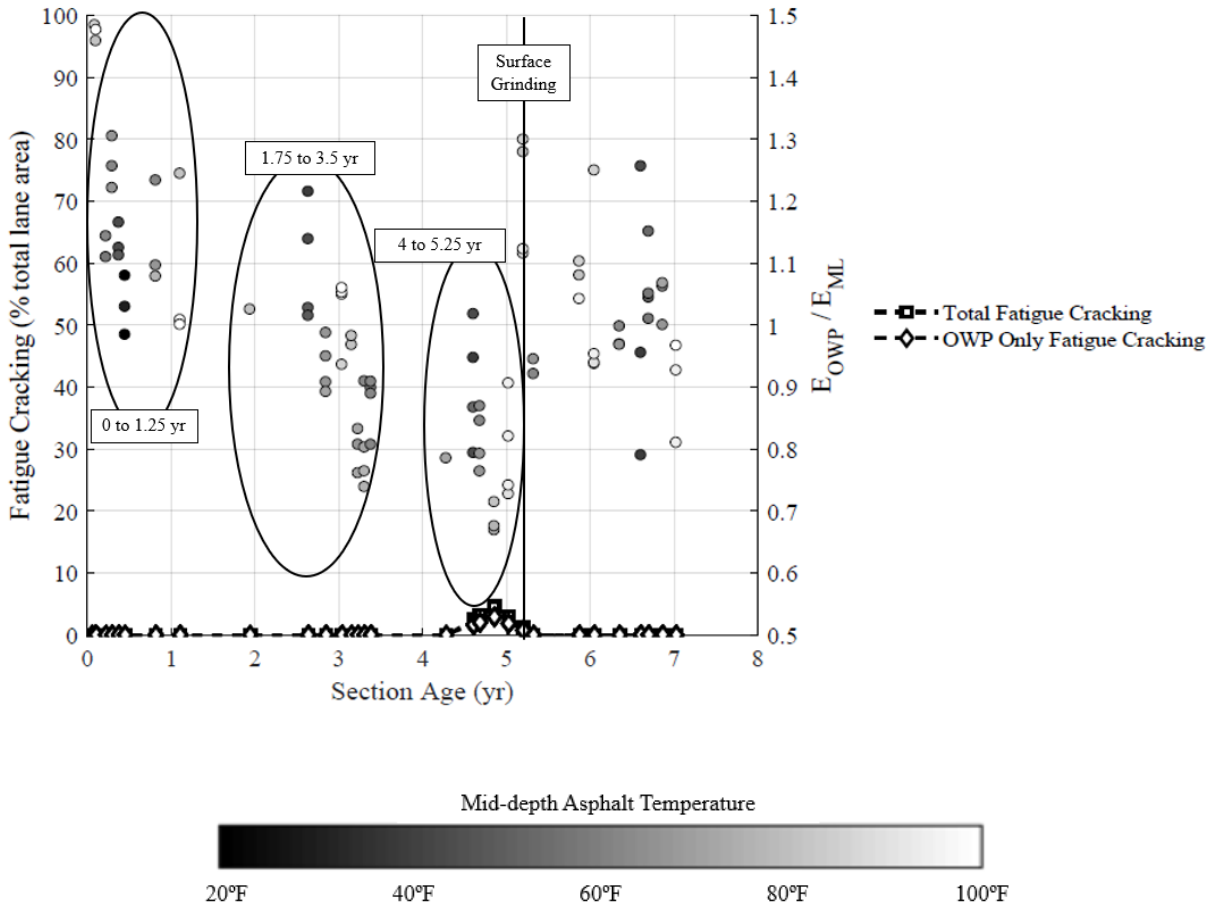

Figure 158. Performance history plot used to establish section age bin categories for two-way ANOVA ($E_{NDT,OWP}/E_{NDT,ML}$, LTPP Section 31-0114, Nebraska).

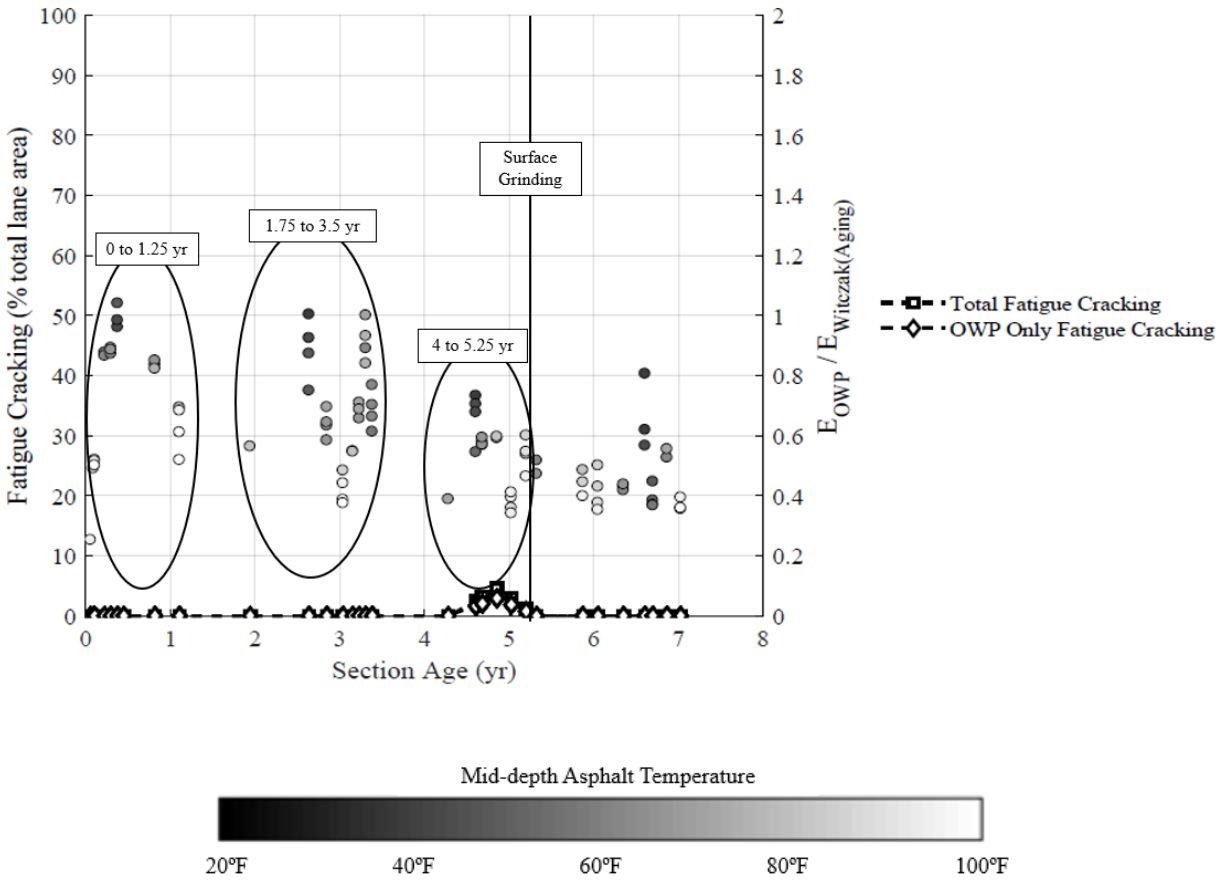

Figure 159. Performance history plot used to establish section age bin categories for two-way ANOVA ($E_{NDT,OWP}/E_{Witczak(Aging)}$, LTPP Section 31-0114, Nebraska).

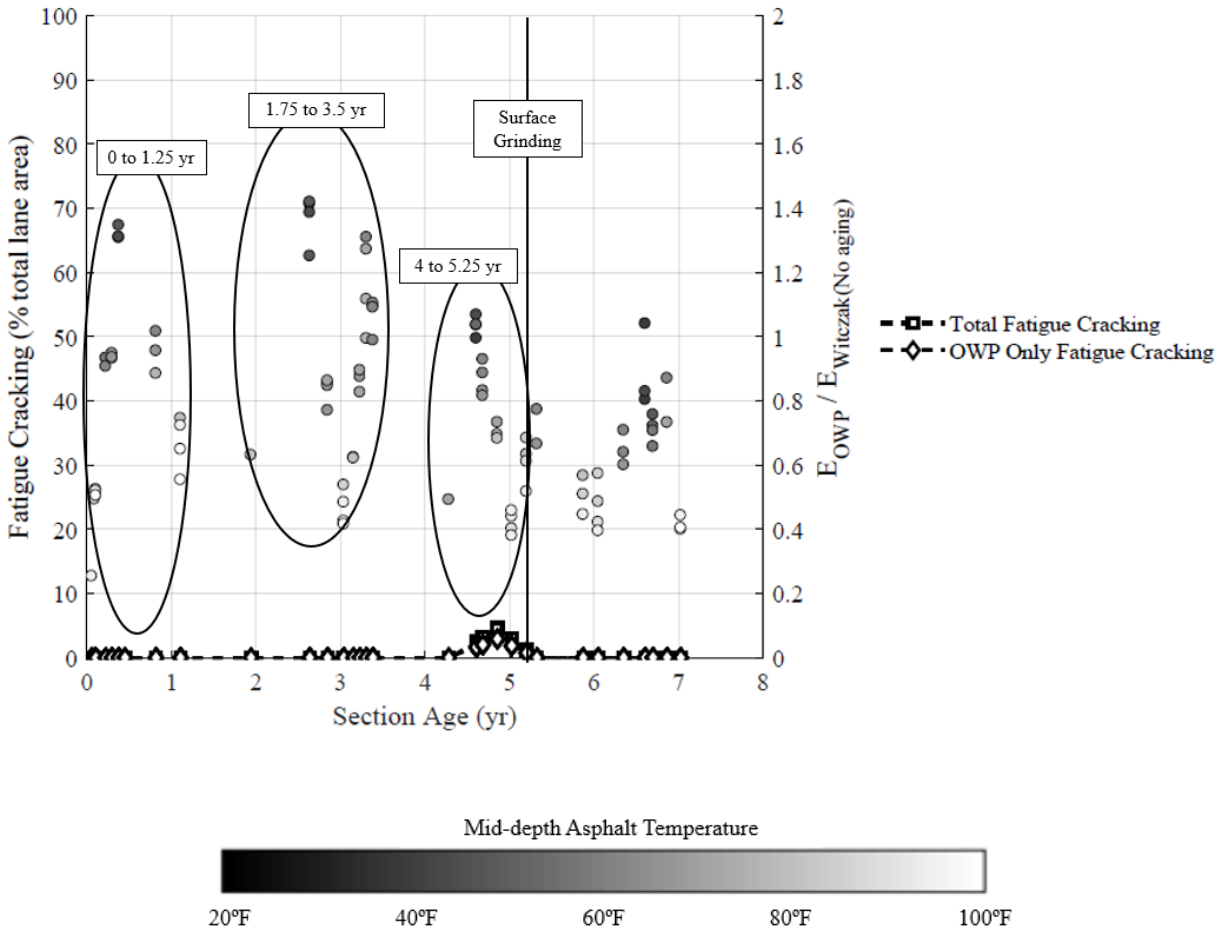

Figure 160. Performance history plot used to establish section age bin categories for two-way ANOVA ($E_{NDT,OWP}/E_{Witczak(No\ aging)}$, LTPP Section 31-0114, Nebraska).

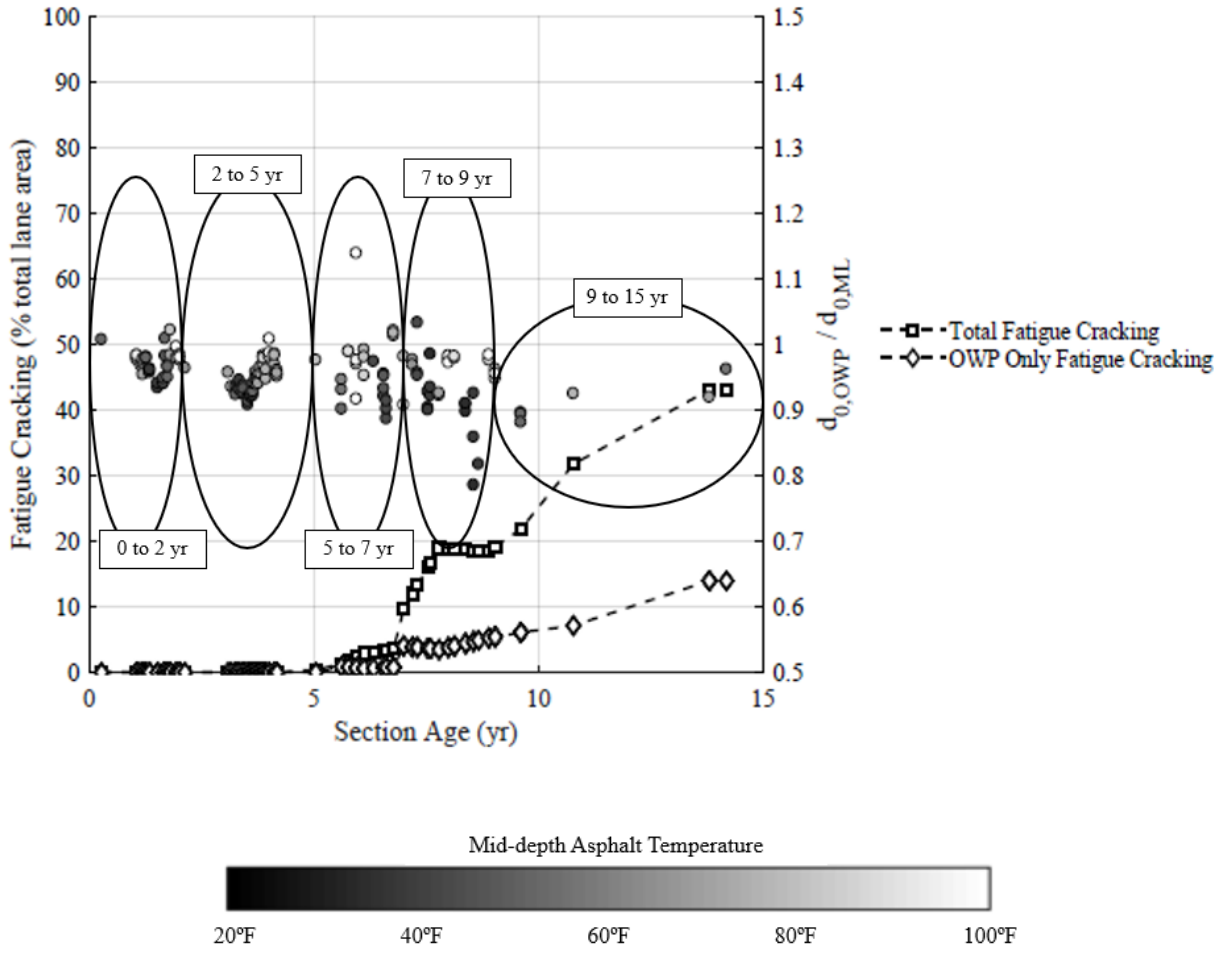

Figure 161. Performance history plot used to establish section age bin categories for two-way ANOVA ($d_{0,OWP}/d_{0,ML}$, LTPP Section 36-0801, New York).

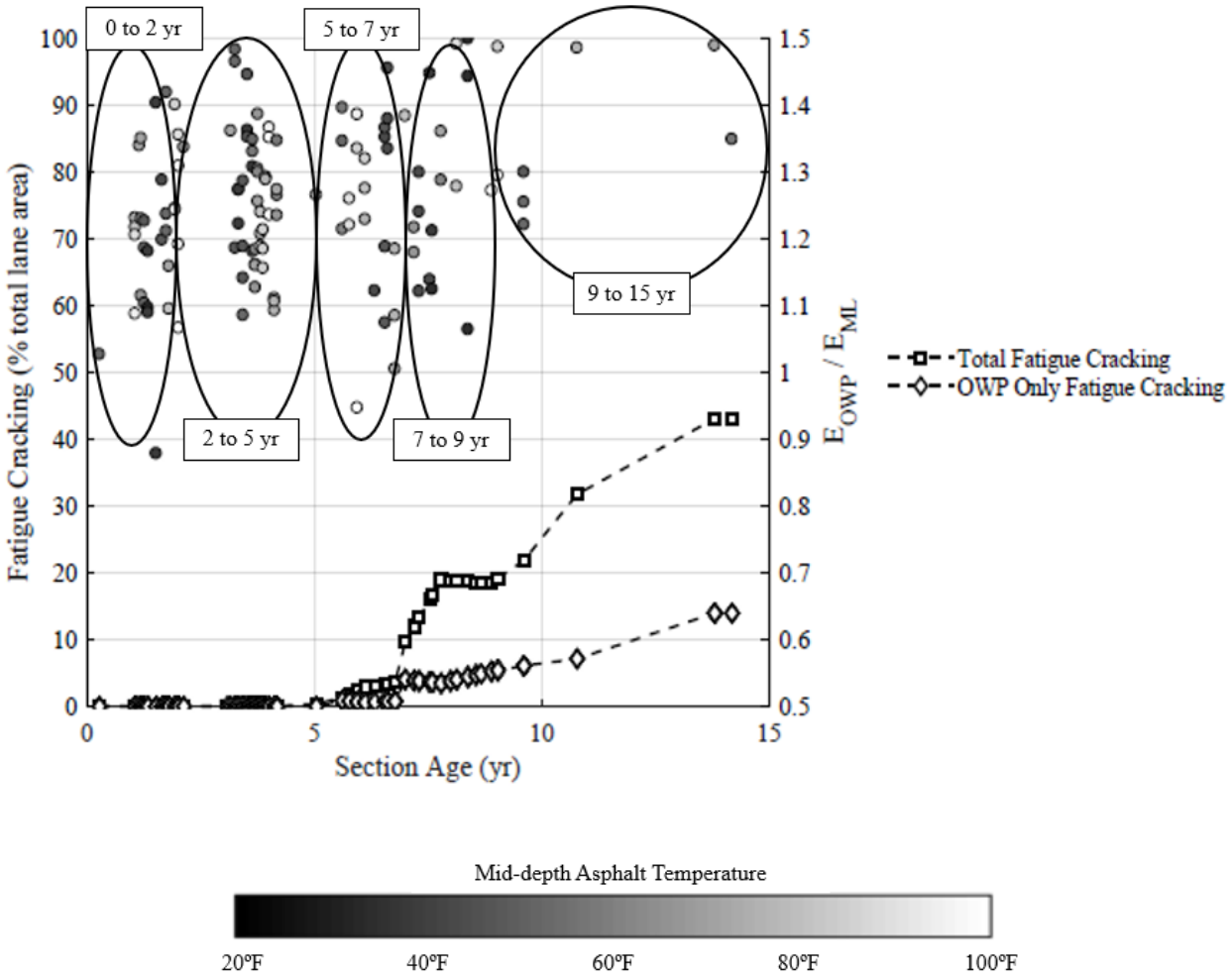

Figure 162. Performance history plot used to establish section age bin categories for two-way ANOVA ($E_{NDT,OWP}/E_{NDT,ML}$, LTPP Section 36-0801, New York).

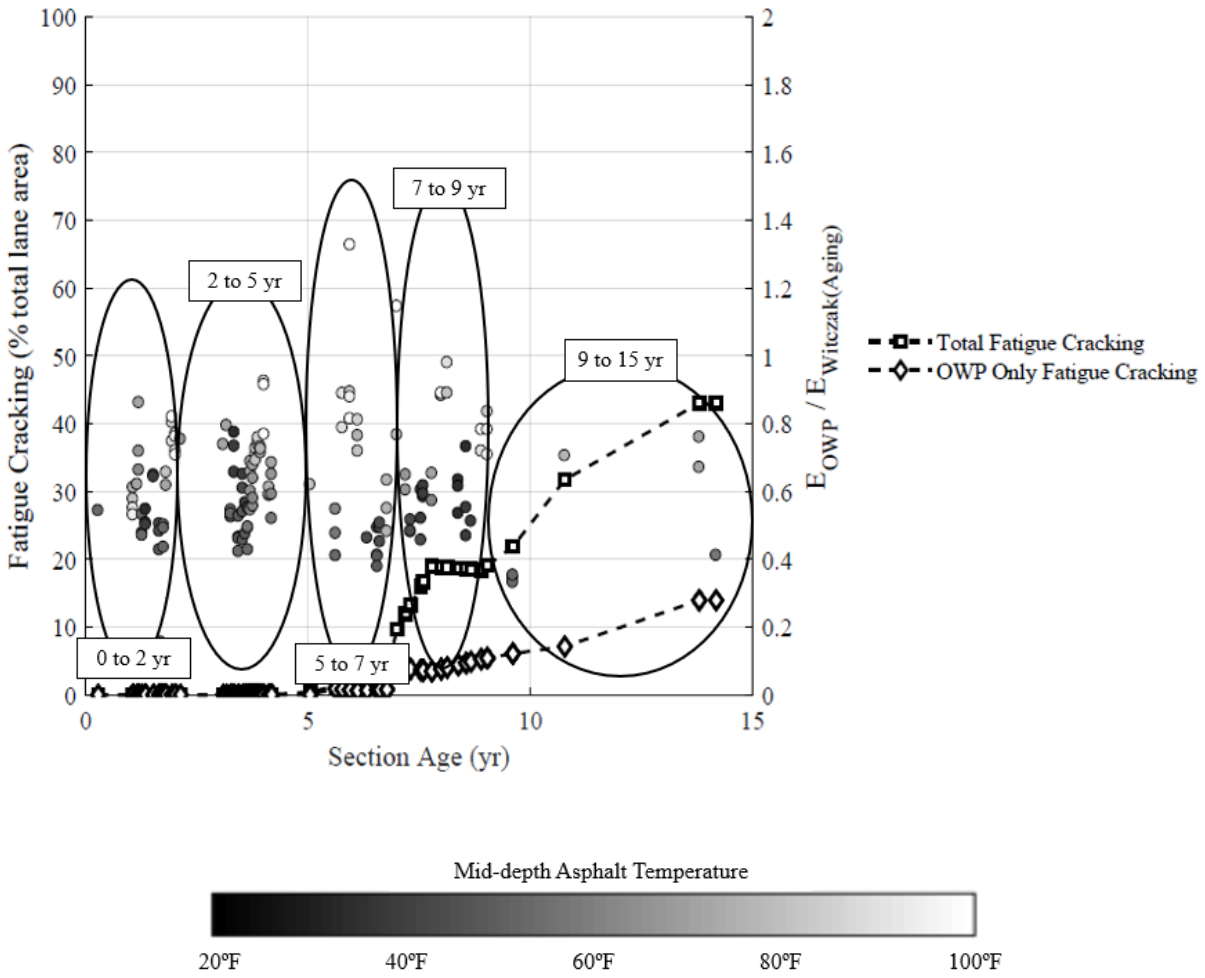

Figure 163. Performance history plot used to establish section age bin categories for two-way ANOVA ($E_{NDT,OWP}/E_{Witczak(Aging)}$, LTPP Section 36-0801, New York).

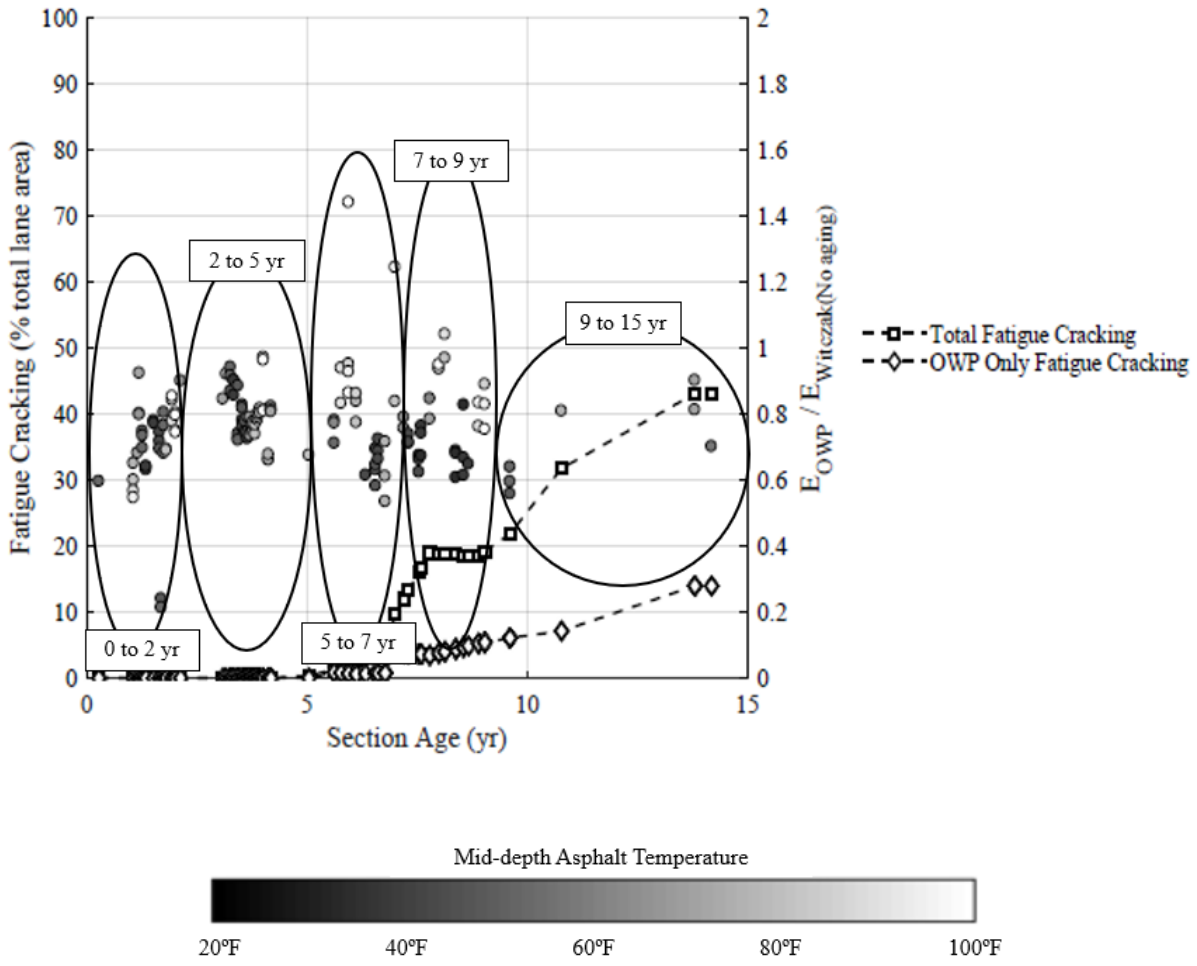

Figure 164. Performance history plot used to establish section age bin categories for two-way ANOVA ($E_{NDT,OWP}/E_{Witczak(No\ aging)}$, LTPP Section 36-0801, New York).

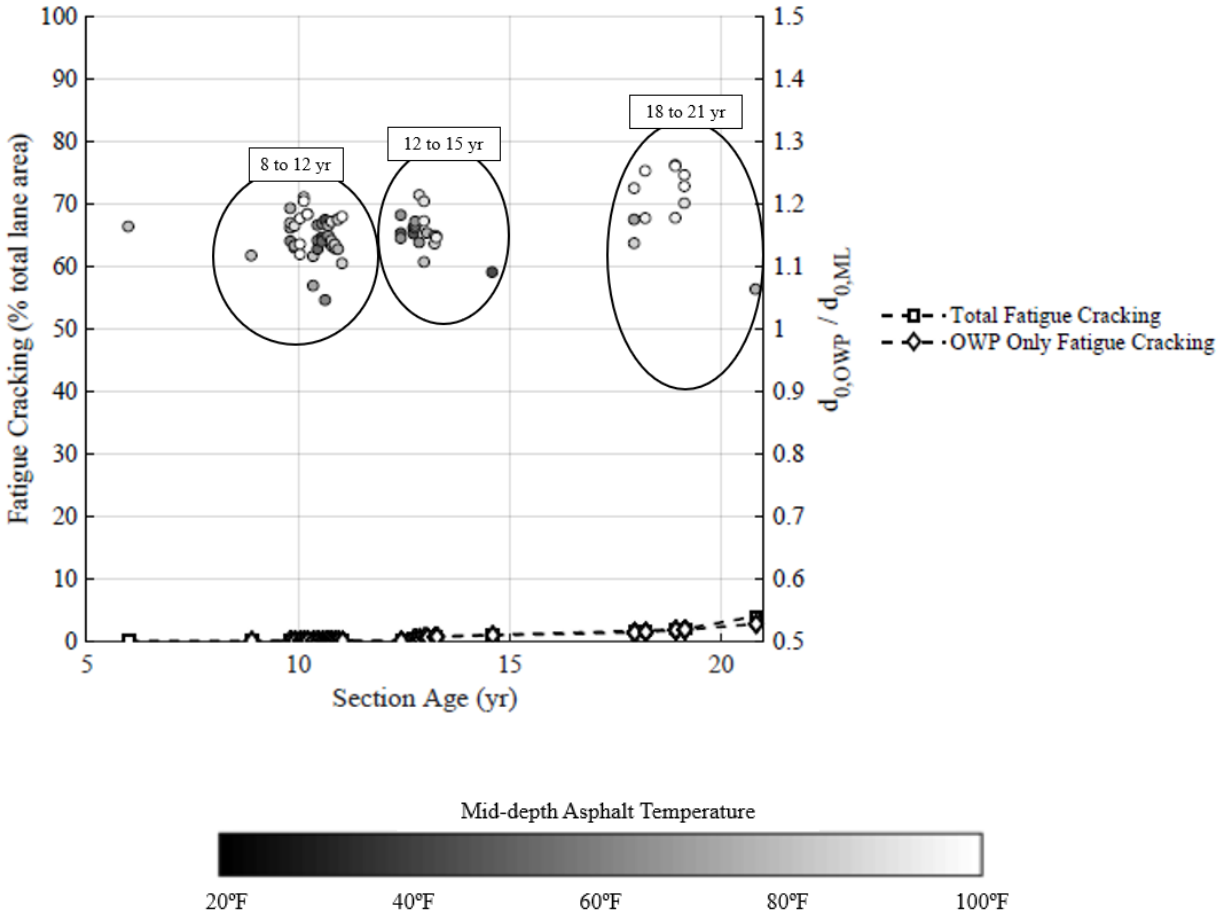

Figure 165. Performance history plot used to establish section age bin categories for two-way ANOVA ($d_{0,OWP}/d_{0,ML}$, LTPP Section 40-6145, Oklahoma).

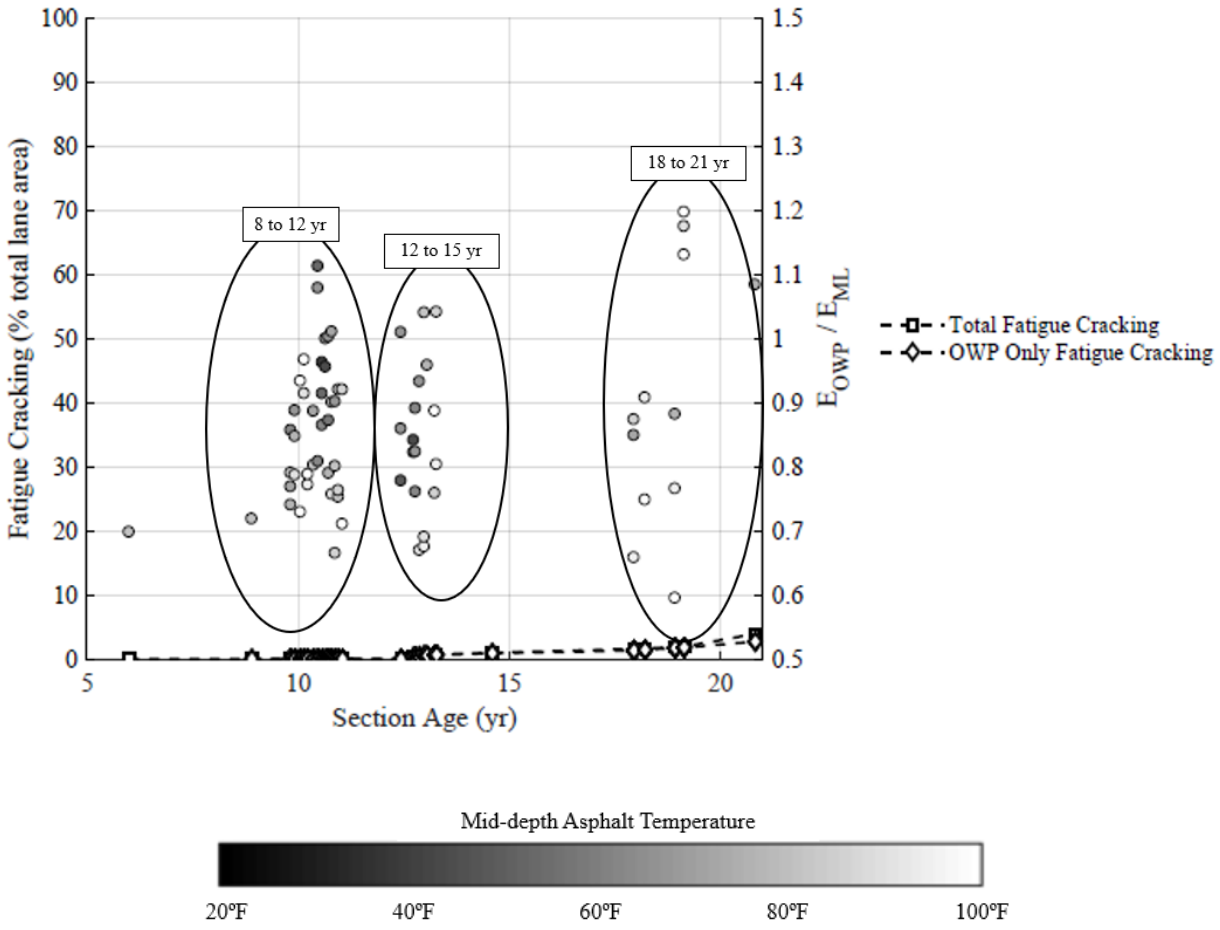

Figure 166. Performance history plot used to establish section age bin categories for two-way ANOVA ($E_{NDT,OWP}/E_{NDT,ML}$, LTPP Section 40-6145, Oklahoma).

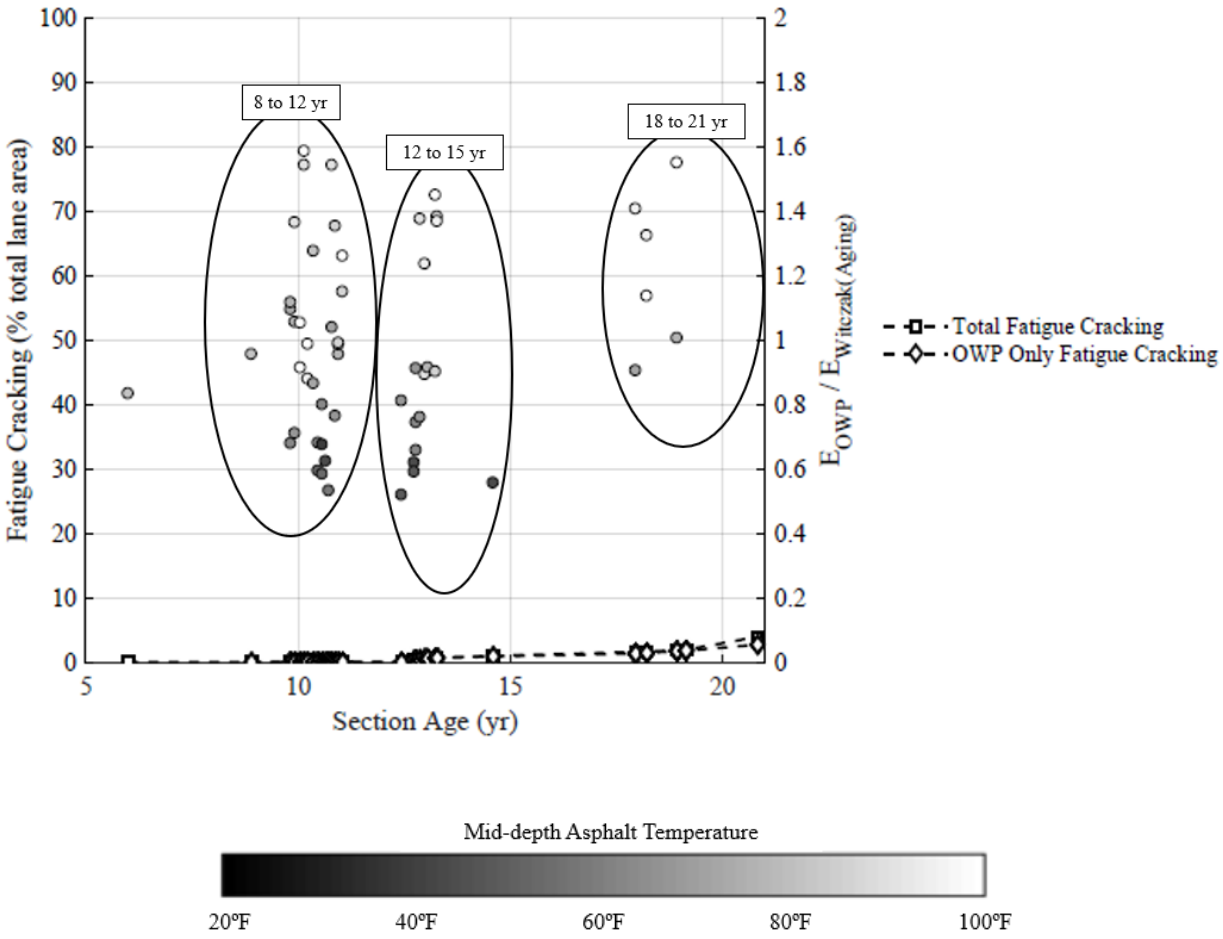

Figure 167. Performance history plot used to establish section age bin categories for two-way ANOVA ($E_{NDT,OWP}/E_{Witczak(Aging)}$, LTPP Section 40-6145, Oklahoma).

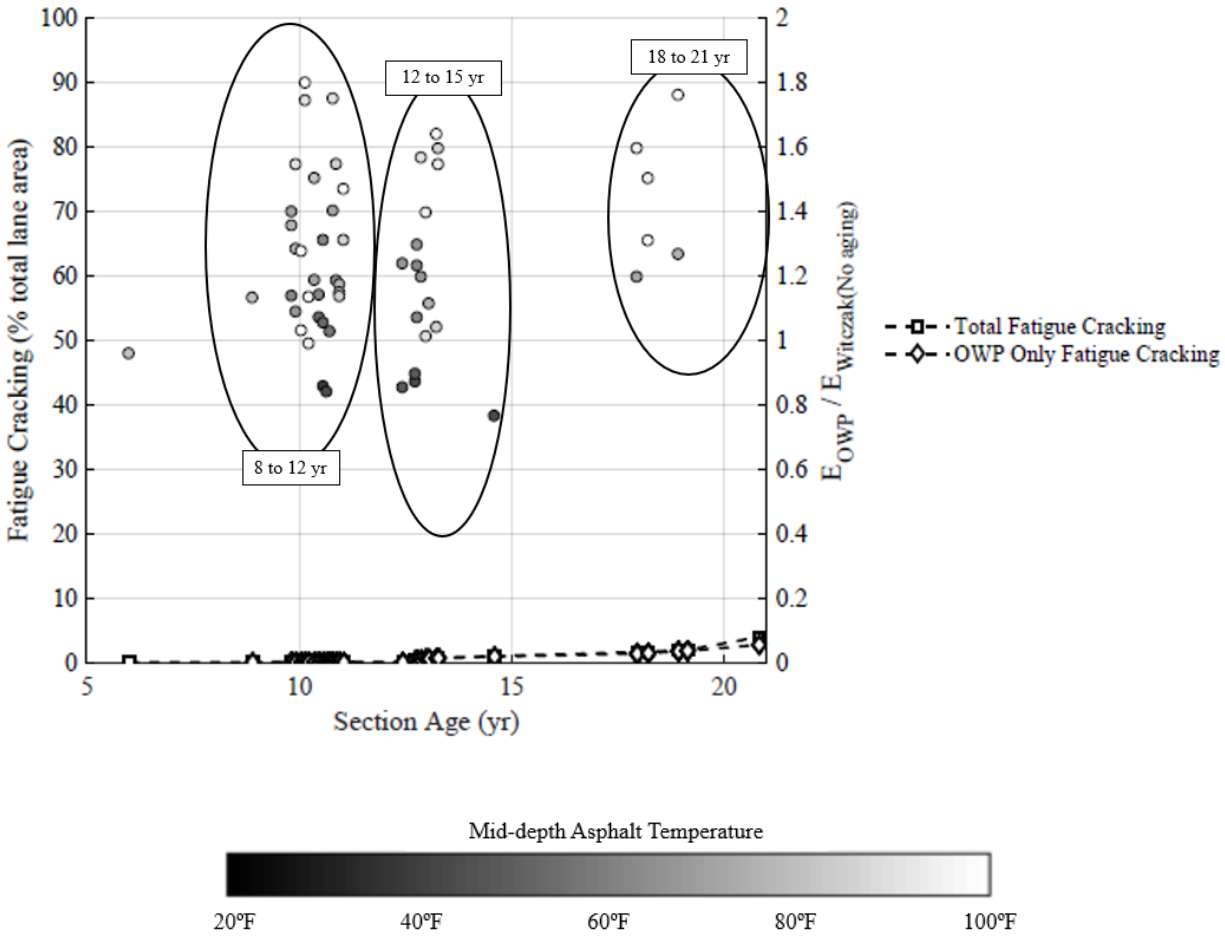

Figure 168. Performance history plot used to establish section age bin categories for two-way ANOVA ($E_{NDT,OWP}/E_{Witczak(No\ aging)}$, LTPP Section 40-6145, Oklahoma).

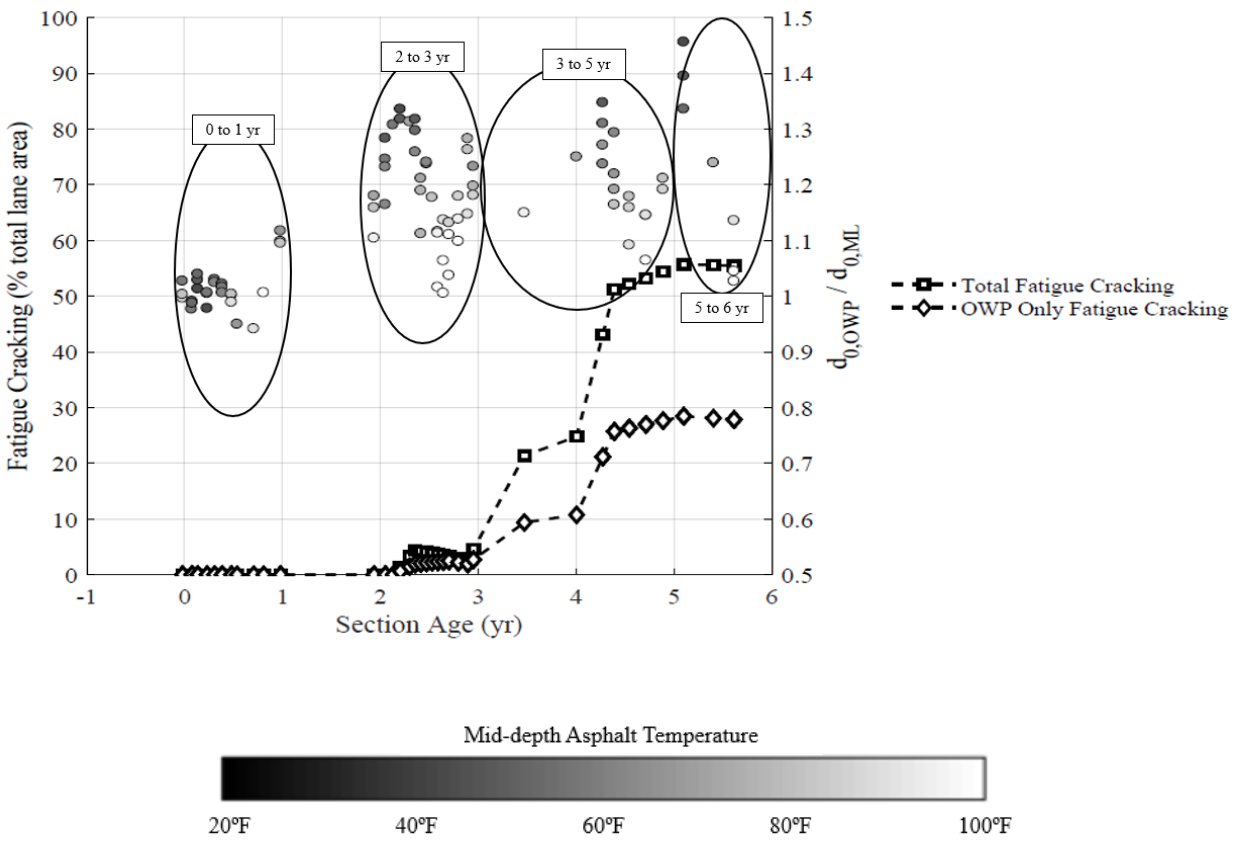

Figure 169. Performance history plot used to establish section age bin categories for two-way ANOVA ($d_{0,OWP}/d_{0,ML}$, LTPP Section 51-0113, Virginia).

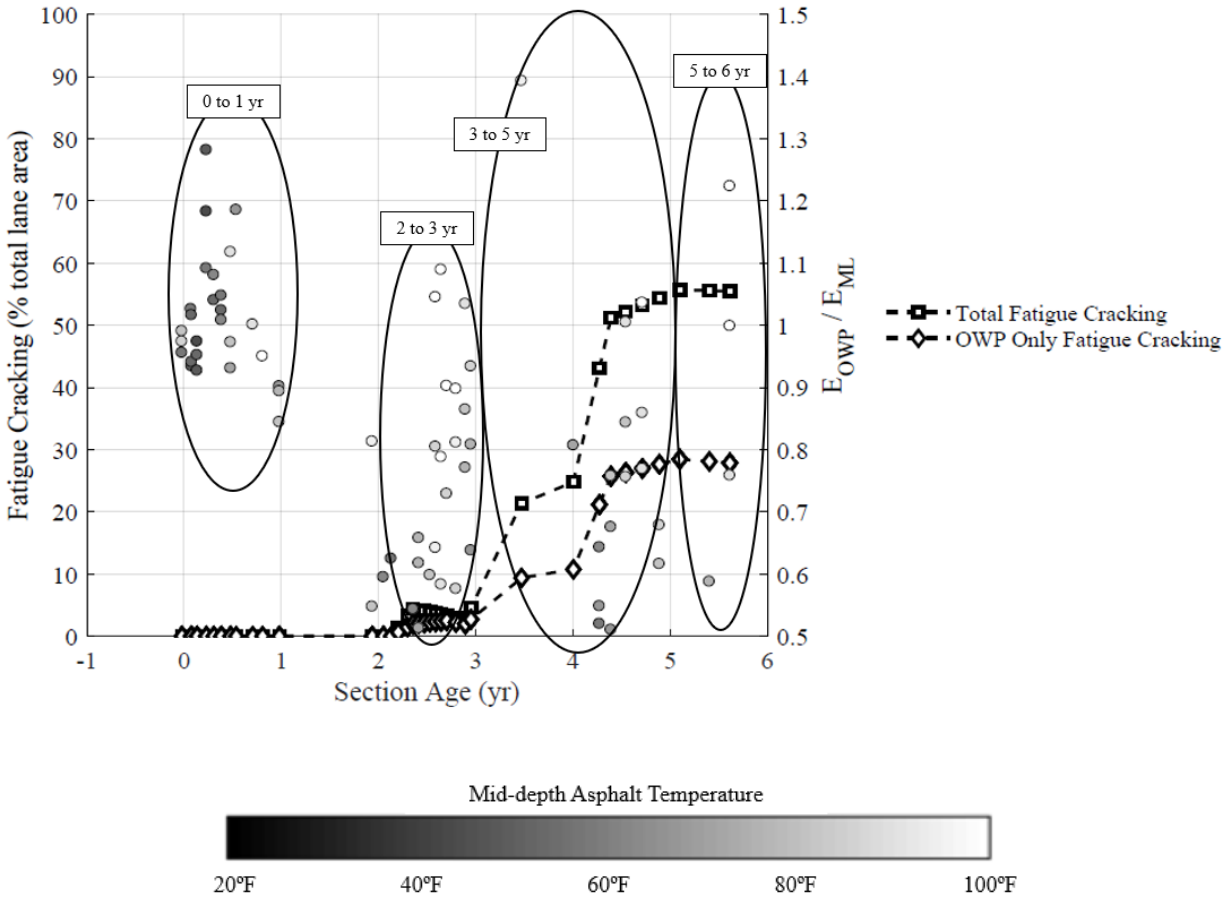

Figure 170. Performance history plot used to establish section age bin categories for two-way ANOVA ($E_{NDT,OWP}/E_{NDT,ML}$, LTPP Section 51-0113, Virginia).

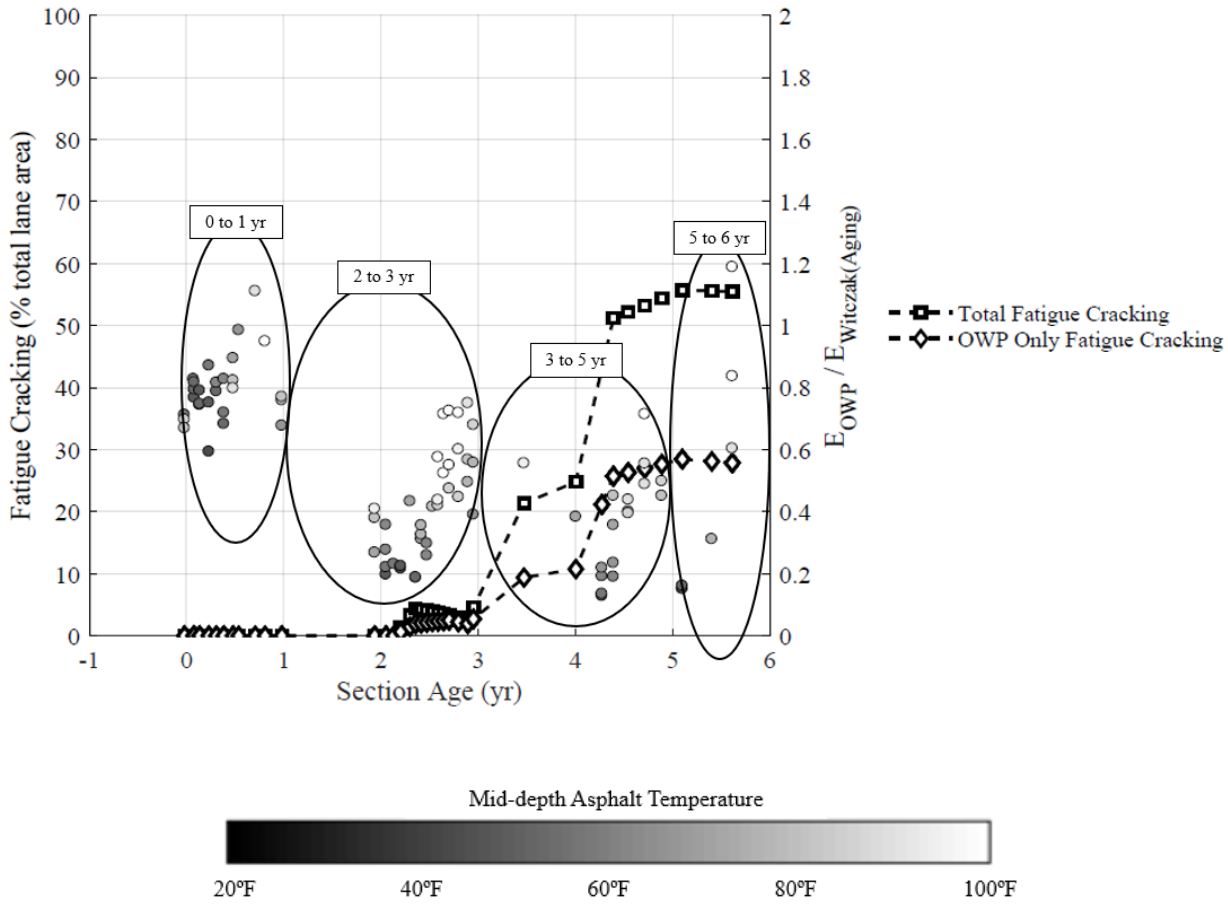

Figure 171. Performance history plot used to establish section age bin categories for two-way ANOVA ($E_{NDT,OWP}/E_{Witczak(Aging)}$, LTPP Section 51-0113, Virginia).

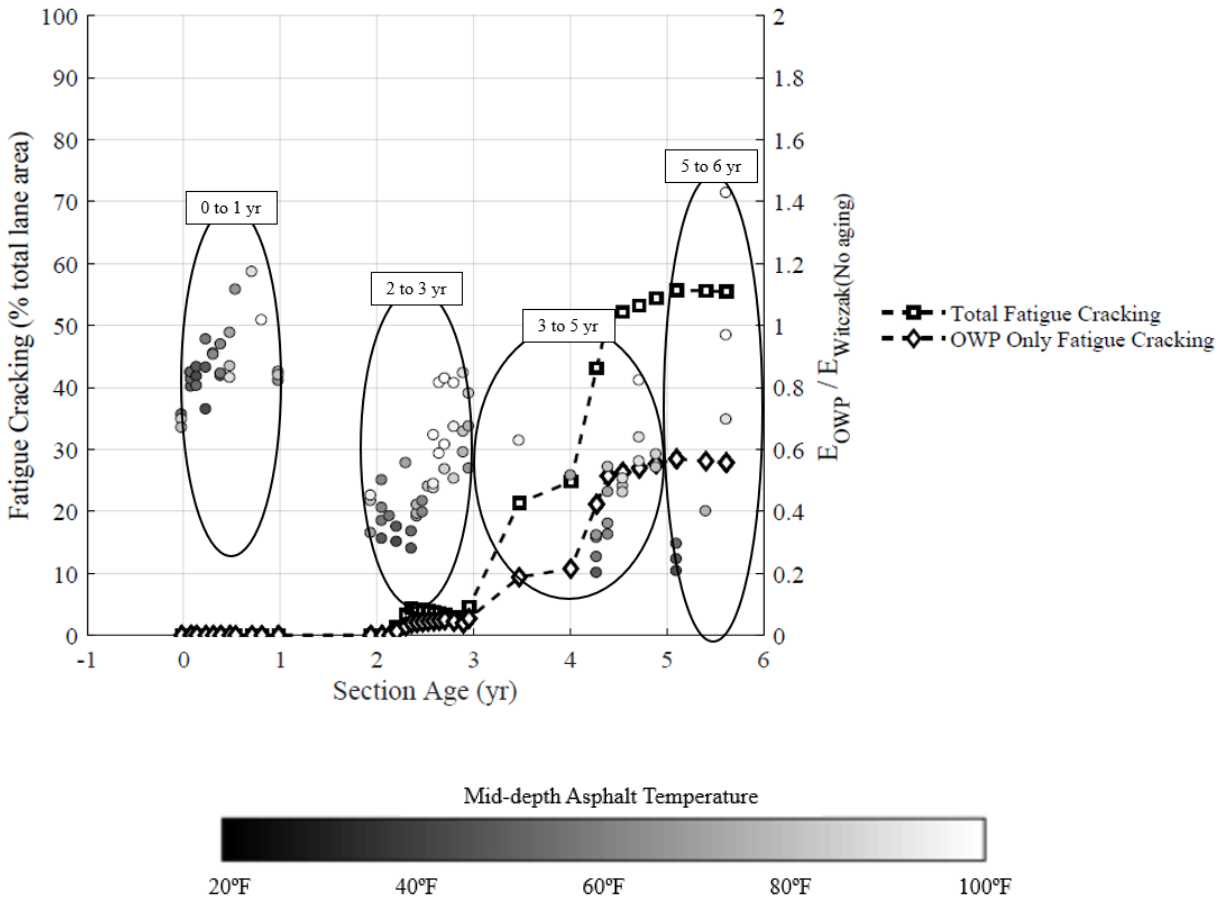

Figure 172. Performance history plot used to establish section age bin categories for two-way ANOVA ($E_{NDT,OWP}/E_{Witczak(No\ aging)}$, LTPP Section 51-0113, Virginia).

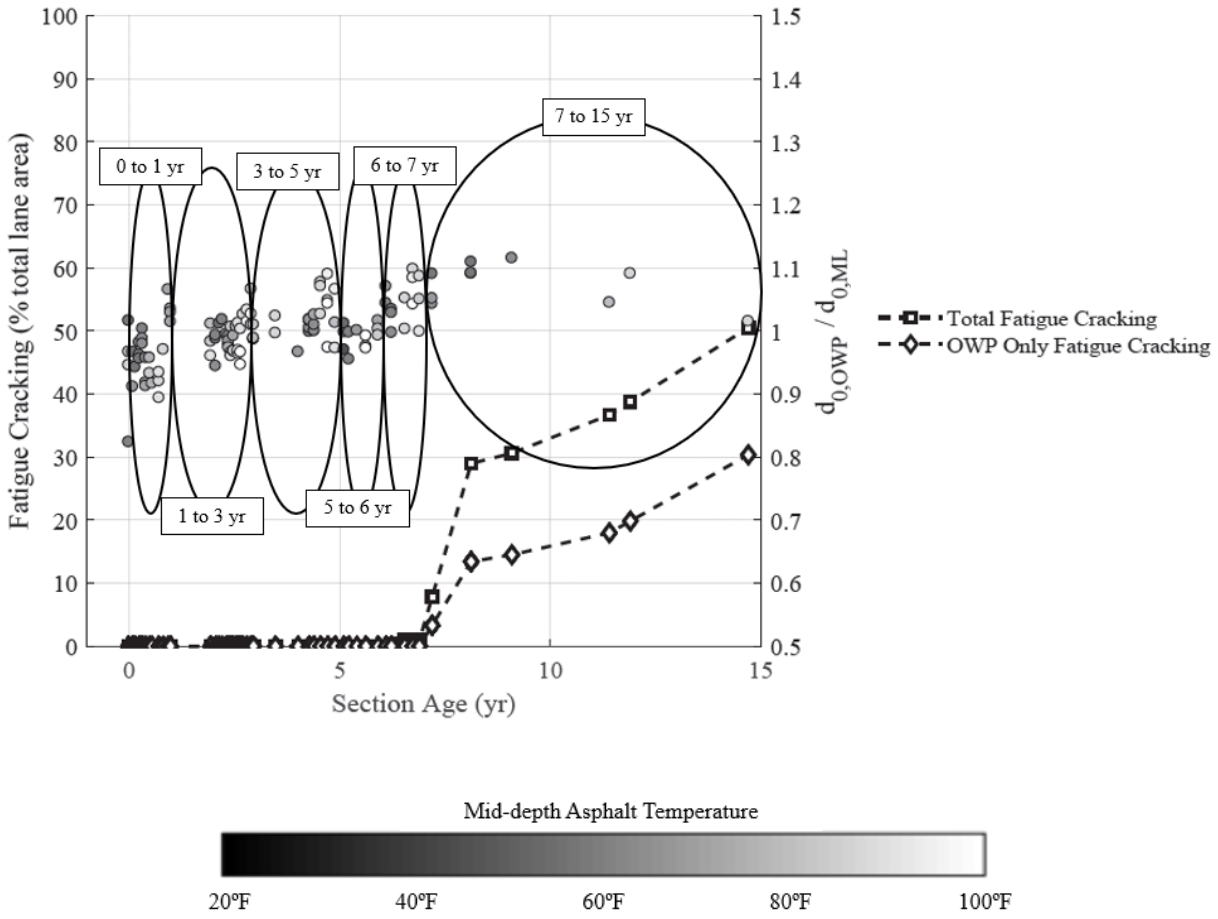

Figure 173. Performance history plot used to establish section age bin categories for two-way ANOVA ($d_{0,OWP}/d_{0,ML}$, LTPP Section 51-0114, Virginia).

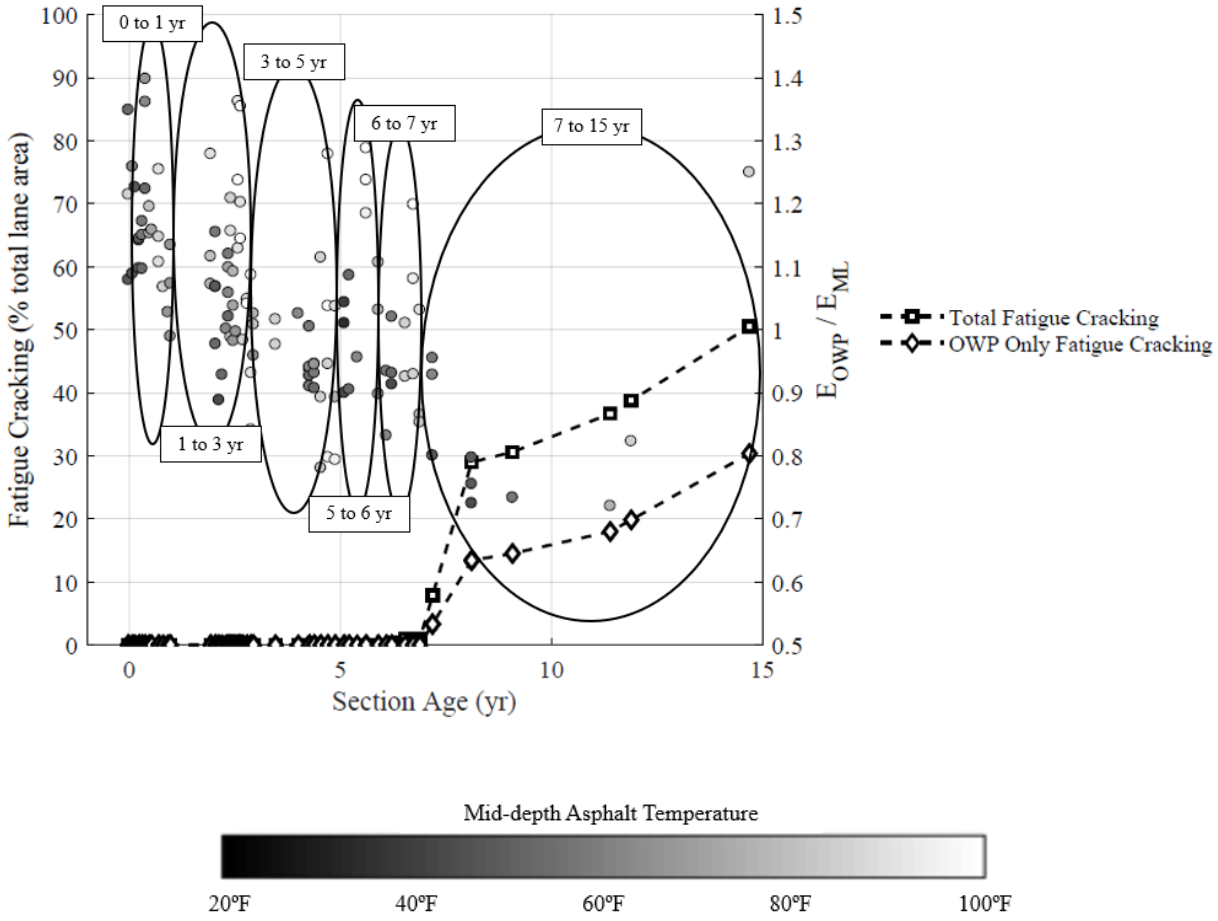

Figure 174. Performance history plot used to establish section age bin categories for two-way ANOVA ($E_{NDT,OWP}/E_{NDT,ML}$, LTPP Section 51-0114, Virginia).

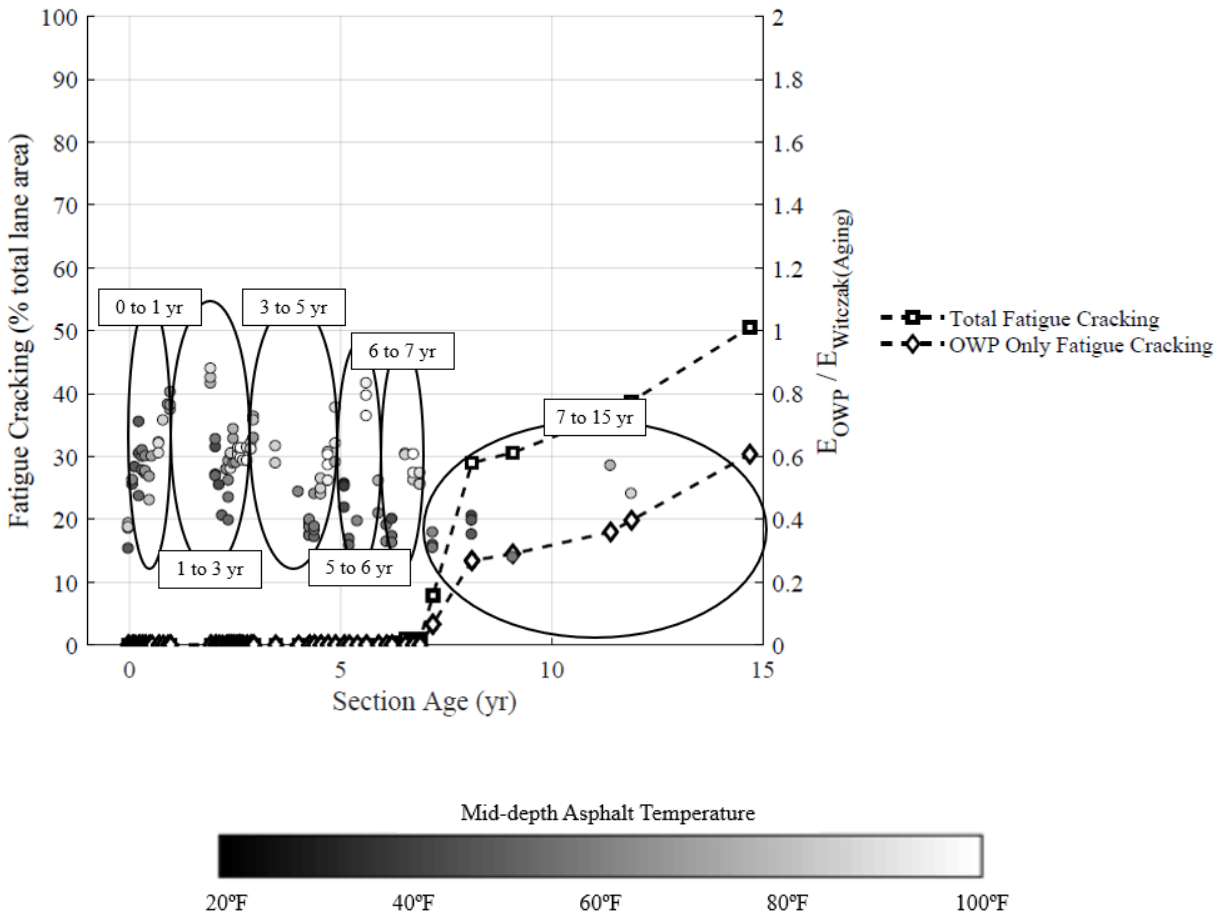

Figure 175. Performance history plot used to establish section age bin categories for two-way ANOVA ($E_{NDT,OWP}/E_{Witczak(Aging)}$, LTPP Section 51-0114, Virginia).

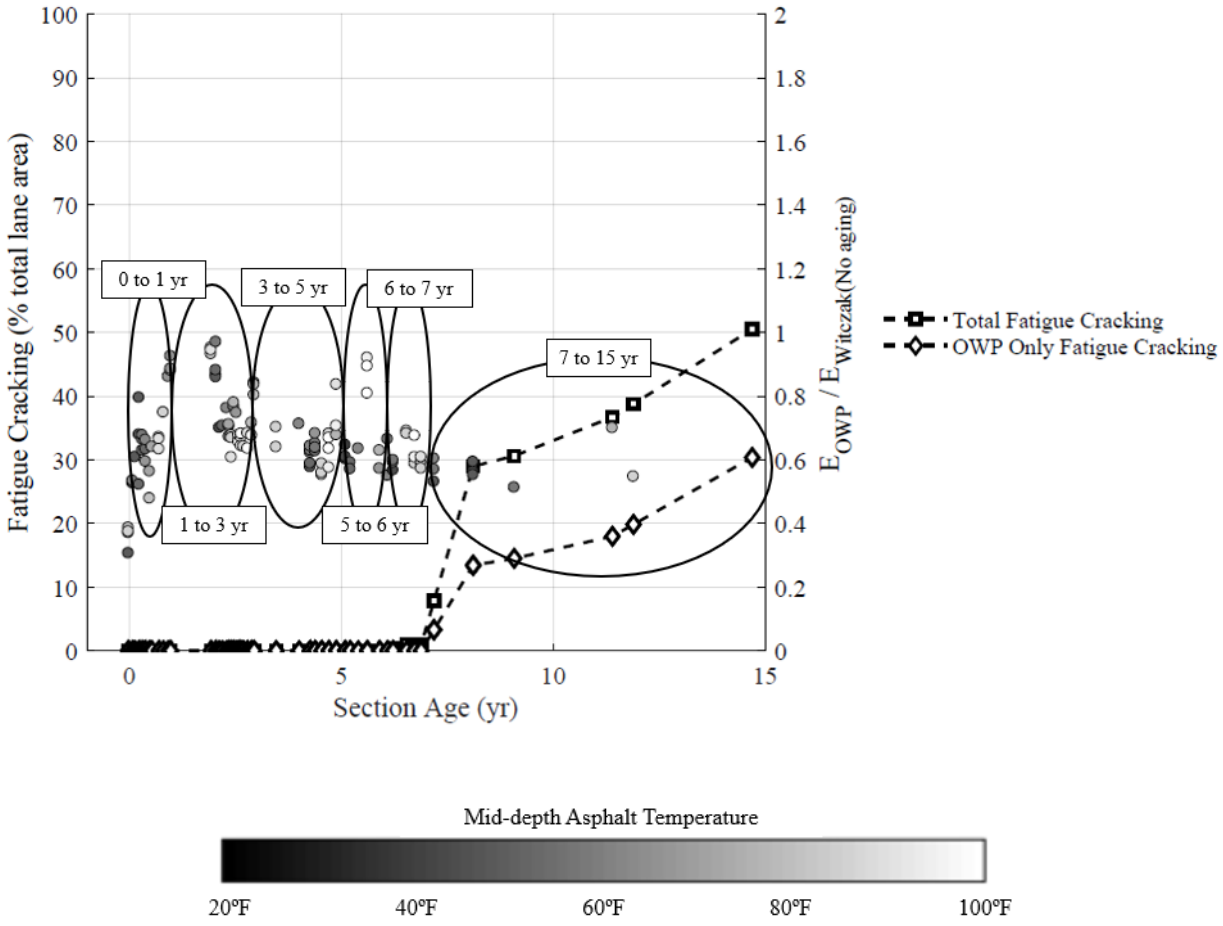

Figure 176. Performance history plot used to establish section age bin categories for two-way ANOVA ($E_{NDT,OWP}/E_{Witczak(No\ aging)}$, LTPP Section 51-0114, Virginia).

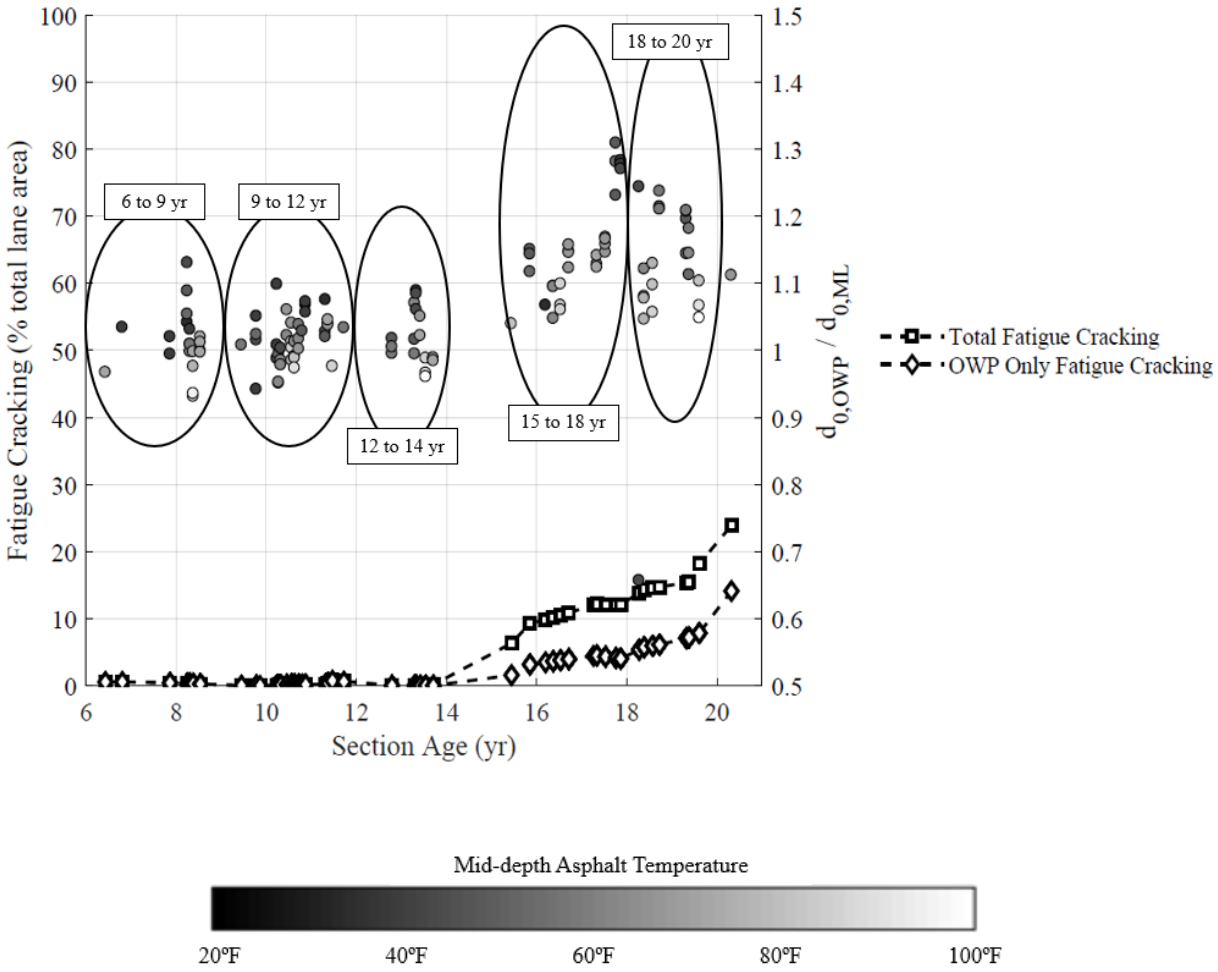

Figure 177. Performance history plot used to establish section age bin categories for two-way ANOVA ($d_{0,OWP}/d_{0,ML}$, LTPP Section 83-1801, Manitoba).

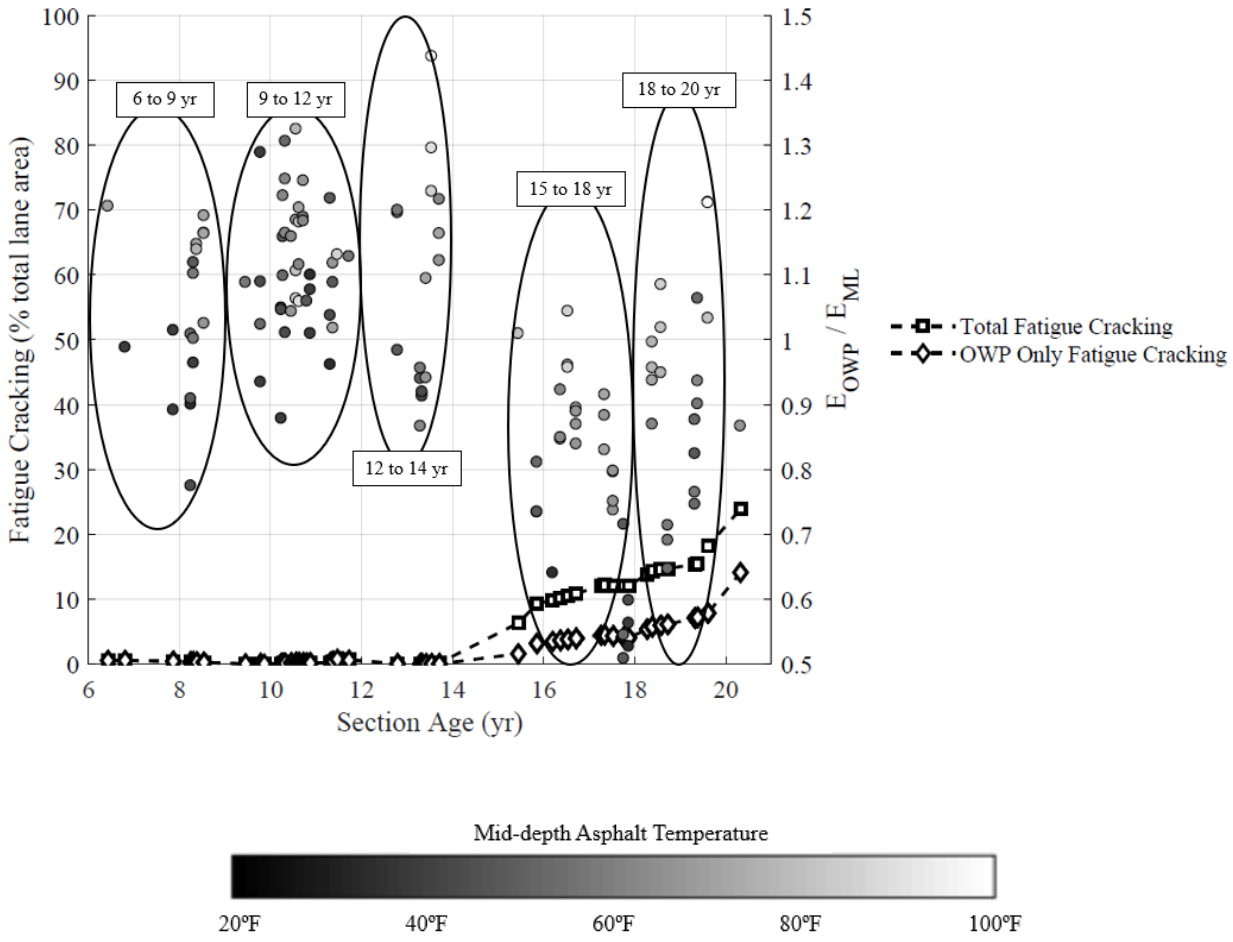

Figure 178. Performance history plot used to establish section age bin categories for two-way ANOVA ($E_{NDT,OWP}/E_{NDT,ML}$, LTPP Section 83-1801, Manitoba).

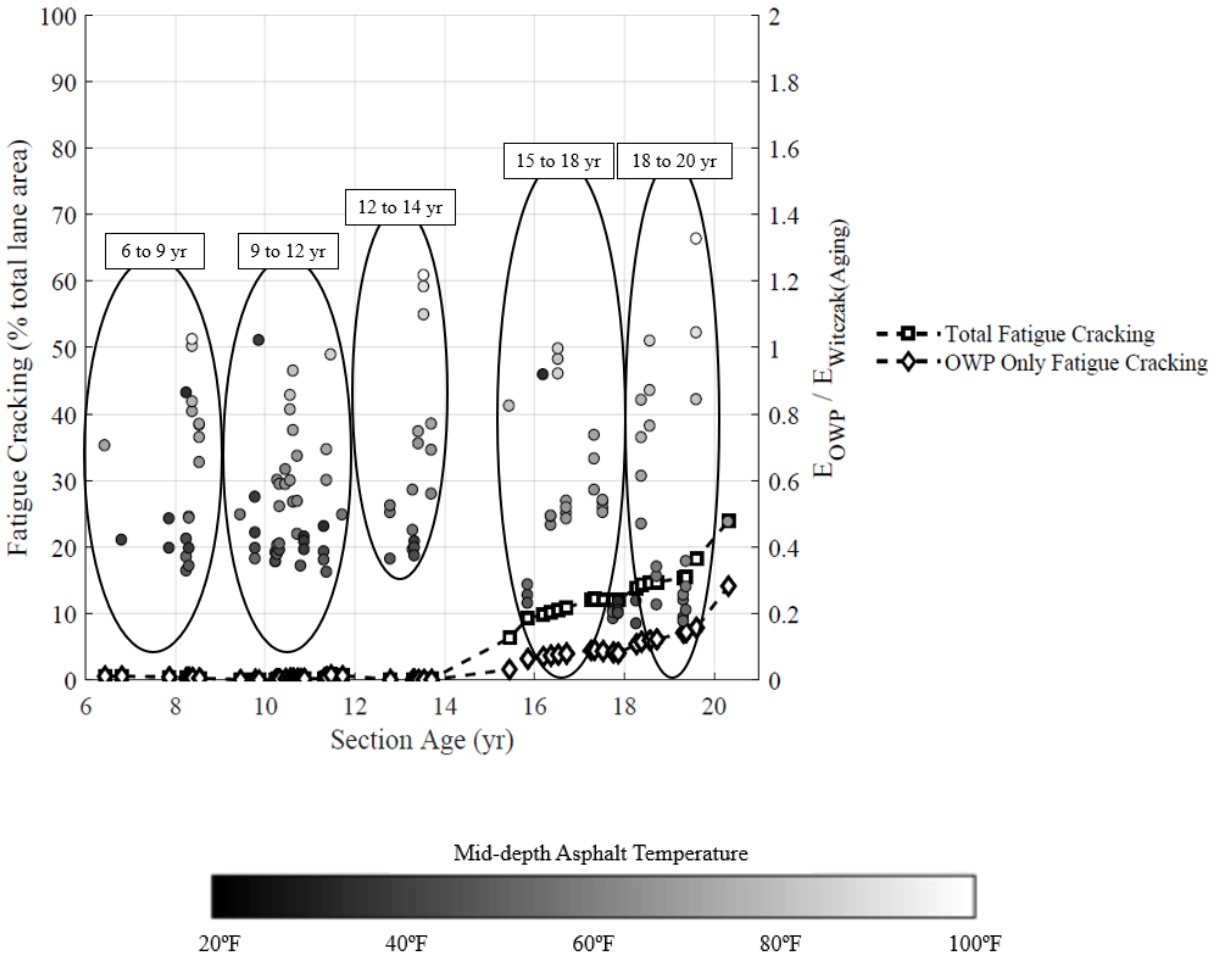

Figure 179. Performance history plot used to establish section age bin categories for two-way ANOVA ($E_{NDT,OWP}/E_{Witczak(Aging)}$, LTPP Section 83-1801, Manitoba).

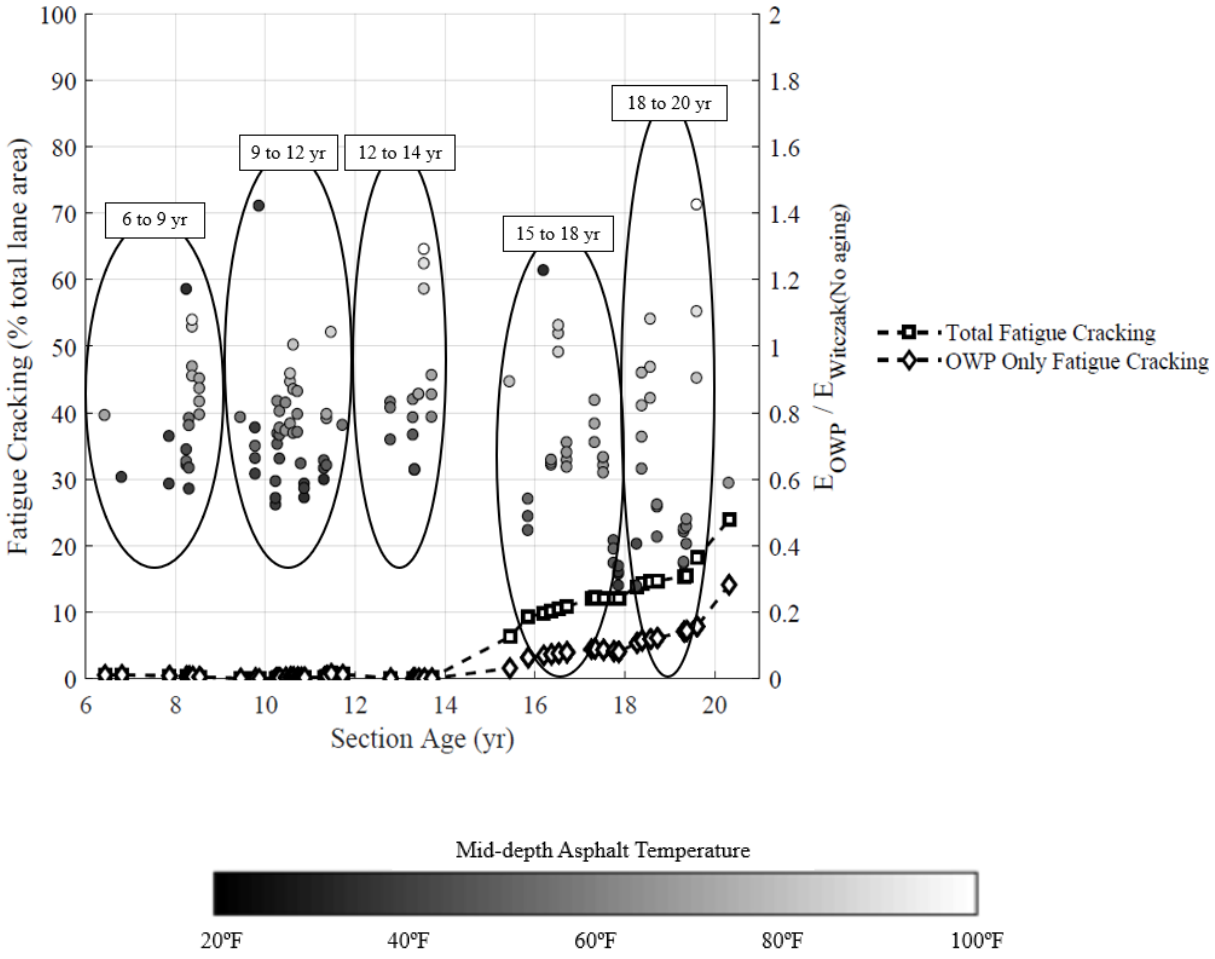

Figure 180. Performance history plot used to establish section age bin categories for two-way ANOVA ($E_{NDT,OWP}/E_{Witczak(No\ aging)}$, LTPP Section 83-1801, Manitoba).

APPENDIX D

PERFORMANCE HISTORY PLOTS USED FOR DETERMINING $E_{NDT(BEST\ FIT)}$

This appendix contains the performance history plots used to determine $E_{NDT(Best\ fit)}$ in Chapter 6. Thirty-five plots are shown, one for each section used in the development of E_{NDT} adjustment factors.

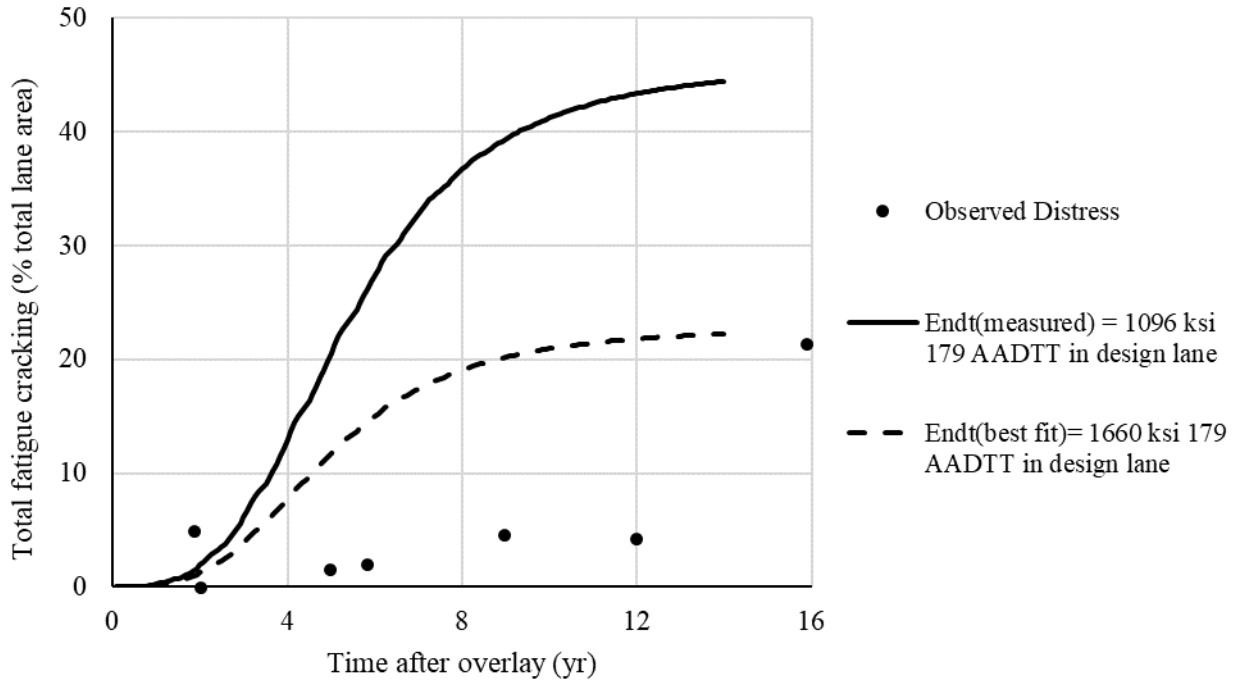

Figure 181. Determination of $E_{NDT(Best\ fit)}$ (LTPP Section 9-1803, Connecticut).

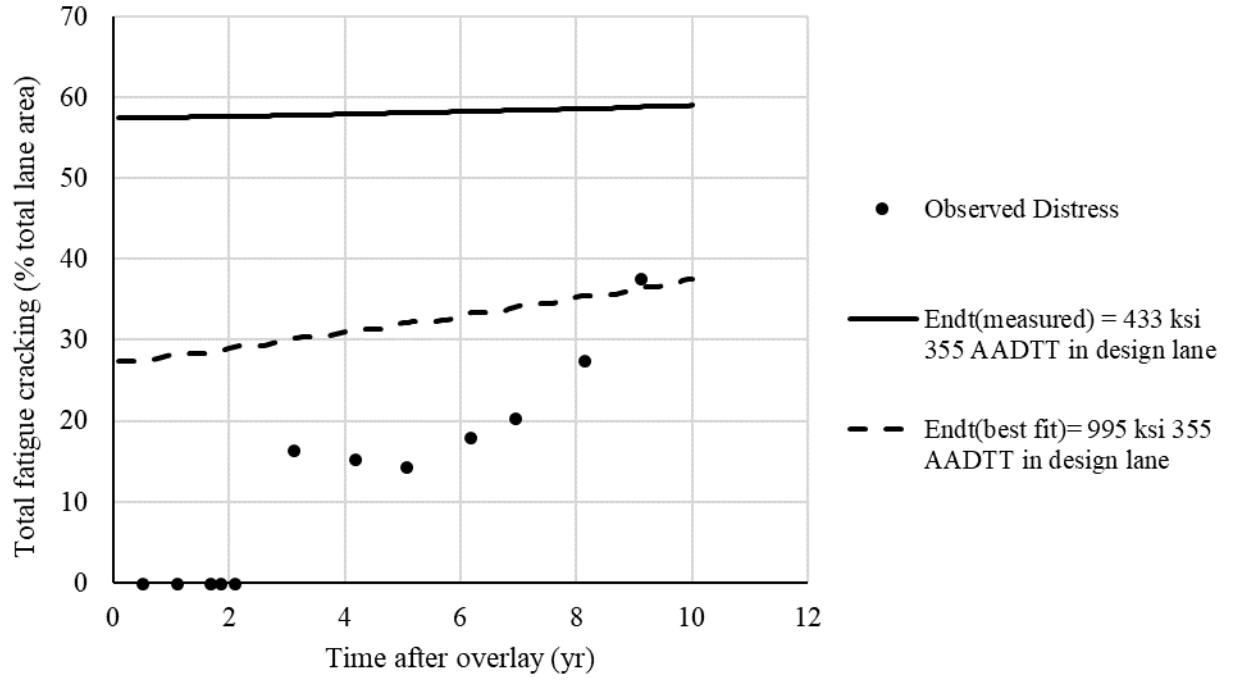

Figure 182. Determination of $E_{NDT(Best\ fit)}$ (LTPP Section 10-0102, Delaware).

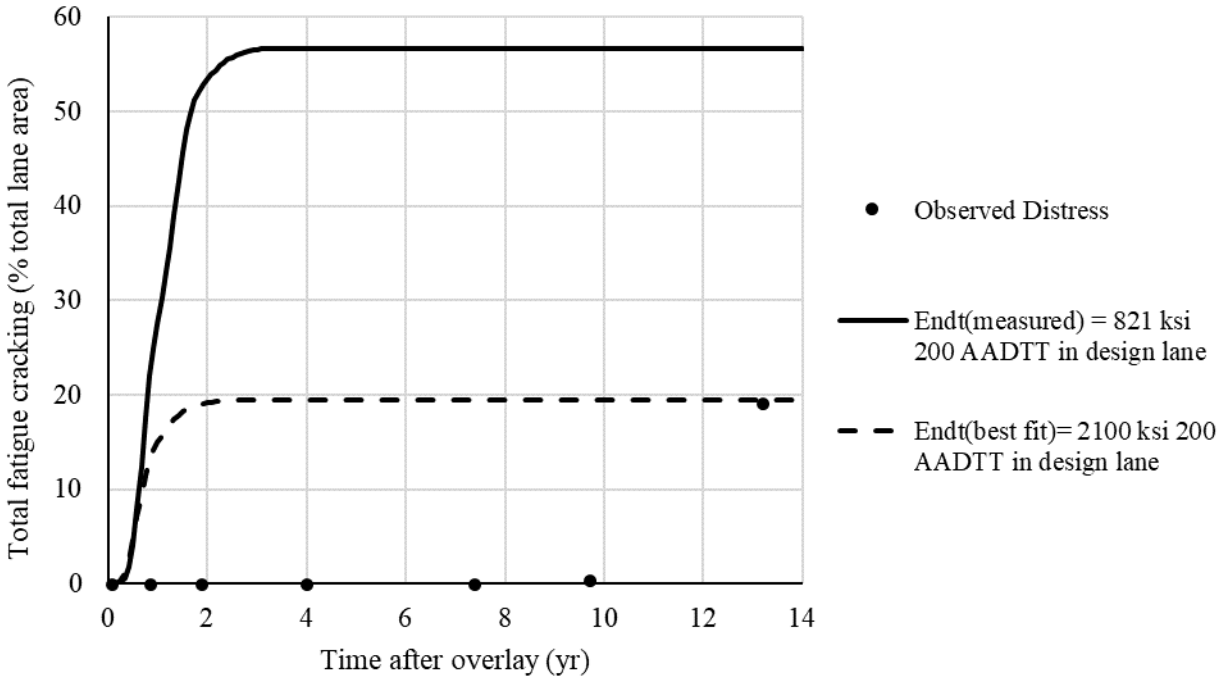

Figure 183. Determination of $E_{NDT(Best\ fit)}$ (LTPP Section 17-A310, Illinois).

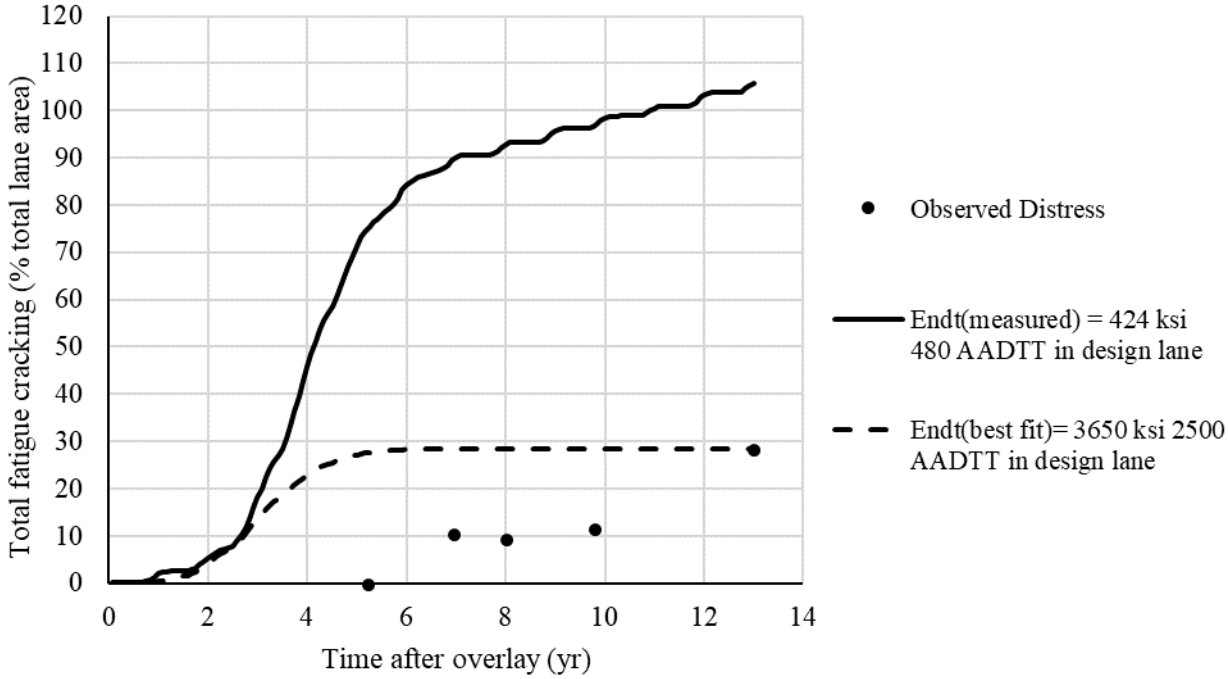

Figure 184. Determination of $E_{NDT(Best\ fit)}$ (LTPP Section 19-1044, Iowa).

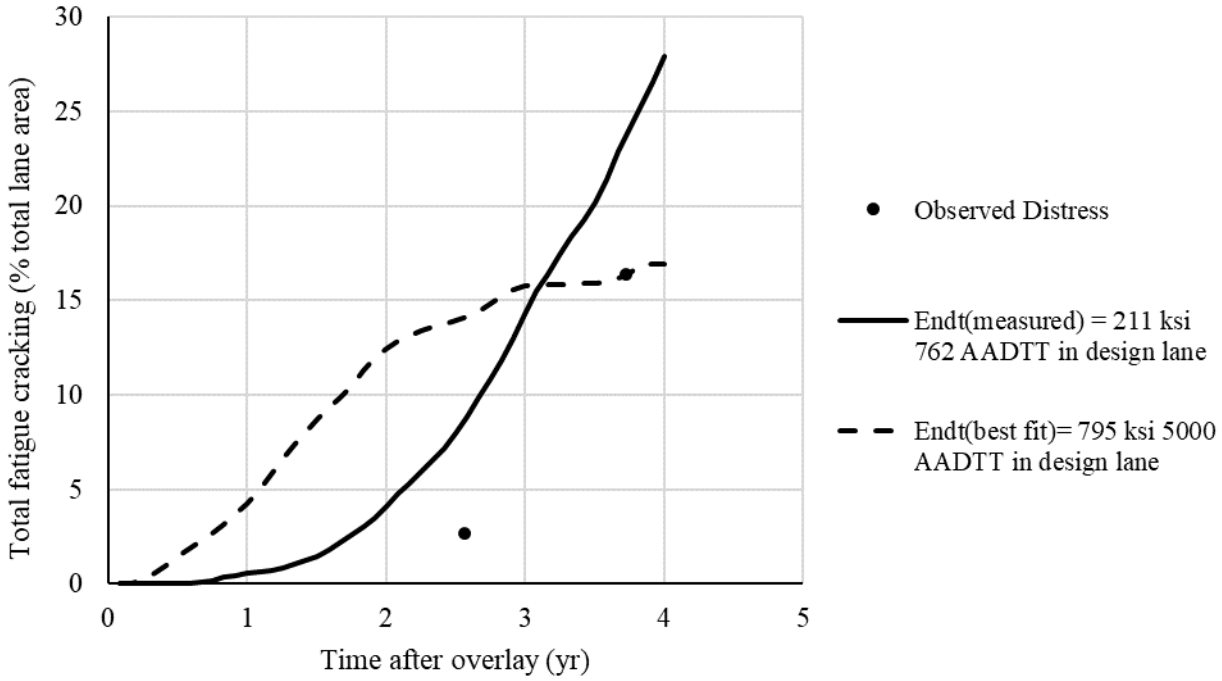

Figure 185. Determination of $E_{NDT(Best\ fit)}$ (LTPP Section 20-0159, Kansas).

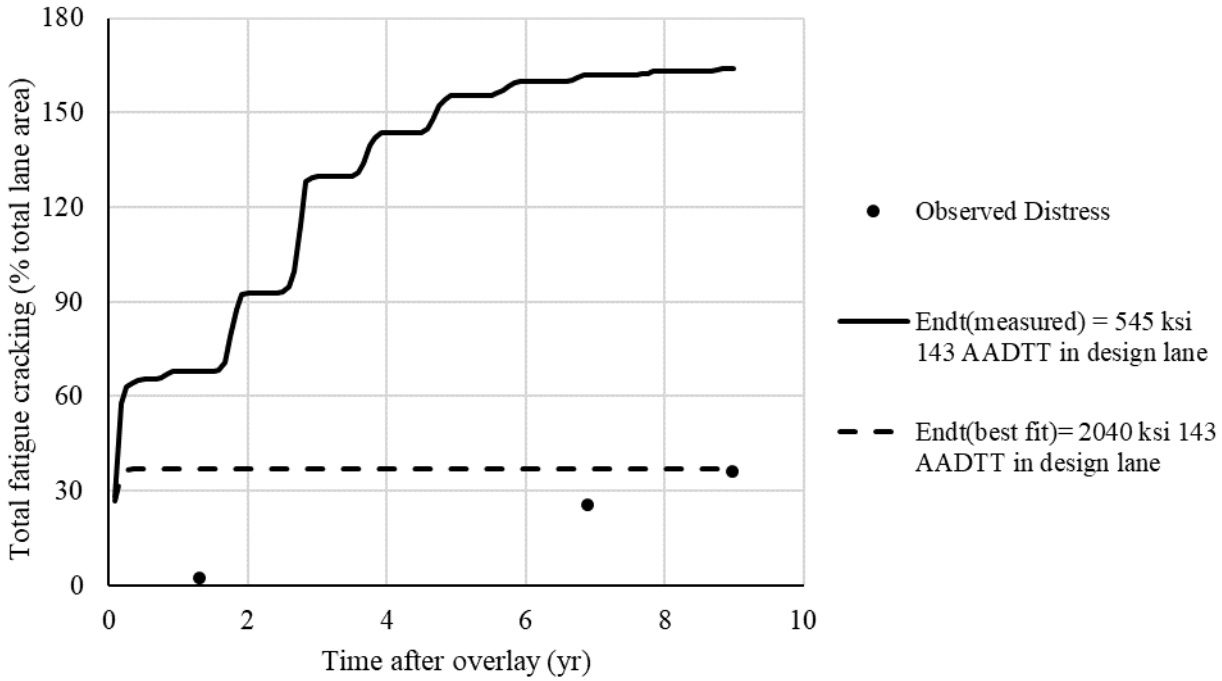

Figure 186. Determination of $E_{NDT(Best\ fit)}$ (LTPP Section 20-1005, Kansas).

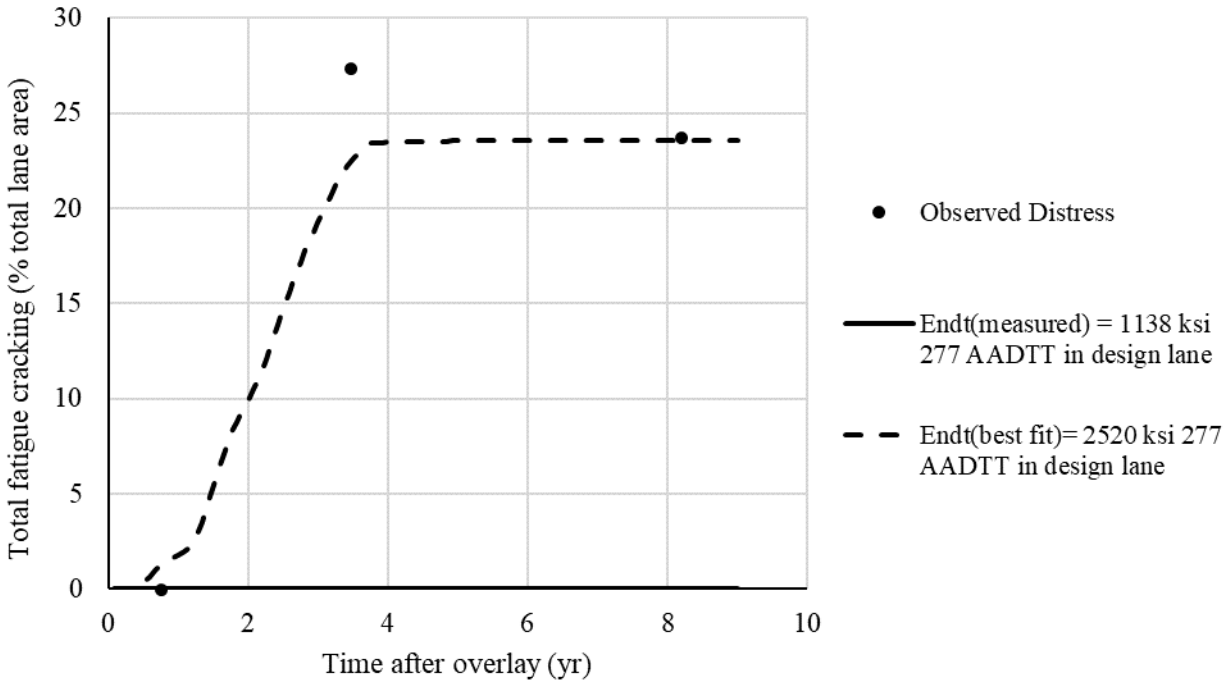

Figure 187. Determination of $E_{NDT(Best\ fit)}$ (LTPP Section 20-1009, Kansas).

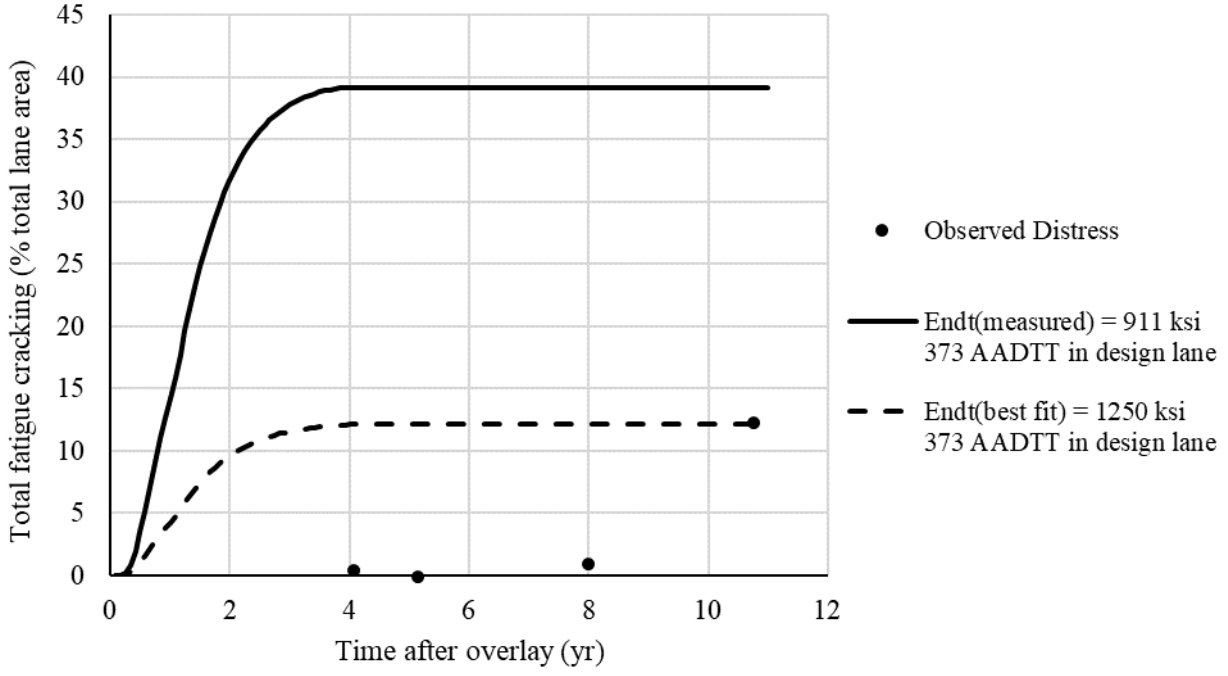

Figure 188. Determination of $E_{NDT(Best\ fit)}$ (LTPP Section 23-1009, Maine).

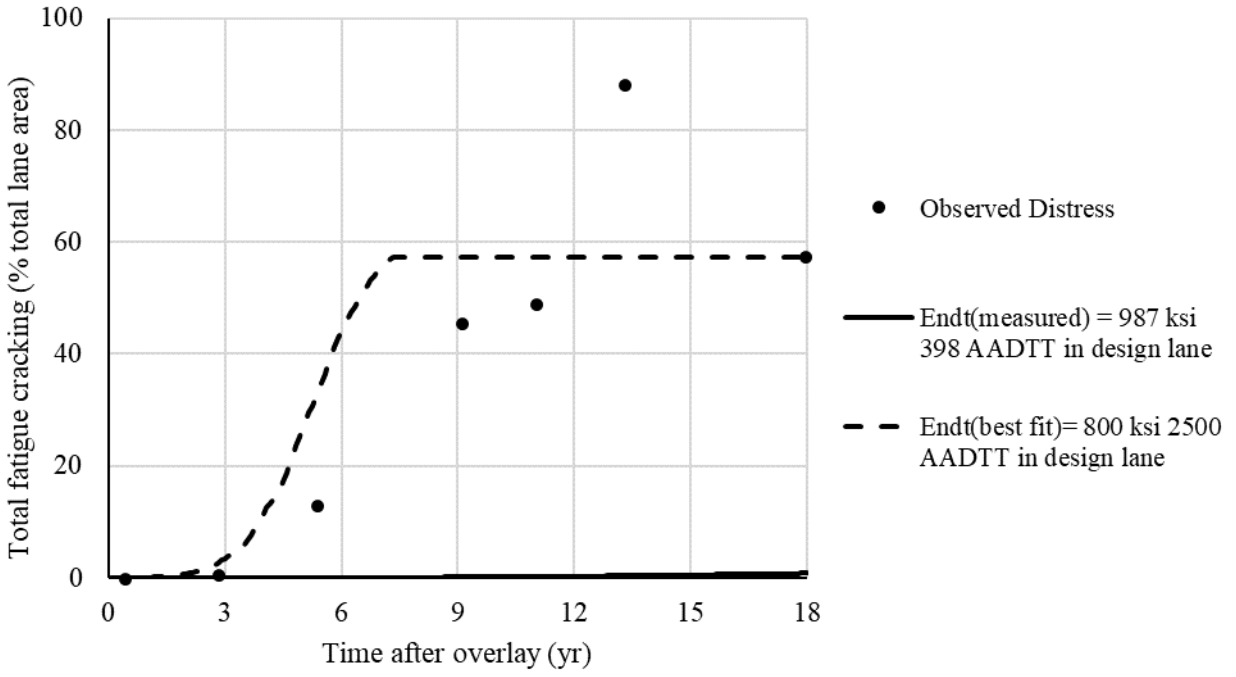

Figure 189. Determination of $E_{NDT(Best\ fit)}$ (LTPP Section 24-1634, Maryland).

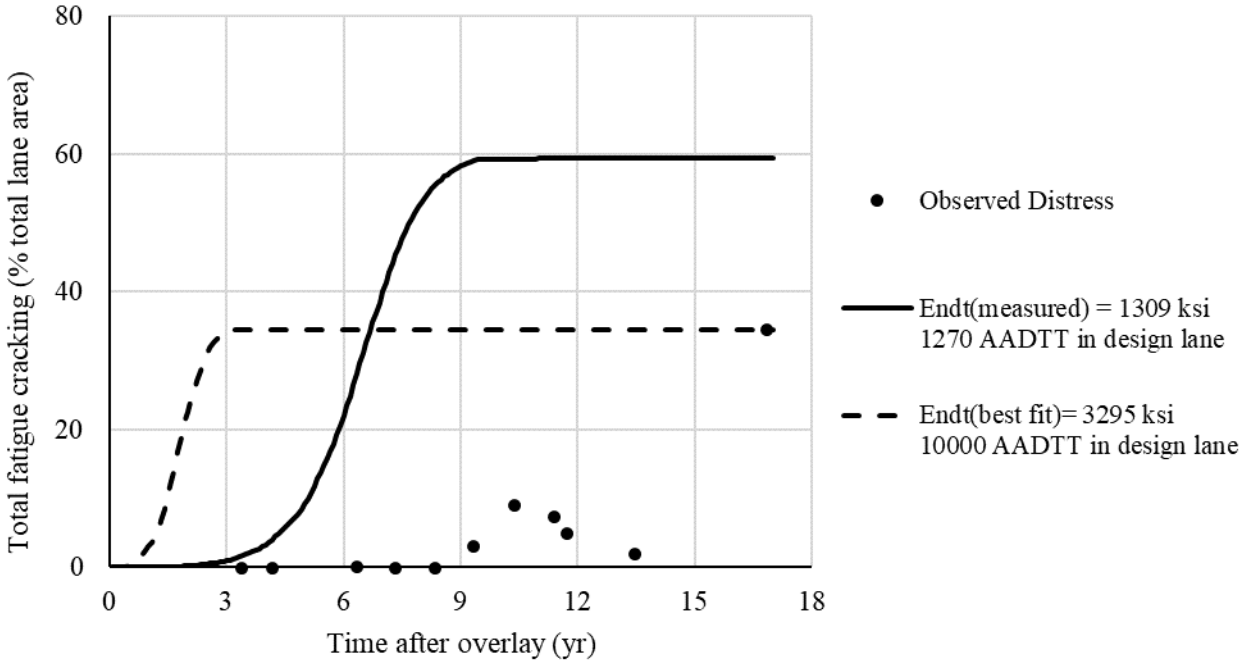

Figure 190. Determination of $E_{NDT(Best\ fit)}$ (LTPP Section 34-0503, New Jersey).

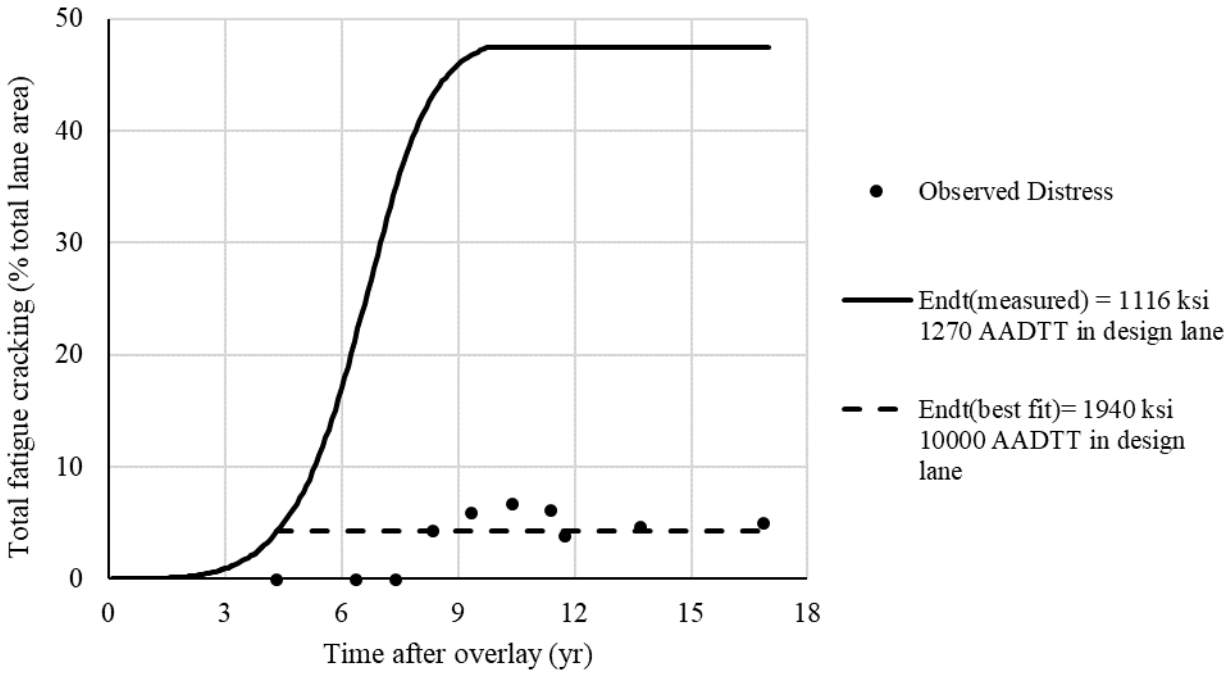

Figure 191. Determination of $E_{NDT(Best\ fit)}$ (LTPP Section 34-0504, New Jersey).

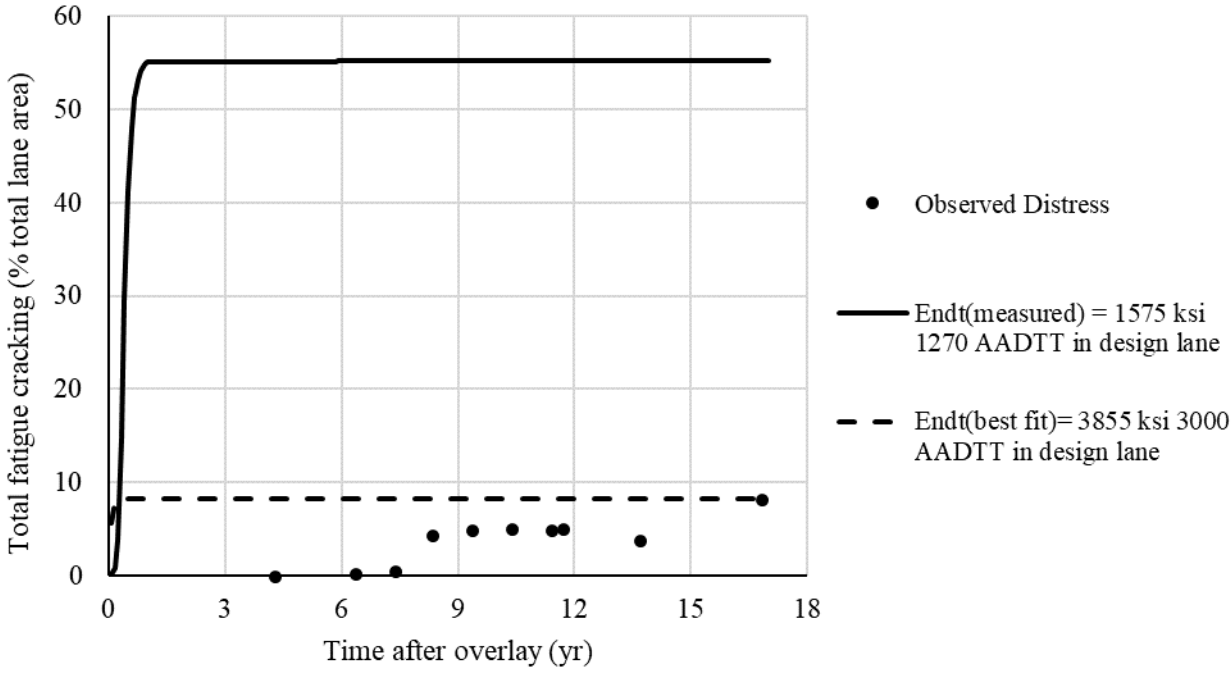

Figure 192. Determination of $E_{NDT(Best\ fit)}$ (LTPP Section 34-0505, New Jersey).

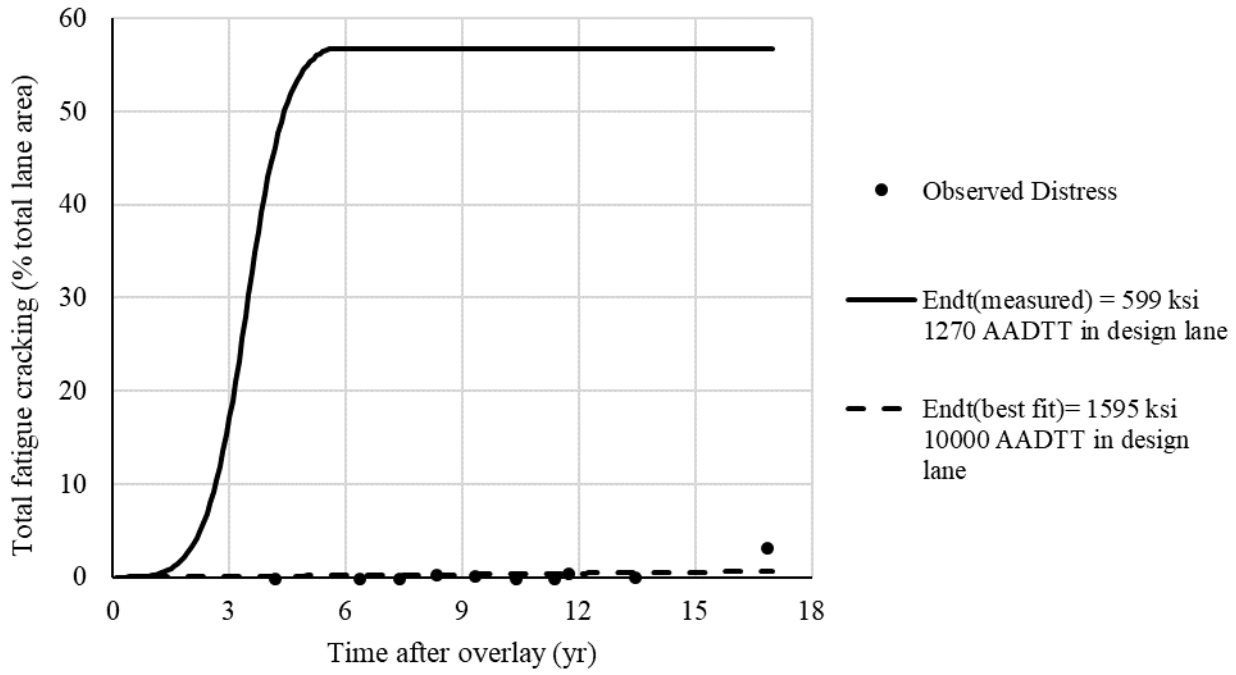

Figure 193. Determination of $E_{NDT(Best\ fit)}$ (LTPP Section 34-0506, New Jersey).

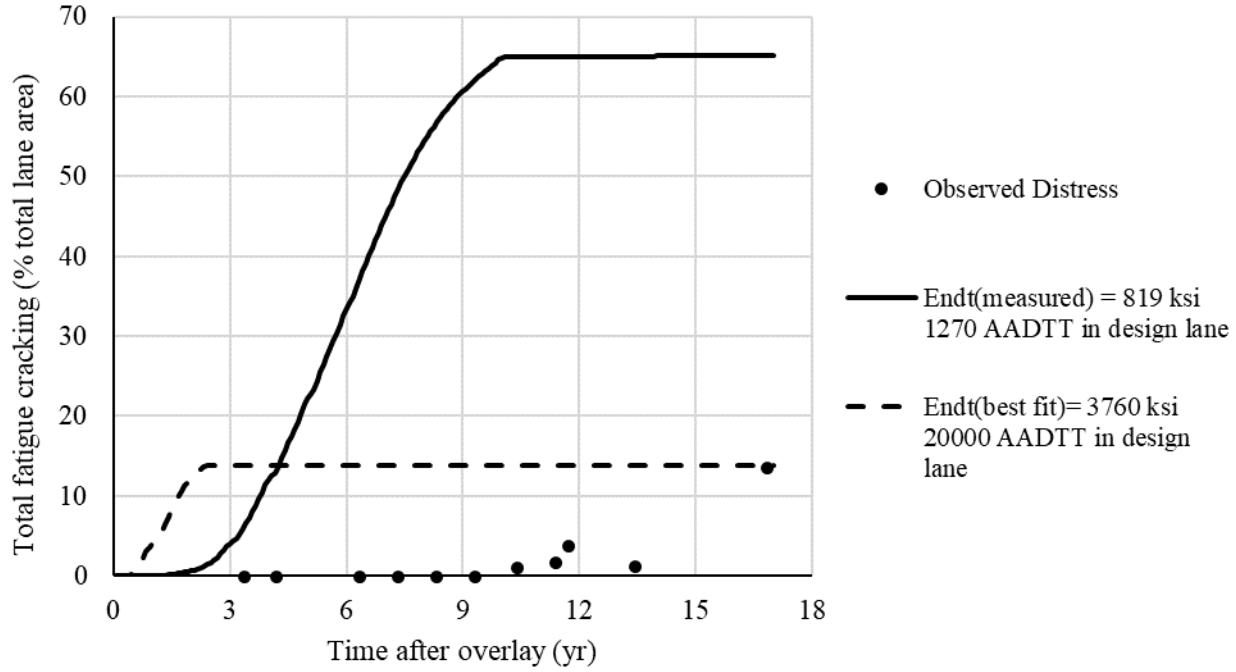

Figure 194. Determination of $E_{NDT(Best\ fit)}$ (LTPP Section 34-0507, New Jersey).

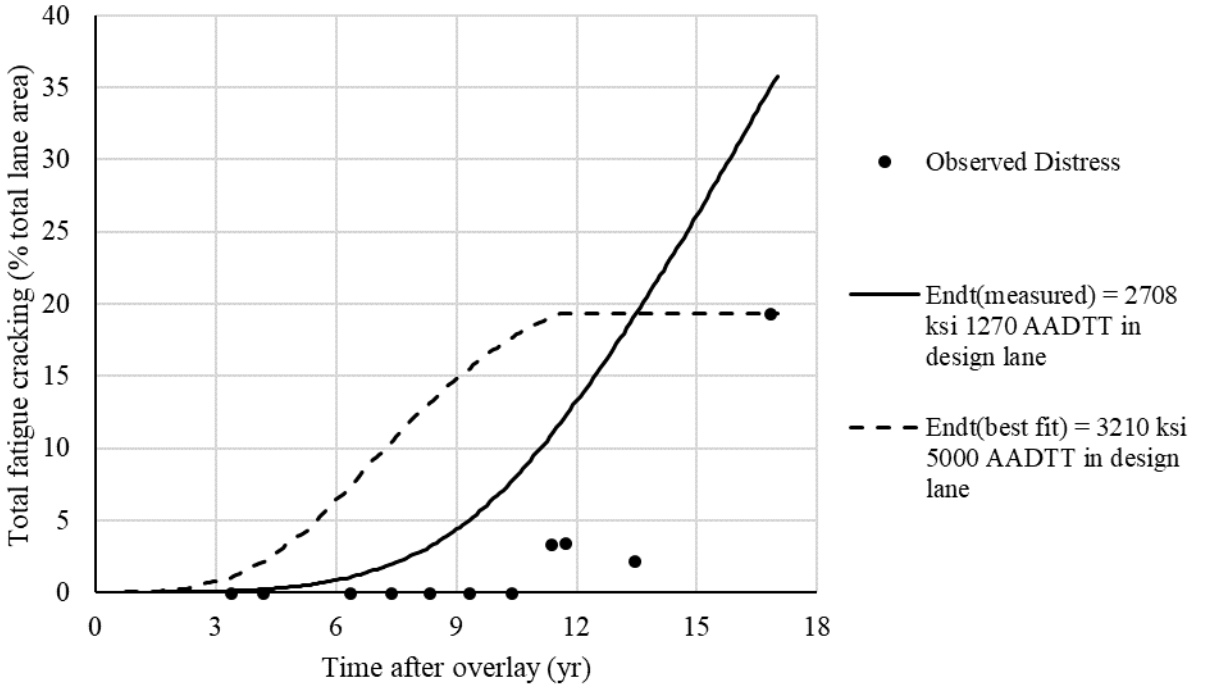

Figure 195. Determination of $E_{NDT(Best\ fit)}$ (LTPP Section 34-0508, New Jersey).

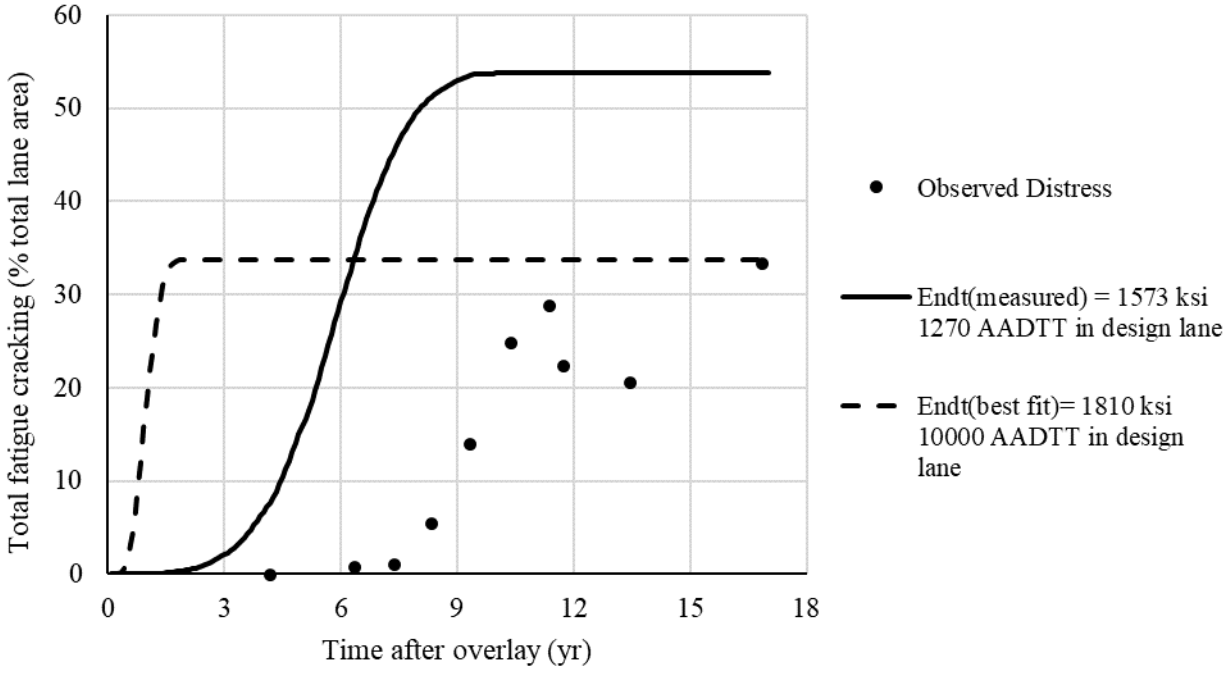

Figure 196. Determination of $E_{NDT(Best\ fit)}$ (LTPP Section 34-0509, New Jersey).

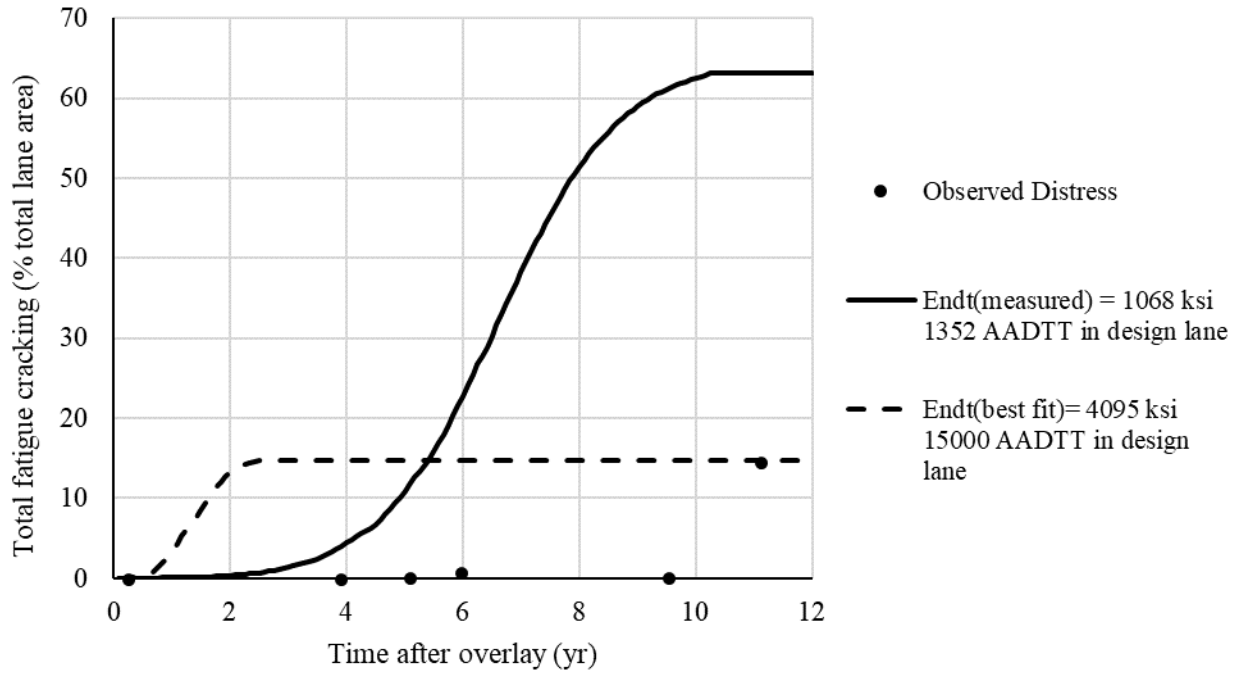

Figure 197. Determination of $E_{NDT(Best\ fit)}$ (LTPP Section 34-0903, New Jersey).

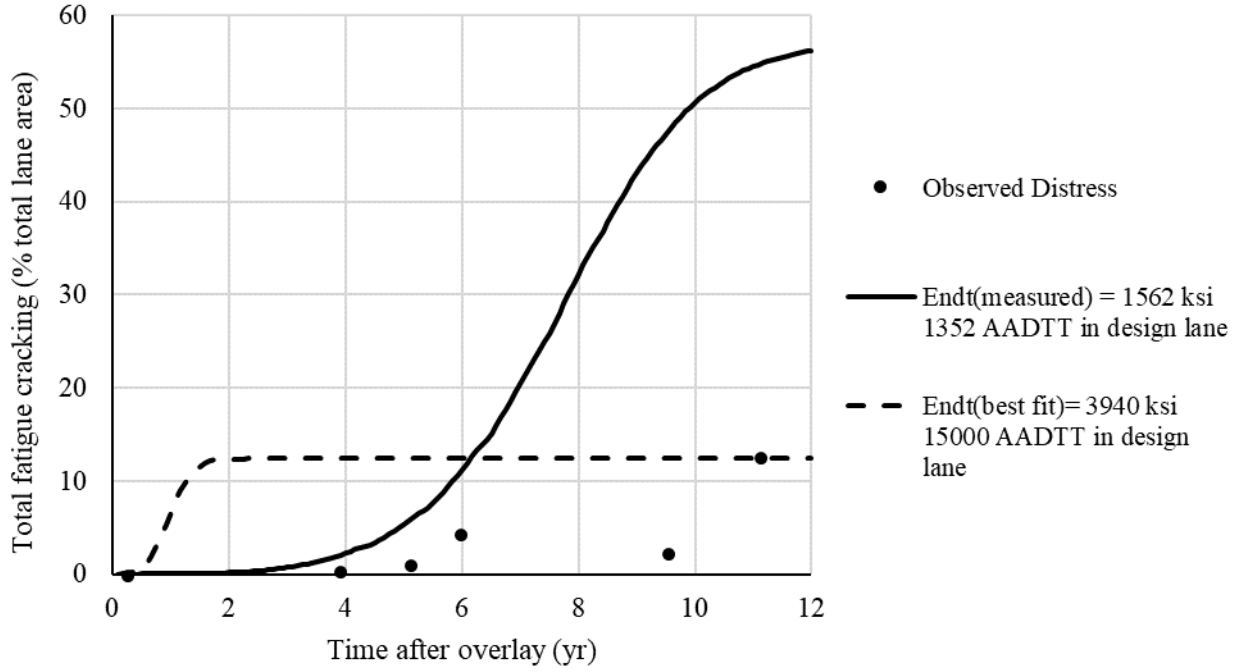

Figure 198. Determination of $E_{NDT(Best\ fit)}$ (LTPP Section 34-0960, New Jersey).

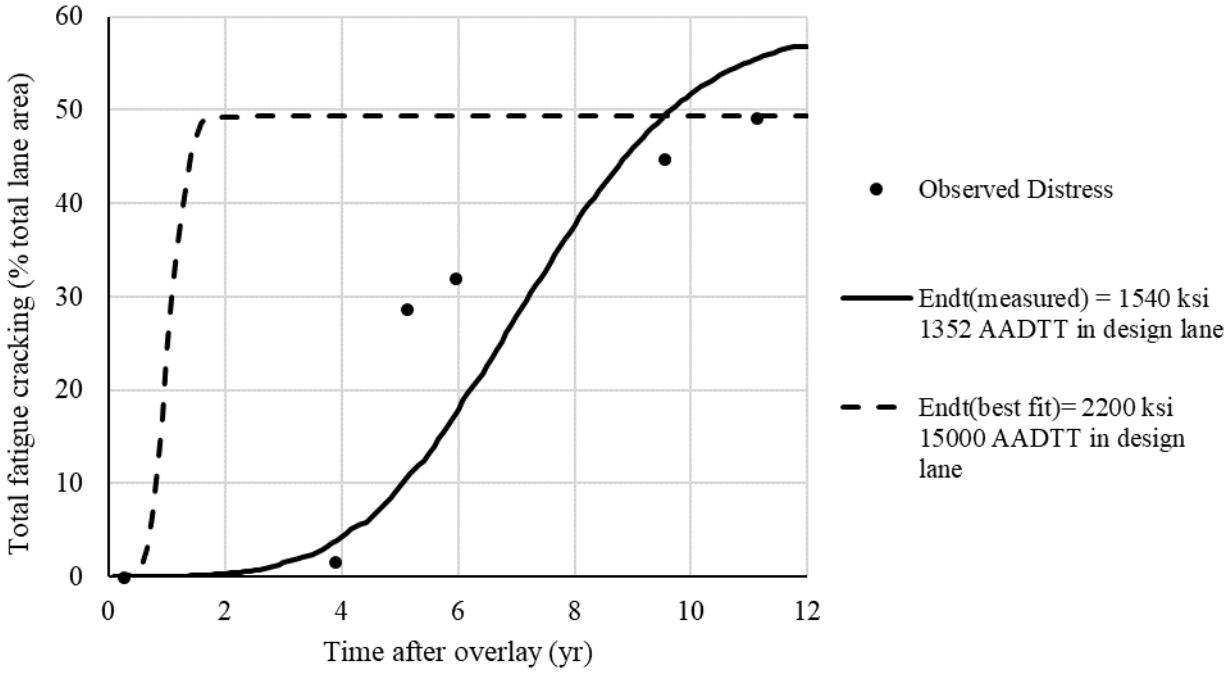

Figure 199. Determination of $E_{NDT(Best\ fit)}$ (LTPP Section 34-0961, New Jersey).

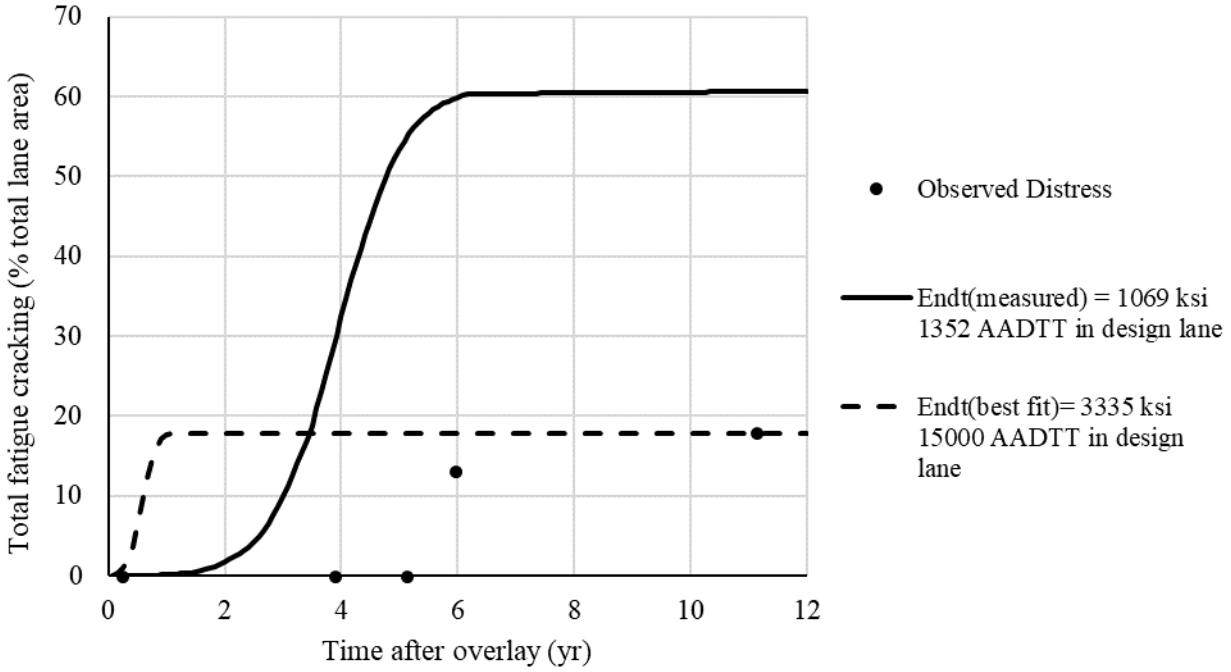

Figure 200. Determination of $E_{NDT(Best\ fit)}$ (LTPP Section 34-0962, New Jersey).

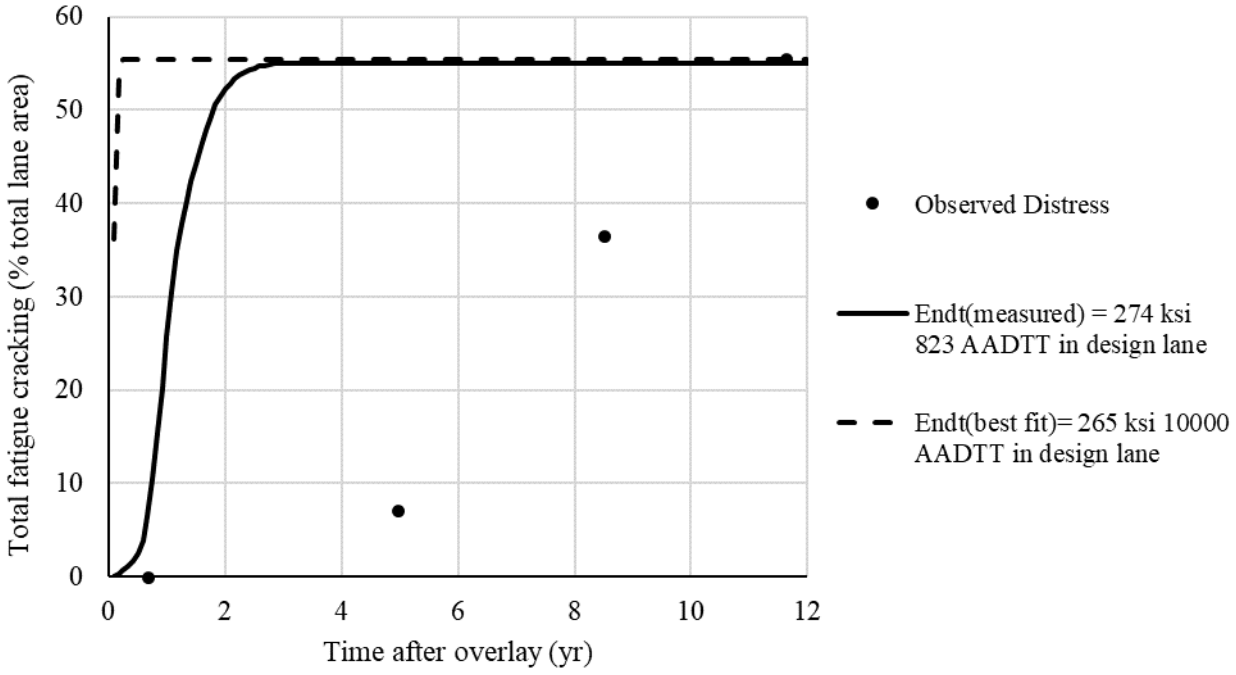

Figure 201. Determination of $E_{NDT(Best\ fit)}$ (LTPP Section 34-1003, New Jersey).

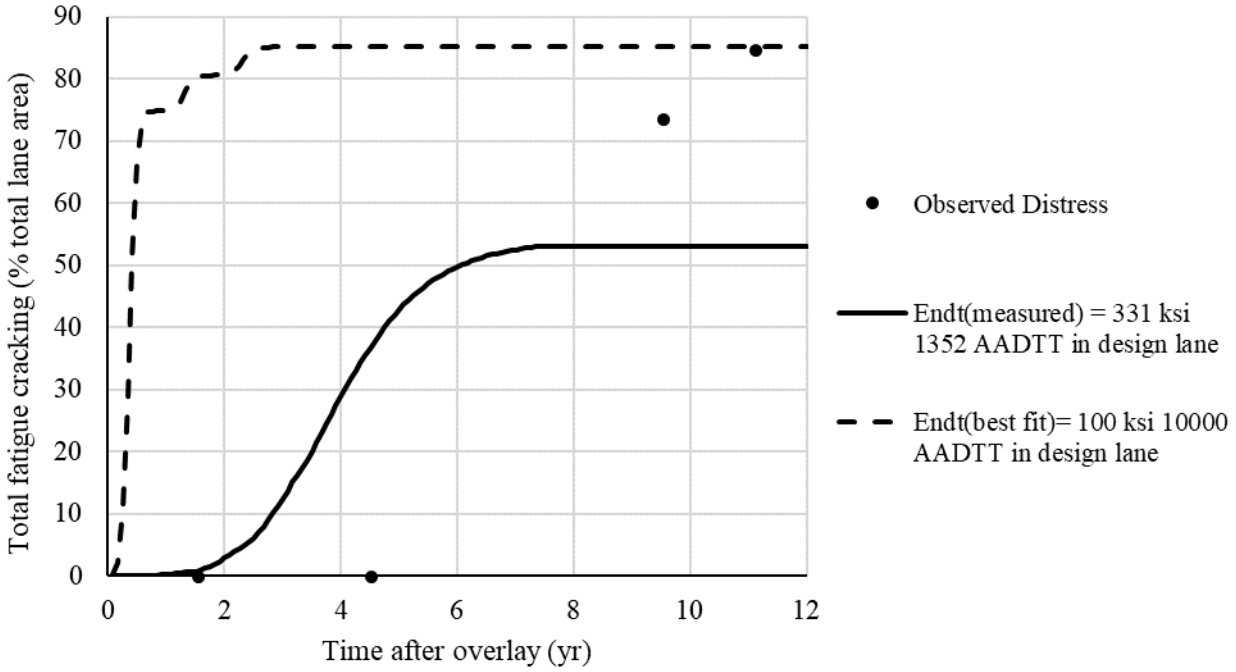

Figure 202. Determination of $E_{NDT(Best\ fit)}$ (LTPP Section 34-1011, New Jersey).

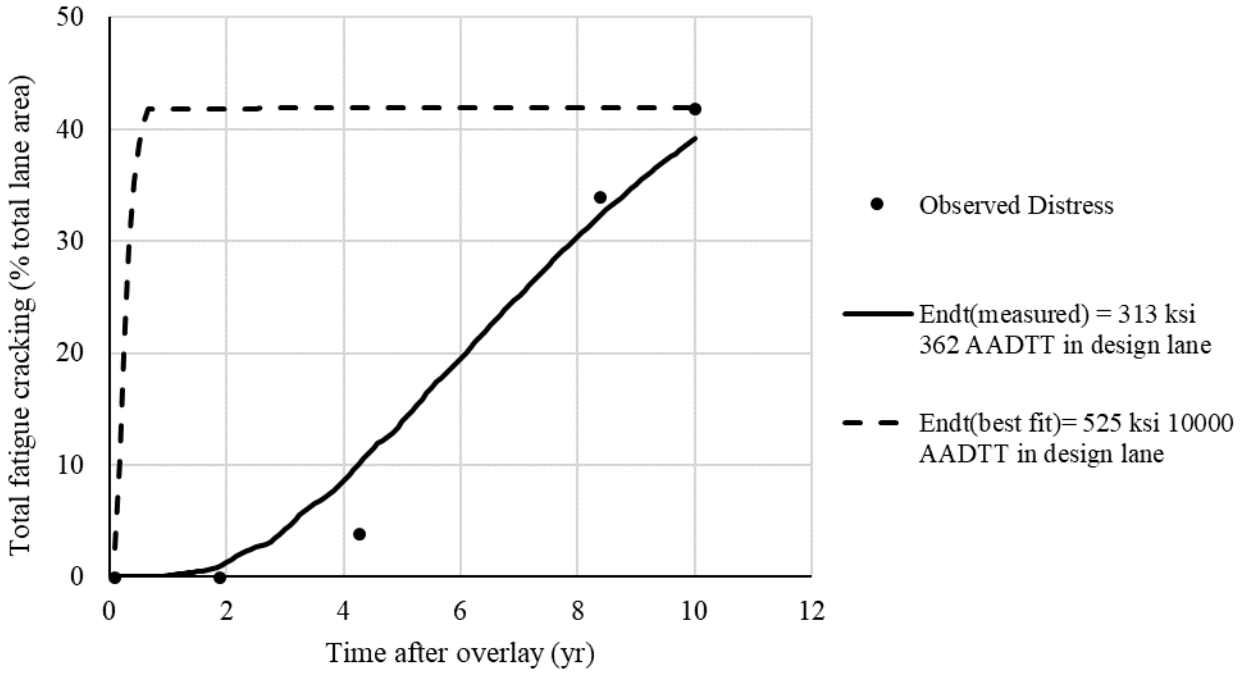

Figure 203. Determination of $E_{NDT(Best\ fit)}$ (LTPP Section 34-1030, New Jersey).

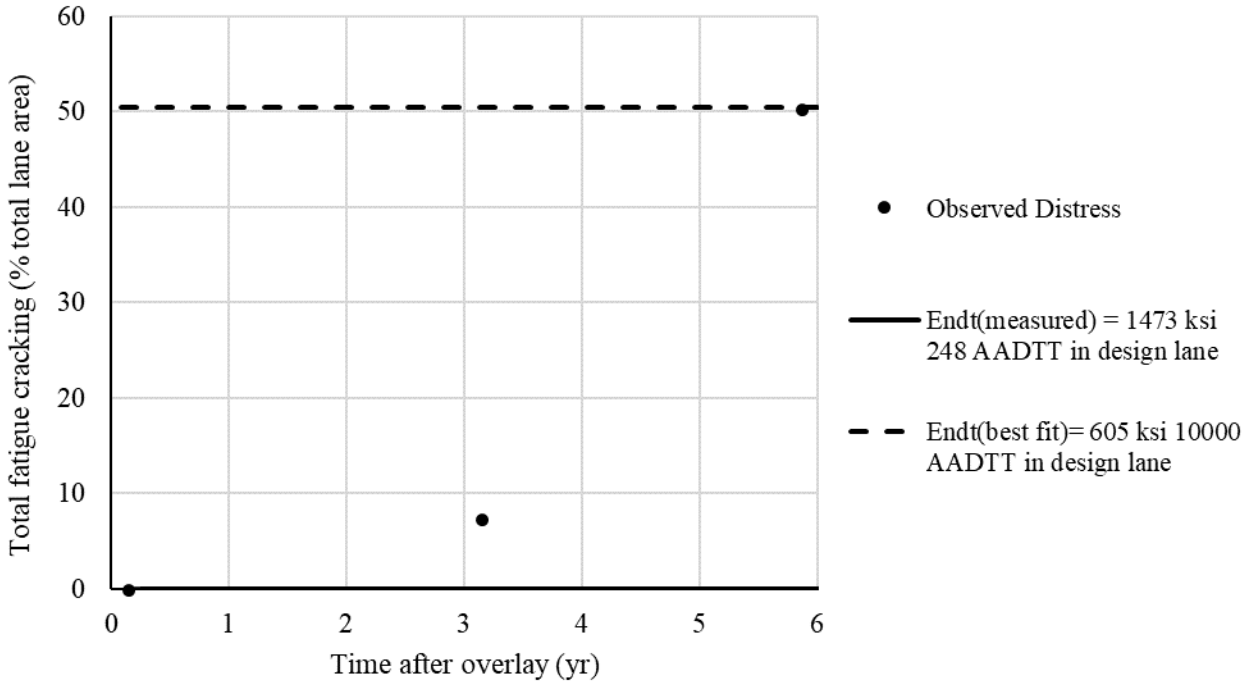

Figure 204. Determination of $E_{NDT(Best\ fit)}$ (LTPP Section 34-1033, New Jersey).

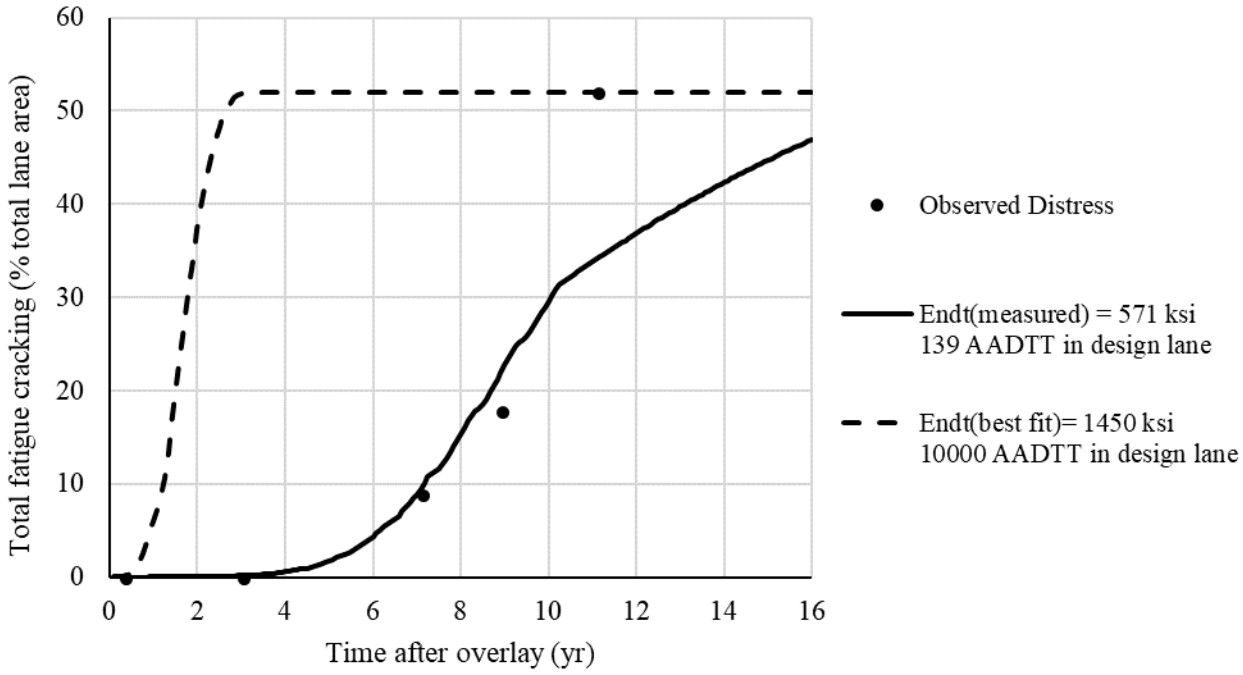

Figure 205. Determination of $E_{NDT(Best\ fit)}$ (LTPP Section 42-1597, Pennsylvania).

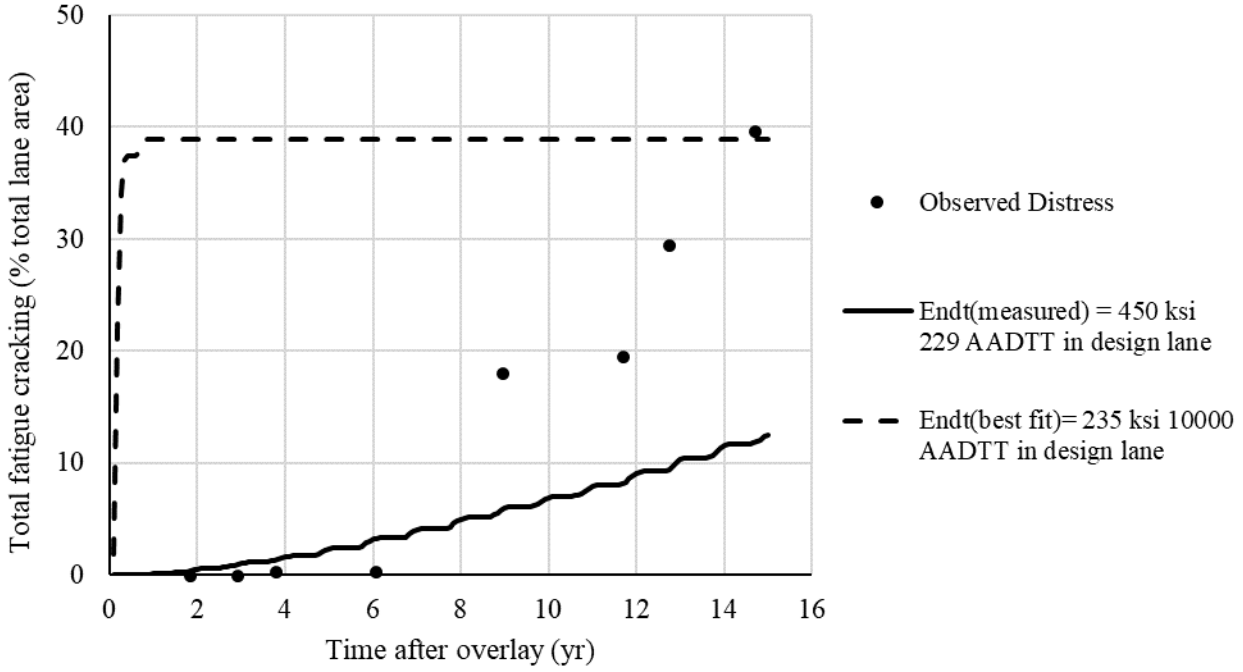

Figure 206. Determination of $E_{NDT(Best\ fit)}$ (LTPP Section 83-0502, Manitoba).

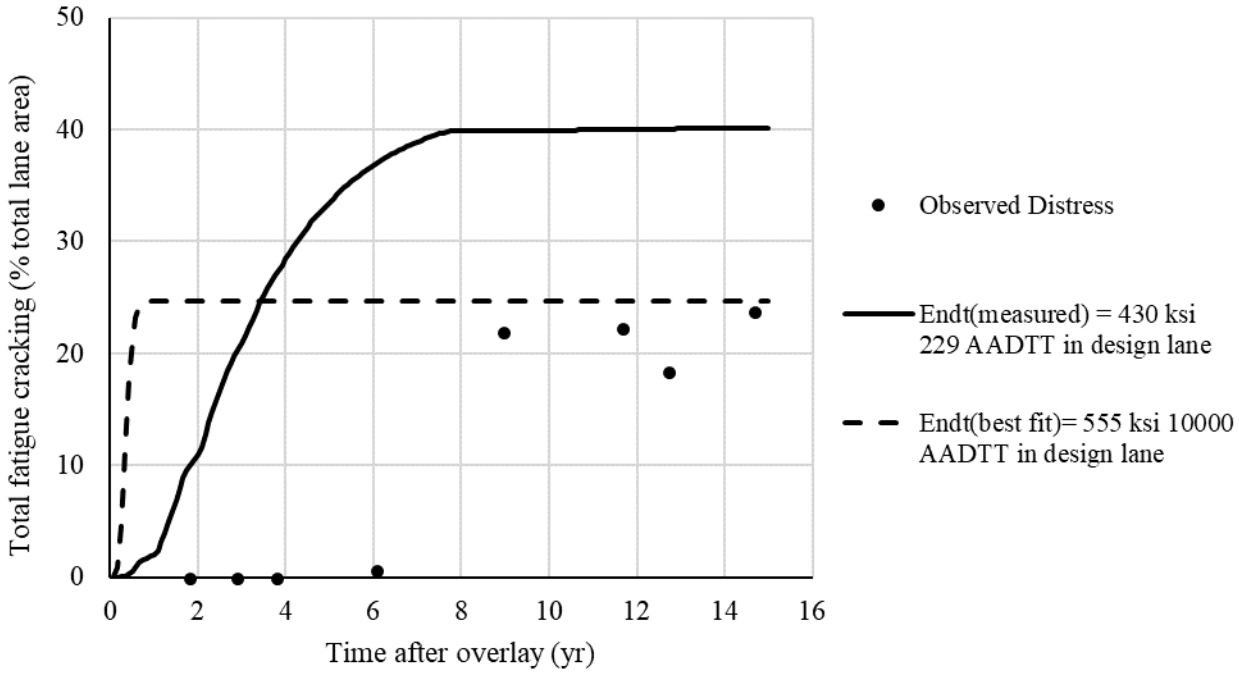

Figure 207. Determination of $E_{NDT(Best\ fit)}$ (LTPP Section 83-0503, Manitoba).

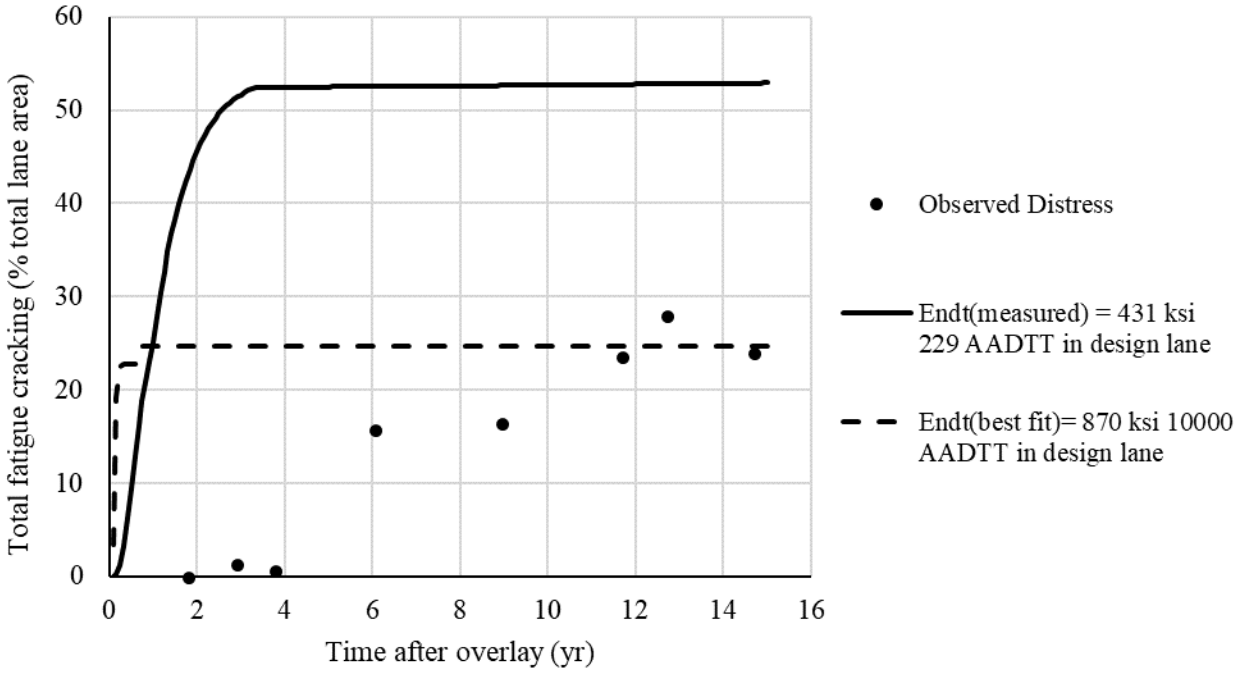

Figure 208. Determination of $E_{NDT(Best\ fit)}$ (LTPP Section 83-0506, Manitoba).

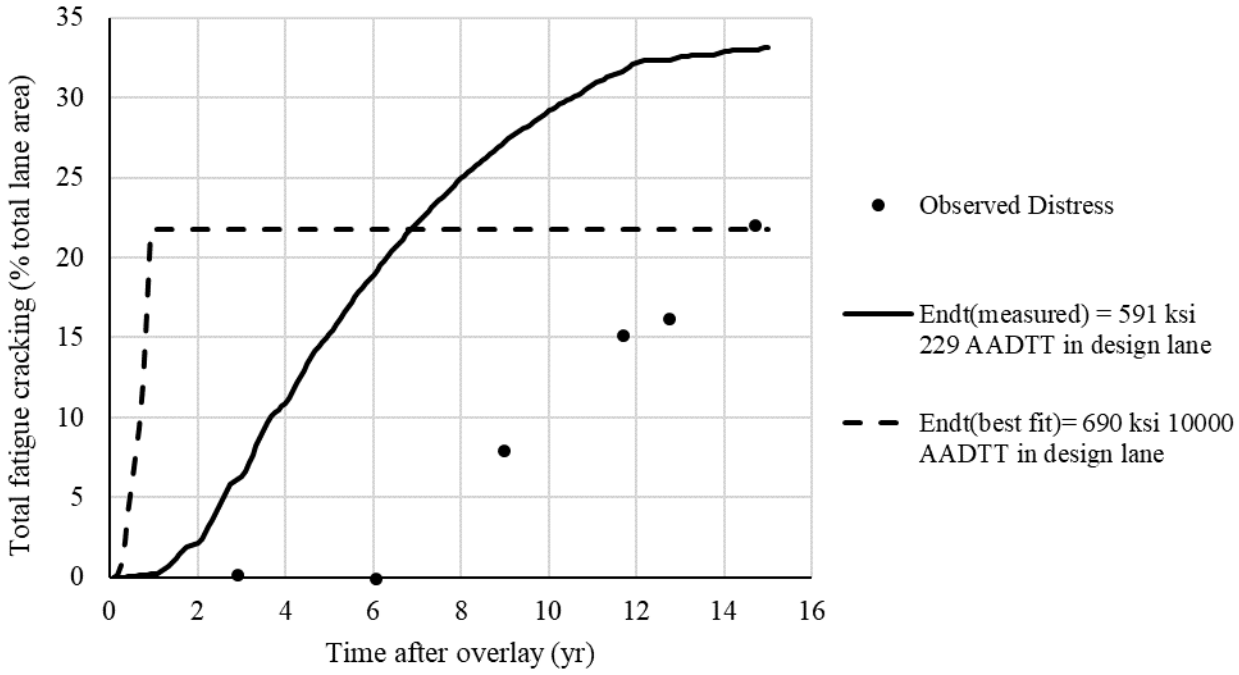

Figure 209. Determination of $E_{NDT(Best\ fit)}$ (LTPP Section 83-0507, Manitoba).

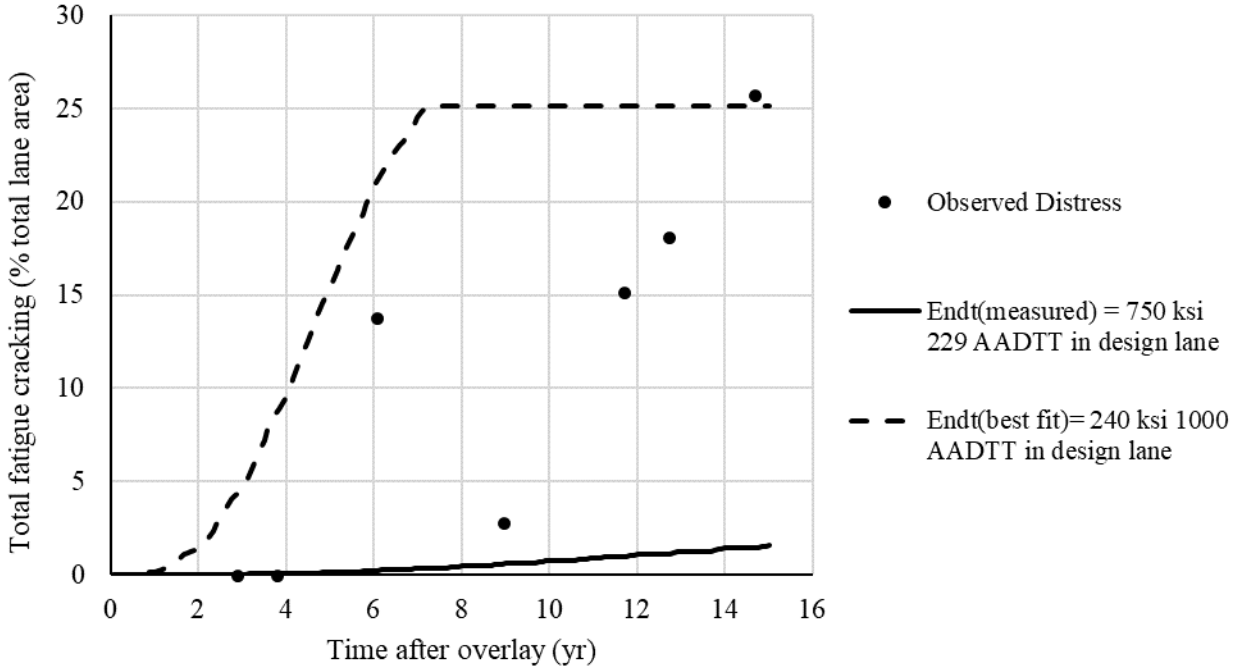

Figure 210. Determination of $E_{NDT(Best\ fit)}$ (LTPP Section 83-0508, Manitoba).

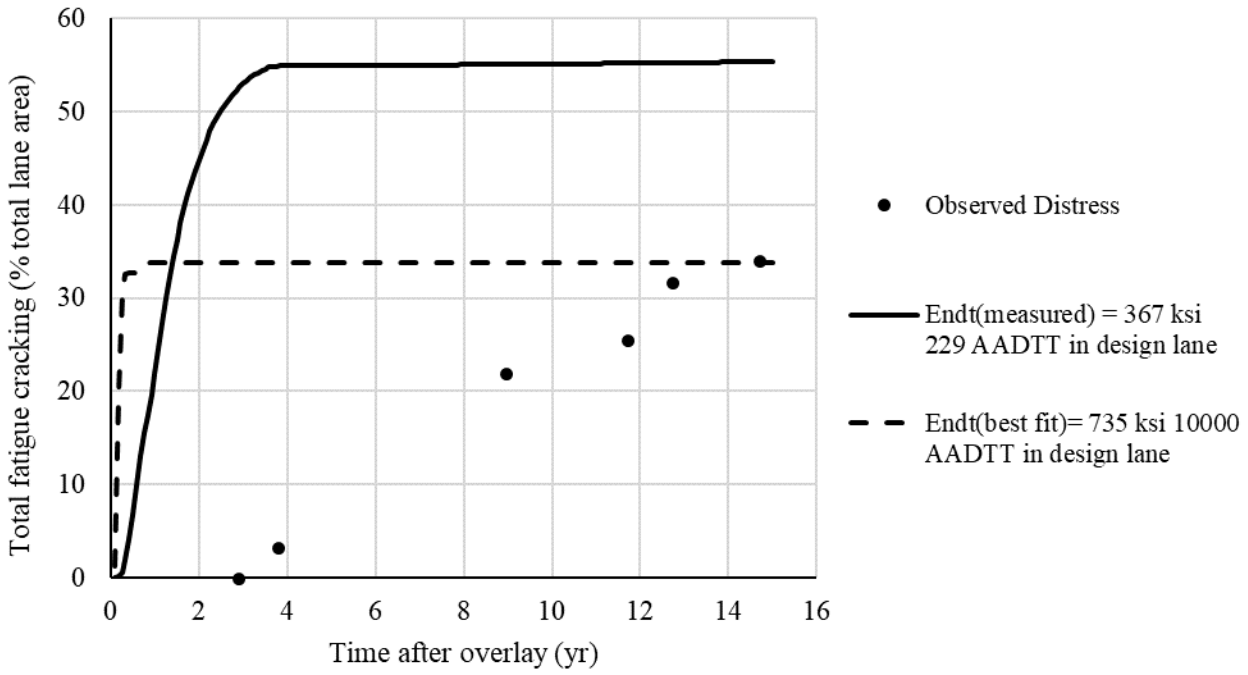

Figure 211. Determination of $E_{NDT(Best\ fit)}$ (LTPP Section 83-0509, Manitoba).

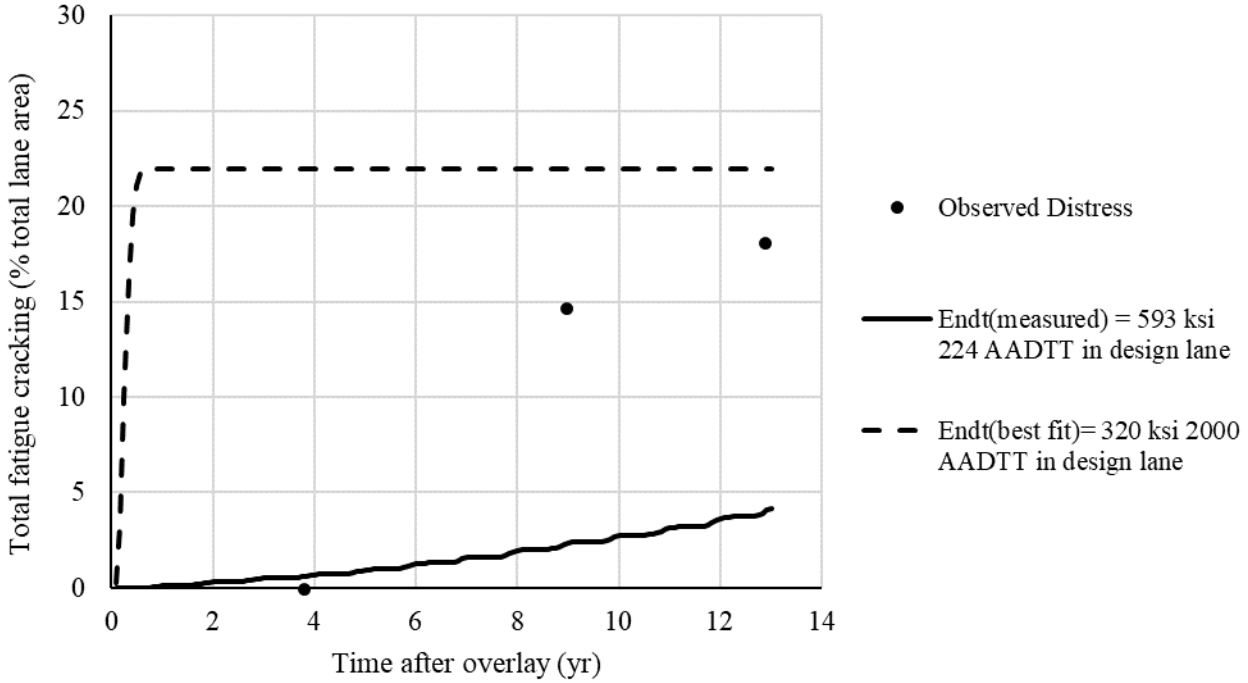

Figure 212. Determination of $E_{NDT(Best\ fit)}$ (LTPP Section 83-6451, Manitoba).

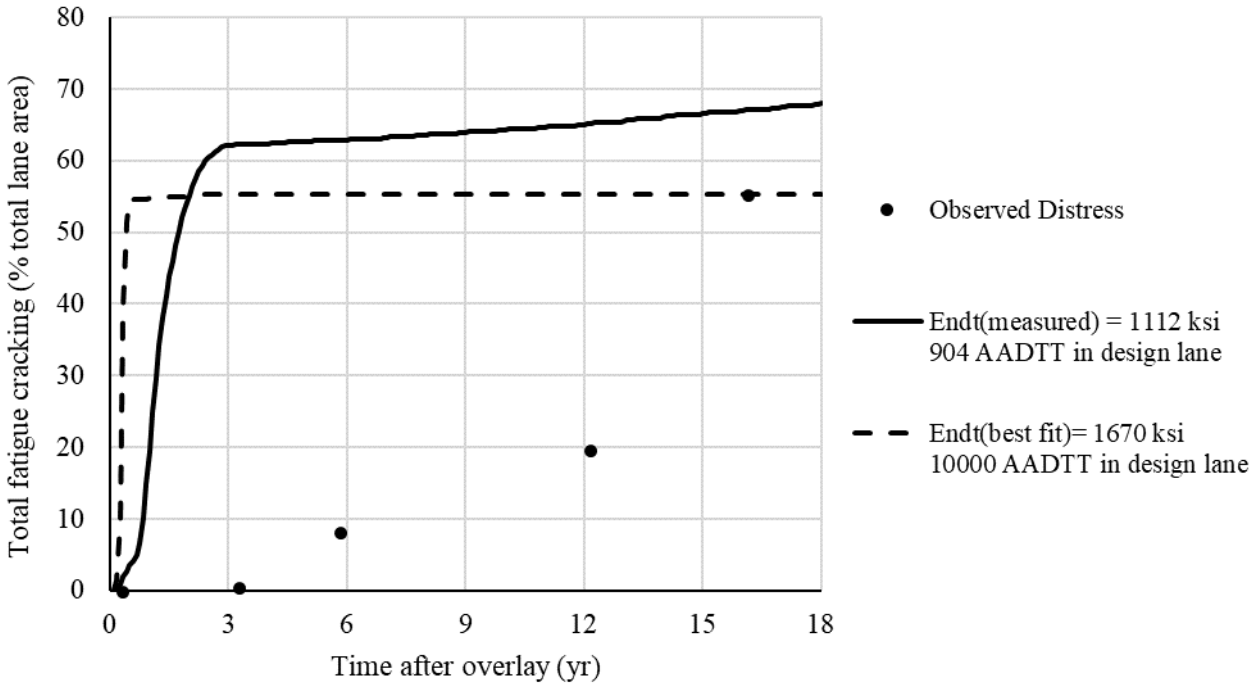

Figure 213. Determination of $E_{NDT(Best\ fit)}$ (LTPP Section 87-1622, Ontario).

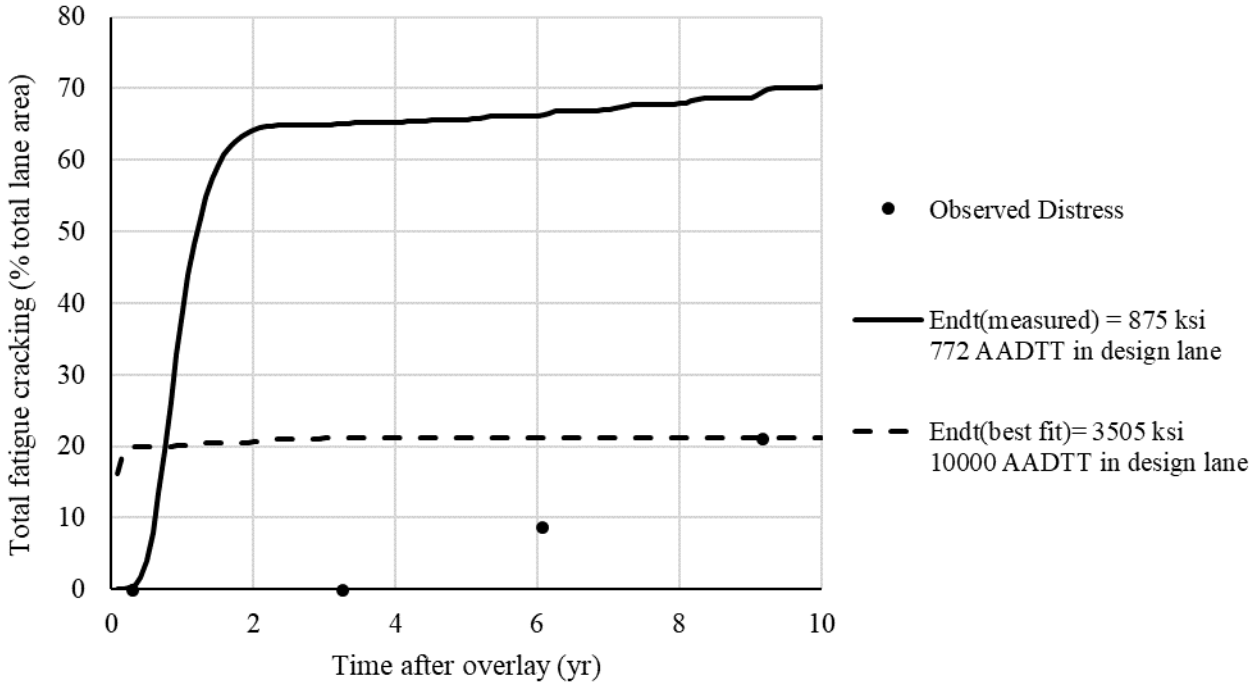

Figure 214. Determination of $E_{NDT(Best\ fit)}$ (LTPP Section 89-1125, Quebec).

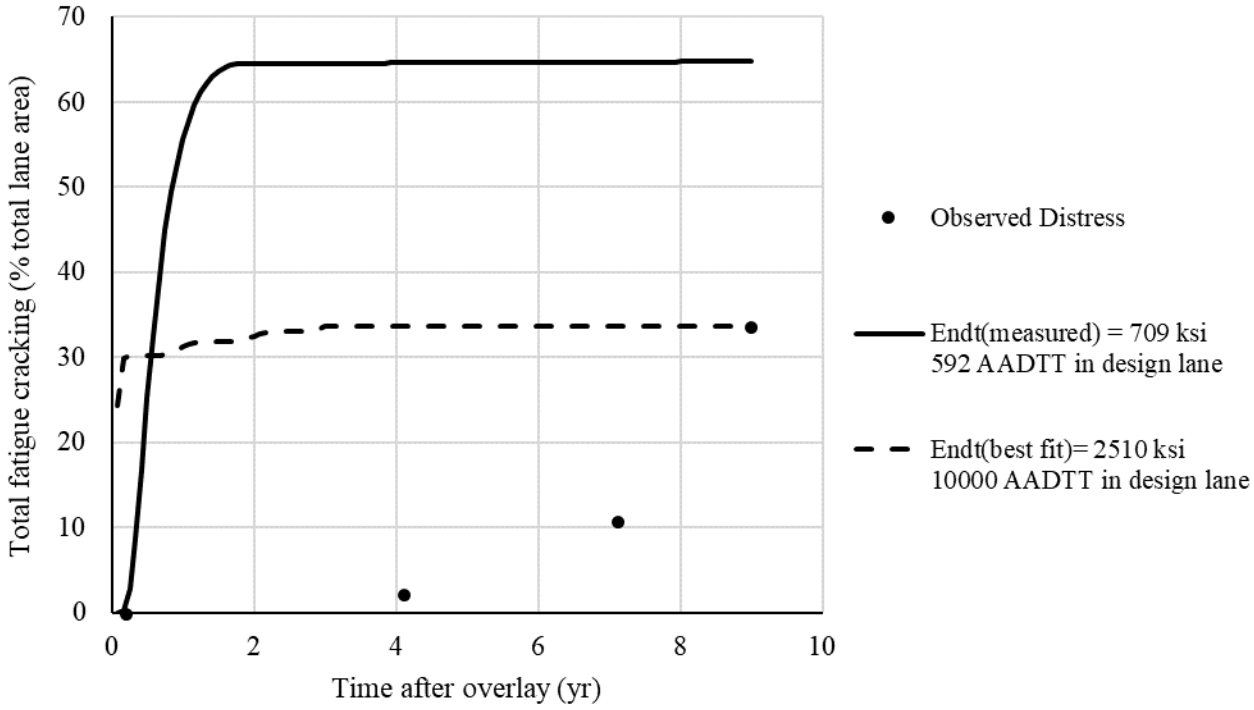

Figure 215. Determination of $E_{NDT(Best\ fit)}$ (LTPP Section 89-1127, Quebec).

BIBLIOGRAPHY

AASHTO. (1993). *AASHTO Guide for Design of Pavement Structures, 1993*. AASHTO Guide for Design of Pavement Structures, AASHTO, Washington, DC.

AASHTO. (2015). *AASHTO T 342-11: Determining Dynamic Modulus of Hot Mix Asphalt (HMA)*. Washington, DC.

Al-Khateeb, G., Shenoy, A., Gibson, N., and Harman, T. (2006). "A New Simplistic Model for Dynamic Modulus Prediction of Asphalt Paving Mixtures." *Journal of the Association of Asphalt Paving Technologists*, 75, 1254–1293.

Andrei, D., Witczak, M. W., and Mirza, M. W. (1999). *Development of Revised Predictive Model for the Dynamic Complex Modulus of Asphalt Mixtures. NCHRP 1-37A*. National Cooperative Highway Research Program, Washington, DC.

ARA Inc. (2004). *Guide for Mechanistic-Empirical Design of New and Rehabilitated Pavement Structures. NCHRP 1-37A*. National Cooperative Highway Research Program, Washington, DC.

ARA Inc. (2015a). *Pavement ME Design Release Notes, Build 2.2*. Applied Research Associates, Inc., Champaign, Illinois.

ARA Inc. (2015b). *Mechanistic-Empirical Pavement Design Guide: A Manual of Practice*. AASHTO, Washington, DC.

ARA Inc. (2017). *Release Notes: Pavement ME Deflection Data Analysis and Backcalculation Tool (Build 1.0)*. Applied Research Associates, Inc., Champaign, Illinois.

ASTM International. (1998). *ASTM D2493: Viscosity-Temperature Chart for Asphalts*. West Conshohocken, PA.

ASTM International. (2011). *ASTM D7369: Standard Test Method for Determining the Resilient Modulus of Bituminous Mixtures by Indirect Tension Test*. West Conshohocken, PA.

Ayyala, D., Lee, H., and Von Quintus, H. L. (2016). *Characterizing Existing Asphalt Concrete Layer Damage for Mechanistic Pavement Rehabilitation Design: Draft Final Report*. Federal Highway Administration, McLean, VA.

Ayyala, D., Lee, H., and Von Quintus, H. L. (2017). “Damage Characterization in Existing Asphalt Layer Concrete for ME Rehabilitation Design.” *TRB 96th Annual Meeting Compendium of Papers*, Transportation Research Board, Washington, DC.

Bari, J. (2005). “Development of a New Revised Version of the Witczak E* Predictive Models for Hot Mix Asphalt Mixtures.” Arizona State University.

Bhattacharya, B. B., Raghunathan, D., Selezneva, O., Wilke, P., Darter, M. I., and Von Quintus, H. L. (2017). *PennDOT Pavement ME Design Preliminary User Input Guide (Draft Report)*. Pennsylvania Department of Transportation, Harrisburg, PA.

Box, G. E. P., and Cox, D. R. (1964). “An Analysis of Transformations.” *Journal of the Royal Statistical Society, Series B*, 26, 211–243.

Bruinsma, J. E., Vandenbossche, J. M., Chatti, K., and Smith, K. D. (2017). *Using Falling Weight Deflectometer Data with Mechanistic-Empirical Design and Analysis - Volume II: Case Study Reports. FHWA-HRT-16-010*. Federal Highway Administration, McLean, VA.

Ceylan, H., Kim, S., and Gopalakrishnan, K. (2007). “Hot Mix Asphalt Dynamic Modulus Prediction Models Using Neural Networks Approach.” *ANNIE 2007, ANNs in Engineering Conference. November 10-14*, St. Louis, Missouri.

Chatti, K., Kutay, M. E., Lajnef, N., Zaabar, I., Varma, S., and Lee, H. S. (2017). *Enhanced Analysis of Falling Weight Deflectometer Data for use with Mechanistic-Empirical Flexible Pavement Design and Analysis and Reccommendations for Improvements to Falling Weight Deflectometer. FHWA-HRT-15-063*. Federal Highway Administration, McLean, VA.

Chen, D. H., Bilyeu, J., Lin, H. H., and Murphy, M. (2000). “Temperature Correction on Falling Weight Deflectometer Measurements.” *Transportation Research Record*, 1716, 30–39.

Christensen, D. W., Pellinen, T., and Bonaquist, R. F. (2003). “Hirsch model for Estimating the Modulus of Asphalt Concrete.” *Journal of the Association of Asphalt Paving Technologists*, 72, 97–121.

Clyne, T. R., Marasteanu, M. O., Li, X., Chadbourn, B., Engstrom, G., and Worel, B. (2004). “Determination of HMA Modulus Values for Use in Mechanistic-Empirical Pavement Design.” *2nd International Conference on Accelerated Pavement Testing*, Minneapolis, MN.

Gedafa, D. S., Hossain, M., Romanoschi, S., and Gisi, A. J. (2010). “Field Verification of Superpave Dynamic Modulus.” *Journal of Materials in Civil Engineering*, 22(5), 485–494.

Johnson, A., Clyne, T. R., and Worel, B. (2009). *2008 MnROAD Phase II Construction Report*. Minnesota Department of Transportation, St. Paul, MN.

Killingsworth, B., and Von Quintus, H. L. (1997). *Backcalculation of Layer Moduli of LTPP General Pavement Study (GPS) Sites. FHWA-RD-97-086*. Federal Highway Administration, McLean, VA.

Kim, Y. R., Underwood, B., Far, M. S., Jackson, N., and Puccinelli, J. (2011). *LTPP Computed Parameter: Dynamic Modulus. FHWA-HRT-10-035*. Turner-Fairbank Highway Research Center, Federal Highway Administration, McLean, VA.

Loulizi, A., Flintsch, G. W., and McGhee, K. (2008). "Determination of In-Place Hot-Mix Asphalt Layer Modulus for Rehabilitation Projects by a Mechanistic-Empirical Procedure." *Transportation Research Record*, 2037(1), 53–62.

Lukanen, E. O., Stubstad, R., and Briggs, R. (2000). *Temperature Predictions and Adjustment Factors for Asphalt Pavement. FHWA-RD-98-085*. Federal Highway Administration, Washington, DC.

Lytton, R. L., and Von Quintus, H. L. (2016). "TRB Webinar - Development and Implementation of the Reflective Cracking Model in the Mechanistic-Empirical Pavement Design Guide." Transportation Research Board, Washington, DC.

Lytton, R. L., Tsai, F.-L., Lee, S. I., Luo, R., Hu, S., and Zhou, F. (2010). *Models for Predicting Reflection Cracking of Hot-Mix Asphalt Overlays. NCHRP Report 669*. National Cooperative Highway Research Program, Washington, DC.

Mateos, A., Ayuso, J., and Jáuregui, B. (2012). "Evolution of Asphalt Mixture Stiffness Under Combined Effects of Damage, Aging, and Densification Under Traffic." *Transportation Research Record: Journal of the Transportation Research Board*, 2304, 185–194.

Miller, J. S., and Bellinger, W. Y. (2014). *Distress Identification Manual for the Long-Term Pavement Performance Program. FHWA-HRT-13-092*. Federal Highway Administration, McLean, VA.

Mirza, M. W. (1993). "Development of a Global Aging System for Short and Long Term Aging of Asphalt Cements." University of Maryland.

MnDOT. (2016). "MnROAD Data." *Minnesota Department of Transportation*, <http://www.dot.state.mn.us/mnroad/data/index.html>.

MnDOT. (2018). *Standard Specifications for Construction*. Minnesota Department of Transportation, St. Paul, Minnesota.

Ovik, J. M., Birgisson, B., and Newcomb, D. E. (2000). *Characterizing seasonal variations in pavement material properties for use in a mechanistic-empirical design procedure*. Minnesota Department of Transportation, St. Paul, Minnesota.

PennDOT. (2015). "Pavement History." *Pennsylvania Department of Transportation*, <http://www.dot7.state.pa.us/PavementHistory/> (Jan. 1, 2016).

Von Quintus, H. L. (2017). "Personal Communication at ASCE International Conference on Highway Pavements and Airfield Technology." Philadelphia, PA.

Von Quintus, H. L., and Killingsworth, B. (1998). Analyses Relating to Pavement Material Characterizations and Their Effects on Pavement Performance. FHWA-RD-97-085. Federal Highway Administration, McLean, VA.

Von Quintus, H. L., Rao, C., and Irwin, L. (2015). *Long-Term Pavement Performance Program Determination of In-Place Elastic Layer Modulus: Backcalculation Methodology and Procedures. FHWA-HRT-15-036*. Federal Highway Administration, McLean, VA.

Rao, C., and Von Quintus, H. L. (2015). "TRB Webinar - Determination of In-Place Elastic Layer Modulus: Backcalculation Methodology and Procedures." Transportation Research Board, Washington, DC.

Rhode, G. T., and Scullion, T. (1990). *MODULUS 4.0: Expansion and Validation of the MODULUS Backcalculation System*. Texas Transportation Institute, College Station, Texas.

Schmalzer, P. N. (2006). *LTPP Manual for Falling Weight Deflectometer Measurements. FHWA-HRT-06-132*. Federal Highway Administration, McLean, VA.

Tukey, J. (1949). "Comparing Individual Means in the Analysis of Variance." *Biometrics*, 5(2), 99–114.

WSDOT. (2005). *EVERSERIES © User's Guide Pavement Analysis Computer Software and Case Studies*. Washington Department of Transportation.

Zapata, C. E., and Cary, C. E. (2012). *Integrating the National Database of Subgrade Soil-Water Characteristic Curves and Soil Index Properties with the MEPDG. NCHRP 9-23A*. National Cooperative Highway Research Program, Washington, DC.